1: Executive Summary

1 Executive Summary

1.1 Science Drivers for the Large Synoptic Survey Telescope

The Large Synoptic Survey Telescope (LSST) will be a large-aperture, wide-field, optical imaging facility designed to address some of the most pressing questions about the structure and evolution of the universe and the objects in it. What is the mysterious dark energy that is driving the acceleration of the cosmic expansion? What is dark matter, how is it distributed, and how do its properties affect the formation of stars, galaxies, and larger structures? How did the Milky Way form, and how has its present configuration been shaped by mergers with smaller bodies over cosmic time? What is the nature of the outer regions of the solar system? Is it possible to make a complete inventory of smaller bodies in the solar system, especially the potentially hazardous asteroids that could someday impact the Earth? Are there new exotic and explosive phenomena in the universe that have not yet been discovered?

These are profound questions, and yet the concept behind the design of the LSST is remarkably simple: conduct a deep survey over an enormous area of sky; do it with a frequency that enables repeat exposures of every part of the sky every few nights in multiple bands; and continue in this mode for ten years to achieve astronomical catalogs thousands of times larger than have ever previously been compiled. The essence of the LSST is wide, fast, deep.

1.1.1 Overview of Science Enabled by LSST

Superior survey capability will open new avenues of research. In formulating the requirements for the LSST, four main science themes have been identified:

1. Constraining the Nature of Dark Energy and Dark Matter

2. Taking an Inventory of the Solar System

3. Exploring the Transient Optical Sky

4. Mapping the Milky Way

These four science topics were chosen because they are the focus of cutting edge research that spans the universe from our own local neighborhood to distant galaxies, the formation of the solar system, the evolution of galactic structure, and cosmology.

These themes fully exercise the technical capabilities of the system, such as photometric and astrometric accuracy and image quality. About 90% of the observing time will be devoted to a deep, wide, fast (main) survey mode. The working paradigm is that all scientific investigations will utilize a common database constructed from an optimized observing program

If the LSST meets the science requirements for these four topics, then it will also meet the requirements for a very broad range of other scientific programs. The LSST Science Book (http;//www.lsst.org/scibook), which was authored by 245 scientists who are currently working with the LSST project, describes many of these programs in detail.

1.2 Major Agency Endorsements

Because of its broad scientific potential, the development of LSST has received strong endorsements in four influential National Academy of Sciences/National Research Council reports:

- ASTRO 2010 - New Worlds, New Horizons in Astronomy and Astrophysics (National Research Council (U.S.). Committee for a Decadal Survey of Astronomy and Astrophysics) selected LSST as the number one priority in ground-based astronomy.
- Connecting Quarks with the Cosmos: Eleven Science Questions for the New Century (National Research Council (U.S.). Committee on the Physics of the Universe. and ebrary Inc. 2003): Reviewed frontier research at the interface of physics and astronomy. Highlighted the capabilities of LSST as a probe of dark energy and dark matter.
- New Frontiers in Solar System Exploration (National Research Council (U.S.) and ebrary Inc. 2003): Reviewed the current status of solar system research and outlined a program of investment for the future. Endorsed LSST for its ability to survey moving objects in the solar system.
- Astronomy and Astrophysics in the New Millennium ((National Research Council (U.S.). Astronomy and Astrophysics Survey Committee. 2001): Reviewed major new initiatives in all areas of astronomy and astrophysics. Endorsed LSST as a high-priority major new project in ground-based astronomy.

As a dark energy experiment, the LSST project has also attracted the interest of the particle physics community. The Dark Energy Task Force (DETF), commissioned jointly by the Astronomy and Astrophysics Advisory Committee (AAAC) and the High Energy Physics Advisory Panel (HEPAP), concluded that a Stage IV Large Survey Telescope (modeled on LSST) could make a major advance in our understanding of dark energy, especially if subtle systematic errors can be brought under control (Albrecht 2006).

On the basis of the DETF report and the results of the LSST CoDR, the Particle Physics Project Prioritization Panel (P5), recommended in 2008 that "DOE support the ground-based LSST program, in coordination with NSF" (Baltay et al. 2008), and this was strongly reaffirmed in the 2014 P5 report (Ritz et al. 2014).

1.3 Conceptual Design of Telescope and Camera

The 8.4 m LSST will be constructed on the El Penon peak on Cerro Pachon in northern Chile. Its three large telescope mirrors will be actively controlled to minimize distortions. The telescope mount will be a compact, stiff structure especially designed to reduce image motion. The LSST Camera - with three refractive lenses and a 9.6 square degree field-of-view - will be the largest digital camera ever constructed. LSST will take pairs of 15-second exposures of each field, separated by a 2 second readout. Operational simulations demonstrate that the LSST can deliver a uniform and deep 18,000 square degree survey with over 5.2 million exposures in ten years. This "movie" out to redshift 3 will open an entirely new window on the universe. LSST will produce on average about 15 Terabytes of data per night. Dedicated facilities will process the image data in near real time. The design of the LSST is described in more detail in Chapter 4.

The LSST Camera and its major subsystems are illustrated in Figure 1-1 below. The Camera provides a 3.2-gigapixel flat focal plane array, tiled by 4K x 4K CCD sensors with 10 µm square pixels. The sensors are deep-depleted, back-illuminated devices with a highly segmented architecture that enables the entire array to be read out within the required 2 seconds. Detectors are grouped into rafts in 3 x 3 arrays, with each raft containing its own dedicated front-end and back-end electronics boards. The rafts are mounted on a silicon carbide grid inside a vacuum cryostat, with an intricate thermal control system that maintains the CCDs at an operating temperature of -100^{o}C. The entrance window to the cryostat is refractive lens L3, the third the three such lenses in the Camera. The other two lenses, L1 and L2, are mounted in an optics structure at the front of the camera body, which also contains a mechanical shutter and a carousel assembly that holds five large optical filters. A sixth optical filter can replace any of the five via a procedure accomplished during daylight hours. The Camera design is described in more detail starting in Chapter 5 and continuing through the remainder of this Report.

This document was produced and revised prior to CD-3. It is periodically updated to reflect significant design changes, but not production status. Thus, while the design description is current, the narrative is a snapshot of R&D and prototyping status prior to CD-3.

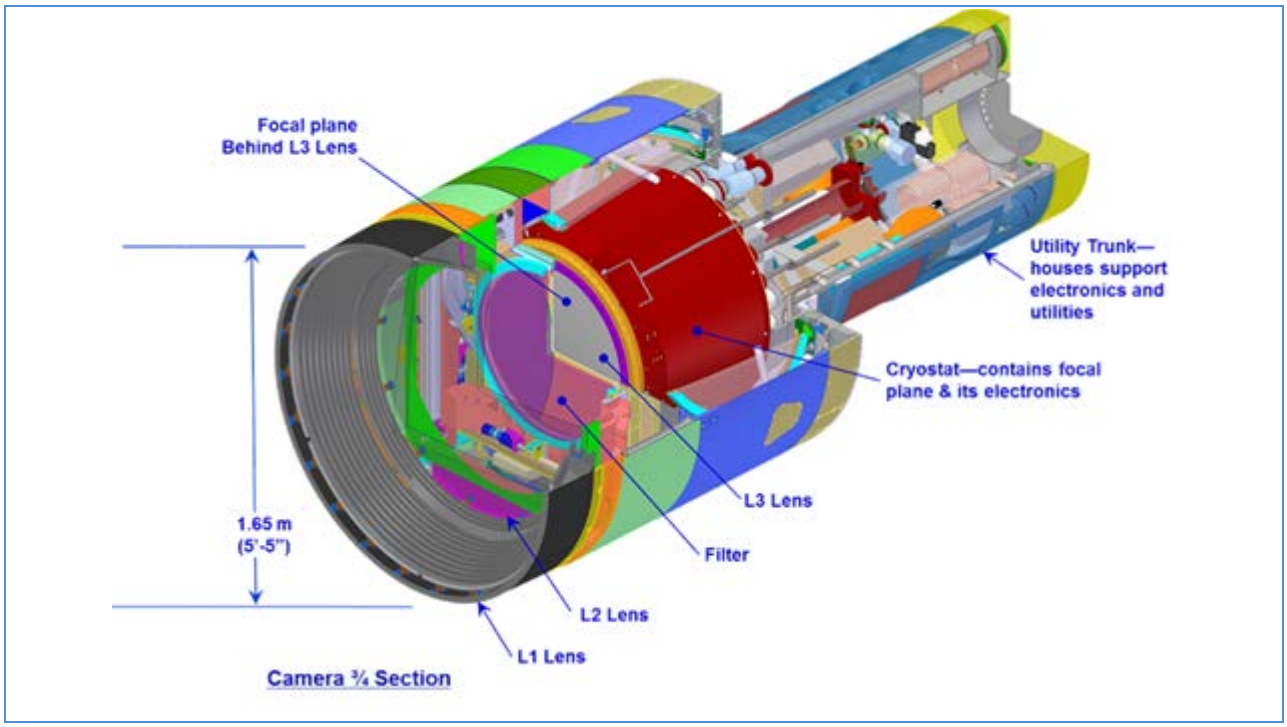

Figure 1-1: High-Level View of the LSST Camera, Showing Major Subsystems (Filter Exchange System Omitted)

1.4 Cost and Schedule

The DOE CD-1 cost range for the LSST Camera is $120M to $175M. The CD-2 approved total project cost is $168M. The construction project has an estimated duration of 5 years.

1.5 Acquisition Strategy

The lead contractor for acquisition of the LSST Camera is Stanford University, which operates SLAC National Accelerator Laboratory under contract with the U.S. Department of Energy.

Major collaborators include the Brookhaven National Laboratory, the Lawrence Livermore National Laboratory, a consortium of U.S. based Universities, and the Institute National de Physique Nucleaire and de Physique des Particules in France.

1.6 References

Albrecht, A. G., Bernstein, G., Cahn, R., Freedman, W. L., Hewitt, J., Hu, W., Huth, J., Kamionkowski, M., et. al. (2006). Report of the Dark Energy Task Force: a joint subcommittee of the NSF-NASA-DOE Astronomy and Atrophysics Advisory Committee (AAAC) and the NSF-DOE High Energy Physics Advisory Panel (HEPAP).

Baltay, C., et al. (Partical Physics Project Prioritization Panel) (2008). US Particle Physics: Scientific Opportunities. A Strategic Plan for the Next Ten Years.

National Research Council (U.S.) and ebrary Inc. (2003). New frontiers in solar system exploration. Washington, D.C., National Academies Press**:** 28 p.

National Research Council (U.S.). Astronomy and Astrophysics Survey Committee. (2001). Astronomy and astrophysics in the new millennium. Washington, D.C., National Academy Press.

National Research Council (U.S.). Committee for a Decadal Survey of Astronomy and Astrophysics. (2010). New Worlds, New Horizons in Astronomy and Astrophysics. Washington, D.C., National Academies Press: 324 p.

National Research Council (U.S.). Committee on the Physics of the Universe. and ebrary Inc. (2003). Connecting quarks with the cosmos eleven science questions for the new century. Washington, D.C., National Academies Press: xvi, 206 p.

Ritz, S. et al. (Particle Physics Project Prioritization Panel) (2014). Building for Discovery: Strategic Plan for U.S. Particle Physics in the Global Context.

2: Science Motivation and Requirements

2 Science Motivation and Requirements

2.1 Overview of Science Requirements for LSST

The LSST is envisioned to be a large, wide-field ground based telescope designed to obtain sequential images covering over half the sky every few nights. The current baseline design (see Chapters 4 and 5) involves a 3-mirror system with an 8.4 m primary mirror, which feeds three refractive correcting elements inside a camera, providing a 9.65 deg^2 field of view sampled by a 3.2 Gigapixel focal plane array. The total effective system throughput (etendue) is expected to be greater than 300 m^2 deg^2. The survey will yield contiguous overlapping imaging of ~ 18,000 deg^2 of sky in six optical bands covering the wavelength range 320–1050 nm. Detailed simulations that include measured weather statistics and a variety of other effects which affect observations predict that each sky location can be visited about 100 times per year, with 30 sec exposure time per visit.

The range of scientific investigations enabled by such a dramatic improvement in survey capability is extremely broad and is summarized in detail in the LSST Science Book (http://www.lsst.org/scibook). However, it is not feasible to make an exhaustive study of the scientific requirements appropriate to all of them. To define quantitative science drivers and resulting requirements on the overall design, four main science themes have been identified:

1. Constraining the Nature of Dark Energy and Dark Matter

2. Taking an Inventory of the Solar System

3. Exploring the Transient Optical Sky

4. Mapping the Milky Way

It is our belief that the analyses encompassed by these four science themes fully exercise the technical capabilities of the system, such as photometric and astrometric accuracy and image quality. The working paradigm at this time is that all such investigations will utilize a common database constructed from an optimized observing program.

Below, we provide broad overviews of the methodologies that will be invoked in the study of dark energy and dark matter, since these are the topics of most interest to the Department of Energy. However, for completeness, we also include short summaries of the science goals for the other three areas. The science requirements that have been derived are made in the context of what we forecast for the scientific landscape in 2022, when LSST will begin its survey. Clearly science will not stand still in the intervening time. Using current plans for smaller surveys and precursor projects one may calculate efficiencies and gauge the likely progress on a number of LSST-related scientific frontiers. Some advances in each area will be made, but the LSST remains the ultimate facility for each key area covered in this chapter.

2.2 Constraining Dark Energy and Dark Matter

Driven by observations, current models of cosmology require the existence of both dark matter and dark energy. One of the primary challenges for fundamental physics is to understand these two major components of the universe. In addition to making a unique map of dark matter structure over half the sky, LSST will probe dark energy in multiple ways, providing cross checks and removal of important degeneracies.

In physical cosmology, dark energy is a hypothetical form of energy that permeates all of space and increases the rate of expansion of the universe. Dark energy is the most accepted theory to explain recent observations that the universe appears to be expanding at an accelerating rate. In the standard model of cosmology, dark energy currently accounts for 73% of the total mass-energy of the universe.

Two proposed forms for dark energy are the cosmological constant, a constant energy density filling space homogeneously, and scalar fields such as quintessence or moduli, dynamic quantities whose energy density can vary in time and space. Contributions from scalar fields that are constant in time are

usually also included in the cosmological constant. The cosmological constant is physically equivalent to vacuum energy.

High-precision measurements of the expansion of the universe are required to understand how the expansion rate changes over time. In general relativity, the evolution of the expansion rate is parameterized by the dark energy equation of state, $w(z) = p/\rho$, the relationship between pressure and energy density as a function of redshift. Measuring the equation of state of dark energy is one of the biggest efforts in observational cosmology today.

An alternative explanation for the accelerated expansion of the universe is that gravity on large scales is not described by Einstein's general relativity. This scenario, at least as radical as the idea of dark energy, is called modified gravity. The experimental approach to testing dark energy can be adapted to test modified gravity, in particular by distinguishing probes of the expansion rate from growth of structure as described below.

2.2.1 Overview of Dark Energy Constraints

LSST will focus on three major techniques for investigating the dynamics of the universe. The first, measurements of cosmic shear through weak gravitational lensing, relies both on the relationship between distance and redshift and on the rate of growth of structure with cosmic time. As such, it simultaneously probes the expansion of the universe and the evolution of the dark matter density field perturbations, which depend on the explicit predictions of general relativity. The rate at which primordial density perturbations grow to form larger and larger structures is very sensitive to the dynamics of the expanding universe.

A second method uses observations of the light curves of Type Ia supernovae. According to the accepted theory, a Type Ia supernova is produced when a white dwarf either accretes sufficient mass from a companion star or collides with another white dwarf, igniting a gigantic thermonuclear explosion. For cosmology, these events are important because they are very bright, which allows for their detection at very large distances, and because their intrinsic luminosities can be inferred from the measured shapes of their light curves. If the intrinsic luminosity of a supernova event is known, then its distance (more specifically, its luminosity distance) can be inferred from its apparent brightness. For any given cosmological model, there is an explicit prediction for the relation between luminosity distance and redshift that can be tested in this way.

Finally, the third technique, measurement of baryon acoustic oscillations (BAO), takes advantage of a feature of fixed scale (in co-moving coordinates) to constrain the angular size versus redshift relation that is also predicted by cosmological models. That fixed scale (~ 150 Mpc) corresponds to the propagation distance of acoustic waves in the early universe prior to recombination of protons and electrons, which decoupled the photon and matter fields. This distance scale remains imprinted on the three-dimensional distribution of galaxies.

Other powerful techniques of probing dark energy will also be implemented with LSST, including the abundance of galaxy clusters and the time delay measured in strong lensing systems. In the interest of brevity we focus only on these three techniques here. This document provides only a summary; more

details of the methods that will be used to study Dark Energy with LSST may be found in the LSST Dark Energy Science Collaboration white paper (http://arxiv.org/abs/1211.0310).

2.2.2 Measurement of Cosmic Shear Through Weak Gravitational Lensing

2.2.2.1 Overview of gravitational lensing

Weak gravitational lensing is the most direct probe of mass distribution in the universe. It has been applied successfully on many different scales, from galaxy halos to large-scale structure. These measurements in turn yield constraints on models of dark matter, dark energy and cosmology. The primary limitation to date has been statistical: Lensing causes a small perturbation to the initially random orientations of background galaxies, so large numbers of background galaxies are required for high signal-to-noise measurements.

Weak lensing (WL) techniques can be used to map the distribution of mass as a function of redshift and thereby trace the history of both the expansion of the universe and the growth of structure (e.g., Hu & Tegmark 1999; Wittman et al. 2000; for a review see Bartelmann & Schneider 2001). Weak lensing of galaxies as a function of redshift probes both the evolution of structure over cosmic time and determines dimensionless ratios of distances versus cosmic time, giving multiple independent constraints on the nature of dark energy. These investigations require deep, wide-area, multi-color imaging with stringent requirements on shear systematics in at least two bands, and excellent photometry in all bands (a requirement shared with BAO). The strongest constraints on the LSST image quality come from this science program. In order to control systematic errors in shear measurement, it is mandatory to obtain the desired depth with many short exposures (which enables reconstruction of galaxy shapes with minimum systematic error). Detailed simulations of weak lensing techniques show that, in order to obtain a sample of roughly 30 galaxies per square arcminute over > 15,000 deg^2, and reach a depth of r > 27.5 (5σ for point sources), with several hundred exposures per field and sufficient signal-to-noise in at least five other bands to obtain accurate photometric redshifts. This depth optimizes the number of measured galaxies in ground-based seeing, and allows their detection in significant numbers to beyond a redshift of 2. It is anticipated that optimal science analyses of weak lensing may also place strong constraints on data processing software.

Gravitational lensing acts as a coordinate transformation that distorts the images of background galaxies near a foreground mass. The transformation can be split into two terms, the convergence and shear. The convergence term magnifies the background objects by increasing their size, and the shear term stretches them tangentially around the foreground mass.

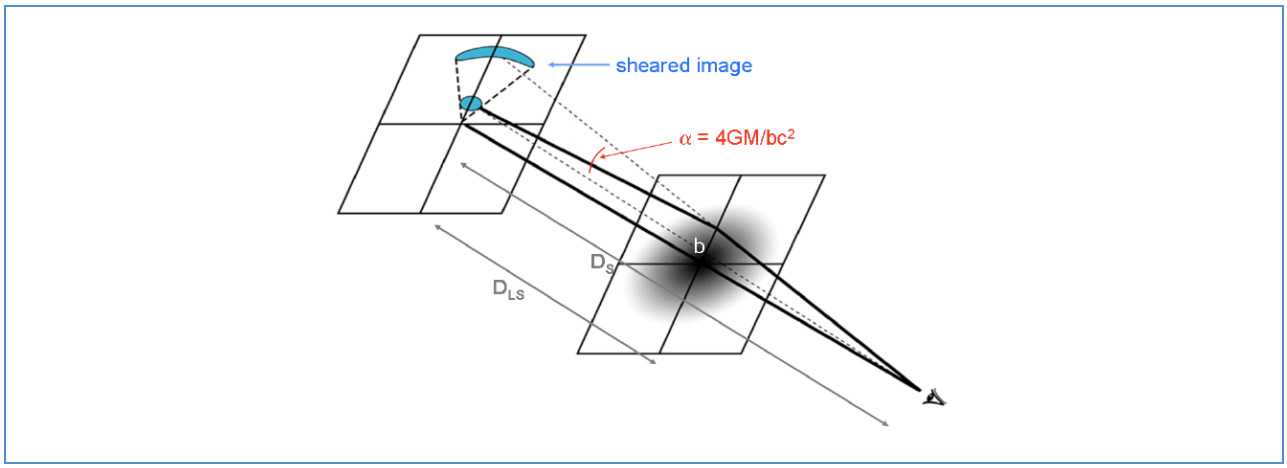

Figure 2-1: Gravitational lensing principle

To measure this tangential alignment, it is necessary to measure the ellipticities of the background galaxies and construct a statistical estimate of their systematic alignment. The fundamental problem is that galaxies are not intrinsically circular, so their measured ellipticity is a combination of their intrinsic ellipticity and the gravitational lensing shear. Typically, the intrinsic ellipticity is much greater than the shear (about an order of magnitude, depending on the foreground mass). The measurements of many background galaxies must be combined to average down this "shape noise". The orientation of intrinsic ellipticities of galaxies should be almost entirely random, so any systematic alignment between multiple galaxies can be assumed to be caused primarily by lensing, if it is not otherwise attributable to the measurement process itself.

A major challenge for weak lensing is correction for the point spread function (PSF) due to instrumental and atmospheric effects, which causes the observed images to be smeared relative to the "true sky". This smearing tends to make small objects more round, destroying some of the information about their true ellipticity. As a further complication, the PSF typically adds a small level of ellipticity to objects in the image, which is not in general random, and can in fact mimic a true lensing signal. Even for the most modern telescopes, this effect is usually at least the same order of magnitude as the gravitational lensing shear. Correcting for the PSF requires building a model for how it varies across the field. Stars in our own galaxy provide a direct measurement of the PSF, and these can be used to construct such a model, usually by interpolating between the points where stars appear on the image. This model can then be used to reconstruct the "true" ellipticities from the smeared ones. Ground-based and space-based data typically undergo distinct reduction procedures due to the differences in instruments and observing conditions.

2.2.2.2 Weak Lensing correlation functions

For weak lensing analyses, the key observables to be extracted from the LSST dataset are shear from galaxy shapes and source redshifts from photometric estimates. These must be derived for as many galaxies as possible, over as wide a range in redshift as possible. Subsequent analysis can be in terms of two- or three-point correlation functions, or shear profiles or mass maps depending on the specific project, but nearly all lensing analyses rest on these two fundamental quantities.

Because large-scale cosmological structures do not have a well-defined location, detecting cosmological gravitational lensing typically involves the computation of shear correlation functions, which measure the mean of the product of the shear at two points as a function of the distance between those points. The shear is a complex variable; its two components are usually combined into two distinct correlation functions.

For current and future surveys, one goal is to use the photometric redshifts of the background galaxies to divide the survey into multiple redshift bins. The low-redshift bins will only be lensed by structures very near to us, while the high-redshift bins will be lensed by structures over a wide range of redshift. This technique, dubbed "cosmic shear tomography", makes it possible to map out the 3D distribution of mass. Because the third dimension involves cosmic time (the light from galaxies further away comes to us from earlier cosmic times), tomographic weak lensing is sensitive not only to the matter power spectrum today, but also to its evolution over the history of the universe, and the expansion history of the universe during that time.

It is important to understand the statistical precision of cosmic shear observables and error propagation in the determination of cosmological parameters. Since cosmic shear probes the projected mass distribution, the statistical properties of the cosmic shear field reflect those of the mass distribution. For the case of the cosmic shear power spectrum, its statistical precision is determined by the covariance that contains three kinds of contributions: the shot noise contamination due to intrinsic ellipticities, and the Gaussian and non-Gaussian sample variances caused by the imperfect sampling of the fluctuations (Scoccimarro et al. 1999; Cooray & Hu 2001; Takada & Jain 2009). A measure of the statistical reach of LSST can be gleaned from Figure A.1 of Clowe et al. (2006b), which shows the shear noise level in 45-minute and 2-hour exposures taken with the 8.2-m VLT in various seeing conditions. These data show that shear noise of 0.05 per square arcminute is easily achievable if the delivered image quality is better than 0.7 arcsec FWHM. This matches the LSST observing plan, which is to take data in r and i (the most sensitive bands and the ones to be used for lensing) when the seeing is better than 0.7 arcsec. For rms = 0.28 per component, this implies Neff = 31 galaxies per square arcmin.

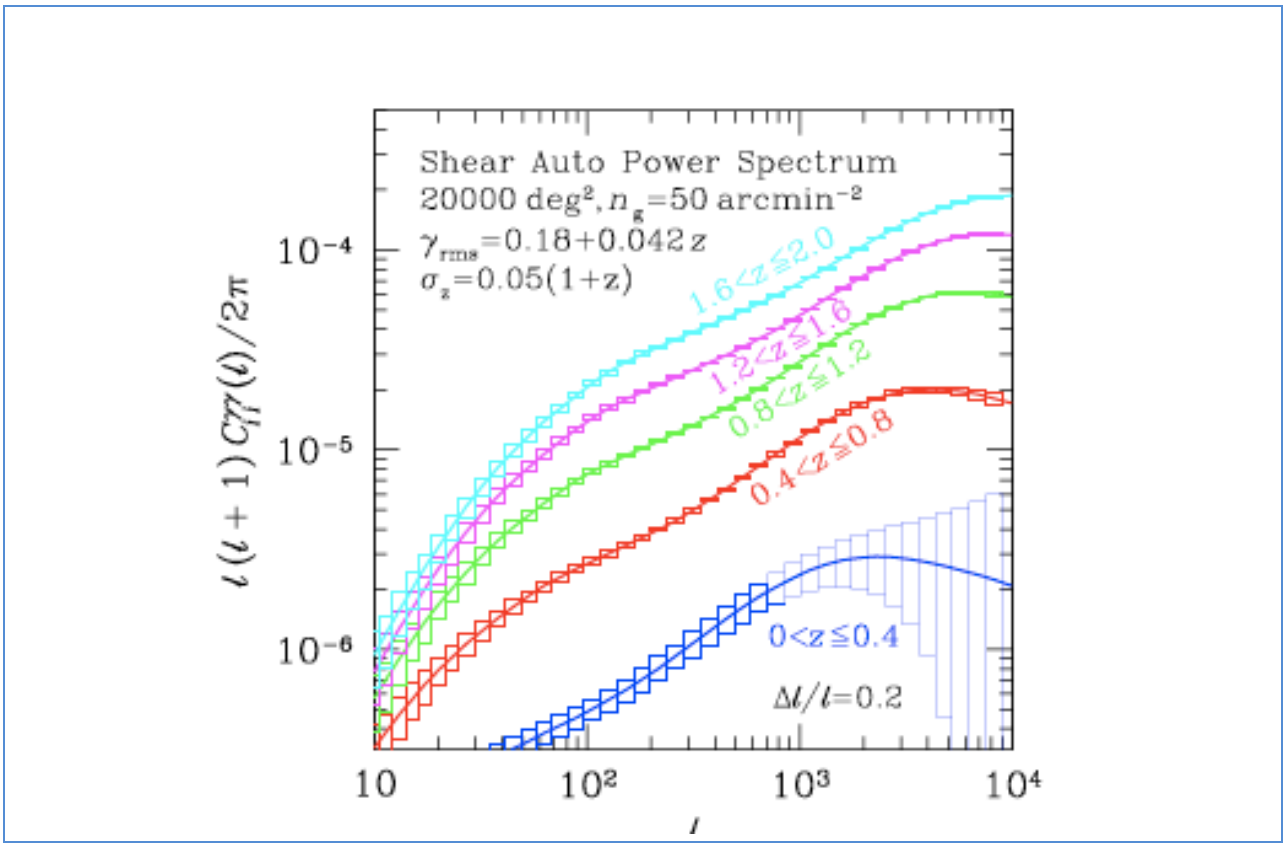

Figure 2-2: The lensing shear auto power spectra constructed from 5 redshift bins (l is the multipole moment of the distribution on the sky). Only the 5 auto-power spectra of each redshift bin among the available 15 cospectra are displayed, and the solid curves show the predictions for the concordance ΕCDM model. The boxes show the expected 1-3/4 measurement error (¢l=l = 0:2) from the full LSST 10-year survey due to the sample (i.e., cosmic) variance which dominates at about l < 1000, and intrinsic ellipticities which dominate at l > 1000 (Zhan 2006).

2.2.2.3 Reducing Systematics

A key issue for this investigation will be the reliability of the photometric redshift estimates. In weak lensing, however, the accuracy and precision of the photometric redshifts (i.e., the mean and standard deviation of the difference between photo-z's and the true redshifts) matter less than how well we know the accuracy and precision. Because the weak lensing kernel is broad in redshift, wide photometric redshift bins may be used. In practical terms, for any photometric redshift (z_p) bin, the most important challenge is in characterizing the true redshift distribution rather than in making that distribution narrow. The science analysis proceeds by integrating over the distribution and is biased only to the extent that the distribution is biased. In the simplified case of a Gaussian distribution, Huterer et al. (2006b) found that the bias and scatter should be known to about 0.003 in each redshift bin. Ma & Bernstein (2008) extended this to arbitrary distributions, which can be represented as a sum of Gaussians, but this more sophisticated analysis did not qualitatively change the result. Huterer et al. (2006b) also investigated the effect of z_p systematics on combined two-point and three-point constraints, and found that requirements are much reduced: with only a 20-30% dark energy constraint degradation, z_p errors could be self-calibrated from the data. However, this assumed a very simple z_p error model, and so may be overly optimistic. It is traditional to measure the z_p bias and scatter by

obtaining spectroscopic redshifts of a subset of galaxies. If this method were employed, the spectroscopic sample requirement is simply to amass a large enough sample to beat down the noise in each bin to less than 0.003(1+z). In this context, Ma & Bernstein (2008) estimate that 10^5 to 10^6 spectroscopic redshifts might be required for LSST, presuming that statistically complete sets of redshifts may be obtained via spectroscopy; however, deep redshift surveys to date have failed to yield secure redshifts of 30-50% of targets, making this path to calibration uncertain. A novel cross-correlation calibration technique described by Newman (2008; see Figure 2-3), has been shown to provide accurate calibrations even with incomplete spectroscopy of only bright objects, however. A more detailed investigation of photometric redshift calibration needs may be found in Newman et al. 2014.

The second major area of concern involves the presence of systematic uncertainties in the galaxy shape determination. There are many contributions to the PSF, including atmospheric turbulence, optical aberrations, perturbations to the alignment of the optics, charge diffusion in the detector, etc. The scale of the residual shear errors that these contributions introduce should be set by the statistical error floors on the co-added data. The level of statistical errors is very roughly equivalent to an rms residual ellipticity of about 0.001, over the range of angular scales relevant for LSST WL science. The residual shear power systematics at all angular scales (after PSF corrections) must be less than 30% of the statistical shear power, including correlations between angle bins.

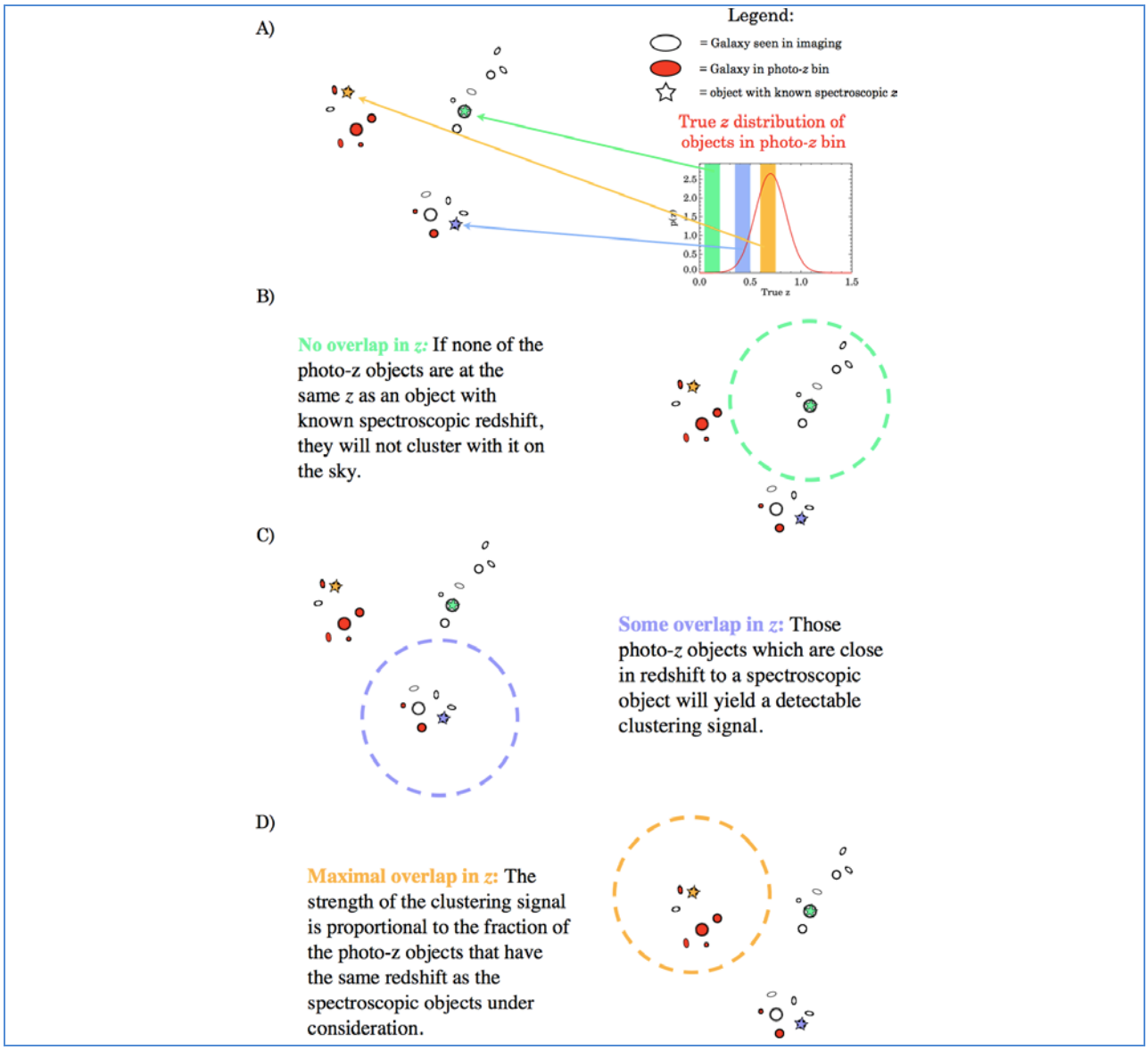

Figure 2-3: Cartoon depiction of cross-correlation photometric redshift calibration (Newman 2008). Panel A) shows the basic situation: we have imaging for many galaxies (circles/ellipses), some of which fall in a photometric redshift bin of interest (red). Galaxies that are near each other in three dimensions cluster together on the sky. We also know the spectroscopic redshifts of a smaller sample of objects (stars). The true redshift distribution for the objects in the photometric redshift bin is here assumed to be a Gaussian with mean 0.7 (plot); the stars are color-coded according to the redshift range the galaxy in question was determined to lie in with the color-coded ranges shown on the plot. B) For spectroscopic redshift objects that do not overlap in z with the photometric redshift objects, there will be no excess of neighbors that lie in the photometric redshift sample. C) If there is some overlap with the true redshift range of the photometric redshift sample, there will be some excess of neighbors around the spectroscopic object that lie in the photometric redshift bin. D) The strength of this clustering signal will be stronger the greater the fraction of the photometric redshift sample lies at the same z as the spectroscopic object in question. Because of this, we can reconstruct the true redshift distribution of the photometric redshift sample by measuring its clustering with objects of known redshift as a function of the spectroscopic z.

2.2.3 Type Ia Supernovae

Type Ia supernovae provided some of the first compelling evidence that the expansion of the universe is accelerating, thereby giving rise to the concept of dark energy, through the dependence of their apparent brightnesses on their actual distance from us. LSST will be a powerful SN factory. Operating in a standard mode of repeated scans of the sky with images taken every few days and with exposures of 30 seconds, LSST will discover on the order of 10^5 Type Ia supernovae annually. The redshifts at which Type Ia supernovae may be detected will be determined primarily by the single-band imaging depth; for the depths listed in Table 2-1, the mean redshift will be z ~0.45 with a maximum redshift of ~ 0.7. Such a sample, when combined with priors from other experiments, can constrain the lowest eigenmode of *w* (i.e. the mean value) in the nearby universe to 1% (limited by systematics). Given their dense sampling on the sky, SNe Ia can also be used to search for any dependence of *w* on direction, which would be an indicator of new physics. Some supernovae will be located in the same direction as foreground galaxy clusters; a measurement of the lensing magnification of the supernova will make it possible to model the cluster mass distribution. Longer exposures (10-20 minutes/band) or denser time sampling in the LSST deep drilling fields should extend the discovery of supernovae to a mean redshift of 0.7 with some objects beyond z ~1. The added statistical leverage on the "pre-acceleration" era will narrow the confidence interval on both *w* and its derivative with redshift.

Spectroscopic follow-up for so many supernovae will be impossible. Exploitation of the data from the LSST will require light-curves that are well-sampled both in brightness and color as a function of time; the fraction of LSST supernovae for which sufficient sampling is obtained will depend on the chosen cadence and dithering strategy. Good-quality light curves are essential both to the search for systematic differences in supernova populations (which may masquerade as cosmological effects) as well as for determining photometric redshifts from the supernovae themselves. Good image quality is required to separate supernovae photometrically from their host galaxies. Observations in at least five photometric bands will be necessary to ensure that, for any given supernova, light-curves in four restframe bands will be obtained. Absolute band-to-band photometric calibration to 1% is adequate, but the importance of K-corrections to supernova cosmology implies that the calibration of the relative offsets in zero points between filters remains a serious issue, as is stability of the response functions, especially near the edges of bandpasses where the strong emission and absorption features from supernovae makes this more of a problem than for stellar spectra.

2.2.4 Baryon Acoustic Oscillations

Acoustic waves propagated in the tightly coupled photon-plasma fluid prior to the recombination of protons and electrons to form hydrogen atoms, in the first few hundred thousand years after the Big Bang; these waves give the Baryon Acoustic Oscillation method of constraining dark energy its name. The distance these waves could travel before recombination creates a characteristic scale: the sound horizon (R_s) in the matter distribution. After recombination, an imprint of this scale remains in the matter and subsequently in the galaxy distributions as an excess of objects separated by a distance R_s (in comoving coordinates). The same acoustic waves give rise to the peaks seen in the CMB temperature fluctuation spectrum, allowing the angular scale of R_s at decoupling to be accurately determined (corresponding to a comoving scale of ~150 Mpc today). Since the BAO are associated with a single

well-defined co-moving distance at all redshifts, they can be used to provide a "standard ruler" for determining the angular diameter distance as a function of redshift relative to the distance to the CMB surface of last scattering, and thereby constrain the cosmic expansion.

There are several advantages of a large photometric redshift survey over existing work with small samples (Eisenstein et al. 2005; Cole et al. 2005; Padmanabhan et al. 2006; Blake et al. 2006): wide coverage (which reduces the sample variance error) and deep photometry (which leads to larger volume, more galaxies, and lower shot noise) with small errors (which significantly improve photometric redshift estimates). Simulations indicate that, with 3 billion galaxy photometric redshifts from LSST, the BAO peaks will be cleanly detected for redshifts ranging from z ~ 0.3–2.7. The corresponding angular diameter distance will be measured to ~ 0.4% accuracy, especially at higher redshift (Zhan, Knox, and Tyson 2009). The requirement for large sample sizes imposed by BAO and WL research is a major driver of the LSST design.

In Figure 2-4, we show the constraints on the dark energy equation of state parameters from the various diagnostics described above, as well as from counts of galaxy clusters (whose abundance is sensitive to the rate of growth of dark matter density fluctuations) both separately and in combination.

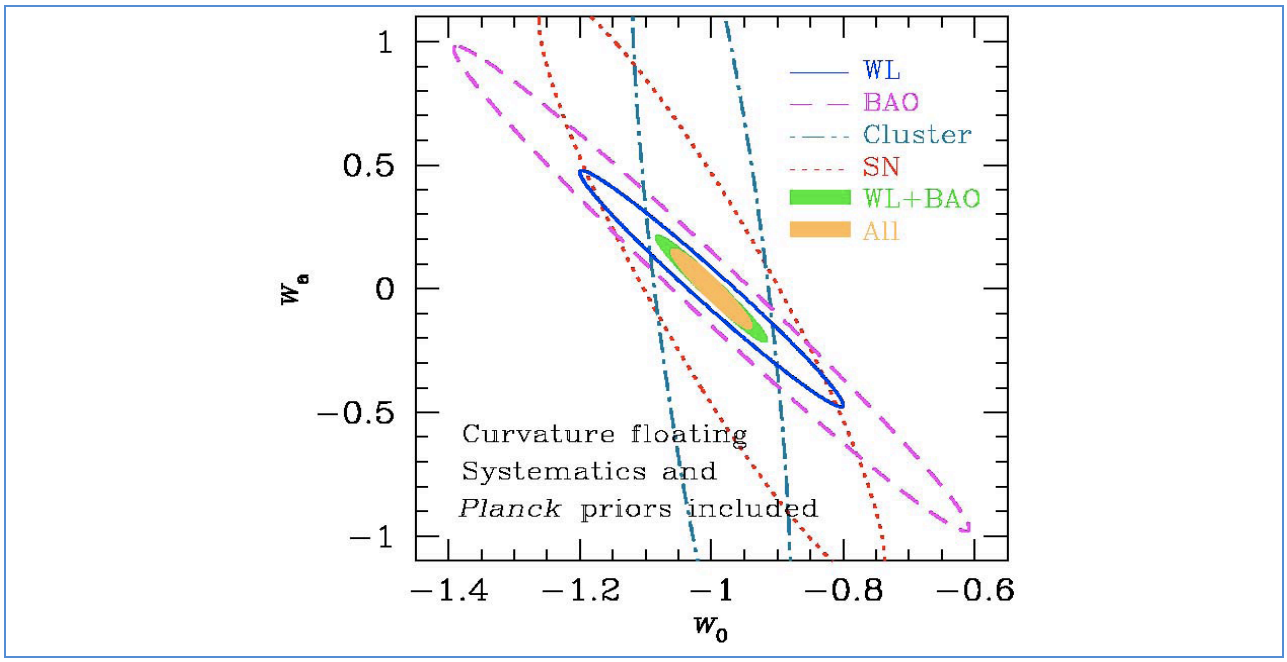

Figure 2-4: Joint w_0–w_a constraints from LSST BAO (dashed line), cluster counting (dash-dotted line), supernovae (dotted line), WL (solid line), joint BAO and WL (green shaded area), and all combined (yellow shaded area). For the purpose of this figure, dark energy has been modeled as a homogeneous and isotropic fluid with the equation of state given by $w(a) = w_0 + w_a(1-a)$, where w_0 is the dark energy density today and w_a is a function of cosmic time or scale factor a. The BAO and WL results are based on galaxy–galaxy, galaxy–shear, and shear–shear power spectra only. Adding other probes such as strong lensing time delay, ISW effect, and higher-order galaxy and shear statistics could further improve the constraints. (See the LSST Science Book for a discussion of these additional techniques.)

2.3 Taking an Inventory of the Solar System

LSST will provide data for millions of small bodies in our Solar System. Previous studies of these objects have led to dramatic changes in our understanding of the process of planet formation and evolution, and the relationship between our Solar System and other systems. These small bodies also serve as large populations of "test particles", recording the dynamical history of the giant planets, revealing the nature of the Solar System impactor population over time, and illustrating the size distributions of planetesimals, which were the building blocks of planets.

The Earth orbits within a swarm of asteroids; some small number of these objects will ultimately strike the Earth's surface. The U.S. Congress mandated that by the year 2008, 90% of the near-Earth asteroids (NEAs) with diameters greater than 1 km be discovered and their orbits determined. Impacts of NEAs of this size have the potential to change the Earth's climate and cause mass extinctions, such as the one credited with killing the dinosaurs. A NASA report published in 2003 estimates conservatively that with then current search techniques, about 70% of the NEAs with diameters larger than 1 km would have been cataloged by 2008. This same report quantifies the risk of impacts by smaller bodies, which have the potential of causing significant ground damage, and recommends reduction of the residual hazard by another order of magnitude as a reasonable next goal. Achieving this goal would require discovery of about 90% of the potentially hazardous asteroids (PHAs) down to diameters of about 140 m. While it is unlikely that any other currently planned facility could achieve this goal within a decade or two, modeling suggests that the LSST is capable of finding 84% of the PHAs with diameters larger than 140 m within ten years.

The search for PHAs puts strong constraints on the cadence of observations, requiring closely spaced pairs of observations two or preferably three times per lunation in order to link observations unambiguously and derive orbits. Individual exposures should be shorter than about 1 minute each to minimize the effects of trailing for the majority of moving objects. Because of the faintness and the large number of PHAs and other asteroids that will be detected, LSST must provide the follow-up required to derive orbits rather than relying, as current surveys do, on separate telescopes. The observations should be obtained within ± 15 degrees of the Ecliptic. The images should be well sampled to enable accurate astrometry, with absolute accuracy not worse than 0.1 arcsec for sources detected with the signal-to-noise ratio SNR > 10. There are no special requirements on filters, although bands such as V and R that offer the greatest sensitivity are preferable. The images should reach a depth of at least 24.5 (5σ for point sources) in the r band in order to probe the ~ 0.1 km size range at main-belt distances. Based on recent photometric measurements of asteroids by the Sloan Digital Sky Survey, the photometry should be better than 1-2% to allow for color-based taxonomic classification.

The LSST can also make a major contribution to mapping Kuiper Belt Objects (KBOs). The orbits of KBOs provide a fossil record of the early history of the solar system; their eccentricities and inclinations contain clues to past perturbations by giant planets. The sizes of the KBOs hold clues to the accretion events that formed them and to their subsequent evolution through collisional grinding, etc. The compositions of KBOs are not identical and are correlated with their dynamical state; the reasons for these differences are not known. Light curves can be used to constrain the angular momentum distribution and internal strengths of the bodies. A more complete sample of KBOs and determination of

their properties can assist with selecting targets for future NASA missions. The survey for PHAs can simultaneously provide the joint color-magnitude-orbital distribution for all bright ($r < 24$) KBOs. The 100 or so observations obtained for each bright KBO can be searched for brightness variations, but modeling will be required to determine how well periods can be extracted from observations made at random times. At the very least, it will be possible to determine amplitudes for many thousands of KBOs, and periods can likely be derived for many of them. Long exposures would be required to push the detection of KBOs to smaller sizes and reach the erosion-dominated regime in order to study the collisional history of various types of KBOs. KBO science would be greatly amplified if a small fraction of the observing time were devoted to hour-long observations in the ecliptic. This same mode of observation may have applications to the study of variable and transient objects. Apart from exposure time limits, the requirements for the KBO science are similar to the requirements for the detection and orbital determination for other Solar System bodies.

2.4 Exploring the Transient Optical Sky

The LSST will open a new window on the variable sky. Recent surveys have shown the power of variability for studying gravitational lensing, searching for supernovae, determining the physical properties of gamma-ray burst sources, etc. The LSST, with its repeated, wide-area coverage to deep limiting magnitudes will enable the discovery and analysis of rare and exotic objects such as neutron star and black hole binaries; gamma-ray bursts and X-ray flashes, at least some of which apparently mark the deaths of massive stars; AGNs and blazars; and very possibly new classes of transients, such as binary mergers and stellar disruptions by black holes. It is likely that the LSST will detect numerous microlensing events in the Local Group and perhaps beyond. The LSST would provide alerts for concerted monitoring of these events, and open the possibility of discovering planets and obtaining spectra of lensed stars in distant galaxies as well as our own. LSST can also provide multi-wavelength monitoring over time of objects discovered by the Fermi Gamma-ray Space Telescope (formerly GLAST). With its large aperture, the LSST is well suited to conducting a Deep Supernova Search in selected areas. LSST will also provide a powerful new capability for monitoring periodic variables, such as RR Lyrae stars, which can be used to map the Galactic halo and intergalactic space to distances exceeding 400 kpc. Since LSST extends time-volume space a thousand times over current surveys, the most interesting science may well be the discovery of new classes of objects.

Exploiting the capabilities of LSST for time domain science requires large area coverage to enhance the probability of detecting rare events; time coverage, since light curves are necessary to distinguish certain types of variables and in some cases infer their properties (e.g. determining the intrinsic luminosity of supernovae Type Ia depends on measurements of their rate of decline); accurate color information to assist with the classification of variable objects; good image quality to enable differencing of images, especially in crowded fields; and rapid data reduction and classification in order to flag interesting objects for spectroscopic and other follow up with separate facilities. Time scales ranging from $\sim$ 1 min (to constrain the properties of fast faint transients such as those recently discovered by the Deep Lens Survey) to $\sim$ 10 years (to study long-period variables and quasars) should be probed over a significant fraction of the sky. It should be possible to measure colors of fast transients on timescales

of a few minutes, and to reach r ~ 24 in individual visits. Fast reporting of likely transients to the community is required in order to facilitate followup observations.

2.5 Mapping the Milky Way

The LSST is ideally suited to answering two basic questions about the Milky Way Galaxy: What is the structure and accretion history of the Milky Way? What are the fundamental properties of all the stars within 300 pc of the Sun?

Standard models posit that galaxies form from seeds planted by the Big Bang with accretion over time playing a significant role in determining their structure. Detailed study of the Milky Way can provide rigorous tests of these ideas, and the LSST will be able to map the 3-D shape and extent of the halo of our Galaxy. Specifically, the LSST will detect F turn-off stars to distances of 200 kpc; isolate stellar populations according to color; and determine halo kinematics through measurement of proper motions at distances exceeding 10 kpc. The LSST dataset can be used to identify streams of stars in the halo that are thought to provide a fossil record of discrete accretion events. The LSST in its standard surveying mode will be able to detect RR Lyrae variables and classical novae at a distance of 400 kpc and hence can explore the extent and structure of our own halo out to half the distance to the Andromeda Galaxy. The proper motions and photometric parallaxes for these stars can be used to characterize the properties of the dark matter halo in which the Milky Way is embedded. The LSST will survey a significant fraction of the Galactic plane, including the Galactic center, and will obtain unprecedented data for studies of star-forming regions.

Is our solar system with its family of planets unique? Or are there many more that contain Earth-like planets within the so-called habitable zone? How do solar systems form? Detailed exploration of our local neighborhood is key to answering these questions. The LSST will obtain better than 3σ parallax measurements of hydrogen-burning stars to a distance of 300 pc and of brown dwarfs to tens of parsecs. These measurements will provide basic information on candidate stars that merit further study in the search for companions, including planets. Residuals from the fits for position, proper motions, and parallax will be searched for the signature of Keplerian motion to identify stars and brown dwarfs with companions and provide fundamental estimates of the mass of the primaries. LSST data will be used to determine the initial mass functions for low-mass stars and sub-stellar mass objects and to test models of brown dwarf structure. The age of the Galactic disk can be inferred from white dwarf cooling curves.

Key requirements for mapping the Galaxy are large area coverage; excellent image quality to maximize the accuracy of the photometry and astrometry, especially in crowded fields; photometric precision of at least 1% to separate main sequence and giant stars; stringent astrometric accuracy to enable parallax and proper motion measurements; and dynamic range that allows measurement of astrometric standards at least as bright as r = 15. In order to probe the halo out to distances of 100 kpc using large numbers of main sequence stars, the total depth (5σ for unresolved sources) has to reach r ~ 27 (assuming 5% photometry in the r band at r = 25.5). To study the metallicity distribution of stars in the Sgr tidal stream and other halo substructures at distances out to at least ~ 40 kpc, the coadded depth in the u band has to deliver 5% photometry at u ~ 24.5. In order to constrain tangential velocity at a distance of 10 kpc to within 10 km/s with the most luminous main-sequence stars (low-metallicity blue

turn-off stars with $M_r = 5.5$), the proper motion accuracy has to be at least 0.2 mas/yr at r = 20.5 (1σ per coordinate). The same requirement follows from the decision to obtain the same proper motion accuracy as Gaia at its faint end (r ~ 20). The LSST will then represent an "extension" of Gaia astrometric measurements to 4 magnitudes greater depth. In order to produce a complete sample of the solar neighborhood stars out to a distance of 300 pc (the thin disk scale height), with 3σ or better geometric distances, parallax measurements accurate to 1 mas (1σ) are required for stars with $M_r = 15$. To obtain 3σ or better geometric distances for T9/Y0 brown dwarfs with z − y colors measured with 10σ or better precision (in coadded data), parallax measurements for sources detected only in y band visits at 10σ significance must have an accuracy of 6 mas (1σ).

In summary, LSST will enable studies of the distribution of numerous main-sequence stars beyond the presumed edge of the Galaxy's halo, of their metallicity distribution throughout most of the halo, and of their kinematics beyond the thick disk/halo boundary, and will obtain direct distance measurements below the hydrogen-burning limit for a representative thin-disk sample.

2.6 Summary of High Level Requirements

The four science themes place a variety of requirements on LSST, as detailed above. Somewhat surprisingly, these can all be met with a common survey, i.e. a single database that is amenable to a set of extremely diverse analyses. In Table 2-1, we summary these requirements at a high level. Further detail can be found in the LSST Science Requirements Document, which is available at http://www.lsst.org/lsst/science/survey_requirements.

Table 2-1: LSST survey requirements

Survey Property	Performance
Main Survey Area	18000 degrees^2
Total visits per unit area	825
Filter set	6 filters (ugrizy) from 320-1050 nm
Single visit	2x15 second exposures
Single visit limiting magnitude	u = 23.5; g = 24.8; r = 24.4; l = 23.9; z = 23.3; y = 22.1
Photometric calibration	< 1% repeatability, absolute, & colors
Median delivered image quality	~0.7 arcsec. FWHM
Transient processing latency	< 60 sec after last visit exposure
Data release	Full reprocessing of survey data annually

2.7 References

Bartelmann, M. and P. Schneider (2001). "Weak gravitational lensing." Physics Reports-Review Section of Physics Letters **340**(4-5): 291-472.

Blake, C., D. Parkinson, et al. (2006). "Universal fitting formulae for baryon oscillation surveys." Monthly Notices of the Royal Astronomical Society **365**(1): 255-264.

Clowe, D., P. Schneider, et al. (2006). "Weak lensing mass reconstructions of the ESO Distant Cluster Survey." Astronomy & Astrophysics **451**(2): 395-U322.

Cole, S., W. J. Percival, et al. (2005). "The 2dF Galaxy Redshift Survey: power-spectrum analysis of the final data set and cosmological implications." Monthly Notices of the Royal Astronomical Society **362**(2): 505-534.

Cooray, A. and W. Hu (2001). "Power spectrum covariance of weak gravitational lensing." Astrophysical Journal **554**(1): 56-66.

Eisenstein, D. J., I. Zehavi, et al. (2005). "Detection of the baryon acoustic peak in the large-scale correlation function of SDSS luminous red galaxies." Astrophysical Journal **633**(2): 560-574.

Halverson, N. W., T. Lanting, et al. (2009). "Sunyaev-Zel'dovich Effect Observations of the Bullet Cluster (1e 0657-56) with Apex-Sz." Astrophysical Journal **701**(1): 42-51.

Hu, W. and M. Tegmark (1999). "Weak lensing: Prospects for measuring cosmological parameters." Astrophysical Journal **514**(2): L65-L68.

Huterer, D., M. Takada, et al. (2006). "Systematic errors in future weak-lensing surveys: requirements and prospects for self-calibration." Monthly Notices of the Royal Astronomical Society **366**(1): 101-114.

Lidz, A., O. Zahn, et al. (2009). "Probing Reionization with the 21 Cm Galaxy Cross-Power Spectrum." Astrophysical Journal **690**(1): 252-266.

Ma, Z. M. and G. Bernstein (2008). "Size of spectroscopic calibration samples for cosmic shear photometric redshifts." Astrophysical Journal **682**(1): 39-48.

Newman, J. A. (2008). "Calibrating redshift distributions beyond spectroscopic limits with cross-correlations." Astrophysical Journal **684**(1): 88-101.

Newman, J. A. et al. (2014). "Spectroscopic Needs for Imaging Dark Energy Experiments." Astroparticle Physics, in press.

Nord, M., K. Basu, et al. (2009). "Multi-frequency imaging of the galaxy cluster Abell 2163 using the Sunyaev-Zel'dovich effect." Astronomy & Astrophysics **506**(2): 623-636.

Reichardt, C. L., O. Zahn, et al. (2009). "CONSTRAINTS ON THE HIGH-l POWER SPECTRUM OF MILLIMETER-WAVE ANISOTROPIES FROM APEX-SZ." Astrophysical Journal **701**(2): 1958-1964.

Scoccimarro, R., M. Zaldarriaga, et al. (1999). "Power spectrum correlations induced by nonlinear clustering." Astrophysical Journal **527**(1): 1-15.

Staniszewski, Z., P. A. R. Ade, et al. (2009). "Galaxy Clusters Discovered with a Sunyaev-Zel'dovich Effect Survey." Astrophysical Journal **701**(1): 32-41.

Takada, M. and B. Jain (2009). "The impact of non-Gaussian errors on weak lensing surveys." Monthly Notices of the Royal Astronomical Society **395**(4): 2065-2086.

Wittman, D. M., J. A. Tyson, et al. (2000). "Detection of weak gravitational lensing distortions of distant galaxies by cosmic dark matter at large scales." Nature **405**(6783): 143-148.

Zahn, O. and M. Zaldarriaga (2006). "Lensing reconstruction using redshifted 21 centimeter fluctuations." Astrophysical Journal **653**(2): 922-935.

3: Requirements Flow Down and Methodology

3 Requirements Flow Down and Methodology

Large, complex engineering projects require a formal systems engineering process to define, manage, control, and document the technical scope of the work. The design and performance characteristics of the LSST Observatory flow directly from the science programs described in Chapter 2. This chapter first summarizes the key science requirements that most impact the overall system design followed by the systems engineering approach used to flow down the requirements to the design. In addition, the error budgets and interfaces that define the system performance and design are summarized.

3.1 System Requirements Flow-Down and Traceability

The LSST Project has developed a requirements flow down hierarchy (Figure 3-1) with the LSST Science Requirements Document (SRD) at the top. Each box in the figure represents a specific part within the requirements view of the System Architecture Model that cleanly maps into one or more documents for review and control.

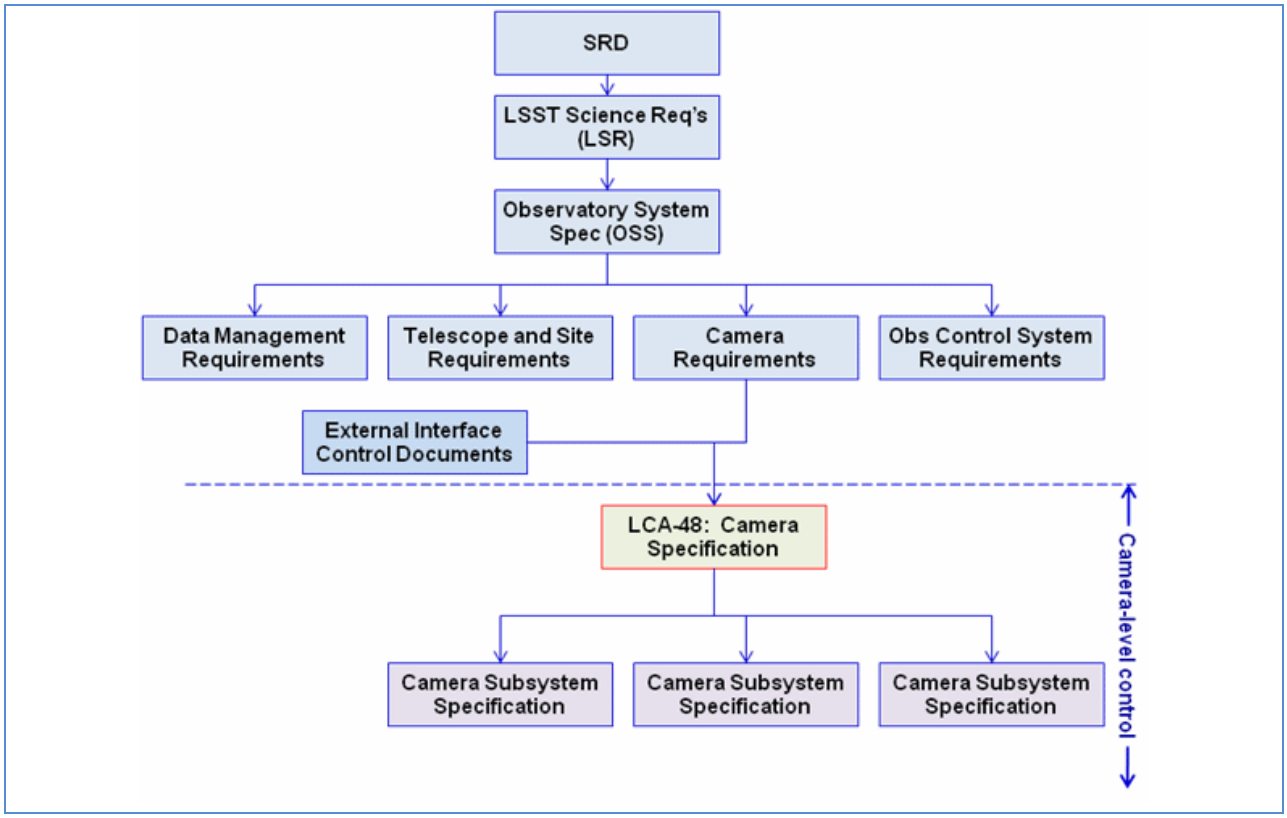

Figure 3-1: LSST requirements flow-down hierarchy, showing flow-down from SRD to Camera subsystem specifications

Within the flow-down hierarchy, additional top-level functional requirements have been derived that provide a high level description of what the LSST is and must do. These in turn have been used to derive the Observatory System Specifications as refined by Operational Use Cases and Definitions, which are satisfied by the overall system architecture. These three parts of the System Architecture Model provide the highest level description of how the LSST will meet its functional and performance requirements and serve as the foundation from which all subsystems derive their requirements.

3.1.1 Science Requirements Document (SRD)

The primary science-derived requirements are specified in the SRD. This document is controlled at the project level and has been approved by the LSSTC Board of Directors. The SRD also enumerates the acceptable bounds for the performance of the LSST survey by providing minimum, design, and stretch goal values for each of the key survey performance parameters. The Project has used the design value in flowing down requirements. The stretch goal is meant to keep some pressure on the engineering efforts without having an adverse impact on the budget and schedule. The minimum value is used to ensure that the science goals of the project are protected. In the event that it is shown that any of the minimum performance specifications cannot be met, a project level internal review is triggered to determine a course of action. To date, it has not been necessary to alter any of the minimum performance values defined in the SRD.

3.1.2 LSST System Requirements Document (LSR)

The LSST System Requirements document (LSR) contains requirements that specify the design point for the LSST survey performance parameters, high-level functional requirements, and overall system configuration parameters. The survey design point in the LSR satisfies the survey performance specifications in the SRD but, where the SRD specifies an allowed range of performance, the LSR specifies a single value within this range as the design point. In nearly all cases, the SRD design value has been adopted as the design point in the LSR.

The LSR establishes the top-level technical definition of the LSST. The LSR also includes the high-level functional requirements needed for conducting the survey and distributing survey data products to the community.

3.1.3 Observatory System Specifications Document (OSS)

The requirements and specifications in the Observatory System Specifications document (OSS) provide the bridge between the SRD and LSR and the detailed requirements for each subsystem. The OSS enumerates functional and performance requirements and quantitative specifications or constraints. Within the OSS these requirements have been organized into 8 topics:

1. The site-specific composition and constraints, including the Summit Facility on Cerro Pachon; the Base Facility in La Serena, Chile; the Archive Site at NCSA; and, a Headquarters Facility located in Tucson, Arizona

2. Common system functions that define survey scheduling, system control, monitoring and diagnostics, maintenance, availability, and system standards

3. Science and bulk data products, performance, and sizing

4. The optical system design specifications, alignment and compensation, stray and scattered light, and image quality

5. Optical throughput efficiency, including the filter definitions, and the 10-year integrated throughput

6. Camera specific system functions and performance specifications

7. Photometric calibration specifications for data products, processing, and performance

8. System-wide timing and dynamic requirements

3.2 Camera Requirements and Budgets

3.2.1 The Camera Requirements and Camera Specification Documents

The Camera requirements flow down from the SRD, with the OSS being the Camera's direct predecessor. Camera Systems Engineering, like the other LSST SE teams, follows current practices to establish that Camera requirements are correctly derived (validatable), define who is responsible for meeting a requirement (separable), and determine how and when a requirement is verified to be met (verifiable).

The Camera's key driving requirements are summarized in Chapter 5.

All observatory-level performance requirements flow down or are allocated out to requirements that show up in the Camera Specification. Camera subsystem requirements are primarily derived from those in the Camera Specification or in external interface agreements and requirements. While the great majority of Camera requirements flow down via the SRD-LSR-OSS hierarchy, certain reliability, integration and test, environmental, and contamination controls requirements are imposed by Camera subsystem constraints and process plans, as illustrated in Figure 3-2.

Quantitative analyses of requirements and expected Camera performance are conducted using simulations and engineering analysis tools. In addition, the Camera project maintains associated error budgets and allocation tables to quantify performance at all system levels. Bottom-up error budgets and performance analyses confirm (i.e., validate) that performance requirements are met by the design.

The remainder of this section lists the Camera requirements categories and their flow-down to Camera subsystems, and discusses Camera allocations and budgets.

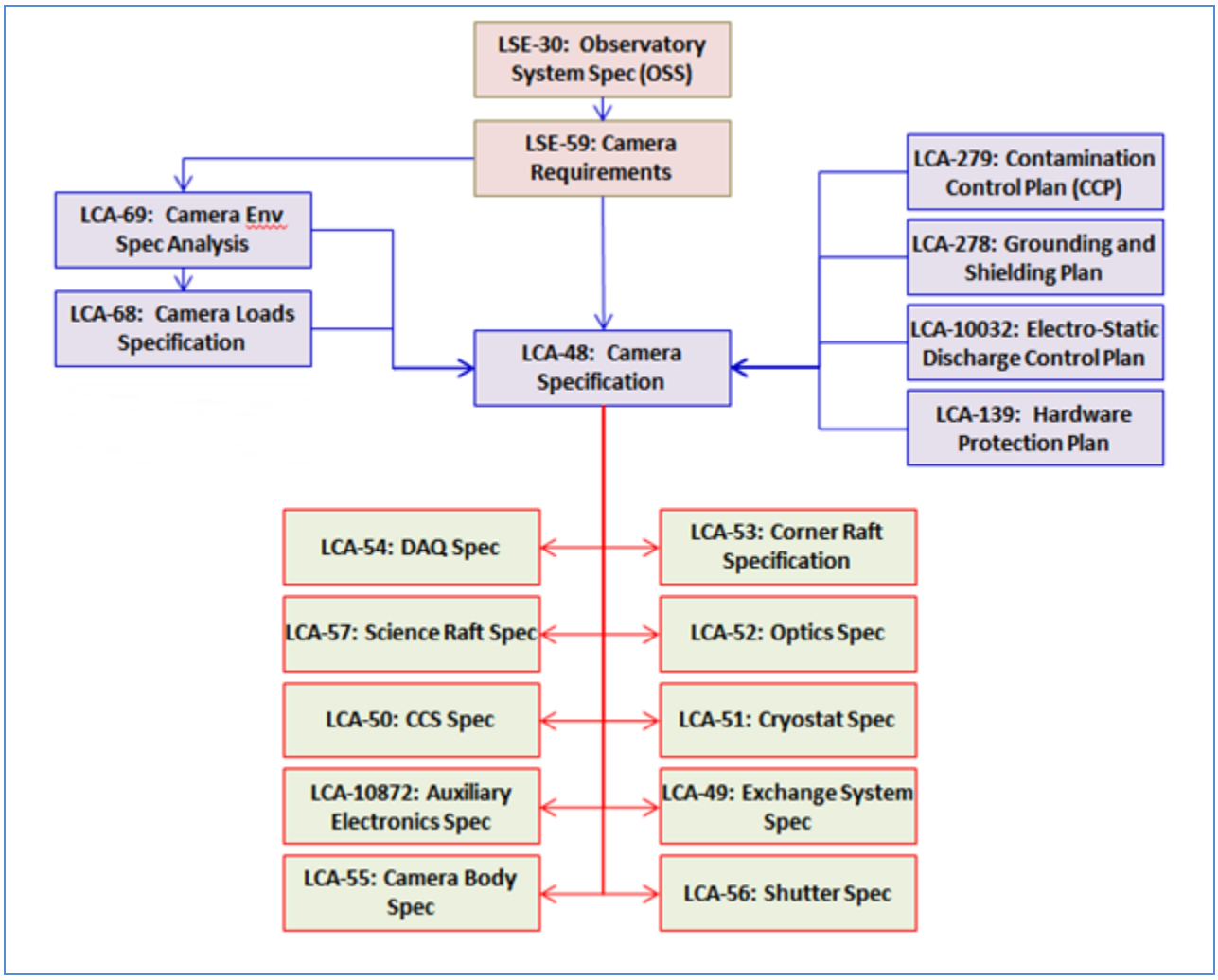

Figure 3-2: Camera and Camera subsystem specification tree, showing sources of requirements outside the flow-down from the SRD

3.2.2 Image Quality

The Camera design must minimize distortions to the image point spread function. Per the formal requirements, the maximum delivered image quality error for the Camera shall be less than 0.30 arc-seconds FWHM. This is the total image quality error allocation to the Camera, from all sources: optics (glass homogeneity and optical figure); the optical assembly (tip, tilt and decenter); distortions imposed by gravity and by thermal, pressure, and vibration effects; and, the detector plane assembly (charge diffusion, flatness). These terms are detailed in the Camera Image Quality Budget (LSST Camera Document LCA-17).

Flowdown of image quality is a combination of analysis at the Camera level to address contributors that cross subsystem boundaries and direct requirements on the optics, science raft, Camera body, filter exchange system and cryostat for positioning and adjustability. Additionally, the Optics subsystem has requirements covering manufacturing tolerances (glass homogeneity and optical figure) and the science raft has requirements covering charge diffusion and sensor flatness.

3.2.3 Throughput

Throughput is defined as efficiency in capturing photons. The requirements are separated into optical throughput and effective area.

Optical throughput requirements address losses as light travels through the Camera and the ability of the CCD to utilize that light. The bottom- up budget (LSST Camera Document LCA-18) for optical throughput defines losses due to contamination (dust and condensation; flows down broadly to a Camera contamination control plan), optics (glass clarity, anti-reflective coatings, filter throughput; these flow down to the Optics subsystem), and sensor quantum efficiency (flows down to the science rafts).

Effective area throughput requirements pertain to the active sensors on the detector plane. The total diameter covered is 634.17 mm, which is equivalent to the diameter of a 3.5 degree circle on the sky. With the total area covered, fill factor must be > 90%. Within the 3.5 degree circle that is active, fill factor must be > 85%. These requirements flow down to the science rafts (which define the efficiency of CCD placement) and cryostat (which defines the spacing between rafts).

3.2.4 Noise

Per the requirement, the electronic noise from the Camera shall contribute no more than 9 electrons per image to each pixel in the data from the science sensor array. This top-level noise budget includes all sources internal to the Camera system that contribute to the base noise in each pixel, including readout noise, residual noise from dark current, additional noise in the electronics, etc.

A bottom-up budget has been generated (LSST Camera Document LCA-32) and is consistent with the allocation.

Noise requirements flow down to the science raft, the designs for which must control contributions from dark current, sensor output amplifiers, and other electronics noise.

3.2.5 Photometric

Photometric requirements specify the characteristics of the Camera needed to support observatory calibration. The characteristics are exposure duration knowledge, filter positioning, gain stability and detector plane temperature knowledge. The gain stability requirement flows to the science raft, with temperature stability support from the cryostat. A science raft level budget (LSST Camera Document LCA-10065) covers gain stability. The detector plane temperature knowledge flows largely to the science raft augmented by system level analysis to account for IR loading. The exposure duration knowledge flows to the shutter. A portion of the filter position repeatability requirement flows to the Filter Exchange subsystem, with the remainder held at the Camera level to account for the motion of the filter relative to the detector plane due to gravity and thermal. This is detailed in a budget in LSST Camera Document LCA-152.

3.2.6 Mass Properties

The mass properties are defined in interface documents with the telescope. The mass, center of gravity and moments of inertia must stay within bounds so that the telescope can meet slew rates and pointing

stability requirements. Additionally there are limits on the added mass during on-telescope servicing operations.

The Camera mass budget is in LSST Document LCA-119. Mass budgets and allocations have been stable for some time. Mass and center of gravity allocations flow down to all subsystems. The Camera inertias are analyzed at the Camera level. Mass is carefully tracked, since margin stands at ~4.5%.

3.2.7 Filter Characteristics

Filter requirements are specified in terms of transmission as a function of frequency (LSST Camera Document LCA-10210). The bandpass is defined as an envelope covering the in-band region and the transitions to the out-of-band region. In those transitions, a relaxed envelope is provided to address the realities of bandpass filter manufacturability. Out-of-band specifications include integrated out-of-band and a requirement on localized (10nm, in wavelength space) regions. Ripple is defined, as well as variations on the bandpass location for positions across the filter. These requirements are intended to control the shape of the filter only; the average transmission requirement is covered by the throughput specification. These requirements flow to the optics.

3.2.8 Optics Prescription

This lengthy set of specifications defines the lens and filter powers and positions relative to the focal plane.

Tolerances for the prescription are constrained by the image quality budget. An iterative approach, allowing precompensation for temperature and pressure, has been used to achieve the desired optical properties.

The requirements provide for a one-time optics spacing and position adjustment prior to the final Camera build.

Flow down is to the optics (governing lens and filter shapes, as well as positioning); Camera body (optics positioning); Filter Exchange subsystem (filter positioning); and the cryostat (positioning).

3.2.9 Stray and Scattered Light

These requirements address the problem of light reaching the detector plane from an unintended source or following an unintended path. They include:

- The prescribed use of surface coatings and baffling. The LSST Project Systems Engineering group uses FRED model to assess observatory performance and provide feedback on the design choices (flow down to Camera body, cryostat, and shutter)
- A derived shutter light tight requirement, which primarily controls impact of leakage during CCD readout (flow down to shutter)
- Definition of the allowed level of specular reflection off each lens surface to minimize ghost images (artifacts caused by multiple reflections off the optics). Throughput budget includes anti-reflective coatings, with budget performance exceeding this spec

3.2.10 Guiding

The Camera is the sole provider of sensor data to a telescope guide loop used to fine tune telescope pointing. The Camera provides data from a small region repeatedly during an image (nominally 50 by 50 pixels at 9Hz). The telescope computes star positions and uses changes in detected star position to estimate and correct pointing deviations. The Telescope team supplies the detailed requirements in the Camera to Telescope ICD (Interface Control Document) (LSST Document LSE-66).

The guiding requirements flow down to the corner raft (for sensor characteristics and readout capabilities), the DAQ subsystem (for data processing) and the CCS (Camera Control System, for corner raft control).

3.2.11 Wavefront Sensing

The Camera is the sole provider of wavefront sensor data to the telescope.

The Telescope team supplies the detailed sensor requirements in the Camera to Telescope ICD (LSST Document LSE-66). Data delivery requirements are specified in the OSS. These requirements include sensor performance, positioning of the sensor relative to the science detector plane, and data delivery requirements (including crosstalk correction).

The wavefront sensing requirements flow down to the corner rafts (sensor specifications), DAQ (data processing, including crosstalk correction), as well as the cryostat and Camera body (for alignment of wavefront sensors to the detector plane).

3.2.12 Crosstalk

The crosstalk requirements define the crosstalk allowed with a raft, the allowed raft-to-raft crosstalk, the number of channels allowed to contribute to raft-to-raft crosstalk and the crosstalk stability. The crosstalk within a raft and crosstalk stability flow down is to the science raft. The raft-to-raft requirements are held at the Camera level.

3.2.13 General Operations

Requirements on high-level Camera operations have been specified.

Commands from OCS (Observatory Control System) include taking images, changing filters and changing configuration. Power -up initialization allows 60 seconds to get to a default condition and be ready to communicate with the OCS (but does not require the ability to take pictures immediately). Engineering mode camera control requires that the CCS control and monitor Camera subsystems when in engineering mode; this mode includes Camera subsystems operating in standalone mode, such as the filter loader.

With respect to Camera telemetry, Camera meta-data availability refers to the protocol used to transfer the telemetry and summarizes the expected content of the telemetry. Camera state notification requires that the Camera report any changes in “major internal state”; those state definitions will be worked out in the Camera behavior/sequence diagram effort. Filter in use status is a derived requirement that the Camera positively identify the filter that is in use. Requirements related to

telemetry analysis require delivery of telemetry analysis tools, which will be developed using an observatory-provided toolbox.

The Observatory Operations team will use this analysis to monitor the camera and will likely refine the tools based on experience

These requirements flow down primarily to CCS for control of Camera behavior and the requirement to report state changes. Derived requirements will flow to most subsystems as determined by the Camera behavior and sequence diagram effort. All systems (except optics) must define health and safety and status telemetry, with the specific list to be generated during the preliminary design phase. Telemetry analysis will follow from Camera integration and test efforts.

3.2.14 Exposure Control

The exposure control requirements address the duration of a standard visit and define boundaries for non-standard visits.

A standard visit is defined as two 15 second exposures. A total of 34 seconds is allocated, starting when the command is received from the OCS and ends when the readout of the second exposure begins.

Non-standard visits are also specified. The Camera must be able to provide a minimum exposure of 1 second and a maximum exposure currently targeted as 1 hour. In addition, the Camera must be able to take bias and dark frames, requiring the ability to read out without integrating and the ability to take exposures without opening the shutter.

Basic operation of the Camera flows down to CCS, DAQ, Corner Raft, Science Raft, and Shutter subsystems. Specific timing allocations flow to the shutter, science rafts and corner rafts.

3.2.15 Filter Exchange Functions

The Camera is required to have five filters on-board at any time, driving the need for an autochanger.

The Camera is also required to swap out one of the five filters in 1.5 hours without removing the Camera from the telescope. The number of filter swap-outs is specified to augment the lifetime requirement.

In addition, the Camera is required to change between filters that are resident on the Camera within 90 seconds. The number of filter changes is specified to augment the lifetime requirement.

Control and overhead specifications flow down to CCS, and all other requirements flow to the Filter Exchange subsystem.

3.2.16 Time Reference

Computer clocks used to produce timestamps shall be synchronized to an observatory master clock. Timestamps shall have an absolute accuracy better than 10 ms with a precision of 1ms (1-sigma) or better.

The requirement flows down to the CCS.

3.2.17 Science Data Readout

This set of requirements defines how the science data (and wavefront data) are provided to the observatory. Each Camera image has a unique identifier. The Camera is to provide both raw and crosstalk corrected science and wavefront data. The crosstalk corrected data is provided within 1 second to support alert processing. Both raw and crosstalk corrected data are persisted for two days and provided on-demand.

These requirements flow down to the DAQ subsystem.

3.2.18 Lifetime, Reliability and Maintainability

Design life requirements for the Camera have been stipulated. Fifteen years provides margin against the full life of the components, from fabrication, integration, commissioning, through operations. The Camera Specification includes cyclic lifetimes for exposure counts and filter changes, which are flowed down from the OSS. Items requiring routine maintenance have been identified and minimum maintenance cycles consistent with observatory maintenance planning have been defined for those subsystems (Shutter subsystem and Filter Exchange subsystem).

The unplanned downtime is addressed by identifying likely hardware failures and identifying mitigations to minimize downtime caused by those failures. Chapter 6 (Camera Architecture) discusses the design features that provide serviceability.

3.2.19 Safety and Protection

Requirements in this category are derived from the Camera Protection Plan (LSST Camera Document LCA-139), Performance and Safety Assurance Plan (LCA-138), and Quality Assurance Plan (LCA-229). They specify aspects of hardware protection, personnel protection, and quality assurance.

The Camera Protection Plan establishes an architecture for what protection is done where, and how system safety status is monitored; defines system-wide hardware and design requirements (electrical and mechanical) to ensure system safety; and, defines the requirements for the Camera protection system and its subsystem elements.

The Performance and Safety Assurance Plan covers personnel safety requirements, giving overarching requirements, which are then flowed to institutional safety implementation plans.

The Performance and Safety Assurance Plan and Quality Assurance Plan will establish quality requirements for protection system elements.

System requirements include details on the required protection functionality and the requirement to handle protection locally.

3.2.20 Thermal Requirements

Thermal requirements:

- Specify the Camera body and utility trunk external skin temperature control capabilities to limit temperature differentials between the Camera and the ambient dome air.

- Define Camera and subsystem component operating, acceptance/marginal, and survival temperatures
- Specify detector plane temperature temporal stability

Temperature requirements are -100°C target for detectors and -40°C for raft electronics, as documented in LSST Camera Document LCA-69, Environmental Specification. The Camera Environmental Specification Supporting Analysis also has design values for components. These design values come from environments at the observatory level, during Camera testing at SLAC and during shipping.

Detailed temperature requirements are defined in each subsystem specification, tailored to the environment for that specific subsystem.

3.2.21 Mechanical Requirements

The mechanical ICD with the telescope (LSST Document LSE-80) provides accelerations, natural frequency, envelopes, mechanical interface details and retroreflector requirements. These requirements are collected in LSE-68, the LSST Camera Loads Specification and appropriately tailored requirements are defined in each subsystem specification.

3.2.22 Power

The ICDs with the telescope (LSST Documents LSE-64 and 65) define power requirements for on-telescope components and off-telescope components. The power allocations are managed in the Camera Power Report (LSST Camera Document LCA-275). These allocations are flowed to all subsystems (except Optics subsystem).

3.3 Camera External Interfaces

The LSST Project management structure is divided into four major technical design teams (1) Telescope & Site; (2) Camera; (3) Data Management; and (4) Observatory Control System. The project Work Breakdown Structure parallels this arrangement.

Early on, the Project identified the major interfaces between the top-level LSST subsystems, along with the interfaces to Education and Public Outreach. This allowed specific design decisions to be made, which were then followed by refinement of the definitions of subsystem components and assignment of their responsible owners.

The interfaces between the top-level subsystems have been assembled into 16 ICDs. These ICDs are key communications documents between the four independent design teams. Interfaces internal to each subsystem have also been identified; these are described in design documents from each subsystem team. The Camera System Engineering team is integrated into the ICD generation process, with Camera subsystem managers or technical leads included in ICD definition when needed.

There are eight interfaces relevant to the Camera project, covered by 12 documents. These are:

1. Camera—Telescope and Site (LSST Document LSE-80), supported by the Mechanical ICD Drawing Between the Camera and Telescope (LSST Document LSE-18)

- Mechanical and thermal interfaces between the Camera and Telescope

2. Utilities and Services (LSST Document LSE-64)

   - Requirements for telescope-provided utilities and services and routing interconnects to the back end of the Camera utility trunk

3. Data Acquisition System—Telescope Control System

   - Wavefront sensor characteristics, data requirements and interactions between the Camera and the Telescope (LSST Document LSE-67)
   - Guide sensor characteristics, data requirements and interactions between the Camera and the Telescope (LSST Document LSE-66)

4. Data Acquisition System—Data Management (LSST Document LSE-68)

   - Data flow from Camera to DM for science and wavefront sensor data

5. Camera Control System—Data Management (LSST Document LSE-69)

   - Information exchanged between Camera and DM through Facilities Data Base

6. Camera Control System—Observatory Control System

   - Observatory Control System communication architecture and protocol (LSST Document LSE-70)
   - Camera command dictionary (LSST Document LSE-71)
   - Telemetry dictionary (LSST Document LSE-74)

7. Facilities (LSST Document LSE-65)

   - Requirements for support facilities and infrastructure for servicing the Camera

8. LSST Observatory Network Design (LSST Document LSE-78)

These interfaces are summarized in Figure 3-3.

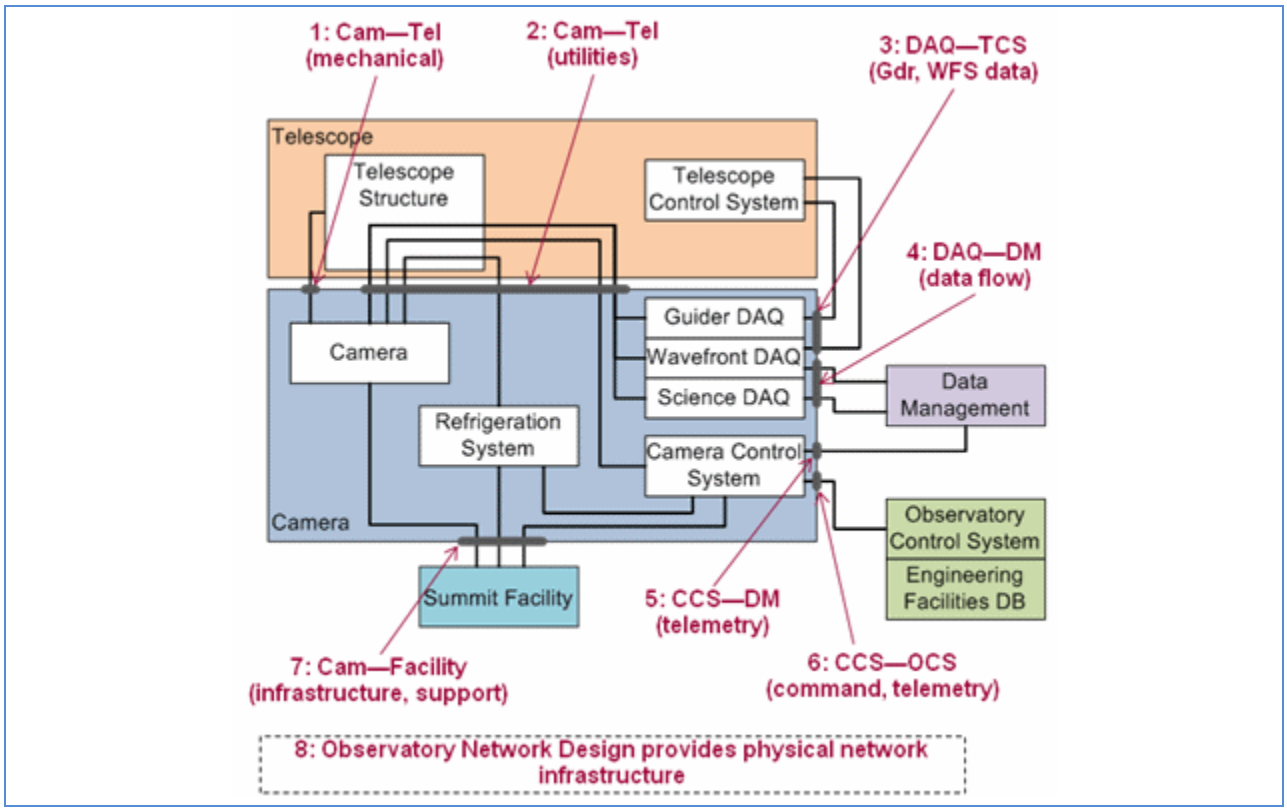

Figure 3-3: Interfaces between Camera and other observatory subsystems requiring formal interface definitions

4: LSST Design Overview

4 LSST Design Overview

This chapter summarizes the LSST's design, drawing largely on the material presented to the NSF at the LSST's Final Design Review and concentrating on those elements of the LSST design most relevant to this Camera Conceptual Design Report.

A large and integrated team of scientists and engineers from the astronomy and particle physics communities has been assembled to translate the LSST concept into an achievable system design. An extensive design and development (D&D) program funded partly by a grant from the National Science Foundation and partly by in-kind resources at the partner institutions has led to a construction ready design. The D&D effort has concluded, and with the signing of a Cooperative Services Agreement with the NSF in August 2014, the onset of construction has been formally established. The project has conducted extensive structural, thermal, and optical analyses of all key hardware subsystems, engaged with vendor interactions to determine manufacturability, developed explicit prototypes of high-risk hardware and software elements, and carried out extensive systems engineering studies. Over 100 technical personnel at a range of institutions are currently engaged in this program. The construction

ready design that has emerged from the D&D effort is summarized in the following paragraphs. Table 4-1 presents a selection of the high-level system design parameters.

The LSST optical design has been optimized to yield a very large field of view (9.6 deg^2), with atmospheric seeing-limited image quality, across a wide wavelength band (320-1050 nm). Incident light is collected by the primary mirror, which is an annulus with an outer diameter of 8.4 m, then reflected to a 3.4-m convex secondary, onto a 5.0-m concave tertiary, and finally into three refractive lenses in a Camera. This is achieved with an innovative approach that positions the tertiary mirror inside the primary mirror annulus ring, making it possible to fabricate the mirror pair from a single monolithic borosilicate glass substrate. The secondary is a thin meniscus mirror, fabricated in an ultra low expansion material. All three mirrors will be actively supported to control wavefront distortions introduced by gravitational and environmental stresses on the Telescope.

The telescope mount is a compact, stiff structure with a fundamental frequency of 8 Hz, which is crucial for achieving the fast slew-and-settle times that the survey strategy requires. The telescope sits on a concrete pier within a 30-m diameter carousel style dome. The dome has been designed with a high degree of ventilation to reduce dome seeing (local air turbulence that can distort images) and to maintain a uniform thermal environment over the course of the night.

The LSST Observatory is sited atop Cerro Pachón in northern Chile, near the Gemini South and SOAR telescopes. This is a developed NSF site, administered by the Association of Universities for Research in Astronomy (AURA).

The LSST Camera provides a 3.2-gigapixel flat focal plane array, tiled by 189 4K x 4K CCD sensors. The sensors are 100 micron thick deep-depleted, back-illuminated devices with a highly segmented architecture that enables the entire array to be read out in 2 seconds. Detectors are grouped into rafts in 3 x 3 arrays, each containing its own dedicated front-end and back-end electronics boards. The rafts are mounted on a silicon carbide grid inside a vacuum Cryostat, with an intricate thermal control system that maintains the CCDs at an operating temperature of -100^{o}C.

The entrance window to the cryostat is the third of the three refractive lenses in the Camera. The other two lenses are mounted in an optics structure at the front of the Camera body, which also contains a mechanical shutter and a carousel assembly that holds five large optical filters. A sixth optical filter can replace any of the five via a procedure accomplished during daylight hours.

The Data Management System (DMS) is configured in three layers: an infrastructure layer consisting of the computing, storage, and networking hardware and system software; a middleware layer, which handles distributed processing, data access, user interface, and system operations services; and an applications layer, which includes the data pipelines and products and the science data archives. The image data will be transferred from the Summit Facility in Chile to a central computing and archiving facility at NCSA over existing high-speed optical fiber network links. Within 60 seconds of acquisition, each visit will be processed to detect transient objects, and alerts are subsequently published as Level 1 data products. On an annual basis all data collected to date will be processed to generate calibrated photometric catalogs and images; these will be released as Level 2 data products.

The rapid visit cadence of the LSST observing program will produce ~15 Terabytes of image data per night, leading to a total image archive over the ten years of operations of more than 100 Petabytes. Processing such an enormous volume of data, converting the raw images into a faithful representation of the universe, and archiving the results in useful form for a broad community of users is a major challenge for the project.

Table 4-1: The LSST Design Configuration Parameters

Parameter	Configuration
System:	
Etendue (A□)	319 m^2degrees^2
Field of View	3.5 degrees in diameter (9.6 square degrees)
Effective clear aperture (On-Axis)	6.5 m (accounting for obscuration & vignetting)
Wavelength coverage (FWHM)	320 nm to 1050 nm
Number of active filters in camera	5
Filter set	u,g,r,i,z,y (5 available on any given night)
Telescope & Site:	
Configuration	3-mirror; alt-azimuth
Final f-ratio & plate scale	f/1.23; 50.0 microns/arcsec
Diameter of optics (physical)	M1 = 8.40 m M2 = 3.47 m M3 = 5.02 m
First camera lens; focal plane diam.	Lens L1 = 1.55 m FPA = 0.64 m
Residual design aberrations (arcsec) *80% encircled energy diameter*	u = 0.25 g = 0.25 r = 0.18 i = 0.18 z = 0.18 y = 0.19
Camera:	
Pixel size; pixel count	10 microns (0.2 arcsec); 3.2 Gpixels
Readout time	2 sec
Dynamic range	18 bits
Camera rotation range	±90 degrees
Focal plane device configuration	4-side buttable, >90% fill factor
Filter change time	120 sec
Data Management:	
Real-time alert latency	60 sec
Raw pixel data/night	15 TB
Yearly data archive rate:	Images: 6.6 PB; Catalogs: 6.5 PB
Computational capacity	Summit Facility (Cerro Pachon): < 1TFLOPS Base Facility (La Serena): 30-54 TFLOPS (yr 1 - 10) Archive Facility (NCSA): 200 - 1100 TFLOPS (yr 1- 10) Data Access Centers (Chile + US) >10% of Total
Communications Bandwidth	Summit to Base Facilities: 2x100 Gb/sec Base to Archive Facilities: 2x40 Gb/sec
Survey Capability:	
Sky coverage	18,000 degrees^2 (Main Uniform Survey); 27,000 degrees^2 (total)
Single-visit depths (point source; 5σ AB mag)	u = 23.5 g =24.8 r = 24.4 i = 23.9 z = 23.3 y = 22.1
Mean visits (2x15 sec. exp.) per unit area	825
Visit distribution over 10 yr (median)	u = 56 g = 80 r = 184 I = 184 z = 160 y = 160
Total visits over 10-year survey	million
Photometry accuracy (rms mag)	repeatability: 0.005; zeropoint: 0.01
Astrometric accuracy at r=24 (rms)	parallax: 1 mas; proper motion: 0.2 mas/yr

The LSST observing strategy will be optimized to maximize the scientific throughput by minimizing slew and other downtime and by making appropriate choices of the filter bands given the real-time weather conditions. A simulator has been developed to evaluate this process, and during the construction phase of the project, it will be transformed into a sophisticated observations scheduler.

4.1 Optical System Design

The LSST optical design, shown in Figure 4-1, is a 3-mirror system that follows the concepts of the well-known Mersenne-Schmidt family of designs that produces large fields of view with excellent image quality (Paul 1935; Baker 1969; Rumsey 1969; Willstrop1984; Angel et al. 2000; Seppala et al. 2002). The effective focal length of the optical system is 10.3 m, producing a final focal ratio of f/1.23. The image plate scale is 50 µm per arcsec. The annular geometry of the primary mirror (M1) produces 33.2 m^2 of on-axis collecting area, equivalent to a 6.5 m diameter unobscured clear aperture. The LSST etendue (including the effects of vignetting) is 319 m^2deg^2.

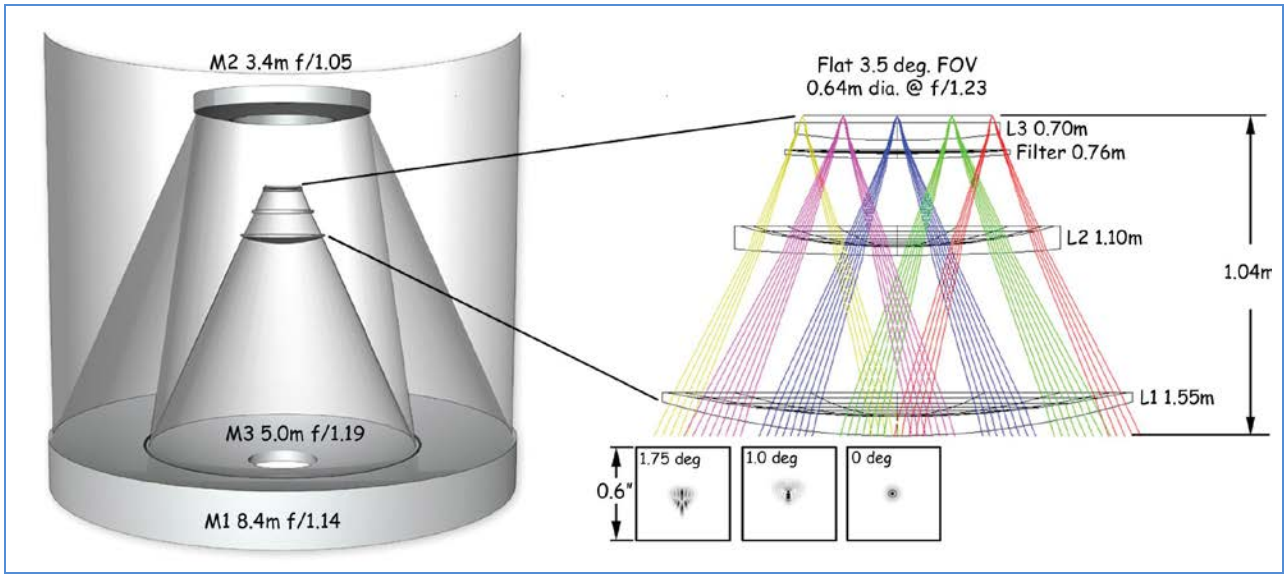

Figure 4-1: The optical design configurations showing the Telescope (left) and Camera (right) layouts. Diffraction images for three field radii, 0, 1.0, and 1.75 degrees, are shown in boxes 0.6 arcseconds square (3x3 pixels).

The M1 is 8.4 m in diameter with a 5.1 m inner clear aperture to accommodate the 5 m diameter tertiary mirror (M3). The relative positions of M1 and M3 were adjusted during the design process to enable fabrication on a single substrate. The two surfaces intersect smoothly within a 50 mm diameter radial band. This region between the mirror clear apertures will be baffled. The 3.4-m convex secondary mirror (M2) has a 1.8 m inner opening to enable LSST Camera installation.

The three reflecting mirrors are followed by a 3-element refractive Camera system, whose 3 lenses – L1, L2, and L3 - correct field flatness and chromatic aberrations. The 3.5-degree field of view (FOV) covers a 64 cm diameter flat focal surface. The selected spectral filter is located between the second and third refractive lens.

The image brightness is constant within 1% to a field radius of 1.2 degrees and gradually decreases outward by about 10% at the 1.75-degree field edge. The intrinsic image quality from this design is excellent. The mean 80% encircled energy is <0.3" in all spectral bands and <0.2" in the r and i spectral bands across the full FOV. The design also has very low geometrical distortion, <0.1% over the full FOV, making the LSST an excellent system for positional astrometry.

There are five aspheric surfaces in the optical design: the three mirror surfaces and one surface each on L2 and L3. The concave asphericity of M1 and M3 are within standard fabrication methods used for astronomical mirrors. During the design process, the asphericity of M2 was minimized to 19 μm of departure from the best-ft sphere to reduce technical challenges in optical fabrication of this large convex optic.

The three fused-silica Camera lenses are large in size, with clear apertures of 1.55 m, 1.10 m, and 0.72 m, but do not present any particular fabrication challenge. The last refractive element, L3, is used as the vacuum barrier to the detector cryostat. The central thickness of L3 is 60 mm to ensure a comfortable safety margin in supporting the vacuum stresses.

The fused-silica spectral filter is located between L2 and the shutter/L3. The 0.76 m diameter filter thickness varies from 13.6-26.6 mm depending on the choice of spectral band and is used to maintain the balance of lateral chromatic aberration. The zero power meniscus shape of each filter keeps the filter surface perpendicular to the chief ray over the full field of view. This feature minimizes shifting of the spectral band wavelength with field angle.

4.1.1 Alignment and Tolerance Sensitivities Analysis

A critical aspect of any large optical telescope design is the ability for the system to achieve the required image quality performance, given reasonable optical tolerances and conditions. Code-V and Monte Carlo techniques were used to evaluate sensitivities to alignment and fabrication tolerances and the ability to compensate for these errors. The 77 parameters defining radii, conic constants, aspheric terms, thicknesses, and rigid-body displacements (LSST Document-1361) were systematically perturbed individually and as an ensemble given expected fabrication, assembly, and operational (i.e. gravity, thermal, and wind loading) tolerances. These simulations were used to generate error budget allocations, system and component tolerances, and provide validation of the compensation strategy. Of the 77 parameters, the system compensation is realized by utilizing static one-time adjustment over axial spacing of two elements and dynamic control over the M2 and Camera assemblies via hexapods in 5 degrees of freedom each (X, Y, Z, eX, and eY) and by actively controlling the surface figures of all three mirrors.

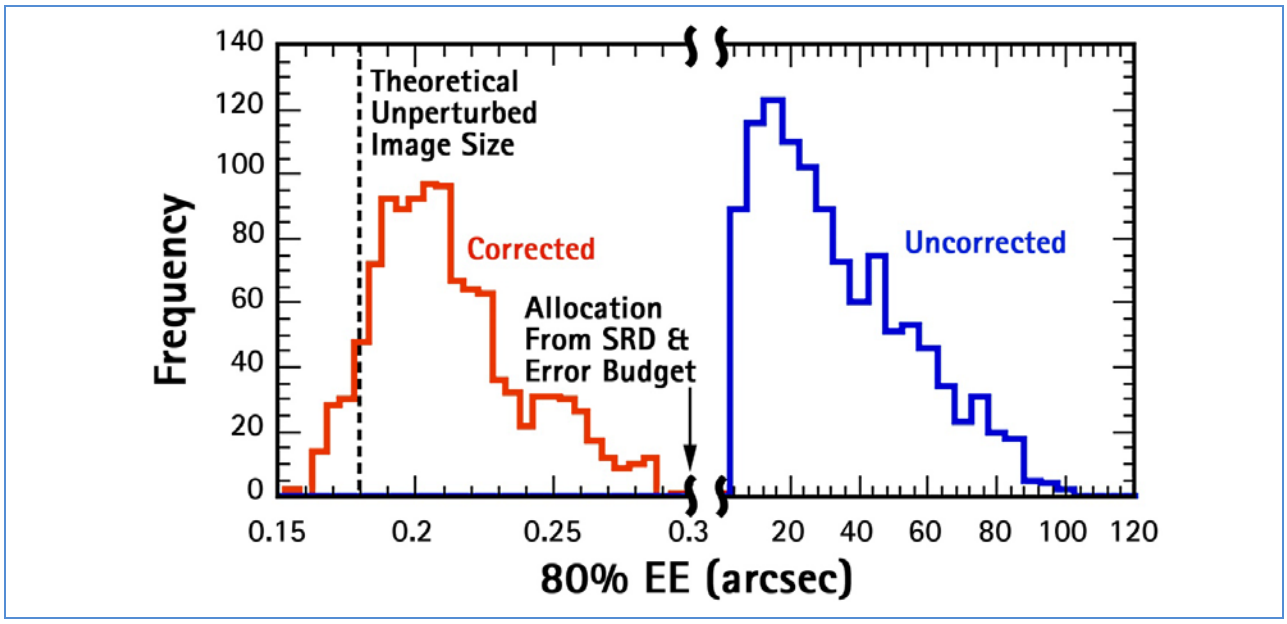

Figure 4-2: Results from Monte Carlo alignment and tolerance simulation including rigid body displacements and mirror surface deformation show the LSST optical system is correctable to the SRD specifications.

Figure 4-2 shows a typical result of the Monte Carlo alignment exercise. The optical system is initially uncorrected (i.e., misaligned) with an 80% encircled energy of 20 arcsec. Using only the compensators discussed above, the system is corrected (i.e., aligned) to a mean encircled energy of 0.2 arcsec. This is comfortably below its allocation in the error budget (0.3 arcsec for the system).

4.1.2 Active Optics System

Mirror figure and alignment control is performed by the Active Optics System (AOS). The AOS utilizes image data from four wavefront sensors embedded in Camera raft towers on the focal plane periphery, look-up tables derived from a model of the mount, and an independent laser tracker alignment system. The fast beam of the LSST optical design results in large single source beam footprints on each of the three mirror surfaces: 100%, 88%, and 74% of the clear aperture on M1 (the entrance pupil), M2, and M3, respectively. Thus, low order surface errors on the mirror cause slowly varying aberrations across the field of view. This in turn allows wavefront sensors from the field edge to accurately determine the necessary corrective measures to maintain the interior image quality. Figure 4-3 shows the basic flow of information, feedback processes, and rates required to maintain high quality images. The Monte-Carlo analysis discussed earlier included wavefront sensing and correctability parameters to qualify the LSST hardware and control approach.

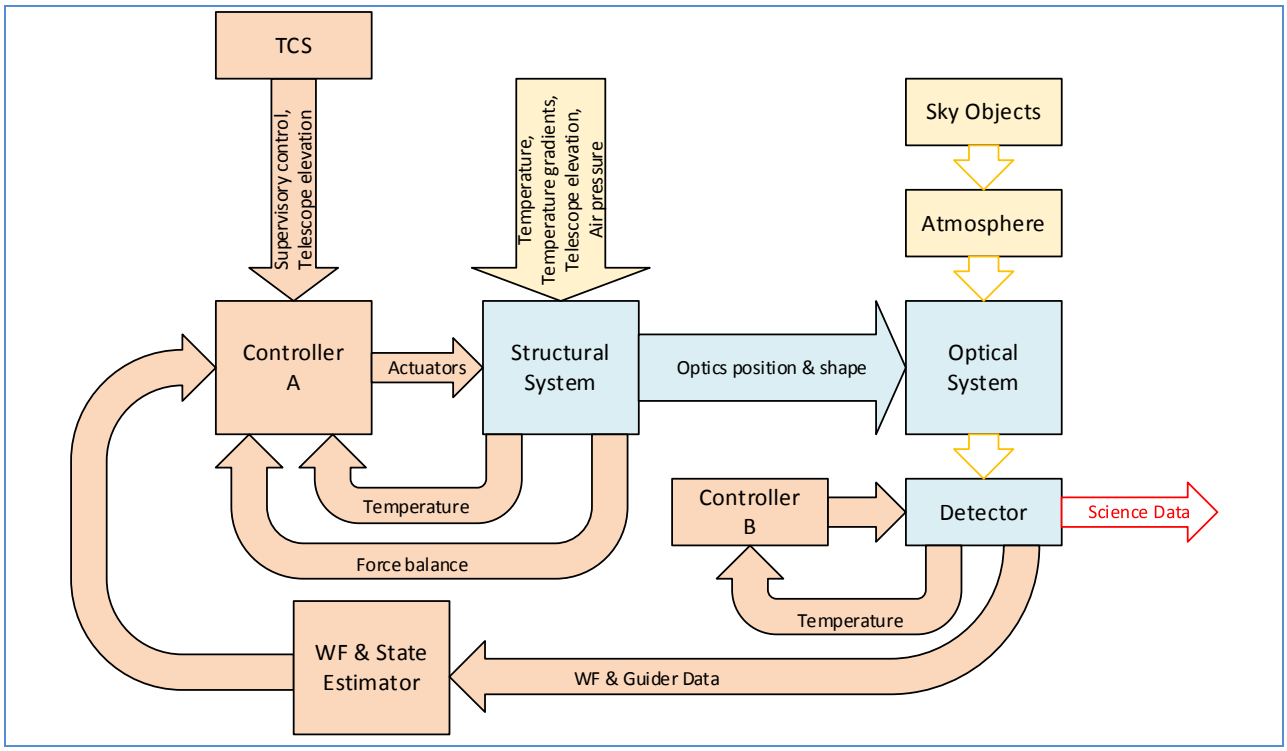

Figure 4-3: Block diagram of the active optics system with major components and control channels

Curvature sensing algorithms (Roddier and Roddier 1991) that have been adapted for the LSST's fast f-number, off-axis sensors and large obscuration have been successfully developed and will be employed to measure wavefront aberrations via the transport of intensity equation. Rigorous analysis has shown that four wavefront sensors on the focal plane periphery (see Figure 4-4) are sufficient to provide active alignment correction in a single iteration and to isolate figure corrections for each mirror (Phillion et al. 2006). The four wavefront sensor detectors will be positioned +/-2 mm about best focus and will be sized to acquire 86 square arcminutes of field. This sky coverage will ensure 100% probability of capturing a star image of sufficient brightness in all filter bands (97% in the u band). Image processing algorithm developed as part of the design and development effort will be used to construct a master intra- and extra-focal image from the many sources that land on each half of the sensor sets. The optical aberrations from the telescope are nearly constant across the wavefront sensors, and the atmosphere is decorrelated from star to star. This allows the residual wavefront error caused by the atmosphere in the 15-second exposures to be effectively eliminated by combining multiple images. This is similar to the approach used routinely on the VISTA Telescope (Clark 2004; Patterson 2004).

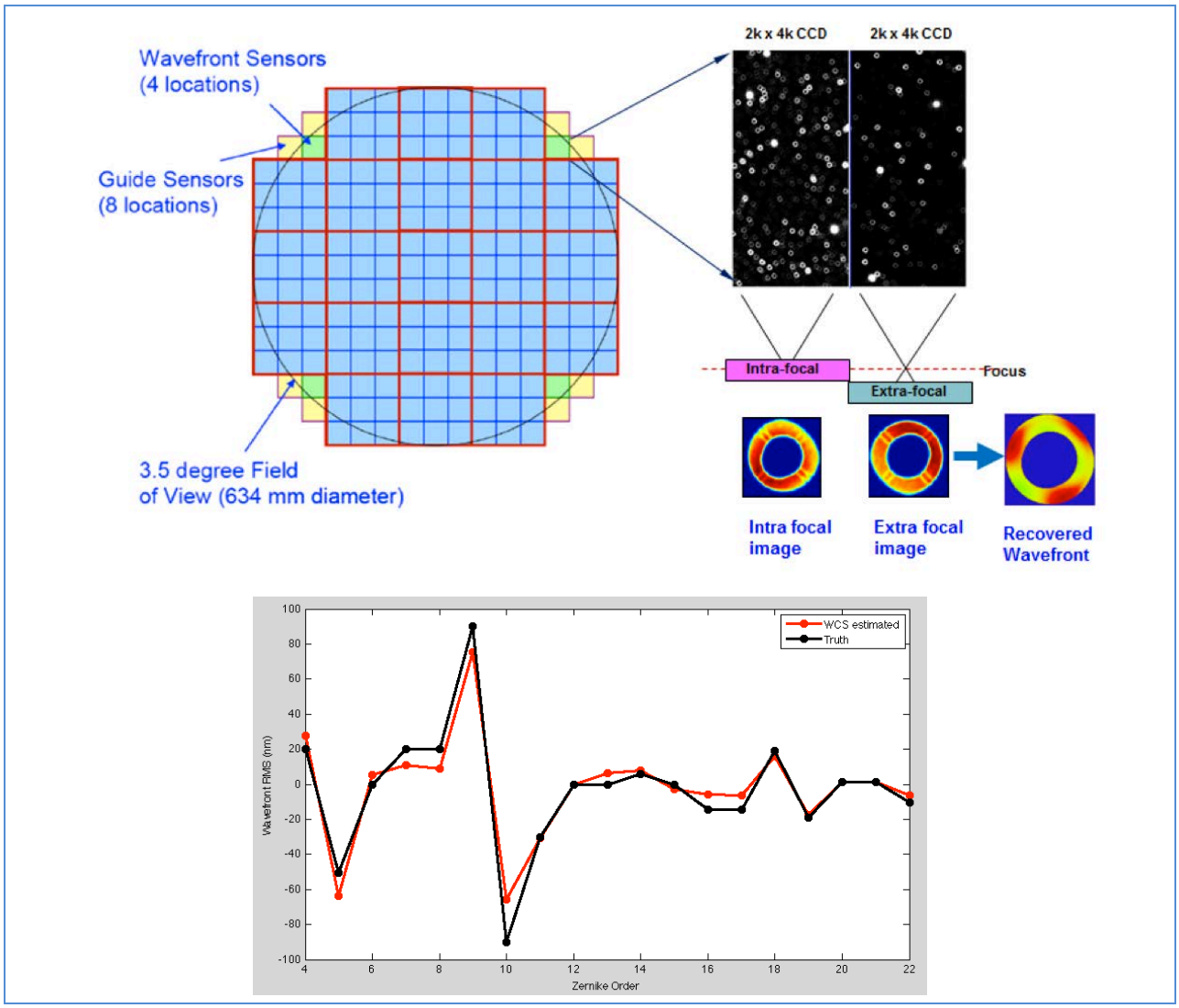

Figure 4-4: The focal plane geometry (upper left) showing the location of the 4 split sensors (green squares) used for the wave front estimation. An example of simulated LSST wavefront sensing images (upper right) and a comparison of the recovered wavefront from the LSST's extended curvature algorithms (lower plot, red line) and the "truth" as calculated from a Zemax optical model (lower plot, black line).

The overall performance of this approach has been demonstrated using an integrated model simulating the entire optical system, structural perturbations from FEA models, atmospheric turbulence and control feedback. In these simulations the computed wavefront aberrations at each sensor are fed to an error reconstruction matrix derived from the pseudo inverse of the sensitivity matrix. The reconstruction determines both mirror figure and rigid body corrections. The control algorithm also places restrictions on competing degenerate modes in order to dampen large displacements and oscillations in the control variables.

Control of PSF ellipticity is of vital importance in controlling systematic errors for the science missions. Ellipticity is tracked in the simulations referenced to 0.6 arcsec atmospheric seeing by convolving the diffraction image with a 2-D Gaussian having a FWHM equal to the seeing. Figure 4-5 shows the results

from simulations indicating that the wavefront feedback and control strategy keeps elipticity within specifications required for the science. Using the limited set of compensators only, the residual ellipticity introduced by the perturbed optical system is well below the SRD specification that 50% of the PSF signatures have a residual ellipticity of 0.04 or less due to all effects.

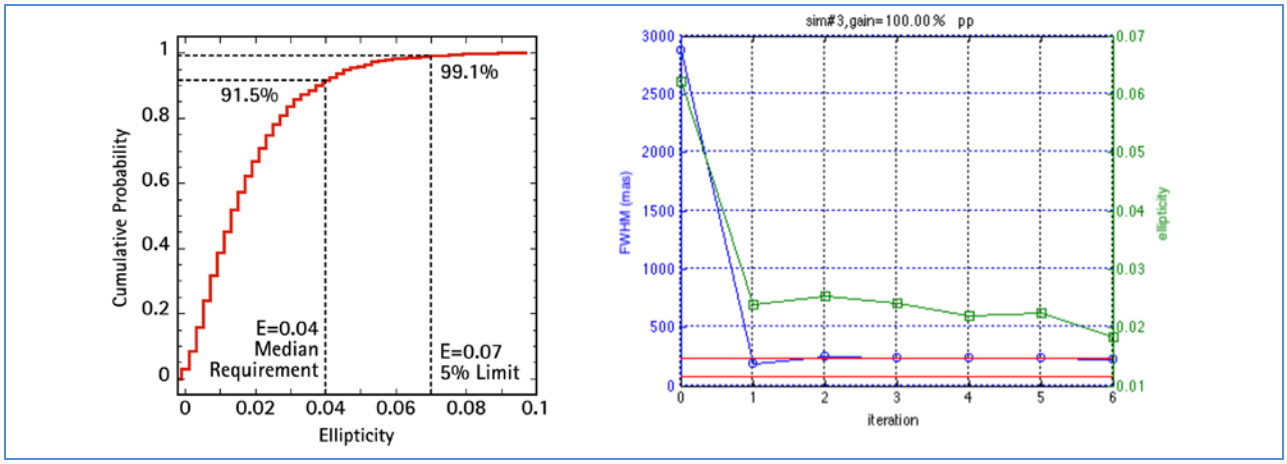

Figure 4-5: Left: The cumulative ellipticity probability predicted by Monte Carlo alignment and tolerance analysis. Right: Simulations using the integrated model show that the convergence of the full width at half maximum (blue line) and ellipticity (green line) in the perturbed optical system occurs in a single iteration of wavefront feedback.

The Camera's inputs to the wavefront correction system are summarized at greater length in Chapter 5. A detailed discussion of the wavefront sensor design is presented in Chapter 9. The architecture of the Corner Rafts is discussed at length in Chapter 11.

4.1.3 Calibration Hardware

The photometric requirements for the survey data place challenging specifications on the functionality of the calibration flat fields and also require that the optical transmission function of the atmosphere be measured. These requirements are achieved by careful attention to the full instrumental throughput characterization via a calibration dome screen and real-time monitoring of the atmosphere with an auxiliary calibration telescope and a bore-sighted IR camera.

4.1.3.1 Dome Screen

The LSST dome screen will uniformly illuminate the entire 8.4 meter telescope pupil over its full field of view at desired monochromatic wavelengths to provide a measurement of the total system throughput from entrance pupil to the digitization of charge in the Camera electronics. This approach accounts for the reflectivity of the mirrors, transmission of the refractive optics and filters, the quantum efficiency of the sensors in the Camera, and the gain and linearity of the sensor read-out electronics (Gressler 2010). The dome screen resides within the enclosures and provides routine operation during calibration cycles.

The dome screen is made with an engineered reflective diffuser illuminated by two rings of projectors located at the top of the telescope structure. The projectors are fed light from a tunable narrow-band laser and broad-band quartz source. The reflected light of this system is itself calibrated using National Institute Standards and Technology (NIST) qualified photodiode detector in lieu of a celestial calibration

source. The individual projector optical systems consist of a fiber-fed collimator, a diffuser and a spatial filter that illuminates the reflective screen with a flat profile. The projected footprint reduces stray light and makes every pixel on the detector integrate the light from every point on the illuminated screen, so the focal plane uniformity is dependent on the diffuser intensity rather than its irradiance.

4.1.3.2 Calibration Telescope

Real-time monitoring of the atmospheric optical transmission function is accomplished with the calibration telescope. This telescope will be located on the small hill adjacent to the main Telescope (-200 m) and at the same altitude. It will be remotely operated from the control room of the main Telescope using the same controls software system. The Calypso telescope mount and mirrors currently located on Kitt Peak will be refurbished, transferred to Chile, housed in a new building, and become the LSST calibration telescope. This telescope is a 1.2 m diameter high image quality and throughput Ritchey-Chretien design that meets the requirements for atmospheric monitoring. A low to mid-resolution spectrometer will be used as the main instrument to measure the atmospheric transmission over the spectral range of the LSST Camera. These data will be fed into a MODTRAN model of the atmosphere and provide a continuous temporal and spatial estimation of the wavelength dependent atmospheric extinction. In addition to the extinction model developed from the calibration telescope, the LSST Telescope will carry a bore-sighted IR camera with a 3-4 degree FOV to provide atmospheric extinction for every science image directly.

4.2 Site

The LSST Observatory is distributed over four sites: the Summit Site, the Base Site, the Archive Site, and the Project Headquarters. Table 4-2 lists the location, features, and function of each site, and the LSST team responsible for the subsystem components at each site. While the sites are geographically distributed, they are all functionally integrated. Dedicated high-bandwidth fiber optic lines connect the summit and base, with the others connected through secure shared networks. Control functions are distributed for operational efficiency and to provide robust, reliable, safe operation.

During operation, the LSST Project will broadcast near real-time transient alerts within one minute of image collection. Digitally processed images and feature catalogs will be available to the U.S. and Chilean communities via the Internet within 24 hours. Full data product releases are scheduled every year.

Table 4-2: The LSST Observatory sites and the functions located at the site.

Site	Location	Features
Summit Facility	El Peñón Peak on Cerro Pachón ridge, Chile	Telescope: service/support bldgs; calibration telescope
Base Facility	La Serena, Chile	Operations Center and infrastructure Pipeline computing facility; backup data storage
Archive Center	NCSA, U of Illinois, Urbana-Champaign	Main computing center and data storage; database archive US Data Access Center
LSST Headquarters	Tucson, Arizona	Corporate and Project Management Data Management and Operations Center

Site	Location	Features
		Education and Public Outreach Center and DAC

The LSST Summit Site is El Peñón peak on the Cerro Pachón ridge in Northern Chile (Figure 4-6). El Peñón is located 400 km north of Santiago and 57 km southeast of La Serena on property owned by the Association of Universities for Research in Astronomy (AURA), Inc. n ridge with El Peñón peak and the two observatories currently in operation there-the 8.2-m Gemini South and 4.1-m SOAR telescopes. The base facility for LSST operations in Chile will be located in La Serena within the AURA owned and operated compound. The archive center will be based at NCSA in Illinois, with the LSST headquarters residing in Tucson, Arizona.

Figure 4-6: A satellite view showing the relation between Cerro Pachón and La Serena. The El Peñón site within the AURA property boundary (dotted yellow) is identified to show the LSST site in relation to SOAR and Gemini South.

Extensive on-site characterization measurements have shown that El Peñón has excellent observing conditions that satisfy the LSST survey requirements. Seeing measurements performed over five years with a Differential Image Motion Monitor (DIMM) have indicated a median zenith pointing image quality of 0.70 arcsec after instrumental correction. The expected median delivered image quality is 0.56 arcsec using an outer scale of turbulence of 26 m computed from a preliminary data analysis of on-site microthermal sensors measurements (Figure 4-7).

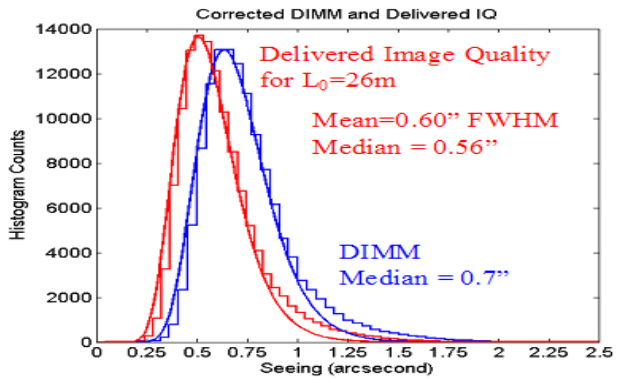

Figure 4-7: The distribution of Differential Image Motion Monitor (DIMM) atmospheric seeing at zenith (blue) and expected delivered image quality for an outer scale turbulence of 26 m (red)

Favorable meteorological conditions exist on site where a predominant northern wind direction dominates the wind rose, with wind speeds mainly between 3 and 12 m/sec. The mean temperature is 11°C (rarely going below freezing) with median temperature gradients during the night below 1°C/hour. Observatory logs for the past ten years show ~85% usable nights on Cerro Pachón.

4.3 Enclosure and Support Building

4.3.1 Summit Facility

The LSST summit facilities, shown in Figure 4-8, will be sited on AURA property atop the El Peñón summit of the Cerro Pachón ridge approximately 1.5 km SSW of the Gemini and SOAR observatories (LSST Document Archive, Document-4741; LSST Document Archive, Collection-2175). Proximity to these two recently completed observatories affords access to developed site infrastructure, proven bearing conditions, and predictable site construction logistics. Access to the site is via the existing main road from below and a 1-km provisional access road; the latter will be improved as required. Utilities (electric power, communications, and water) will be extended approximately 1.3 km from the common Cerro Pachón utility yard near Gemini. An existing shared dormitory and dining facility on Cerro Pachón will be expanded as needed to accommodate LSST requirements.

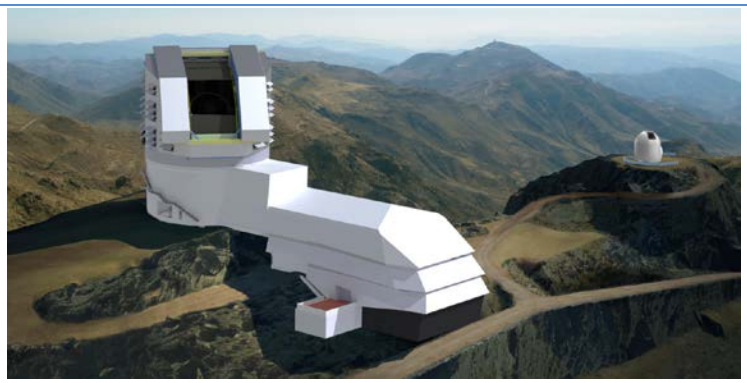

Figure 4-8: Artist's rendering of the LSST and dome enclosure with the attached summit support buildings and the LSST calibration telescope shown on an adjacent peak

The support facility consists of three primary elements: the Telescope lower enclosure, a platform lift, and an attached service and operations building. The overall layout is designed to keep heat-producing equipment and conditioned spaces, such as the control room and computer rooms, away from the Telescope area; the linear design also allows for efficient, protected circulation of equipment and personnel.

The layout of the main level of the service building is shown in Figure 4-9. Almost all maintenance of the optics and Camera for the LSST will be performed here. Mirror recoating and major Camera maintenance can be carried out concurrently in order to minimize downtime.

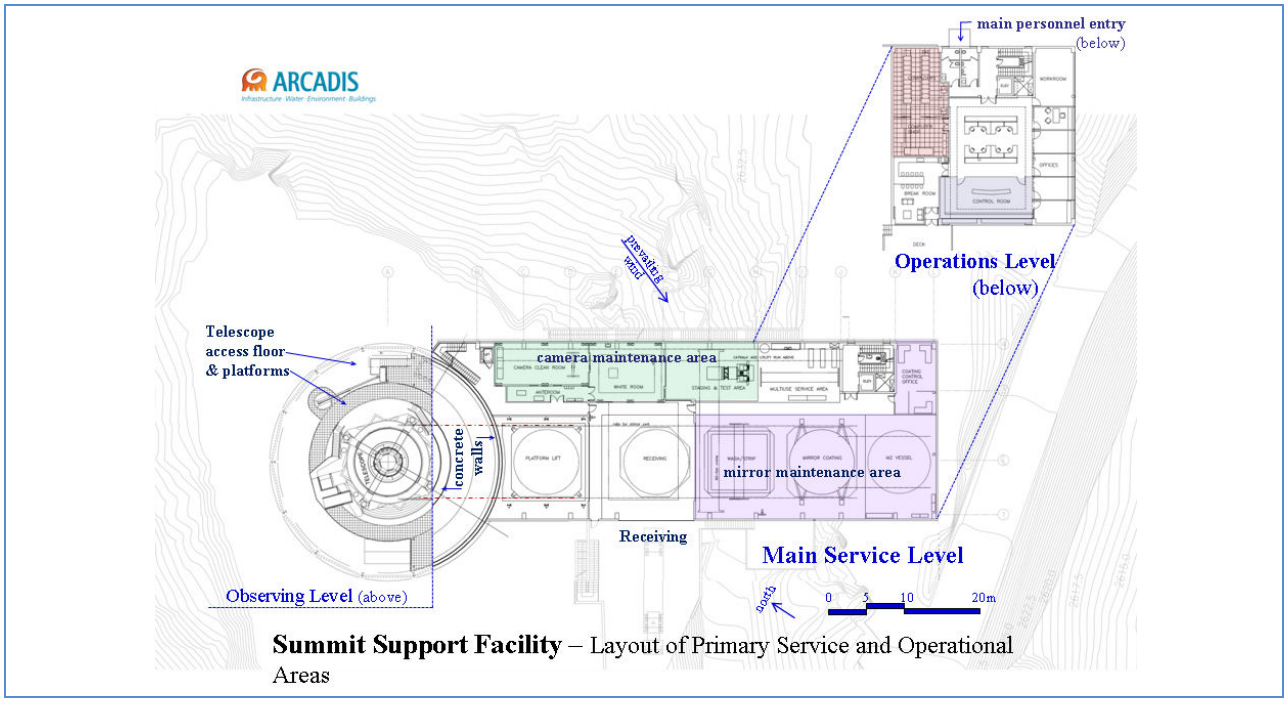

Figure 4-9: Layout of Primary Service and Operational Areas in the Summit Support Facility

The summit facility includes the control room, data/computing room, and offices. These conditioned spaces are located at the farthest end of the building, 70 m away and 25 m below the telescope base. A personnel elevator provides access to the service building above, both at the main service floor level and at a mezzanine level where an interior corridor leads directly to the telescope enclosure.

4.3.2 Telescope Dome

The telescope dome will be a rotating cylindrical structure, 30-m in diameter, supported by a fixed lower enclosure (LSST Document Archive, Document-2550). In addition to its normal functions of protecting the telescope against weather and providing housing for support, maintenance, and other equipment, the LSST dome satisfies the critical need for light baffling necessitated by the telescope's wide field-of-view and the system's rapid retargeting cadence. This is achieved by continuously “crawling” the enclosure in azimuth and the wind/light screen in elevation in between the rapid repositioning of the telescope mount. The major components of the dome are:

- Carousel: The primary protective shell of the dome; a faceted, cylindrical housing made of insulated metal panels supported on a structural steel framework.
- Observing aperture shutters: Two L-shaped sliding doors that open to provide an 11-m diameter observing slit.
- Wind screen/light baffle: The wind/light screen serves as a light baffle to form an 11-m aperture and provides the first level of protection against wind and extraneous light sources.
- Ventilation: Openings in the vertical faces of the carousel with operable louver panels to allow controlled natural ventilation of the telescope area during observing configured with baffle structures to prevent direct light passage.
- Rotation system: The drives, wheels, and control system that rotate the dome slit to any required azimuth position. The observing cadence, which is dictated by the science requirements, demands faster than normal dome drive speeds and special strategies, as described below.
- Dome crane: A 20-ton bridge crane mounted to the arch girders of the dome, which is used to service the Camera and other telescope-mounted equipment.
- Rear Access door: A 10-m wide service door at the back of the dome to allow passage of the mirrors and Camera onto a platform lift for conveyance to and from the service areas below.

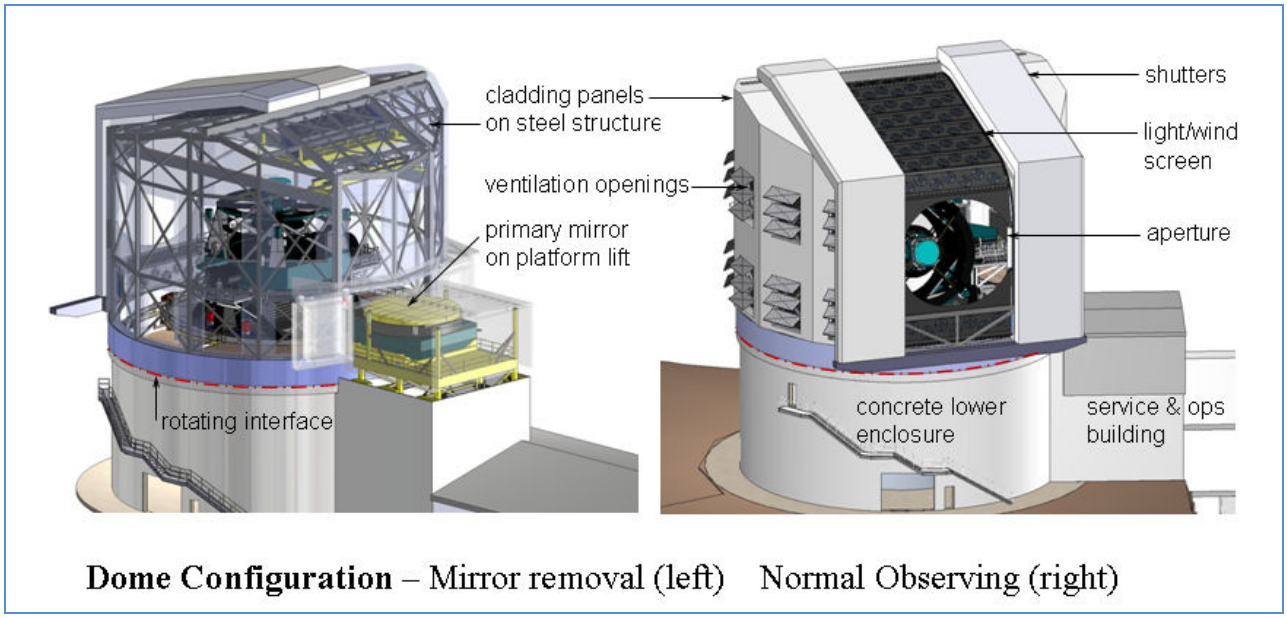

Figure 4-10: Mirror removal configuration (left) and normal observing (right)

The dome design provides adequate space for internal handling operations and interfaces with an exterior platform lift, while minimizing interior air volume and keeping the structure lightweight and agile. The views of the dome depicted in Figure 4-10 show the normal observing configuration (right) and the position used for removal of the primary mirror (left). Removal of the mirror and Camera are the two maintenance activities requiring the most radial space.

4.4 Telescope Mount

The LSST telescope is a compact, stiff structure with a powerful set of drives, making it one of the most accurate and agile large telescopes ever built (LSST Document Archive, Document-2255). The mount is an altitude over azimuth configuration (Figure 4-11). The telescope structure is a welded and bolted steel system designed to be a stiff metering structure for the optics and a stable platform for observing (Neill and Krabbendam 2010). The primary and tertiary mirrors are supported in a single cell below the elevation ring; the Camera and secondary mirror are supported above it. The design accommodates some on-telescope servicing as well as efficient removal of the mirrors and Camera, as complete assemblies, for periodic maintenance.

The stiffness of this innovative design is key to achieving a slew and settle time that is beyond the capability of today's large telescopes. The motion time for a nominal 3.5-degree elevation move and a 7-degree azimuth move is five seconds. In two seconds, a shaped control profile will move the telescope, which will then settle down to less than 0.1 arcsec pointing error in three seconds. All sky pointing performance will be better than 2 arcsec, an important efficiency parameter. Accurate pointing is key to tracking performance which, particularly for the LSST's wide field-of-view, directly impacts trailing and imaging systematics.

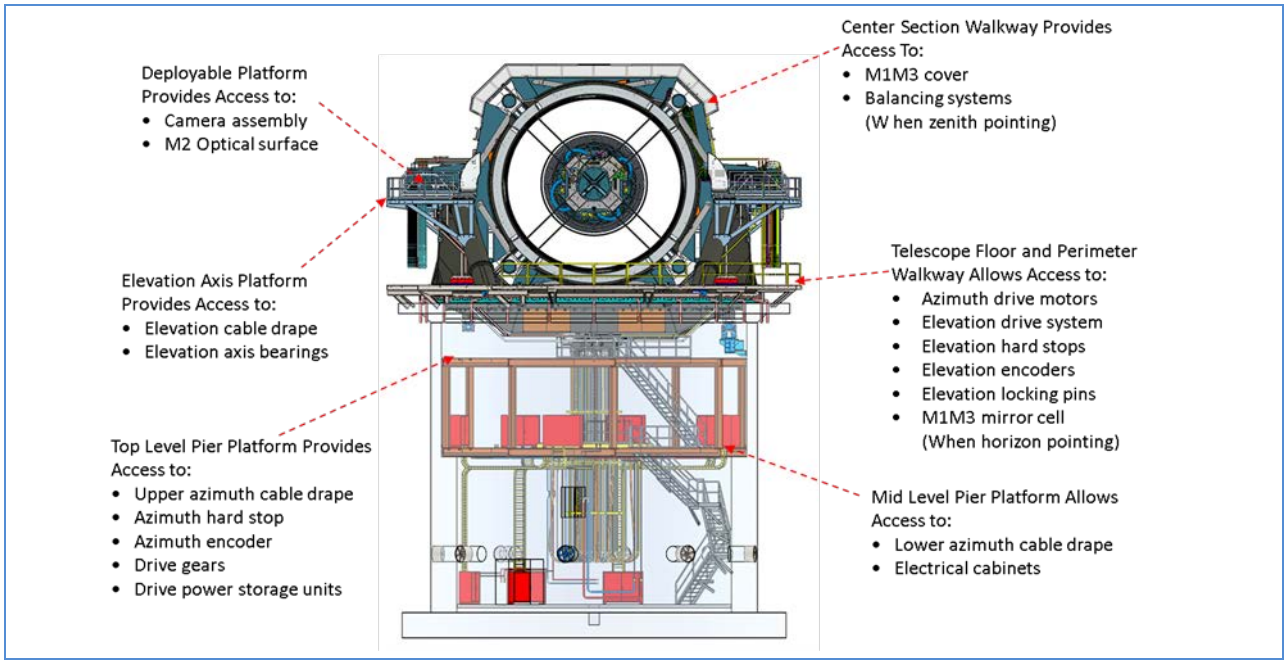

Figure 4-11: Configuration of the Telescope mount showing several subsystems and key attributes with a translucent pier.

The top end assembly, shown in Figure 4-12 in cross section, provides the support system for the Camera and the secondary mirror (Neill and Krabbendam 2010). These systems will be mounted on independent hexapods to adjust rigid body positions in 5 degrees of freedom providing high accuracy and repeatability (LSST Document Archive, Document-3589 and Document-9129). The Camera support will also include a rotator to provide +/- 90 degrees of motion for de-rotating the field-of-view during tracking.

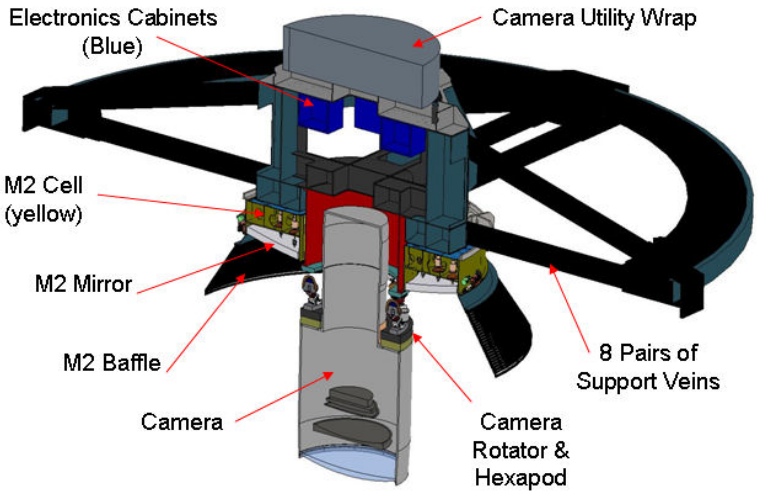

Figure 4-12: This 21-ton assembly, supported with 16 thin struts for minimal optical obstruction, carries the Camera and secondary mirror

The Telescope is outfitted with light baffles and surface treatments necessary to prevent out-of-field and incident light from reaching the focal plane.

1. Top End Ring Light Baffle
2. Mid Level Light Baffle
3. Center Section Light Baffle
4. M1 to M3 Transition Baffle
5. Top End Pier Scraper Vanes
6. Center Section Scraper Vanes
7. M2 Baffle

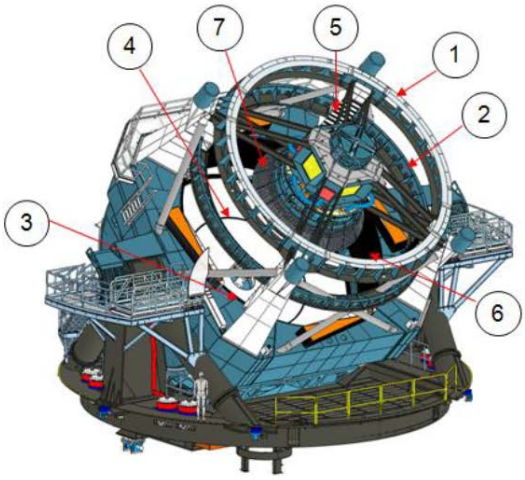

Figure 4-13: This 21-ton assembly, supported with 16 thin struts for minimal optical obstruction, carries the Camera and secondary mirror

Figure 4-14 shows the system stray light model, developed in FRED™, which was used to assess this critical wide-field issue. A point source transmittance calculation has evaluated the out-of-field stray light rejection and secondary ghost image performance. The design's critical surfaces have been identified.

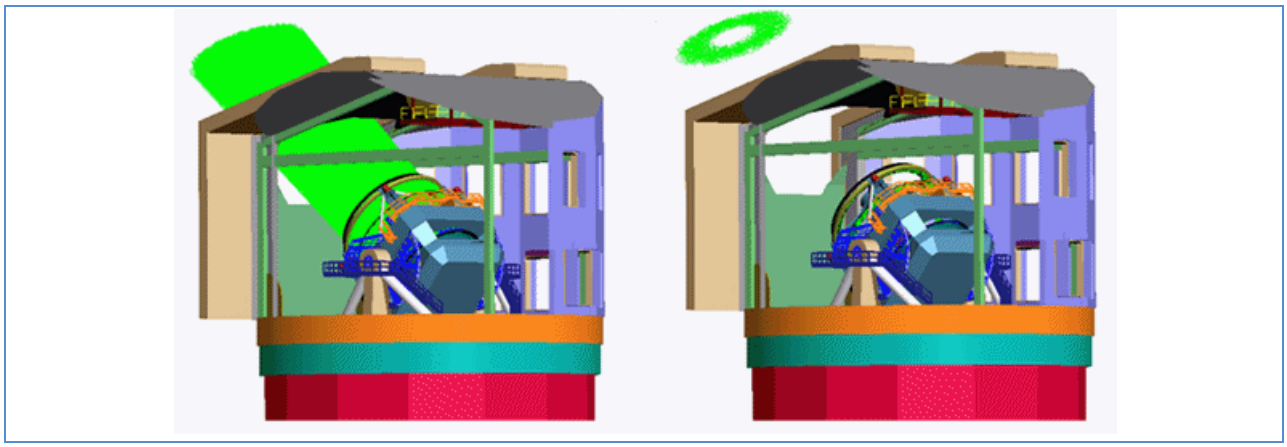

Figure 4-14: Detailed LSST FRED model analyzed for stray light and ghosting performance of the system. Green in the figure represents all projected light paths as seen by the detector.

4.5 Observatory and Telescope Control Systems

The LSST will include an Observatory Control System (OCS) to orchestrate and control all aspects of the observatory operation, including science observations, calibration, engineering, monitoring, and maintenance. The OCS is responsible for high-level observatory operations, including user interfaces, scheduling, resource allocations and system monitoring as shown in Figure 4-15. Through the OCS, the LSST system can be started, monitored, adjusted and stopped, both locally and remotely. The OCS also provides the connecting infrastructure for the system. It is the physical "glue" and coordinator of the subsystems in the LSST: the telescope control system (TCS), the Camera control system (CCS), the data management system (DMS), and the calibration/auxiliary control system (CACS) (Schumacher 2008).

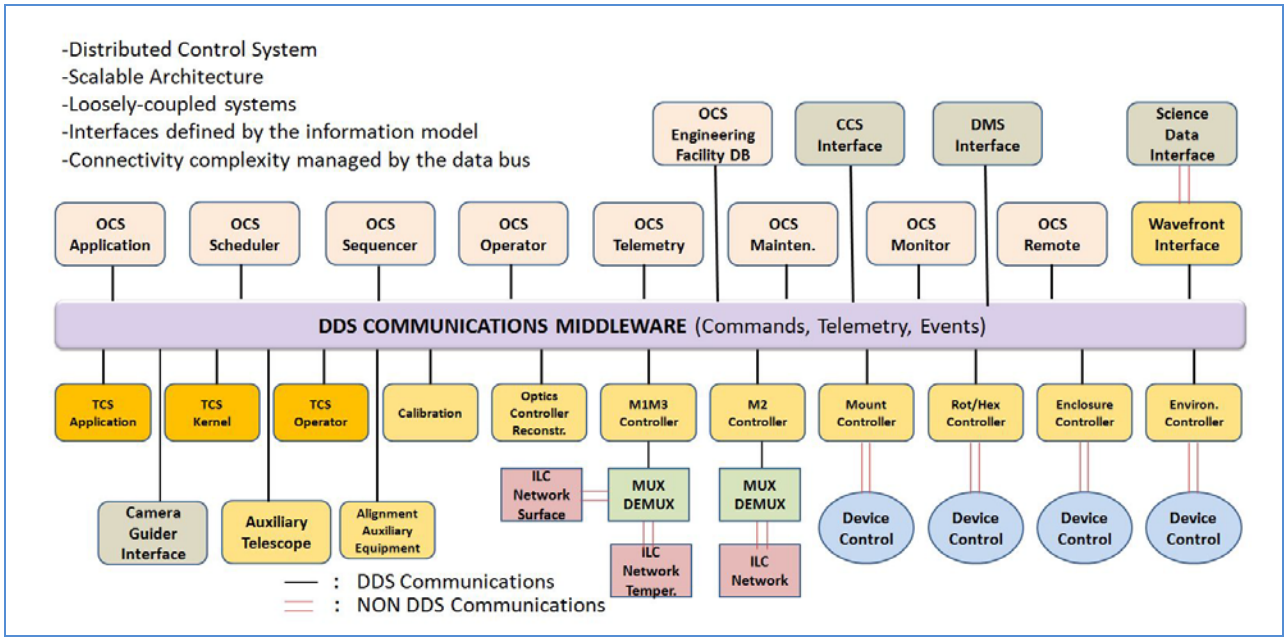

Figure 4-15: The LSST control architecture is based on a distributed control system using communications middleware.

There is a regular daily cadence to the operations of the observatory in terms of data acquisition, engineering, calibration, and science. The OCS must support all these activities, including the handover between them. An operator taking responsibility for the telescope at night must be able to see at a glance what the state of the control system is, just as an engineer on the morning shift needs to know how the telescope and instrument have been left by the night time users.

The Camera has critical interfaces to the Telescope Control System. The TCS is responsible for the control of the Telescope assembly and associated hardware, to accomplish the tasks of acquiring a target on the sky, tracking it during an observation, and correcting wavefront aberrations. The TCS is the central coordination facility for the delivery of high quality field images to the Camera. It is responsible for the precise pointing and tracking calculations necessary to observe a certain field. The TCS does not itself operate any mechanical component; rather it delegates this responsibility to the various telescope subsystems and manages them according to the observation requests. The TCS itself will be controlled either directly by a Telescope operator, or by commands initiated by the Observatory Control System (OCS). Its role, therefore, is to act as intermediary between the observer(s) and the Telescope hardware, translating high level user commands into low level subsystem commands.

4.6 Data Management System

The data management challenge for the LSST Observatory is to provide fully-calibrated public data to the user community to support the frontier science described in Chapter 2, while simultaneously enabling new lines of research not anticipated today.

Processing and storage activities are distributed across four types of DMS centers: the Mountain Summit, Base Center, Archive Center, and Data Access Centers. Connecting all the facilities are long-haul communications networks.

The principal functions of the DMS are to:

- Process the incoming stream of images generated by the Camera system during observing to archive raw images, transient alerts, and source and object catalogs. As the crosstalk-corrected image data is received at the Base Center, it is processed for alert generation. At the same time, the raw images are transferred from the Mountain Summit to the Base Center and are streamed to the Archive Center over the course of the night and the next day; the transfer must be completed before observing is started for the next night.
- Periodically process the accumulated survey data to provide a uniform photometric and astrometric calibration, measure the properties of fainter objects, and classify objects based on their time-dependent behavior. All data releases are archived for the entire operational life of the LSST archive.
- Periodically create new calibration data products, such as bias frames and flat fields, which will be used by the other processing functions.
- Make all LSST data available through an interface that utilizes, to the maximum possible extent, community-based standards such as those being developed by the International Virtual

Observatory Alliance (IVOA). Provide enough processing, storage, and network bandwidth to enable user analysis of the data without Petabyte-scale data transfers.

LSST images, catalogs, and alerts are produced at a range of cadences in order to meet the science requirements. Alerts are issued within 60 seconds of completion of the second exposure in a visit. Image data will be released on a daily basis, while catalog data will be released at least twice during the first year of operation and once each year thereafter.

Two general classes of events can trigger an alert. The first is an unexpected excursion in brightness of a known object or the appearance of a previously undetected object such as a supernova or a GRB. The astrophysical time scale of some of these events may warrant follow-up by other telescopes on short time scales. These excursions in brightness must be recognized by the pipeline, and the resulting alert data product sent on its way within 60 seconds. The second event class is the detection of a previously uncatalogued moving solar system object. The LSST scheduler system may not generate another observation of this object for some days; again, prompt follow-up may be appropriate, but in this case, a one-hour latency is acceptable.

Image data are read out and cross-talk corrected on the Summit and delivered via fiber link to the DMS Base Site by the Camera Data Acquisition System (DAQ). Each Camera image, which must be read out in 2 seconds, is 6 Gigabytes in size. The Observatory must be capable of operating for a specified period without Base Camp support; therefore, the Camera DAQ subsystem provides a storage array capable of buffering up to two days of images (~60 Terabytes) using a storage system that satisfies stringent failure requirements. The Camera DAQ subsystem delivers cross-talk corrected images as they are taken as well as buffered “raw,” uncorrected image data on request from the DMS. Images are “tagged” with sufficient metadata to uniquely identify them in time and space, with time tagging at sufficient resolution to allow correlation with any Observatory event.

4.7 References

Angel, et al. (2000). “Design for an 8-m Telescope with a 3 Degree Field at f/1.25: The Dark Matter Telescope” in van Breugel, W. and J. Bland-Hawthorn (2000). Imaging the Universe in Three Dimensions. Imaging the Universe in Three Dimensions.

Baker, J. G. (1969). "On Improving Effectiveness of Large Telescopes." Ieee Transactions on Aerospace and Electronic Systems **Aes5**(2): 261-&.

Clark, P., P. Berry, et al. (2004). Wavefront sensing within the VISTA infrared camera, SPIE.

Filippenko, A. V. (1982). "The Importance of Atmospheric Differential Refraction in Spectrophotometry." Publications of the Astronomical Society of the Pacific **94**(560): 715-721.

Gressler, W. J., P. Doherty, et al. (2010). Calibration dome screen for the Large Synoptic Survey Telescope, SPIE.

LSST Document Archive, Document-1361 Monte Carlo Simulation of the LSST v3.0 Optical Design.

LSST Document Archive, Document-221. PSF ellipticity caused by uncorrected atmospheric dispersion. Technical Study.

LSST Document Archive, Collection-2175. Construction Documents for the Summit Support Facility.

LSST Document Archive, Document-2255. LSST Mount Study.

LSST Document Archive, Document-2550. Technical Review of Dome Design.

LSST Document Archive, Document-2554. Wavefront curvature sensing. Technical report.

LSST Document Archive, Document-3589. Camera Hexapod and Rotator.
LSST Document Archive, Document-4741. Camera Telescope Facility ICD.
LSST Document Archive, Document-9129. LSST Secondary Mirror Assembly Hexapod.
Neill, D. R. and V. L. Krabbendam (2010). LSST Telescope mount and pier design overview, SPIE.
Patterson, B. A. and W. J. Sutherland (2003). Analysis of curvature sensing for VISTA, SPIE.
Paul, M (1935). Corrective systems for astronomical reflectors. Rev. Opt. Theor. Instr., **14**: 169
Phillion, D. W., S. S. Olivier, et al. (2006). Tomagraphic wavefront correction for the LSST, SPIE.
Roddier, F. and C. Roddier (1991). "Wavefront reconstruction using iterative Fourier transforms." Appl. Opt. **30**(11): 1325-1327.
Rumsey, N.J. (1969). Optical Insruments and Techniques. Oriel Press, Newcastle.
Schumacher, G. and F. Delgado (2008). The Large Synoptic Survey Telescope middleware messaging system, SPIE.
Seppala, L. G. (2002). Improved optical design for the Large Synoptic Survey Telescope (LSST), SPIE.
Willstrop, R. V. (1984). "The Mersenne-Schmidt - a 3-Mirror Survey Telescope." Monthly Notices of the Royal Astronomical Society **210**(3): 597-609.

5: Camera Design Overview

5 Camera Design Overview

5.1 Introduction

This chapter summarizes the baseline design of the LSST Camera, covering Camera subsystems in their functional categories: optics, focal plane systems, thermal control and vacuum systems, filter exchange and shutter mechanisms, controls and DAQ.

Chapter 3 discussed the requirements driving this design. Chapters in the remainder of this Report provide a detailed discussion of each of the subsystems introduced herein.

5.2 Key Driving Requirements

The LSST Camera will be the largest digital astronomical camera ever built and, as such, its design presents a number of challenges. LSST's scientific requirements lead to demanding constraints on sensor architecture, optical throughput, precision, and the sophistication of the read-out electronics. In addition, given the fast optical beam (f/1.23), Camera tolerances on the assembly and alignment of the focal plane and optics are tight. The LSST science missions require precise knowledge and control of both the size and shape of the delivered PSF.

Key requirements on the Camera are listed in Table 5-1.

Over the past several years the LSST team has worked to minimize the risk that critical Camera components might not fully meet the technical performance or schedule needs of the project. The two main Camera components in this category are the sensors and filters.

The LSST science requirements preclude the use of any existing sensor design. In addition to the need for extended red response and small point spread function, the fill factor, full well capacity, as well as readout speed and noise of the sensor have the most impact on LSST science performance. LSST has generated a set of sensor performance requirements derived from the science requirements. These performance requirements dictate sensor specifications that exceed current technology, so an R&D program was initiated to implement a new design. Evaluation of these novel sensors is now complete. The sensor design is summarized at greater length in Section 5.3.3; a full treatment of the design and a discussion of results from the R&D and evaluation program are discussed in detail in Chapter 8.

Table 5-1: Key Driving Camera Requirements

Parameter	Requirement	Notes/Rationale
Image quality budget allocation	0.30 arcsec.	Includes all optics, focal pane flatness, and sensor charge diffusion

Parameter	Requirement						Notes/Rationale
Focal Plane Flatness	±11 microns						Derived from image budget
Charge Diffusion	Point spread < 5 microns rms						Derived from image budget
Mass properties							
Total mass	≤ 3060 kg						Affects frequency response of telescope
Moments of Inertia about CG	$MOI_x, MOI_y \leq 3500$ kgm^2 ; $MOI_z \leq 1000$ kgm^2						Affects requirements on rotator and hexapod support
Camera Timing:							
Sensor Readout	≤ 2 seconds for 3 Gigapixel readout						Derived from cadence timing requirement.
Internal filter change	<90 seconds						30 sec. of the 120 sec. system rqmt. is allocated to the rotator on the telescope for repositioning the camera.
Shutter Timing	<5 msec (goal)						300 msec is the official requirement; the Project aims to meet a 5 msec goal. Derived from photometric budget. Requirement on error of knowledge of exposure time over full FOV.
Camera Throughput	u	g	r	i	z	y	
Hardware integral	0.065	0,170	0.135	0.097	0.065	0.024	Averaged over the upper filter envelope.
Total camera allocation (%)	23.5	45.4	49.1	46.3	42.1	12.6	Derived from camera allocation; detector QE minus contamination and condensation.
Sensor QE (%)	41.0	78.0	83.0	82.0	75.0	21.0	

The LSST ideal filter curves have been generated to facilitate the analysis of the total system throughput for the different passbands. The six filters that will be used for LSST are based on the Sloan Digital Sky Survey filters and are capable of supporting a large set of observing objectives. Wide, steep slopes of the filter passbands with high throughput were required as well as low out-of-band transmission. The baseline filter component is described in Section 5.3.1 and then presented in detail in Chapter 7.

5.3 Design Overview

The LSST Camera, shown in Figure 5-1, contains a 3.2-gigapixel focal plane array comprised of 189 4Kx4K CCD sensors with 10 µm pixels. The sensors are deep depletion, back-illuminated devices with a highly segmented architecture that enables the entire array to be read out in 2 seconds. The detectors are grouped into 3 x 3 arrays called "rafts." All the rafts are identical; each contains its own dedicated raft electronics boards, which fit within the footprint of the raft sensors. The rafts and associated electronics

are mounted on a silicon carbide (SiC) GRID inside an evacuated Cryostat, with an intricate thermal control system that maintains the CCDs at an operating temperature of -100°C. The GRID also contains four sets of guide sensors and wavefront sensors at the edge of the field.

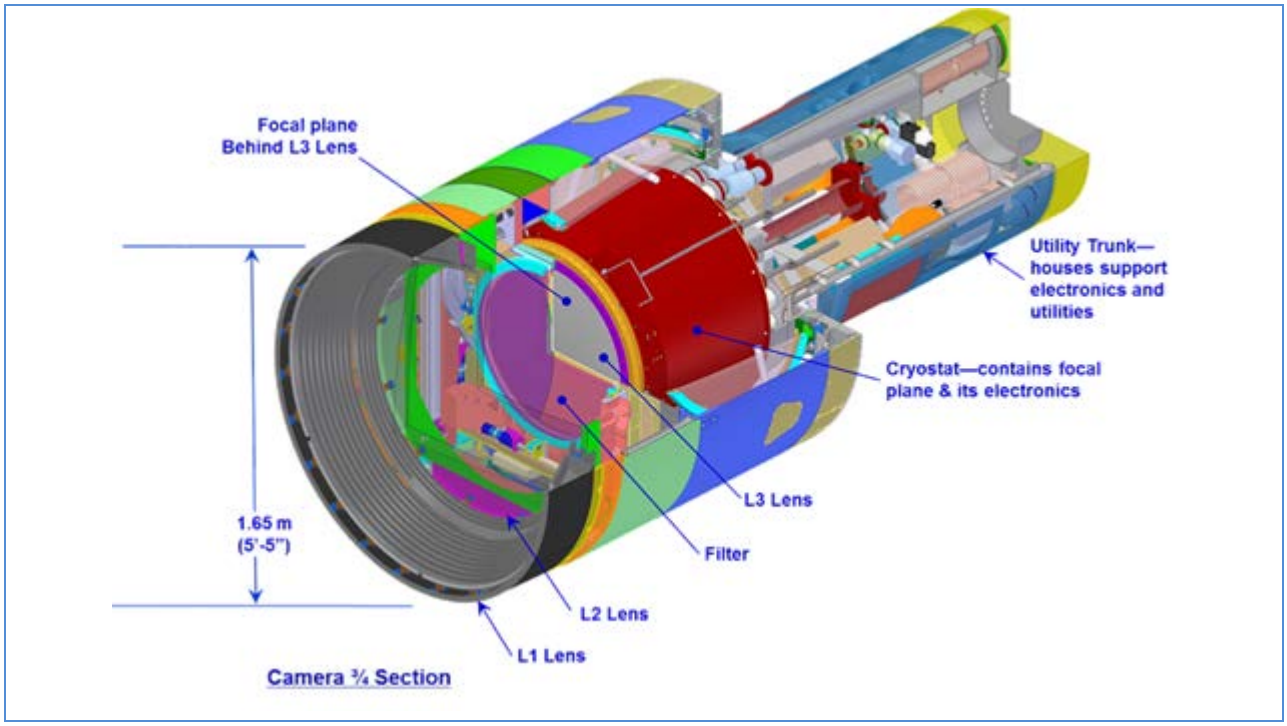

Figure 5-1: Top-level View of the LSST Camera, Showing Major Components

The entrance window to the Cryostat is the third of three refractive lenses. The other two lenses are mounted at the front of the Camera Body. The Camera Body also contains a mechanical shutter and a Filter Exchange system holding five large optical filters, any one of which can be inserted into the Camera field of view for a given exposure. A sixth optical filter will also be fabricated; this filter can replace any of the five via a daytime procedure.

5.3.1 Camera Optics

This section provides a high-level description of the Camera optical design. For analysis of the mechanical, thermal, and contamination control concerns related to the optics, see Chapter 6. A detailed treatment of the refractive optics and filters themselves is presented in Chapter 7.

5.3.1.1 Refractive Optics

The Camera refractive optics consists of three fused silica lenses (L1, L2, L3) with clear apertures of 1.550 m, 1.102 m, and 0.722 m, respectively. L1 has an edge thickness of 3.4 cm and a center thickness of 8.2 cm. L2 has a central thickness of 3.0 cm. The space between L2 and the filters is 34.9 cm, which is adequate for accommodating the filter interchange. L3 is the vacuum barrier for the Cryostat containing the detector array. L3 has a central thickness of 6.0 cm, which provides a sufficient safety margin against fracture due to the pressure differential across it.

The Camera optics design can meet all design requirements using fused silica substrates. The Corning manufacturing process for fused silica can produce glass of the required size and quality. Although the required lenses are large, a substantial industrial base exists for fabricating them, and the LSST requirements are consistent with optical elements that have been produced for other programs. A key aspect of the fabrication involves the testing of wavefront distortion. Wavefront distortion will be measured interferometrically utilizing null tests. The L1, L2, and L1/L2 assembly null tests will incorporate computer generated holograms as null correctors and to verify alignment.. All null tests use a retro-reflecting mirror to test the lenses in double pass transmission. A perfect point source is re-imaged onto itself with a wavefront error less than 1/20 wave at 633 nm.

The optic mounts provide the interface between the lenses and the structures that support them. These interfaces have been designed such that adjustments between the frame and optics are not needed. A one-time adjustment is available to the vendor between the L1 cell and L2 cell through a shim within a three point kinematic interface. The lenses will be installed in their mounts and requirements verified prior to delivery to the integration group. In terms of optical correction, L1 and L2 are the most significant optical elements in the Camera. Their alignment to one another is therefore critical and the assembly is tested and delivered as a single unit to minimize optical error and reduce on-site integration requirements . In order to preserve optical alignment, the L1-L2 assembly struts are spaced to enable access to components without removing the assembly from the camera body.

Finite element modeling has confirmed design of an independently stiff housing to which both the L1 and L2 lenses attach. Between the housing and L1 and L2 are radial-motion flexures, which allow for differential thermal expansion. Each optic will be measured first by itself and then in the mount during fabrication.

5.3.1.2 Filters

The filters consist of multi-layer dielectric interference coatings deposited on fused silica substrates. The first surface of the filter is normal to the chief ray for all field points in order to keep the angles of the light rays passing through the filters uniform over the entire range of field positions. The filter thickness and the curvature of the second surface are optimized for image quality.

The current LSST filter complement (u,g,r,i,z,y) is modeled on the system used for the Sloan Digital Sky Survey (SDSS), which has been successful in a variety of applications (e.g., photometric redshifts of galaxies, separation of stellar populations, photometric selection of quasars, among others). Extension of the SDSS system to longer wavelengths (y-band) is necessary to increase the effective redshift range that will be achievable with the LSST due to deeper imaging. The addition of a u-band improves the robustness of photometric redshifts of galaxies, stellar population separation, and quasar color selection, and will provide significant additional sensitivity to star formation histories of detected galaxies.

5.3.2 Focal Plane Components

This section provides a high-level description of the Camera focal plane design. For analysis of the mechanical, thermal, and contamination control concerns related to the focal plane, see Chapter 6. Other detailed treatments of subsystems introduced here are covered in:

- Chapter 8 for science sensors
- Chapter 9 for guide and wavefront sensors
- Chapter 10 for the science rafts
- Chapter 11 for the corner rafts

The 3200 cm^2 unvignetted field of view of the Camera is tiled with a mosaic of 21 identical square rafts configured with science sensors and an additional four triangular rafts carrying wavefront sensors and guiders (Figure 5-2).

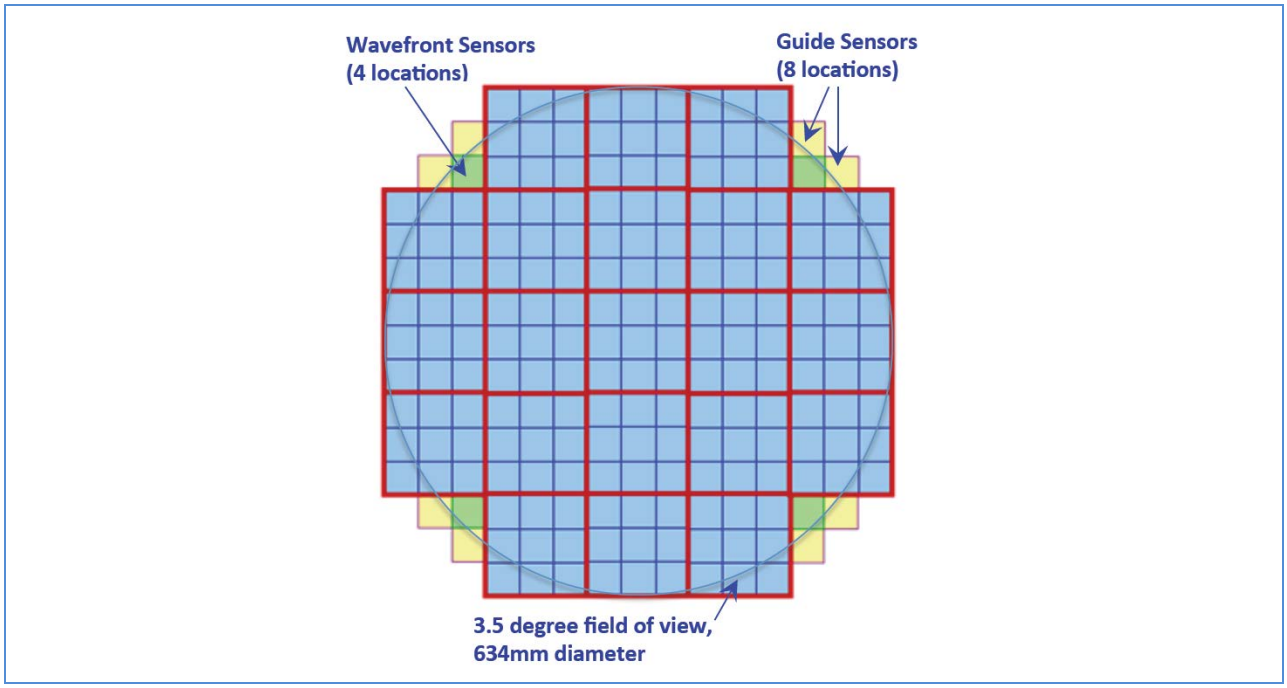

Figure 5-2: Focal Plane Organization. With its 189 sensors, the focal plane of the Camera images 10 square degrees of the sky per exposure.

5.3.2.1 Sensor Design

The science sensor array is the main element of the Camera and the sensor design is directly influenced by LSST's unique science requirements. The interaction between sensor performance and key science requirements is shown in Table 5-2.

Table 5-2: Relationship of Sensor Performance Characteristics to Science Requirements

	single visit image depth (D1, DB1)	image quality (S1)	photometric repeatability (PA1)	survey area (Asky)	visit distribution (Nv1)
quantum efficiency	X				X
read noise	X				
dark current	X				
cosmetics				X	
diffusion PSF	X	X			
flatness	X	X			
QE and PSF stability			X		
fill factor .				X	
readout time				X	X
reliability/time to repair				X	X

The design for the LSST sensors specifies an over-depleted silicon thickness of 100 µm (tradeoff of NIR QE and charge diffusion), coplanarity of ±9 µm (to stay within LSST's small focal depth), a pixel size of 10 µm (0.2 arcsec at LSST's plate scale), and segmented full-frame architecture with sixteen amplifiers per CCD (to give 2 second readout with less than 8 e- rms read noise). High resistivity bulk silicon technology, seldom used in commercial CCDs, is required for this application. The package design is also critical for achieving the flatness, thermal stability, and close-butting requirements. While each of these parameters has been achieved in individual devices, the LSST sensors will be the first to incorporate the full set of performance parameters in a single sensor optimized for surveys. A concise table of requirements is given in Table 5-3.

Table 5-3: Key Sensor Performance Requirements

Parameter	Value
Pixel size	10 µm
Depleted silicon thickness	100±5 µm
Format	4K x 4K pixels
Segmentation	Sixteen 2000 row x 500 col sub-arrays

Parameter	Value
Total no. of output amplifiers	16
Readout time	2s
Read noise	< 8 e^-
Height of imaging surface above baseplate	13.000 ± 0.009 mm
Quantum efficiency, 350 nm	40%
Quantum efficiency, 500 – 900 nm	80%
Quantum efficiency, 1000 nm	21%

The LSST Project has completed a multi-year R&D effort on sensor development. Two suppliers have successfully produced prototype sensors meeting LSST specifications, and in June 2014 the Project awarded the first production contracts. Prototype results are discussed in more detail in Chapter 8.

5.3.2.2 Raft Towers

The sensor packages are assembled into raft "towers", illustrated in Figure 5-3. The functions of the Science Raft Tower are to provide:

- Precise mechanical location and support for the CCD array
- Electronics to control and read out the CCDs
- Thermal management of the CCDs and front end electronics

Mechanical requirements are extremely stringent and include locating the CCD imaging surfaces to within a narrow flatness envelope and with gaps of 0.25 mm between adjacent CCDs. As a result of the fine segmentation of the CCDs, the Science Raft Tower has to implement all electronic functions of a 144-channel CCD controller in a volume contained within the projected footprint of the Raft. Although low-power ASICs are used, their total power dissipation is significant and must be removed from the Cryostat through adequate thermal paths. Finally, the imaging surfaces of the CCDs must be protected from contamination by condensable materials in the electronics enclosures.

The science raft tower module (RTM) is the modular building block of the camera focal plane and consists of three major assemblies:

- The raft-sensor assembly (RSA) is a 3 x 3 mosaic of science CCDs in precision packages, mounted on a silicon carbide baseplate. The RSA also includes temperature sensors, resistive heaters, and flexible electrical and thermal connections.

- The Raft Electronics Crate (REC) houses three circuit boards (REBs) and contains copper planes providing the thermal path for cooling the RSA and the CCDs.

- The Raft Electronics Board (REB) contains custom video processing and clock/bias buffering electronics plus video digitizing, clock sequencing, bias generation, temperature sensing, and interfacing to the control and data acquisition systems.

All components of the RTM are contained within the camera cryostat vacuum space. The RSA and REC are maintained at an operating temperature of around -100ºC. This temperature is chosen as a compromise between sensor dark current and near-IR quantum efficiency. The REBs operate at a warmer temperature, to reduce the load on the cryo cooling system and to allow the use of standard commercial electronics. The power dissipated on the REBs is extracted via a cold plate that is held at -40C. To prevent volatile contaminants from condensing on the CCD imaging surfaces several precautions are taken: The circuit boards and components are tested for low outgassing of volatiles, CCDs are never allowed to be the coldest surfaces in the cryostat, and the REC includes a conductance barrier to minimize molecular flow towards the CCDs.

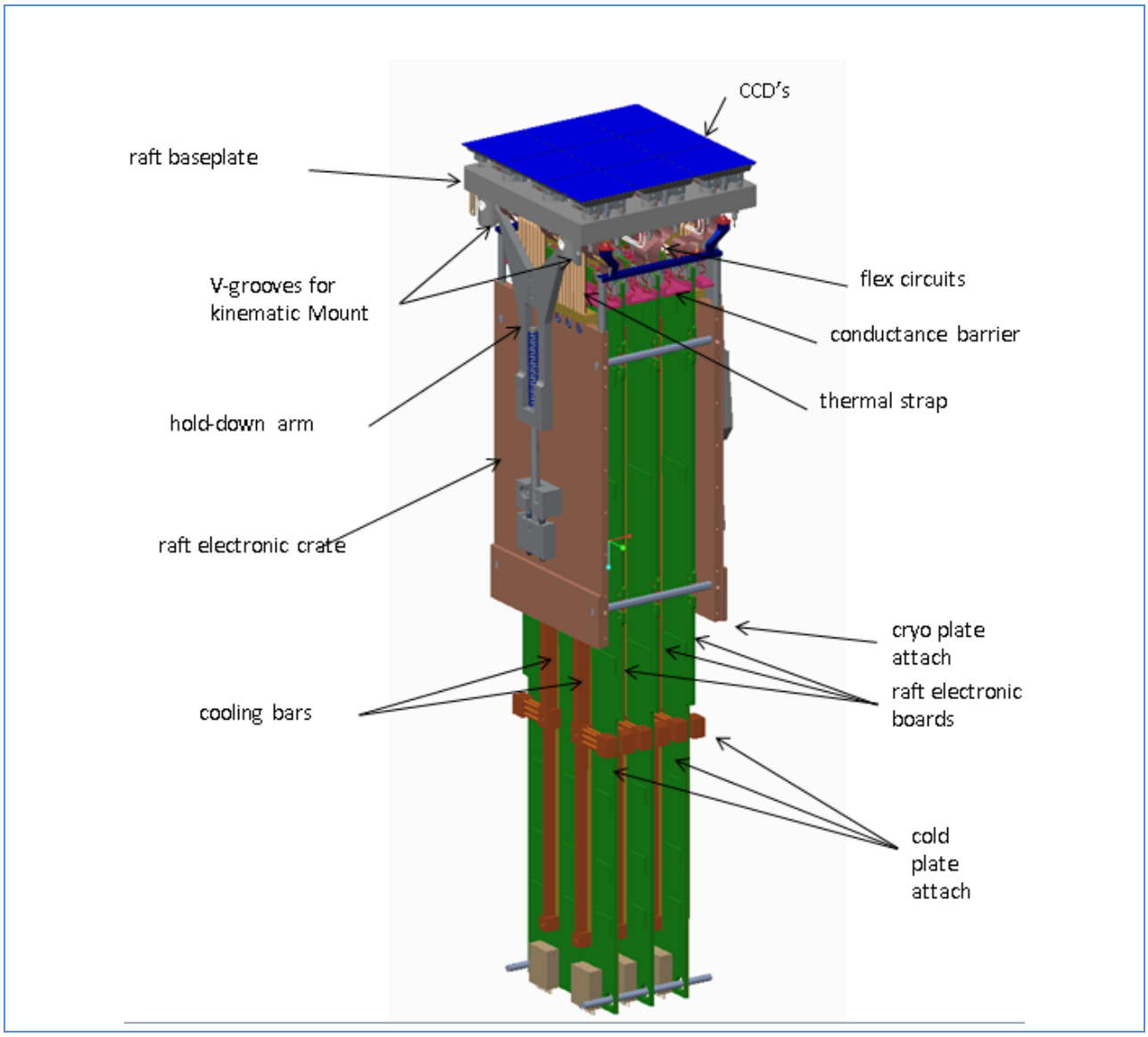

Figure 5-3: The Science Raft Tower showing 3x3 array of CCDs

5.3.3 Focal Plane Electronics

The major electronics subsystem is the readout of the CCDs in the science array. The electronics also include readout of the auxiliary CCD wavefront and guide sensors, temperature and voltage monitoring, as well as the electronics hardware located outside the cryostat that implements the Camera controls system and the power supplies and network interfaces that support the sensor readout and control functions.

5.3.3.1 Science Array Readout

The architecture of the science array readout is dictated by the four science requirements: 1) low read noise, 2) high dynamic range, 3) fast readout, and 4) low and stable cross-talk.

A salient feature of the readout is its raft-oriented structure. Each raft of nine CCDs has an independent electronics package. All of the raft based readouts are driven by a common clock to ensure strict synchronicity across the entire focal plane array. The readout electronics are located within the cryostat because of the high degree of segmentation in the sensors, which requires approximately 150 bond pads per sensor. The 189 science sensors plus four wavefront and eight guide sensors have some 30,000 connections to the electronics. Inclusion of the entire electronics chain within the cryostat reduces the number of high vacuum feed through connections by two orders of magnitude and allows the electronics to fit within the camera envelope. Close proximity of the front end electronics to the CCDs also permits short interconnections to be used, which minimize power, noise, and crosstalk. To control contamination due to outgassing from cables and electronics boards, the project has carried out extensive materials testing of component parts and has developed procedures to guarantee compliance with those requirements.

There are a total of 3024 video channels in the science array that are processed in parallel at a rate of 550 kpix/sec to achieve a frame read time of 2 sec at a power budget of about 300 mW/channel.

5.3.3.2 Raft Electronics Board (REB) design

One REB handles all readout and control for three CCDs. The video signal chain consists of a custom, eight-channel correlated double sampler (the ASPIC) and commercial operational amplifiers and 18 bit ADCs. The clocking and biasing of the CCDs is handled by commercial devices. Each CCD requires two ASPICs. Control of timing and movement of data is performed by a commercial medium scale Field Programmable Gate Array (FPGA). All timing is based upon a common central clock in order to synchronize the readout across the focal plane. Auxiliary functions such as temperature measurement, heater control and various diagnostics are implemented with commercial devices also controlled by the FPGA. High speed data moves from the FPGA via a copper link to outside the cryostat where it is converted to an optical signal and sent via long fibers to the DAQ system on the ground.

5.3.4 Cryostat

This section provides a high-level description of the Camera Cryostat. For analysis of general vacuum, thermal, and contamination control concerns affecting Camera performance, see Chapter 6. A detailed treatment of the Cryostat is presented in Chapter 12.

The Cryostat (Figure 5-4) structurally supports, thermally controls, and provides the contamination free environment that houses the Science and Corner Raft towers comprising the focal plane array.

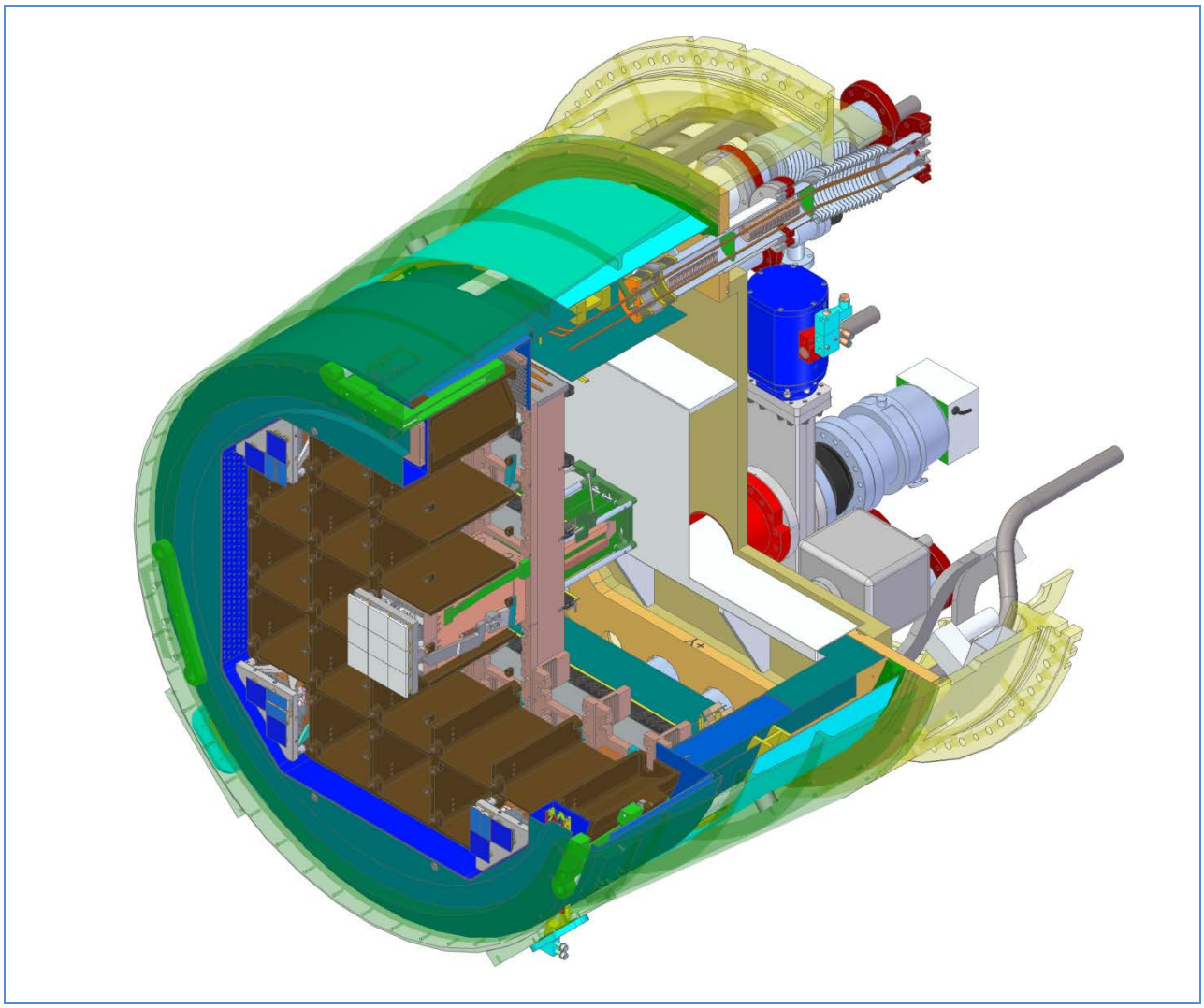

Figure 5-4: The Cryostat housing holds the Grid assembly. The Raft Towers are mounted into the square slots of the Grid.

The rafts holding the sensors are kinematically mounted to the grid assembly, where the SiC structural material and grid flexures provide mechanical isolation and minimize gravity and thermally-induced distortions. Sensor and electronics heat is removed by the Cryoplate, operating at -130 °C, and the cold plate operating at -40°C, both of which are cooled and controlled by a refrigeration system whose components lie in the utility trunk and the support building. Finally, the cryostat housing, along with the L3 entrance window, comprise a vacuum vessel which provides a base operating pressure of < 10^{-6} Torr for thermal insulation of the sensors and electronics. The structural support, thermal control, and clean insulating vacuum supplied by the cryostat provide the isolated and controlled environment needed for optimal operation of the focal plane array. Each of these functions is described in detail, below.

5.3.4.1 Structural Support: Kinematic Coupling and Grid

The cryostat structure is designed to provide a stiff support for the science sensors, while isolating them from the effects of external loads and environmental changes. The science and corner rafts are mounted

directly to an 18 cm deep SiC grid structure by way of ball-and-vee groove kinematic couplings, and held in place with pre-loaded compression springs. Prior to integrating the rafts, ceramic balls are installed onto the grid and aligned such that each of the three balls per raft form a plane, itself co-planar with all other balls across the grid. Rafts are assembled in advance with each of the nine individual sensors aligned to be co-planar and accurately offset from the plane defined by the vees in the bottom of the Raft. During Raft integration into the Cryostat, the kinematic features are coupled, providing very accurate and repeatable alignment of the detectors to form the single large focal plane. If necessary, any subsequent re-alignment can be accomplished by removing and re-lapping the ball support nests. The kinematic coupling design has been demonstrated to provide extremely repeatable positioning of rafts that is insensitive to differential contraction of materials during cool-down. Furthermore, the spring mounting system ensures a uniform and very stiff pre-loading that minimizes deflections of the structure while isolating the rafts from external load changes and distortions in the grid.

The grid itself forms the structural backbone of the support system. Because the camera must operate over a range of azimuthal and rotational orientations, the grid must hold the focal plane flat despite changes in bending and shear loads. As Figure 5-5 shows, maximum out-of-plane distortions have been held to less than 0.21 µm, using contraction during cooldown, reduction of the heat leak into the cold mass, and isolation of the grid from external loads imparted by distortion of the outer cryostat housing.

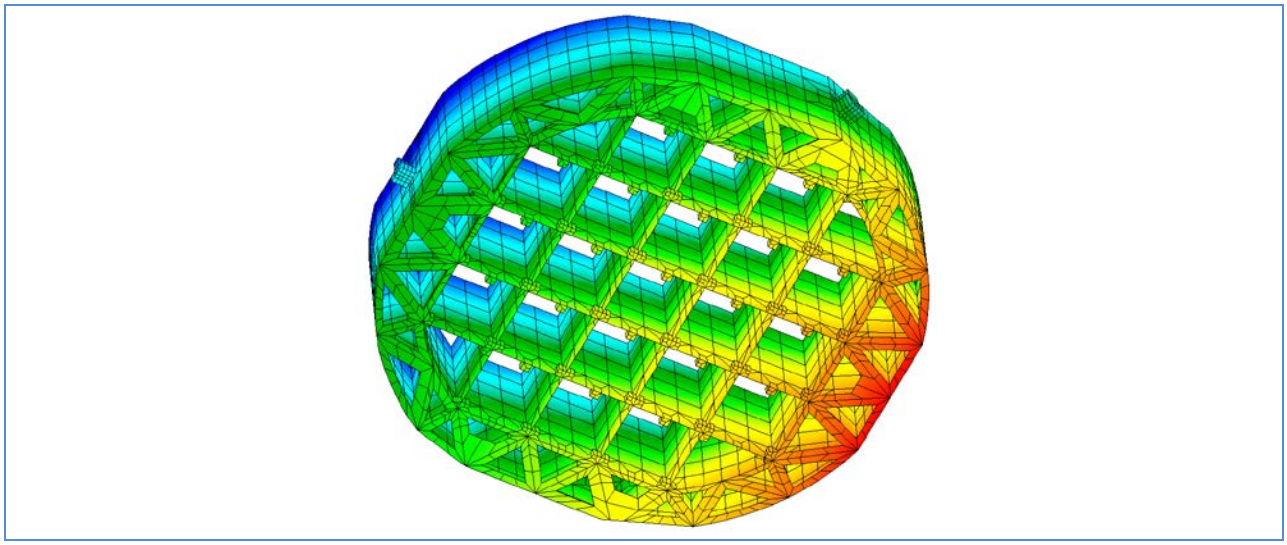

Figure 5-5: Grid distortion plot, with Camera at 30° elevation from zenith and no rotator angle, maximum peak to valley distortion = 0.21 µm

The grid is fabricated from a form of silicon carbide ceramic that provides the optimal combination of material and fabrication properties. SiC has a very high stiffness-to-weight ratio, coupled with a moderately high thermal conductivity and very low coefficient of thermal expansion. This combination of properties is not found in any metal, but is exactly what is needed for the optical bench-like structure required by this application.

While the grid and kinematic coupling support system provide the ideal structural design to allow us to meet our tight flatness requirements, they also allow for rapid, safe, and repeatable mounting of the

raft tower elements during system integration. The pre-loaded kinematic mounts provide very predictable interfaces that impart only gravity loads on the structure, while the mount design is simple and safe to mate up. This will help minimize the need for adjusting the position of rafts during integration, while reducing the risks associated with handling the delicate and high-value sensors.

5.3.4.2 Thermal Control: Cryo and Cold Plates

The cryo and cold plates remove heat generated inside the cryostat and provide a stable thermal environment for the sensors and grid support structure. The cryo plate also provides the mechanical support for the Raft Electronics Crates (RECs). The cryo plate, operating at -130ºC, removes over 500 W of process heat generated by the operation of the sensors and the radiant heat impinging on themfrom the warm L3 lens. This is conducted back through the REC structure - bypassing the grid-to the cryo plate, where it is removed by refrigerant running in channels through the cryoplate. Likewise, the -35ºC cold plate removes process heat generated by the REBs. Both plates include temperature sensors and heaters to stabilize their temperatures and speed the warm up of the cryostat.

The cryo and cold plates are fed by separate refrigeration compressor systems located in four environmentally controlled cabinets under the telescope mount assembly. These systems supply high-pressure mixed refrigerants at ambient temperature that are then expanded in capillaries housed in the counterflow heat exchanger module behind the cryostat. They are then flowed through the plates where the refrigerant absorbs the heat. The refrigerant returns to the compressors at ambient temperature after leaving the heat exchangers. The refrigeration system is discussed in more detail below.

Other than heat removal, another important function provided by the cryo plate thermal control system is thermal isolation of the grid and sensor rafts. The grid is cooled by two thermal straps running down to the cryo plate within each bay. The cryo plate itself includes radiation shrouds that surround the grid on all sides, including a picture frame around the front perimeter. These shrouds intercept radiant heat from the warm cryostat housing and conduct it back to the cryo plate, which significantly reduces the overall heat load on the grid. The low heat load on the grid, coupled with the use of low-expansion SiC, results in extremely low thermally-induced distortions due to both cool-down contraction and residual temperature gradients in the grid. Our thermal-distortion analysis predicts that even under worst-case heat-loading conditions, the maximum expected out-of-plane distortion of the grid due to temperature gradients is on the order of tens of nanometers, factors of 100 below our tightest requirements.

5.3.4.3 Vacuum Environment: Housing and Feedthroughs

The cryostat housing is a conical aluminum vessel, approximately 94 cm diameter at the base and 74 cm long. Contamination due to outgassing by the various components contained in the cryostat is a concern because of the possibility that desorbed materials will migrate to the cold sensor surfaces and modify the quantum efficiency of the detectors. To minimize this effect, the interior of the vessel is cleaned and baked out, and all flanged penetrations are either welded or contain double Viton O-ring seals. Furthermore, the cryostat has been divided into regions with low-conductance barriers.

The cryostat housing is closed out with flanges on the front and back ends. The front flange of the vessel supports the L3 lens, which carries the atmospheric pressure differential while being clamped between Viton gaskets around its perimeter. The rear flange is comprised of an outer annulus containing high density signal, instrumentation, and power feedthroughs, and inlets and outlets for vacuum-insulated refrigerant lines. The central octagonal part of the rear flange supports a turbo-molecular pump, a residual gas analyzer head, vacuum valves, and vacuum instrumentation. The octagonal plate is removable to provide access for inserting or removing raft towers.

5.3.5 Camera Body and Mechanisms

This section provides a high-level description of the camera body and of mechanisms built to provide Camera exposure control and filter exchange. For general principles of the Camera's mechanical design, see Chapter 6. Other detailed treatments of subsystems introduced here are covered in:

- Chapter 15 for Camera Body
- Chapter 13 for Filter Exchange
- Chapter 14 for Shutter

5.3.5.1 Camera Body

The aluminum back flange and outer housing provide interfaces and supports for most of the camera components. The back flange mounts to the telescope rotator around two bolt circles. The annular flange has a large central hole in it, through which the cryostat is inserted into the camera, and off of which the cryostat and filter carousel are supported. The flange is flat in this inner region, but flares out to a triangular cross-section at its outer diameter to stiffen the interface and reduce deflection. Cut-outs in the cross-section provide pockets for carousel motors and control electronics, and for routing cables out of the camera. The camera housing mounts around the outer perimeter of the flange with another bolt circle.

The housing fully encloses the back-end two-thirds of the camera volume. Cut-outs in the housing provide access to the inside of the camera for maintenance, but the portholes are sealed off during normal operation. At the front end of the housing, a flange stiffens the free end and provides a structural mounting interface. The shutter mounts to this interface ring, as well as the struts that support the L1/L2 assembly. The auto changer bolts and pins into a cut-out in the front end of the housing, adding stiffness to the housing and closing out the notch.

Finally, a gas-tight shroud bridges between the front end of the housing and the L1/ L2 assembly support ring. This completes the hermetic seal of the camera volume to ensure that it remains clean and thermally stable.

5.3.5.2 Shutter

The shutter for the LSST camera lies tightly packaged between the L3 lens/cryostat window and the filter. It controls the length of time that the sensors on the focal plane are exposed to an image while blocking out all stray light when closed during read-out of the CCD sensors. The shutter is a double-acting guillotine-like device, where plates move across the focal plane to start and end an exposure. Guillotine shutters have been used on a number of cameras, but tight lateral space constraints have

forced us to segment the one-piece shutter into two pieces, as shown in Figure 5-6. The two blades are stacked up when the shutter is open, then slid over the field of view in a coordinated telescoping motion to close.

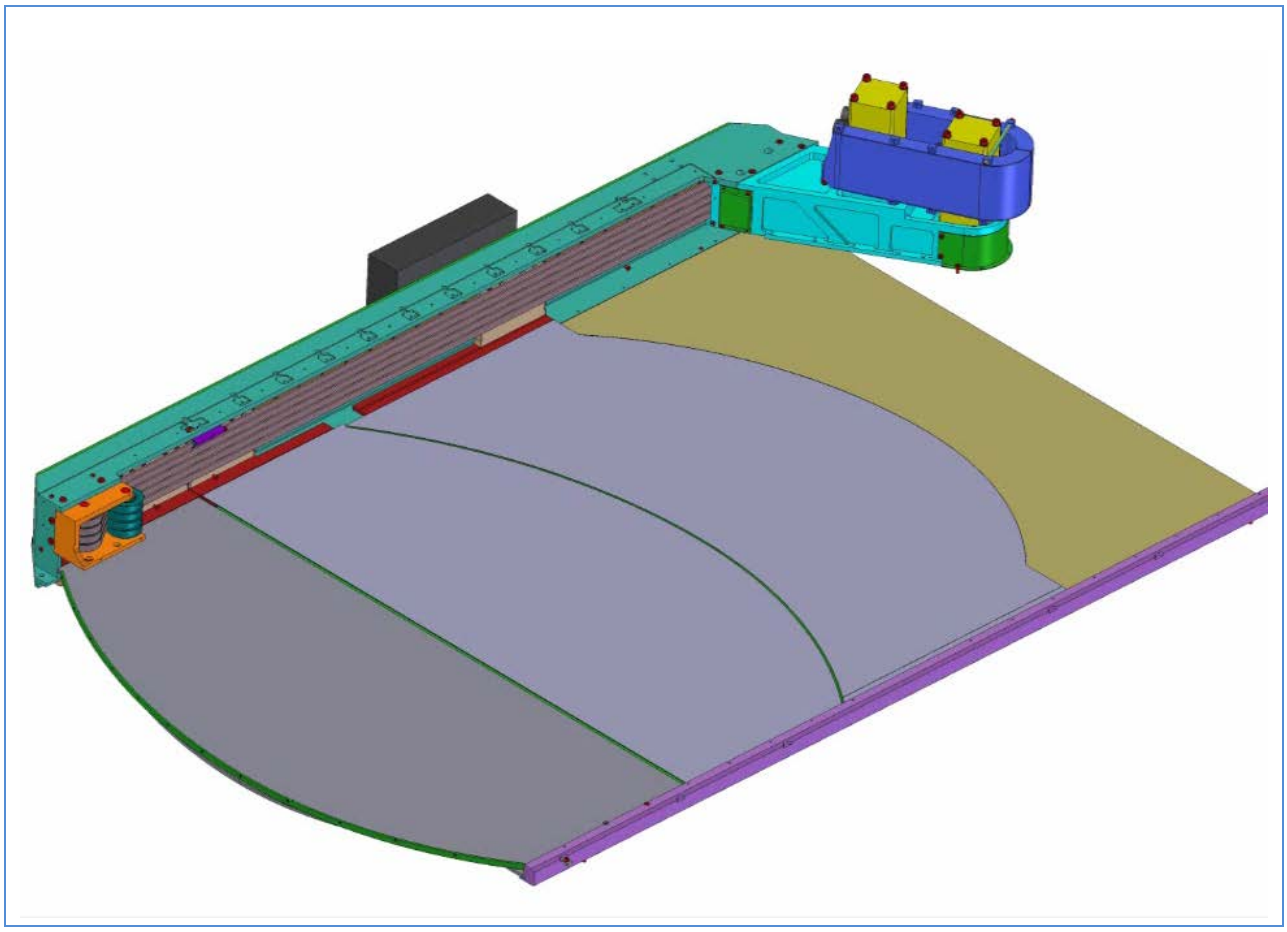

Figure 5-6: Shutter in Closed Configuration.

To maintain exposure time uniformity across the FOV, two sets of blades are used. The first moves off to one side to clear the FOV to start the exposure, then the second set of blades occludes the FOV by coming on from the opposite side, and traveling in the same direction as the first. For the next exposure, the process is reversed. This provides a more uniform exposure time for all pixels, since the first pixel exposed by the trailing edge of the first blade set is also the first blocked by the leading edge of the second.

5.3.5.3 Filter Exchange

The Filter Exchange system provides the capability to change filters remotely during the course of nighttime Telescope operations. Given the survey nature of LSST and the multiple science programs that the observatory is supporting, filter changes will be a regular occurrence during a typical night of operation. Thus, the filter exchange system must reliably and safely change filters quickly and with minimal impact on the nightly observing schedule.

The Camera houses five on-board filters for fast-90 second-filter changing during nightly viewing, and includes the capability for swapping in a sixth filter during a daytime maintenance access. The Filter Exchange system includes three sub-assemblies to provide this functionality. The Carousel stores filters that are not in use inside the clean environment of the camera housing, arrayed in an annulus around the outside of the Cryostat. It rotates to move filters into position for placing them on-line when needed. The selected filter is moved into the FOV by the Auto Changer. This mechanism includes rails that support wheeled trucks that hold a filter and shuttle it from its slot in the Carousel, forward and around the edge of the Cryostat and L3 lens, to the on-line position between the L2 and L3 lenses.

Finally, a manual Filter Loader is used for swapping in a sixth filter during daytime access. The Filter Changer engages with the internal Auto Changer rails to ensure a clean, smooth, and safe hand-off of the filter. All three of these assemblies ensure that the large-diameter filters are handled safely, and can be accessed and brought on-line quickly to maximize viewing time.

5.3.6 Camera Control System (CCS) and Data Acquisition (DAQ)

This section provides a high-level description of the CCS and DAQ subsystems. Additional detail is provided in the CCS discussion, Chapter 16, and the DAQ discussion, Chapter 17.

The CCS and DAQ together provide the core functionality for orderly collection of images from the focal plane and their transfer to the clients. The CCS controls and coordinates the various Camera subsystems. The DAQ acquires, processes, and buffers incoming data and makes it available to the clients.

5.3.6.1 Camera Control System (CCS)

The CCS interacts with the LSST observatory and human operators, receiving commands and sending and receiving the data necessary for coordinated operations.

• It makes sure that operations, both during science and calibration modes, proceed efficiently.

• It monitors Camera performance, maintaining a stable Camera environment and reporting errors.

• It provides human interfaces both to display status information and to provide test, diagnostic, and debug capability.

The core CCS infrastructure component provides a set of buses used to transport messages between components. The types of messages include commands, status, and logging and alarms. The infrastructure includes mechanisms to control device access and dependencies between components.

The CCS controls the Camera via a set of "CCS subsystem" software modules. Each module is a Java process that uses the bus infrastructure defined above to receive commands and communicate status information. These modules also communicate with the Camera subsystem hardware, possibly using private or proprietary protocols. Complex Camera subsystems (e.g., the DAQ and the Filter Exchange system) will require several modules. In those cases, a higher-level module will coordinate their operation. During engineering or diagnostic operation, each subsystem is capable of autonomous operation.

The control of CCS is implemented via "consoles". A CCS console is a Java process that is capable of receiving instructions (e.g., from the OCS or a human), issuing commands to CCS subsystems, and displaying responses, telemetry, and other Camera status.

5.3.6.2 Data Acquisition (DAQ)

The Camera's DAQ provides a direct connection and interface with the sensors and electronics contained within the camera's Focal-Plane-Array (FPA). Pixels are digitized with 18 bits of precision. In nominal operation both science and wave-front sensors are exposed for 15 seconds and readout completely in 2 seconds, while a subset of the pixels from each of the eight guider sensors are exposed and readout with a faster cadence averaging 9 HZ. With respect to its FPA the DAQ System must satisfy four necessary functions:

- Acquire, buffer and catalog its acquired pixel data.
- Provide both buffered and streaming access to these data.
- Generate and distribute a common system reference clock.
- Provide access to its electronics for the purpose of configuration, monitoring & control.

These two functions are expressed through a set of four different services. These services allow:

- Notification, through subscription of incoming data.
- Retrieval of buffered data for both science and wave-front sensors.
- Access to streaming interface for guiding.
- Access to FPA electronics for purposes of configuration, monitoring & control.
- Management of reference clock and timing.

Users access these capabilities through application-specific-software on commodity hardware. Any such software is considered a DAQ system Client. The execution platform for a client is a Host. A host is a commodity processor operating under LINUX connected to the DAQ system through a 10-Gigabit Ethernet. Clients gain access to the various DAQ services through a set of DAQ system provided software Interfaces. These interfaces hide from the client the underlying communication mechanisms implemented between host and DAQ system.

These relationships are summarized in Figure 5-7 below.

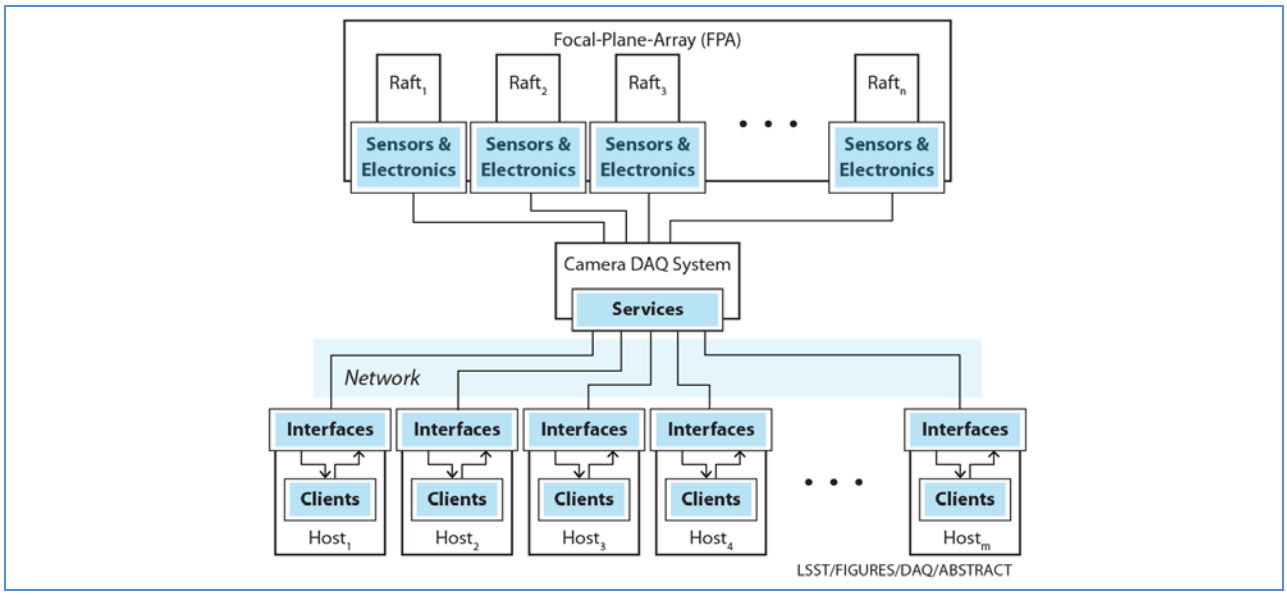

Figure 5-7: Abstract model of the DAQ system and its interfaces

5.3.7 Operations

5.3.7.1 Control, Timing and Telemetry

Overall control of the Camera has been allocated to the CCS.

During Observatory operations, the CCS will accept commands from the OCS and will control the Camera activities accordingly. All activities on the Camera (with the exception of low level interactions between the DAQ and DM and DAQ and telescope) are sequenced by the CCS. The sequences that the CCS controls are

1- Power up
2- Vacuum/thermal initialization
3- Exposure control
4- Filter changes (both external and internal)
5- Thermal control

The CCS gathers engineering telemetry from the Camera subsystems. That engineering data (as well as data from the CCS itself) is passed to the OCS, where it provides part of the metadata used to interpret the science data. The OCS will perform the detailed health checks on that data (including trending), while the CCS performs a monitoring and alarming function to alert the operators of specific conditions.

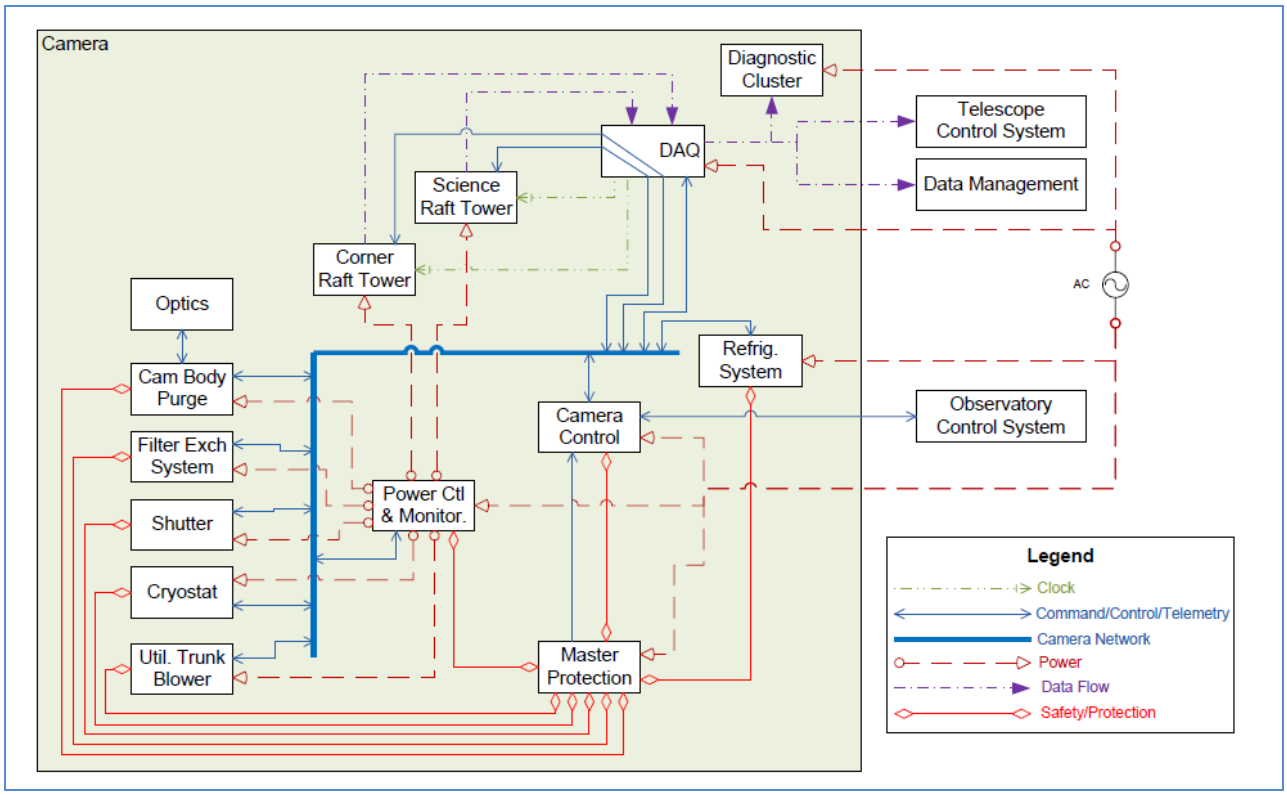

Figure 5-8: Camera logical block diagram

The CCS also provides the ability to control the Camera in absence of other observatory subsystems. This capability will be used during Camera level integration and test as well as for Camera maintenance during operations.

5.3.7.2 Exposure control

The exposure sequence taken by the observatory is separated into visits. The standard visit consists of a telescope move to the desired position and two 15 second exposures. For efficiency, the readout of the second of the two exposures is in parallel with the move to the next visit position. The Camera is given the command to start the visit and sequences its internal operations to implement the two exposures of the visit.

The Camera allocation for this activity is 34 seconds. The primary drivers for the timeline are shutter motion, 15 second exposure, and readout times. The control interactions between these activities are in the millisecond regime. Note that the 15 second nominal exposure actually takes 16 seconds. This is caused by the finite shutter opening time. The CDD clear and shutter initialization occur just before the start of the visit in parallel with the telescope slew.

The OCS initiates the activity by sending a command to the CCS. The CCS provides a positive response to the OCS and directs any overhead activity needed to get ready for the exposure. The CCS then performs a CCD clear. The CCS then directs the shutter to open. As the shutter opens, the science sensors and wavefront sensors begin to integrate the incoming light and continue to do so through the exposure. In

contrast, the guide sensor is repeatedly read out during the exposure and provided to the telescope guide system.

5.3.7.3 Data Flow

The data flow for the Camera is allocated to the Rafts and to the DAQ. The Rafts digitize the signal and forward that data to the DAQ. The DAQ processes that data and routes it to either the DM or the Telescope Control System. Three sensor systems generate data (science, guider and wavefront). The science and wavefront data are used by DM. The wavefront and guider data are used by the Telescope Control System.

Science data is provided in both raw and processed form. Processing corrects for crosstalk and the data is provided near real time to subscribers. The raw data is persisted by the DAQ and provided on demand. Raw science data is persisted for over 2 days to allow Observatory operations during loss of communications between the mountaintop and Data Management system in the Base Station.

While some metadata naturally accompanies the science, wavefront and guider data, the CCS compiles additional metadata to define the Camera state, health and engineering data. This metadata follows a separate path from the CCS through the OCS to the engineering and facility database.

Data from Science and Corner Rafts are routed as copper signals through feedthroughs in the Cryostat. After a short run (to minimize possible interference) those signals are converted from electrical to optical. The light fibers are routed out of the Camera, through the telescope and down to the DAQ in the computer room. The DAQ communicates to the DM and the telescope control system through 10Gbit-Ethernet.

5.3.7.4 Guide/Wavefront Sensor System

The Camera provides the guide and wavefront sensors for the telescope. This has the advantage of eliminating the alignment offsets that would occur if those sensors were outside the complete optical path.

The Camera provides four wavefront sensors, one on each corner of the focal plane. The wavefront sensor is a split detector with a step in the z direction so that half of the detector is above the focal plane and the other half is below the focal plane. The characteristics of the out-of-focus images on the two halves are used by the telescope to determine the relationship of the science focal plane to the ideal focus. Processing is used to compensate for slow variations and is not carried out in real time.

The Camera provides eight guide sensors, two in each corner of the focal plane. Each guide sensor is a single CCD that is used real time during the exposure to tune the telescope pointing. The camera to telescope interactions have been carefully thought through to ensure an efficient control loop architecture. The telescope defines a small window for each sensor. The camera reads out those windows from each guide sensor at 9 Hz when the shutter is open and feeds the raw data to the telescope. The telescope generates the guide star centroids from each window and uses that position information in the control loop for the telescope pointing.

The control loop is somewhat complicated because the guide sensors are behind the shutter and only exposed when the shutter is open. The design approach addresses this startup transient (as well as imprecise telescope pointing to account for large traverses) by starting with a larger window for the first readout of a guide image. The telescope uses that larger window to determine the location of a smaller window to use for the remainder of the exposure. The achieved sampling rates, noise and latencies have been analyzed by the LSST Telescope team and positive margin demonstrated.

5.3.8 Camera Integration and Test

This section provides a high-level discussion of the Integration and Test subsystem. The individual subsystem chapters provide details on assembly and test at the subsystem level. Chapter 19 provides a complete description of the I&T effort.

Camera Integration and Testing (I&T) will be carried out in a new clean room in the IR-2 hall at SLAC. The facility includes approximately 2000 square feet of class 1000K clean room, 1500 square feet of office space and a 160 square foot cooled server room. Inside the clean room a dedicated air-handling system provides temperature and humidity control, with HEPA filtration and top-down air flow. The clean room also includes a full-coverage anti-static floor and grounding points throughout for personnel electrostatic discharge (ESD) control and equipment safety grounds. Other features include nitrogen and air purge systems, a wet-pipe sprinkler system, remotely-accessible temperature and humidity monitoring with automated alarm system.

Facility use plans and support equipment designs have been developed along with the design of the Camera. This was partially necessitated by the large physical size of the Camera. Step-by-step integration processes have been developed for the large sub-assemblies, and each step was evaluated for height, floor-space, and access constraints within the facility clean rooms as well as future space available on summit. Integration sequence evaluation was also performed to assess the requirements and configuration for the support fixturing that is needed. This has resulted in a comprehensive list of the support hardware, along with requirements imposed on the hardware to fulfill its function during the I&T process.

Finally, integration sequencing was used to inform the design of the Camera hardware itself. Many design features and implementation choices of the hardware design have been driven by the integration planning process in order to ensure that all hardware can be safely and precisely integrated, accessed by the appropriate fixtures and test equipment, and safely tested in its as-installed configuration.

The Camera will be assembled from pre-tested and verified sub-assemblies and components. To reduce technical and schedule risk associated with the integration process, care has been taken to develop modular designs for all components that can be pre-verified with bench testing. This assures that only fully-performing modules are integrated into the overall Camera and reduces the risk of test failures and problems during the integration and test process. Modular designs also serve to reduce the complexity of the component interfaces and reduce the time for integrating, servicing, and removing a component.

Camera integration work is divided into four phases. First, raft towers are loaded into the cryostat, and the detector plane array is incrementally tested. This process is repetitive, with timing largely driven by

the availability of science raft towers. Dedicated fixtures and test equipment will be used to standardize and control the process, thereby reducing the risk of damage. The utility trunk will be integrated during this process to provide the system electronics and refrigeration system connections needed for cryostat cold-testing. Initially, the utility trunk will be detached from the rest of the cryostat, but ultimately it will be mounted to the back end of the cryostat housing for final testing.

During integration of the rafts onto the grid, a non-contact metrology station is utilized in the clean room. Two commercial non-contact laser triangulation heads are mounted together on an XY stage which is supported off the cryostat stand. One head measures the distance to a reference flat and the second head measures the distance to the camera sensor surface. This two sensor method removes z-jitter effects by determining distance between a reference flat and measured surface rather than distance between the head and triangulation head alone.

After closure and pump down of the cryostat, measurements are taken through the flat optical window (L3 replacement), substituting one head for a longer range laser-head with 1 µm precision and applying fixed corrections for the optical path. After the cryostat is fully loaded and L3 installed metrology may be repeated once more.

In parallel with cryostat integration, the shutter and exchange system will be integrated into the Camera body. These large subsystems will be fully tested prior to delivery, so the integration process involves mounting and mechanical alignment, then re-testing of the systems in their final configuration.

Once the cryostat is fully integrated and the Camera body loaded, the two major assemblies are joined by sliding the cryostat into the Camera body. The two assemblies are only coupled at the back flange of the Camera, so the integration process is straightforward. The L1-L2 assembly is also mounted during this final integration phase.

The final step of Camera I&T is system-level verification testing. This will be accomplished through a series of targeted tests. First, optical component positions will be measured to ensure they are correctly aligned. Then, the Camera Calibration Optical Bench (CCOB) will be used to verify both optical performance of the Camera and to characterize any ghost imaging and the effects of stray and scattered light.

6: Camera Architecture

6 Camera Architecture

6.1 Introduction

The Camera design is described at a high level in Chapter 5, and details of its subsystems are addressed in the remaining chapters of this Report. This chapter discusses architectural aspects that cut across subsystem boundaries, addressing the Camera as:

- An optical system
- A focal plane system
- An integrated structural system
- A system requiring integrated power distribution

This chapter also describes the Camera Protection System.

6.2 The Camera Optics System

Chapter 5 describes the optical design of the Camera. The design of the Camera lenses and filters is covered in detail in Chapter 7. This section addresses cross-cutting mechanical, contamination control, and thermal aspects of the optical design.

6.2.1 Mechanical Considerations

The Camera design includes important considerations to improve the optical behavior of the system. These considerations include designing for the control of stray and scattered light, implementing thermal design features, and including provisions for correcting for mirror as-built figure errors.

6.2.1.1 Control of Stray and Scattered Light

The large aperture and wide field of view of the Camera allow for accepting a considerable amount of on-axis celestial light, but also off-axis scattered light. Furthermore, the sharply converging light cone inside the Camera means that there are many non-optical elements visible through the L1 lens that can potentially reflect scattered light back onto the detector plane. These potential sources of stray and scattered light are handled both by clearly defining the optical path geometry and carefully choosing surface treatments. The optical path geometry is defined in two ways, both of which can be seen in

Figure 6-1. First, knife-edge aperture rings clearly demark the outer diameter of the field of view at the entrance window, as well as before the L2 lens, before the filter, and entering the cryostat at the L3 lens. These aperture rings clear glancing-angle stray light entering the Camera just off the main beam. Second, higher-angle stray light is captured by a set of veined baffling rings between L1 and L2. These stair-stepped baffles reflect stray light back away from the field of view onto absorbing surfaces. The baffles and aperture rings provide geometrical barriers to prevent stray and scattered light from reflecting off of Camera structural elements and back to the detector plane.

Apart from geometric design considerations, all surfaces with a view of the main field of view volume are also treated with light-absorbing surface treatments. For many surfaces, this involves coating surfaces with high-emissivity, low reflectance black paint. Inside the cryostat, surfaces are treated with similar low-reflectance surface treatments that are compatible with our vacuum.

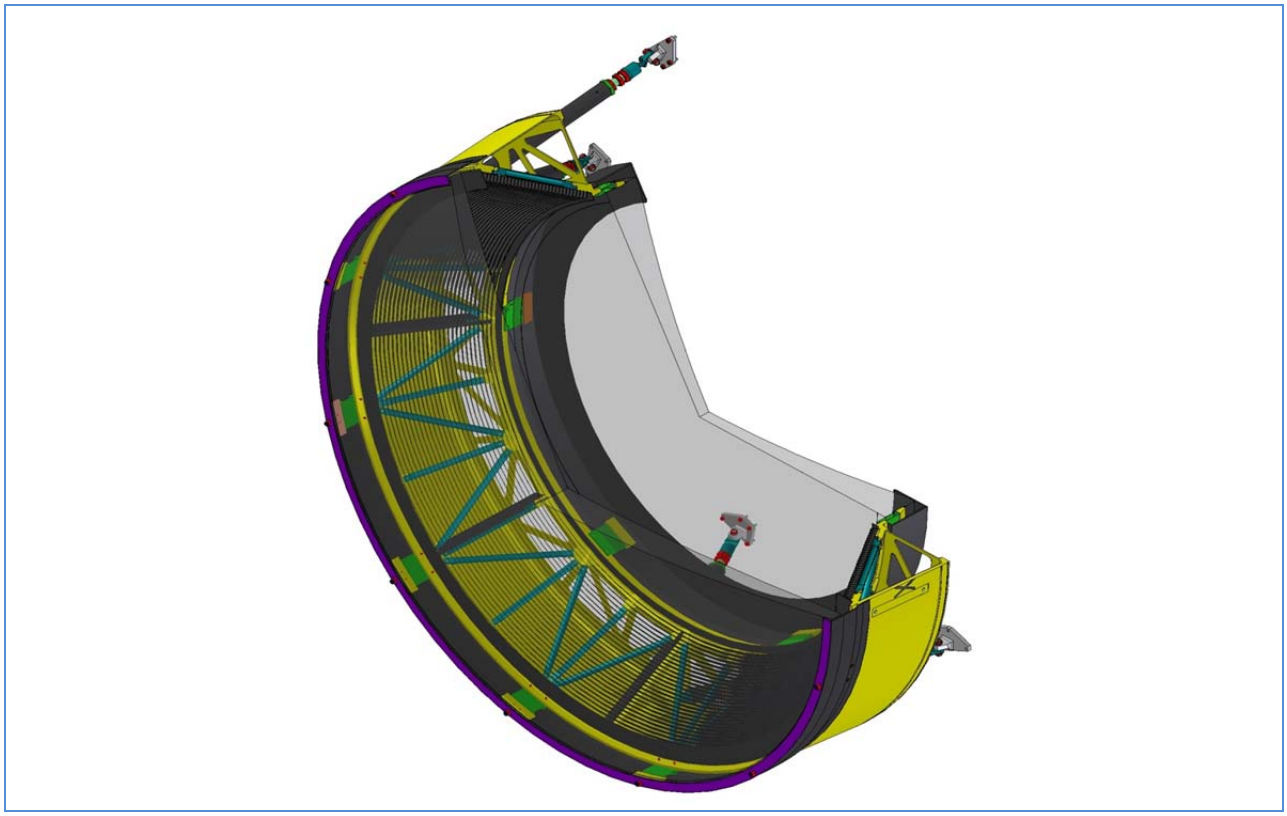

Figure 6-1: Section of the L1-L2 Assembly, showing aperture rings at the entrance and in front of L2, along with light baffle rings between the lenses and a light trap around the perimeter of L2

6.2.1.2 Athermal Design Considerations

The Camera must be able to fully function over a broad range of altitude and rotation angles, but also over a broad temperature range. Furthermore, inside the cryostat the cold mass must be able to operate at its low working temperature while maintaining alignment to the room-temperature lens. The Camera design includes four design features to “athermalize” the design, ensuring that it can function over its entire operating temperature range.

First, at the largest scale, the cryostat and Camera body are both made from aluminum to match their coefficients of expansion (CTE). The L1-L2 assembly is supported off the front of the Camera body by very low CTE carbon fiber struts, ensuring that as the Camera warms and cools, the relative axial spacing between the lenses remains unchanged.

Inside the cryostat, two additional features are used. Flexures are used both for structural and thermal isolation, but also to allow for shrinkage of the cold mass during cooldown. The radially-flexing flexures allow for contraction but maintain the cold structure centered on the bore of the cryostat. Flexures are used to support the Grid, Cryo Plate, and Cold Plate, ensuring that all three remain centered on the boresight. Furthermore, for the Grid in particular, low-CTE materials have been used to reduce the magnitude of thermal motion during cooldown. The Grid itself is manufactured from very low CTE Silicon-Carbide, while its support flexures are made from titanium for improved thermal insulation and flexing ability, as well as its moderate CTE. These reduce the overall magnitude of motion of the detectors and best-fit detector plane to the warmer lenses outside the cryostat.

6.2.1.3 Adjustment Capability

The final optical design capability added to the Camera is the ability to optically correct for as-built figure errors in the mirrors. This is done by leaving provision to adjust the relative position of the L3 lens with respect to the detector plane, as well as the ability of moving the L1-L2 assembly with respect to the filters, L3, and the detector plane. These provide two knobs to turn to improve overall focus image quality. For the detector plane to L3 lens separation, this adjustment is made by adjusting the stand-off distance between the support Grid inside the cryostat and the common front flange that supports both the L3 lens and the Grid. For the L1-L2 assembly, the adjustment capability is built into the range of the six-strut support system, allowing this spacing to be tuned at any time.

6.2.2 Camera Contamination Control

Outside of the cryostat cold mass, the remainder of the Camera volume also requires a clean operating environment. There are two primary reasons for this need for cleanliness. First and foremost, any particulate or outgassing materials could be deposited on one of the lens or filter surfaces inside the Camera. While this does not significantly affect the image quality, long-term contamination can impact the overall system throughput, reducing the Camera's sensitivity to faint objects. Furthermore, the surfaces of the optics inside the Camera are not easily accessible and are difficult to clean, so the Camera environment must be clean enough to obviate the need for cleaning at intervals less than yearly.

The second motivation for maintaining a clean environment inside the Camera is that this needs to be compatible with our clean room facility cleanliness. During maintenance, the Camera will be moved into on-site clean room facilities and opened up for preventative maintenance and any repair. This will expose the contents of both the Camera and utility trunk to the clean rooms. Given the large number of trapped volumes and difficult-to-clean regions of components in both volumes, it will not be practical to re-clean them if they were to get dirty or contaminated. Thus, our plan is to clean them at the component and sub-assembly level, then keep them clean during normal operation.

6.2.2.1 Camera Volume Cleanliness

As part of the Camera design and planning process, we have invoked four design principals to provide for the cleanliness of components in the Camera body and reduce the risk of contamination of the optics. First, the Camera body and supporting structures completely encompass the Camera volume, including all of the Camera optics, in a sealed and clean environment. Thus, the clean innards of the Camera are completely isolated from the dirty dome environment surrounding the Camera, keeping all of the optics except the first surface of the L1 lens in a relatively pristine state.

Second, all components being installed in the Camera body are being designed to meet cleanliness requirements for a class 10,000 clean room (ISO Class 7). This constrains the choice of materials to those that do not shed particles and with low outgassing levels to prevent "fogging" due to outgassing of highly volatile plasticizers in some materials.

Third, the Camera is using a "good-neighbor policy" to address contaminants at their source. In short, if subsystem hardware is likely to produce contaminants, then they are expected to provide for reducing the rate of production to acceptable levels, cleaning up the contaminants, or trapping them to prevent them from spreading. This principal is being used in the design of the shutter and filter exchange system, where elements of the motion control systems will wear, possibly generating particulate contamination.

Finally, many components with a higher contamination risk have been located in the utility trunk, where contamination is less of a concern. This includes the ducting and instrumentation racks for the Camera purge systems, as well as much of the control, communication, and power electronics for the Camera and cryostat components. While these components will be cleaned and kept clean, their geometries make them prone to collecting contaminants. Keeping these out of the Camera volume will reduce the risk of contamination introduced by them affecting the optics.

6.2.2.2 Purge Systems

Other than the passive design and materials choices we have made to maximize the cleanliness in the Camera volume, we have also implemented active purge systems to continuously clean the air in the volume and remove any particulate contamination that may have been introduced or created. Actually, two purge systems are used in the Camera volume to further isolate electronics and other heat-producing components, as well as stabilize the temperature of components and remove contaminants.

The Mechanism Purge system constitutes a volume completely isolated from the Camera volume. It actively cools power and control electronics and motors mounted on the exchange system and shutter units mounted in the Camera volume. These heat-producing components are completely contained in electronics boxes and shrouds and are actively cooled with cooled air.

The Camera Volume Purge system then filters and conditions the air in the Camera volume proper. The entire volume operates at a very slight overpressure to reduce the chance of contaminants entering the clean volume, and the entire air volume is recycled through a heat exchanger and filters to clean the air of volatiles and particulates and to stabilize its temperature. Desiccants also ensure that the dew point is sufficiently low to keep the humidity of the air controlled and reduce the risk of condensation on the cold L3 lens outer surface.

6.2.2.3 Clean Access

During normal operation, the design principals and active purge system are expected to produce a very clean environment inside the Camera. However, during routine maintenance, personnel could introduce contaminants into the clean volume while working in the dome. This is especially a risk during filter swap-out, which will happen on a regular basis. To both keep the filters clean and reduce the risk of contaminating the Camera volume, the filter loader has been designed to maintain the hermetically-sealed volume during a swap-out. Thus, a filter will be swapped out without exposing the Camera volume, the outgoing filter, or the incoming filter to the dome environment.

Besides swapping filters, maintenance activities are also expected to require access to the mechanisms to check for wear or troubleshoot a problem. For this, we will lower a clean tent over the entire Camera and purge it with dry filtered air, essentially establishing a clean micro-climate around the Camera. After cleaning the outside of the Camera, we can then access the clean inner volume through hatches and removing the sealing shroud, using clean room protocols to carry out the maintenance work.

To limit the amount of access needed to the Camera volume, much of the on-board electronics have been moved to the Utility Trunk. These are also accessible for replacing a damaged board, but the Camera volume does not need to be accessed to perform this maintenance.

6.2.3 Camera Thermal Control

Outside the cryostat, component thermal control is a concern for two reasons. The primary driver for maintaining thermal control of the Camera is that since the Camera sits in the main beam of the telescope in front of the M2 mirror, differences between the Camera skin temperature and that of the dome air will create natural convection plumes between the mirrors. Plumes produced by large temperature differences would have an impact on the delivered image quality of the telescope optical system, especially when the wind speed is low or the telescope is pointed into the wind when there is little flushing of the dome air.

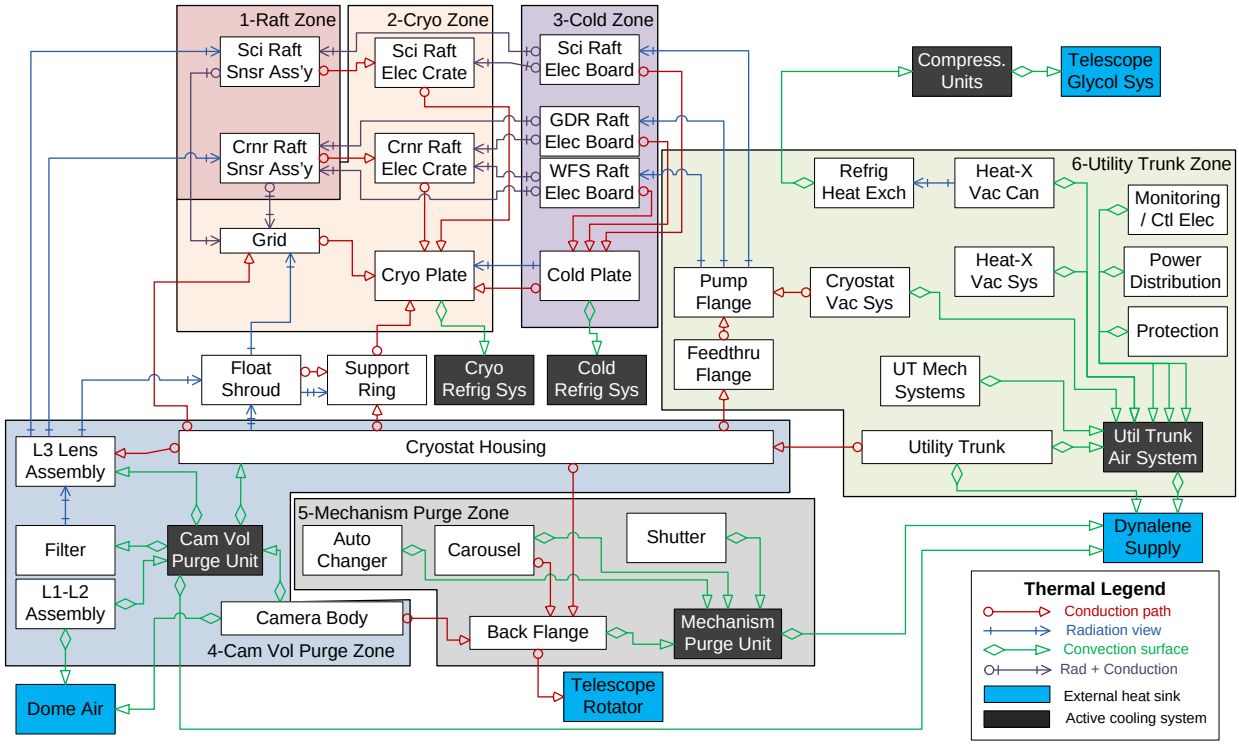

Figure 6-2: Camera thermal block diagram

The Camera skin and internal temperatures also need to be controlled to reduce natural convection cells inside the Camera. Here, the L3 lens will operate colder than any other components since it is radiating heat to the cold mass inside the cryostat. This constant cold source could produce natural convection plumes inside the Camera much as cold windows do in a house.

6.2.3.1 Passive Thermal Management Features

Temperature control is handled first by removing heat-producing elements from the Camera volume. Most power-consuming elements—including controllers and single-board computers—have been moved to the utility trunk to eliminate the source of heat. The remaining heat sources include only the motors and controllers that operate mechanisms in the shutter and filter exchange system. While the shutter and carousel motors, in particular, are relatively high-powered motors, their duty-cycle is low so their average power draw is on the order of a hundred Watts, total. This heat is removed by forced air from the Mechanism Purge system.

6.2.3.2 Active Control

The Camera Volume Purge system is used to stabilize the skin and volume temperature and remove the process heat produced by the few remaining components. The net heat load inside the volume is close to zero, since the average heat generated by the low duty-cycle motors is offset by the constant ~100 W cooling provided by the L3 lens. The primary issue is to maintain a uniform-temperature volume throughout the Camera.

The purge system provides the source of constant-temperature air to stabilize the Camera temperature. Temperature-controlled, dry, filtered air is blown in from the purge cabinet in the utility trunk through channels on the outer housing of the Camera forward to the front end, where it exits the channels and is blown onto the inside surface of the L1 lens. This actively stabilizes the skin and L1 lens temperature to match the dome temperature, allowing the Camera to track the outside air temperature as it changes during the night.

From the front end of the Camera, the purge air filters back past the L2 lens and then is removed near the back end. For the L3 lens, jets of temperature-controlled purge air are blown across the surface of the lens. This provides a constant-flow air curtain that re-heats the air cooled by the lens and breaks up any natural convection cells before they can start.

This combination of general purge flow and targeted temperature stabilization is expected to provide a uniform and controlled thermal environment inside the Camera volume

6.3 Camera Focal Plane System

As introduced in Chapter 5, the Camera uses CCDs organized in a focal plane built up from Science and Corner Raft Towers. This focal plane is housed in the cryostat. CCDs for science imaging as well as Telescope guiding and wavefront correction are covered in detail in Chapters 8 and 9. The Science and Corner Raft Towers that form the focal plane are covered in Chapters 10 and 11, respectively. The cryostat is covered in Chapter 12.

This section addresses thermal and contamination control aspects of the focal plane design.

6.3.1 Detector Plane Thermal Control

6.3.1.1 Thermal Control Requirements

Thermal control of the detector plane and other components of the cryostat cold mass has been a primary design driver in the development of the cryostat design.

Thermal control requirements can be loosely grouped in three classes. First, the cold mass thermal control system must be able to remove a considerable amount of heat from within the cryostat. Up to 1650 W of heat is generated by the raft electronics, radiated from the warm L3 lens, or leaked in from the cryostat wall through conduction along support members or radiation.

Despite this large heat load, the detectors on the focal plane must be held at -100 °C, stable over multiple nights and uniform over the large area of the field-of-view. These requirements ensure that the CCD sensors operate in a stable environment, to minimize thermally-induced variations in their performance that would impact the precision of their calibration.

Finally, despite the relatively high heat loads and temperature stability requirements, the elements providing structural supports for the detectors cannot distort across the field of view. Thus, heat conduction paths must be well-understood to ensure that thermally-induced distortions of the Grid due to temperature gradients do not move sensors off the focal plane.

6.3.1.2 Sensor Thermal Control

The challenging thermal requirements of the detectors and cold mass in the cryostat are met by four design considerations that have been used in the development of the design discussed herein. These considerations are outlined below, while details of the component design and thermal behavior are left to the individual subsystem chapters later in this Report.

The primary architectural consideration taken to address the tight thermal requirements has been to separate the Cryostat cold mass into three thermal zones. First, the raft electronics boards (REBs) have been thermally and structurally separated from the raft electronics crate and rafts, and mounted on their own Cold Plate. These account for 1100 W of the total 1650 W, which is removed by a dedicated refrigeration system tied to the Cold Plate. The Plate operates at -40 °C, largely to reduce the gas load from the electronic boards and help maintain a clean environment inside the cryostat. Heat removal at this temperature is relatively straightforward, and is accomplished by a dedicated refrigeration system.

The second and third thermal zones are tied to the Cryo Plate, which operates at -130 °C. The raft electronics crate structures are bolted to the Cryo Plate, and both are directly cooled by a low-temperature mixed-gas refrigeration system. The system uses compressors on the ground to deliver high-pressure room-temperature gas to the back of the cryostat, where it is pre-cooled then expanded through tiny orifices to cool it to our operating temperature and liquefy it. This cold liquid then flows through tubes in the Cryo Plate, where it boils as it absorbs the waste heat. The system provides a number of advantages over alternative options. However, one significant advantage is that using phase-transition to remove heat provides a more stable and uniform temperature over single-phase heat removal. This ensures that the Cryo Plate temperature is uniform across the plate, providing a constant and uniform thermal ground plane for all 25 raft towers.

The Raft Sensor Assemblies (RSAs) form the third thermal zone inside the cryostat. The rafts are thermally connected to the front end of raft electronics crates through flexible thermal straps to accommodate relative thermal contraction between the Grid and Cryo Plate. This produces a relatively large temperature gradient from the sensors all the way back down the conduction path to the Cryo Plate. While the relatively long, higher-resistance conduction path produces a large temperature gradient between the Cryo Plate and sensors, it provides thermal isolation of the sensors with respect to thermal transients elsewhere in the system.

This isolation of the sensors is coupled with active temperature control provided by temperature sensors on the CCDs and resistance heaters on the rafts. These components are used for active feedback control of the sensor temperature. The control loop responds both to the small transients in heat load due to changes in heat dissipated by the CCDs themselves, as well as variations in the radiant heat load on the surface of the sensors from the L3 lens. Feedback control will also be able to stabilize the sensors from long-period fluctuations in the temperature of the Cryo Plate itself. While much of this variation will be damped out by the relatively high thermal mass of the intervening sidewall copper plates, small fluctuations of the sink temperature of the rafts could still affect the sensor temperature.

In summary, the overall thermal design principals and implementation, as well as the active thermal control loop, provide a very uniform and stable thermal environment for the sensors on the focal plane.

6.3.1.3 Control of Thermally-Induced Distortions

The thermal path described above is designed to assure that the CCDs on the focal plane operate in a stable thermal environment. However, the parallel thermal paths for the sensors and raft electronics described above also serve to reduce the possibility of thermally-induce distortions of the detector plane. This is because the thermal path to remove the 1100 W of heat from the REBs and thermally stabilize the sensors is completely decoupled and isolated from the structural path that supports the sensor rafts to the Grid and out to the cryostat wall. This largely eliminates all thermal gradients in these key structural elements, significantly reducing the possibility of thermally-induced distortions which could warp the plane of detectors and move them off the focal plane.

The primary structural element supporting the RSAs is the Grid. The RSAs are supported off of the Grid by way of ball-and-vee kinematic couplings which are very stiff but have a very high thermal resistance. Thus, very little heat flows across this joint. In contrast, the Grid is thermally coupled directly to the Cryo Plate by two thermal straps in each of its 25 bays. These straps mount midway up the Grid structure and remove what little heat is conducted or radiated onto the Grid, while providing a stable and uniform temperature sink. Mounting the straps on the neutral axis of the Grid ensures that for generalized radiant heat loads, any temperature gradients in the Grid will be relatively balanced about the neutral axis, thereby neutralizing their effects on out-of-plane distortion.

Beyond isolation of thermal paths from structural load paths and thermal sinking of the Grid, the final design element incorporated to reduce thermally-induced distortions in the Grid is to thermally isolate it from all possible heat sources. This has been done by surrounding the Grid with an actively-cooled thermal shroud to significantly reduce the radiant heat load from the warm cryostat housing. The shroud mounts around the perimeter of the Cryo Plate and extends to the front of the cryostat, then around the front perimeter of the Grid, where it profiles the perimeter of the sensors. This essentially blocks all view angles from the warm cryostat housing to the Grid, significantly reducing the radiant heat load on the perimeter surfaces of the Grid and the attendant temperature gradients and distortions.

Figure 6-3 shows the predicted thermally-induced out-of-plane distortion of the Grid, due to a worst-case heat load around the perimeter of 16 W/m^2. The total expected heat load is about 1/5 this design load. The expected thermal distortion of the Grid in normal operation is 12nm (out of plane), but a worst case scenario (e.g., loss of a cooling loop) may produce up to 250nm out of plane distortion. Further analysis and detailed design discussion is continued in Chapter 12. The result of the thermal control design considerations is a structural load path that is isolated both from the process heat loads and ambient radiant heating, producing a thermally stable structural path to support the sensors on the focal plane.

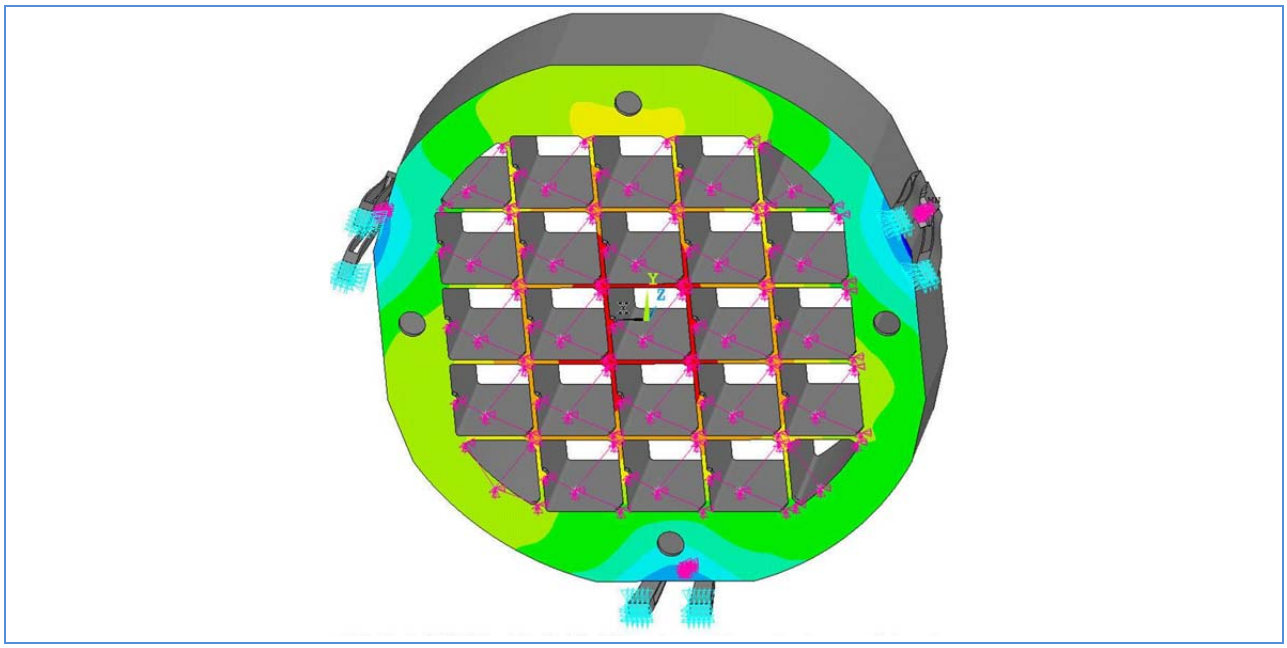

Figure 6-3: Thermally-induced out-of-plane distortion of the Grid due to perimeter radiant heat loading; the maximum distortion is 12 nanometers for a worst-case radiation heat load of 16 W/m^2

6.3.2 Cryostat Contamination Control

6.3.2.1 Introduction

As introduced above, all of the sensor electronics are located inside the cryostat to reduce signal length, minimize overall power dissipation on the sensors, and reduce crosstalk. However, this introduces challenges to ensure that the evacuated cryostat volume remains clean and that the sensors are not damaged by possible contaminants introduced into the vacuum. This hazard has been addressed in three ways: the thermal control systems, design of the vacuum system, and a program to reduce the possibility of contamination ever occurring.

6.3.2.2 Thermal System

The cryostat has been segmented into four separate thermal zones. The -130C Cryo Plate and shroud serves as the coldest of the thermal zones, to provide a stable low-temperature heat sink for the RSAs and for cryo pumping. The CCDs on the focal plane form the second thermal zone. This is intentionally not the coldest zone, to reduce the cryo-pumping load on the CCD's. A -40C Cold Plate forms the third thermal zone, thermally grounding the electronics for each raft. Keeping these electronics cold reduces their gas load in the cryostat. The fourth thermal zone is the warm cryostat wall and L3 lens inside face. Only these metal and glass surfaces remain warm, to reduce the gas load and the possibility of contamination.

The four thermal zones in the cryostat are independently controlled, to protect the optical surfaces during cool-down and warm-up sequences.

6.3.2.3 *Materials Qualification Process*

The final element of the contamination control plan is a qualification process for all materials that are planned for use in the cryostat. This has been used to qualify materials for use in the cryostat, define baselines for outgassing rates for the material, and to establish cleaning and bake-out protocols needed for parts made from the material. All materials used in the cryostat have gone through this qualification process and through cleaning and bake-out procedures appropriate for the material are being used in process travelers as parts are fabricated, cleaned, and assembled.

6.4 Camera Structural System

The Camera structural design has been guided by four overarching principles that have been derived from high-level requirements. First, the Camera and its components have been developed to be compact to meet tight packaging constraints. Next, support members have been optimized to provide stiff structures with compact flow of forces. Third, a by-product of this is that the structural design is structurally efficient. Finally, sometimes in opposition to the first three principles, the Camera and its subsystems are modular. These four principles are expanded on in the following sections, along with the requirements driving them and the effect on Camera structural design details. Please refer to Figure 6-4 for a structural block diagram of the Camera.

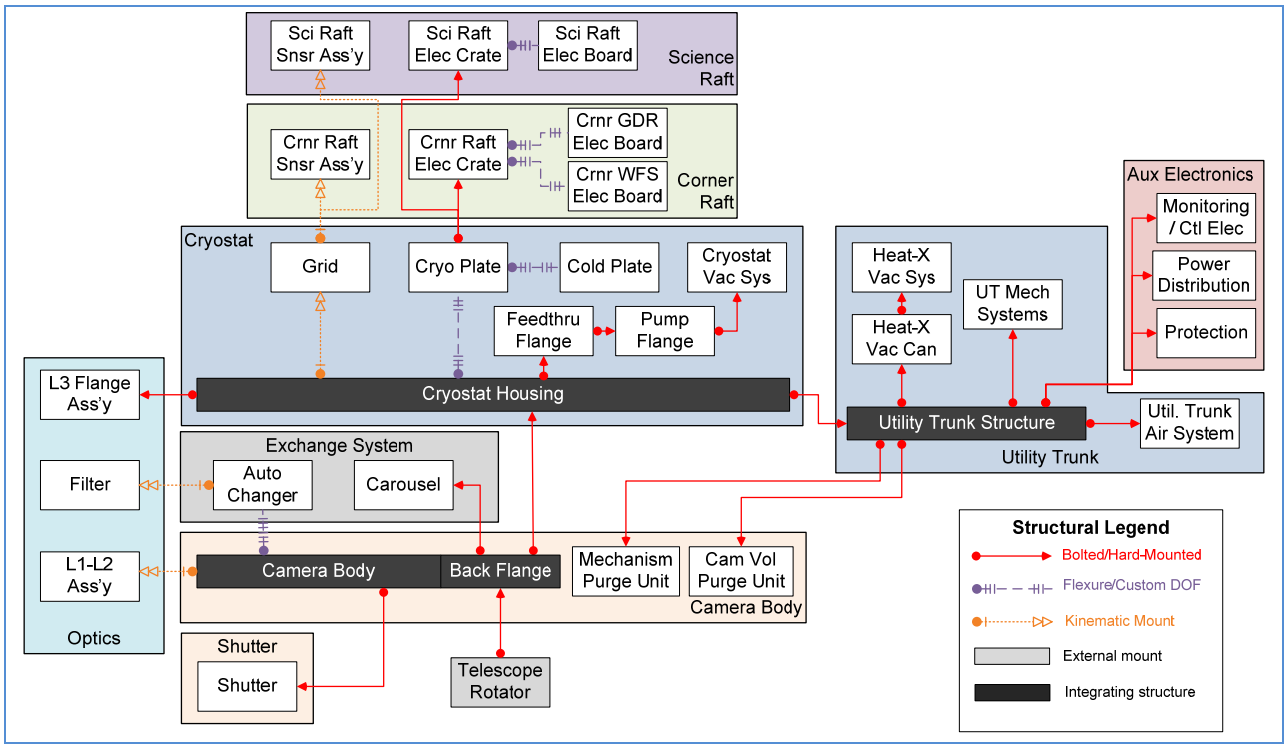

Figure 6-4: Camera structural block diagram

6.4.1 Packaging Volume

The Camera and its subsystem elements have been designed to tight packaging constraints. These are borne out of three driving requirements. First, the Camera is cantilevered out from the telescope top end assembly through the bore of the M2 mirror and into the main beam of the telescope. Thus, its

outer envelope is constrained by the optical design of the telescope and the location of the light cones for incoming light. Second, the Camera acceptance angle is very large and is part of a short focal length optical system, meaning it accepts a considerable amount of light over a large angle and delivers it down to the focal plane. Staying out of the way of this incoming light volume constrains the design of all components forward of the detector plane. Third, the short focal length of the optical design results in optical elements being spaced very closely together inside the Camera. Especially given the large diameter of the clear aperture through the Camera, the spacing between optical elements produces challenges in the design of both the optics supports as well as the design of the ancillary components around them.

These packaging constraints have produced a very compact design of all sub-assemblies of the Camera. This starts with the toroidal structure of the L1-L2 support ring which fills the entire triangular section between the M2-M3 light cone on the outside and the incoming L1-L2 light cone on the inside of the Camera. Further back, the changer-carousel exchange system concept is driven almost exclusively by the need to store five filters onboard the Camera while still staying within the bore of the M2 mirror. More conventional filter changer systems used on other Cameras, such as sliding filters, filter wheels, or filter cartridges stored in decks would impinge significantly into the incoming light in our optical design. However, the changer-carousel design elegantly provides the motions needed to store and exchange filters while staying within the packaging constraints.

Inside the cryostat, packaging constraints are borne out largely by the need for a minimum of 85% packing fraction of active pixels in the field of view. This has led to the four-side buttable CCD design, along with designing the support electronics to fit within the footprint of the sensor rafts, thereby not contributing to any loss of active area.

6.4.2 Structural Stability

Camera element structures have been designed to be very stable in the face of changing structural and thermal loads. This is the result of two driving requirements. First, our overall image quality is critical to meeting high-level science requirements, but motions and distortions of the optics introduce errors that impact the image quality. Second, as the telescope is re-pointed and the Camera rotated on its mount, changes to the orientation of the Camera with respect to gravity will cause further misalignment. While the telescope guide system can correct for some of these misalignments, there will still be residual errors that cannot be corrected. These must be minimized to maximize image quality and keep it as uniform as possible over the full range of altitude and Camera rotational angles.

Structurally stable features have been incorporated into nearly all aspects of Camera component designs. At the most fundamental level, many key structural elements have been designed to maximize stiffness and incorporate smooth, compact flow of forces. This is most easily seen in the tapered, conical shape of the Camera and cryostat housings, shown in Figure 6-5. For both, the tapered shape transmits the weight of the L1-L2 assembly—for the Camera housing—and loaded Grid—for the cryostat housing—back to its mounting point. Early analysis for both showed that a simple cylindrical design did not produce an adequately stiff structure.

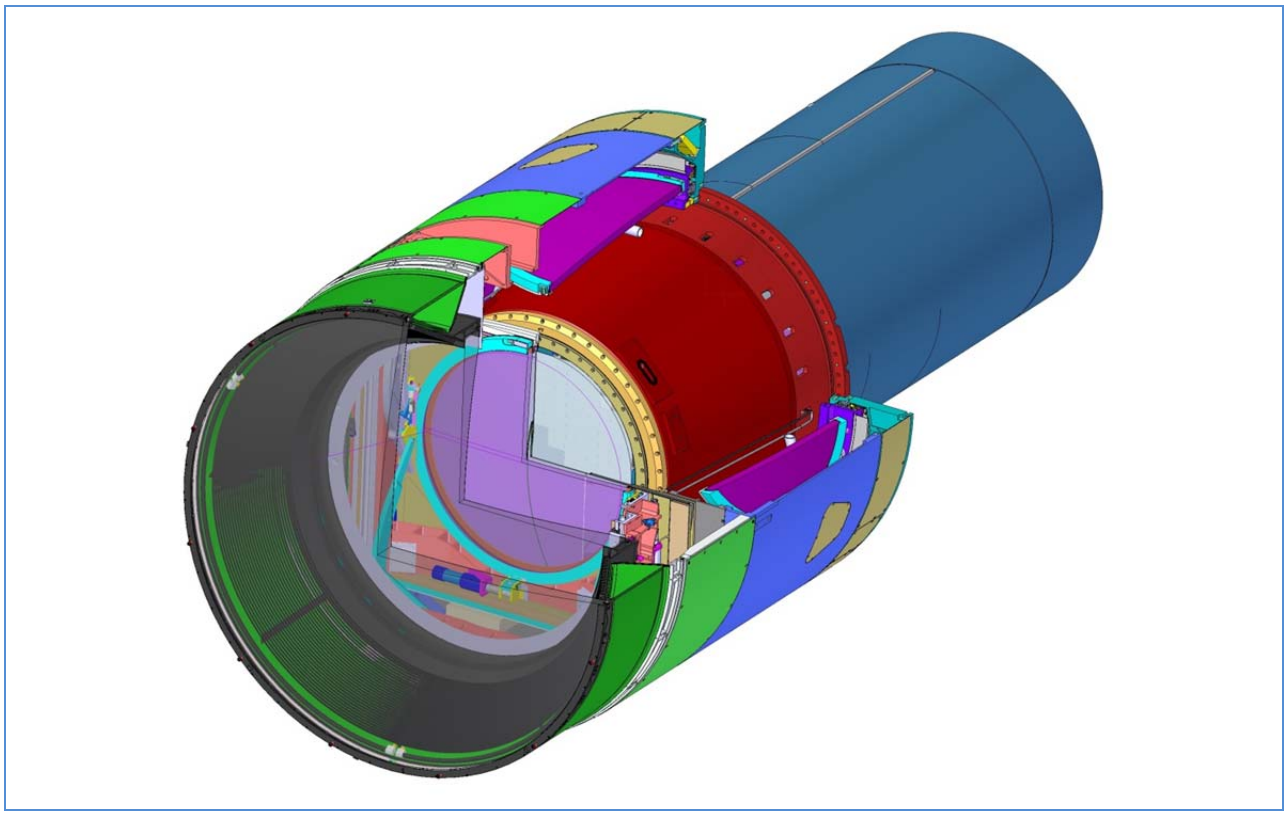

Figure 6-5: Section of the Camera, showing tapered Camera and cryostat housing, as well as the closed triangular section of the L1-L2 structural ring

Furthermore, closed sections have been used throughout to maximize the bending stiffness of members for a given cross-sectional area available. Two areas where closed sections are used to considerable benefit are the Grid and L1-L2 support ring. As shown in Figure 6-6, the Grid is comprised of a 5x5 array of relatively empty bays with marginal structural stiffness. However, a “picture frame” structure surrounds this empty region to provide the considerable stiffness needed to preserve the flat detector plane. This picture frame structure is made of a closed rectangular section with internal cross-cutting webs to further improve stiffness. Likewise, the L1-L2 structural ring is comprised of a closed triangular cross-section to maximize resistance to bending as well as twisting.

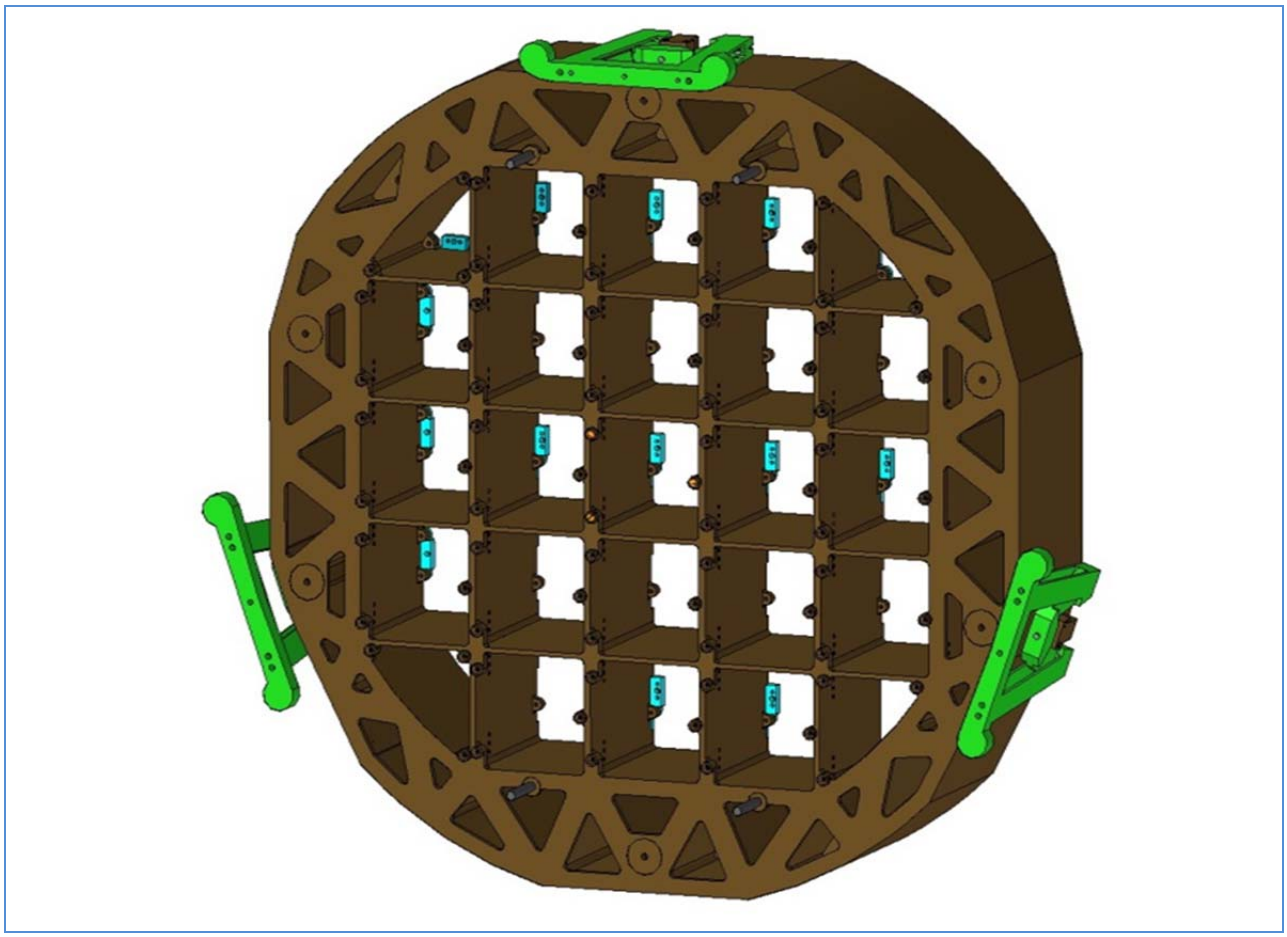

Figure 6-6: The Grid assembly, showing the box structure of the perimeter frame and the flexure support, one part of the kinematic support for the Grid

Kinematic connections are the third design element used throughout the Camera to improve structural uniformity. At a minimum, two elements must be connected such that all six degrees of freedom are constrained, but often some of these degrees of freedom are over-constrained, which allows for the transmittance of forces and torques across the interface that can distort and stress components on the other side. This externally-applied distortion must be factored into the component design, which leads to larger structural elements. Such connections are particularly suspect in handling thermally-induced distortion, especially if the connecting elements are not the same material.

To avoid these pitfalls, the Camera uses kinematic connections throughout. The L1-L2 assembly is mounted to the Camera housing using a six-strut hexapod. The Grid is mounted to the cryostat housing with three radially-oriented flexures, to prevent cryostat distortion from imparting loads or deflections on the Grid. Filters are supported in the Auto Changer and Carousel using a ball/cup and ball/slot kinematic mount, to ensure that small track misalignments in the Changer do not impart loads on the filter frame and glass. Rafts are mounted to the Grid using three radially-oriented vee-blocks, both to isolate the CCDs from stresses due to raft distortion and to accommodate differential contraction between the rafts and Grid. The Auto Changer is mounted to the Camera housing using a near-kinematic

series of connections, to allow for on-telescope removal. In all of these joints, kinematicity leads to more predictable structural performance and isolation of structural load transfer across the joint.

6.4.3 Structural Efficiency

A by-product of designing for a compact volume with high structural stability is that the resulting designs are very structurally efficient. This is particularly important for the Camera, since it is cantilevered off the telescope top end, and its mass directly impacts the natural frequency and dynamic response of the top end assembly. The Camera mass allocation is 3060 kg. However, 1540 kg or fully half of this weight is accounted for by purely functional elements of the Camera—lenses, sensors and support electronics, filters and changer, and shutter. Another 290 kg is used for infrastructure elements such as vacuum, thermal, and environmental control, while 1100 kg of the total is used for primary structural elements. Thus, only 38% of the total mass is used for primary structure, which is remarkably efficient given the difficult structural loading and load cases of the Camera.

6.4.4 Modularity

The final principal guiding the Camera design is the modularity of Camera subsystem elements. In short, the Camera includes three primary integrating structures: the Camera body, cryostat, and utility trunk. All other components are modular assemblies that are mounted to one of these structures. This design principal has been used to improve efficiency for integration, testing, and follow-on servicing of components during operation. The modules are intended to be assembled and pre-tested prior to integration, to allow for much more streamlined integration with less risk of test failure at higher levels of assembly.

6.5 Camera Grounding and Shielding

The control of unwanted currents, the shielding of sensitive components and the prevention of unwanted electrical interference in sensitive circuits such as the CCD readouts is a well-developed but paradoxically not well-understood science. Most textbooks consider the simple case of a single sensitive detector connected to some form of readout as shown in Figure 6-7. The rules developed from this simple case – single point grounds, isolation of detector and front end amplifier from other components, separately isolated power feeds for each element – work well. This case, however, breaks down in critical ways when the number of detector elements becomes “large” and where those elements are inextricably intertwined with each other and, even more problematically, intertwined with other mechanical or electrical parts of the system. For LSST, with some three thousand low noise channels in a circle larger than half a meter in diameter, we are well into the territory of the intertwined and need to consider a range of mechanical and thermal as well as electrical issues to arrive at an optimal solution. A more exhaustive discussion of the philosophy and issues is found in the LSST Camera Grounding and Shielding Plan, but the main features of the baseline solution are presented here.

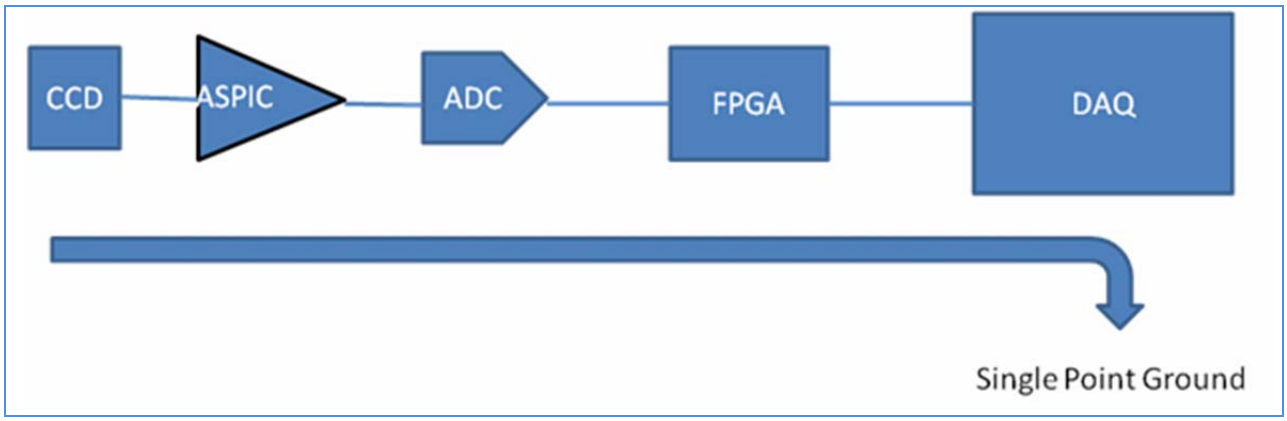

Figure 6-7: Power distribution design: simple case of a single sensitive detector connected to some form of readout

6.5.1 Ground Reference for the Focal Plane

A primary initial question for any system is what is the "reference" point for system "ground". To what point or surface are all the electrical potentials referred? In the specific case of the science raft (and corner raft) towers, the question is largely decided by thermal considerations. The science (and corner) rafts are cooled by refrigerant flowing in a massive metal plate – the Cold Plate – and the thermal connection between the raft tower structure and the Plate needs to be of a low thermal impedance. The metallic conducting parts of the raft towers (and the Plate) are made from copper in order to minimize the thermal impedance. If one were to try to electrically isolate each raft from the Cold Plate, that electrical isolation would necessarily increase the thermal impedance and, because of the relatively large area of the mating metallic surfaces and the inherent capacitance across any electrical isolation, the electrical isolation would only be at relatively low frequencies. Thus the simplest plan is to make the Cold Plate copper the reference "ground" surface for the raft electronics – this guarantees a low impedance thermal and electrical path but implies some mild requirements for the mechanics.

As the Cold Plate is the reference "ground" it is important to not allow stray currents to flow through or across it, and so the Cold Plate must be electrically isolated from the cryostat and any other mechanical structures. This implies electrical breaks in the flexures mounting the Plate to the cryostat walls and electrical breaks in the piping carrying the refrigerant in and out of the cryostat. However, once those isolating structures are in place we have a nearly ideal multi-channel electrical environment. Each Raft tower is powered by floating power supplies (independent current returns for each supply) and the communication to and from the RCM is by way of LVDS signaling with its very relaxed common mode voltage requirement. Each raft tower is then a 144 channel (or 48 channel for the Corner Raft Tower) readout system which is only electrically connected to the other raft towers through the ground reference at the Cold Plate as indicated very schematically in Figure 6-8. Of course within a Raft Tower it is essentially impossible and would be unwise to attempt to treat each channel separately. Already at the CCD sensor level the channels are intertwined with common substrates and bias structures. In the electronics, eight channels share a single ASPIC and a given sensor is handled by two sides of the same REB board. In this intertwined situation the general rule changes to one of keeping a common very low impedance reference for all channels so that even if there were to be circulating currents from one area

to another across that ground surface, the potential differences are, perforce, insignificant – for instance if one can maintain μΩ impedances, even mA stray currents cause only μV level shifts (remembering that the LSB for the LSST ADCs is a few μVs). In this case we are helped significantly by the simultaneous requirement for low thermal impedances – the additional copper mass required for the thermal transfer serves to lower the electrical impedance even more.

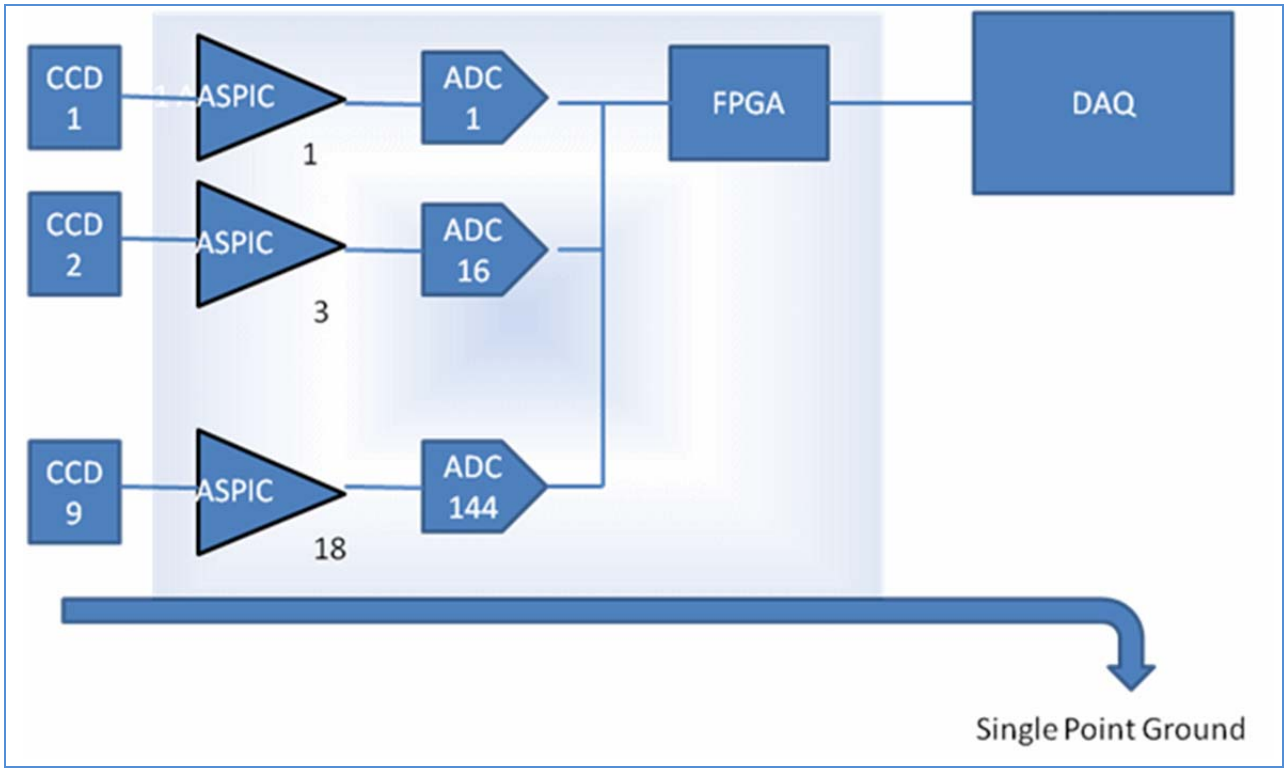

Figure 6-8: Power distribution design: parallel readout of multiple detectors connected to a readout chain. The RCC's, of course, necessarily share their ground reference on a board to board basis with the Science Raft Tower and so the Cold Plate is a second massive metallic part of this reference ground surface. The Cold and Cryo Plates are not, of course, tied together mechanically with low impedance paths because of the significant thermal difference between those two plates. However, both Cryo and Cold Plates are electrically isolated from the cryostat and other conductors in that volume with provision for a single point connection to be made between those plates and the cryostat shell using a high thermal and relatively low electrical impedance connection. In fact a number of different points around the Cryo/Cold Plates and along the cryostat interior are planned to be available for this connection in case there are unpredicted sensitivities to one particular connection scheme.

6.5.2 Shielding for the Focal Plane

In addition to possible interference from the conducting current paths discussed above, one also needs to worry about radiated energy (RF) causing interference in a sensitive electronic system. A Faraday cage is a simple and highly effective prophylactic measure in most such cases. At first glance the cryostat would seem as if it might form an effective cage until one realizes that L3, the final lens in the LSST optical system, is a nearly ¾ m diameter hole in the "cage". Clearly, shielding of the CCDs and the front end electronics is not such a simple matter. Nevertheless, it is possible to put a nearly complete shield around all the electronics even if the CCDs themselves must remain uncovered. The raft electronics crate in the science raft tower is, effectively, an all copper box around four sides of the electronics and

the vacuum conduction barrier (an aluminum Kapton or copper Kapton laminate) between the front of the boards and the rafts covers the CCD side of the crate. Only the back end of the electronics boards is not shielded and even there the Cryo and Cold Plates form a nearly complete shield. This “shield” is, of course, the same as the reference “ground” and that is not, in a text book sense, ideal but in practical terms it can be expected to be very good indeed and similar to successful high density channel count systems in recent HEP (High Energy Physics) detectors. The remaining weak spot – the CCDs themselves – must be protected by the design of the electronics system, the design of the Camera and the design of the telescope and observatory. Fortunately the exposure is only for relatively high frequencies as the CCDs are 4 cm x 4 cm and so operate as moderately efficient receiving antennas only over frequencies above some hundreds of MHz. As the front end signal processing uses correlated double sampling with time constants of order hundreds of nanoseconds, any potential RF pickup from the CCD is cancelled to very high order. The other side of the issue is to ensure that the environment does not contain any aggressor devices with frequency emissions in the bandpass of interest during sensitive times and, fortunately, essentially all possible RF emitters for some kilometers around are part of the LSST Observatory and so under our control.

6.5.3 Best practice signal distribution

In addition to controlling low- and high-frequency signal paths that might disturb the low noise measurements, it is also useful to establish a set of standards or practices to avoid any iatrogenic degradation of the sensitive system and, as a side benefit, improve signal integrity in even the less sensitive parts of the Camera. Historically, the most important areas of concern are signal transmission (radiated and received energy) and power supplies (conducted noise).

The single most important step in signal transmission is the use of differential lines (as opposed to single ended signaling) and the second most important step is the use of the lowest possible voltage swing. Therefore, all the high speed digital signaling within the cryostat and, largely, outside the cryostat, is accomplished using LVDS (Low Voltage Differential Signaling). Signals only used for initial system configuration or emergency response are exempt from this requirement. In addition, the analog transmission of the CCD video signal is fully differential as is the digitization. The advantage of differential signaling is well known, but perhaps a brief reminder is in order – as a differential line carries both positive and negative going excursions, the cancellation of those excursions in the far field regime results in essentially zero radiated energy while in the near field regime radiation can be easily controlled by distance rules and the location of “ground” plane surfaces. Similarly, an external disturbance moves both positive and negative lines in similar ways and so the common mode rejection of the receiving differential amplifier removes such disturbances.

In terms of power supplies, the most important challenges are isolating “noisy” entities from sensitive ones. To that end the LSST Camera power system is organized to provide separate power regulation (and conversion where needed) to each sub-system and to divide those sub-systems into separate “clean” and “dirty” branches (see Chapter 18 for more details). Insofar as possible loads are provided with isolated power (i.e. power return is not via “ground” but via a separate and isolated power return line) and this is strictly true for all loads in the cryostat – the most sensitive region. The goal is prevent

any possibility that variations in load in one area are reflected in variations in potential in a separate area.

6.5.4 Current flows in mechanical structures

The final area of noise mitigation is a set of rules applying to all metallic and insulating structures within the Camera. In order to prevent an isolated conductor from acting as a receiving or transmitting antenna it is necessary to attach all conducting structures to some fixed potential – so, for instance, all of the mechanical parts of the Camera body and utility trunk will be electrically connected either as a consequence of their mechanical assembly or, if not guaranteed by the mechanical assembly technique, by an explicit conductor to some fixed potential. In addition, and perhaps less obvious, it is useful to control large insulating structures as they can accumulate charge which, eventually, reaches a discharge potential and produces a spark. Wherever possible, large insulating structures are avoided and where that is not possible, static control measures are taken to avoid discharges – for example the dry air bathing the lens structures will be sufficiently ionized to avoid high potential charge build up and insulating fluids will be carried in conductive plumbing.

6.6 Camera Protection System

6.6.1 Introduction

The Camera Protection System (CPS) is a key functional system of the Camera that provides active mitigation of Camera hazards by preventing a mishap from occurring or stopping one in the process of occurring, thus preventing damage to Camera hardware or insult to the environment. The CPS operates completely independent of CCS control, providing core protection for all elements of the Camera needing it. During normal operation and maintenance of the Camera, the CCS ensures safe monitoring and control of all Camera systems. However, Camera protection activities are intended to be performed regardless of the state of the CCS.

Note that the CPS provides the last and strongest line of a tiered defense against the occurrence of a mishap. The Camera's first defense against a mishap is in the design, analysis, and testing of Camera components. This includes developing a clear understanding of functional requirements, a process by which the design and manufacturing plans are reviewed and approved as meeting those requirements, and verification test plans to ensure that the as-built hardware meets expectations. Second, Camera hardware is protected by a clear monitoring, communication, command, and control system that orchestrates all Camera actions. The CCS actively monitors the condition of all systems within the Camera and compares operating parameters with preset allowable limits. This provides early warning of trends in hardware operation that could result in a mishap, as well as immediate emergency action to prevent a mishap if thresholds are exceeded. Finally, the CPS system includes hardware interlocks and switches, monitored and controlled by PLC's to safe systems in the event that CCS controls fail or otherwise do not function as needed.

6.6.2 CPS Architecture

Development of the Camera Protection Protocol List has led to the development of architecture for the CPS.

Six local protection zones have been identified, which correspond with six functional elements needing protection. These functional elements are:

- Exchange System—including the Carousel, Auto Changer, and Filter Loader as well as the supervisor that controls interaction between them
- Shutter—Shutter mechanism, which includes two blade sets
- Power Management—low-voltage AC-DC and DC-DC transformers and voltage regulation system providing power at discrete voltages for the Raft Towers and other systems
- Camera Body—purge environmental control system as well as access-control hatches and monitoring of rigid-body motions of the Camera
- Cryostat—vacuum, thermal, and environmental control of the cryostat
- Refrigeration System—compressors and ancillary equipment on the ground, providing high-pressure refrigerant for cooling components in the cryostat

While these six protection zones do not encompass all hardware within the Camera, they include all monitoring and control needed to protect the Camera against all hazards listed in the Protection Protocol List.

The Master Protection Module (MPM) implements protocols that require monitoring in one protection element and action taken in another.

The MPM and local functional elements must operate completely independent of the CCS and its local controllers. However, the two systems are interconnected to a limited extent. Figure 6-9 shows a generic subsystem device, along with its control elements and protection elements.

On the control side, the local Hardware Control Unit (HCU) communicates with the CCS using the Camera Ethernet bus, then converts high-level commands to low-level instructions which are sent on to the Local Device Controller (LDC) and the hardware device or actuator. Part of the HCU control function involves monitoring of sensors on the hardware for feedback control, status, and health.

On the protection side, the protection module (Local Protection Module (LPM) or MPM) controls and monitors the protection system sensors and switches within the hardware and generates interlock permit signals. Note that the mechanism for protection system control is through interlocks on the actuator power. This is the only low-level connectivity allowed between the protection and control systems. If a sensor is needed both for protection interlock and control, then by definition it is considered a protection system sensor.

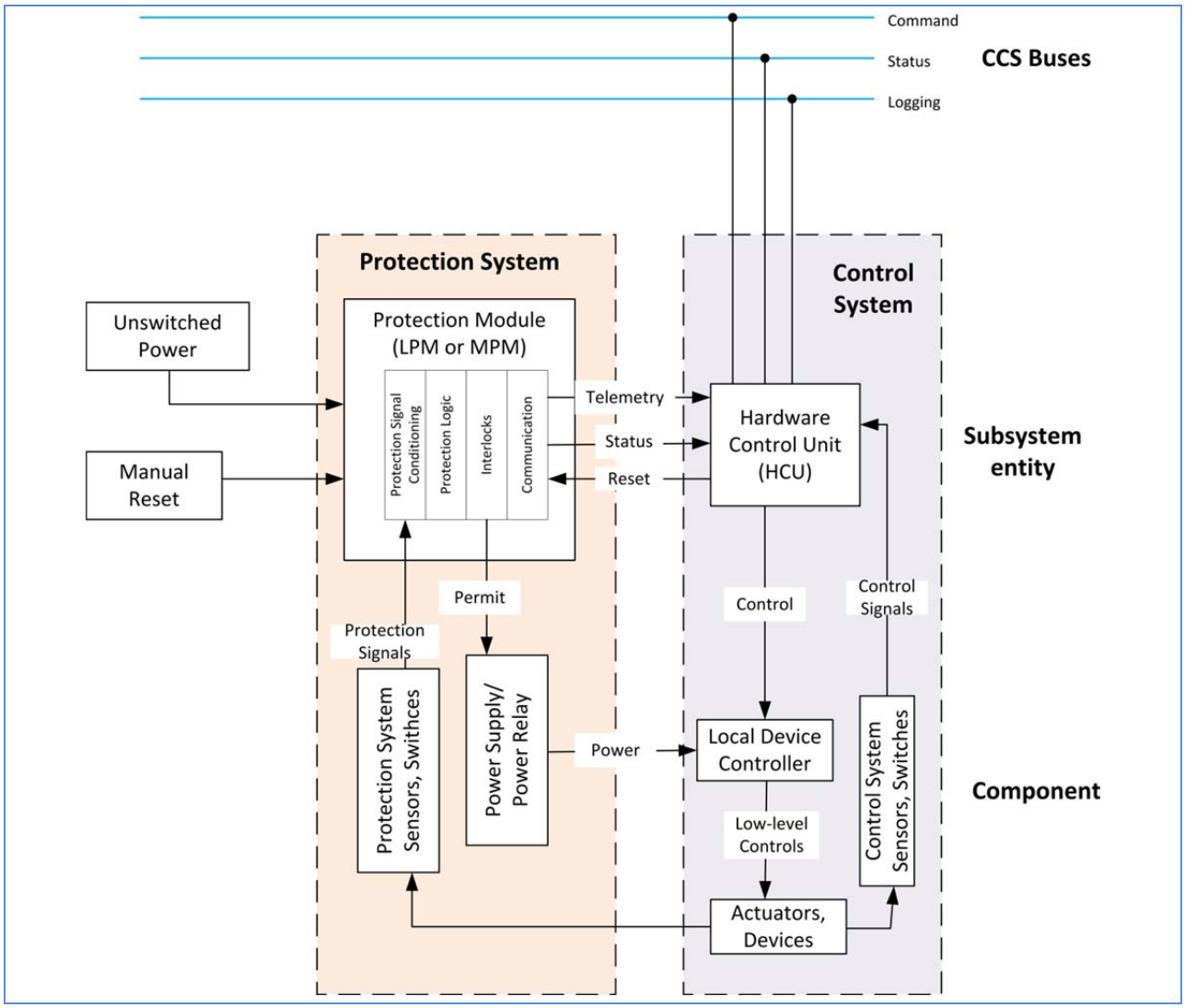

Figure 6-9: Interrelationship between CCS and CPS elements for a generic functional subsystem.

The HCU receives telemetry from the LPM and can use the conditioned sensor information for its control, but "sharing" of signals is not permitted. The HCU monitors the status of all signals from the LPM, as well as the status of any permit signals emitted by the LPM. These are communicated back to the CCS and the control room, so that protection status is always available. Note that this is a monitoring function only. The MPM and LPMs are hosted on Hardware Protection Units (HPUs), which are typically PLCs. Multiple LPMs may be hosted on one HPU.

8: Science Sensors

8 Science Sensors

8.1 Introduction

The instrument performance of the LSST Camera will be dominated by the focal plane sensors. Significant advances over the previous state-of-the-art were required to achieve the broadband high sensitivity, fast readout, and exquisite image quality demanded by the LSST's ambitious science goals. At the same time, the imager must be stable and robust to ensure a consistent high level of data integrity throughout the survey, and to avoid unnecessary downtime for maintenance and repair. A set of requirements has been defined (described in the next section), and a prototyping and testing program has been underway since 2005.

Since the sensor delivery rate is a pacing item on the project's critical path, we have received CD3a approval to proceed with the procurement of CCDs that meet project requirements. This decision was supported by our extensive sensor prototyping program, and by careful characterization of prototype devices by the LSST sensor team. The sections that follow document the considerations that are the underpinning of our sensor specifications and design choices.

Technology for visible light imaging is rapidly evolving and several candidate devices have been considered for use in the LSST focal plane. Charge-coupled devices (CCDs) are considered the performance benchmark in photography, scientific, and industrial imaging and have a long heritage in ground- and space-based astronomy. Monolithic CMOS sensors are fabricated using modified versions of standard CMOS integrated circuit processes and are becoming competitive with CCDs in several market segments. Hybrid p-i-n/CMOS sensors attempt to overcome the limitations of monolithic CMOS sensors by bump-bonding a p-i-n diode array to a readout integrated circuit (ROIC or multiplexer) fabricated in a conventional mixed-signal CMOS process. Both types of CMOS sensors differ from CCDs in having circuits which perform charge-to-voltage conversion within each pixel rather than transporting charge to a small number of amplifiers at the periphery of the array. CMOS sensors also take advantage of the native highly-integrated on-chip electronics to provide flexible readout modes, electronic shuttering, and low power dissipation.

Monolithic CMOS has several drawbacks for low-light, high dynamic range imaging encountered in astronomy. To stay within the fabrication capabilities of an IC line, these devices are typically produced with thin (1 – 10 µm) sensitive thicknesses, limiting their red sensitivity. More importantly, by incorporating readout electronics within each pixel the light-sensitive area is less than 100%. Deposited microlens arrays are often used to increase the effective fill factor in front-illuminated configurations (the majority of applications for CMOS sensors are front-illuminated). Low noise can only be achieved by use of special processes which allow pinned photodiode, four-transistor circuits that perform in-pixel correlated double sampling (CDS). Although initially expected to benefit from low-cost CMOS manufacturing processes, the accommodations needed to achieve good imaging performance have required specialized, low-volume foundries, similar to CCDs.

Hybrid p-i-n/CMOS detectors are made as a sensor-chip assembly, where the photosites are a p-i-n photodiode array fabricated on thick, high-resistivity, back-biased silicon to which the readout

integrated circuit (ROIC) containing a pitch-matched array of pixel amplifiers is bump-bonded. By decoupling the fabrication processes of the sensing and readout structures, both can be optimized independently. These sensors are back-illuminated, have 100% pixel fill-factor, and can use thick silicon to achieve good sensitivity in the red. Non-destructive readout (multiple reads can be performed without pixel reset) permits noise reduction and cosmic ray rejection by sampling multiple times during exposure, and in-pixel reset circuitry can function as an "electronic shutter," eliminating the need for mechanical shuttering. Since charge is not shifted from the photosite to the amplifier sense node, there are no issues of charge transfer inefficiency (especially significant for devices operated in a radiation environment). On-chip electronics permits flexible readout modes as in monolithic CMOS, at the expense of some loss of fill-factor for buttable imagers. This technology is an offshoot of infrared staring arrays using InSb or HgCdTe as the photosensor, which are extensively used in military surveillance and targeting applications as well as in IR astronomy.

Silicon-based visible hybrid p-i-n/CMOS arrays have seen only limited use in astronomy to date (Bai, et al. 2008, Dorland et al. 2007, Simms, et al. 2007). Performance is similar to CCDs, but limitations have been found: read noise is not as low as CCDs operated at equivalent frame rate; dark current density has been relatively high; there are significant numbers of isolated dark pixels due to bump bond failure; bright defect density is higher than in CCDs; and, there is coupling between adjacent pixels through mutual capacitances, resulting in pixel-pixel correlation artifacts. Residual image charge has been observed [Dorland] at the level of 8e-/pix/s at 120K which persists for several hours after 100X full well illumination. Another concern related to oversaturated illumination is permanent threshold shift of the input transistor of the 3.3V ROIC. At high illumination levels and with the substrate biased to minimize charge diffusion, the pixel's sense node will rise towards the substrate (most positive) potential. The gate oxide of the source follower may be stressed beyond its rated breakdown voltage or may suffer permanent threshold shift, by an amount which depends on detector bias, temperature, illumination level, integration time, and frame rate.

Although hybrid and monolithic CMOS sensors are promising technologies offering features that would simplify some engineering aspects of LSST's large-area focal plane, concerns about performance, technological maturity, and high cost led us to choose CCDs as the baseline technology for the science array. In the design and development phase of the project we have procured prototype sensors from two vendors who have demonstrated their ability to produce sensors that meet our requirements.

8.2 Science Sensor Requirements

The key requirements for LSST sensors are wideband quantum efficiency (QE) extending beyond 1 μm in the red, control of point spread function (PSF), and fast readout using multiple amplifiers per chip operated in parallel. In addition, LSST's fast optical system (f/1.23) places severe constraints on focal plane flatness. At the chip level this involves packaging techniques to minimize warpage of the silicon die, and at the mosaic level careful assembly and metrology to achieve a high co-planarity of the sensor tiles. A summary of the science drivers and the implications for sensor technology is given in

Table 8-1.

Table 8-1: Science requirements impact on imager technology

Large field of view implies physically large focal plane (64cm ϕ)	Modular mosaic focal plane construction	21 rafts × 9 4Kx4K CCDs/raft 189 CCDs total 3.1Gpix
Broadband, high spectral sensitivity	Thick silicon sensor, back illuminated, AR coat	100µm thickness for IR sensitivity Thin conductive window with AR coating
Seeing-limited image quality	Internal electric field to minimize diffusion	High resistivity, biased silicon (> 3 kΩ-cm, -50V)
Fast readout (2s) with low noise (5 - 8 e^-)	Highly parallel readout electronics	16 amplifiers/4K CCD
Fast f/1.2 beam, shallow depth of focus	Tight alignment and flatness tolerance	Flatness: 5µm Alignment(z axis): 10µm
Plate scale 20”/mm	Small pixels, close butting	Pixel: 10µm Chip-chip gap: 250µm

8.2.1 Quantum Efficiency Requirements

The quantum efficiency requirement for the sensors derives from the Science Requirement DB1, single visit image depth per band in fiducial observing conditions, combined with the expected throughput of the telescope and Camera optical elements. The allocation to the sensors is shown in the following table.

Table 8-2: Sensor QE allocation derived from throughput requirements in six bands

Filter	Wavelength (nm) red – mid - blue	5σ limiting mag (SRD DB1)	QE requirement (band averaged)
u	336 – 357 – 379	23.9	0.41
g	417 – 477 – 537	25.0	0.78
r	567 – 622 – 676	24.7	0.83
i	706 – 755 – 803	24.0	0.82
z	833 – 871 – 909	23.3	0.75
y	939 – 1004 – 1069	22.1	0.20

The quantum efficiency of the sensors is limited by three factors: reflection from the entrance surface, absorption in the bulk of the sensor, and possible recombination losses (dead layer) near the entrance window. These losses have different effects in different parts of the wavelength range. The only practical material system for optical sensors in this wavelength range is silicon, and the properties of silicon are assumed in the following discussion.

The reflectivity of bare silicon to light at normal incidence ranges from 32% in the near IR to over 54% in the UV. Antireflection coating the silicon surface can cut down the reflection loss to much lower levels, and with sufficient number of layers of proper thickness and refractive index, can reduce reflection levels to a few percent across the full LSST band 320 – 1100nm. However, the absorption length for red light is a strong function of wavelength and temperature, reaching over 100 µm at and beyond 950nm at

-100°C (Rajkanan et al. 1979). To meet the QE requirement in the z and y bands, therefore, thick silicon is needed: at least 83 µm if the operating temperature is -120°C and no AR coating is applied. At warmer temperature and with an AR coating that reduces losses to the 5% level in y band, the thickness could be reduced to 50 µm to achieve the same QE.

8.2.2 Image Quality Requirements

8.2.2.1 Image Size and Ellipticity

The LSST optical system is designed to deliver point source images whose diameter at the focal plane is less than 10µm (50% encircled energy) in the absence of atmospheric seeing. Science requirement S1 specifies that the final image quality will be dominated by the atmosphere, i.e. that the system contribution to the delivered image quality never exceeds 15% degradation due to hardware. For median site seeing of 0.6"full width at half max (FWHM), this means the telescope plus Camera can contribute no more than 0.38"FWHM to the point spread function (PSF). The allocation to the Camera is 0.3" FWHM, which corresponds to a one-sigma width of 6.4µm for a Gaussian profile.

Charge Diffusion

The sensor will contribute to image size increase due to several mechanisms, the most important of which is charge diffusion. In a thick, back-illuminated silicon sensor, charge generated near the entrance surface must be transported to the potential wells on the electrode side for collection. In particular, short wavelength light is absorbed very near the entrance surface (within the first µm for $\lambda < 500$nm) and the photogenerated charge must be transported across the full silicon thickness. In the time taken to move to the electrode side the charge will experience lateral diffusion, increasing the effective image size. It is important to minimize the transit time by ensuring that a high electric field exists throughout the sensor. If any portion of the silicon thickness is undepleted, i.e. field-free, lateral diffusion will increase significantly (Holland, et al. 2003). Therefore, the entire silicon thickness must be fully depleted by applying sufficient voltage to the back (entrance) surface. The full-depletion voltage is:

$$V_{depl} = \frac{qN_D t^2}{2\varepsilon_{Si}}$$

Where q is the electron charge, N_D is the dopant density, t is the thickness, and ε_{Si} is the dielectric constant of silicon. For 100µm sensor thickness, full depletion is only possible at reasonable voltage if the doping concentration is below 10^{13} dopants/cm^3. Higher resistivity material will deplete at lower voltage, and it is desirable to operate the sensor above full depletion to increase the electric field strength, reduce the transit time, and thereby limit lateral diffusion.

Carrier drift velocity in high-resistivity silicon is limited by phonon scattering and is strongly dependent on temperature. At the field strengths expected in the overdepleted LSST sensors, carrier velocity saturation must be taken into account as well.

In our CCDs the depletion voltage will be applied between the entrance surface and the buried channel on the electrode side, and will have a linear dependence on thickness $E(x) = E_0 + Ax$ according to the

straightforward solution of Laplace's equation in 1D. We can then express the transit time of carriers generated at the entrance surface as:

$$t = \int_0^d 1/velocity(E(x), T)dx$$

Lateral diffusion of photogenerated charge will result in a Gaussian PSF profile with a width that is a function of the diffusion coefficient for free carriers at temperature T. The resulting PSF is shown in Figure 8-1 as a function of thickness, temperature, and carrier type.

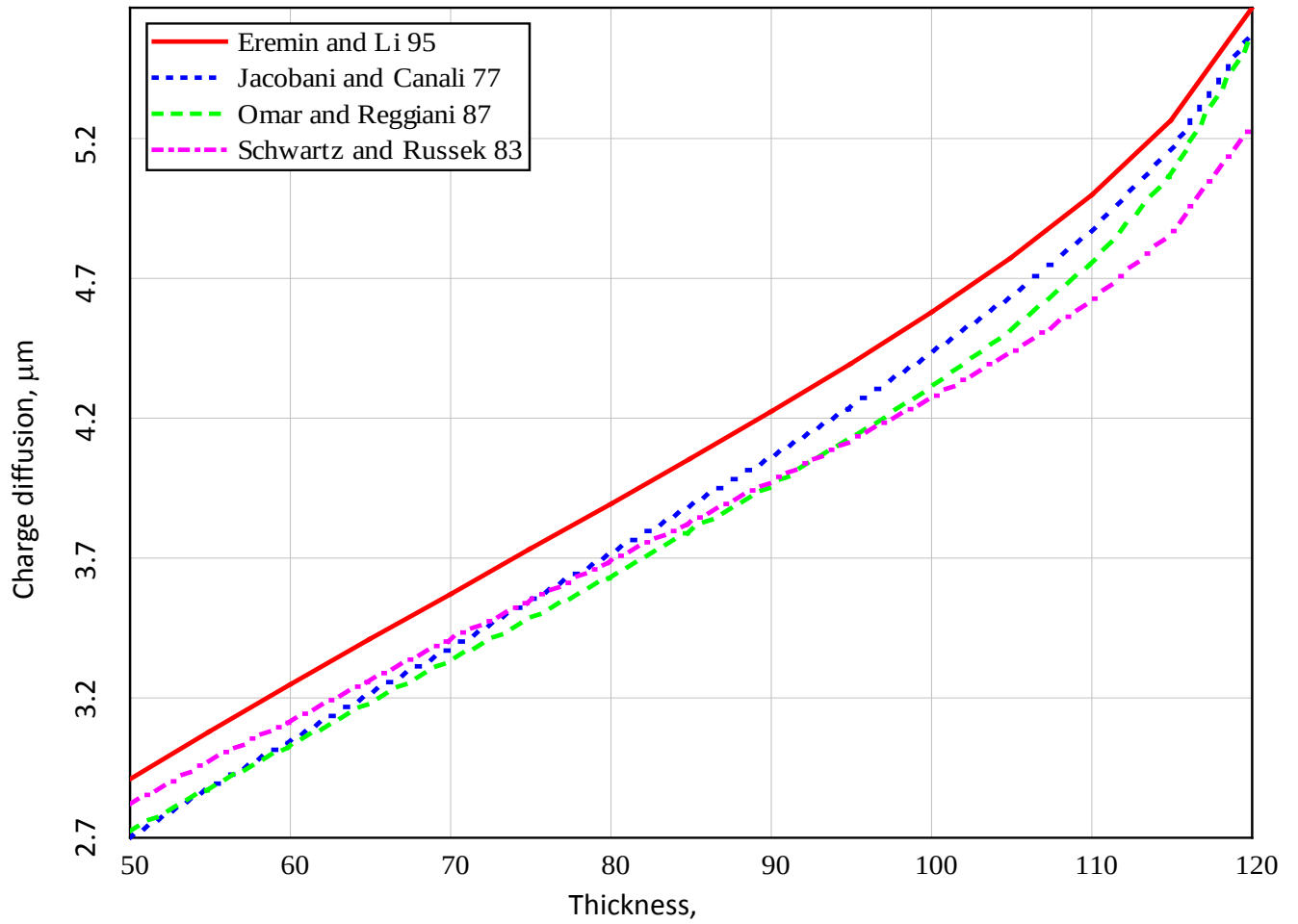

Figure 8-1: Charge diffusion PSF vs. thickness for p-type substrate CCDs. Four parameterizations of the velocity-field-temperature function have been compared. For this analysis the parameters were T=173K, ρ=3kΩ-cm, V=-50V, photoconversion at the entrance window side.

In Figure 8-2, charge diffusion is compared for 50-, 100-, and 150µm-thick sensors on p-type and n-type material as a function of the applied substrate voltage. For a given thickness and temperature, diffusion is smaller for sensors fabricated on n-type silicon. This is because the saturated drift velocity of holes is comparable to that of electrons, hence their transit times are similar, while the diffusion coefficient for holes is about three times smaller than that for electrons.

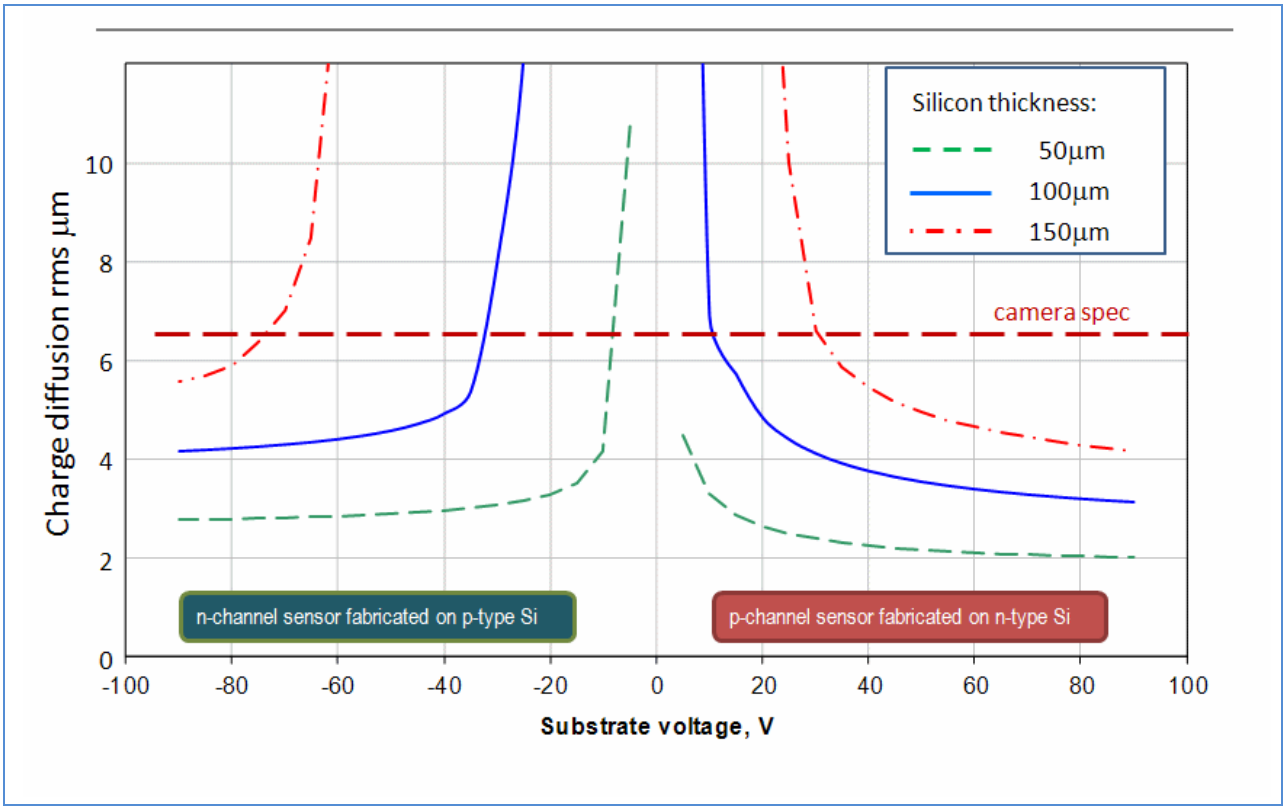

Figure 8-2: Charge diffusion PSF vs. substrate voltage

Charge Transfer Inefficiency

In CCD sensors, the image size and ellipticity will also be affected by charge transfer inefficiency (CTI) and charge trapping. In the simplest case CTI is uniform, i.e. each shift transfers a fraction (1-CTI) of the charge in a given pixel, leaving the remaining charge behind in the original pixel. In general, CTI can have different values in the vertical and horizontal shift directions, and the number of shifts may differ depending on the array format. Figure 8-3 shows the effect of vertical CTI on image size for a CCD with 2000 rows. For CTI in the range 10^{-5} or better, the impact on PSF is less than 2% increase. Depending on the relative values and number of shifts in each axis, CTI will also induce ellipticity into the point spread function.

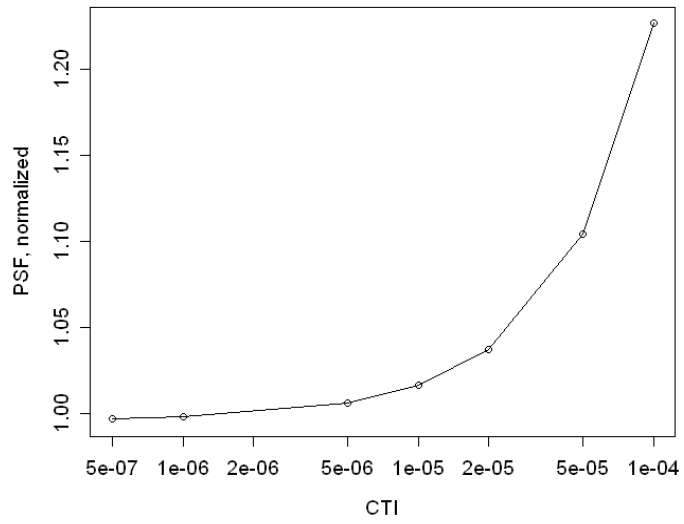

Figure 8-3: PSF broadening due to charge transfer inefficiency)

Beam Divergence in Silicon

In a low-f number optical system like LSST, light is incident on the sensor at large angles from the normal. Figure 8-4 shows an optical raytrace result from the LSST f/1.23 configuration. Because of the high index of refraction of silicon, the light "cone" has a smaller half-angle inside the silicon than in air. The lower half of the figure shows the absorption of light of two wavelengths. For long wavelengths where the light absorption length is much greater than the sensor thickness, the light is absorbed almost uniformly, while shorter wavelength light is strongly absorbed at the surface.

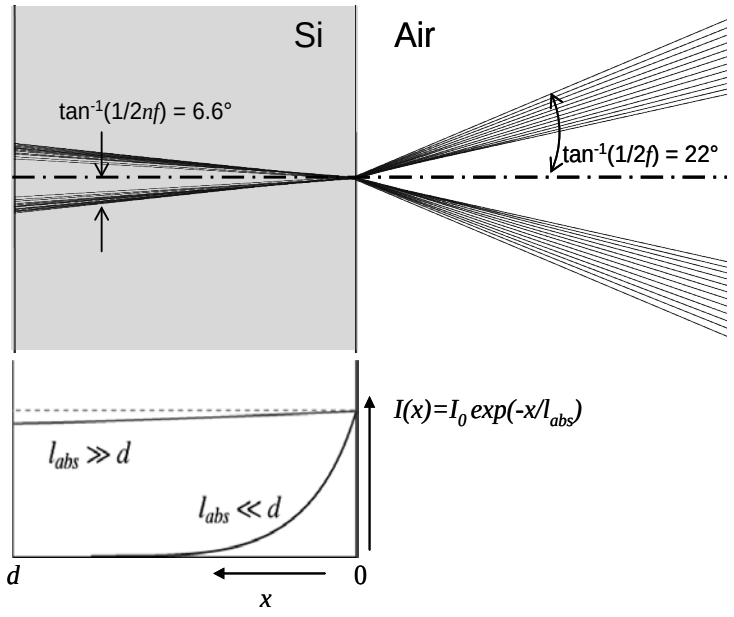

Figure 8-4: PSF broadening due to divergent optical beam in silicon

To evaluate this effect, we performed Monte-Carlo simulations for absorption lengths of 2, 10, 50, 100, 200, and 300 µm and for sensor thicknesses from 50 to 250 µm. For each configuration, ten thousand rays were traced into a thick silicon layer and the depth of conversion was selected according to the appropriate exponential probability distribution. The resulting ionization distribution was then projected onto the collecting surface, with the effect of diffusion optionally included based on the drift distance of each electron and using the expressions developed in the previous section.

This method can also be used to study the optimum position of the focal plane. Because of the weak absorption at long wavelengths, the projected charge distribution on the electrode side of the sensor can be made smaller by displacing the focal plane in the direction of the incoming light. Figure 8-5 illustrates the effect. When the sensor is displaced towards the incoming rays, long-wavelength light comes to a focus within the body of the sensor and the projection of the generated charge forms a smaller spot. The amount of focal plane displacement is highly sensitive to wavelength and also depends on temperature. In operation, the focus of the telescope can be adjusted separately for observations in each passband.

Non-Flatness and Z-height Variation

By design the optical focal plane of LSST is nearly flat across the 64cm diameter. The physical focal plane, a mosaic of roughly 200 sensors, is also designed to be flat. However, at the fast focal ratio of f/1.23 the depth of focus is small. The image quality allocation for focal plane non-flatness is 53 milliarcsec FWHM, which corresponds to 17 µm peak-to-valley z-height variation if uniformly distributed. This variation will have contributions from non-flatness of the silicon surfaces of the sensors, and from the tip-tilt and piston of the sensors when mounted to their supporting structures (rafts and grid). The spatial scale of the flatness variation impacts the uniformity of the point spread function across the field. The LSST image processing software can accommodate a variable point spread function, as long as the variation is not at high spatial frequency.

8.2.2.2 Full Well Capacity

The charge capacity of a pixel is limited to the depth of the charge-collecting potential wells, the pixel area, and the number of collecting phases It is desired to have a full-well charge capacity at least 90,000 electrons, in order to image sources eight magnitudes brighter than the single-visit five-sigma limit without saturation. This will enable 16th magnitude photometric standard stars to be used for calibration. We also establish a maximum full well specification in order to ensure that we can accomplish crosstalk correction, by keeping full well within the dynamic range of the analog signal chain.

8.2.2.3 Dark Current and Cosmetic Defects

Dark current accumulates in all pixels during exposure, and its shot noise will contribute to the signal to noise ratio. In LSST, the dark current requirement is not demanding because of the short (15 second) exposure time. The noise budget is set by sky noise, which will be greater than 6.5 e- rms in all bands. Therefore, for dark current shot noise to be negligible the dark current rate should be less than 2 e-/s/pixel or about 0.3pA/cm^2, a rate readily achievable in high resistivity silicon diodes with moderate cooling.

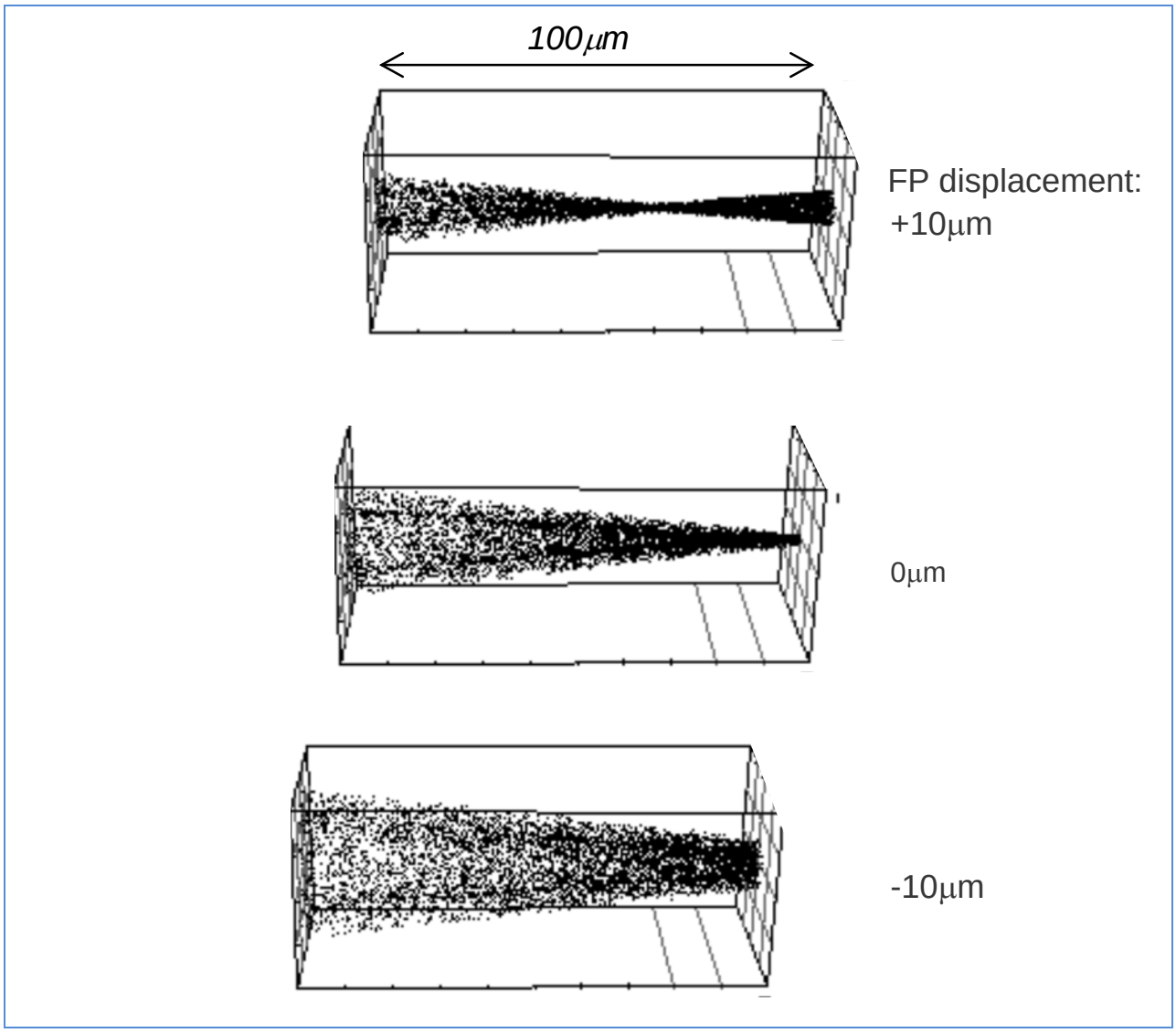

Figure 8-5: Effect of divergent light cone on PSF in the NIR

Every sensor will have a wide variation of dark current, and bright defects with emission rates greater than 6000 e-/pix/s (1nA/cm^2) will saturate in a 15s exposure, causing blooming. The region affected by this bloomed charge will be unusable for science, causing a loss of effective fill factor. LSST requires that no more than 0.5% of pixels be unusable due to high dark current, low photoresponse, or presence of column traps.

8.2.3 Electrical Requirements

8.2.3.1 Read Noise and Readout Time

As stated in the previous subsection, the noise budget is set by the lowest sky noise expected in normal imaging. This occurs in u-band with no moon, where the sky signal will be roughly 45e-/pixel per exposure, corresponding to a Poisson noise of 6.7e- rms. The read noise of the sensor is required to be less than 8e- rms to avoid degrading the signal-to-noise ratio set by the sky in 95% of images.

For CCD sensors, the Camera's mechanical shutter is closed during readout. LSST's high throughput goals demand that the closed-shutter time be minimized. The allocation for the readout time is 2 s.

8.2.3.2 Linearity

The sensor nonlinearity is required not to exceed ±2% for signal levels from 1000 e- to the full well limit, driven by requirements on photometric accuracy.

8.2.3.3 Crosstalk

Electrical crosstalk can be created by capacitive coupling between amplifiers on the sensor, between signal wires in the interconnect, or by poor isolation from the power supply or bias circuits. LSST intends to perform a crosstalk correction in real time, but the required accuracy will be difficult to attain if the sensor crosstalk is high. Therefore, a goal of 2×10^{-4} has been established. Optical crosstalk other than multiply-reflected light is expected to be negligible, and the optical design has no in-focus ghost images.

8.2.3.4 Power Dissipation

The maximum IR heat load on the focal plane has been analyzed to be less than 82 W from the warm cryostat window (L3) and walls. Power is dissipated in the sensor by the on-chip amplifiers and also by resistive losses in the clock lines during readout. To minimize the load on the cryosystem, the on-sensor power dissipation should be minimized .

8.2.4 Fill Factor and Pixel Size Requirements

Contributions to the fill factor of the focal plane include the non-imaging area of the sensor (guard rings, back window contact, amplifiers, busses, bond pads, etc.), gaps between sensors, and defective pixels. LSST has allocated 8.6% fill factor loss to non-imaging area of the silicon die and an additional 0.8% to gaps between sensors.

The plate scale of LSST is 20 arcseconds/mm. In order to properly sample the expected best seeing of 0.4" FWHM, a pixel size of $\frac{FWHM}{3} \div PlateScale$, 10µm is appropriate.

8.3 Optimization of the Sensor Design

8.3.1 Silicon Thickness

As discussed above, the silicon thickness choice is a tradeoff between quantum efficiency and point spread function. A detailed modeling study of thickness optimization for point sources has been made (O'Connor, et al. 2006). The analysis in (O'Connor, et al. 2006) assumed a requirement of 25% QE at λ = 1000nm and considered PSF contributions from beam divergence and charge diffusion. In the y-band (970 – 1060nm] the detection limit was found to have a broad optimum for thicknesses in the range 125 – 150 µm in the absence of atmospheric seeing; when seeing of 0.7" is included it completely dominates the S/N ratio. For the u, g, r, i, and z bands the sensitivity is nearly independent of thickness, since light absorption occurs within the first 20µm of silicon. Subsequent models have concentrated on quantifying the relation between QE and charge diffusion, using new parameters for the diffusion model. The results are shown in Figure 8-6. For the conditions assumed in this analysis, the internal QE at λ = 1000nm is 27% and charge diffusion contributes a Gaussian PSF with a one-sigma width of 4.6µm.

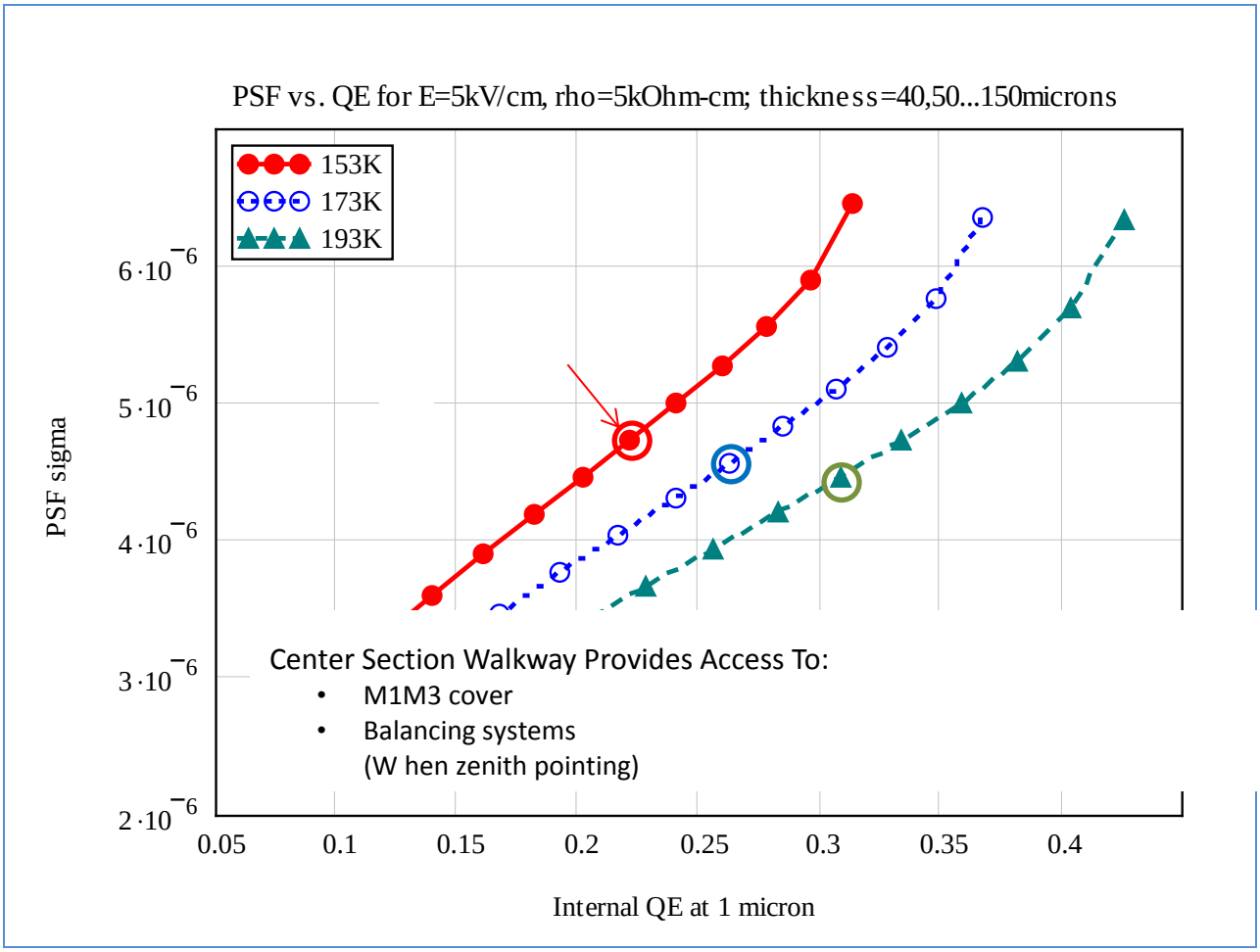

Figure 8-6: 1000nm QE vs. charge diffusion PSF(m)

8.3.2 Charge Collection Polarity

Historically, astronomical back-illuminated CCDs have been produced using p-type epitaxially-grown silicon layers, with resistivity in the range of 10-20 Ω-cm, on low-resistivity p-type substrate wafers. After frontside fabrication, the device is bonded to a handling wafer epi-side down, and the substrate is removed by selective etching, leaving the active epitaxial layer whose thickness is typically 10-20 µm. Thicker high-resistivity CCDs were originally produced on n-type silicon, which is more readily available in ultra-high resistivity and offers better radiation tolerance (Holland, et al. 2003). More recently thicker devices have also been fabricated on bulk p-type material (Jorden, et al. 2006, Jorden, et al. 2010, Boggs, et al. 2007). As discussed elsewhere, p-channel CCDs (those fabricated on n-type material) have less charge diffusion than n-channel devices of the same thickness and substrate bias, since the diffusion coefficient for holes is smaller than that of electrons while their saturated drift velocities are similar. Drawbacks of p-channel CCDs include higher persistent image requiring an erase cycle between exposures and poorer noise performance of the on-chip source follower amplifier. It has also been noted that p-channel CCDs exhibit higher dark current and more bright defects than n-channel devices, so they often require operation at lower temperature; however these characteristics may be

technological rather than fundamental and their effects may be reduced with improving material and process quality. We have selected a sensor thickness of 100 microns.

8.3.3 Segmentation

Survey speed is decreased by the time taken to read out the focal plane after each exposure, but increasing the pixel rate degrades read noise. To meet the goal of 2s readout time for the full focal plane while keeping the read noise below 5 electrons rms, the sensor is divided into segments read out in parallel. In the tradeoff analysis the detector size is assumed to be 4K X 4K, the readout time is constrained to be 2s, and we estimate the noise performance of the detector based on a simple noise model of the source follower transistor, per Figure 8-7(a). The choice of 16 segments (1Mpix per segment) and 550 kpix/s provides the necessary performance. The arrangement of the segments can be chosen to provide a large contiguous imaging area, as shown in the CCD conceptual layout in Figure 8-7(b).

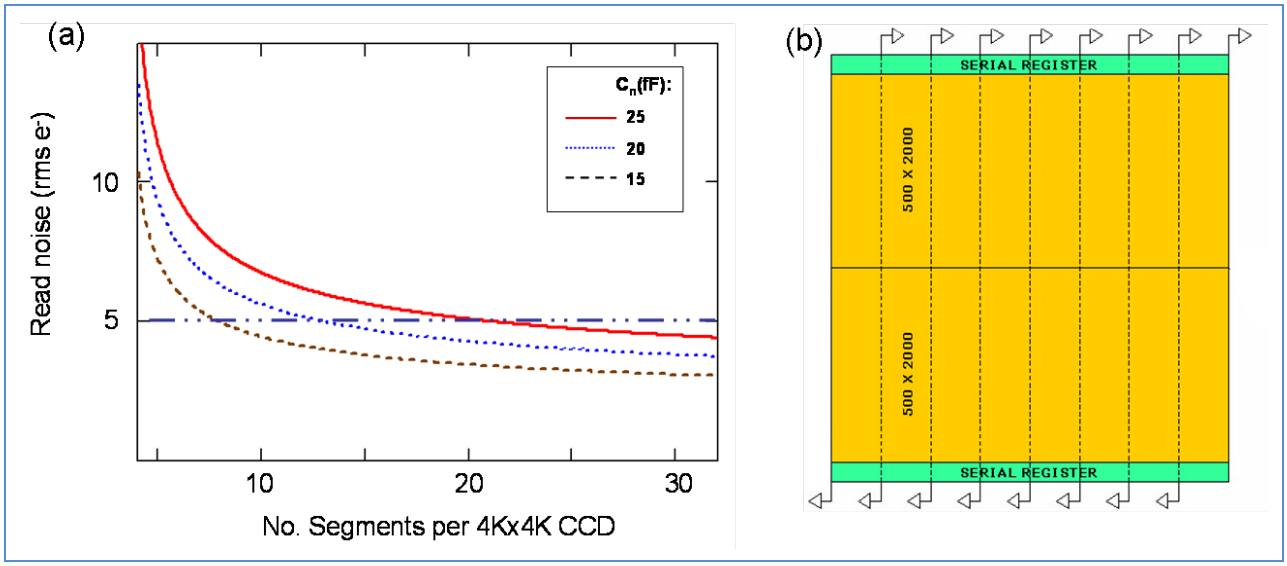

Figure 8-7: (a) Estimated read noise for a 4K x 4K sensor constrained to 2s readout time. Increasing the segmentation allows the clock rate, and hence the read noise, to be reduced. Noise estimates are based on CCD output transistor properties with three values of sense node capacitance. (b) Proposed layout of a 16-fold segmented, 4K x 4K CCD for fast, low-noise readout

8.3.4 Packaging

LSST's fast optics, large mosaic focal plane, and highly parallel readout electronics lead to the need for a highly specialized CCD package:

- The shallow depth of focus demands strict control of the imaging surface z-height
- 4-side buttable packages are required with small chip-to-chip gaps to minimize dead area
- Electrical interconnect for 16 video outputs, plus clock and bias connections must be accommodated without introducing crosstalk or otherwise compromising signal integrity
- Good thermal contact to the raft baseplate is necessary

The science sensor package is therefore a critical component and its design will significantly contribute to the CCD performance in this application.

8.3.4.1 Mechanical Design

For a fully depleted CCD, the non-imaging periphery has to include space for the amplifiers, electrical bus lines, bond pads, and field-terminating structures (guard rings). Experience with silicon detectors for particle tracking indicates that the guard ring area should be about 2.5 times the chip thickness to keep lateral fields in the substrate negligibly small. We adopted a raft geometry with a pitch of 42.25mm between CCDs in x and y. The package physical dimension will be no greater than 42mm x 42mm, leaving maximum gaps of .25mm between packages on the raft. This gap spacing is feasible if the package x-y-theta position is constrained by a pair of alignment pins and corresponding holes in the raft baseplate. Our design ensures this to be the case.

In most mosaic focal planes, sensors have at least one edge which cannot be closely butted to an adjacent device because the package requires extra space for wirebond connections to the sensor die; hence a new type of packaging is required for LSST. In Figure 8-8(a), the backthinned CCD is shown attached to a ceramic support with the edges of the chip cantilevered beyond the edge of the support to expose the bond pads on the front side (Derylo et al. 2006). Wirebonds connect these pads to traces on the ceramic support. In Figure 8-8(b), the CCD is bump-bonded to the ceramic support (Lesser and Tyson 2002). Both styles allow a high fill factor to be attained, since the connections to the CCD bond pads are made without consuming any area outside the chip periphery.

The gap between the outermost imaging pixels on adjacent chips is then equal to the package-to-package gap (0.25mm nominally) plus the width of the non-imaging region of the CCD (minimum of 0.25mm). Practical chip designs will require wider non-imaging peripheries on at least two edges to accommodate the amplifiers and serial registers. The gap between the outermost imaging pixels on adjacent chips will then be in the range of 0.75 - 1.8mm, equivalent to 15 - 37 arcsec**.**

Imaging surface flatness of 5-10 µm peak-to-valley has been achieved by several groups using chip flatteners which hold the imaging surface against a highly polished vacuum chuck during epoxy cure (Lesser and Tyson 2002). In LSST the imaging surfaces of all chips in the mosaic must be coplanar, so the packages must have tight parallelism and absolute height tolerances to the mounting surface, and this alignment must be preserved upon cooldown. Precision machining, athermal construction, and three-point mounting with built-in adjustability are mandatory for the LSST sensor packages.

8.3.4.2 Thermal Design

The heat path for thermal IR from the cryostat window and power dissipated by the clocks and on-chip source followers is through the package frame and mounting points to the raft baseplate, which in turn is cooled through copper straps to the cryoplate. A total of about 0.8W must be removed through this thermal path, and a thermal impedance of less than 5C/W is required.

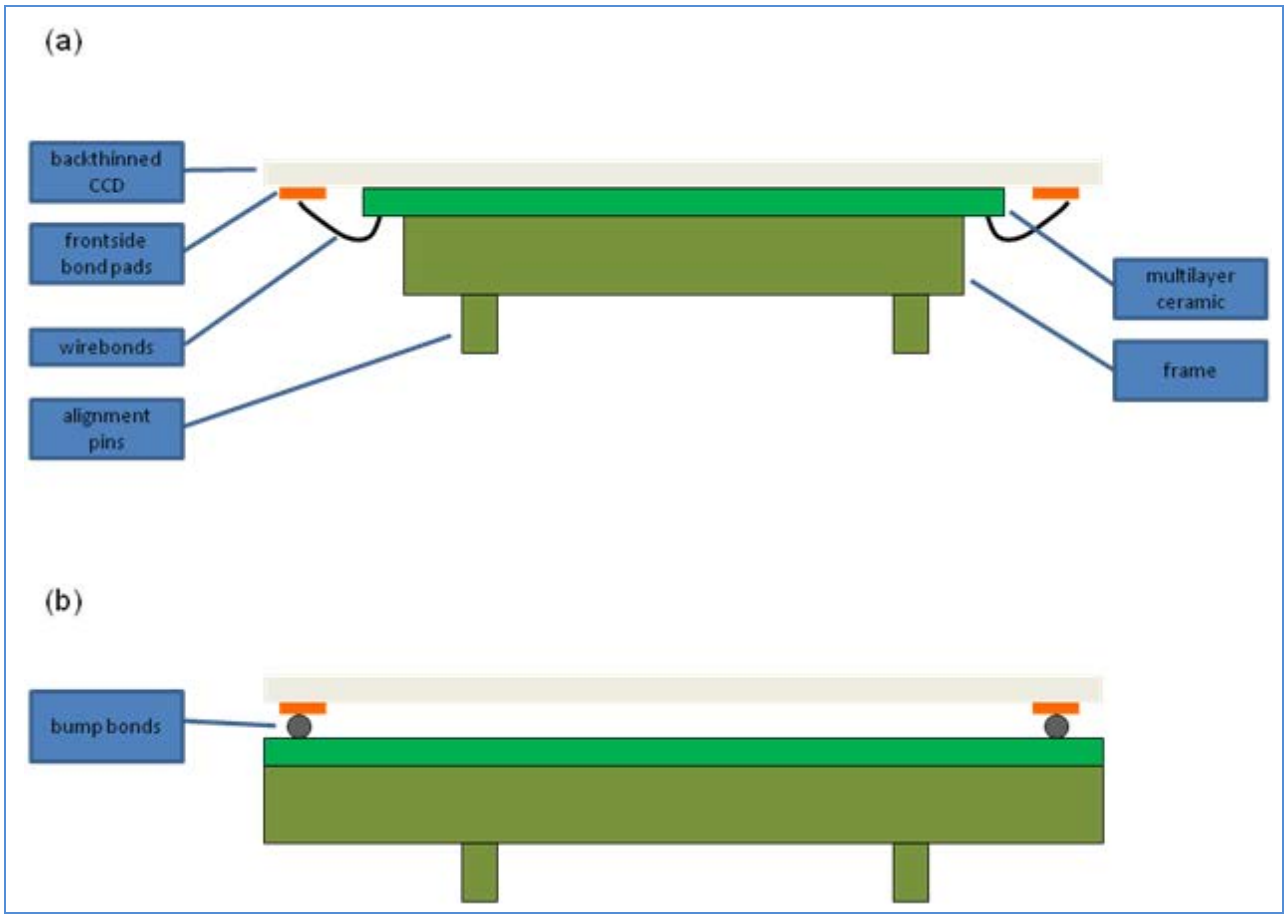

Figure 8-8: Buttable package construction

8.3.4.3 Electrical Interface Design

In the four-side butting arrangement of the LSST focal plane, the electrical connections must exit the sensors without extending past the 42 x 42mm boundary of the imaging surfaces. Each CCD will have a signal interface consisting of a complement of 70 to 100 wires on flexible printed circuit cables to the front end electronics. Many of these signals (amplifier outputs and drain bias) are highly susceptible to crosstalk, electromagnetic interference, and capacitive loading so the wiring interface must include short traces wherever possible to minimize capacitance; tightly-coupled return paths for signal currents; independently-buffered, low-impedance drive for the output drain and output gate (the signals most likely to induce crosstalk between segments); isolation between segment video outputs and between video and clock signals.

8.4 Sensor Development and Risk Mitigation

The performance demanded of the LSST science sensors has required a multi-year development program consisting of modeling and trade studies followed by prototype fabrication and testing. Details of the modeling effort have been reported in a number of publications (Lesser, Tyson 2002; Starr et al. 2002; Geary et al 2006; O'Connor et al 2007; O'Connor et all 2006) and led to the sensor design described in the previous section. This in turn was endorsed by the CD3a review process that authorized procurement of these long lead items.

8.4.1 Phase 1: Technology Demonstration

Recognizing the long lead time for semiconductor device development, the LSST project provided early funding for technology demonstration and prototyping. Phase 1 began in 2006 with the award of contracts to three vendors with the goal of addressing the most pressing technical challenges early. In this phase, both CCD and hybrid pin-CMOS devices were under consideration. The key objective of Phase 1 was fabrication of imaging structures on 100um-thick, fully-depleted silicon with a transparent conductive entrance window; vendors were given the option of selecting an appropriate format and packaging scheme for their demonstration devices. By 2008 all three vendors had completed demonstration devices which were evaluated in LSST labs. The characteristics and performance of the Phase 1 devices have been reported in detail in 2008 (Simms et al. 2007; O'Connor et al. 2008) and are summarized in Table 8-3.

Table 8-3: Results of Phase 1 prototypes. Dark current and full well results normalized to (10µm)^2 pixel area. Dark current measured at 180K. Read noise measured at 150kpix/s

Vendor	Device Technology	Format	Pixel Size (µm)	Outputs	Dark Current (e-/pix/sec)	Full Well (1000 e-)	Read Noise (e- rms)
e2v	CCD	2K x 4.5K	13.5	2	0.02	99	22
ITL/STA/DALSA	CCD	4k X 4k	10	16	<.03	90	15 - 25
Teledyne Imaging Sensors	Hybrid pin-CMOS	4k X 4k	10	32	6	55	13

Note that all the prototypes were fabricated on thick bulk, high resistivity silicon thinned to 100 µm and were able to achieve full depletion as indicated by the small extent of charge diffusion from x-ray conversions. All devices showed high sensitivity at near-IR wavelengths generally following the theoretical behavior for pure silicon. In the visible there were differences in quantum efficiency due to the use of different antireflection coatings on the prototypes. None of the devices were offered in buttable, high fill-factor packages in this phase.

Devices produced in Phase 1 were evaluated at LSST labs at BNL, Stanford, and Harvard-CfA. In addition, three on-sky tests were done on 1.2 – 2.4m telescopes at Kitt Peak. These telescope tests were aimed at exercising the new devices in realistic observatory conditions and comparing their imaging performance to existing instruments. Preliminary results from the prototypes show that standard instrument signature removal and data reduction techniques can be used.

The hybrid pin-CMOS device from Teledyne was fully functional and was found to be suitable for a number of astronomical investigations, primarily telescope guiding. However, it suffered from performance anomalies to a greater degree than the new CCDs (Simms et al. 2007, Simms 2009). These included image persistence, interpixel capacitance and interpixel charge transfer, high dark current, high number of nonfunctional pixels, and high read noise. Nonlinearity was also exhibited with a complex behavior depending on operating conditions. Although subsequent developments at Teledyne have resolved several of these issues, we judged that the benefits of hybrid pin-CMOS technology did not outweigh the performance limitations at the current state of technological maturity.

8.4.2 Phase 2: Full Prototypes

In February 2008, the LSST Corporation issued a Request for Proposals for CCD prototypes meeting the full set of optical, electrical, and mechanical specifications. The required deliverables included design reports, package mechanical samples, fully operable prototypes, and a manufacturability demonstration calling for operational devices from at least 2 lots of wafers to be manufactured with acceptable yield.

Awards were made to two vendors, e2v and ITL (with STA and Teledyne-DALSA). The fully-buttable packages offered by the two vendors differ in design and material choice but are each compatible with the raft mounting and alignment hole pattern of the raft. Illustrations of the packages are shown in Figure 8-9.

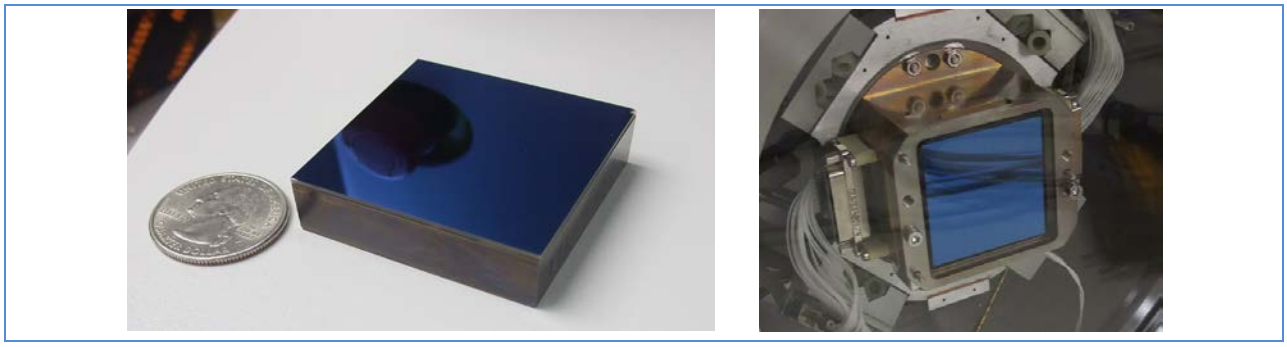

Figure 8-9: Phase 2a mechanical sample CCDs. Left: ITL/STA/DALSA. Right: e2v.

A total of 33 devices were delivered, 60% of which were operable and the remainder mechanical grade. During the course of the Phase 2 contracts, both vendors iterated their design and fabrication processes several times to achieve optimized performance. Electro-optic and physical metrology testing has verified that sensors from either vendor can meet LSST specifications. Detailed results were presented at the sensors Final Design Review, May 1-2 2013 (Stubbs et al. 2013). An illustrative selection of those results is shown in Figures 8-10 to 8-13. In addition to demonstrating the key performance parameters, the device-to-device reproducibility is very good (Figures 8-11, 8-12, 8-13) as required for obtaining adequate yield in a large production program.

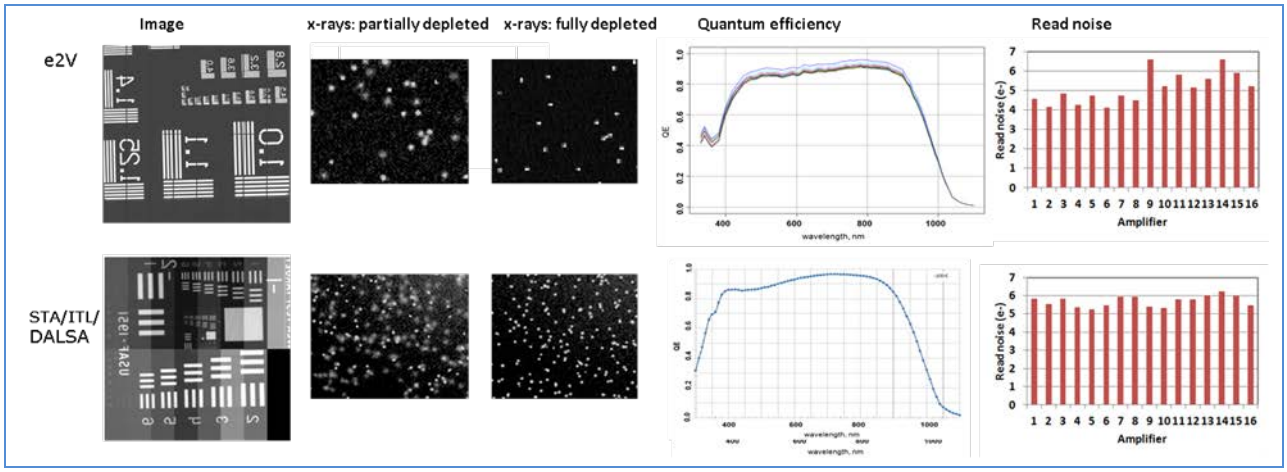

Figure 8-10: Selected results form Phase 2 sensor prototypes. Top: e2v. Bottom: ITL/STA/DALSA

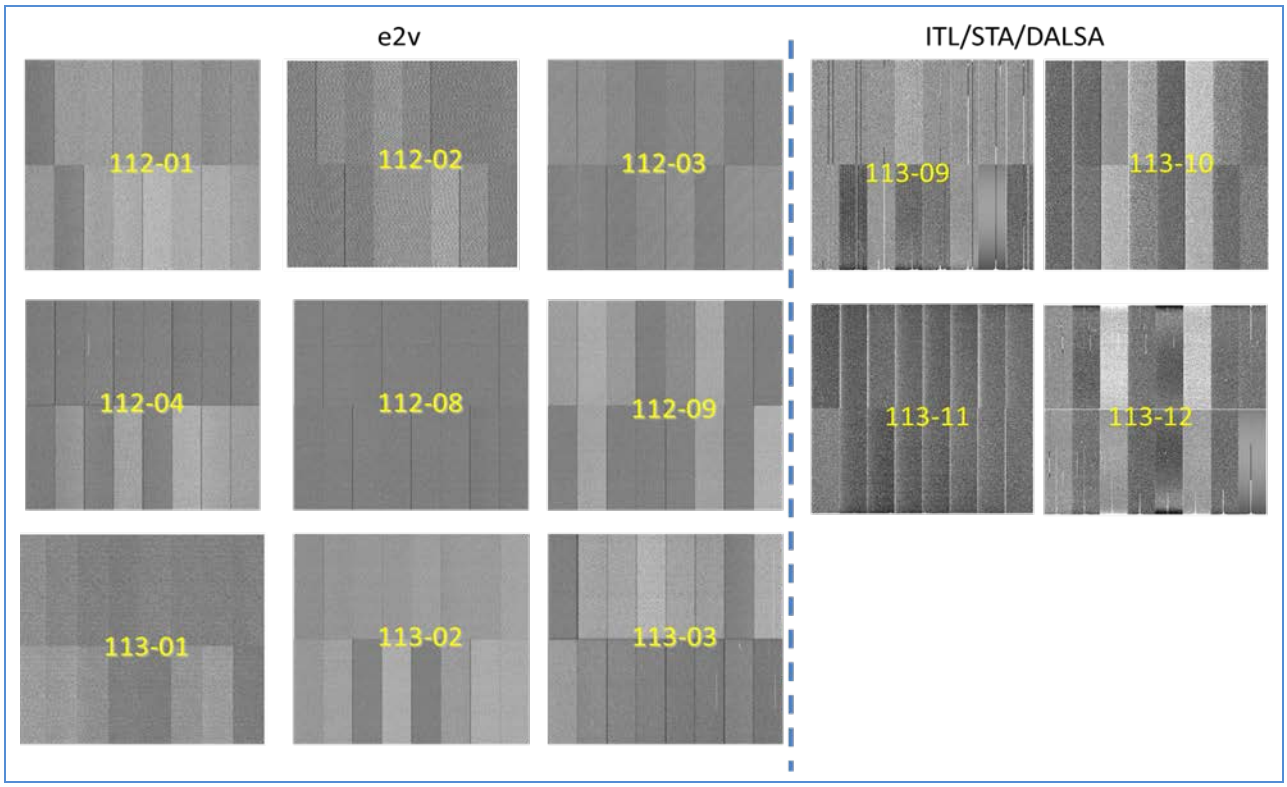

Figure 8-11: 500s dark frames, taken at -100C

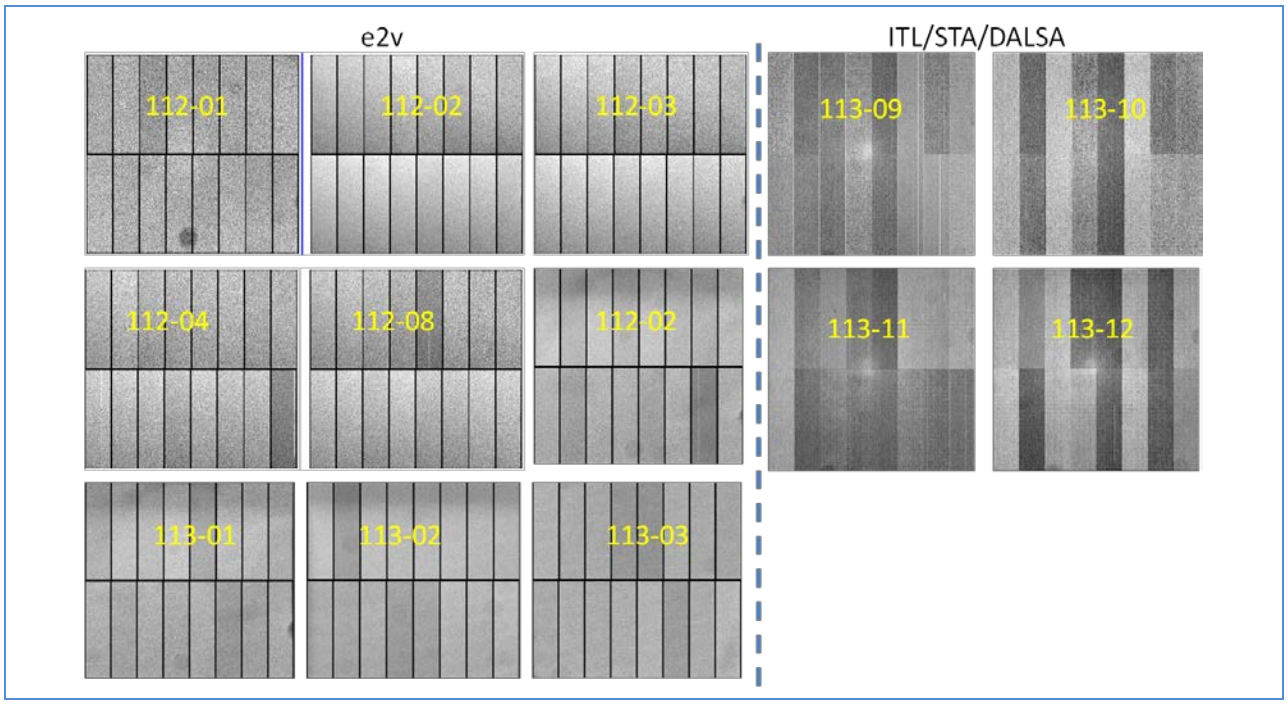

Figure 8-12: Midband flat fields, -100C

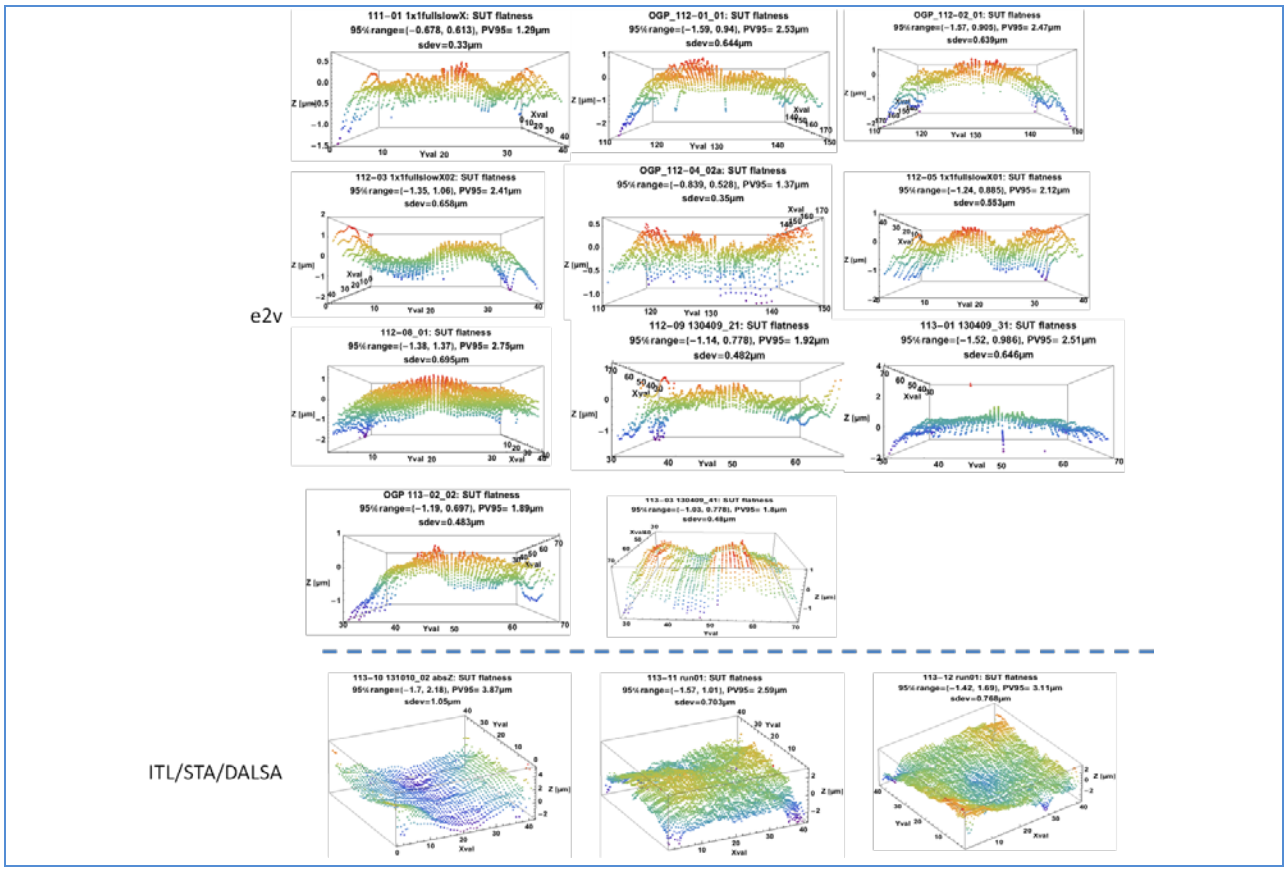

Figure 8-13: Flatness profiles of delivered sensor prototypes. The 95% peak-to-valley flatness for these devices is 2.40 ± 0.64μm

8.4.3 Summary of Prototype Sensor Development

A sustained program of prototype development lasting seven years has been concluded with two vendors demonstrating sensors meeting all LSST performance goals: 16-output, 4Kx4K devices which meet the key requirements of dark current, quantum efficiency, read noise, point spread function, and flatness. The CD3a Review committee recommended that LSST proceed to first article procurement, which is now under way. First article procurement contracts have been issued to the two vendors that produced qualifying prototype devices in 2014.

8.4.4 Risk Mitigation

We have attempted to mitigate the most serious sensor-related risks that could threaten either the science performance of the Camera or the schedule and budget of the construction project. Most importantly, we have sought to fund multiple vendors with manufacturing experience during the prototype development phases. Having more than one qualified supplier will permit flexibility in case of performance issues. By requiring each vendor to not only meet identical performance specifications but also compatible mechanical mounting features, we preserve the ability to change suppliers late in the development process. The prototype development program has been carefully phased to allow technological expertise to be gained incrementally. The sensor specifications have been stable except for minor changes in the QE profile for 4-plus years, and explicit descriptions of the special requirements

of LSST have been provided through documents and reviews to minimize misunderstanding. The remaining risks to the LSST program associated to sensors are considered minor.

8.5 References

Bai, Y., J. Bajaj, et al. (2008). Teledyne Imaging Sensors: silicon CMOS imaging technologies for x-ray, UV, visible, and near infrared, SPIE.

Boggs, K., R. Bredthauer, et al. (2007). Development of fully depleted scientific CCDs for astronomy, SPIE.

Derylo, G., H. T. Diehl, et al. (2006). 0.250mm-thick CCD packaging for the Dark Energy Survey Camera array, SPIE.

Dorland, B. N., G. S. Hennessy, et al. (2007). Laboratory and sky testing results for the TIS H4RG-10 4k × 4k 10-micron visible CMOS-hybrid detector, SPIE.

Geary, J., D. Figer, et al. (2006). The LSST sensor technologies studies, SPIE.

Holland, S. E., D. E. Groom, et al. (2003). "Fully depleted, back-illuminated charge-coupled devices fabricated on high-resistivity silicon." Ieee Transactions on Electron Devices **50**(1): 225-238.

Jorden, P., K. Ball, et al. (2006). Commercialization of full depletion scientific CCDs, SPIE.

Jorden, P. R., M. Downing, et al. (2010). Improving the red wavelength sensitivity of CCDs, SPIE.

Kotov, I. V., A. I. Kotov, et al. (2010). Study of pixel area variations in fully depleted thick CCD, SPIE.

Lesser, M. P. and J. A. Tyson (2002). Focal Plane Technologies for LSST, SPIE.

O'Connor, P., J. Frank, et al. (2008). Characterization of protojournal article LSST CCDs, SPIE.

O'Connor, P., V. Radeka, et al. (2006). Study of silicon thickness optimization for LSST, SPIE.

O'Connor, P., J. Geary, et al. (2007). "Technology of the LSST focal plane." Nuclear Instruments and Methods in Physics Research Section A: Accelerators, Spectrometers, Detectors and Associated Equipment **582**(3): 902-909.

Radeka, V., J. Frank, et al. (2009). "LSST sensor requirements and characterization of the prototype LSST CCDs." Journal of Instrumentation **4**.

Rajkanan, K., R. Singh, et al. (1979). "Absorption-Coefficient of Silicon for Solar-Cell Calculations." Solid-State Electronics **22**(9): 793-795.

Simms, L. M., D. F. Figer, et al. (2007). First use of a HyViSI H4RG for astronomical observations, SPIE.

Simms, L.M. (2009). HYBRID CMOS SIPIN DETECTORS AS ASTRONOMICAL IMAGERS, Ph.D. dissertation, Stanford University

Starr, B. M., C. F. Claver, et al. (2002). LSST Instrument Concept, SPIE.

Stubbs, C.W. , O'Connor, P. et al. (2013) LSST Camera Sensors Final Design Review, available: https://confluence.slac.stanford.edu/display/LSSTCAMREV/Sensors+Final+Design+Review%2C+May+1-2%2C+2013

9: Guide and Wavefront Sensors

9 Guide and Wavefront Sensors

9.1 Introduction

As discussed in Chapter 3, the Camera provides sensor data to a Telescope guide loop used to fine tune Telescope tracking. This guide loop uses changes in detected star position to estimate and correct tracking deviations. The Telescope team supplies the detailed requirements to the Camera. In addition, the Camera provides wavefront sensor data to the Telescope.

The Camera Project has chosen a baseline design in which CCDs provide both guide and wavefront sensor data; these CCDs and their readout infrastructure are mounted on Corner Rafts located in the periphery of the focal plane. This chapter covers those CCD readout characteristics relevant to guide and wavefront data collection; since the guide sensors are identical to and the wavefront sensors are closely modeled on the science data sensors, readers are encouraged to consult detailed information on the science sensors in Chapter 8 for additional information. Chapter 11 provides a thorough discussion of the Corner Raft mechanical and electronics architecture.

9.2 Guide Sensing

9.2.1 Guider Requirements and Interfaces

The LSST Telescope has critical requirements on tracking error to meet image quality specifications, and will require closing a guiding loop between the Camera and a Telescope servo control. The Camera Guider subsystem consists of eight guiding sensors located at the edge of the 3.5 degree field of view. All eight sensors will be read simultaneously at a high rate (up to 9 Hz), and centroids from each will be fed to the telescope and rotator servo controls, for real-time tracking error correction.

The critical parameters needed by the Telescope Subsystem are centroid noise, centroid frame rate, and transport delays. The centroid noise needed by the telescope for effective guiding constrains the read noise of the Guide sensor as well as the integration time. This in turn, combined with required frame rate, constrains the readout time.

Observatory seeing conditions combined with the expected uncertainty in the telescope rotators define the size of the guide window needed around a guide star candidate and are expected to be of the order of a 50x50 pixel window.

9.2.2 Guide Sensor Design

The Guider subsystem will use sensors acquired during science sensor procurement. They will meet exactly the same CCD specifications as the sensors used on the science sensor array. This allows Guider sensor development to leverage significantly from the science sensor development program. However, windowing and readout requirements differ significantly between guiding readout and science rafts, giving the Guider subsystem a distinct readout sequence and cadence. In addition, windowing requirements make image smear an important consideration for guide sensing.

9.2.2.1 Guide Sensor Readout Sequence

A detailed discussion of the guide sensor readout electronics package is provided in Corner Raft design description in Chapter 11.

Operationally, windowed readout of a full-frame CCD consists of four steps: integration; shifting the charge in the guide window to the output amplifier; reading the selected pixels; and clearing parasitic charge from the ROI before beginning the next integration. The cycle must be repeated at a 9 Hz rate to meet the guiding requirement for LSST.

As described in Chapter 5, the Camera CCD sensor is a full-frame 4K × 4K device with 10μm pixels (0.2″/pixel) organized as 16 independent 2K × 0.5K segments, each with individual readout. The parallel (vertical) and serial (horizontal) clocks are common to all segments. The parallel clock readout rate is limited by RC time constants on the polysilicon parallel clock lines; the manufacturer estimates the minimum parallel (row) transfer time to be 16 μsec. In normal operation the serial clock rate is limited by the allowable readout noise. The relation between pixel read rate and noise may be estimated as:

$$R_{ON}(f) = \frac{1}{2}\sqrt{C_n(1+\frac{f}{f_0})}$$

where R_{ON} is the read noise in rms electrons, C_n is the sense node capacitance in femtoFarads (assumed to be 16fF for our device), $f = 1/t_{ss}$ is the readout frequency, and f_0 is a flicker noise corner frequency (150kHz for this technology). The science sensors are read out at about 540kpix/s giving an R_{ON} of less than $8e^-$. The serial register can be clocked more rapidly when low-noise readout is not necessary, as when clearing charge. Based on CCDs with similar characteristics (e2v technologies plc, CCD231-84 Datasheet) we estimate a fast serial clock rate of t_{sf} = 400ns per pixel. We also have the opportunity and ability to bin the guide sensor readout, thereby reducing the effects of read noise.

The time to read out an ROI window can be precisely estimated, as described below in Section 9.4.1. The overall readout time necessary to retrieve the guide window size needed by the telescope is between 1.24ms to 35 ms based on the location of the window. This is consistent with the integration time specified for this device derived from the centroid noise after processing.

9.2.2.2 Image Smear

An important source of centroid error in CCDs is image smear during charge shift and readout; that is, while the window is shifted to the readout amplifier and read out with open shutter.

The guide window "box" will accumulate additional photoelectrons due to photons (from sky, sources, or stray/scattered light) or cosmic rays that are incident on pixels along the path taken by the guide window charge during its transport to the readout register. Those pixels are a small fraction (never more than 0.2%) of the sensor area and so the probability of them intercepting another bright source is low; in general the location of bright sources will be known in advance and the guide star can be chosen to avoid these interfering sources. Flux from sources dimmer than the guide star could contaminate the centroid. However, smeared charge from such sources is only integrated during the time the ROI window is shifted across their PSF. For any given pixel in the ROI, the time spent shifting across an interfering source to the integration time is t_{par}/T_{int} = 16µs/75ms = 2.1×10^{-4}. Hence, the amount of smeared, structured charge that could interfere with the centroid estimate will be negligible. Sky background flux is low (less than 200 e^-/s/pixel) and unstructured; it will add a constant signal to all pixels in the window which will not contribute to centroid error. Lastly, since the streaked charge due to row transfers is deterministic, we can always choose to make an appropriate subtraction, but we do not expect for this to be necessary.

The most significant source of smear is the guide star itself. As pixels are shifted through the guide window they will accumulate flux from the guide star, but the flux will be mis-registered. Consider the simplified diagram shown below, which depicts a 5 × 5 pixel ROI centered on a guide star at CCD row 3.

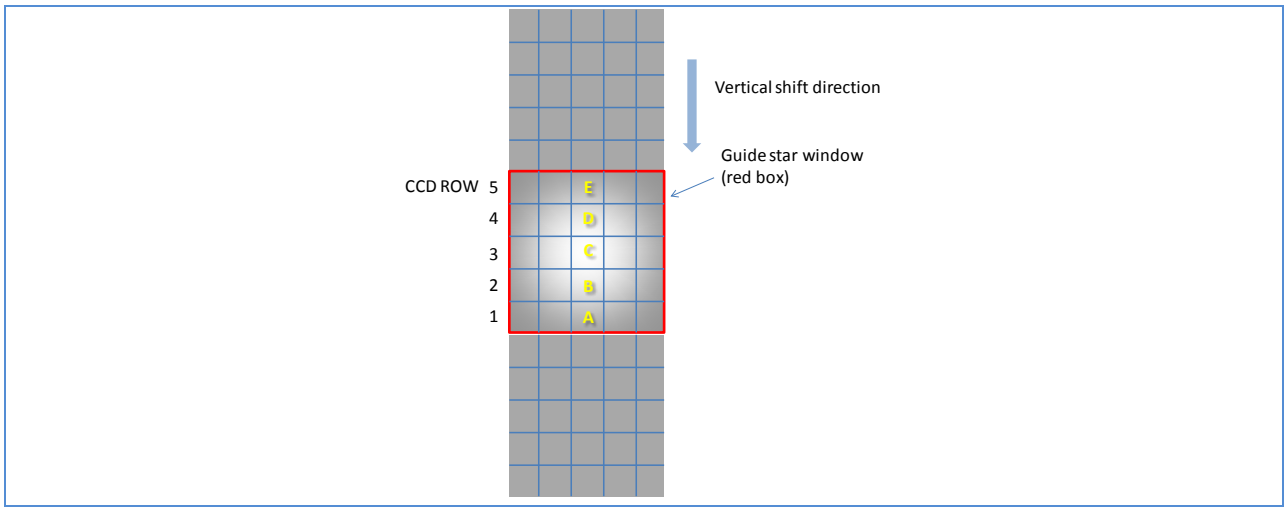

Figure 9-1: Simplified illustration of ROI with guide star centered at CCD row 3.

The vertical shift direction is indicated by the blue arrow. Yellow labels A-E denote charge packets that will be read out. Figure 9-2 below illustrates the readout sequence. Before integration the situation is as shown in Figure 9-2(a). The last four cycles of the clear phase are shown in Figure 9-2(b-e), during which the charge packets A-E are exposed to flux from the guide star (we assume that all sources of flux other than the guide star are insignificant.)

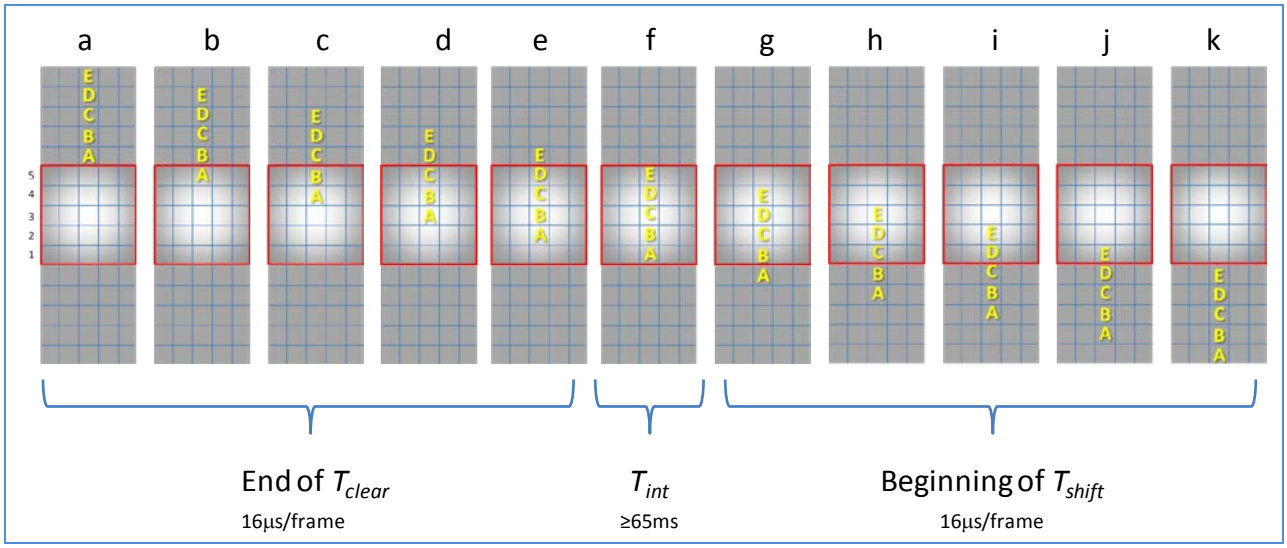

Figure 9-2: Charge packets A--E are shifted into and out of the ROI region. The smeared charge from the CLEAR and SHIFT phases adds to a constant offset which does not affect the centroid.

The obvious symmetry of the readout sequence through the ROI argues that the smeared charges from the clear and shift phases cancel out, as long as atmospheric transparency does not vary on the row transfer rate timescale, leaving only a constant term in each pixel which will not contribute to centroid error. This intuition is borne out by the analysis presented in 9.4 below

9.3 Wavefront Sensing

9.3.1 Wavefront Sensing Requirements

The LSST Telescope experiences aberrations from its three mirrors due to changing gravitational forces and thermal drifts. Those changes are corrected by actively controlling the surface shape and position of each mirror with actuators. The active optics system does not correct for the rapidly changing atmospheric turbulences as would an adaptive optics system operating at higher temporal frequencies. The LSST wavefront sensor integration time is 15 seconds (same as the science sensor array). Our objective is to compensate figure and positioning errors in the three-mirror LSST optical train, not to correct for atmospheric turbulence with an adaptive optics system (doing so over the wide field of LSST is simply not practical)). Because three different mirrors have to be controlled, different field angles must be used to tomographically reconstruct the wavefront data. It has been shown that four wavefront sensors collecting data on reference stars in a square geometry is conceptually sufficient to perform the tomographic reconstruction by using a Zernike expansion to parameterize the aberrations at each of the mirror surfaces. This, combined with the expected ability of finding a suitable star for each wavefront sensor, has driven the wavefront sensor to be located at 4 field angle collection points (at the corner raft location) and cover the equivalent of two science sensor areas at each location. Because of the fast f number of the overall LSST optical system, the wavefront sensors have to be co-located with the science sensor in the focal plane.

Curvature wavefront sensing has been chosen as the baseline method for LSST based simplicity and large effective field of view. Additionally the desire for using similar infrastructure as the science sensors for packaging, data readout, processing and transport has also supported this choice since it is easily implemented using CCDs. We will effectively break a science sensor in half, and place one half above and one below the nominal telescope focal plane. The format of the wavefront sensors is very similar to the main science and guide sensors, allowing us to capitalize on the electronics and packaging engineering that has been developed for the science rafts.

A curvature wavefront sensor uses the difference in intensity between the intra and extra focal stellar image, allowing one to estimate the second derivative (or curvature) of the local wavefront. Traditionally, curvature wavefront sensors image the same star on either side of focus by pistoning the sensor. In LSST, a split detector was chosen as the baseline design, one half at an intrafocus location and one half at an extra focus location, imaging different stars at two nearby field locations. The value of the defocus distance is a parameter that needs to be carefully chosen, and is a balance between too much blur from the atmosphere for small offsets and not enough signal-to-noise ratio for large offsets. While not extremely sensitive to the absolute defocus, the design needs to have a good knowledge of the actual location of the two half-sensor devices as well as a local uniformity driven by the size of the defocused stars on the sensor. Those two requirements, besides driving metrology calibration requirements, define the flatness of each sensor as well as the tolerancing of the split sensor assembly. The signal to noise ratio needed and related to the offset chosen between the intra and extra focal half sensors is also a driver for the selected sensor and was chosen to match the science sensor performance.

9.3.2 Wavefront Sensor Design

LSST requires four wavefront sensors assemblies (each assembly comprises two devices) located in the Corner Rafts at the periphery of the focal plane (see below).

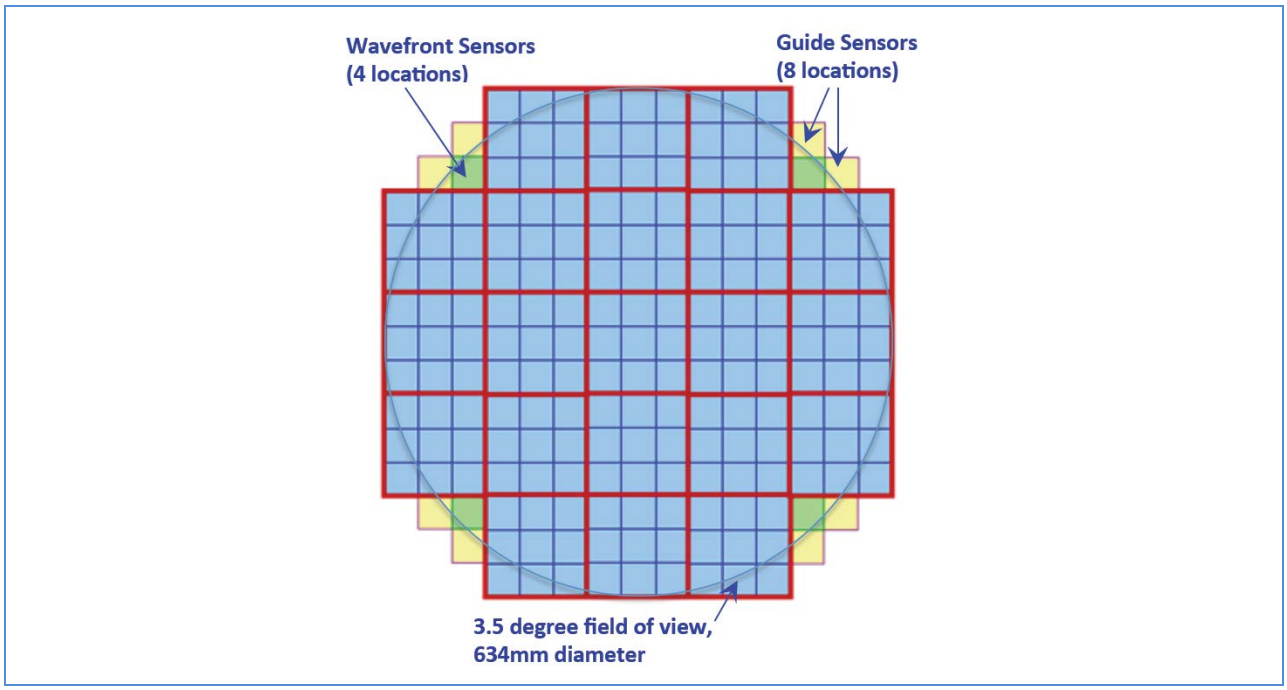

Figure 9-3: Organization of the Camera focal plane, showing wavefront sensor locations

A depiction of a wavefront sensor device is shown in Figure 9-4 below. Two 2K x 4K segmented CCD devices will be packaged and offset relative to the Science focal plane to produce intra and extra focal images as an assembly. Wavefront sensor CCDs will share the layout and processing of the Science sensors, and have similar performance as Science CCDs regarding quantum efficiency, point spread function, read noise, and readout speed.

The primary LSST science sensors are high-rho sensors of roughly 4096X4096 format, with two registers and eight outputs at top and bottom. The wavefront sensor assembly will be a pair of packaged devices of approximately 4096X2048 format, co-mounted with a specified step height difference on a supporting step-plate. Each 4096X2048 device is equipped with eight outputs from one register.

The existing science sensor package concept will be used, with a similar packaging approach but in half the size for each wavefront sensor device. The support block and ceramic concept will be unchanged and adapted to accommodate the 2kx4k pixel form factor. The die size for a 2kx4k device is expected to be 41.58 X 21.35 mm. There is a gap between the last image row and the edge of the package of about 0.68 mm. This means that at least 680 µm of the central gap is not available for imaging, which is acceptable with the requirements. In addition the flex cable lengths are slightly different from the science sensor cables to accommodate the increased length and reversal of one of them.

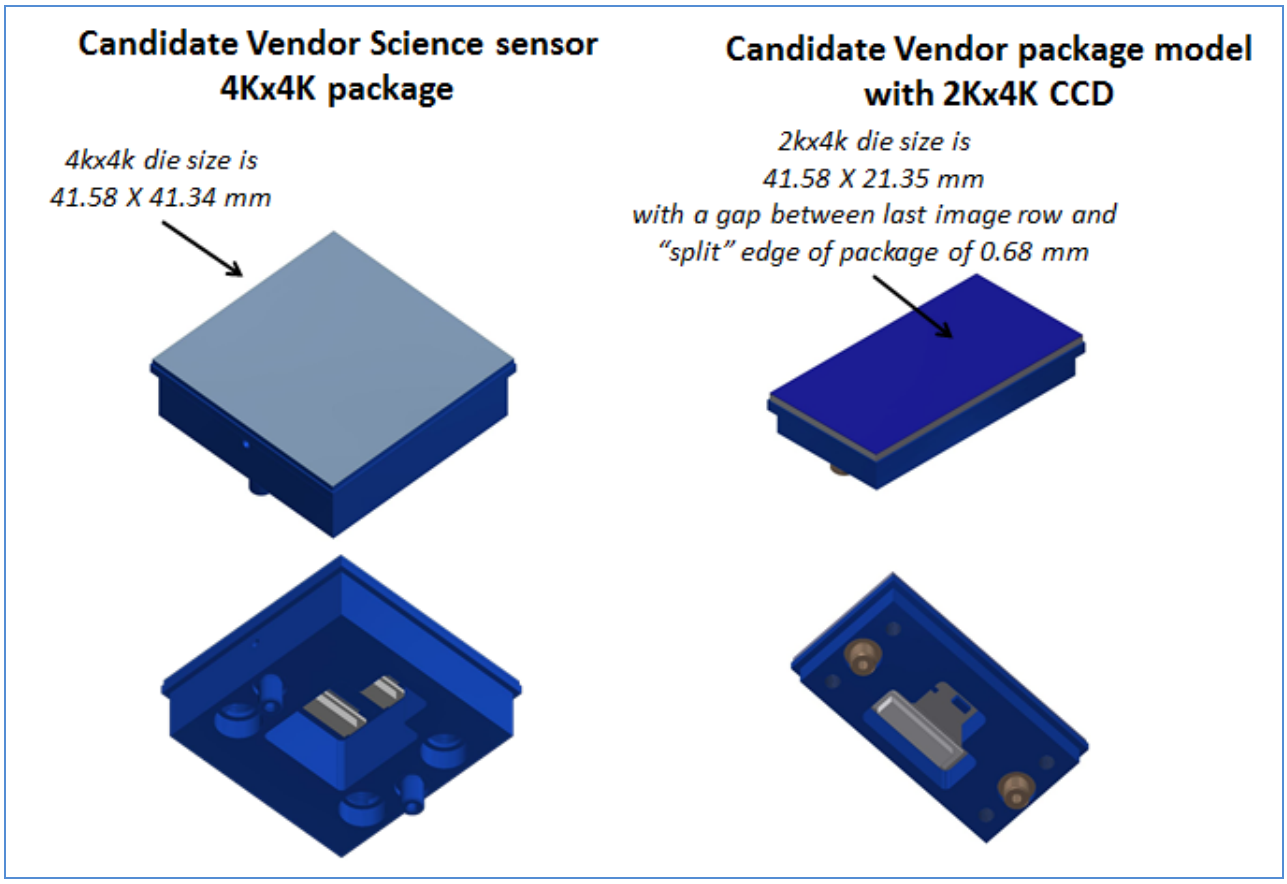

Figure 9-4: Wavefront sensor (right) device compared against science sensor (left).

Accurate wavefront sensing is critical for LSST to reach its science goals. Simulations performed at LLNL predicted the method would work, and this has been confirmed by the LSST team based in Tucson as part of the algorithm prototype testing effort under way (See Angeli et al, SPIE 9150). To develop confidence for the LSST wavefront sensing method, an optical wavefront testbed has been built (depicted in Figure 9-5). It has a capability of producing aberrated images that can be used to develop wavefront reconstruction algorithms or to improve existing ones. Low order aberrations such as astigmatism and coma are introduced into a collimated beam by means of different lens configurations. A special focusing lens (f/1.23) provides an LSST-like fast beam. A CCD camera with pixel size (9 µm) similar to the LSST Science sensors (10 µm) records the images. Moving the camera in and out of focus provides defocused images.

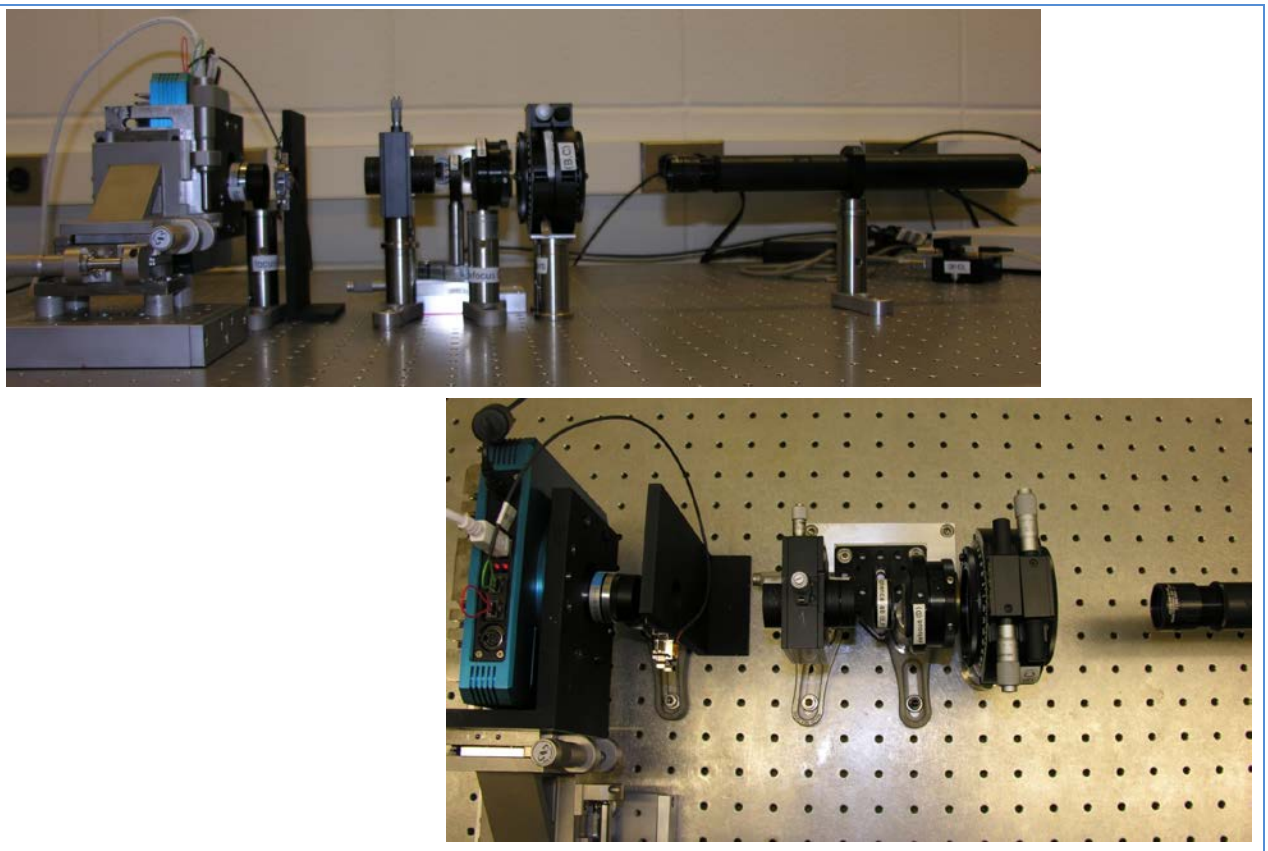

Figure 9-5: Optical wavefront testbed

Images taken with the testbed, by displacing the camera ± 1mm out of focus, are shown in Figure 9-6 below. To simulate the LSST central obscuration a mask is used to block the central beam. Centrally obscured images are also shown in Figure 9-6 as donuts. Recording images from the camera on each side of focus enables reconstruction of wavefront aberrations.

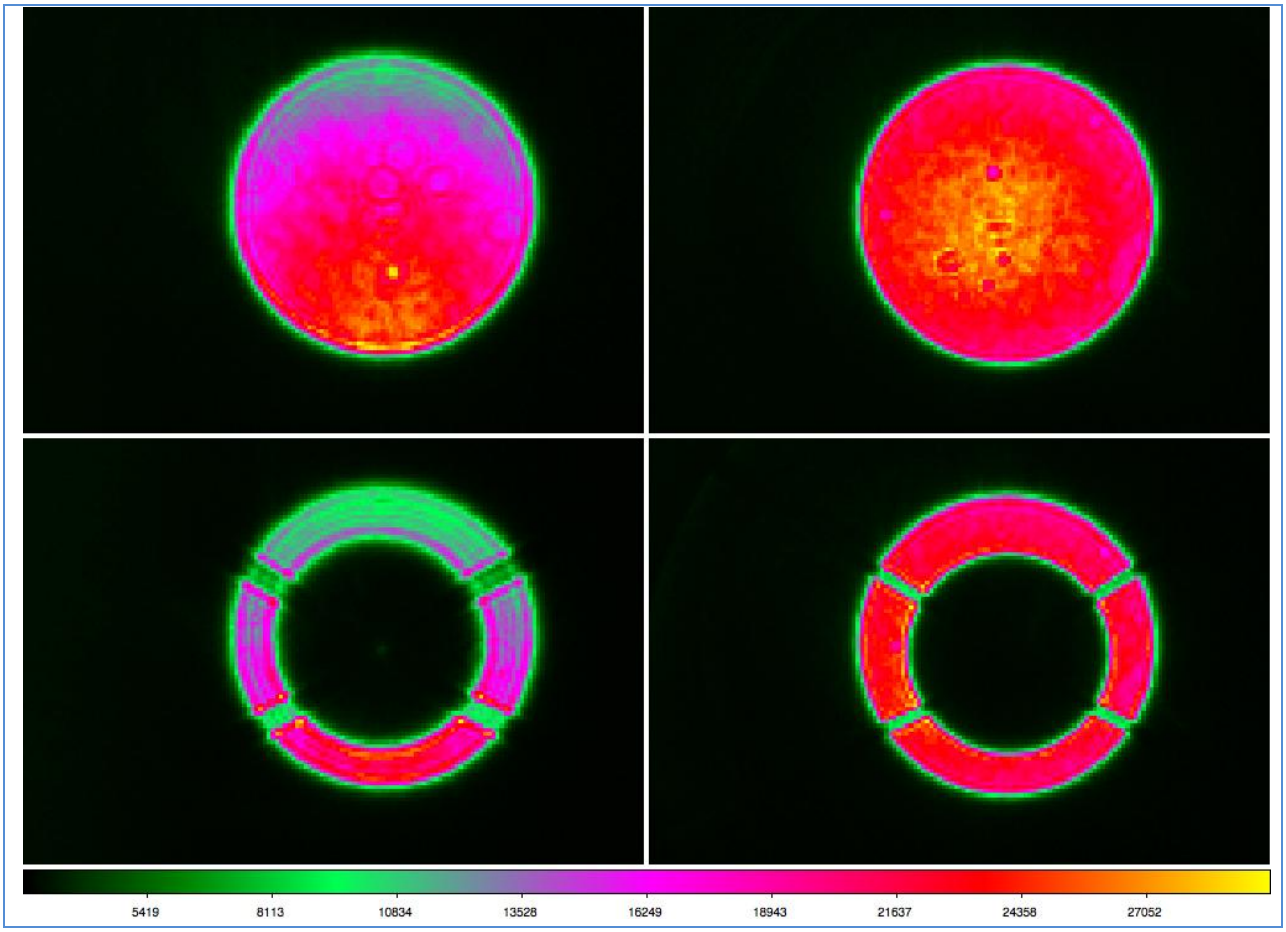

Figure 9-6: Images acquired with the optical wavefront testbed. Images are with (below) and without a central obscuration (above).

9.4 Supplemental Analysis

9.4.1 Guide Window Readout Time

The time to read out an ROI window can be estimated.

Let us denote the following quantities:

$N_x = 2002$	number of rows per segment
$N_y = 522$	number of columns per segment (including prescan)
$6 < N_{pixy} < 25$ seeing and binning	size of ROI window in row direction; adaptive depending on
$N_{pixx} = N_{pixy}$	size of ROI window in column direction
$0 < N_{off\text{-}y} < N_y - N_{pixy}$	offset of corner of ROI from amplifier in row direction
$0 < N_{off\text{-}x} < N_x - N_{pixx}$	offset of corner of ROI from amplifier in column direction

t_{par} = 16µs vertical row transfer time

t_{sf} = 0.4µs fast serial shift time per pixel

t_{ss} = 1.9µs serial pixel rate for low noise readout

Then the times for the components of the window readout cycle will be:

INTEGRATE: T_{int}

SHIFT: $T_{shift} = N_{off\text{-}y} \times t_{par} + 3N_x \times t_{sf}$

READ: $T_{read} = N_{pixy} \times (N_{off\text{-}x} \times t_{sf} + N_{pixx} \times t_{ss} + t_{par})$

CLEAR: $T_{clear} = N_{pixy} \times t_{par}$

During T_{shift} the serial and parallel clocks are operated at t_{sf} and t_{par} respectively while the Reset Gate (RG) is held high to remove charge; readout sampling and digitizing are not operated. Because $t_{par} < N_x \times t_{sf}$ there will be multiple rows of charge building up in portions of the serial register. The second term in the expression for T_{shift} accounts for the need to clear accumulated charge from the register after completing the $N_{off\text{-}y}$ line transfers, before starting the ROI readout.

During READ the N_{pixy} lines of the ROI window are read out using the normal science sequencing, except that the serial register may be clocked at a fast rate (t_{sf}) until it reaches the first column of the ROI window.

Time T_{clear} is necessary to remove accumulated charge from the image area pixels in the ROI, because those pixels will be accumulating charge during the previous T_{read} sequence which can last several milliseconds.

9.4.2 Charge Smearing During Readout of the Guide Window

The guide window readout sequence is illustrated above. Some terms in the following analysis are defined in Section 9.4.1 above.

During guide window readout, charges accumulated will be:

$$Q_{Acl} = t_{par} \times (F_5 + F_4 + F_3 + F_2)$$

$$Q_{Bcl} = t_{par} \times (F_5 + F_4 + F_3)$$

$$Q_{Ccl} = t_{par} \times (F_5 + F_4)$$

$$Q_{Dcl} = t_{par} \times F_5$$

$$Q_{Ecl} = 0$$

where F_i is the guide star flux in CCD row *i*, in the center column of the ROI. Figure 9-2(f) above shows the position of the charge packets during integration. They acquire charge

$$Q_{Aint} = T_{int} \times F_1$$

$$Q_{Bint} = T_{int} \times F_2$$

$$Q_{Cint} = T_{int} \times F_3$$

$$Q_{Dint} = T_{int} \times F_4$$

$$Q_{Eint} = T_{int} \times F_5$$

Figure 9-2(g-j) shows the first four cycles of the SHIFT phase. The pixels acquire charge:

$$Q_{Ash} = 0$$

$$Q_{Bsh} = t_{par} \times F_1$$

$$Q_{Csh} = t_{par} \times (F_2 + F_1)$$

$$Q_{Dsh} = t_{par} \times (F_3 + F_2 + F_1)$$

$$Q_{Ecl} = t_{par} \times (F_4 + F_3 + F_2 + F_1)$$

The total charge that reaches the readout is then:

$$Q_A = (T_{int} - t_{par}) \times F1 + t_{par} \times (F_5 + F_4 + F_3 + F_2 + F_1)$$

$$Q_B = (T_{int} - t_{par}) \times F2 + t_{par} \times (F_5 + F_4 + F_3 + F_2 + F_1)$$

$$Q_C = (T_{int} - t_{par}) \times F3 + t_{par} \times (F_5 + F_4 + F_3 + F_2 + F_1)$$

$$Q_D = (T_{int} - t_{par}) \times F4 + t_{par} \times (F_5 + F_4 + F_3 + F_2 + F_1)$$

$$Q_E = (T_{int} - t_{par}) \times F5 + t_{par} \times (F_5 + F_4 + F_3 + F_2 + F_1)$$

i.e. the smeared charge from the CLEAR and SHIFT phases cancel, leaving only a constant term in each pixel which will not contribute to centroid error.

9.5 References

George Z. Angeli ; Bo Xin ; Charles Claver ; Douglas MacMartin ; Douglas Neill ; Matthew Britton ; Jacques Sebag ; Srinivasan Chandrasekharan; Real time wavefront control system for the Large Synoptic Survey Telescope (LSST). Proc. SPIE 9150, Modeling, Systems Engineering, and Project Management for Astronomy VI, 91500H (August 4, 2014); doi:10.1117/12.2055390.

Baker, K. L. and L. G. Seppala (2010). Shack-Hartmann wavefront sensing performance evaluation for active correction of the Large Synoptic Survey Telescope (LSST), SPIE.

e2v technologies plc. CCD231-84 Datasheet "CCD231-84 Back Illuminated Scientific CCD Sensor".

Gressler, W. J., C. F. Claver, et al. (2005). LSST Wavefront and Alignment Sensing. American Astronomical Society Meeting Abstracts. **37:** 1205-+.

LSST Document Archive, Collection-886. LSST Baseline Optical Design.

LSST Document Archive, Document-10055. Functional Assessment of Alternate Configurations for the Curvature Wavefront Sensors for the LSST Camera

Manuel, A. M., D. W. Phillion, et al. (2010). "Curvature wavefront sensing performance evaluation for active correction of the Large Synoptic Survey Telescope (LSST)." Optics Express **18**(2): 1528-1552.

Rodigas, T., C. F. Claver, et al. (2007). A Prototype Automated Wavefront Sensing Pipeline for the LSST. American Astronomical Society Meeting Abstracts. **38:** #137.117-+.

10: Science Raft Towers

10 Science Raft Towers

10.1 Introduction

Unlike most astronomical imagers, LSST's mosaic camera will be constructed from 21 identical modules, known as "rafts". This choice is motivated by the large area of the focal plane (3217 cm^2 unvignetted field) and issues of integration, test, and maintainability. The alternative option, a monolithic structure supporting the entire complement of sensors and electronics, leads to difficulty accessing the central portion of the array during construction and repair. Each raft module can be operated as an autonomous, fully functional, and testable camera. In view of the long production time for sensors, series production and testing of the rafts streamlines and reduces risk for the project. By maintaining a set of hot spares, the mean time to repair the camera in the event of sensor or electronics failures can be minimized. A diagram of the focal plane layout is shown in Figure 10-1.

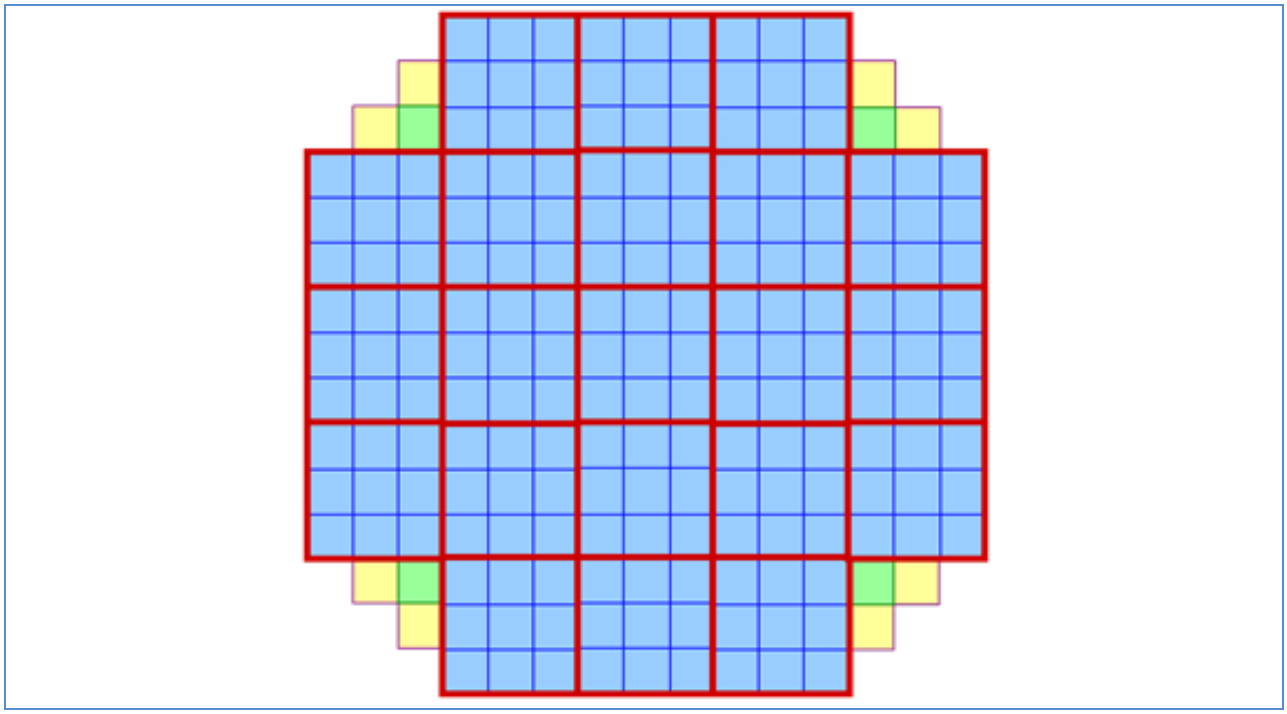

Figure 10-1: Focal plane organization: science sensors (blue), guide sensors (yellow), wavefront sensors (green), Science Raft boundaries (red).

10.2 Requirements

The Science Raft Tower Module must provide:

- • Precise mechanical location and support for the CCD array
- • Electronic support functions to control and read out the CCDs
- • Thermal management of the CCDs and electronics.

Mechanical requirements are extremely stringent and include locating the CCD imaging surfaces to within a narrow flatness envelope and with gaps of 0.150 mm between adjacent CCDs, and 0.250mm between CCDs on adjacent rafts. As a result of the fine segmentation of the CCDs, the Science Raft

Tower Module has to implement all electronic functions of a 144-channel CCD controller in a volume contained within the projected footprint of the Raft. Although low-power ASICs are used, their total power dissipation is significant and that power must be removed from the Cryostat through adequate thermal paths. Finally, the imaging surfaces of the CCDs must be protected from contamination by condensable materials in the electronics enclosures.

10.3 Science Raft Tower Module Design Description

The science raft tower module (RTM), shown in Figure 10-2, is the modular building block of the camera focal plane and consists of three major assemblies:

- The raft-sensor assembly (RSA) is a 3 x 3 mosaic of science CCDs in precision packages, mounted on a silicon carbide baseplate. The RSA also includes temperature sensors, resistive heaters, and flexible electrical and thermal connections.

- The Raft Electronics Crate (REC) houses three circuit boards (REBs) and contains copper planes providing the thermal path for cooling the RSA and the CCDs.

- The Raft Electronics Board (REB) contains custom video processing and clock/bias buffering electronics plus video digitizing, clock sequencing, bias generation, temperature sensing, and interfacing to the control and data acquisition systems.

All components of the RTM are contained within the camera cryostat vacuum space. The RSA and REC are maintained at an operating temperature of around -100^{o}C. This temperature is chosen as a compromise between sensor dark current and near-IR quantum efficiency. The REBs operate at a warmer temperature, to reduce the load on the cryo cooling system and to allow the use of standard commercial electronics. The power dissipated on the REBs is extracted via a cold plate that is held at -40C. To prevent volatile contaminants from condensing on the CCD imaging surfaces several precautions are taken: The circuit boards and components are tested for low outgassing of volatiles, CCDs are never allowed to be the coldest surfaces in the cryostat.

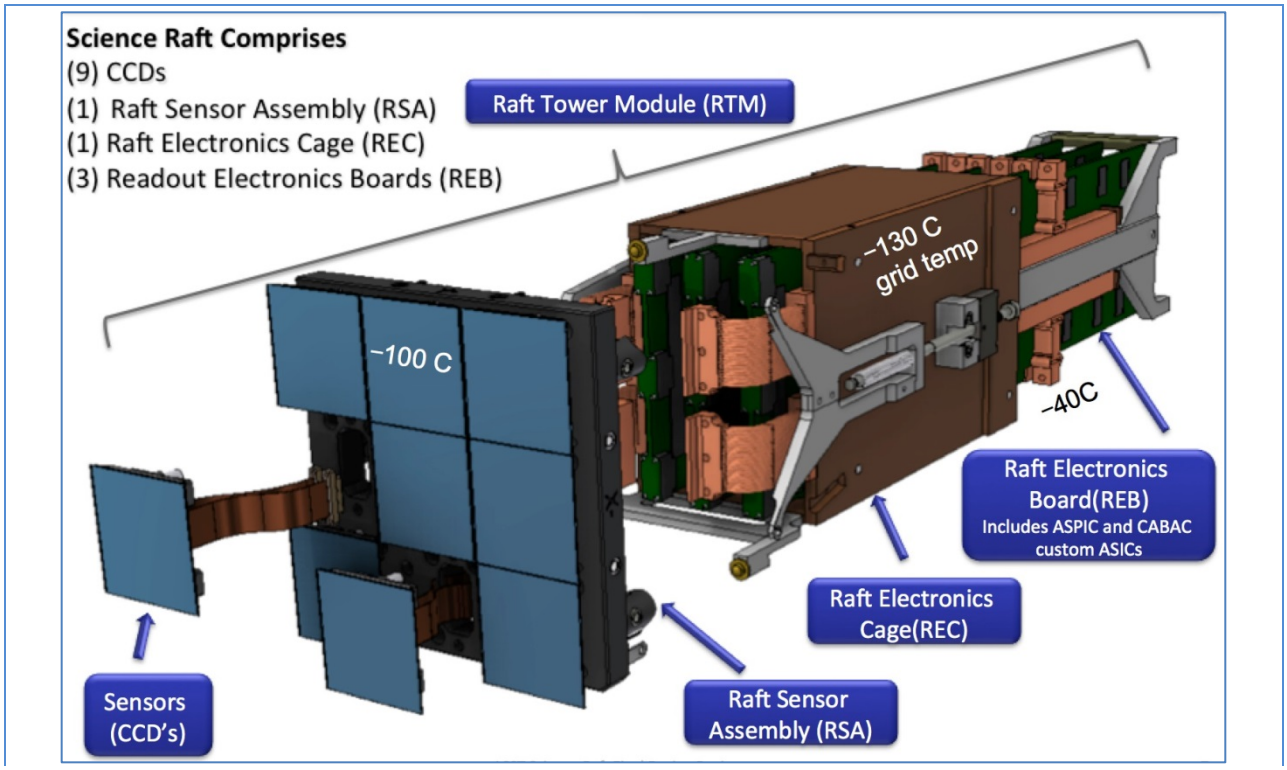
Science Raft Comprises
(9) CCDs
(1) Raft Sensor Assembly (RSA)
(1) Raft Electronics Cage (REC)
(3) Readout Electronics Boards (REB)
Raft Tower Module (RTM)
~130 C
grid temp
~100 C
~40C
Raft Electronics
Board(REB)
Includes ASPIC and CABAC
custom ASICs
Raft Electronics
Cage(REC)
Sensors
(CCD's)
Raft Sensor
Assembly (RSA)

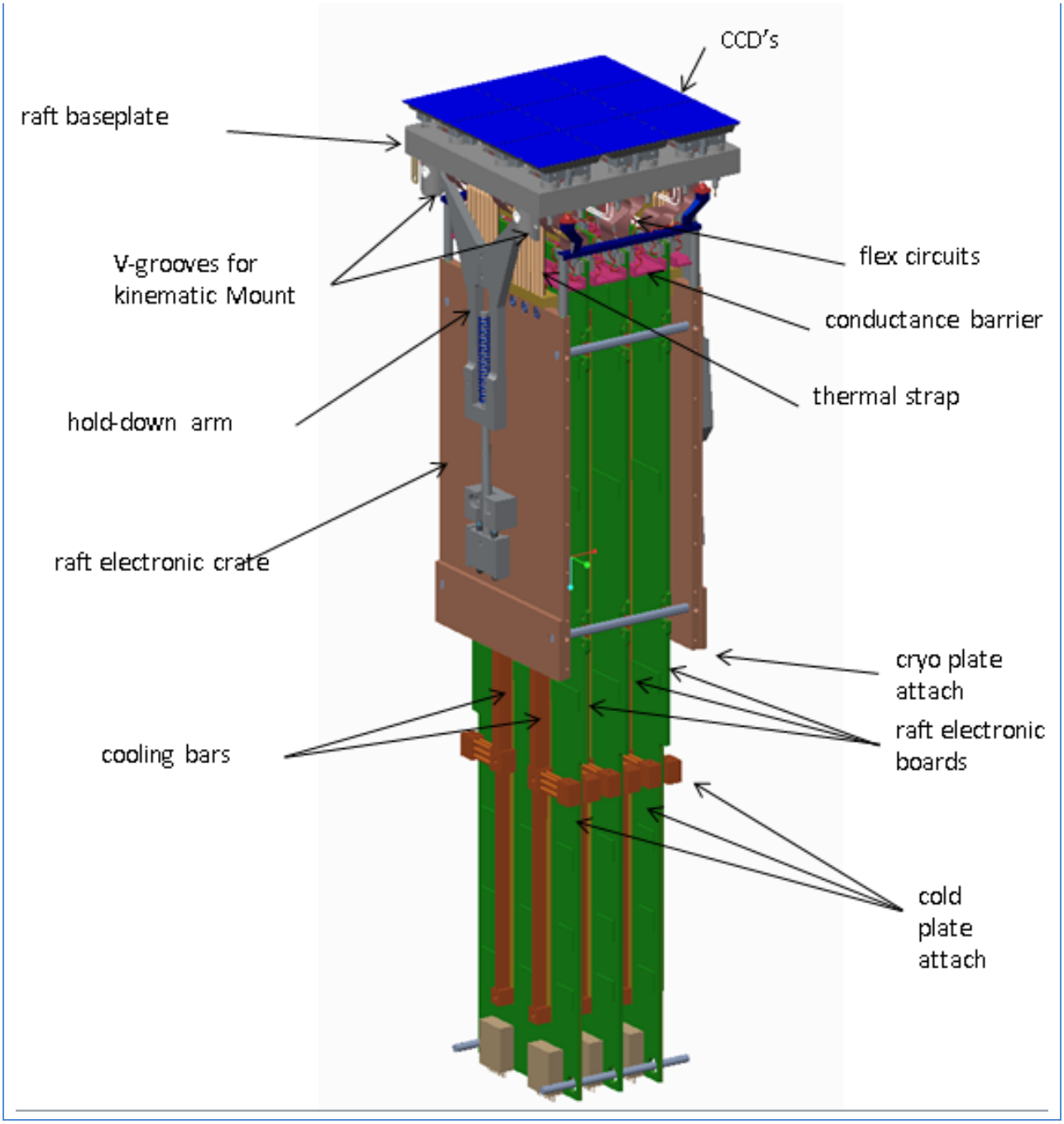

Figure 10-2a,b: Exploded (a) and perspective (b) views of and LSST science raft

10.3.1 Raft Tower Electronics

The function of the Science Raft Electronics is to fully support the nine CCDs that reside on a raft. It must provide all biasing and clocking signals, amplification and low noise analog signal processing, digitization, data collection, and transmission of image and metadata to the DAQ. Finally, it must provide flexible timing and control in a manner that is precise, predictable, and programmable under control of the Camera Control System. In addition, it is subject to the specifications articulated in LCA-57, and related documents. Some key performance parameters are summarized in Table 10-1.

Table 10-1: Key Science Raft electronics specifications

Specification	Value
Read time	2 seconds
Read noise	9 electrons rms
Blooming full well capacity	Not to exceed 175k electrons
Dynamic range	18 bits
Crosstalk	$2x10^{-3}$
Gain Stability, one hour	0.1%
Linearity	3%
Focal plane temperature measurement absolute value	+/- 1.5°C
Focal plane temperature measurement stability	+/- 0.15°C
Focal plane temperature resolution (LSB)	= < 0.05°C
Contribution to image quality, FWHM	0.3 arcsec
Vertical range for 95% of the pixels on a raft	+- 10 microns relative to height datum

Each of the sensors in the Science Raft comprises 4k x 4k pixels, or 16 Megapixels total. To simultaneously meet the read time and read noise specifications, the sensors have been divided into 16 segments of 1 Megapixel, each with its own output amplifier. This allows readout to proceed at an average rate of ~550k pixels/second, a rate which has been shown to be compatible with the noise requirement. This segmentation results in 144 parallel streams of image data for each raft. The raft dimensions of 127mm x 127mm results in extremely tight packaging requirements for the 144 parallel channels of analog signal processing, A to D conversion, and data collection.

The Science Raft Electronics also has the responsibility for monitoring and reporting a variety of metadata such as supply voltages and currents, precision temperature measurements, and operating raft heaters to maintain focal plane temperature. In addition, a significant ability to diagnose problems *in situ* is part of the design.

Each Science Raft contains a 3 x 3 array of science sensors and forms an integral unit along with its accompanying Science Raft electronic package. The focal plane consists of 21 such Science Raft electronic packages and four Corner Raft electronics packages, described in Chapter 11.

10.3.2 Electronics architecture

The functionality of the Science Raft Electronics is contained on three Raft Electronic Boards (REBs) which hold the analog functions and digital electronics that provide clocks and biases to three CCDs and handle the 48 channels of video output from those CCDs. Each REB also provides power regulation, monitoring of voltages and currents and conversion of the 48 streams of digitized video data into a single high speed link that is connected to the DAQ system as shown in Figure 10-3.

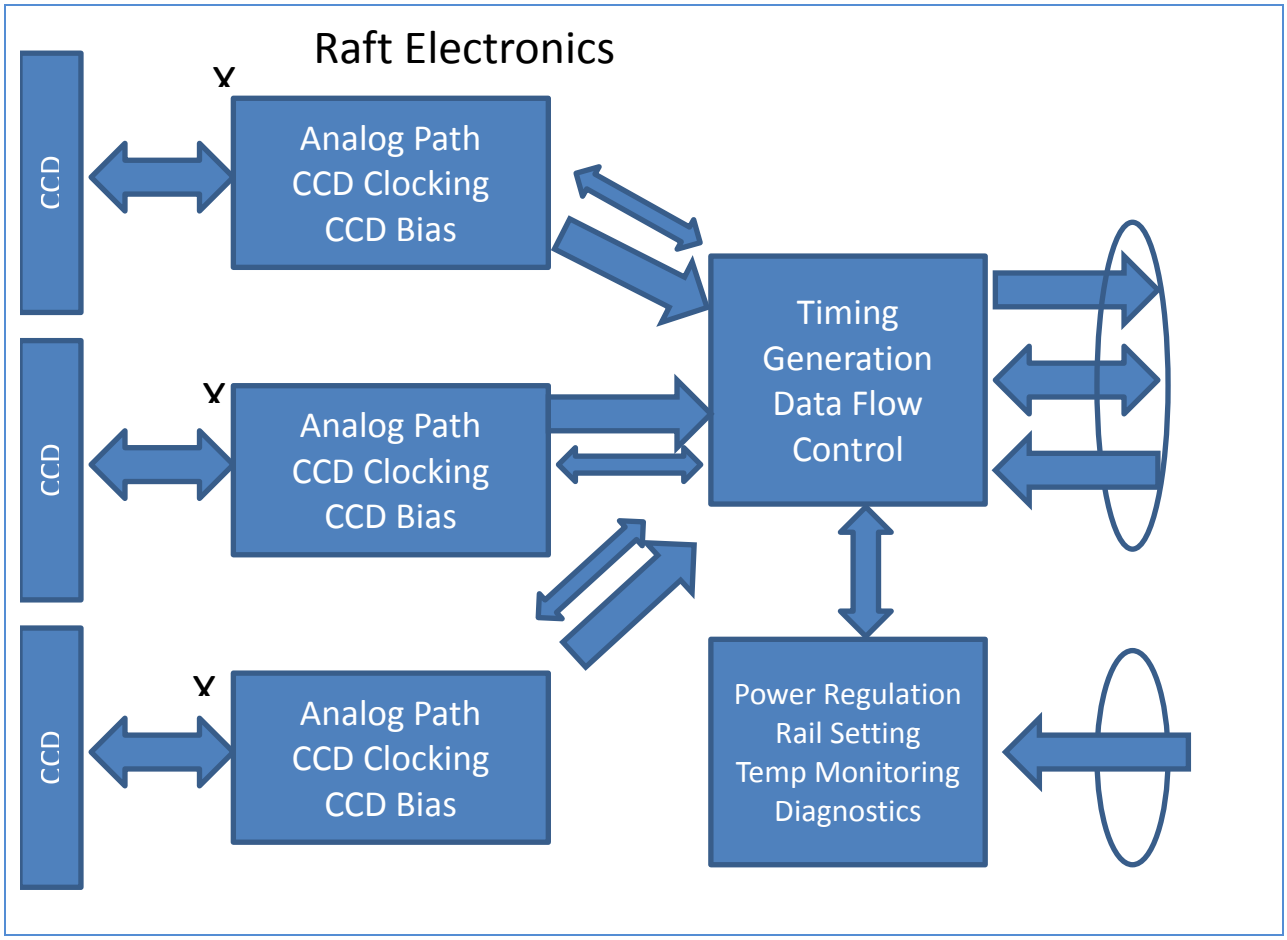

Figure 10-3: Raft electronics board (REB) block diagram

A significant feature of the Science Raft Electronics is that each raft, and indeed each REB, can function as an autonomous readout and control system for nine (or three) CCDs. The raft and three REBs can function as a fully autonomous 144 Megapixel camera, when connected to an LSST-style DAQ system.

To mitigate potential crosstalk and pickup noise issues, all twenty one science rafts in the focal plane operate fully synchronously. The requisite synchronicity is maintained by distributing a master clock for the entire focal plane. A real time microcontroller, implemented in a Xilinx FPGA on each REB, fans out timing and gating signals to the custom ASICs and commercial ADCs at an accuracy of order a few nanoseconds and with a jitter less than 100ps.

A block diagram of the overall mechanical assembly is shown in Figure 10-4.

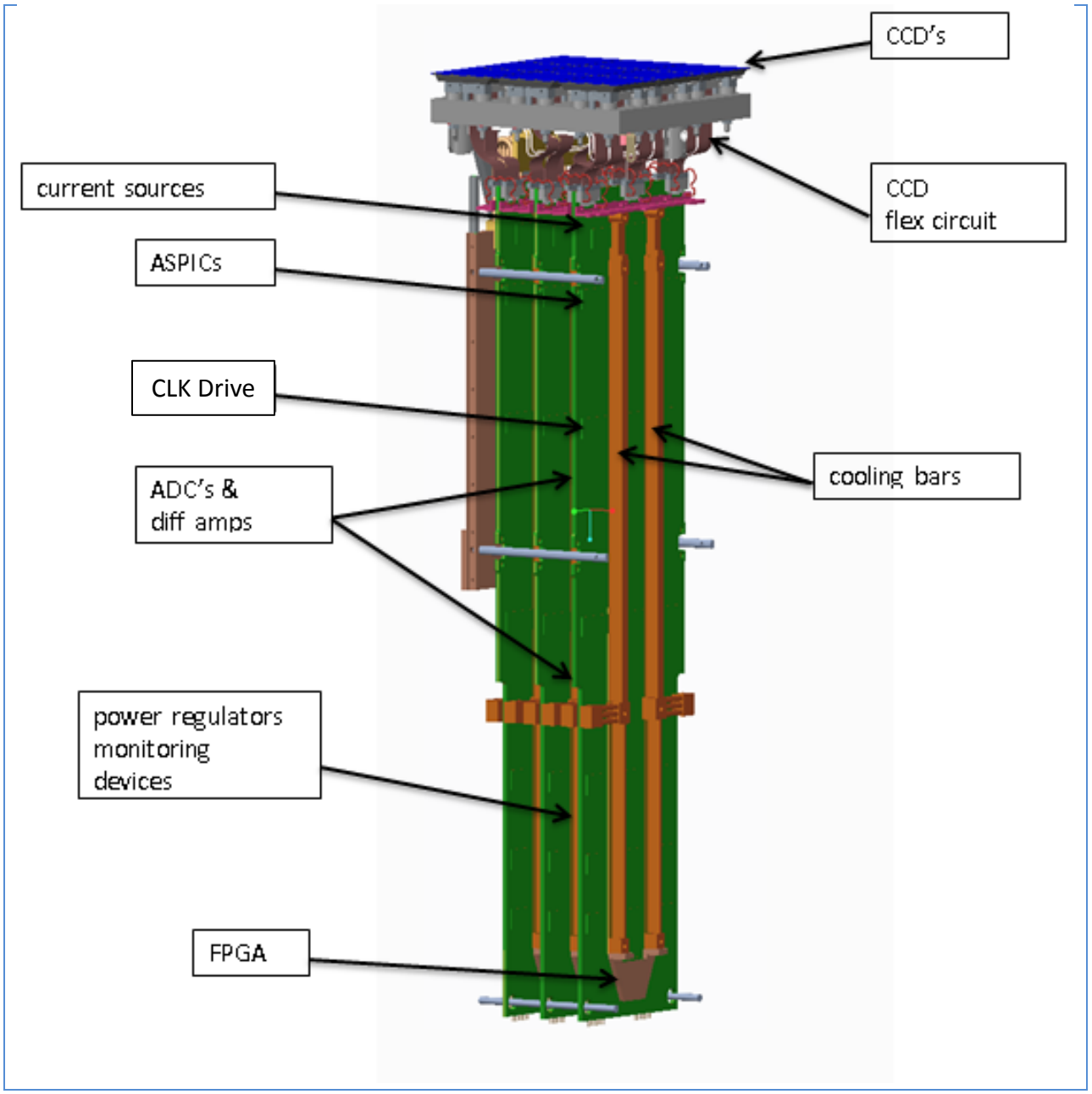

Figure 10-4: Block diagram of overall science raft electronics

10.3.3 Location of electronics

The physical location of the main electronic systems is a significant issue which is dependent on a number of important factors. One factor is how much, if any, of the electronics should reside within the cryostat, and how much should be placed outside.

The pin-count on the sensors themselves is an important consideration. Each of the science sensors has of order 150 bond pads, each of which requires connection to the readout electronics. There are thus in excess of 30,000 bond pads in the focal plane requiring connections and consequently one motivating factor in determining the electronics location is the desire to avoid this large number of vacuum

feedthroughs in the cryostat. Secondly, we know that a large contributor to crosstalk is in the cable connection between the Science Sensors and the electronics. Each sensor cable has multiple video channels with conductor to conductor capacitance. That this capacitance is a source of crosstalk implies that video cables should be as short as possible and for signal amplification to be located as close to the focal plane as possible. Further, transmission of analog signals from the first amplification point should be differential if they are to span any reasonably long distances. Thus, at a minimum, we require over 6,000 differential video connections exiting the focal plane.

Other connections required for clock driving, biasing, and power, quickly escalate the total to well over 10,000 connections. In addition, given the optical design of the telescope, the electronics package must reside in the shadow of the focal plane. Given those factors, the LSST design has located the full readout chain inside the cryostat – minimizing sensor cable length and vacuum penetrations at some cost in additional in-cryostat electronics cooling. Given the large channel density, analog amplification and low noise signal processing requires ASIC technology.

10.3.4 Custom Analog Electronics

The very front of the electronics system is responsible for providing clock signals and bias voltages to the CCDs and then taking the voltage signals from the CCD output amplifiers through an amplification and correlated dual sampling stage to prepare the CCD video signals for digitization. The video chain functions are accomplished by a custom integrated circuit – the Analog Signal Processing Integrated Circuit (ASPIC), which provides preamplification and correlated double sampling for eight channels of CCD output.

In the baseline, the clock drivers and positive bias generators were also contained in a second custom chip, the CABAC. However, design problems in the second version of the CABAC necessitated a significant redesign effort which, while largely successful, did not provide much schedule margin. During the chip redesign effort, a backup solution using all commercial parts was created and prototyped. As the commercial solution was shown to fully satisfy all LSST requirements, it has been adopted as the new baseline.

Both the ASPIC and the commercial clock and bias drivers are mounted on the front (CCD end) of the REB custom printed circuit that serves three CCDs – six ASPICs and three bias/clock drivers per REB. The other significant block at the CCD end of the electronics chain is the current source, one for each of sixteen output segments in a CCD, implemented using a low noise FET.

The ASPIC has as its goal to amplify and process the signal coming from the focal plane CCDs in order to optimize the signal-to-noise ratio before digitization.

Each ASPIC contains eight channels and is implemented in the AMS 0.35um 5V CMOS process. The chip operates down to -100°C and provides processed differential signals to the commercial 18-bit ADC.

The architecture chosen for the LSST camera signal processing is a Dual Slope Integrator (DSI). Dual slope integrator processing combines correlated double sampling with CCD signal integration.

Correlated double sampling, eliminating reset noise, removes kT/C and 1/f noise while integration removes thermal noise. A block diagram of one ASPIC channel is shown in Figure 10-5.

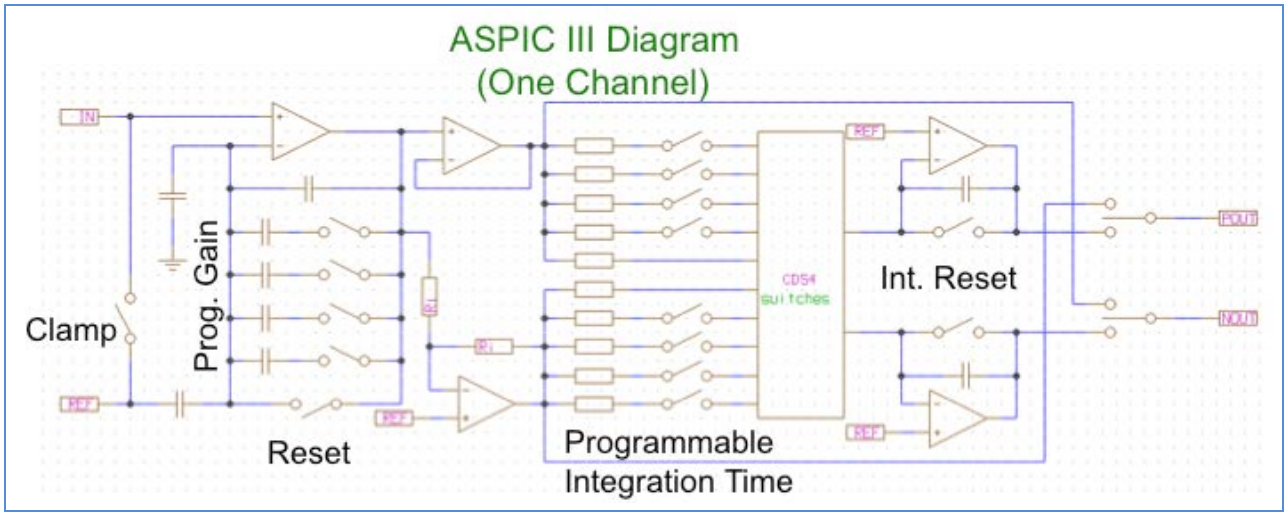

Figure 10-5: ASPIC channel block diagram

The correlated double sampling is performed by integrating first the CCD reference signal just after reset and then the charge signal with opposite polarity during the same integration time as shown in Figure 10-6. The difference of these two integrations provides the CCD signal with the kT/C and 1/f noise contributions suppressed.

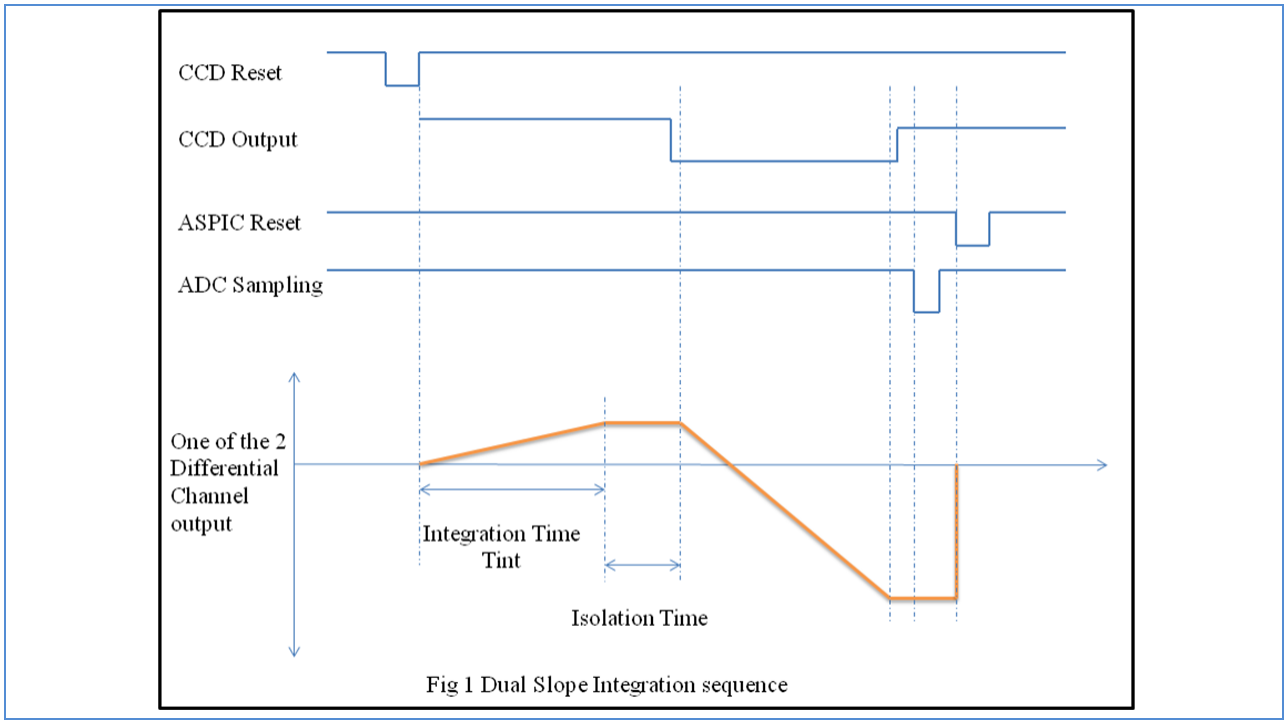

Figure 10-6: Dual slope integration sequence

The CCD will be AC coupled to the ASPIC through an external capacitance. A large clamp switch has been integrated to perform a DC level restore regularly; this large switch will provide a very low resistance, around a few hundred ohms.

The ASPIC has been designed to meet the following requirements as part of the overall electronics requirements:

- Operates at a temperature down to 173 K, required running temperature 223-300 K. ASPIC will include a temperature probe.
- Noise: @ 500 ns integration time for an input of 5.75 μV/e- and a gain of 1.9 : < 2.3 e- (requested) , 1.8 (goal)
- Operation @ 0.1 – 1 Mpixels/s , nominal 550 kpixels/s
- 0.05% maximum crosstalk between channels @ 550 kpixels/s, (goal 0.01 %)
- gain 1.7 to 6 , for a nominal gain of 1.9 compatible with a 180k e^- full well capacity for 5.75 μV/e-
- 0.5% linearity requested , 0.3% goal
- Output load 25pF // 1kΩ
- Differential output, +/-2.5 V from ref
- Operating voltage 5V with central reference V_{ref} = 2.5V
- Power dissipation ≤ 38 mW/channel

The ASPIC implements a power down feature which allows a significant reduction in dissipated power during non-readout periods (below 2 mW used per channel for the ASPIC in idle mode). Use of this feature is not part of the REB baseline.

10.3.5 Raft Electronics Board (REB)

The REB that services a set of three of the CCDs on a raft is a complex 16 layer board with blind and buried vias about 104 x 419 x 2.5 mm with surface mounted active and passive components on both surfaces. A fully stuffed prototype REB2 is shown in Figure 10-7. – the CCD connectors are on the left , the current sources are just to the right of those connectors, the ASPIC chips are next, followed by a CABAC0. Eight differential amplifier and ADC blocks follow. The blank space to the right of the ADC blocks is for attachment of the cold bars and then power supplies, DACs, auxiliary ADCs and other monitoring blocks are followed by a large 400 pin connector that takes the daughter board (DREB) holding the FPGA. In the latest version (REB3) the FPGA is integrated into the common REB substrate as we now know that in this topology no measureable noise is injected in the video chain by the digital activity.

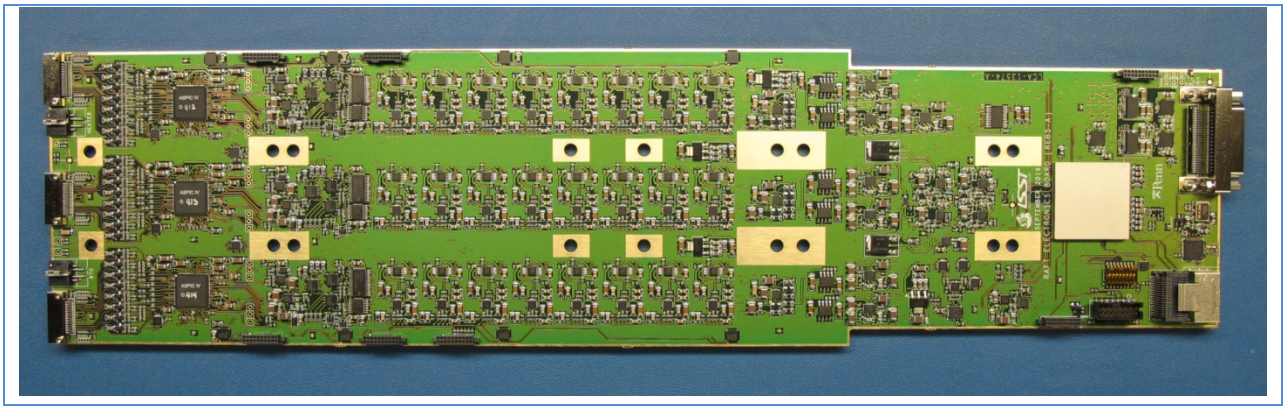

Figure 10-7: Production raft electronics board

10.3.6 Digitization and Control Electronics

The output of the ASPIC is sent as a differential analog signal to a commercial differential buffer and 18-bit ADC for digitization. The ADC is rated for 1 MS/s but for LSST is run at the LSST pixel rate of 550 kpix/s. This pixel data is fed as 48 individual serial streams directly into the FPGA where the firmware formats the data into packets to be sent out via the high speed electro-optical link to the DAQ hardware in the Observatory Control Room. At the same time, sequencer logic in the firmware provides direct control of the timing of all the circuitry involved in the video chain – parallel and serial CCD clocks, clamps, resets, ramp up and ramp down for the correlated double sampling in the ASPIC and ADC convert – all based upon a common 100 MHz clock distributed from the DAQ hardware to each REB. In addition there are numerous “housekeeping” tasks such as providing programmable voltages required by the CCD for biasing, monitoring temperature sensors distributed on the REB, Raft and sensor packages, and preparing meta-data packets for transmission to the DAQ. Each of the “housekeeping” devices is controlled by an independent serial bus from the FPGA so that it is possible to read a precision temperature from a sensor mounted RTD while setting a new clock rail voltage while monitoring the input voltage.

In addition to supporting the analog video chain and housekeeping circuits as described above, the REB also provides:

- A hardware serial number
- DACs and power op amps to control raft based heaters
- Precision 5V and 2.5V references for the video chain
- DACs and power op amps to provide rail voltages for the parallel, serial and reset clocks.
- Heavy internal ground planes plus externally mounted Cu bars to carry heat from the REB to the cold plate
- Auxiliary ADC channels to measure bias voltages, drain currents and power regulator currents and voltages.
- Protection circuitry to allow the back substrate bias to be clamped to ground until a logic signal is sent from the FPGA
- Diode reverse voltage protection on all sensitive CCD nodes.

The basic functionality of the REB has been demonstrated (as of May 2015) at the three-CCD level, with ASPIC III and CABAC0 versions of the ASICs. The commercial clock driver circuitry was successfully demonstrated using a modified corner raft board in June of 2015.

10.4 Science Raft Tower Module Mechanical Design and Analysis

10.4.1 Introduction

The raft tower serves several purposes. It is the mechanical structure that houses and protects the raft electronic boards (REB's) that interface with the CCDs, it serves as the heat sink path to the cryofluid plate, it helps to prevent VOCs liberated from the electronics from contaminating the CCD image surface, and it provides an initial platform on which the sub-assembly of the raft and its CCDs can be supported before inclusion in the camera cryostat. The tower concept allows the design of the focal plane to be modular, and it is a replaceable unit within the cryostat. There are 21 science Raft Tower Modules (RTMs).

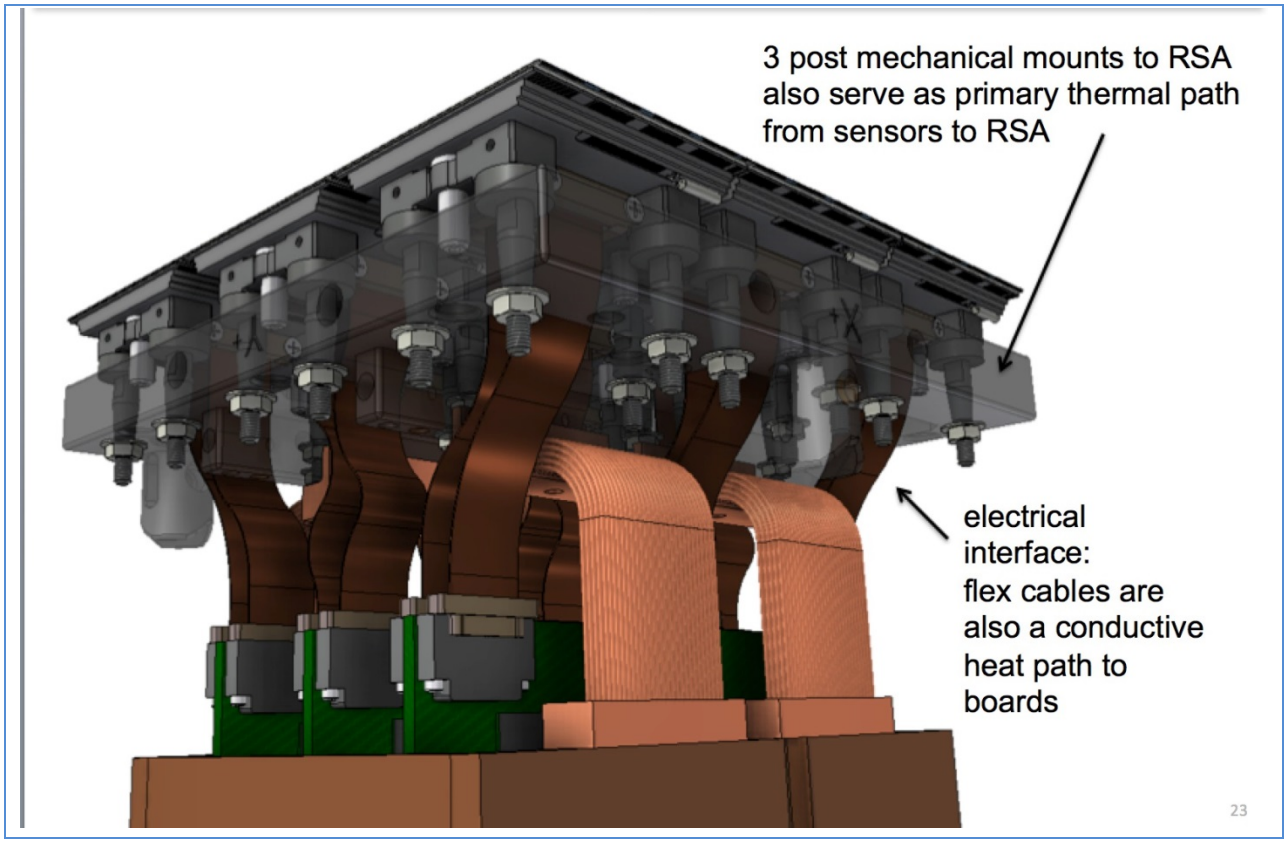

Figure 10-8: Detail of a raft science assembly (RSA).

The tower has a smaller "footprint" than the Raft/CCD sub-assembly. While the RSA is 126.5mm on each side, with the CCD's forming a 127.0mm square, the tower envelope forms a rectangle 116.0mm x 117.0 mm. The larger dimension includes the extremities of the spring hold-downs. Note: The grid bay opening is 120.0mm square. The RTM's total height is 476 mm from the focal plane to its extremities, before installation in the cryostat (final installation of the tower increases this dimension by 4 mm, as

the RTM is mated with the kinematic supports on the grid and the cage walls are pulled up off the temporary supports and mated with the cryoplate). Each of the 21 RTMs has a total mass of 9.8 kg.

The materials for the RTM must satisfy several requirements. Of prime importance is excellent mechanical stability over a +20 to -100°C temperature range, high thermal conductivity, and low thermal expansivity. In addition, low-temperature strength and ductility, good machinability, low density to reduce static and dynamic mass, and availability in small production volumes are also desirable.

10.4.2 Interaction between Tower and Raft/CCD

The tower is connected electrically and thermally to the Raft/CCD sub-assembly, as shown in Figure 10-9,but it must remain uncoupled from it mechanically as much as possible so that mechanical distortions of the image plane are avoided. Electrically, the mechanical isolation is accomplished by using polyimide film pigtails with copper traces between the CCDs and the REB's. Pigtails are permanently affixed or manually connected to the CCD, with a nano-connector at the other end.

From the time of Raft Tower Module (RTM) build-up until installation in the cryostat is complete, the tower is the sole support for the Raft/CCD sub-assembly. During this period, features on the tower walls engage the underside of the raft so that there exists a stable, reproducible position of the raft on the tower in all axes. This is especially important during the installation of the RTM into the cryostat in order to avoid collision of its CCDs with those of the previously installed RTMs, as they come in very close proximity.

10.4.3 Thermal Connections

The total electrical power dissipated on each raft tower is approximately 60 Watts. This comes from four sources: radiated heat from lens L3 onto the focal plane; amplifiers and clocks on each CCD; the makeup heaters that regulate the RSA temperature, and heat generation from electronic functions on the REB. Nearly all the heat on the REB, (operating between -20 degrees and +8 degrees Celsius), is removed via conduction into copper bars attached to the REB, and then through semi-flexible straps to the cold plate, which is cooled to -40C by a refrigeration loop. A small amount of heat leaks into the RSA portion via the flexible circuits and the heater wires. The heat on the RSA, (operating at or near -100 degrees Celsius) which is from the CCD amplifiers and clocks, radiation from lens L3, and the heat leak from the electronics via the flex circuit, is removed by flexible conductors, and then transferred by conduction through the REC walls, then to the cryoplate that is maintained at -130C, and finally into the cryofluid.

The REC walls are thick copper plates to allow good heat transfer from the flexible thermal straps on the RSA baseplate to the bolted interface at the cryoplate. To provide reliable thermal contact conductance, mating surfaces will be gold plated. Bolted connections will have Belleville springs and lock washers to accommodate thermal contraction and cyclic thermal ratcheting effects.

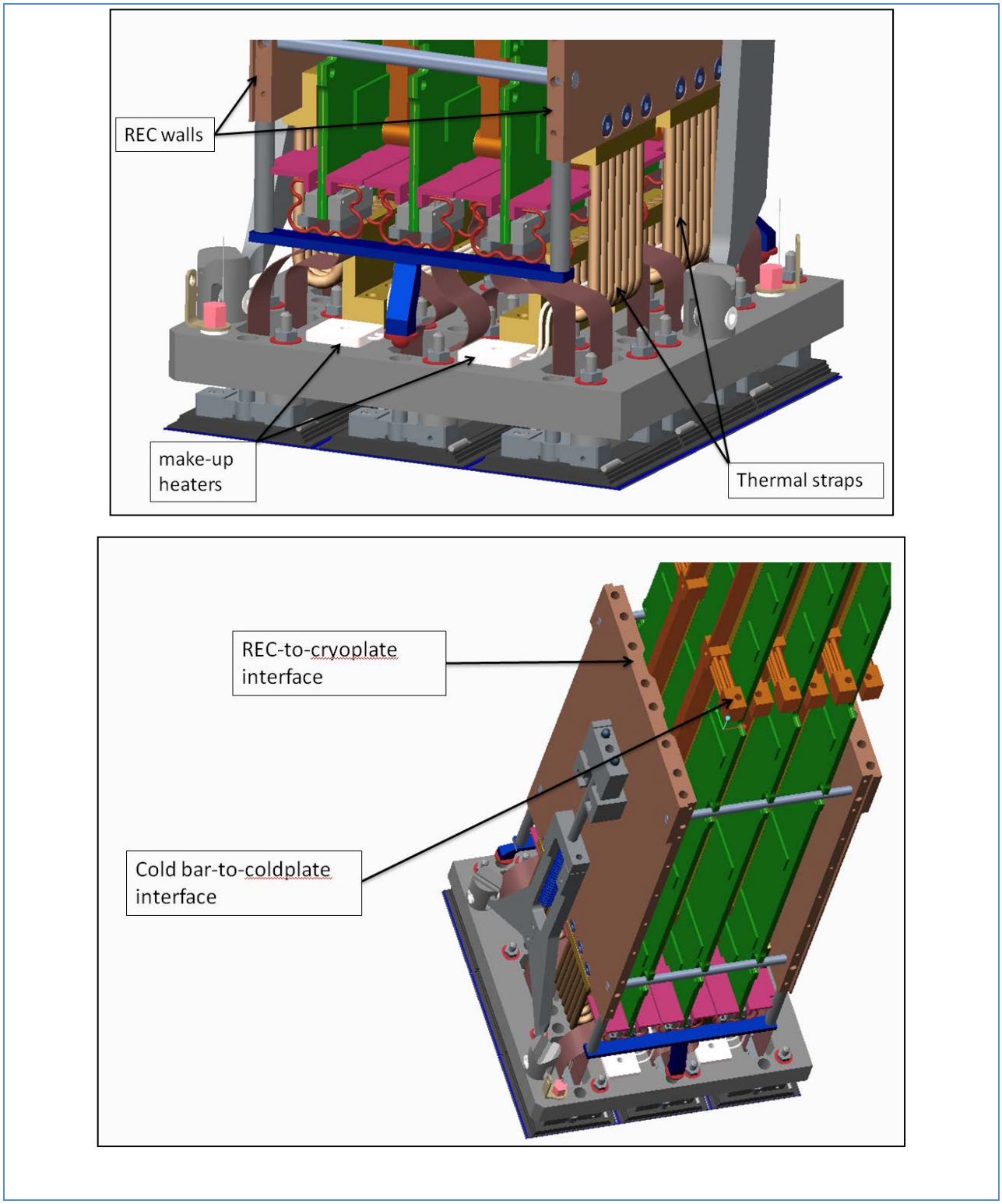

Figure 10-9: Thermo-mechanical mounting details for RSA and RTM

The components on the raft electronics boards REB's generate approximately 180 W of power (all three boards) that is removed through the cooling bars into the cold plate. The board material is an

FR4/copper sandwich to aid in lateral heat conduction. The cold bars are attached to the cold plate with semi-flexible straps. Mechanical compliance is obtained by using sliding clamped joints between each board at its edges.

Finite element modeling of the temperature distribution across the REB during operation has been generated, and matches our measured REB2 values within 5C. The modeled surface distribution of REB temperatures is shown in Figure 10-11.

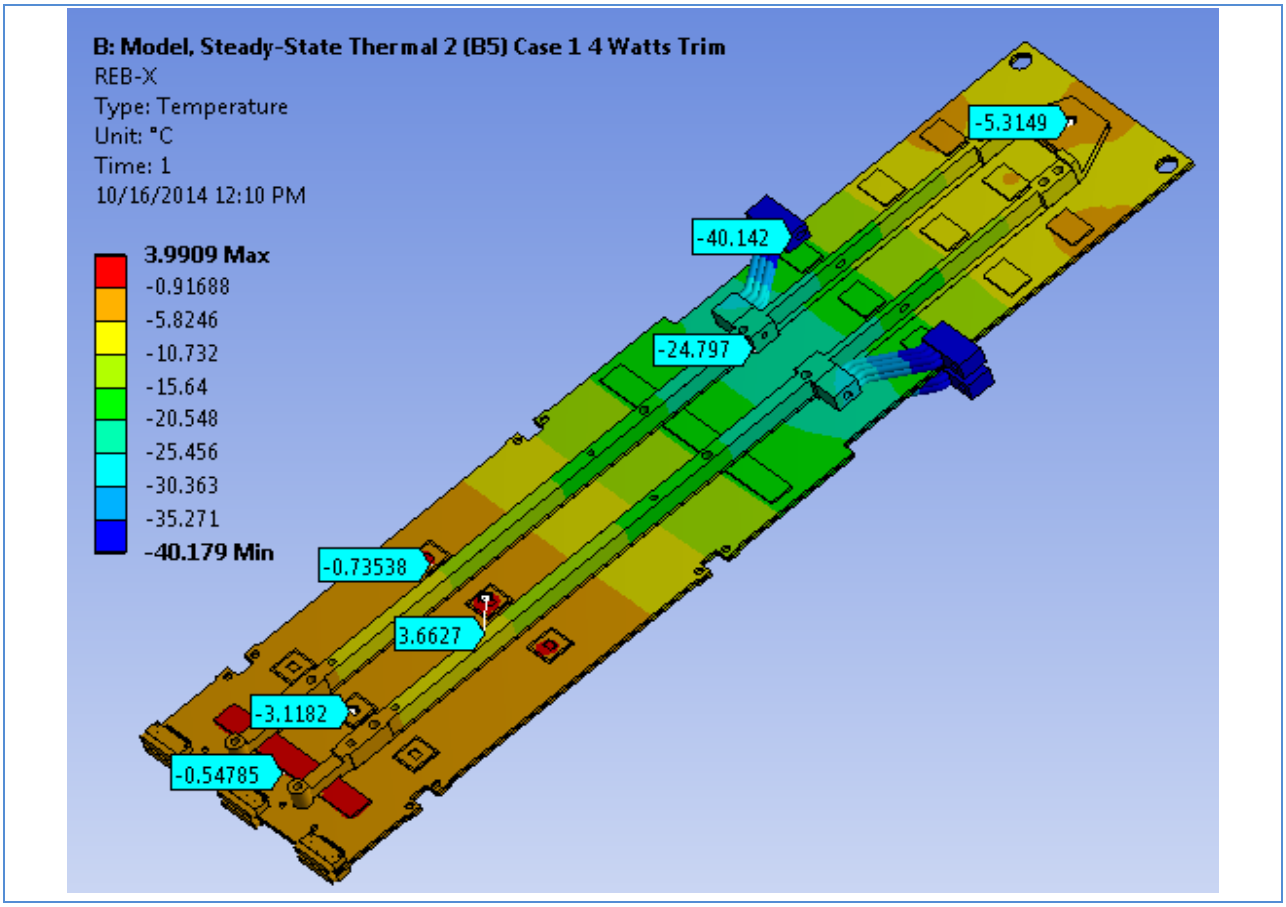

Figure 10-10: Science raft electronics board (REB) thermal design, showing equilibrium temperature distribution for cold plate held at -40C

10.4.4 Hold-Down Design

The raft is designed to be supported in the cryostat on a three-ball kinematic mount. The balls and their cup mounts are an integral part of the cryostat's support grid whose lattice-like structure forms "bays" into which each RTM is installed. V-grooves in the three raft mounts engage these balls. A total spring load equivalent to 5g is imposed on the raft to assure unchanging contact pressure in all camera attitudes and slewing motions, this load being applied directly over the center of each ball to eliminate bending forces within the raft. The mechanical components designed to apply this load are called the "raft hold-downs". There are two hold-downs per RTM, positioned on two opposite sides of the tower.

While there must be the inherent electrical and thermal connections from the Raft/CCD sub-assembly to the tower, it is advantageous to mechanically uncouple the RSA from the tower in order to eliminate as many sources of image plane distortion as possible. For this reason the forces of the hold-down springs are not allowed to remain reacted by the tower (as they are during RTM build-up), but are instead transferred to the support grid after the RTM is installed on the cryogenically-cooled cryoplate. Once decoupled, the tower (REC) position is independent of the RSA position. Furthermore, neither static deflection of the grid due to weight, nor thermal motion during transient cool-down, can have any effect on the position nor shape of the raft on the kinematic mount after this decoupling is accomplished.

To transfer the spring load from tower to grid, each hold-down employs a captive screw. There is very limited access to the area inside each grid bay and total inaccessibility from the image plane side of the RTM, so the screw is actuated through cut-outs provided in the cryoplate. Rotating each screw the specified number of turns compresses the spring the appropriate amount and completes the load transfer from tower wall to grid bay wall.

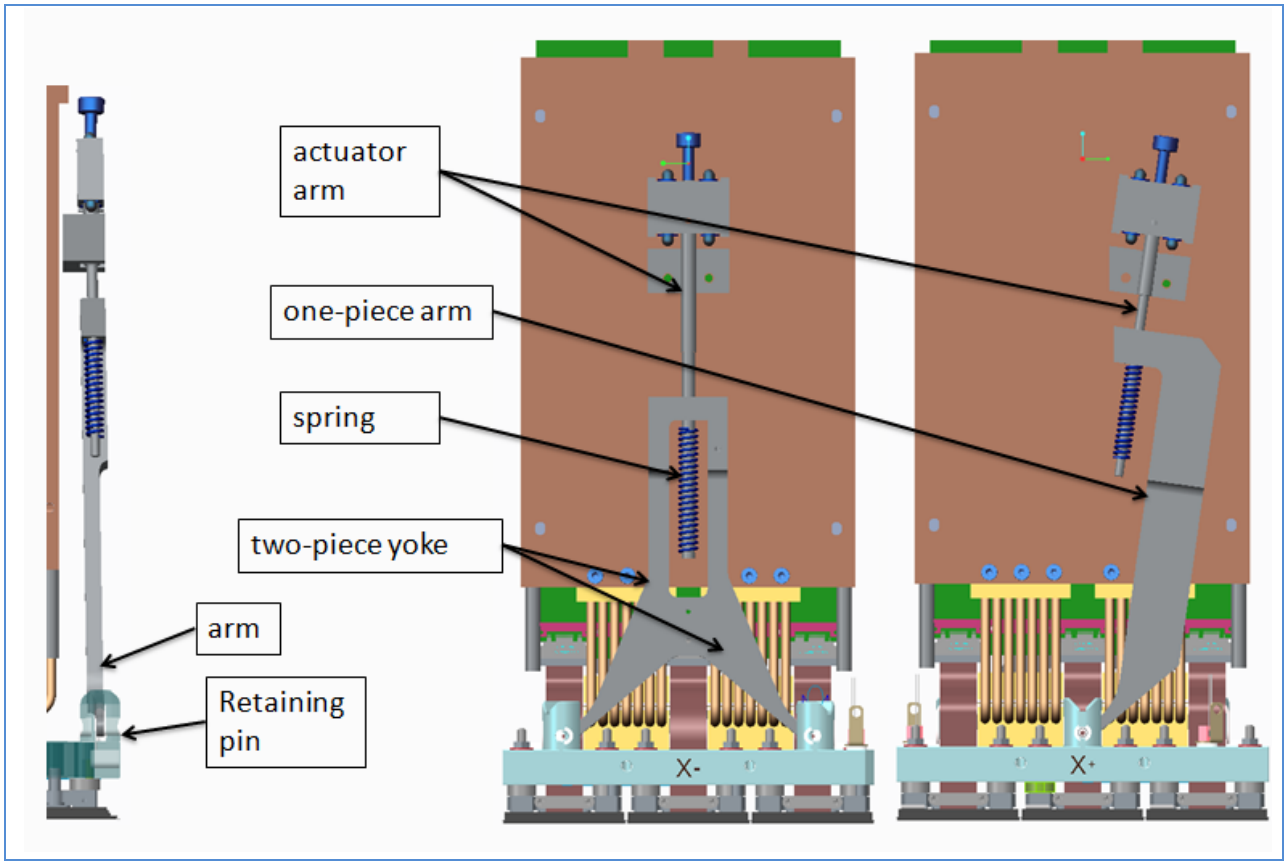

Figure 10-11: Hold-downs, both in one figure

The maximum stress in either hold-down is on the backside of the arm. The highest localized von Mises stress in this location is around 81 MPa (yield strength for 304 SST material used for the arm is ~240 MPa). The average shear stress on the pin attaching the hold down to the raft is 28 MPa).

10.4.5 Conductance Barrier

The purpose of the conductance barrier is to provide some measure of isolation between the area around the REB's and the image plane. Thermal excursions of the REB's may cause outgassing to occur. If volatiles are allowed to reach the image plane, they could condense there, impairing CCD function. Though not a hermetic seal, the conductance barrier is intended to cause enough resistance to flow between those two areas so that molecules will eventually find their way to the vacuum pumps/getters instead.

The conductance barrier is made in overlapping pieces that attach to each REB and form the complete barrier.

10.4.6 Thermal and Mechanical Analysis

ANSYS FEA software has been used along with many hand calculations and spreadsheets, to determine the thermal and mechanical response of the RTM to the loads imposed on it. Analysis simulations of steady state and transient thermal, static structural and modal / vibration have been run. The model analyzed is a robust compilation, including all materials and interfaces between components within the complex assembly. Where applicable, and without reducing accuracy, some simplifications and de-featuring have been implemented for enhancing convergence and reducing run time. The simplifications involve eliminating features (such as threads) and parts insignificant to the thermal, stress, and deflection responses, and combining some mated parts into new single parts where possible. However, the simplified model itself is not all that simple, primarily due to the fact that the mechanical supports and thermal paths of the CDDs are not mirror symmetric about either transverse axis. Therefore, the entire RTM must be modeled to obtain accurate results. This work is ongoing, but results-to-date are presented.

The thermal path from the focal plane to the heatsinks is through the CCD sensor supports. Extensive testing was performed to characterize the thermal contact impedance, and this was verified through FEA analysis. Analytical assumptions and results matched well before and after testing, and have been refined for the high-fidelity thermal model in use. An illustration is provided in Figure 10-11.

10.4.6.1 The FEA Model

The cryofluid passage surfaces in the plate are set to -130^{o}C, consistent with the fluid properties.

The coldplate temperature is set to -40 degrees C, also consistent with the properties of that fluid.

Imperfect conductivity across mating part faces is accounted for in ANSYS Workbench by manually entering conductance values based on the materials mated. The values chosen have been taken from various published sources, as well as from the results of the contact resistance testing performed, and represent average-to-conservative values as shown in Table 10-2.

Table 10-2: Conductivity across various part faces in the cryoplate to Science Raft Tower Module interface

Contact Conductances		
Value		Applied to joints
∞	W/m^2-C	soldered joints
10,000	W/m^2-C	Cu to Cu, Si to Si, etc. with good contact
2000	W/m^2-C	Cu to SS and all bolted connections
5000[2]	W/m^2-C	Cu to CeSiC
2500[3]	W/m^2-C	CeSic to CeSiC
1000[3]	W/m^2-C	Cu to G-10

1 Apiezon-N or Indium applied as interposer; 2 Based on data for Cu/Si joint, no interposer; 3 estimate

The heat inputs to the focal plane from lens L3 plus CCD chip functions (applied to surface), and from CCD amplifiers (applied to actual locations of amplifiers within the CCD substrate), are indicated in Figure 10-12; the heat inputs to the REB's are shown in Figure 10-13. There are three such boards per tower. The FPGA side of the board is shown (The other side does not have the FPGA. All other components are mirrored).

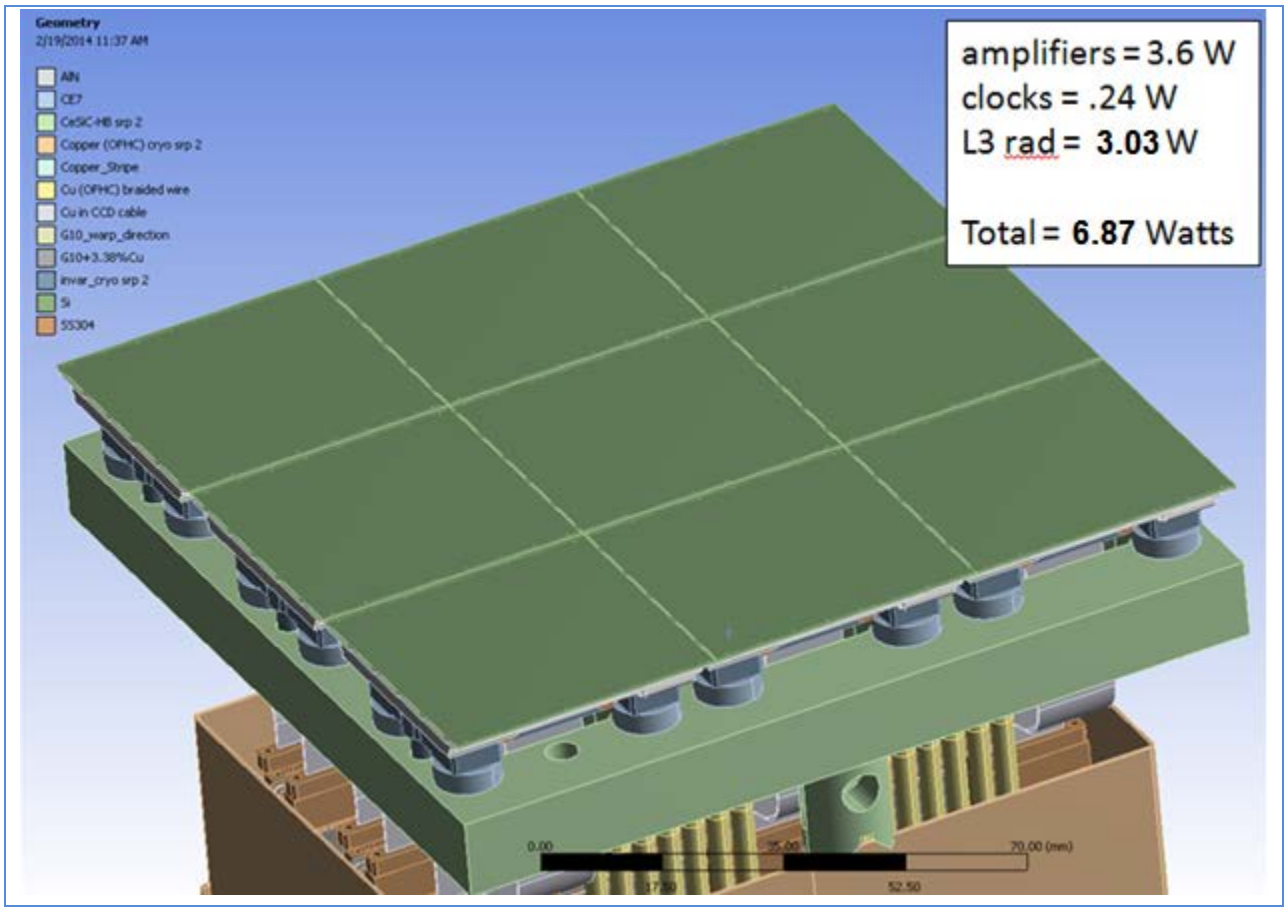

Figure 10-12: Thermal model, focal plane inputs

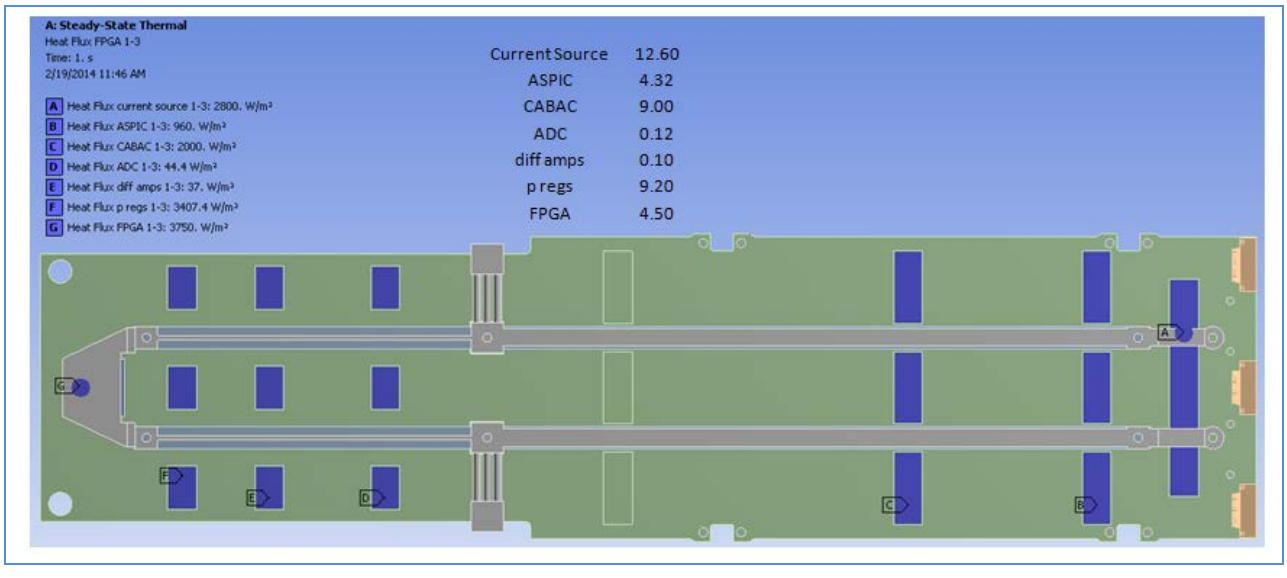

Figure 10-13: Thermal model, REB inputs

10.4.6.2 Steady State Thermal Analysis

From an initial temperature of 22°C, the model cools to an equilibrium condition governed by the cryoplate, the heat inputs, the materials chosen, and the conductances assigned. The resulting overall temperature profiles of the Raft/CCD sub-assembly components are shown in Figure 10-14 below. The raft surface shows an expected temperature gradient, cooler toward the middle, reflecting the cooling paths connected toward the center underside of the part. The maximum and minimum temperatures across the focal plane surface are -98.6°C and -100.7°C, respectively. This is consistent with the goal temperature of -100°C, and with the allowed temperature differences across the focal plane.

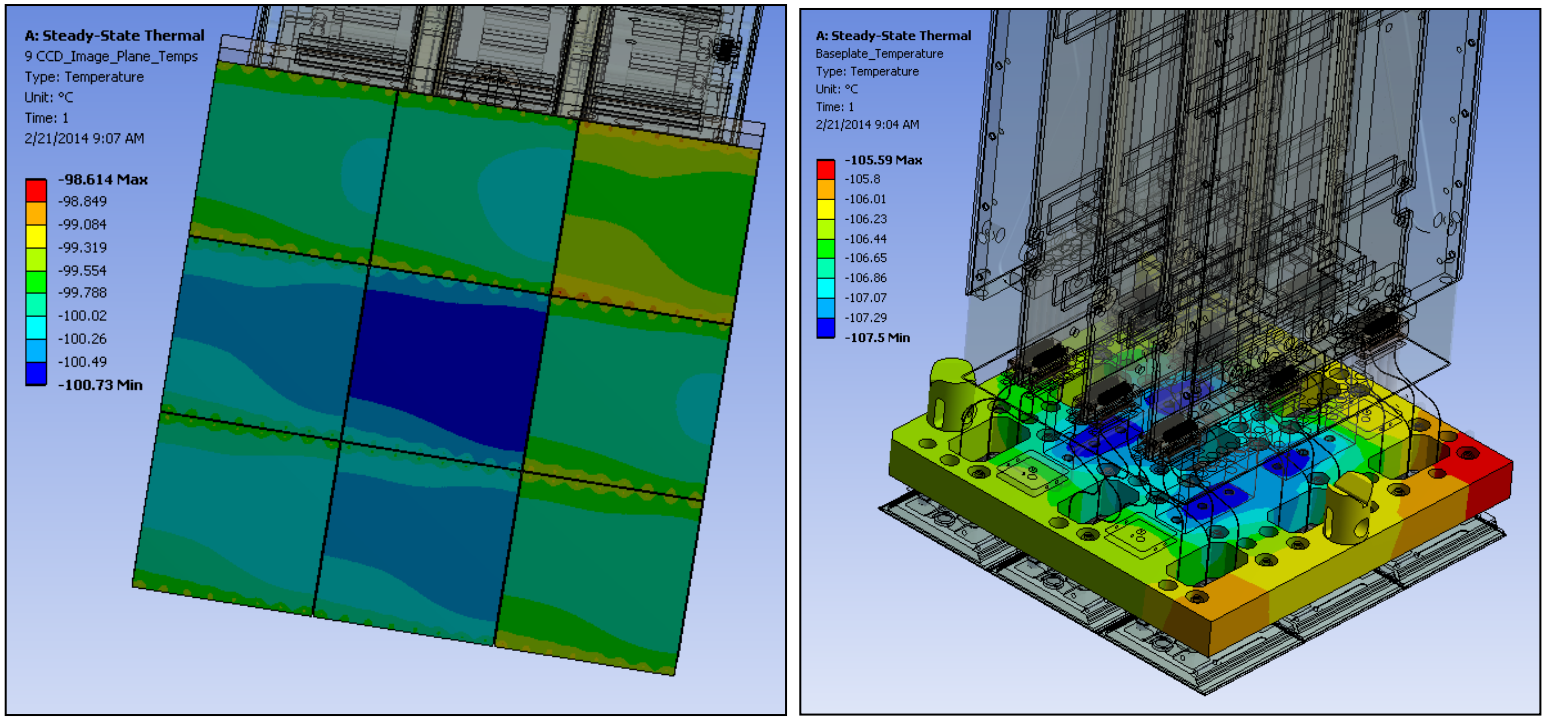

Figure 10-14: Modeled raft/CCD sub-assembly temperatures

The temperature profiles of the tower and its components (REB's, thermal straps, tower walls) are shown in Figure 10-15. Again one sees the cooler REB regions near the cold plate attachment points with a maximum delta T along the REB of about 30 degrees, well within the requirements of the electronics.

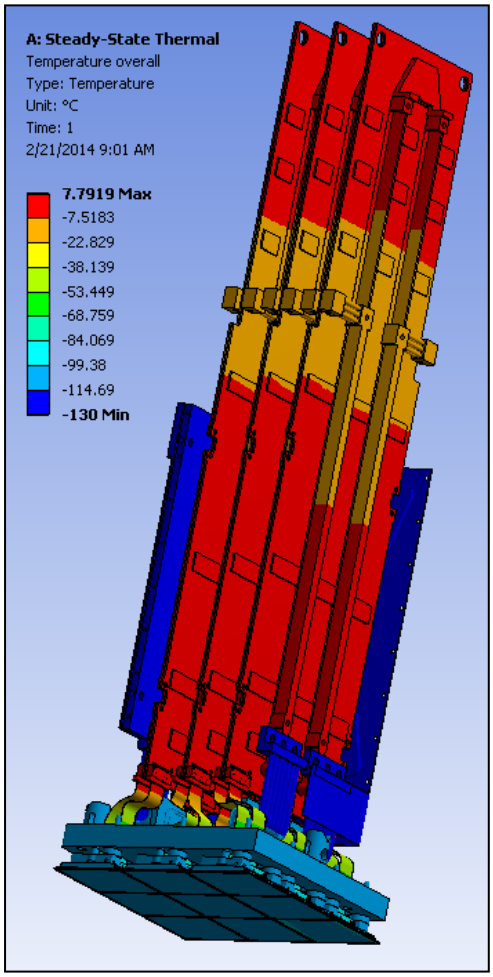

Figure 10-15: Tower steady-state temperatures

10.4.6.3 Static Structural Analysis

This analysis was run to determine the deflection of the focal plane due to gravity and the hold-down forces alone. It gives a baseline for comparison with the deflection that includes thermal effects. The gravity direction is applied perpendicular to the focal plane surface and directed away from it, simulating the camera pointing toward earth.

The flatness of the raft surface is 119 nm, with the crown of the bow in the center area of the raft and parallel to the ribs underneath, as expected. Each CCD is bowed individually about 640 nm, which masks the raft bowing to a large degree. The larger amount of bowing in the CCDs is primarily due to the single unsupported corner of each CCD. All of these deflections meet specifications.

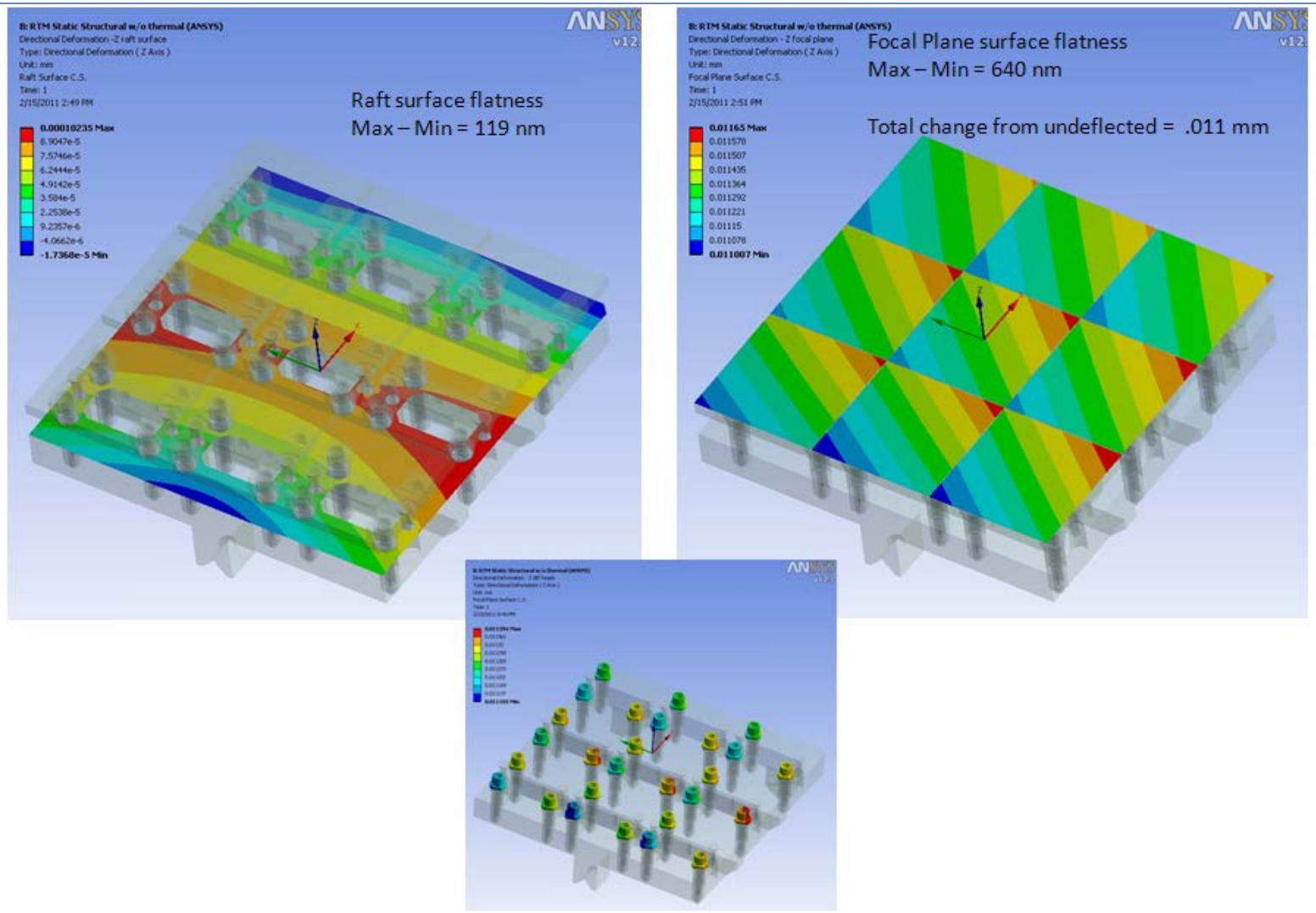

Figure 10-16: Gravity deflection

10.4.6.4 Static Structural Analysis

Looking at raft motion from the underside shows that the kinematic mounts as modeled are properly allowing raft contraction to occur along the v-grooves. In addition, the stress plot shows that the Von Mises stress at these grooves is very low. Both of these conditions are important to verify that deflections in the raft are occurring for reasons that are appropriate, not by improper over-constraint. This model presently does not include the frictional effects between the mounting balls and the v-grooves.

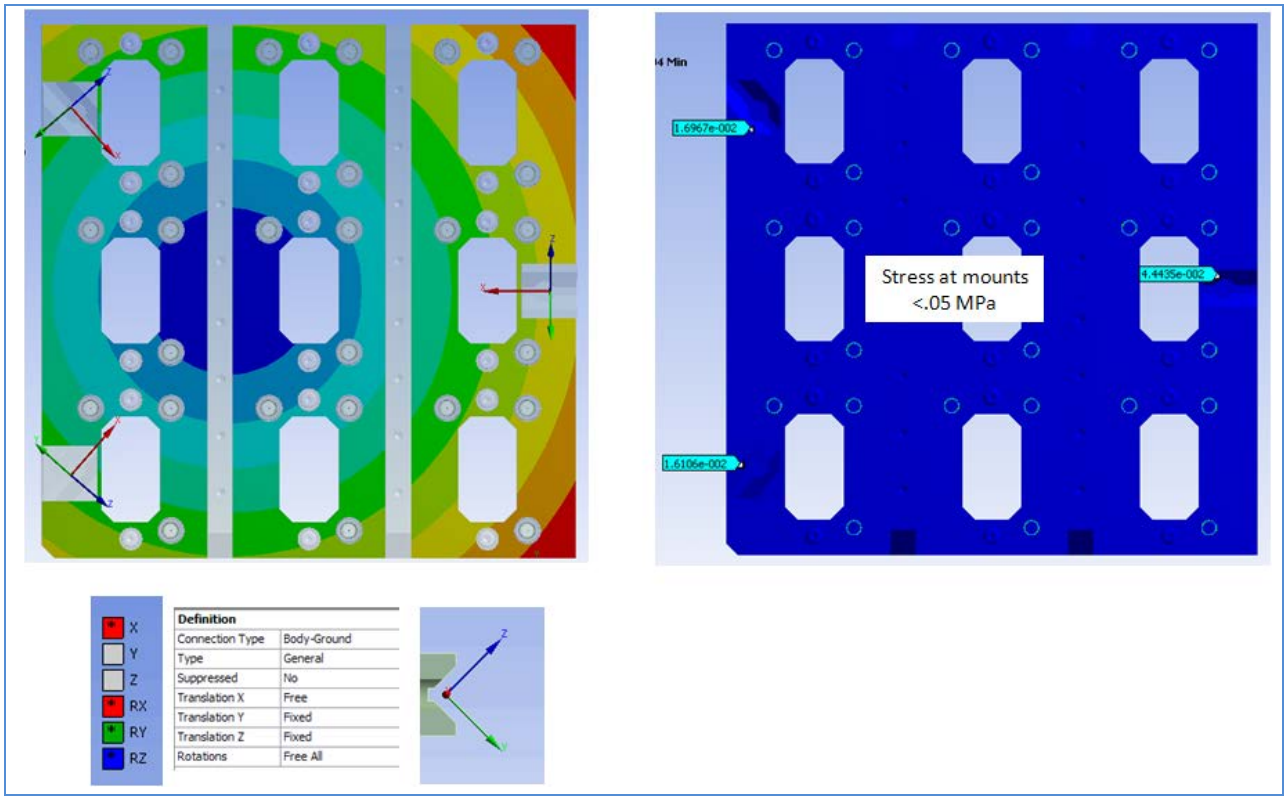

Figure 10-17: Kinematic mounts

Figure 10-18 shows the deflection of the Raft surface with the thermal contraction and the mechanical response superimposed. The resulting flatness is well within tolerance (.013 mm requirement). The total height change of ~.005 mm can be accommodated in the design.

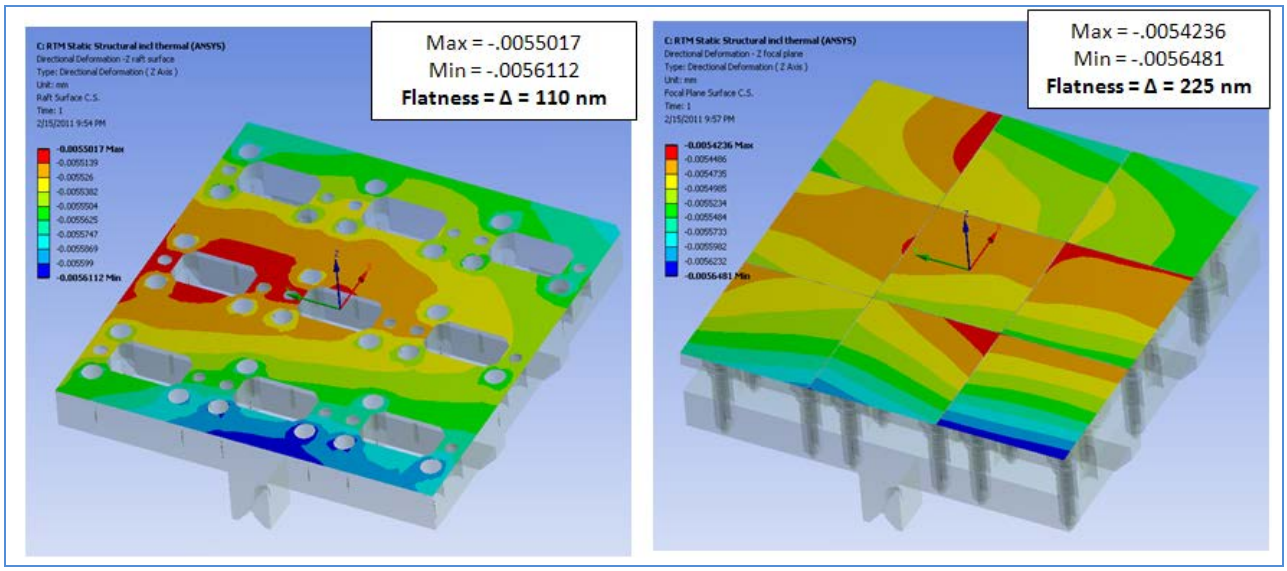

Figure 10-18: Raft surface deflection, mechanical plus thermal

10.5 Science Raft Tower Module (RTM) Assembly

The LSST camera project plan calls for the RTMs to be assembled and tested at BNL, and then shipped to SLAC for integration into the LSST instrument. This section describes the plans for the assembly of RTMs.

10.5.1 Raft Tower Assembly and Test Facility BNL

A ~1750 sq. ft. ISO 7 cleanroom has been built in the BNL physics building (see Figure 10-19).

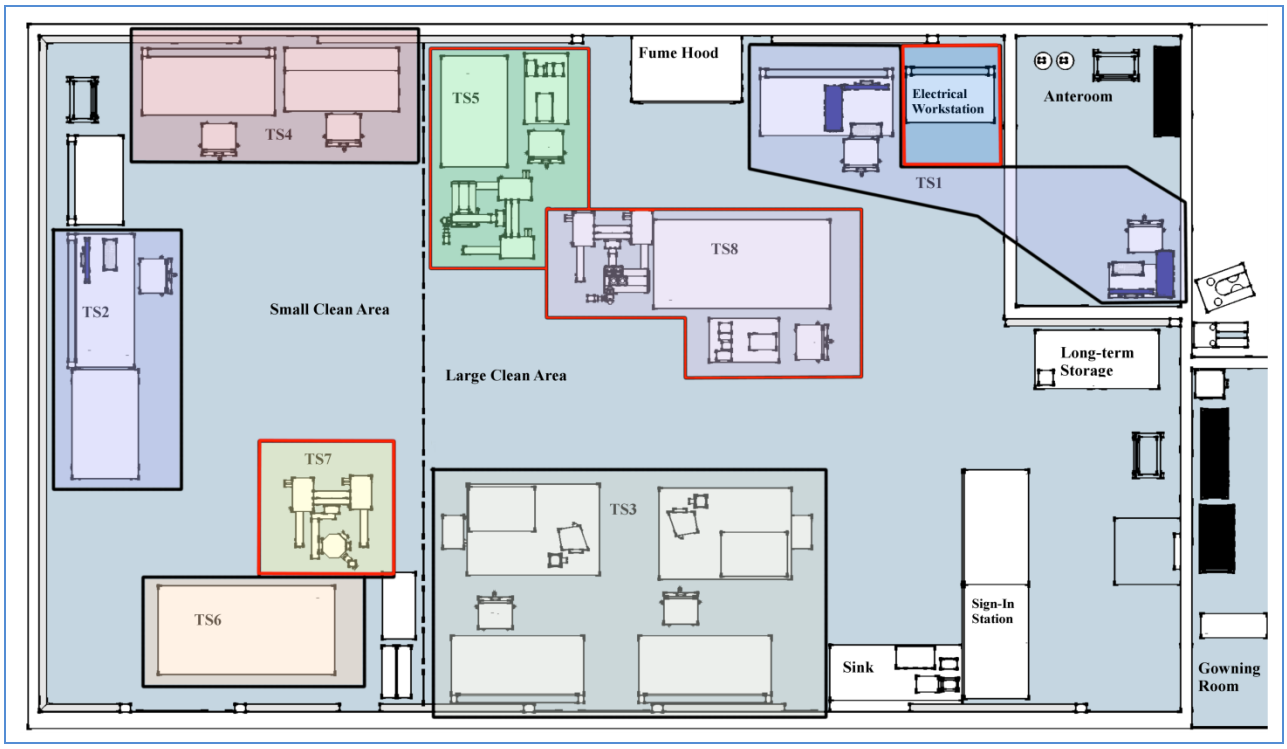

Figure 10-19: Raft assembly cleanroom design

Construction funds were provided by Scientific Laboratories Infrastructure (SLI) program within the DOE Office of Science for the construction and revitalization of general purpose infrastructure as part of a series of major lab and office space renovations that will improve facilities in the Physics (PO) and Chemistry departments at BNL.

Acceptance testing of the CCDs, construction of the 25 raft planes of 9-CCD sensors, metrology tests, integration with raft-electronics, and final raft testing will take place within this facility. In order to meet schedule objectives for science raft construction over a 2-1/2 year funding period, the facility will have two dedicated single CCD-test stations, two metrology stations, two raft assembly stations and a station for conducting qualification tests of a fully integrated RTM. The room is separated by an ESD-protective curtain to partition the space and offer an environment that is better controlled due to limited activities in that area. This space contains almost all the work requiring sensor surface exposure to air. A laminar flow hood is to be used during testing and assembly steps which require the most amount of exposure, i.e. RSA assembly.

10.5.2 Assembly sequence

Providing a detailed description of the assembly process is outside the scope of this chapter. What follows are the highlights of the major test and assembly steps, as outlined in Figure 10-21

The assembly procedure begins by populating the raft with nine tested CCDs, all of which have previously been checked for flatness and statistically sampled for electro-optical performance. Specialized measuring equipment and dedicated tooling is then used to check the mosaic flatness of the nine CCDs on the raft. After performing tests and checks, the Raft/CCD sub-assembly protective tooling

is installed around the raft to encase the CCDs and the raft is ready for further assembly. The protective tooling also provides mounting features during subsequent work.

The two thick copper tower walls are the paths for heat removal from the RTM. The two walls orthogonal to them complete the mechanical structure. To assure final coplanarity of the mounting surfaces of the heat path copper walls to the cryoplate, all four walls are pre-assembled and held in position relative to each other via precision dowel pins in the corners, then the copper mounting surfaces are pre-machined as an assembled unit. The walls are then disassembled but are kept together as a set. The dowel pins, asymmetrically placed to allow reassembly of the four walls in only one orientation, guarantee proper mating to the cryoplate.

The Raft Tower Module (RTM) assembly uses the Raft/CCD sub-assembly (RSA) as a base during construction. During assembly, the image plane (CCD Silicon) faces down and is covered by protective tooling. The polyimide flexi-cables and their integral nano-connectors are facing up, where they are placed through the openings of their respective conductance barriers. The nano-connectors are mated to the REBs in a prescribed order to best facilitate access to each connector. The copper REC walls are assembled around the REBs. The REB attachment to the REC utilizes an attachment system to allow for thermal expansion, as the REBs are at a different temperatures than the REC walls. The distal end of each hold-down arm is attached to each of the three raft mounting points, followed by the completion of each hold-down assembly. Each hold-down mechanism is adjusted to provide a defined pre-load between the REC and the RSA assembly using a temporary support structure. After the RTM performance is measured and qualified, it is placed into a custom designed environmentally controlled crate that is used for shipment and long-term storage.

Description	Type	N/A Cleaning (Wet/Plazma)	N/A Cleaning (Air)	N/A Component and Subassembly Registration	TS1 Receive and Inspect	TS2 Mechanical Metrology (Component)	TS3 EO Testing (Sensor)	TS4 RSA Assembly	TS5 Mechanical Metrology Warm/Cold (RSA & RTM)	TBD REB Electronics Test (REB Test)	TS6 RTM Electro/ Mechanical Assembly	TS7 Dewar and Vac/Cryo (TS5 & TS8)	TS8 EO Testing (RTM)	N/A Package and Shipping (to SLAC)
Sensors	Component			X	X	X	X	X						
Raft Base Plates	Component	X		X	X	X		X						
RSA Thermal Straps	Component	X		X	X			X						
Trim Heaters	Component		X	X	X			X						
RTDs	Component		X	X	X			X						
Hardware (Screws, Nuts, etc.)	Component	X		X	X			X			X			
Misc. RTM Fab Parts	Component	X		X	X						X			
REBs	Component		X	X	X					X	X			
REB Thermal Straps	Component	X		X	X						X			
REC Walls	Component	X		X	X						X			
RSA	Assembly		X	X				Assembly	X		X			
RTM	Assemply			X					X		Assembly		X	X

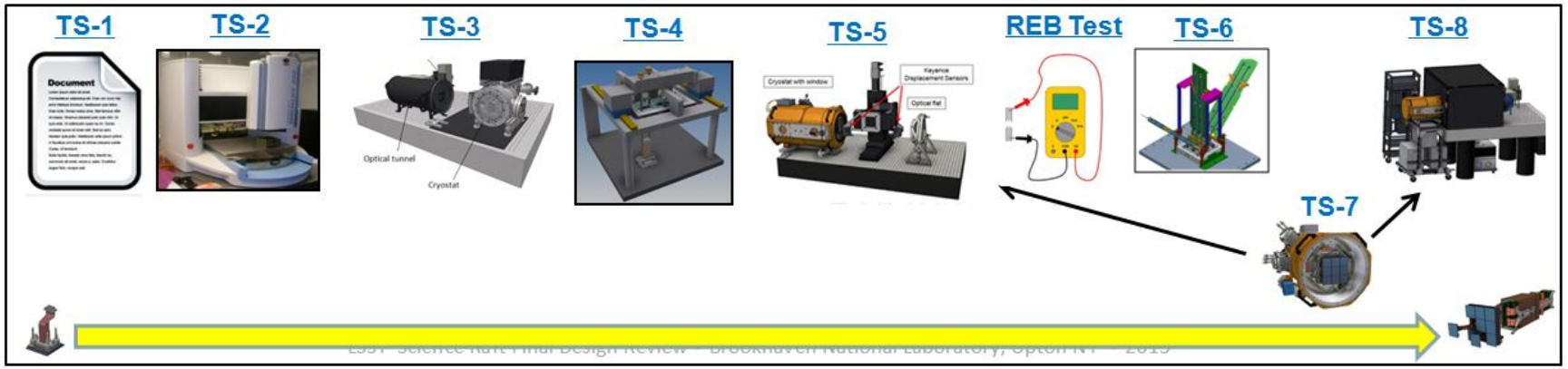

Figure 10-20: Abbreviated science raft tower module assembly sequence

11: Corner Raft Towers

11 Corner Raft Towers

11.1 Introduction

Four special purpose rafts, called corner rafts, are mounted at the corners of the LSST science Camera, and contain wavefront sensors and guide sensors. A single design can accommodate two guide sensors and one split-plane wavefront sensor integrated into the four corner locations in the camera. Although contained within the LSST Camera, the corner rafts have a broader role in the operation of the telescope.

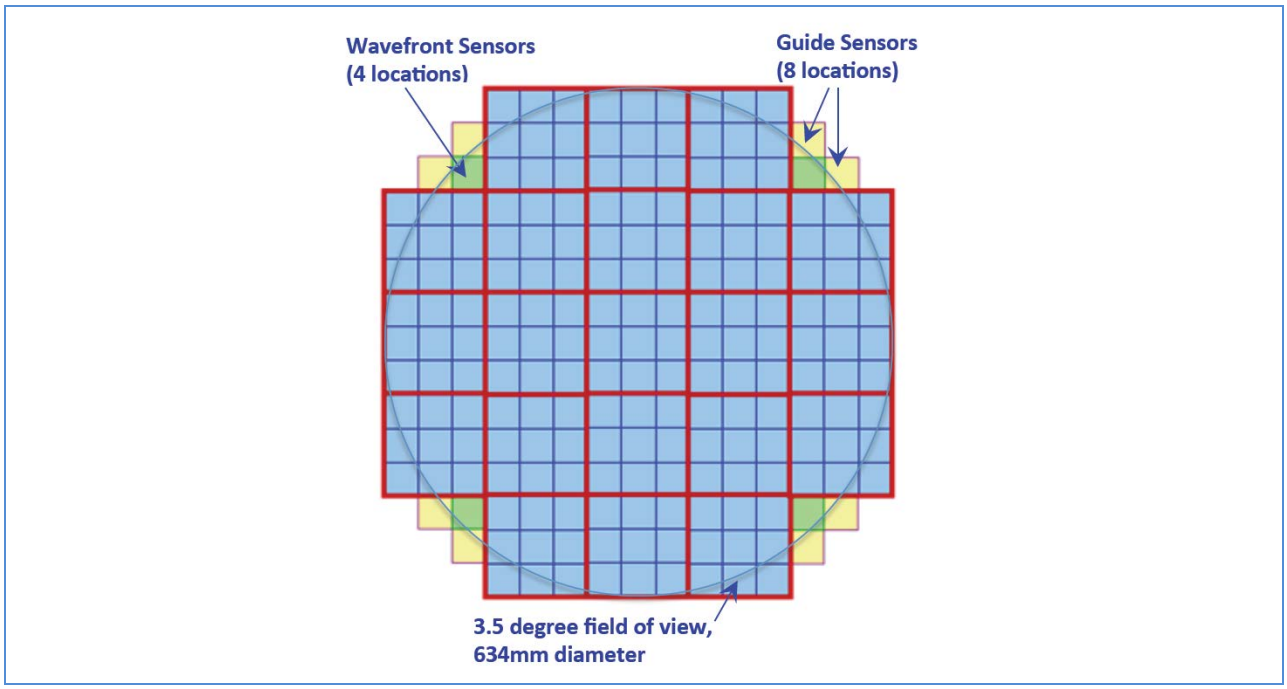

Figure 11-1: Focal plane layout

11.2 Requirements

The location of the corner raft is dictated by the requirement that the wavefront sensor cover 4 field angles in a square geometry with the highest possible atmospheric de-correlation in order to reconstruct the phase at each mirror. The guide sensors have a similar requirement. This has driven the corner raft to be located at the edge of the field and therefore at the edge of the sensor array. Thus the corner raft sub-system has a triangular cross section as opposed to the square cross section of the science raft. Similar to the science rafts, many of the design challenges relate to packaging the required functionality in a tightly constrained volume.

Another driver is related to the leveraging of the electronics system and infrastructure (such as thermal management and mechanical stability) from the science raft development effort. The challenge for the corner raft is to re-package the electronics chain used for the science sensor CCDs such that it

accommodates the corner raft geometry while maintaining the logical functionality of the design. Interfaces to the cryo plate and cold plate and the contamination control features of the corner raft also have to be similar to the science raft.

The precision required in the placement of the sensors has been shown to be similar to that required for the science sensors and therefore most of the design principles and mechanisms are similar to those used in the science raft.

11.3 Corner Raft Design Description

11.3.1 Role of the Corner Raft in the Overall LSST

The corner raft sub-system is responsible for acquiring curvature wavefront data for the active optics system. The corner raft must acquire intra and extra focal images at 4 locations at the edges of the focal plane that will be used by the Telescope Control System to estimate the wavefront and, through reconstruction, provide inputs to the active optics controller. Images are collected in parallel with the science images and follow the corresponding exposure time and cadence (nominally 15 second exposure and 2 second readout time). The current specification requires flexibility to adjust the intra to extra focal separation up to 4.8mm from the nominal 4mm separation. This will be set at the time of final assembly based on final analysis and tests.

Table 11-1: Wavefront sensor specifications

Key requirement	Value
Pixel Size	10 µm square pixels
Readout Noise	10 e- rms
Intra/Extra focal sensor separation	4 mm +/-0.1 mm
Integration time	15 s
Readout Time	2 s
Sensor Flatness/z-axis tolerance	+/-15 µm

The corner raft sub-system is also responsible for acquiring small images centered on selected bright stars at a nominal 9Hz rate. These images are used to estimate the pointing variation during the exposure and provide input to the telescope control tracking system. The guider system interface specifies the performances of the guide sensors as described in Table 11-2.

Table 11-2: Guide sensor specifications

Key requirement	Value
Pixel Size	10 µm square pixels
Readout Noise	9 e- rms
Integration time	50 ms
Frame Rate	9 Hz
Window size	50 x 50 pixels
Sensor Flatness/z-axis tolerance	+/-30 µm

Number of Guide Sensors	8

The guide sensor specifications have been set to ensure that the servo loop jitter for point spread functions on the sky better than 0.6 arc-sec FWHM will be less than 0.02 arc-sec FWHM. Based on the servo-loop implementation, this requirement can also be expressed as a single guide sensor rms centroid accuracy of 0.04arc-sec = 0.2 pixels with worst case flux of 800e- (u-band)

11.3.2 Corner Raft Architecture within the LSST Camera

The corner raft subsystem will provide images from 8 guide sensors and 4 wavefront split sensors. The images are collected at the focal plane by those sensors. The sensors are readout by the analog electronics located in the corner raft towers. The electronics in each corner raft tower reads the data from the sensors, processes and digitizes the signals, and transmits the digitized data to the data acquisition (DAQ) systems over a high speed serial interface (PGP link). The DAQ provides access to the wavefront images to either the Telescope Control System (TCS) for close loop operation or to the data management system for archival storage. The DAQ provides access to the guide star image data and the guide system is responsible for computing the star centroid location and estimating the changes as they are measured at 9Hz. The telescope decides whether the information is used to close the loop or not, depending on the current mode of operation. The Observatory Control System (OCS) initiates commands resulting in images being acquired by the corner raft sub-system. The OCS coordinates with the Camera Control System (CCS) for camera specific actions including the corner raft operating steps and the TCS for active control.

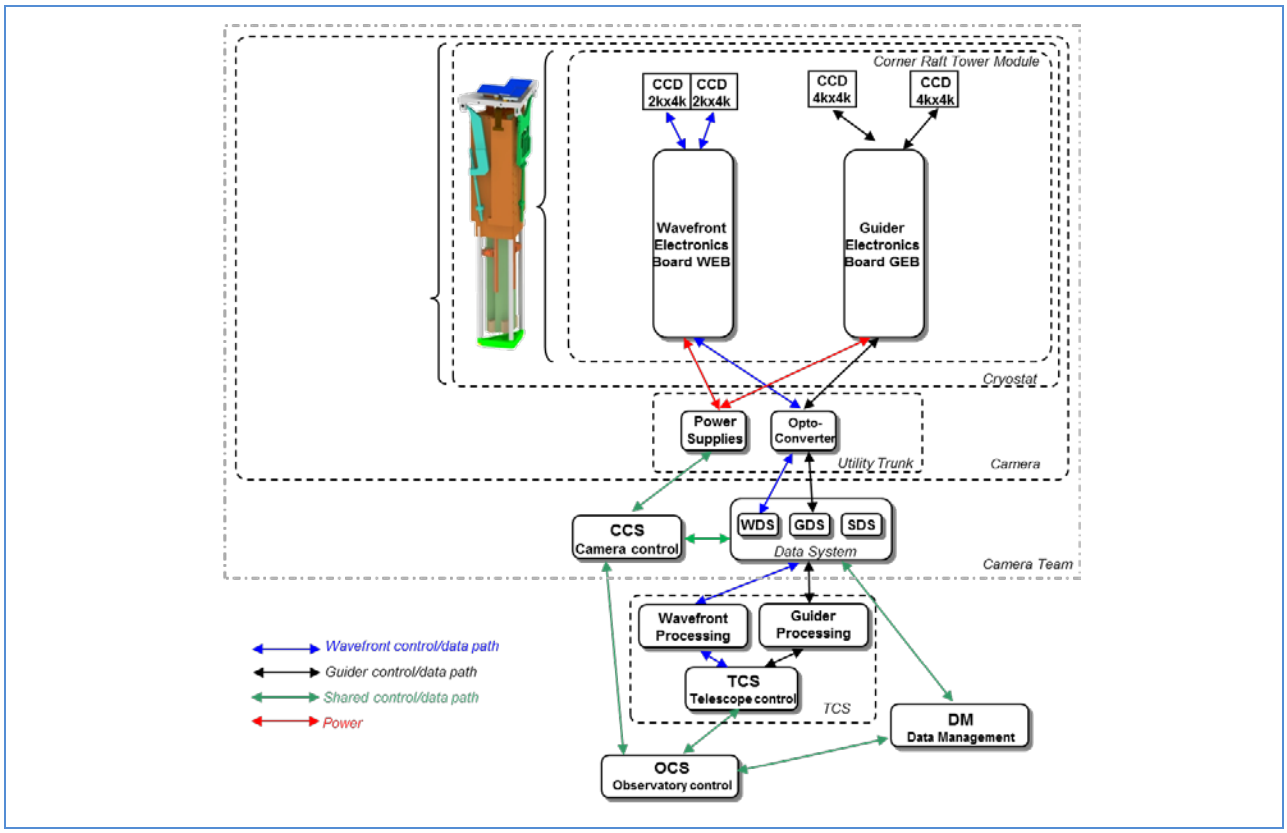

Figure 11-2: Corner raft system component block diagram in the context of the LSST Camera and telescope

11.4 Corner Raft Tower Mechanical Design and Analysis

11.4.1 Corner Raft Sensor Assembly

Each sensor package will be mounted to the corner raft structure by means of 3 threaded studs + 2 pins, Belleville washers and locking nuts. Removable, thermally-conductive spacer/shims will be used to set the height of the sensor surfaces above the corner raft. Identical corner rafts will be mounted in four corner locations on the GRID structure (which also supports the science rafts) by means of an adjustable 3-point ball-and-vee kinematic mount design. The concept for this mount system is shown in Figure 11-3.

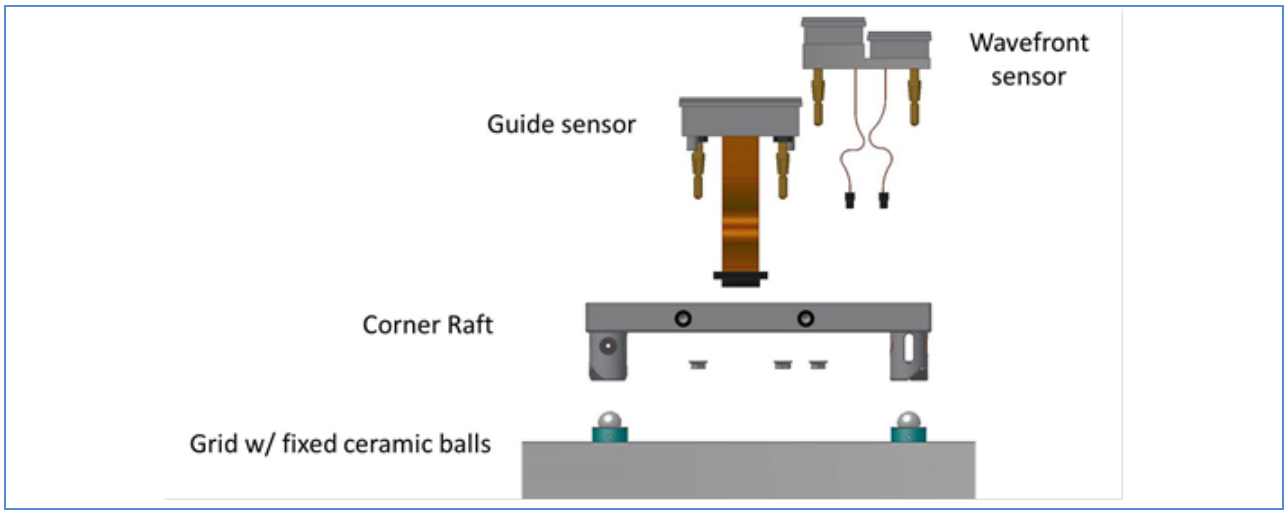

Figure 11-3: Side view of sensor-to-corner raft-to-grid mounting scheme

Two guide sensors are located in each of the 4 corner rafts (total of 8 guide sensors). The baseline design for guiders uses 4K x 4K LSST science CCD sensors with 10 micron pixels. The CCD sensors are deep-depletion, back-illuminated devices with a highly segmented architecture. The readout electronics are mounted on a custom printed circuit board and housed inside a metal enclosure for EMI shielding and heat transfer to the cold plate. A pair of flat flex cables (identical to those used connectivity in the science CCD array) mates to circuitry on the back-side of the CCD sensor package, and terminates in a pair of 37-pin Nano-connectors for connection to the readout electronics board.

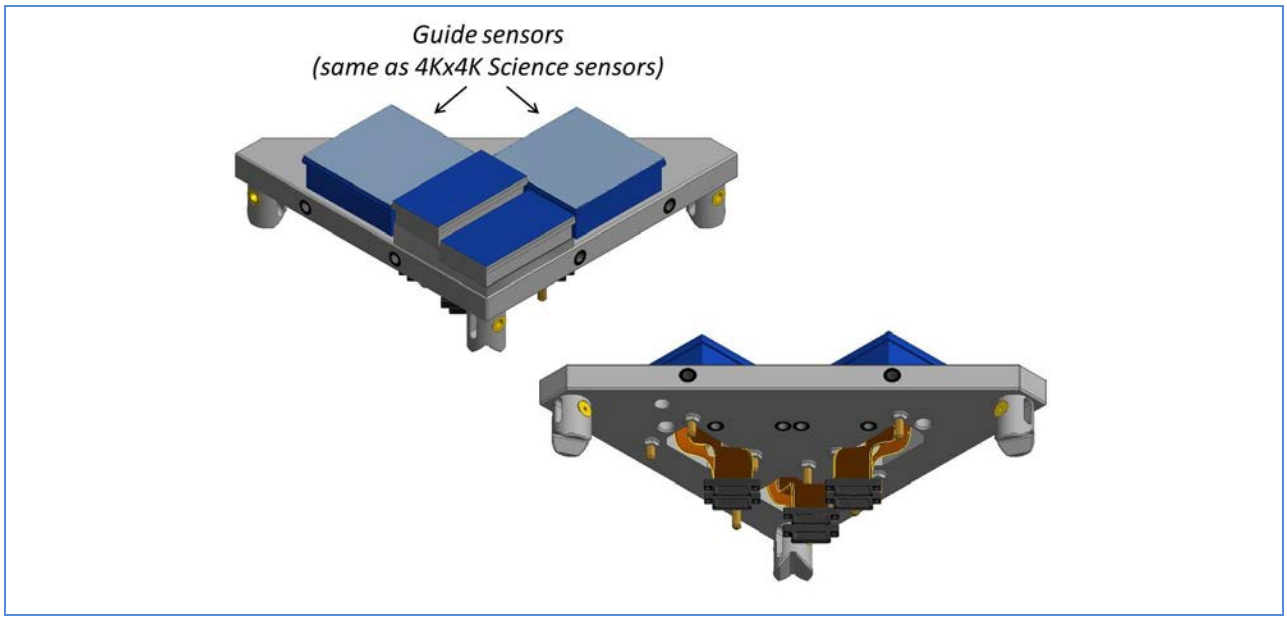

Figure 11-4: Guide and wavefront sensor assemblies on the corner raft

LSST requires four wavefront sensors located in the corner rafts at the periphery of the focal plane. A depiction of the wavefront sensor concept is shown in Figure 11-5. Two 2K x 4K segmented CCDs packages will be mounted on a “step plate” and offset relative to the science focal plane to produce

intra and extra focal images. An offset of roughly +/- 2mm from the science focal plane is anticipated. Wavefront sensor CCDs will share the layout and processing of the science sensors, and have similar performance as science CCDs regarding quantum efficiency, point spread function, read noise, and readout speed. Detailed mechanical specifications such as fill factor, flatness, parallelism of the intra and extra focal sections, and temperature sensing will be validated by laboratory measurements.

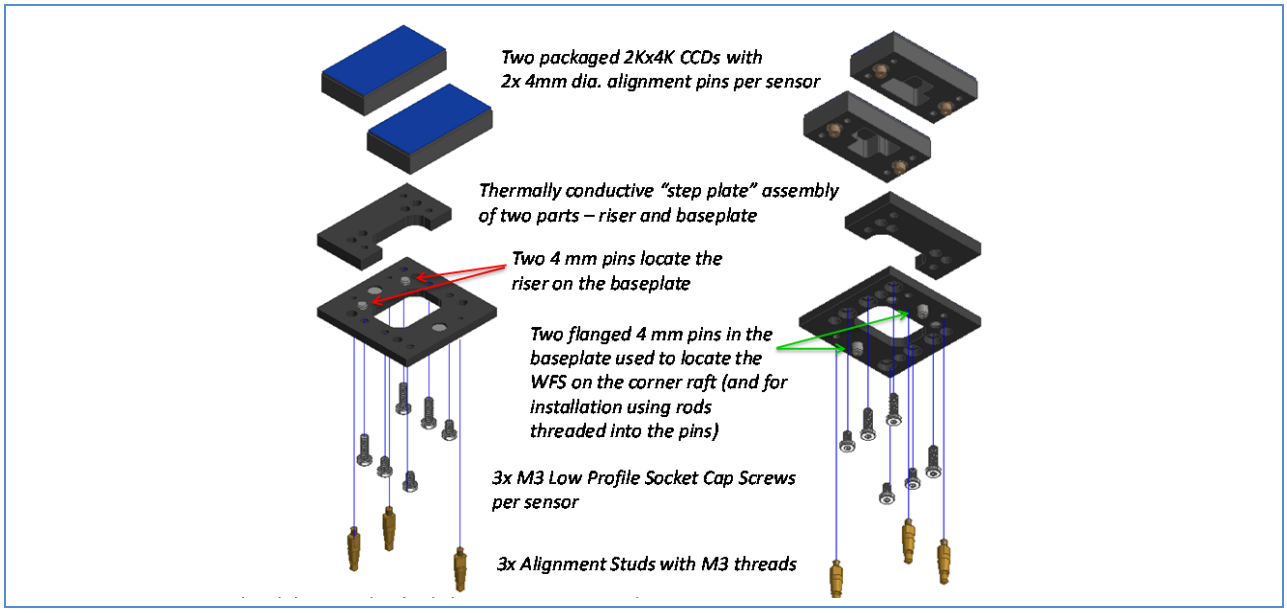

Figure 11-5: Wavefront sensor assembly

The wavefront sensor mechanical alignment is tied to the science sensor array best fit plane as it is a critical component of wavefront correction. The details of the overall mechanical alignment requirements applicable to the corner raft are shown in Figure 11-6.

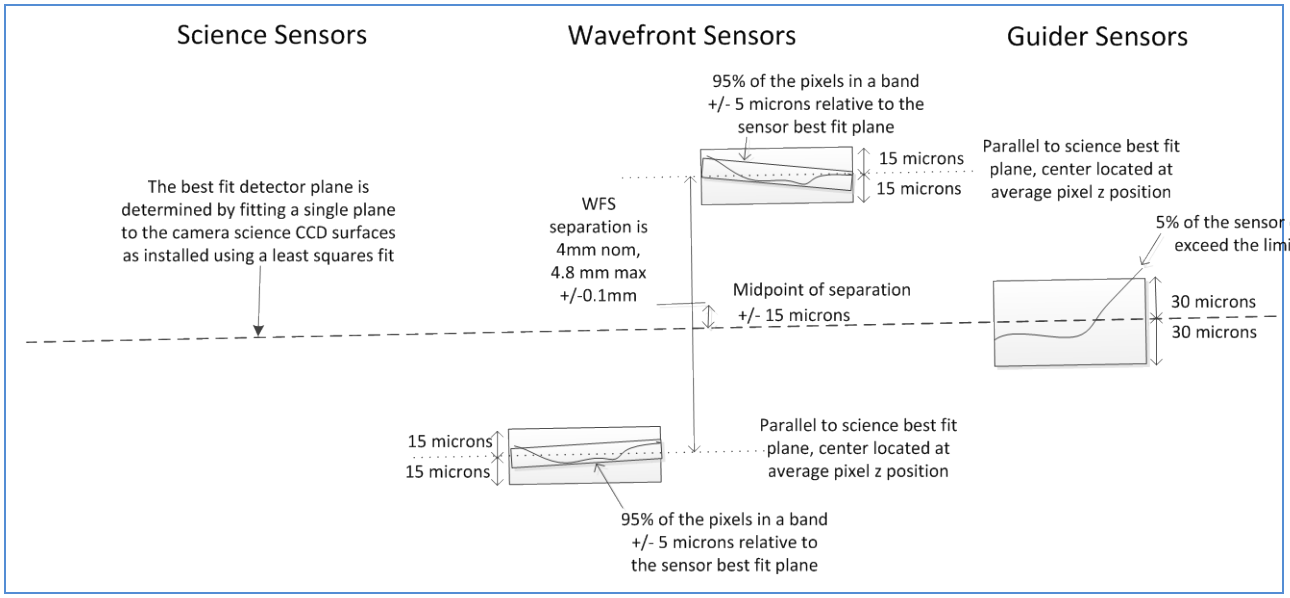

Figure 11-6: Corner raft sensor mechanical alignment and tolerance requirements

The back side of the corner raft features three radially-arrayed vees ground into the Raft material. The vees uniquely define the position of the corner raft with respect to silicon-nitride ceramic balls that are fixed in cups mounted on the grid. This forms a kinematic connection that isolates the corner (and science) rafts from grid distortion due to external dynamic and transient loads, assembly tolerances, and to the expected thermal motions due to differential contraction during cooling. The corner rafts are held in position by springs that pre-load the corner rafts against their kinematic coupling to the grid, producing a uniform, invariant loading. The deflection of grid and corner raft due to the spring loading is compensated for during initial integration, and remains unchanged in operation, independent of camera orientation and temperature.

The grid, science rafts, and corner rafts will be manufactured from a silicon-carbide ceramic matrix composite. This material is used for lightweight and stable space-borne structures, including focal planes, optical benches, and mirrors. The high modulus, high thermal conductivity, near-zero expansion coefficient and improved fracture toughness of the ECM CeSic material makes it ideal for the grid, science raft, and corner raft structures. A closed-loop thermal control system will be used to adjust the temperature of the corner rafts, thereby maintaining a suitable and stable operating temperature for the sensors.

11.4.2 Corner Raft Tower Concept

Each corner raft tower contains one wavefront sensor and two guide sensors and dedicated electronics. The mechanical and thermal design of the corner rafts is as similar as possible to the science rafts.

The electronics for operating the wavefront and guide sensors are packaged within the volume behind the detectors, similar to the science raft configuration, in a corner raft electronics crate (CREC) “Tower.” Electrical connections between sensors and front-end electronics boards are made by flat flex circuit cables. The electronics boards are thermally connected to the cold plate at about -40C by thermally conductive straps. The grid supports as little mass as possible—only the sensor rafts and their supports—to reduce gravity induced deflections. The tower is supported by a neighboring cryogenically-cooled Cryo Plate at about -130^{o}C temperature. Each corner raft is thermally connected, but structurally decoupled, from the tower by use of thin copper thermal straps to remove the electrical and radiant heat load from each corner raft and conduct it back to the cryo plate. Details of the design for corner raft/towers for the LSST camera are shown below.

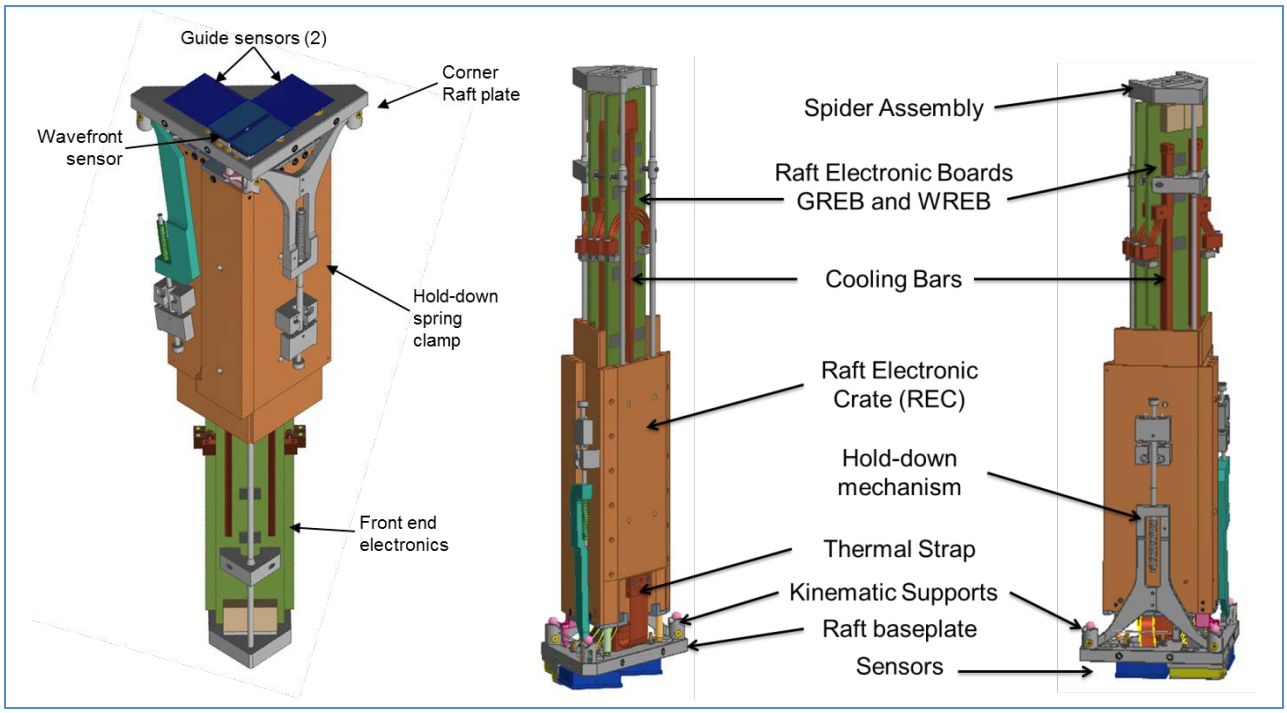

Figure 11-7: CAD model of the corner raft tower

11.4.3 Mechanical Interfaces

11.4.3.1 Cryo Plate Interface

The corner raft tower is a mechanical enclosure that contains the readout electronics boards for the wavefront and guide sensors and has a smaller "footprint" than the corner raft. The tower is fastened to the cryo plate by a series of screws to provide mechanical support as well as the thermal path from corner raft CCDs to the cryo plate. The CRT also acts as a barrier to contaminants outgassed from electronics that could degrade the image quality of the CCDs (see Figure 11-8).

The corner raft WREB (wavefront readout electronics board) and GREB (Guider readout electronics board) are passed through a triangular-shaped opening in the cryo plate during installation of the corner raft tower module (CRTM) in the cryostat. Access to the captive screws for the two corner raft hold-down mechanisms is through cut-outs in the cryo plate adjoining the opening for the WREB and GREB.

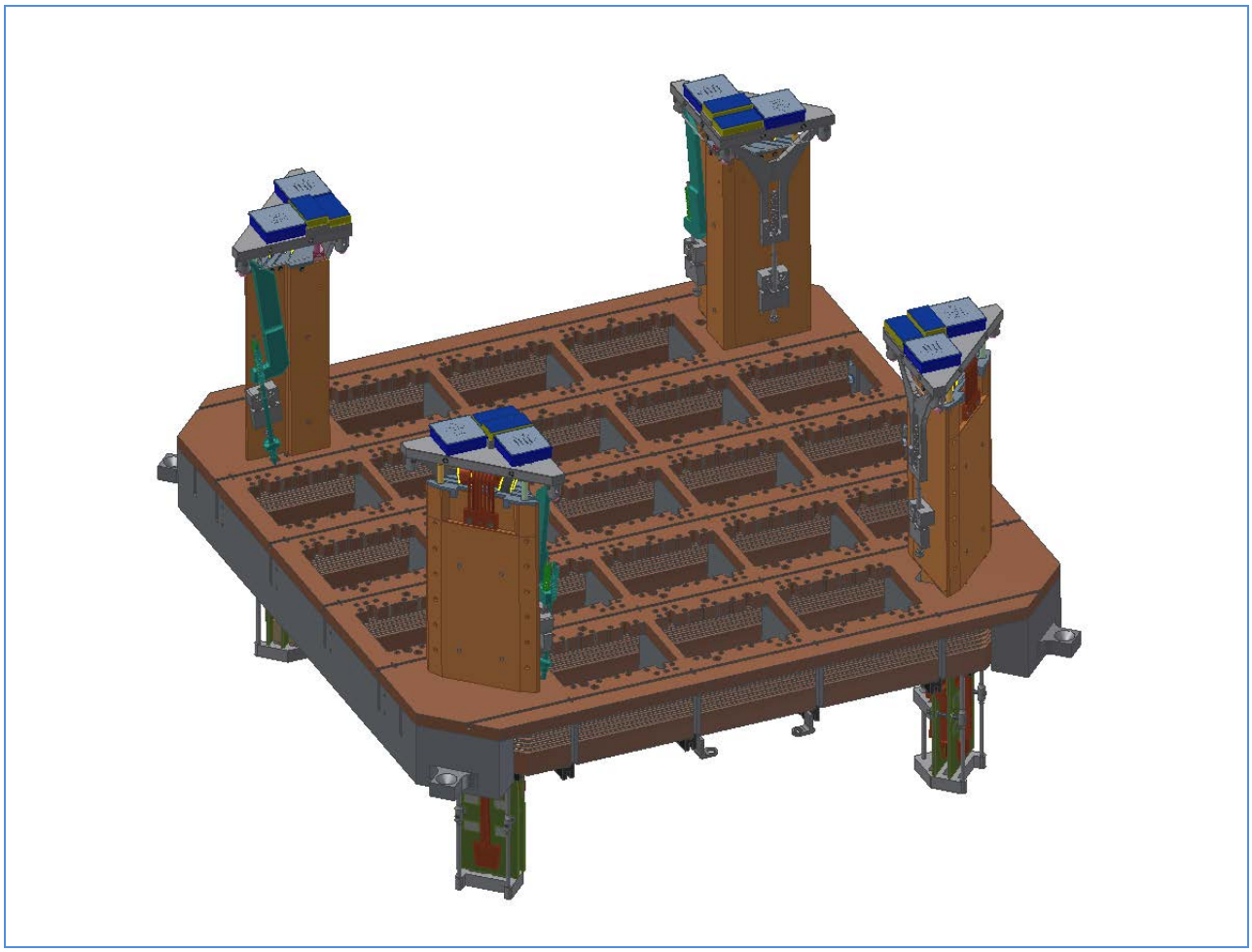

Figure 11-8: Corner raft to cryo plate interface

11.4.3.2 Cold Plate Interface

The corner raft tower is a mechanical structure that houses the readout electronics boards. Thermal connections are made between cold bars on the WREB and GREB and cold plate "fingers" during installation of CRTMs into the cryostat (see Figure 11-9). Copper blocks at the ends of copper braided wire cables (connected to the cold bars on the REBs) are retracted within the profile of the REBs during insertion of the CRTMs into the cryostat, then extended and fastened to the cold plate fingers.

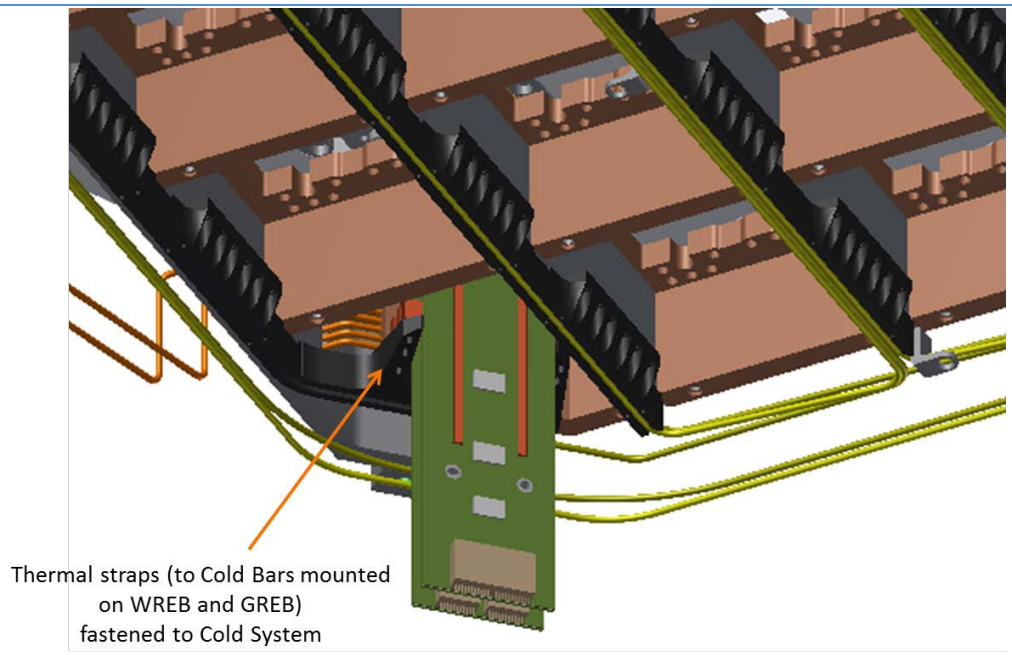

Figure 11-9: Corner raft to cold plate interface

11.4.3.3 Cryostat Interface

The designs for the mechanical and thermal interfaces between the corner rafts and the cryostat are as similar as the possible to the interface designs for the science rafts. The mechanical interface between the corner raft and the grid provides precise mechanical location and support for the corner raft sensors with respect to the focal plane. The mechanical and thermal interfaces between the cryostat and corner raft towers support the electronics to control and read out the CCDs and provide the thermal paths for removal of the heat from the corner raft CCDs and electronics without adversely affecting the performance of the science raft subsystems.

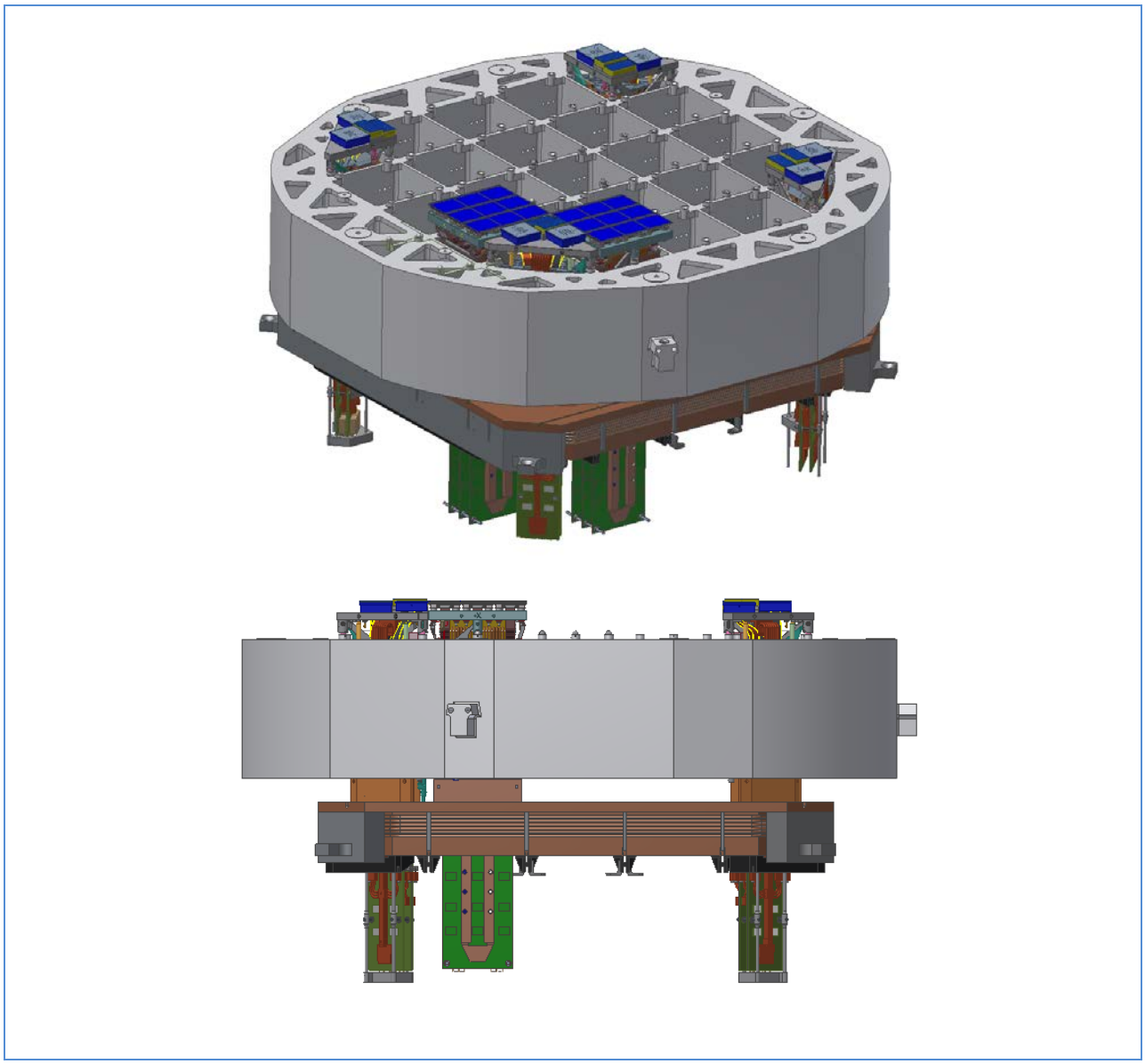

Figure 11-10: Corner raft to cryostat interface

11.4.4 Thermal and Structural Analysis

Thermal steady-state finite element analysis results of a simplified corner raft tower model, with average REBs power (23.5W), 2.7W heat load on the corner raft sensor assembly, and temperatures at the cryo plate interface fixed at -130°C and at the cold plate interface fixed at -40°C, are shown in Figure 11-11. Makeup heat of ~0.5W from ohmic heaters mounted on the backside of the corner raft are required to raise the temperature of the sensors to -100°C. A closed-loop thermal circuit will be used to adjust the make-up heat on each corner raft to maintain a stable operating temperature for the sensors with varying thermal loads.

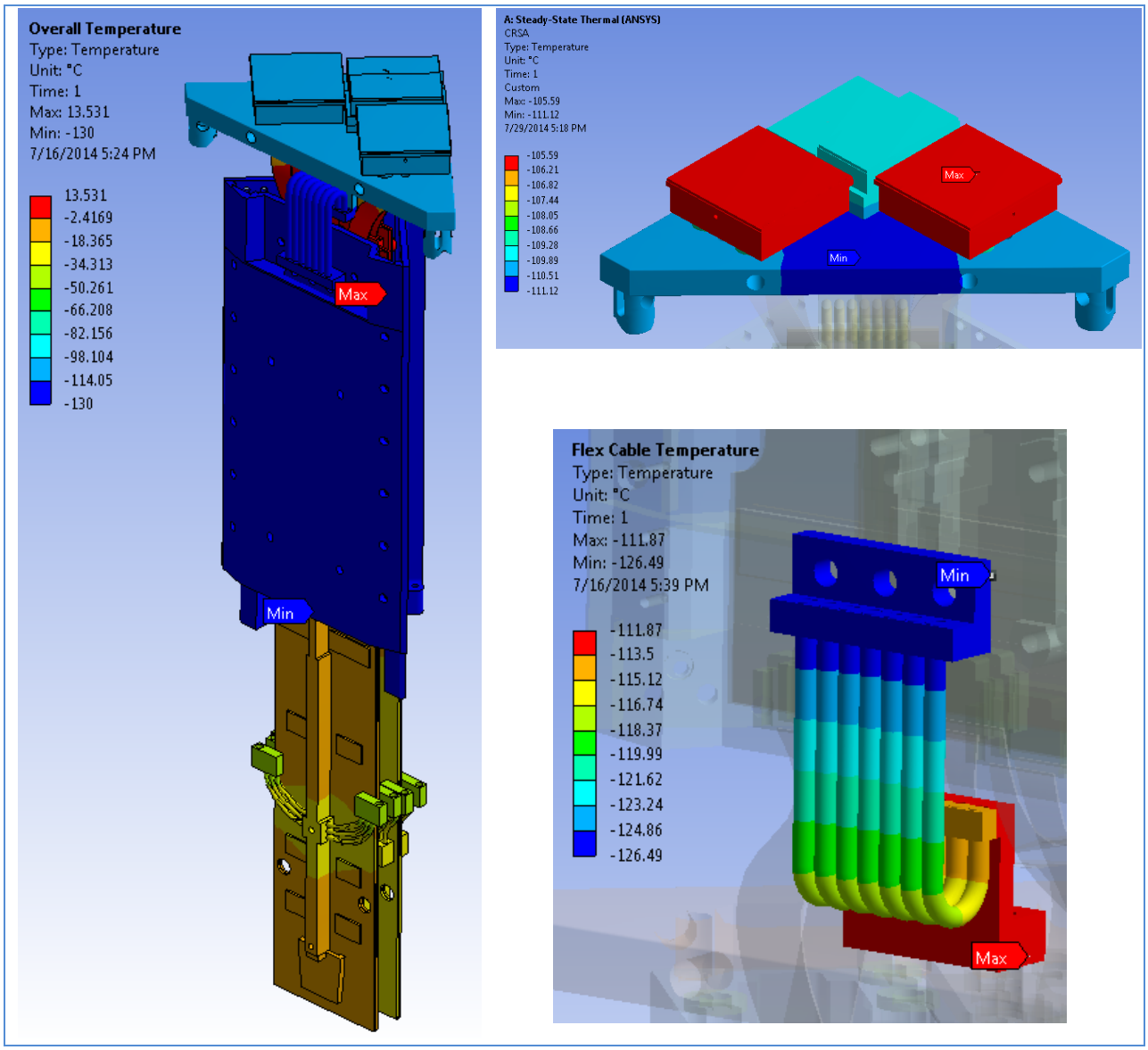

Figure 11-11: Corner raft tower thermal analysis results

Preliminary structural finite element analysis of a simplified corner raft and sensors model, with the corner raft kinematically supported by the vees on fixed balls, and including thermal loads, gravity and applied spring forces, results in a “z-axis” deformation of the corner raft and sensor surfaces of ~1 µm, meeting requirements.

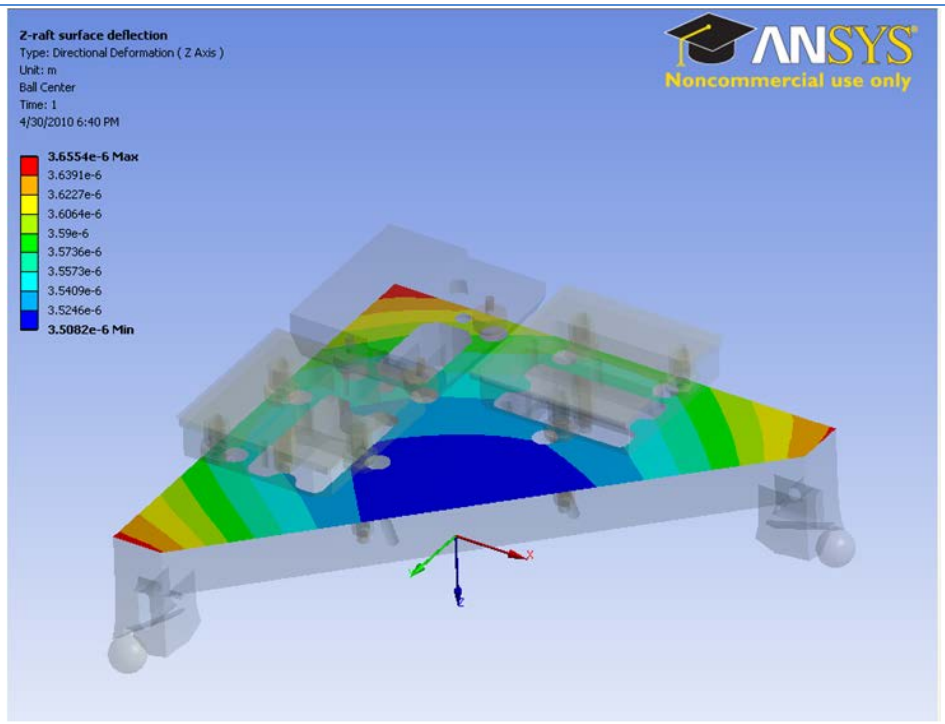

Figure 11-12: Corner raft structural analysis results

11.5 Corner Raft Tower Electronics

Data acquisition and control for the wavefront and guide sensors are managed using the same infrastructure as for the Science detectors. The corner raft tower contains four ASPIC ASICs for reading the two guide sensor data and two ASPIC ASICs for the split wavefront sensor. The ASPIC implements the CCD readout and was developed specifically for LSST. The electronics used to read the CCD sensors are schematically nearly identical to the science electronics and are simply re-packaged to accommodate the smaller footprint and reduced numbers of channels.

11.5.1 Guide Sensing Electronics Architecture

The corner raft tower electronics provides all CCD biasing and clock signals, CCD signal amplification and low noise analog signal processing, digitization, data collection, and transmission of image and metadata to the DAQ. The corner raft tower electronics also has the responsibility for monitoring and reporting a variety of metadata such as supply voltages and currents, precision temperature measurements, and operating raft heaters to maintain the focal plane temperature. In addition, a significant ability to diagnose problems *in situ* will be part of the design. The video data from the CCDs will be transmitted via two high speed serial links (one for both guide sensors, one for the wavefront sensor) to the DAQ system. Analogous to the dual functionality of the corner raft (guiding and wavefront sensing) the electronic is partitioned into 2 PCBs: one for the operation of the two guide sensors at high frame rates with a total of 32 analog channels (GREB for Guider Readout Electronics Board) and one for the operation of the wavefront sensor with 16 channels (WREB for Wavefront Readout Electronics Board). The two different CCD types (for guide sensor and wavefront sensor) will be very similar in terms of

segmentation and readout and therefore will be interchangeable with respect to the electronics. Therefore it is foreseen to utilize the same basic electronics block for both PCB types. Still, some optimization for the specific functionality will be implemented, especially to support the fast shift and region of interest readout for the guide sensors. The CCDs will be connected to the readout boards via polyimide flex leads. Length and layout of this connection is critical for noise and crosstalk performance.

11.5.2 Guide Sensor Electronics

The guide sensor electronics is based on the science sensor electronics and is responsible for providing clock signals and bias voltages to the CCDs as well as processing and digitizing the CCD output signals. The design uses the ASPIC integrated circuit to amplify and process the signal from the CCDs. The required CCD bias voltages and clock waveforms are generated by the DCBS block. The CCD back-side bias is generated by an external power supply but a dedicated switch to enable this voltage is included on the board. The circuitry is identical to the science sensor design, but the implementation is re-packaged to fit the diagonally shaped corner raft tower. The guide sensor electronics services 2 CCDs and therefore is organized with two video stripes (each stripe using two ASPICs and 16 ADCs). Additionally, during operation the sequencing electronics is operated at 9Hz to meet the guide servo loop requirements.

The two guide CCDs are serviced by an electronics board as shown in Figure 11-13.

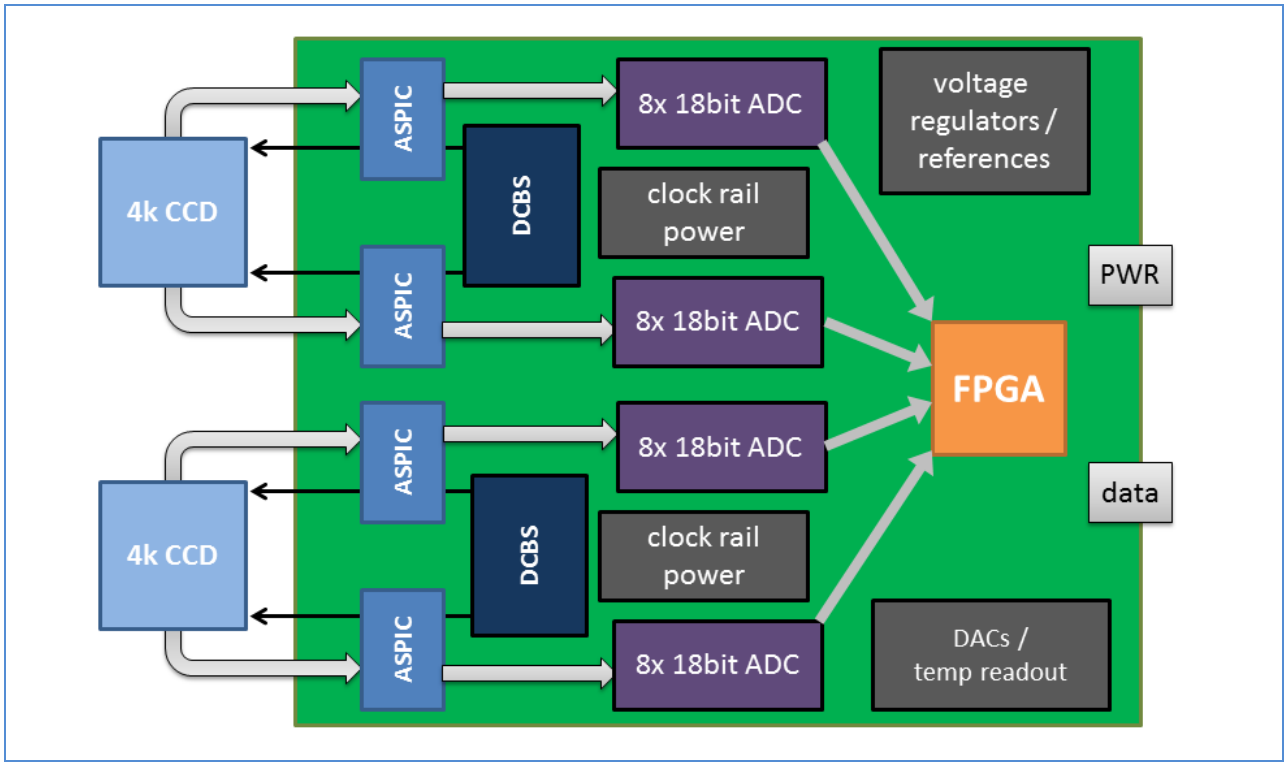

Figure 11-13: Guider readout electronics block diagram

Even though the 2 guide sensors located in each corner raft are controlled using a single board, their sequencing will be concurrent but different to accommodate different guide windows locations. Each

guide sensor board also provides temperature sensing near various components on the board. Support for temperature monitoring and heating of the corner raft is also available in a similar fashion to the science REB capabilities. Power supplies, bias voltage, as well as clock signal filtering are also available.

The FPGA firmware is reconfigurable via the DAQ interface. Register content in the FPGA is accessible via the GDS interface and this interface is used to handle the instruction set updates and meta-data transfers (a few tens of words) defining CCD and ASPIC clock structure.

Guide CCD operations are controlled by a synchronous readout processor implemented within the FPGA of the guide sensing electronics. The microcode for this processor is downloaded through the DAQ so that the processor is completely unaware of the purpose of any particular code. This architecture is particularly useful in the case of the guide sensor for two reasons. First, the same electronics design used in the science sensor electronics can be re-used in the corner raft with only changes to the downloaded firmware needed. Second, the windowed operation can be simplified or upgraded by loading new code to the electronics as needed.

The guide sensing CCD sequences are more complicated than science raft sequences, but it is expected that the code would be the same except for guide window coordinates. A possible guider sequence implementation compatible with the overall guider timing is given below:

- Set up the sequence microcode without guide window coordinates
- Download window coordinates to registers
- Execute single frame read with large window
- Download smaller guide window
- Execute frame reads until told to stop

11.5.3 Guide Sensing Electronics Interfaces

11.5.3.1 Power Supply Interface

As shown in the table below, the power distribution system (PDS) provides a number of different potentials to the guide sensing back-end electronics in the corner raft – similar voltages as used in the science rafts, but at lower maximum current. Each supply is floating and is separately adjusted and monitored. The adjustment, monitoring and on/off sequencing of the supplies is controlled by CCS.

The PDS has separate power supply groups for each of the 21 science rafts and for each of the four corner rafts. In general, the power used in the corner raft, as in the science rafts, is regulated at the point of load to further reduce interference – for instance the ASPIC uses a separate low dropout linear regulators to take A_VDD from about 6V to the 5.0V and 3.3V required by the chip. Bias and clock rail voltages are regulated with OPAMPs and emitter follower output transistors.

Table 11-3: Power supply voltages

Voltage(V) (nom.)	Current(A) (peak)	Name	Description
6.0	1.5	V_ANA	Analog power
5.0	1.0	V_DIG	Digital power
5.0	1.0	V_HTR	Power for raft heaters
+14 (e2V) +8 (ITL)	0.8	V_CLK_H	Auxiliary power for clock rail generation
-2 (e2V) -8 (ITL)	0.8	V_CLK_L	Auxiliary power for clock rail generation
32	.13	V_OD	CCD bias generation power
12	0.7	V_dPHI	CCD parallel clock amplitude
-70	.002	V_bias	Adjustable 0 to -70V – CCD bias

11.5.3.2 DAQ Interface

The guide sensing electronics interface to the DAQ System through via their Source Communication Interface (SCI) firmware block. The corner raft is by default in reset mode, where the pixels are continuously read and their charge reset. After the shutter opens, the raft initiates readout of 50x50 pixel windows to be read at 9Hz. Based on the location in the CCD segment, the readout time can range from 1.25 msec to 35 msec and the fixed 50 msec integration time is accounting for this range. It has been shown that, as long as the start of integration on all sensors is synchronized within 1 msec, the servo loop rejection ratio and bandwidth is appropriate for guiding. All windows are read out such that their integration start times are all synchronized within 1msec. As data are read out by the raft, they are forwarded to the telescope for centroid finding computations and servo loop control.

11.5.3.3 Wavefront Sensing Electronics Architecture

The wavefront sensors electronics is physically independent from the guide sensor electronics and has their own independent board; however, they are co-located within the mechanical crates. The wavefront sensor electronics architecture is nearly identical to that for readout of each of the two guide sensors on the GREB. The wavefront sensor electronics operates independent of the guider electronics.

For electronics readout purposes, the split wavefront sensor of two 2kx4k pixels is seen as a unique 4kx4k sensor. This allows the electronics to operate fully synchronously with the science electronics as they share the same integration time. This guarantees that the potential cross-talk and pickup noise issues are limited and similar to the science sensor operation so that the identical cross-talk correction algorithm and processing chain can be used.

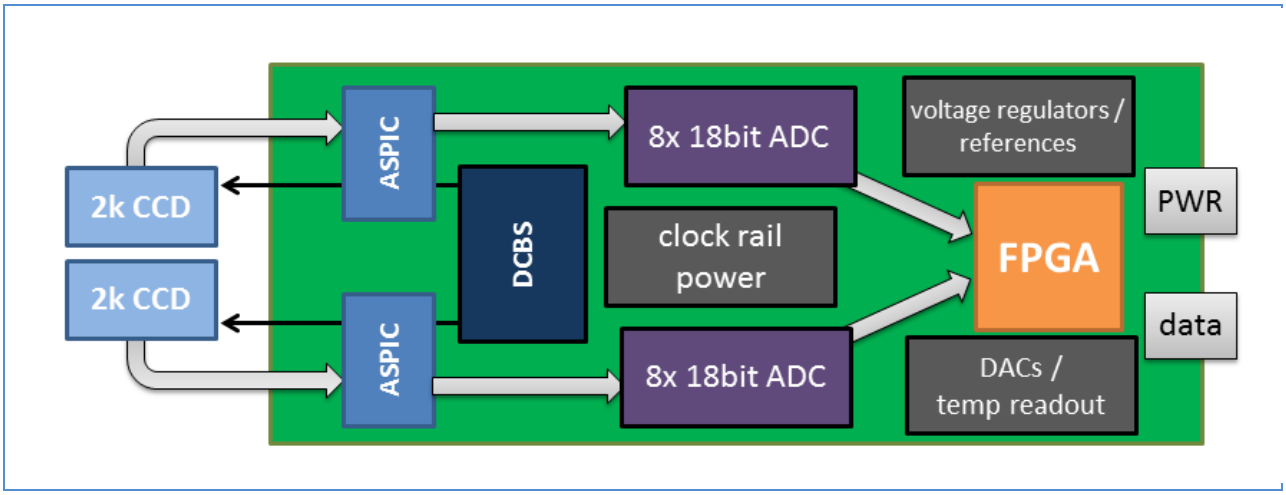

Figure 11-14: Wavefront sensing electronics block diagram

11.5.4 Wavefront Sensing Readout Electronics

As mentioned previously, the wavefront sensing electronics is based on the science sensor electronics and is responsible for providing clock signals and bias voltages to the CCDs as well as output signal processing and digitization. The circuitry is practically identical to the guide sensor electronics but the implementation is re-packaged to fit the diagonally shaped corner raft tower and simplified to a single strip due to the need of controlling a single equivalent 4kx4k sensor. In contrast to the guide sensor electronics, this board will not include trim-heater circuitry.

The split CCD sensor, constructed of two identical CCDs, in a corner raft tower is serviced by a wavefront readout board (WREB) as shown in Figure 11-14.

11.5.5 Wavefront Sensing Electronics Interfaces

11.5.5.1 Power Supply Interface

The power distribution system provides a number of different potentials to the wavefront sensing electronics in the corner raft. Those voltages are identical to those provided for the guider.

11.5.5.2 Timing Interface

The wavefront sensor timing is generated by the FPGA on the WREB and the timing programs are loaded via the DAQ system. The wavefront sensing FPGA operates identically to the science sensor FPGA as the readout is done at the same time with the same timing.

11.5.5.3 DAQ Interface

The interface between wavefront sensing electronics and the DAQ System is identical to the interface between the Science REB and the DAQ System.

11.6 Assembly and Test

Given that LSST is a survey telescope, the mechanical and electrical systems must be reliable, with a high up-time. All mechanical and electrical sub-assemblies will be functionally and performance tested prior to installing in the corner raft towers, minimizing the risk of early failures and the need for disassembly

during subsequent camera integration and commissioning. Sensors and electronic sub-assemblies are modular and self-contained, allowing them to be installed, removed, and serviced with minimal disturbance of neighboring components.

After assembly and system testing, each corner raft tower will be integrated into the LSST Camera. The same procedure and installation tooling on a gantry motion control system envisioned for integration of science raft towers will be used for integration of corner raft towers into the Camera cryostat.

11.6.1 Assembly Sequence

Corner raft-specific assembly fixtures and procedures are adaptations from science raft assembly. Sensors will be assembled into corner rafts in a face-down orientation to allow easy access to the installation mechanism and to minimize the potential for surface contamination and accidents. Installation rods are screwed onto the ends of two of the threaded stud legs on the sensor package. Using a handling fixture, the sensor package with flex cables attached is pulled into contact with the corner raft. The taper on the rods is designed to fully engage the mounting holes in the corner raft before the sensor package overlaps any neighboring sensors.

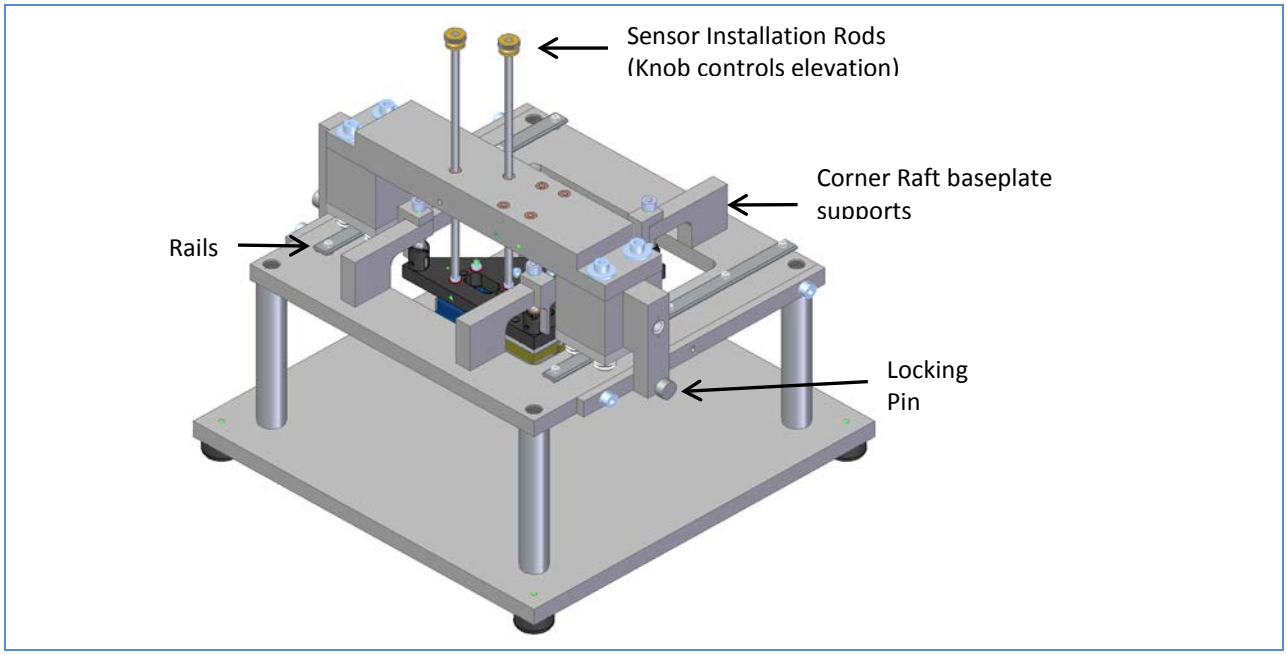

Figure 11-15: Wave front and guide sensor insertion tooling

After sensors are installed and leveled in the corner raft, a protective lid will be fastened to the corner raft sensor assembly (CRSA) to protect the sensors from particulates and contamination. The thermal straps, readout electronics, tower sides, and spring-loaded yoke hold-down sub-assemblies are progressively connected to the CRSA (see Figure 11-16). A conductance barrier (to separate the ultra-clean focal plane from the support electronics) is formed during assembly by the installation of bar-shaped parts between thermal straps and sensor flex cables across the front end of the tower.

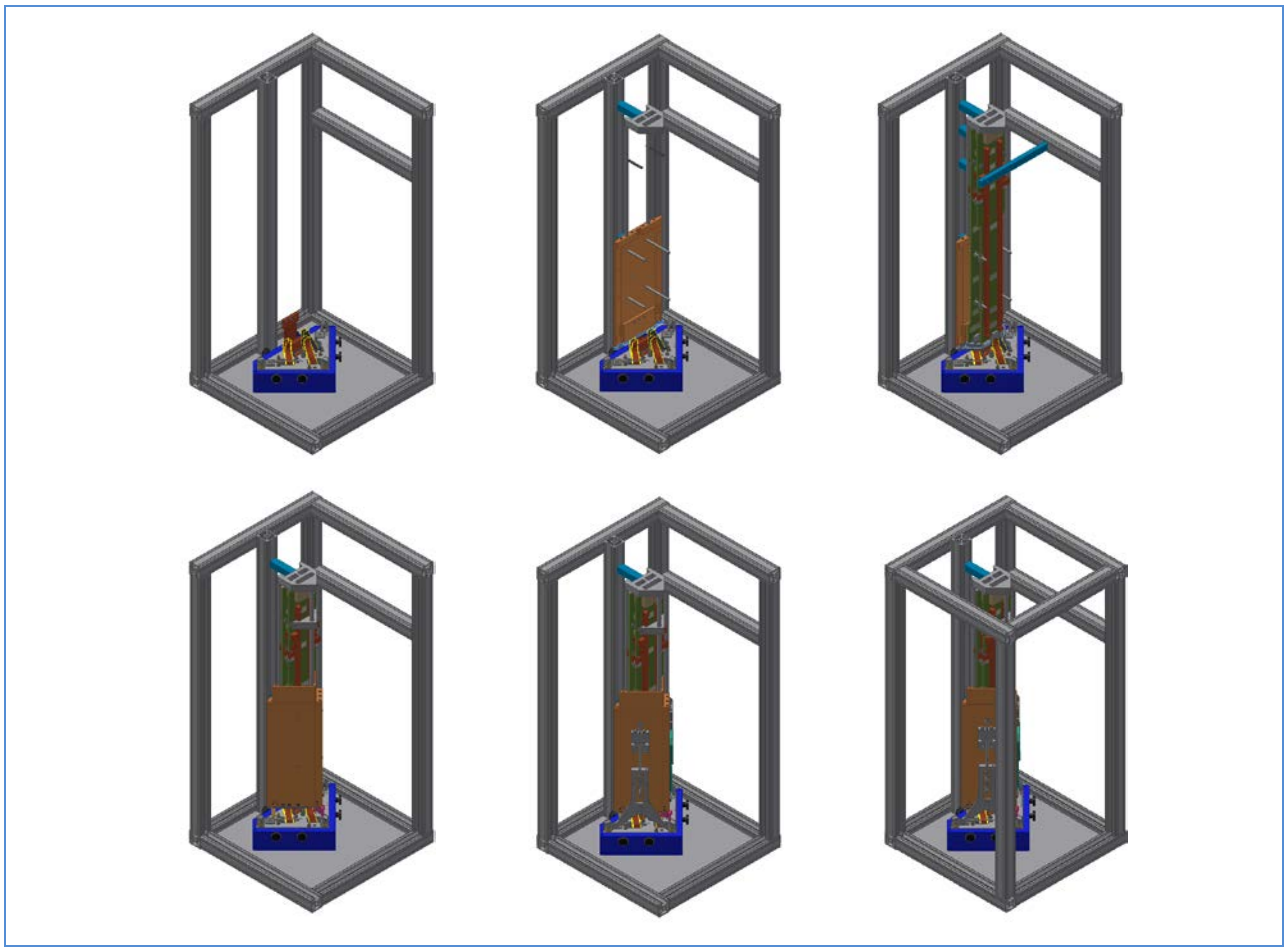

Figure 11-16: Corner raft tower assembly sequence

11.6.2 Corner Raft Installation into the Camera

Corner raft towers are modular and designed to use the same tooling and insertion, mounting, connecting, and testing processes developed for installation of the science raft towers into the cryostat.

As with the integration of science raft towers, corner raft towers are inserted into the corner bays of the grid and cryo plate from below, with the cryostat pointed downward in its integration stand. An insertion arm on the XYZ-gantry is extended down through the cryostat and fastened to the back-end of the corner raft tower. The corner raft tower is pulled into the cryostat through the grid; making small adjustments with the XYZ-gantry to maintain alignment during insertion (see Figure 11-17).

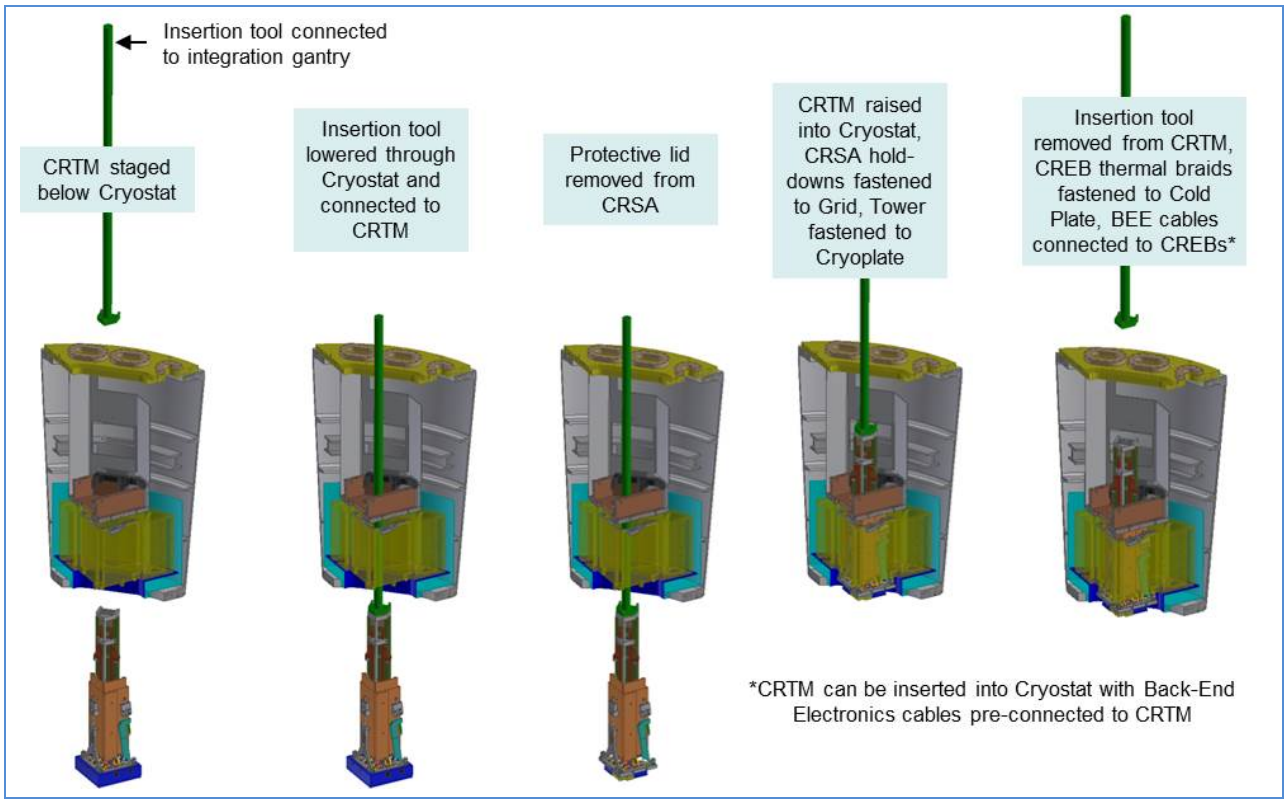

Figure 11-17: CRTM installation into the cryostat

As the corner raft reaches its mounting location, V-blocks on the corner raft contact the balls on the grid, lifting the corner raft off the temporary supports on the tower. The tower is pulled an additional ~4mm into the cryostat until its back end contacts the cryo plate. The same pre-loaded spring hold-down mechanism design for the science rafts is used to allow this relative motion between the corner raft and tower. The tower is the fastened to the cryo plate with screws, and the insertion arm is disconnected from the back of the tower and retracted from the cryostat.

Mechanical installation is completed by transferring the load of the hold-down springs from the sides of the Tower to support points on the back of the grid. This load transfer is accomplished by engaging the captive screws on the grid into the hold-down mechanisms to lock the corner raft into place on the grid.

Following mechanical integration, the corner raft tower is electrically integrated by connecting the vacuum feedthrough pigtail connectors to the back of the electronics boards. Testing using equipment connected to the pigtails on the outside of the cryostat will be performed to verify that all internal connectors are mated as well as ensure that all corner raft tower systems are functional.

12: Cryostat

12 Cryostat

12.1 Introduction

The Cryostat subsystem includes the cryostat body plus all the on-Camera and off-Camera components that support the cryostat vacuum vessel. The cryostat is closed by the last optical element (L3) and holds the Camera focal plane sensors and sensor readout electronics in an appropriate environment. The Cryostat subsystem also includes all the utilities (vacuum, purge, contamination control, and refrigeration) necessary to accomplish this. For completeness, the subsystem also includes the utility trunk structure itself.

12.2 Cryostat Subsystem Requirements

The highest-level requirements on the Cryostat subsystem are indicated in Table 12-1 and fully specify the subsystem. The cryostat specifications were derived largely from the image quality and throughput requirements imposed on the Camera and the environmental and safety requirements from the telescope. The cryostat enclosure also provides the mechanical and environmental support for the last refractive optical element (L3) of the telescope.

Table 12-1: High-level cryostat subsystem requirements

Requirement	Predecessor/ Traceability	Title	Requirement Description
			Performance Requirements
C-CRYO-200	C-368	Cryothermal temperature	The cryo thermal system shall provide a cryoplate at nominal -130°C so as to maintain the FPA at -100°C design temperature
C-CRYO-002		Cryothermal Power	The cryo thermal system shall be capable of removing a total of 540 watts from the cyrostat
C-CRYO-213	C-369	Coldthermal Temperature	The cold thermal system shall provide a cryoplate at nominal -40° C so as to maintain the Raft Electronics Crates (RECs) at -40° C design temperature
C-CRYO-214		Coldthermal Power	The cold thermal system shall be capable of removing a total of 1500 watts from the coldplate
C-CRYO-226	C-CRYO-002	Vacuum FPA Region	The cryostat vacuum environment in the region of the FPA shall be sufficient to insure less than 5 monolayers of condensable gas accumulation on the FPA surface between annual servicing.
C-CRYO-228		Vacuum thermal insulation	The cryostat nominal total pressure in the cryo and cold thermal regions shall be in the molecular flow regime
C-CRYO-229		Vacuum reliability	All demountable elastomer-sealed vacuum flanges shall provide redundant (main and guard) sealing with inter-volume for leak check-pump-backfill between the main and guard seal.

Requirement	Predecessor/ Traceability	Title	Requirement Description
C-CRYO-234		Vacuum reliability	The cryostat vacuum envelopes shall have no fluid (water, refrigerant, etc.) to vacuum joints
C-CRYO-249		Cryo FPA planarity	The total FPA planarity under all cryostat derived conditions and effects (assembly error, measurement error, load and orientation, thermal) shall be less than 5 microns, RSS.
C-CRYO-250	C-CRYO-249	Cryo FPA planer zenith	The cryostat - grid elements for support of the RSA rafts -FPA shall be provided planer to <4 microns RSS when measured with cryostat oriented to zenith pointing at 20C (room temperature)
C-CRYO-401	C-003	L3 position adjustability	The cyrostat shall provide a one-time adjustment of the L3 interface position by +/- 3.5mm
		Camera Interfaces	
C-CRYO-248	C-190	Contamination	The cryostat components shall be compliant with the Camera Contamination Control Plan (LCA-279)
C-CRYO-303	C-227	Cryostat assembly weight	The cryostat assembly mass shall not be greater than 580 kg.
C-CRYO-286	C-375	Local Protection	Protection from mechanical and electrical failure shall be handled locally within the system
C-CRYO-287	C-224	Commanding from CCS	The cryostat shall support commands from the CCS to power-up and initialize, to pump down, to repressurize, to cool down and to warm up as defined in the Cryostat to CCS ICD (LCA-316)
C-CRYO-299	C-001	Lifetime	The cryostat shall be designed to operate for at least 15 years

To accomplish this, the Cryostat subsystem is divided into four main functional elements; 1) cryostat body, 2) vacuum and purge system, 3) refrigeration system, and 4) utility trunk. The on-Camera elements are shown in Figure 12-1.

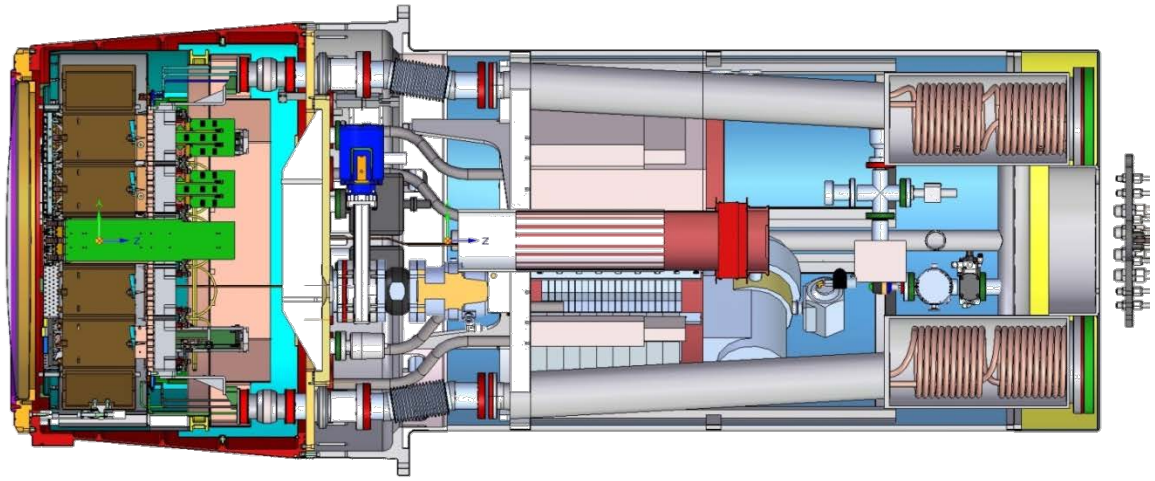

Figure 12-1: Half section of the cryostat and utility trunk.

A section view of the cryostat body is shown in Figure 12-2.

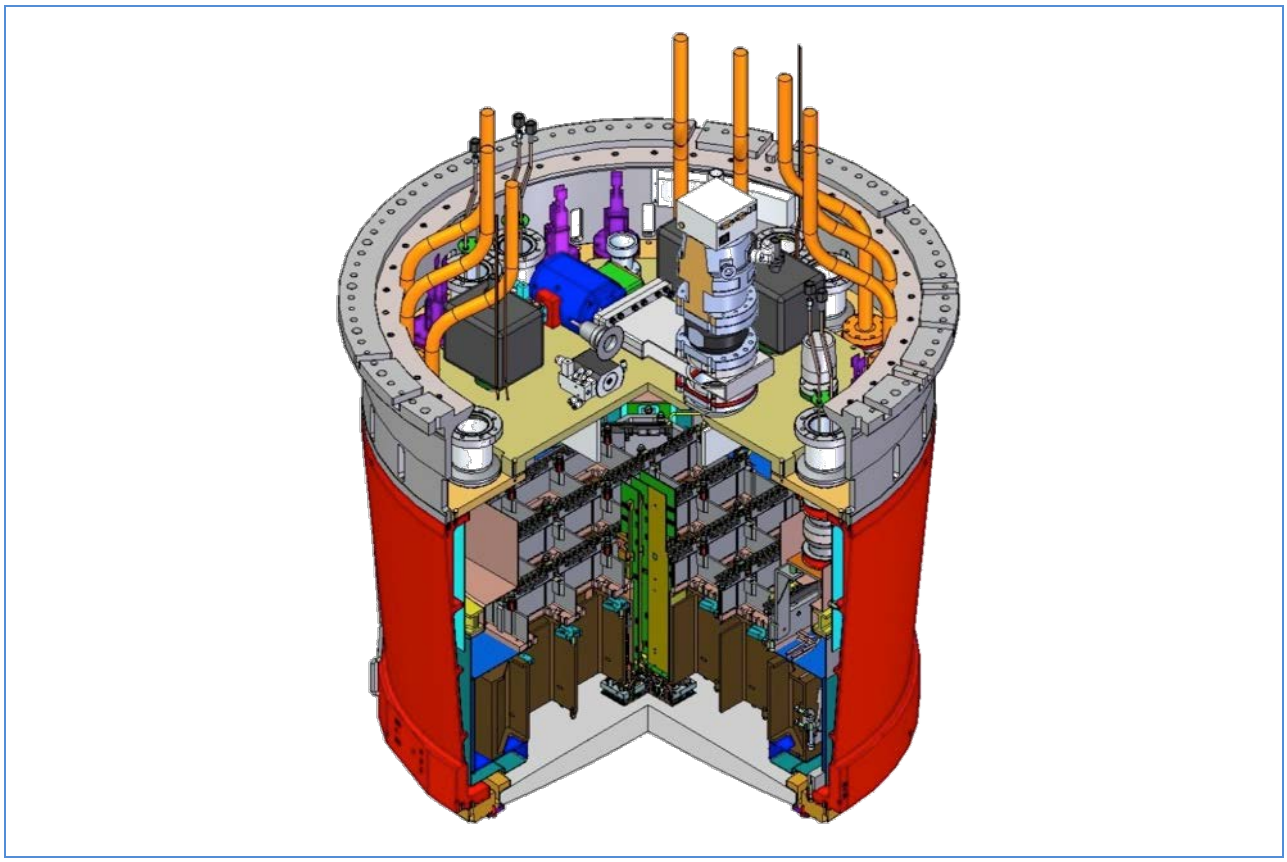

Figure 12-2: Detail quarter section view of cryostat body

The cryostat body is a largely self-contained vacuum vessel closed at the front by the L3 refractive optic and vacuum pumped at the rear. It houses and cools the science raft and corner raft readout electronics, and provides the stable mechanical and thermal platform for the focal plane. Analog and digital signals exit the rear of the cryostat body into the utility trunk. Refrigeration lines enter and exit the rear flange as well.

The utility trunk provides support hardware for the cryostat, housing power supplies, instrumentation, vacuum hardware, and support electronics that do not reside within the cryostat body vacuum enclosure. The utility trunk also supports the on-Camera elements of the refrigeration system.

The refrigeration system provides cooling for the sensors and readout electronics within the cryostat body. A schematic of the modular refrigeration system is shown in Figure 12-3.

The refrigeration system has major components (counterflow heat exchangers, valves) in a distinct vacuum space (heat exchanger module) starting at the rear of the utility trunk, and vacuum-compatible super-insulated transfer lines that traverse the utility trunk and connect to the back of the cryostat. In addition, there are components (compressors, water-cooled condenser, oil separators, fractionators etc.) on the ground in the utility room. Room temperature fluid and gas lines run between the utility room and the Camera.

12.2.1 Vacuum Requirements:

The cryostat body is a vacuum vessel at ambient dome temperature that is used to insulate the cold focal plane and readout electronics from conductive and convective heat losses. A pressure 10^{-5} to 10^{-6} Torr is sufficient for this purpose and is achieved wherever warm seals are required in the vessel by using redundant O-ring seals with pumpouts between the seals.

However, the driving requirement of the vacuum system is not the vacuum required for insulation, but rather the partial pressure of condensable molecules (e.g.: H_20, high molecular weight non-volatile residue (NVR), etc.) in the focal plane region at the front of the cryostat body. These molecules can be cryo-pumped onto the cold focal plane and inside surface of L3, and subsequently absorb incident light over a wide spectrum of wavelengths. The change in light transmission must be small over periods between calibrations (the observing night) and ideally small over the longer time between scheduled warmups and maintenance of the cryostat. The requirement for the vacuum in this region is then set by flow-down from the image quality budget and to some extent by the throughput budget (to the extent that observing time may be lost due to unscheduled warmups of the focal plane).

While laboratory measurements are ongoing, it appears that the partial pressure of H_2O in the focal plane region must be ~ 10^{-8} Torr to reduce condensable buildup to the few nm/year range. This obviates the need for periodic warmups to drive off and remove by pumping any built up layers.

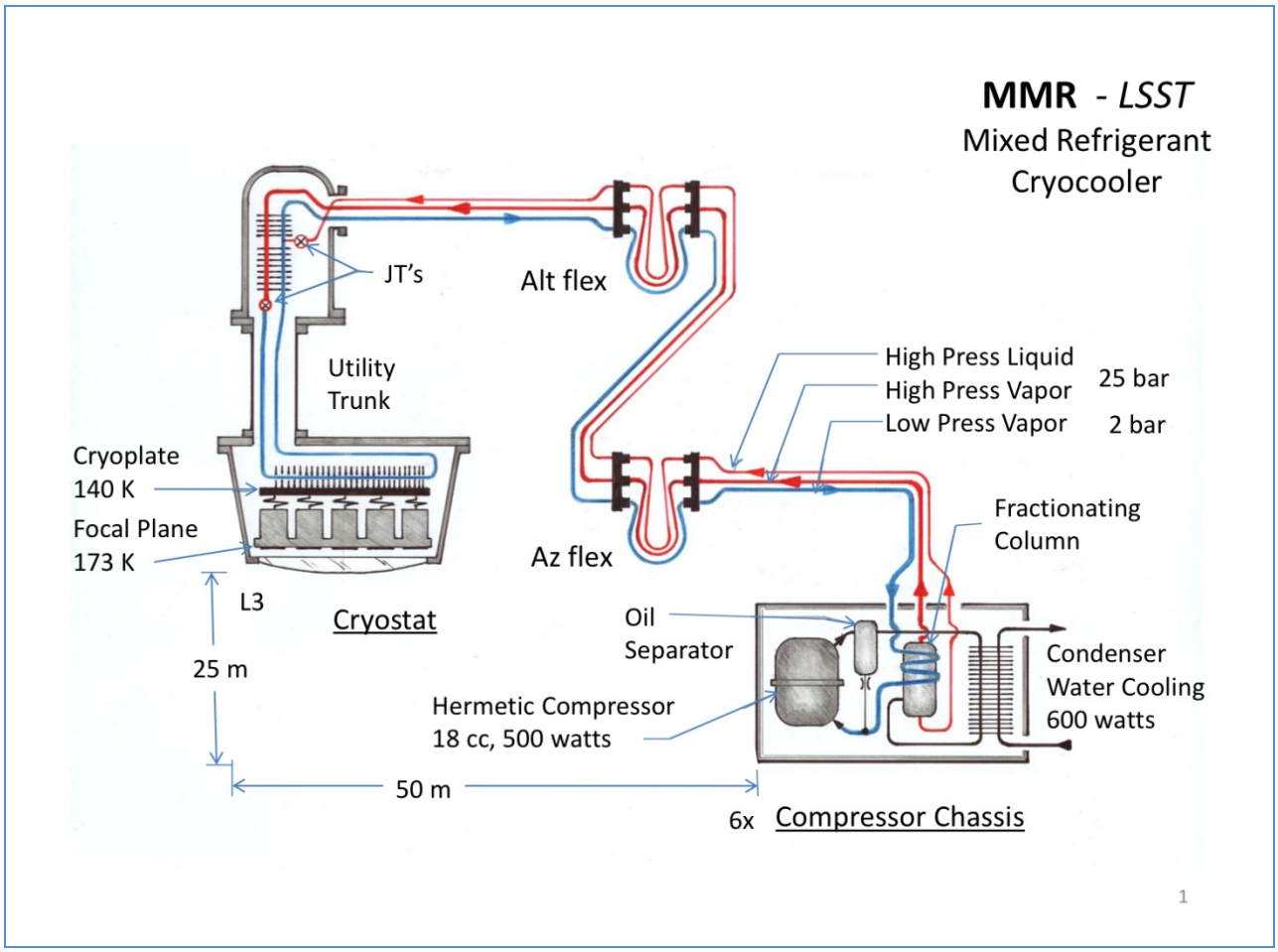

Figure 12-3: Schematic of mixed refrigerant cryogenic system (original proposal)

12.2.2 Contamination Requirements:

Contamination (particulate and chemical/non-evaporable) in the cryostat body can lead to degradation of the image quality, through absorption and scattering of light on the focal plane. The requirement is set by the Image Quality budget. Particulate (dust) contamination will be controlled by enforcing a clean room environment for assembly.

Non-evaporable chemical contamination has a similar requirement as water (discussed in 12.2.1) but should be easier to enforce as elements of the cryostat body will be cleaned for high-vacuum and to a large extent are bakeable at > 85°C (the first water point) prior to integration. During integration and testing however, the cryostat body will be filled with the 21 science raft towers and four corner raft towers that include the readout electronics and the signal and power cable assemblies. This represents a large surface area of materials that cannot be baked out above the water-point, and the contamination requirements must therefore be set within the relevant subsystem. The subsystem must be delivered to the Integration and Test team for verification before the subsystem is inserted into the otherwise clean and tested cryostat.

12.2.3 Thermal Requirements:

The driving thermal requirement is the need to operate the CCD sensors at -100°C with sufficient uniformity and stability across the focal plane in order to achieve suitable and stable sensor quantum efficiency without frequent recalibration of the system. In addition, to process heat (front end electronics), there is radiation through L3 and from the warm walls of the cryostat body, and a small amount of conduction from the mechanical supports of components inside the cryostat to the walls and front flange of the vessel. In total, approximately 540 W of heat must be removed by the cryoplate at -130°C, using a mixed refrigerant system.

The readout electronics are held at their required operating temperature via the coldplate, held at -40°C utilizing a mono-refrigerant system. Approximately 1500W must be removed by this system.

12.2.4 Mechanical Requirements:

The driving mechanical requirement is the specification for the contribution of the Cryostat subsystem to the focal plane's location and planarity. In particular, the planarity allocation to the cryostat is 4 µm peak-to-valley due to ball array planarity and 5 µm total RSS due to all cryostat-related effects.

The interpretation of this requirement is that these are the residual non-calibratable, non-correctable contributions that may arise from the following:

- Distortions of the cryostat as whole off the support ring and hexapod, due to changes in the gravitational vector during normal telescope operation,
- Irreducible kinematic support ball planarity achievable due to fabrication and assembly tolerances in the components and measurement system.
- Gravitational distortions of the grid due to changes in the gravitational vector during normal telescope operation.
- Grid distortions due to residual thermal non-uniformities during normal Camera operation.
- Uncorrected errors in the initial integration of rafts onto the grid due to measurement accuracy, or kinematic mount non-reproducibility.
- Changes in the raft position due to finite kinematic mount stiffness and variation in the gravitational vector during normal telescope operations

12.2.5 Electrical Requirements:

There are two driving requirements addressing electronics within the cryostat body. The Cryostat subsystem must comply with the Camera Grounding Plan, and in particular that the common reference ground is at the coldplate, and the electronics within the cryostat body have grounds isolated from all other elements of the cryostat. The second requirement is the need to pass a large number of digital signal and power supply cable assemblies between the readout electronics in the cryostat vacuum enclosure and the utility trunk through the rear vacuum wall of the cryostat.

12.2.6 Other Requirements

In addition to the formal requirements described in the previous paragraphs, the cryostat in general is required to survive for 15 years of operation with scheduled servicing fitting largely within the regularly scheduled telescope downtimes.

Accordingly, cryostat integration and serviceability have led to the requirement that the cryostat design is modular with respect to the raft tower modules. In particular, all cryostat grid readout electronics bays must be accessible for integration and service from the rear of the cryostat, in any order, without removing adjacent raft tower modules and with only minimal uncabling.

In general, access to the inside of the cryostat for servicing and repair will require removal of the Camera from the telescope and relocation to a clean and dry environment, with a warmup and purge cycle prior to opening. Access to the utility trunk is also minimal during telescope operation, as it sits largely within the M2 mount.

12.3 Cryostat Design Description

12.3.1 Cryostat Structural Design

12.3.1.1 The Cryostat Housing (Vacuum Vessel)

The cryostat housing is an aluminum pressure (vacuum) vessel shaped as a conical frustum. It is ~74 cm long, ~65 cm diameter at the front entrance (L3 flange) and ~95 cm diameter at the back end. The wall thickness is ~ 6 mm along the conical sides. The housing is cantilever, supported from the rear flange via a support ring (see Figure 12-4). The housing is a monolithic construction, machined from a single cylindrical ring forged aluminum 6061-T6 alloy blank.

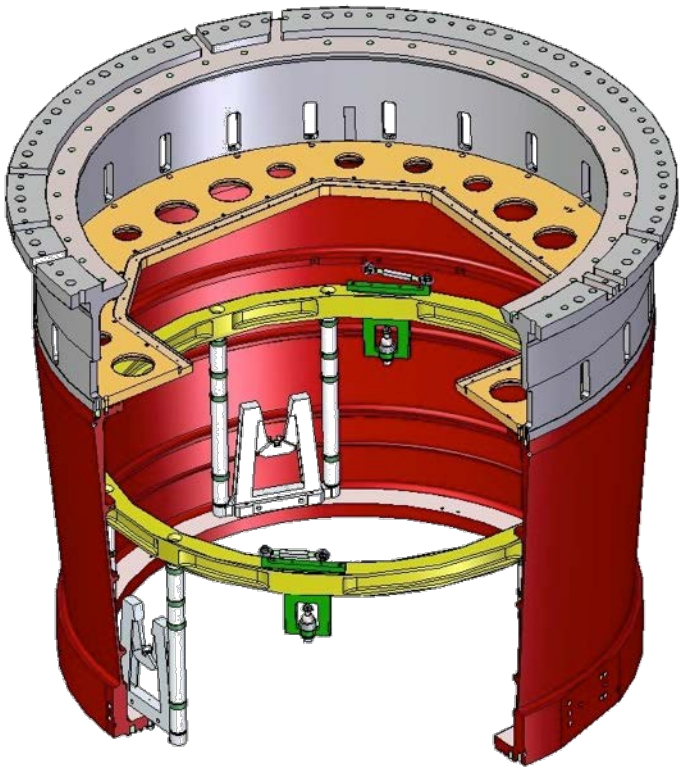

Figure 12-4: Quarter section view of cryostat body internal support structure and rear support ring

The front of the cryostat is closed by the L3 optic assembly (~6cm thick L3 refractive optic and integration ring) (see Figure 12-5).

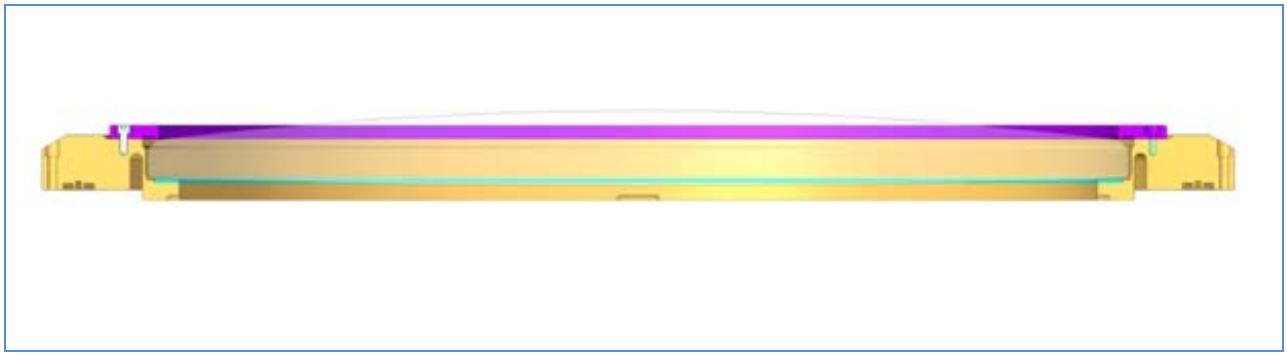

Figure 12-5: L3 and L3 flange cross section

The lens is mounted in the annular integration ring and vacuum sealed with dual redundant Viton gaskets to form a double O-ring seal with the cryostat body front flange. The region between the seals is actively pumped. The L3 assembly is subject to the warm Camera body environment on one side and the cold focal plane on the other. The perimeter of the integration ring is bolted to the warm cryostat housing, establishing the vacuum seal at that interface. During integration and testing of the cryostat, the L3 optic assembly will be replaced with an aluminum blank off flange. During Camera integration and test the L3 refractive optic will be replaced with an optical flat to provide for the focal plane metrology.

The front flange of the cryostat also provides support for the grid, via three titanium flexures.

The back of the cryostat is closed by an aluminum flange system consisting of an outer electrical-data feedthrough flange and an inner pump plate (see Figure 12-6). The outer feedthrough flange is an annular ring ~2cm thick which contains all the power, data, instrumentation and refrigeration vacuum via assemblies. It is installed and tested prior to raft tower integration.

The inner part of the annulus has an octagonal opening that gives clear rear access to the science raft and corner raft bays for integration and servicing. This opening is ultimately sealed by the “pump plate,” which contains all the on-Camera high vacuum pumping, gauging and valuing components. The pump plate is installed following completion of integration of the raft tower modules in the cryostat.

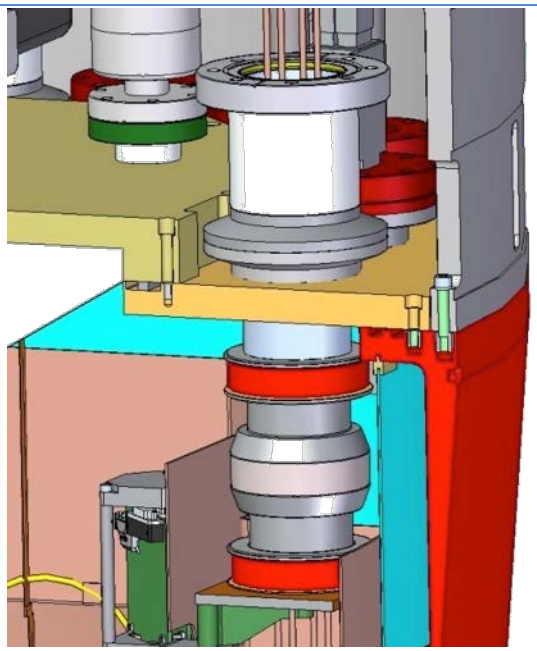

Figure 12-6: Detail of rear flange and cryo feed through – the outer feedthrough flange is on the right in mustard and the inner pump plate is on the left in greenish yellow

Additional high pressure backing pumps will be located in the utility trunk. Both the inner feedthrough flange and the pump plate vacuum seals are redundant O-rings systems similar to that employed with the L3 optic assembly. During integration and testing, a simpler blank version of the pump plate will be used.

All remaining sealing of the cryostat vacuum enclosure will be completed using all metal systems (e.g.: Conflats) including the power, data and refrigeration feedthrough assemblies and the pumps, gauges and valves.

12.3.1.2 Cryostat as an Optical Bench for the Focal Plane Sensors

The cryostat housing mechanically supports two primary elements of the system:

- the grid,
- the cryo-cold plate

All loads and load variation during telescope pointing through these elements within the cryostat must be accomplished in a fashion that limits influences on the precise alignment, height and lateral position of the focal plane.

The grid (see Figure 12-7) is the rigid ~65cm diameter, 18cm thick Silicon Carbide optical bench structure that mechanically supports and maintains the positioning and precision alignment of the 21 science raft and four corner raft sensor assemblies (RSAs) that make up the focal plane and guide sensors. SiC ceramic (variety HV) is chosen for its large stiffness to weight ratio, comparatively low density, and excellent thermal properties (high thermal conductivity and low coefficient of thermal expansion (CTE).

Held at the cryoplate temperature, it provides is a significant element of the thermal system establishing the uniform thermal environment for the RSAs.

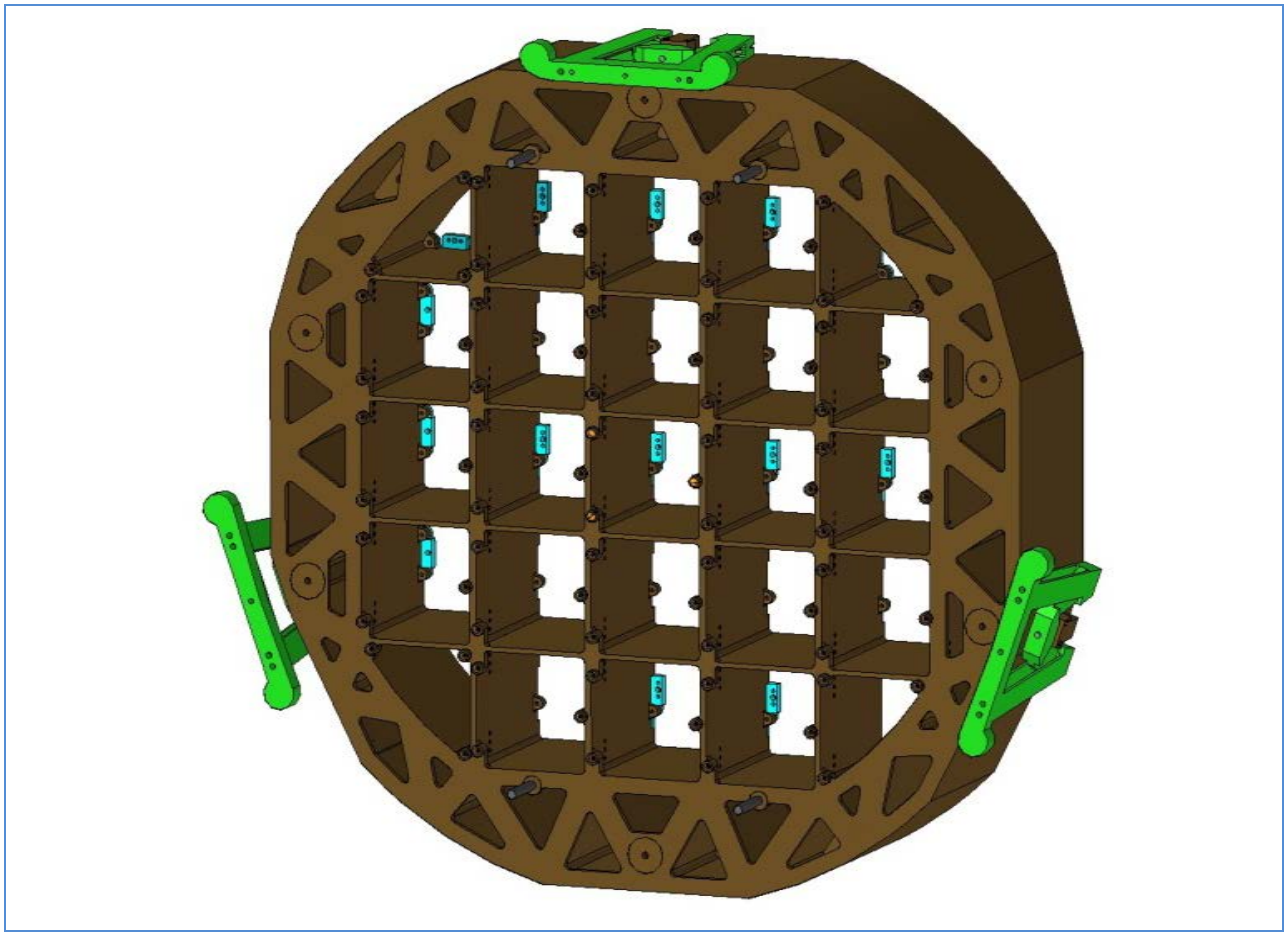

Figure 12-7: The grid with support flexures

The grid itself is mechanically supported and pre-aligned to the front of the cryostat body by three titanium flexures (Figure 12-8). These attach to the grid via a precision ball and groove kinematic mount. Titanium is used here for its stiffness (reducing rigid body motion of the grid under a varying gravity vector-during telescope pointing) and low thermal conductivity (reducing the conductive heat leak from the body). In this manner, the grid and RSAs that it supports are transmitted to the cryostat body in a controlled and reproducible fashion. The flexures also take out the differential contraction of the grid and cryostat body during cooldown.

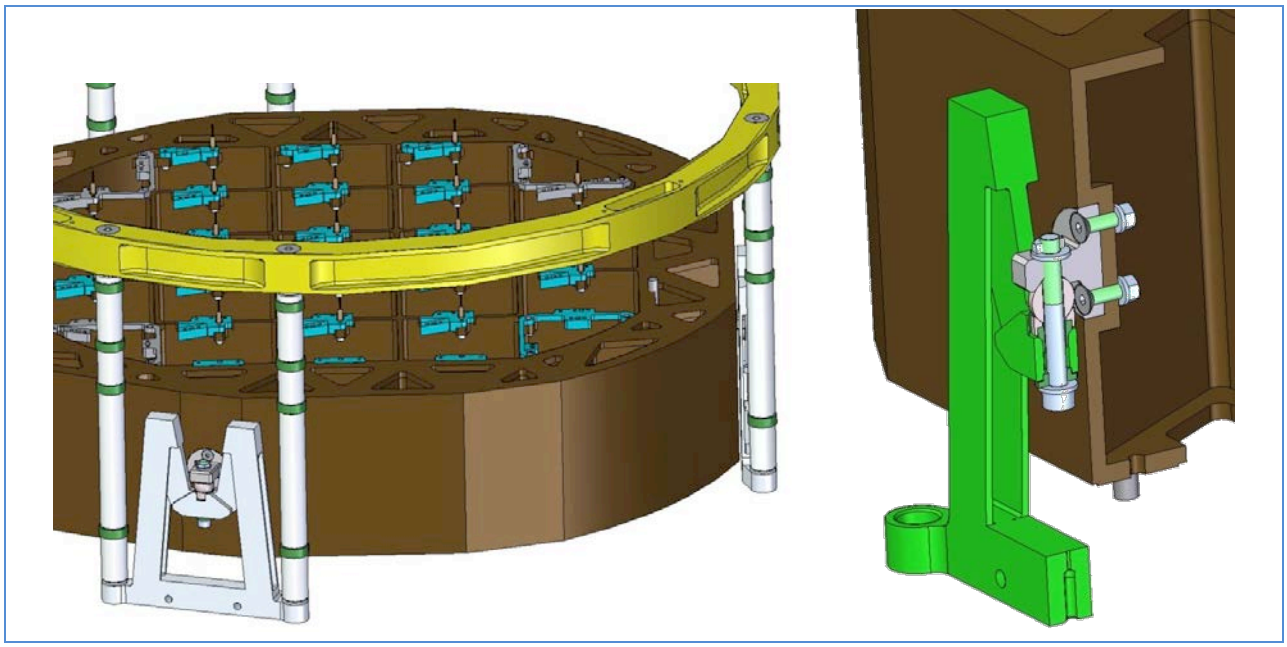

Figure 12-8: Grid flexure mounted to grid

In keeping with the grounding requirements, the grid is electrically isolated from the cryostat body by ceramic washers in each of the flexure connections.

Each of the 21 science raft sensor assemblies and four corner raft sensor assemblies (25 RSAs) are supported and positioned on the front face of the grid by means of a ball and vee kinematic coupling system (Figure 12-9).

Nine CCD assemblies are pre-aligned on a sensor raft plate. Both the sensor height relative to the vee-grooves and the sensor to sensor planarity are tightly controlled. Each RSA kinematic mount is uniformly held to the grid with a load of ~12N per support ball. This load is isolated to the grid and RSA via a hold-down and load transfer system at the base of each raft tower bay in the grid (Figure 12-10). This load transfer decouples potential effects of distortions in the cryostat body and/or the cryoplate from the grid and RSAs.

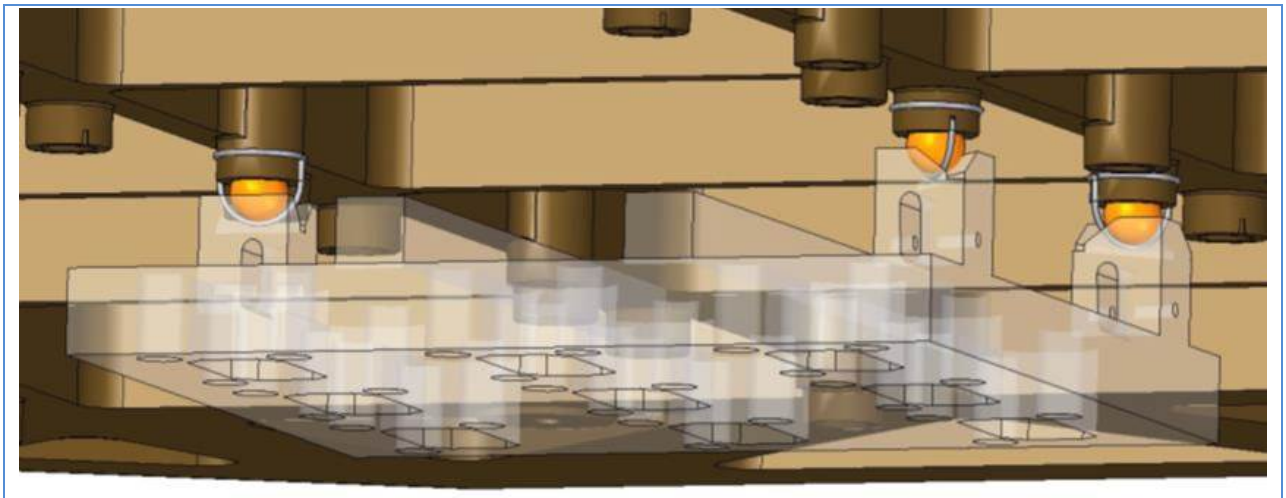

Figure 12-9: Raft-grid kinematic mount rendition

The cryoplate sits immediately behind the grid. While its primary function is to remove heat (at -130^{o}C) from the raft sensor assemblies (RSAs), its mechanical function is to support the load of the raft electronics boards (REBs) supported inside the raft electronics crates (RECs) without influencing the sensor plane positioning or planarity. After integration into the cryostat, these RECs are only loosely coupled mechanically to the sensor plane via flex cables and thermal straps.

During integration of the raft tower modules (consisting of the RSAs and RECs as a preassembled package) into the cryostat, the load transfer of the RSAs from the REC to the grid is accomplished by detaching spring loaded hold down assemblies from their temporary mount on the side of the REC to hold down features on the grid. The REC having already been bolted to the cryoplate (Figure 12-11), the cryoplate is in turn attached to the body of the cryostat by the four flexures and four lateral struts.

These flexures also support the cold plate, which is mounted from the cryoplate via thermally resistive standoffs. (Figure 12-12), The flexures provide compliance of the joint to the cryostat body when both plates contract during cool down while maintaining accurate and tightly controlled positioning of the cryo-cold plate assembly. These flexures are electrically isolated by ceramic washers from the cryostat body, to meet the grounding and shielding requirements of the cryo-cold plate assembly.

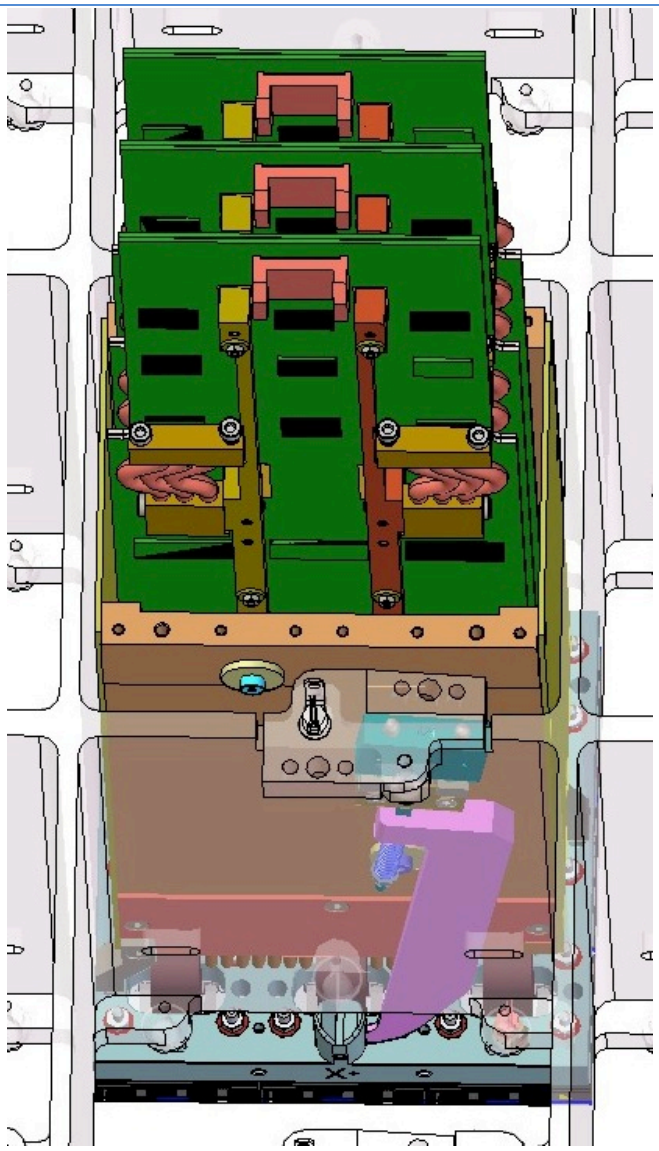

Figure 12-10: Hold down features at the base of the grid

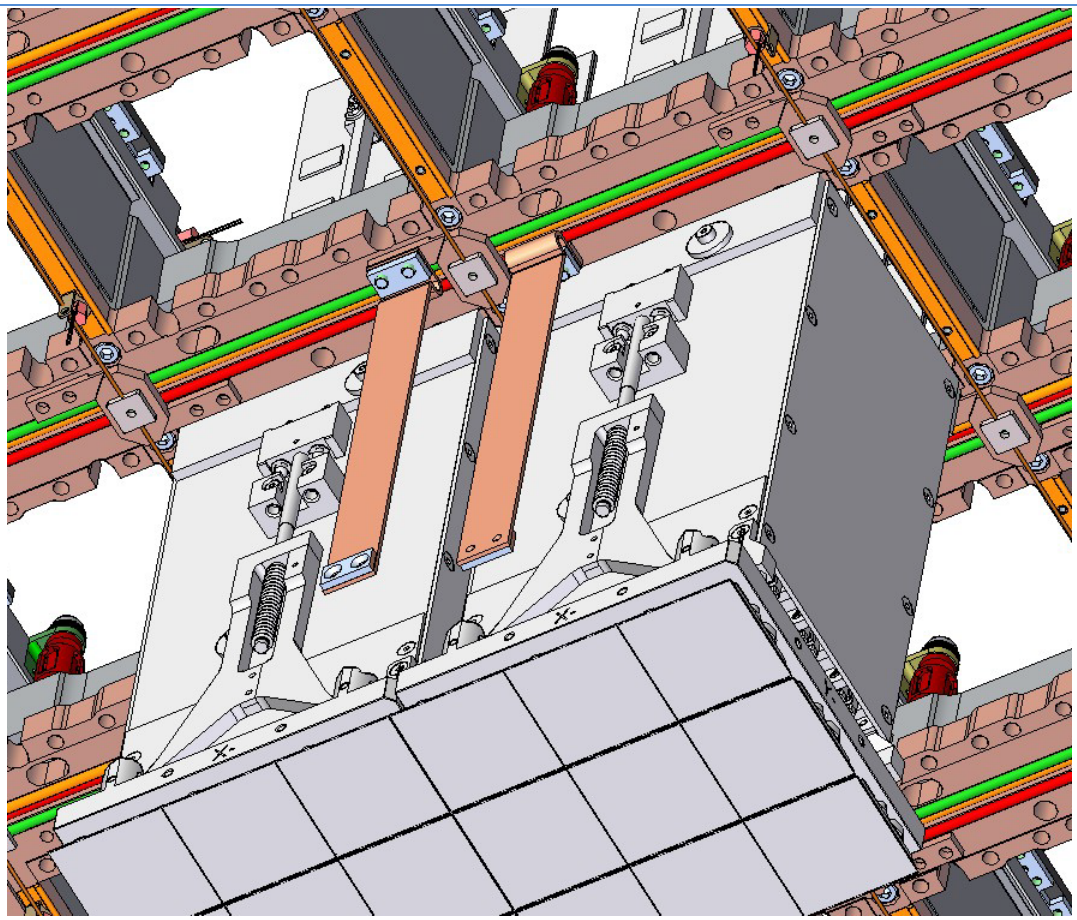

Figure 12-11: Detail of bolted joint of raft electronics crate to cryoplate

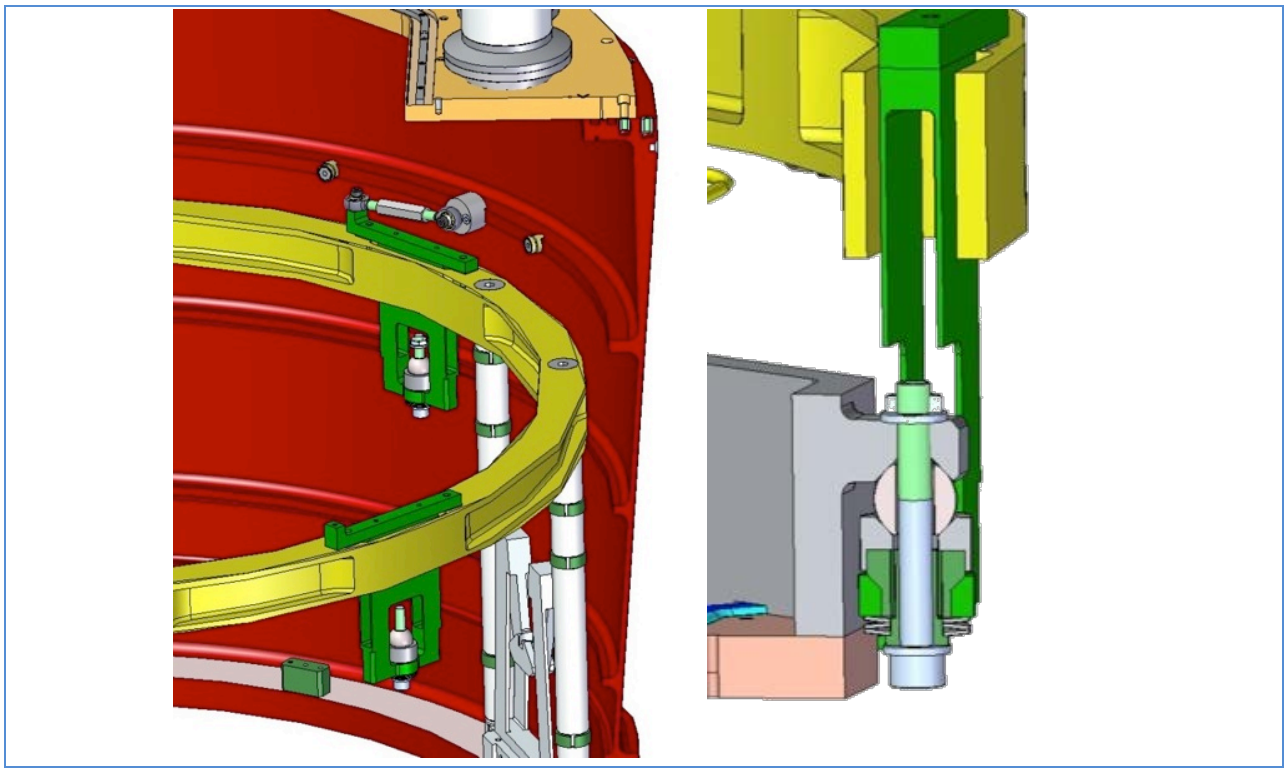

Figure 12-12: Cryoplate and coldplate support column, support ring, flexures. And lateral struts. Cross section of flexure

12.3.2 Cryostat Thermal Design

12.3.2.1 Cryostat from a Thermal Perspective

The cryostat subsystem hardware establishes the thermal environment for the sensors and readout electronics inside. The cryostat is within the confines of the Camera body enclosure. Thermal requirements of Camera body elements dictate that the cryostat housing be maintained at near ambient dome temperature.

An insulating vacuum reduces conduction from the comparatively warm surfaces of the cryostat enclosure (housing) to the cold grid, cryoplate and coldplate internal elements. The flexures which support those elements inside the housing provide low conductance paths from the warm housing. A system of warm, cold and thermally “floating” shrouds within the cryostat assists in maintaining the required stability and uniformity of the grid, cryoplate and coldplate, while minimizing radiative load on the cold internals from the warm housing surfaces.

The L3 optic, which establishes the forward vacuum barrier of the cryostat enclosure via its attachment to the warm housing, represents a radiative thermal load on the sensors. Conversely the cold sensors cool the L3 optic. The radial distribution of this radiative flux is shown in Figure 12-13. Careful design of the L3 optic mount ring and cryostat internal shrouding has ensured that thermal gradients within the L3 optic do not adversely affect its optical performance and load on the cryostat internals and cryo-cooler is limited.

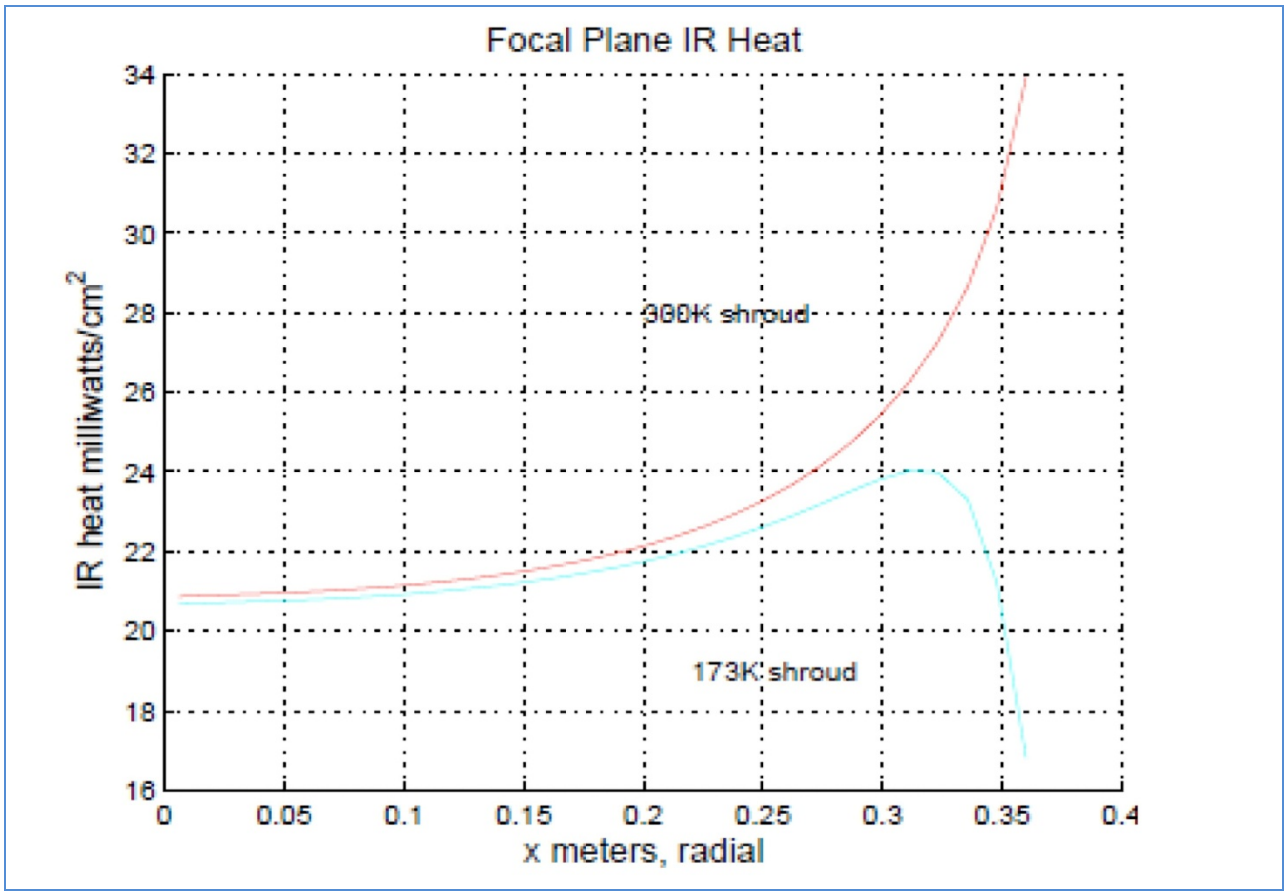

Figure 12-13: Radiation from L3 onto focal plane, comparing cold and warm perimeter shrouds shows cold perimeter shroud reduces flux at larger radii, radial flux variation due to effect of thermal profile in L3

From a thermal perspective the raft tower module (RTM) is constructed of "cryo" elements and "cold" elements. The cryo elements are the raft sensor assembly (RSA) and the raft electronics crate (REC). The cold elements are the readout electronics boards and attached cooling bars.

When the RTMs are assembled in the cryostat, the RSAs are supported from the grid, and the RECs are supported from the cryoplate. The CCDs, assembled on the RSA, are cooled via flexible thermal straps between the RSA and the REC and the copper structure of the REC walls bolted to the cryoplate. There is a maximum 30C temperature differential allowed between the cryoplate (-130C) and the sensors at their design temperature of -100C. Prototypes and modeling suggest this number will be somewhat smaller, allowing the cryo system to operate at a temperature a few degrees warmer.

The most critical thermal requirement is that the sensor drift over the observing night must be limited to a few tenths of a degree C to avoid drifts in the absolute quantum efficiency between daily calibrations. The stability of sensor temperature is maintained by coarse make-up (trim) heaters on the cryoplate and fine make-up heaters on the RSA's. The cryoplate has a long (tens of minutes) time-constant because of its thermal mass, the coarse make-up trim heaters maintain cryoplate temperature stability to less than 1C by closed loop control reading temperature sensors mounted on the cryoplate. Accordingly, stabilization of small temperature drifts of the sensors is accomplished by local temperature sensors

mounted directly on the CCDs and fine control local make-up heaters mounted on the individual RSAs via a closed control loop.

The cold raft electronics boards (REBs) are mounted within the REC from low conductivity thermally compliant supports. The temperature of the REBs is maintained by the coldplate (-40°C) via flexible thermal connections to the cooling bars bolted to the REBs. The coldplate is supported on low thermal conductivity standoffs from the backside of the cryoplate.

Cold plate thermal stability is maintained at less than 1C drift by a trim heater system similar to that used on the cryoplate.

Avenues of thermal load on the cryo system (-130C) from the comparatively warm cold system (-40C) are: the electronics interface cables connecting the cold CCDs to the warm REBs, the cabling connecting the fine trim heaters on the cold RSAs to their power supplies on the warm REBs, the support system mounting the warm REBs within the cold REC, the support system mounting the cold plate from the cryoplate and the radiative loads between cryo and cold elements with a non-zero view factor.

These thermal loads on and between the cryo cooler system and the cold cooler system, in addition to the parasitic radiative and conductive loads discussed earlier and the process power dissipated in the sensors and readout electronics, are carefully considered and controlled in the integrated thermal design of the cryostat. Full thermal accounted is summarized in Table 12-2. The total load on the Cryo system is thus ~540 W and the cold system is ~1500 W when trim heaters are on full capacity.

Table 12-2: Cryostat thermal loads

	Sink	Source	Type	Transfer Mechanism	Q (Watts)
Process and parasitic thermal load	Sensor	REB	Process Load	Conduction	79
	Sensor	L3	Parasitic Load	Radiation	78
	Sensor	REB		Conduction	55
	Cryoplate (REC)	REB's		Conduction	60
	Cryo-shroud	L3		Radiation	5
	Cryo-shroud	Housing		Radiation	10
	Grid (flexure)	Housing		Conduction	9
	Cryoplate (flexure)	Housing		Conduction	6
	Cryoplate	Coldplate		Radiation	15
	Cryoplate	Coldplate		Conduction	18
	Cryoplate (REC)	REB's		Radiation	75
	Total Load				410
	Temperature Stability Trim				20
	Margin (or absolute temperature trim)				110
	Refrigeration Capacity (6 @ 90W/ea)				540

The grid temperature is maintained by the cryoplate via a system of flexible thermal straps which connect the two. Thermal gradients in the grid have the potential to influence the sensor alignment and must therefore be controlled. To help reduce gradients, the grid is fabricated from silicon carbide, a ceramic having high thermal conductivity and very low thermal expansion coefficient. The grid is also enclosed within a cryoshroud thermally tied to the cryoplate. The function of the cryoshroud is to minimize the effects of spatial varying radiation loads from the warm cryostat walls, which have the potential to create thermal gradients within the grid and subsequent geometric distortions.

Finally, the distribution of temperatures in the cryostat also influences the cleanliness of the focal plane through the cryo-pumping of residual water or other condensable molecules in the cryostat. The thermal environment has been arranged such that the focal plane will never be the coldest surface in

the cryostat. This is true during normal system operation, system cool-down, and warmup and during non-typical conditions such as in the event of any loss of heating from electronics during maintenance periods or power failures.

12.3.3 Cryostat Vacuum Design

12.3.3.1 Cryostat from a Vacuum, Purge and Contamination Standpoint

A schematic of the complete vacuum and purge system for the cryostat is shown in Figure 12-14

There are two primary vacuum systems for the Camera. One maintains the cryostat enclosure and one maintains the thermally insulating vacuum for the refrigeration heat exchanger enclosure. In addition, there is a small ancillary system that evacuates the small inter-seal volumes between the redundant elastomer seals in the L3 optic, and the rear feedthrough plates that close the cryostat.

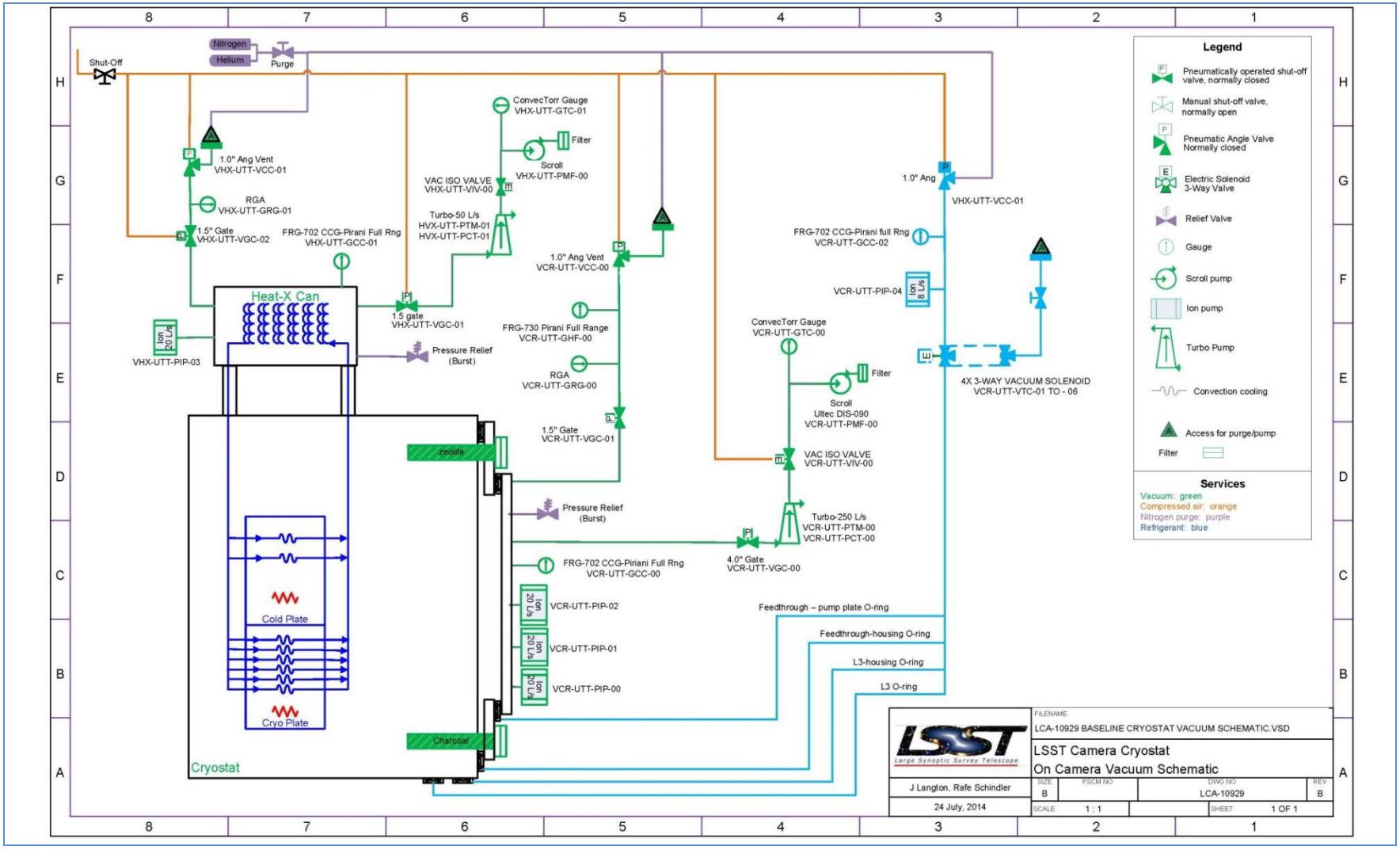

Figure 12-14: The cryostat vacuum and purge system

These systems are completely distinct and do not interact with each other. A purge – gas system is connected to each of these vacuum systems to allow controlled venting and purge.

12.3.3.2 Cryostat Vacuum

The cryostat has the most stringent vacuum requirements. Table 12-3 lists statistics for the significant materials within the cryostat, the quantities and expected gas loads based on initial tests conducted in the Material Test facility (see below).

Table 12-3: Materials in the cryostat

Material	Total surface area (cm^2)	Total Outgassing Rate (Torr-L/sec/cm^2)	Water Outgassing Rate: (torr-L/sec/cm^2)	Total Outgassing (torr-L/sec)	Water Outgassing (torr-L/sec)
Adhesive	7	1.7E-8	1.8E-11	1.2E-07	1.3E-10
Al2O3 Ceramic	130	1.0E-9	2.5E-10	1.3E-07	3.2E-08
Aluminum	177000	2.0E-10	3.0E-11	3.5E-05	5.3E-06
Aluminum Nitride	4400	1.0E-10	2.5E-11	4.4E-07	1.1E-07
CE7 Al-Si Alloy	1800	5.0E-10	2.5E-11	8.8E-07	4.4E-08
Epoxy	250	1.00E-09	1.00E-10	2.5E-07	2.5E-08
FR4	61000	1.0E-9	1.7E-10	6.1E-05	1.0E-05
Fused Silica	10500	9.00E-10	5.00E-11	9.3E-06	5.2E-07
Kapton	47000	5.7E-10	1.2E-11	2.7E-05	5.6E-07
OFE Copper	151000	1.0E-10	9.4E-12	1.5E-05	1.4E-06
Silicon	3700	5.0E-09	1.0E-11	1.9E-05	3.7E-08
Silicon Carbide	68000	1.0E-9	2.5E-11	6.8E-05	1.7E-06
Stainless Steel	86000	1.0E-10	5.0E-12	8.6E-06	4.3E-7
Titanium	9500	5.0E-10	1.2E-11	4.7E-06	1.1E-07
Tungsten Carbide	150	1.0E-10	2.5E-11	1.5E-08	3.8E-09

Material	Total surface area (cm^2)	Total Outgassing Rate (Torr-L/sec/cm^2)	Water Outgassing Rate: (torr-L/sec/cm^2)	Total Outgassing (torr-L/sec)	Water Outgassing (torr-L/sec)
	620000			**2.9E-04**	**2.07E-05**

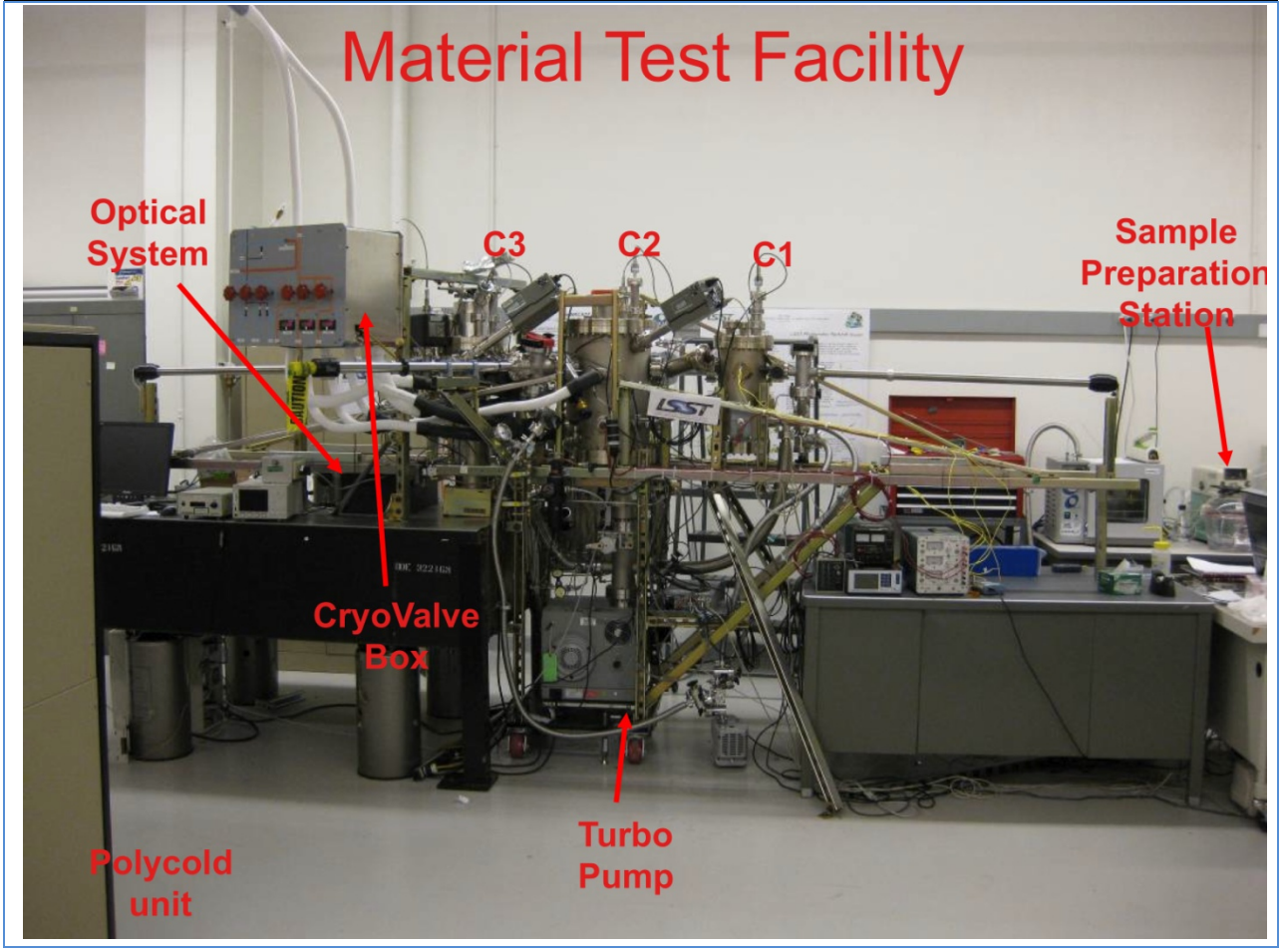

Figure 12-15: Material Test Facility

A base pressure of 10^{-5} to 10^{-6} Torr is needed for vacuum insulating the warm walls from conduction to the cold surfaces within. The vacuum system should be able to bring the base pressure below 10^{-5} Torr at room temperature and to ~10^{-6} Torr when cooled down. The more stringent requirement is the need to maintain high lifetime throughput of the Camera system by limiting the accumulation of condensable material and non-volatile residue (NVR) molecules on the focal plane.

Nominally, a throughput less than 10^{-8} Torr L/sec of condensables and NVR from their source, dominated by the REBs and associated cabling in the rear of the cryostat, into the focal plane region will limit accumulation to acceptable levels.

Through careful selection and processing of materials coupled with proper design of the vacuum system elements within the enclosure, we expect the quantity of matter of concern (i.e.: water and material with atomic mass greater than 44 AMU) reaching the focal plane to have extremely low partial pressure resulting in acceptable accumulation levels on the focal plane.

To satisfy these requirements, the cryostat and the vacuum systems have incorporated four features:

- Material selection and processing: All materials used in the cryostat will be qualified for use based on tests in the Material Test Facility. This will include the preparation, handling and storage of the material. Before being introduced into the cryostat, during integration, the properties of each element will be re-tested to insure compliance with expectations.

  During setup of the cryostat, a clean dry environment will be insured; both through the properties of the clean room and with a dry inert gas (N2) purge system.

- Cryostat internal system design: The cryostat enclosure concentrates all the pumping at the backend of the cryostat where the largest potential sources of contaminates reside (see Figure 12-16).
- Cryostat pumping: The primary vacuum pumping in the rear of the cryostat is an installation of three 20 liter per second sputter ion umps.

  One of these ion pumps will be configured for pumping noble gas, predominantly Argon. A secondary pumping system is located on the feedthrough flange and incorporates a mix of evaporable getters (warm molecular sieve), chosen to maintain the clean vacuum by selective pumping of water and evaporable getters (cold activated charcoal), which pump more broadly than the sieve. This getter system is located to intercept molecules originating in backend region of the cryostat.

  As a third means of maintaining the vacuum environment, during non-observing times the cryostat can be pumped by a turbo-molecular pumping system consisting of a 250 liter per second TMP backed by a dry scroll pump located in the Camera utility trunk. The TMP will have vibration isolation which might allow use during observing, if necessary. The Turbo-molecular pumping system also provides an in-situ capability to evacuate the cryostat from atmospheric pressure.

- Finally, the temperature distribution in the cryostat has been arranged to reduce as much as possible the cryo-pumping action of the focal plane. In particular, the cryoplate, cryoshroud and grid will be held between 15 and 30 ^{0}C colder than the focal plane. The focal plane view factor to warmer surfaces (the periphery of L3 and the cryostat body near the front flange) has been limited to the greatest extent possible by inclusion of a close fitting cryoshroud “top hat”.

12.3.3.3 Refrigeration System Vacuum

The refrigeration system vacuum is purely an insulating vacuum for the heat exchanger modules and transfer lines from the individual heat exchangers to the back flange of the cryostat, where they pass

into the cryostat enclosure via the cryo-feedthroughs. A 20 liter per second ion pump will be used for holding the vacuum after the system is roughed down. This system will provide 10^{-5} Torr scale vacuum.

The heat exchanger vacuum enclosure can also be pumped during non-observing periods by a turbo-molecular pumping system consisting of an 80 liter per second TMP backed by a dry scroll pump located in the Camera utility trunk.

The elastomer seal inter-volume pumping system consists of an 8 liter per second sputter ion pump connected to the various redundant O-ring seals via a series of three way valves and stainless steel tubing. The three way valves provide leak checker interconnect and helium supply to complete independent integrity checks of all elastomer seals, both inner and outer, at each location. This system will be roughed from atmosphere by off-Camera pumping using the same interconnect valves and plumbing used by the leak checker and helium supply.

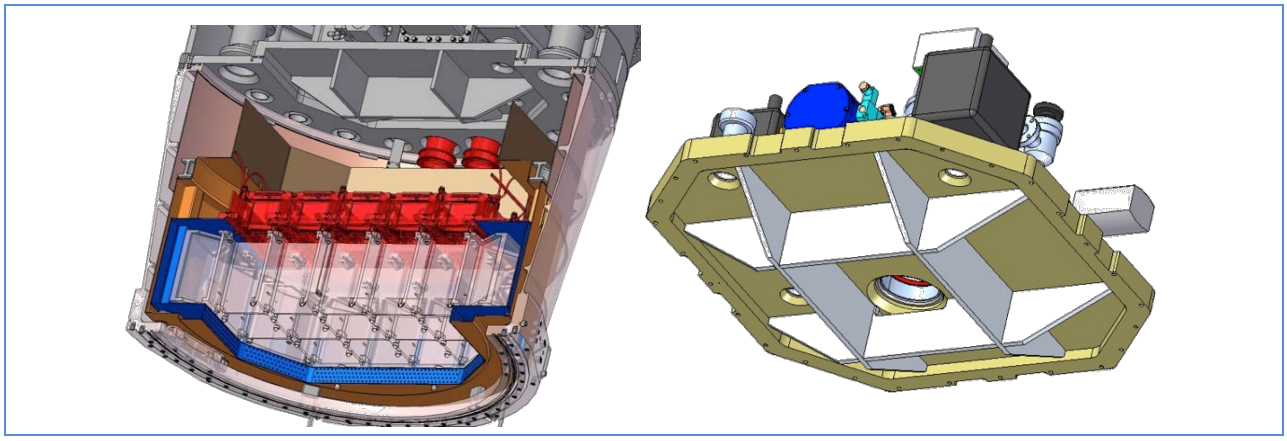

Figure 12-16: Vacuum regions in the cryostat showing open backend region to the pump intakes.

12.3.3.4 Purge System

The purge system contains a source of dry nitrogen with pressure regulation and temperature control and a mass flow meter for monitoring. This will reside on the ground in the utility room and be plumbed to the Camera via spare refrigeration transfer lines. For safety, a pressure relief valve and rupture disk will also be present to prevent the accidental over-pressuring of any part of the system.

12.4 Cryostat Mechanical Design and Analysis

12.4.1 Grid and Grid Flexures

The backbone structure for assembling, supporting, and aligning the CCD focal plane in the LSST cryostat is designated the grid. The grid provides a flat, rigid, and stable mechanical support surface for the focal plane CCDs (pre-aligned on individual rafts) , while operating in all orientations (zenith to ~30 degrees from the horizon) and transitioning from ambient (+20^{o}C) to operating (-130^{o}C) temperature. To achieve this requires the design of a compact structure (due to space constraints within the cryostat housing), of a material with extreme rigidity, low density (due to mass constraints on the Camera), high thermal conductivity and low thermal expansion coefficient over the operating range.

The investigation of possible materials for the grid included numerous metal alloys and ceramics. The best match is a class of materials based on silicon carbide ceramic. ECM- Munich produces a version of silicon carbide designated HB-CeSic® which, considering the very large transverse dimensions and thickness of the grid, is ideal. HB-CeSic® has a density of ~3 g/cm3, comparatively high thermal conductivity (~120W/m K) and a low thermal expansion coefficient (2.1x 10^{-6} /K at room temperature to below 0.4 x 10^{-6} /K at operating temperatures). HB-CeSic® has a modulus of ~350 Gpa giving a stiffness to weight ratio approximately five times that of stainless steel (type 304), which is excellent.

The thermal properties help to ensure stability and reproducibility of the mechanical structure, in particular the critical metrological properties of the focal plane kinematic support elements. Thermal isolation of the grid from the warm cryostat housing by the cryoshroud, and the warm readout electronics within the raft tower modules further increases long term mechanical reproducibility of the kinematic mounts that provide the focal plane alignment.

The ECM HB-CeSic® is produced by starting with a proprietary non-directional carbon fiber felt that is pressed into a phenolic-like block. It is "green machined" in this state to final dimension, with allowance made for the well-known geometric effects of the final processing. The ability to execute precise, final dimension machining of the material at the green body stage allows for complicated monolithic structures at a comparatively low cost. The part is then fired ("pyrolized") to reduce the phenolic to carbon. The component is then transformed into silicon carbide by reaction of the carbon matrix in a furnace, where liquefied polycrystalline silicon is infused in an exothermic reaction at ~1200^{o}C.

The detailed design of the grid and the firing process is subjected to detailed thermal analysis to accommodate the silicon infusion reaction's thermal requirement. After cooling, the resulting structure is sand-blasted to remove unreacted silicon scale and inspected to insure uniform silicon infusion. The final fabrication process is diamond tool grinding of high precision features, such as the backside of the grid, and the focal plane kinematic support interfaces.

An extended grid engineering and manufacturing development effort has been completed in cooperation with ECM and has resulted in modest changes to the early design of the grid. Rigidization of the structure by use of "hammerhead" shaped web structures allowed better access for silicon infusion and control of reaction temperature. Changes were made to the interface bosses for the support flexures to reduce high load point stresses. And finally the focal plane kinematic support features (i.e.: "ball cups") were incorporated into the structure of the grid as a monolithic components, whereas previously these features were to be fabricated separately and mounted and adjusted at cryostat assembly. The incorporation of the ball cups into the grid structure has significantly improved the location and planarity precision possible while simplifying the metrological setup during I&T.

The final part of the grid development program was the manufacture and testing of a "Single Bay Grid" to verify the results of the engineering and manufacturing development program.

12.4.1.1 Detailed Grid Features and Design

Figure 12-17 shows the top and side views of the grid.

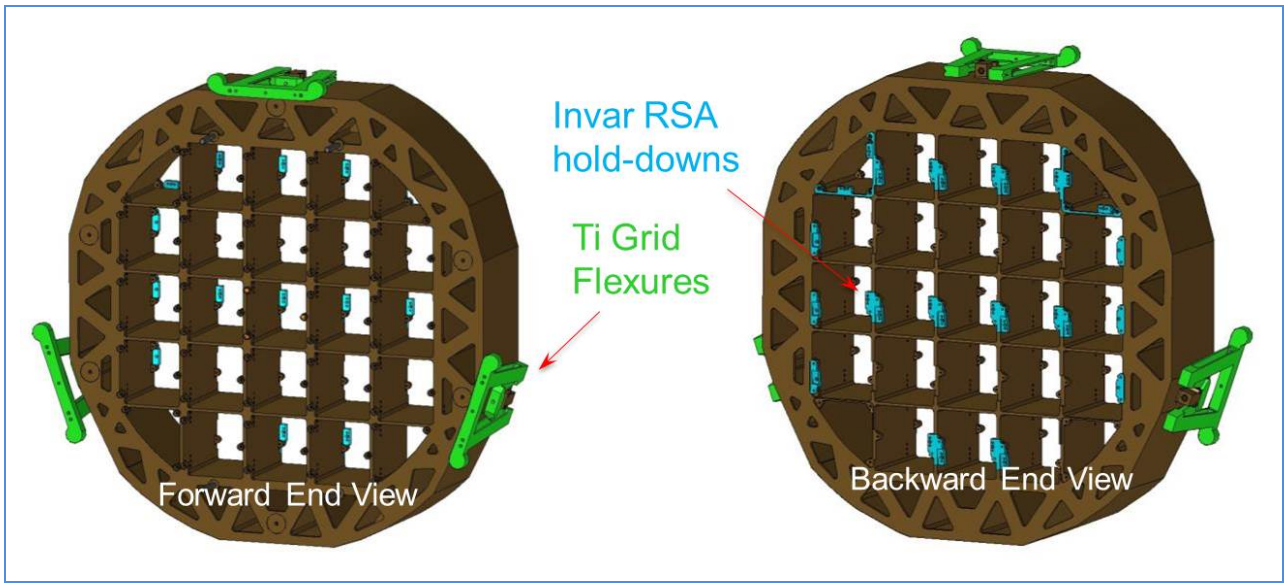

Figure 12-17: Grid top and bottom views

The basic design is an egg-crate like structure 180 mm thick that has 21 individual rectangular "bays" (each approximately 12cm x 12 cm) to accommodate the science raft tower modules and four triangular-like bays for the corner raft tower modules. The assembly (grid, flexures and auxiliary hardware) weighs about 64 Kg. Wall thickness throughout the grid is 7mm. Finite element analysis of the grid structure indicated the need for additional stiffening to prevent mechanical distortions due to the changing gravity vector, which would impact the focal plane alignment. This was accomplished by adding a perimeter of cells which, unlike the instrumented bays, are largely covered on the top and bottom with a SiC plate. The plate has cutouts to allow access for the SiC fabrication steps, in particular the infusion of silicon to the backside of the grid bay walls and outer-perimeter walls. Access must also be available for subsequent sandblasting and removal of silicon scale and dust. The 180mm high perimeter walls are completely closed to provide stiffness.

The grid is mounted from the front flange of the cryostat housing by three flexures which provide kinematic support and thermal isolation of the grid from the warm housing (see Figure 12-18).

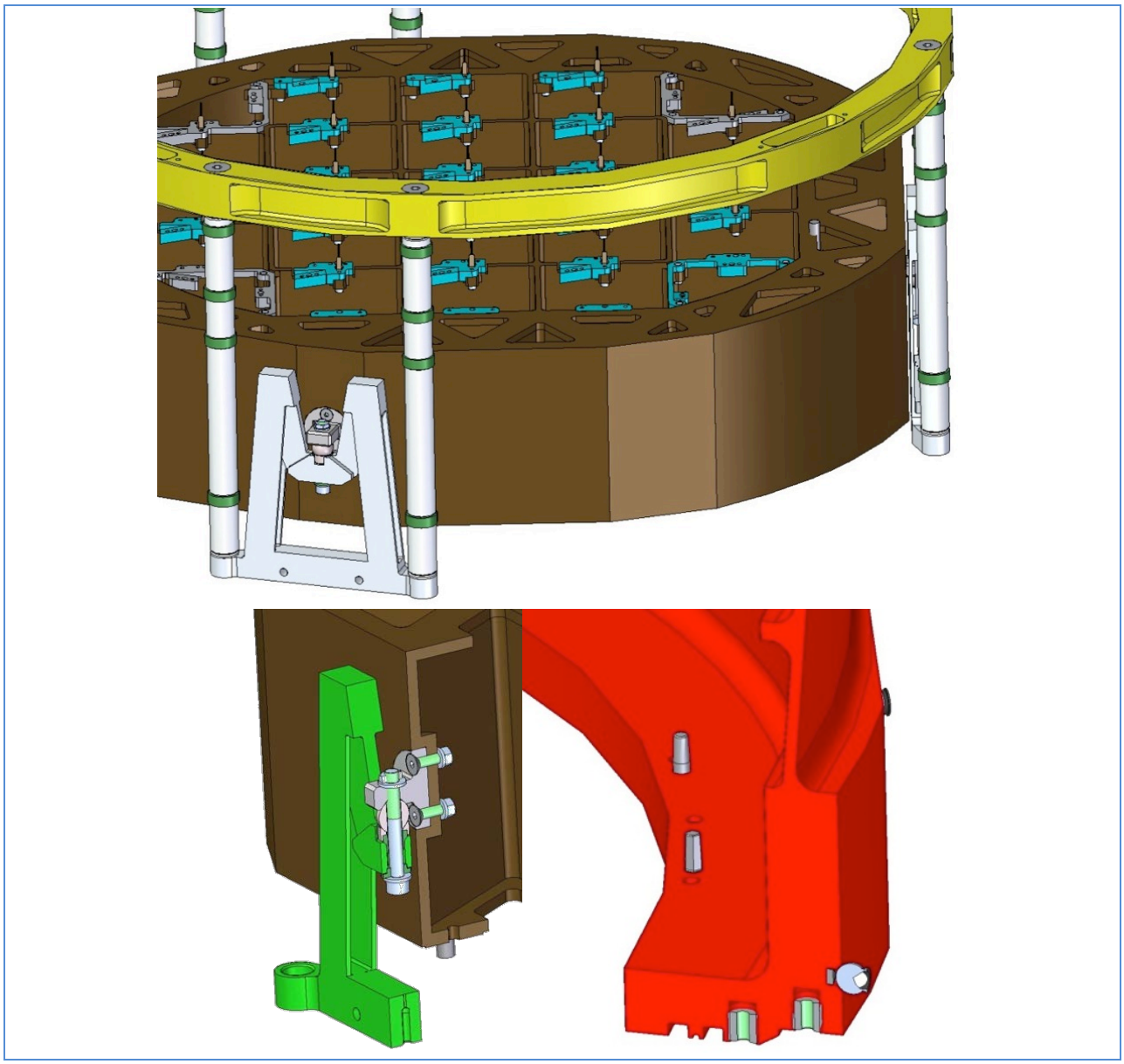

Figure 12-18: Grid flexures with detail of the kinematic coupling to the grid

Titanium is chosen for the flexure for its stiffness and relatively poor thermal conductivity. This and the large thermal resistance of the kinematic coupling on the grid end of the flexure help reduce the heat load on the grid. The flexures interface the grid with a ball in cup coupling allowing initial adjustment and subsequent reproducibility in the alignment of the grid to the cryostat. The mating of the coupling is via a ceramic ball sitting in an invar boss that is fixed in a receiving feature in the grid perimeter.

While the grid bays are completely open on the top and bottom, each has a number of additional features to interface with the science and corner raft sensor assemblies and the cryoplate. Those features are:

- Each bay has three circular bosses (approximately 12 mm diameter) with precision ball cup ground in place at the top surface which provides the kinematic mounting point for the RSA interface. These bosses stand proud of the nominal grid surface by about 12 mm and are ground with the ball cup features such that the grid focal plane support ball array lies in a common plane within 4 µm across the grid. The balance of the interface will be a ceramic ball in the cup feature mating with V-grooves on the SiC ceramic raft plate.
- Each bay also has thru-holes on two opposing walls to provide anchor points for thermal straps, which run down through the bay to the cryoplate. Compliance is generated in the strap by a bend at the cryoplate side. The straps provide uniform cooling of the grid by the cryoplate to reduce thermal gradients and subsequent geometric distortions (see Figure 12-19). Metal inserts will be bolted into the holes and, to insure a high level of temperature uniformity across the grid, an intervening thermal transfer material will be included between the thermal strap and the ceramic.

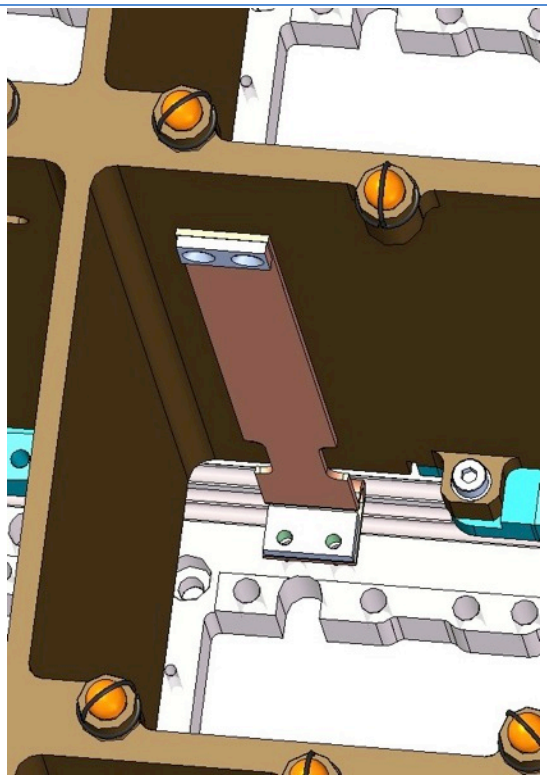

Figure 12-19: Thermal strap mounting

- Each bay also has two features at the bottom on opposing walls for mating with an RSA load transfer device. That is a part of the mechanism providing an RSA's hold down tension to the grid via a spring mechanism. The hold down elements will be separately machined invar parts that bolt into features in the bottom of the grid. This will obviate the need for precise machining of the SiC and avoid developing high load / stress points on the ceramic itself during the insertion and tie-down of the rafts. The hold down interface to the RSA tensioning mechanism provides for the load transfer during raft tower module (RTM) integration in the cryostat.

- Finally, the grid will have a modest number of additional attachment points for thermal instrumentation.

12.4.1.2 Structural and Thermal Analysis of the Grid

The grid structure as described has undergone finite element analysis (FEA) to confirm its stiffness, and to avoid high stress regions in the ceramic. This FEA also allows us to determine the range of distortions under varying load orientations with respect to gravity that it will be subjected to in operation. A thermal-mechanical analysis has also been performed.

In operation, the Camera rotates from zenith to close to the horizon, placing the front of the focal plane in an almost vertical down looking orientation. It will also rotate about Z, +/-90 degrees, meaning either the X or Y axis of the grid may lie close to the vertical plane. In practice, errors in image quality are dominated by the atmosphere within ~30 degrees from the horizon. Figure 12-20 shows the peak to valley out of plane distortion of the face of the grid for 1g gravity loads in the three directions. The subsequent maximum out of plane distortion of the raft surface is found to be-250 to +310 nm.

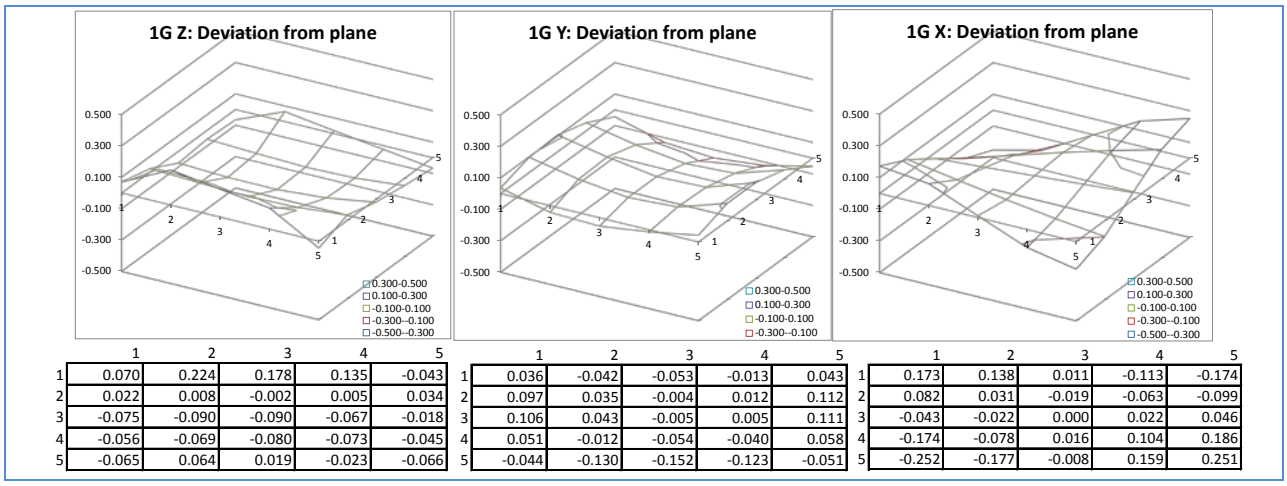

	1	2	3	4	5
1	0.070	0.224	0.178	0.135	-0.043
2	0.022	0.008	-0.002	0.005	0.034
3	-0.075	-0.090	-0.090	-0.067	-0.018
4	-0.056	-0.069	-0.080	-0.073	-0.045
5	-0.065	0.064	0.019	-0.023	-0.066

	1	2	3	4	5
1	0.036	-0.042	-0.053	-0.013	0.043
2	0.097	0.035	-0.004	0.012	0.112
3	0.106	0.043	-0.005	0.005	0.111
4	0.051	-0.012	-0.054	-0.040	0.058
5	-0.044	-0.130	-0.152	-0.123	-0.051

	1	2	3	4	5
1	0.173	0.138	0.011	-0.113	-0.174
2	0.082	0.031	-0.019	-0.063	-0.099
3	-0.043	-0.022	0.000	0.022	0.046
4	-0.174	-0.078	0.016	0.104	0.186
5	-0.252	-0.177	-0.008	0.159	0.251

Figure 12-20: Grid distortion from 1g in X, Y and Z

A preliminary thermal analysis of the grid was performed including conduction through the flexures, cold straps, kinematic mounts, and modeling the radiation environment in the cryostat. This was first done to optimize the temperature uniformity of the grid by adjusting the placement of the straps, and subsequently to examine the effects of residual non-uniformities introduced by the cryoplate.

By careful positioning of the two thermal straps in each grid bay, and from bay to bay, it was possible to reduce lateral and longitudinal temperature gradients in the grid to < 0.45°C even with the allowed variations in the cryoplate temperature distribution itself (+/-1.0°C).

A thermal-mechanical analysis was performed including the changes induced by conduction through the flexures, radiation on the perimeter and front face of the grid, and conduction to and radiation from the RSA's. Assuming a uniform temperature cryoplate, the worst case grid distortion itself amounts to only ~220 nm, which leads to a maximum out of plane motion of the rafts of about 23nm after removing an average offset. Figure 12-21 shows a summary of the deviations across the grid bays.).

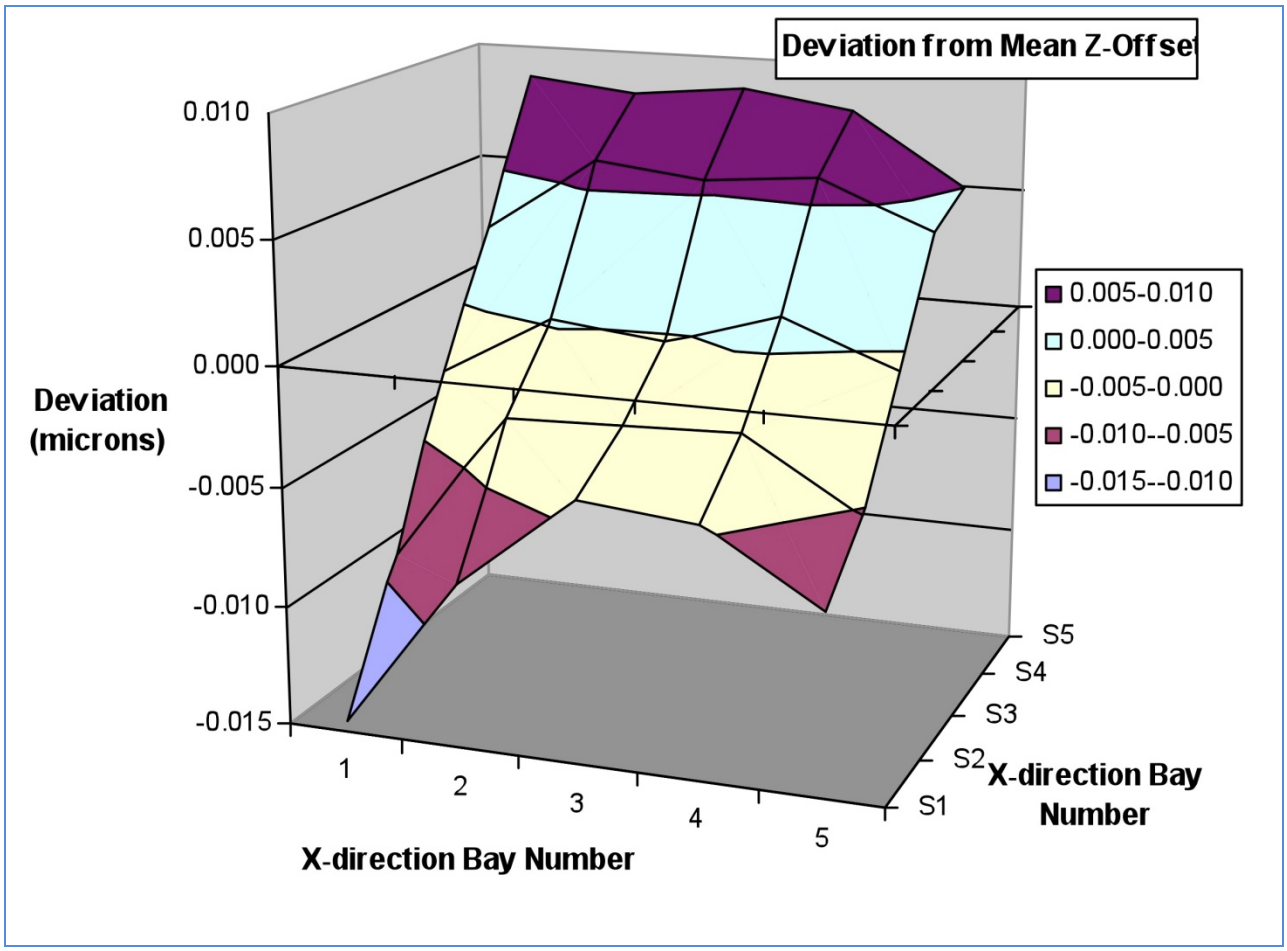

Figure 12-21: Thermally induced deviation of raft surfaces from mean Z offset

The same analysis was repeated with a non-uniform cryoplate influencing the grid temperature (see Figure 12-22). The additional grid distortion is in the 10 nm range, and total distortions remains below 0.23 µm.

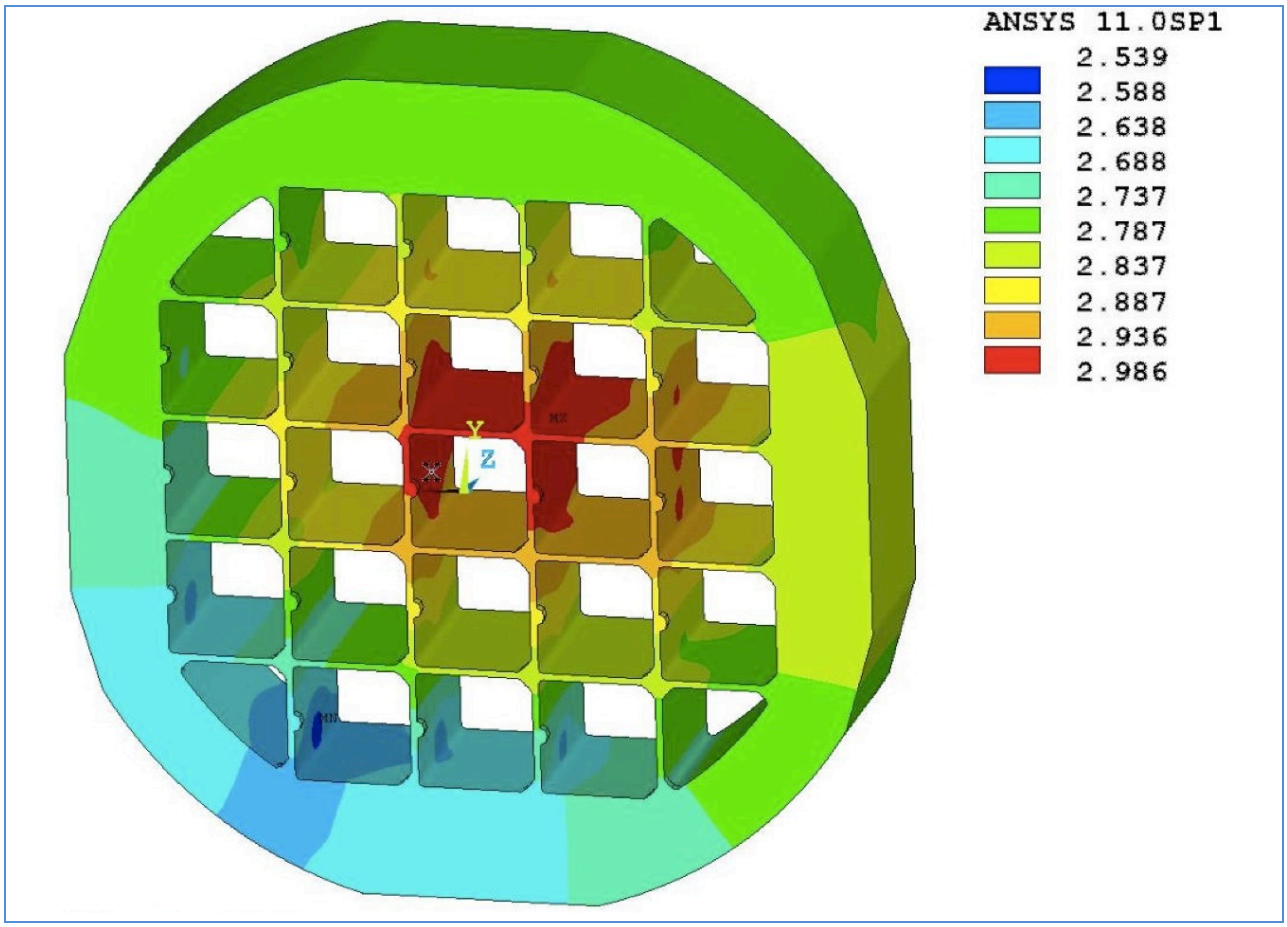

Figure 12-22: Temperature distribution in the grid

12.4.1.3 Grid Development

Development work on the grid is complete and procurement of the long-lead time fiber material has begun. The design and manufacturing development effort has been verified by construction of an HB-CeSic unit designated the "single bay grid". The single bay grid (see Figure 12-23) is a subscale prototype containing a single grid bay surrounded by a structure similar to the perimeter of the real grid. All the critical features of the grid are present in this prototype (raft kinematic mounts –ground coplanar), raft hold downs and thermal strap mounts. Thus it has allowed the testing of the SiC fabrication process and all the mechanical, thermal, and metrological performance requirements of the grid and flexures.

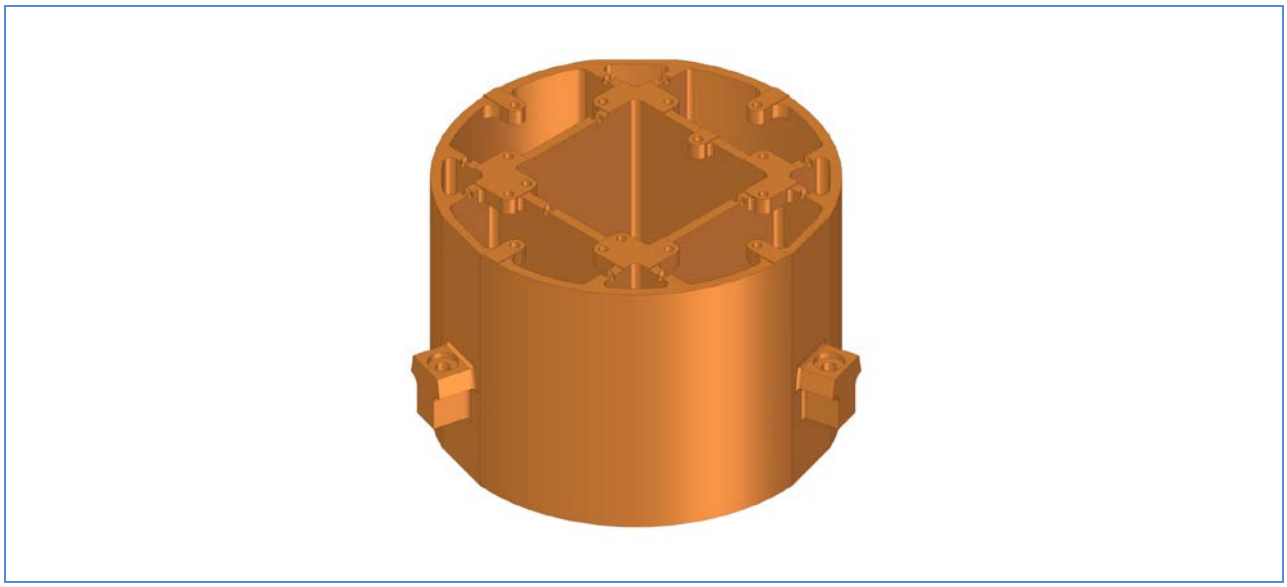

Figure 12-23: Single bay grid

The single bay grid has been used in the metrological kinematic support test stand that served to verify the stiffness, repeatability and precision requirements of the RSA kinematic support system.

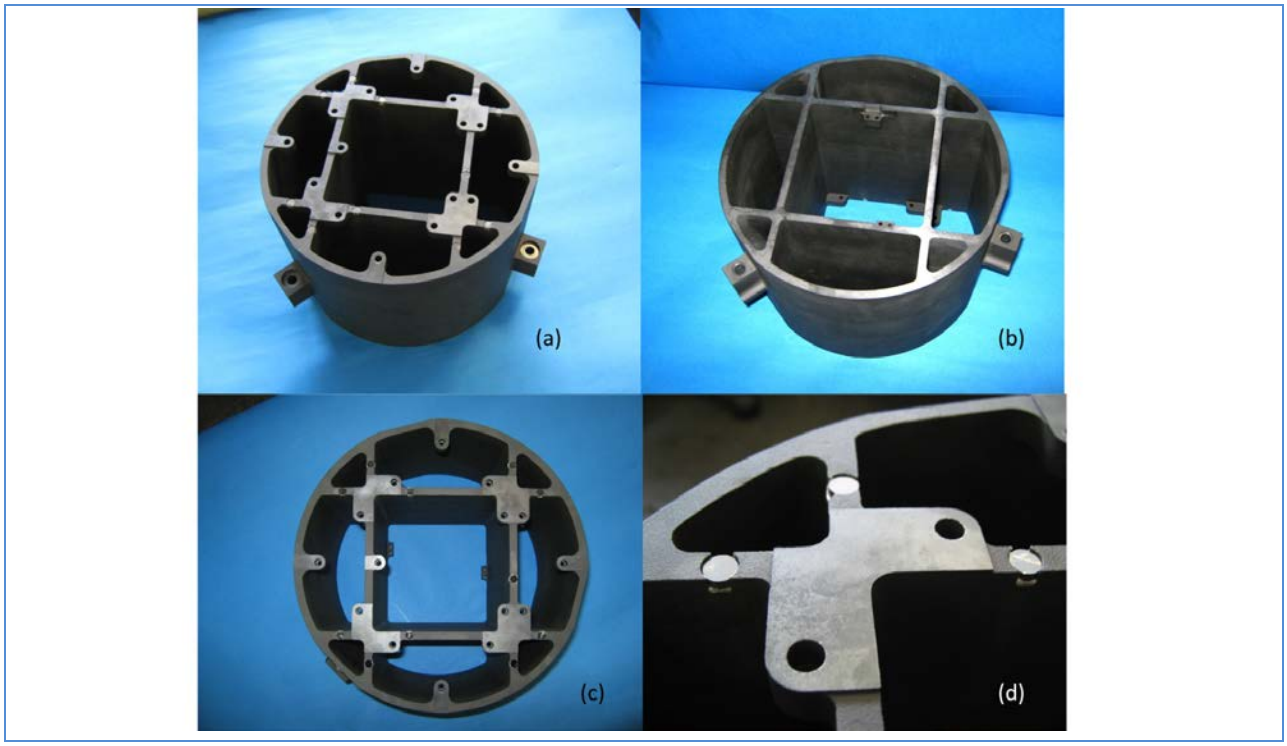

Figure 12-24: Single bay grid after arrival at SLAC

12.4.1.4 Grid Flexures (Interface to Cryostat Body)

The grid is supported from the front flange of the cryostat housing by three titanium grid flexures (Figure 12-18). The three flexures interface to the grid via a ball in socket coupling which provides electrical isolation of the grid from the body of the cryostat. The mating part of the coupling is a ceramic ball sitting in an invar lug that is bolted and glued into a socket in the grid itself. It is manufactured separately and then mechanically attached and bonded into the grid after the Si-infusion (see Figure 12-25).

The invar grid-lug captures the ball, analogous to the raft-grid kinematic mounts. The insert helps to reduce hoop stress directly on the ceramic. Titanium is chosen for the flexure for its stiffness and its relatively poor thermal conductivity (~22W/m·K). It also has a relatively low thermal expansion coefficient (8.5×10^{-6} /K). At operating temperature there is an ~ 116°C temperature drop across the flexure however the heat leak of each flexure is only about 1.4 W because of the small cross sectional area and thermal resistance of the flexure webs.

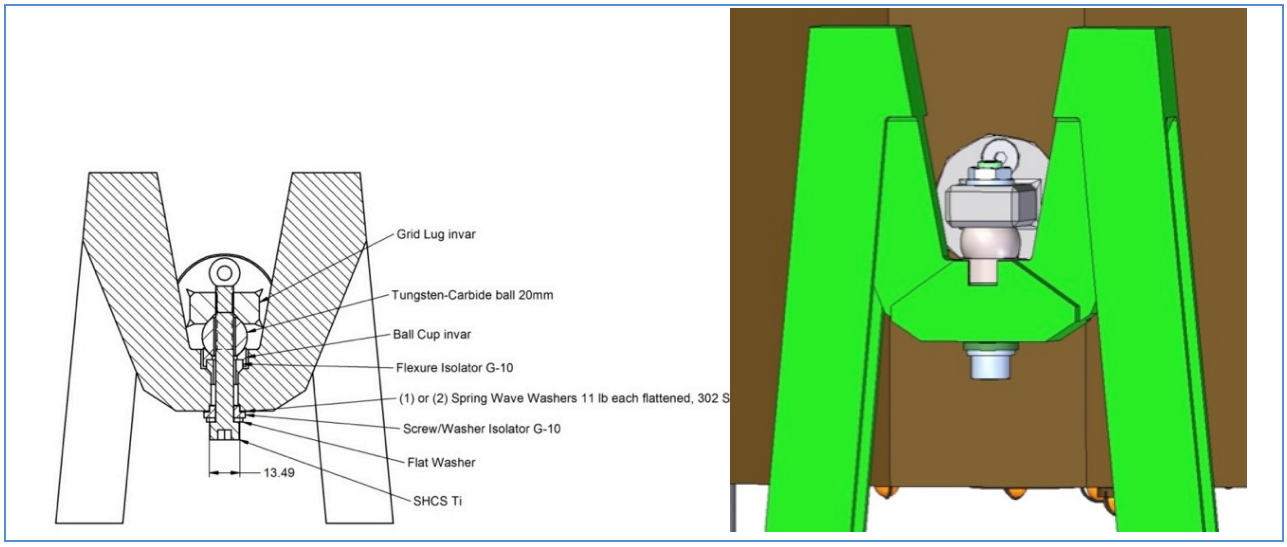

Figure 12-25: Detail of the flexure kinematic mount

Finite element analysis of the flexures carrying the loaded grid (see Figure 12-26) shows that they are operating far from failure. Finite element analysis also shows that the distortions of the grid due to the flexures (inertial and thermal) are negligible and the rigid body motion of the grid due to thermal shrinkage of the flexures will be < 1.6 µm. This motion is removed by shimming or by repositioning of the hexapod.

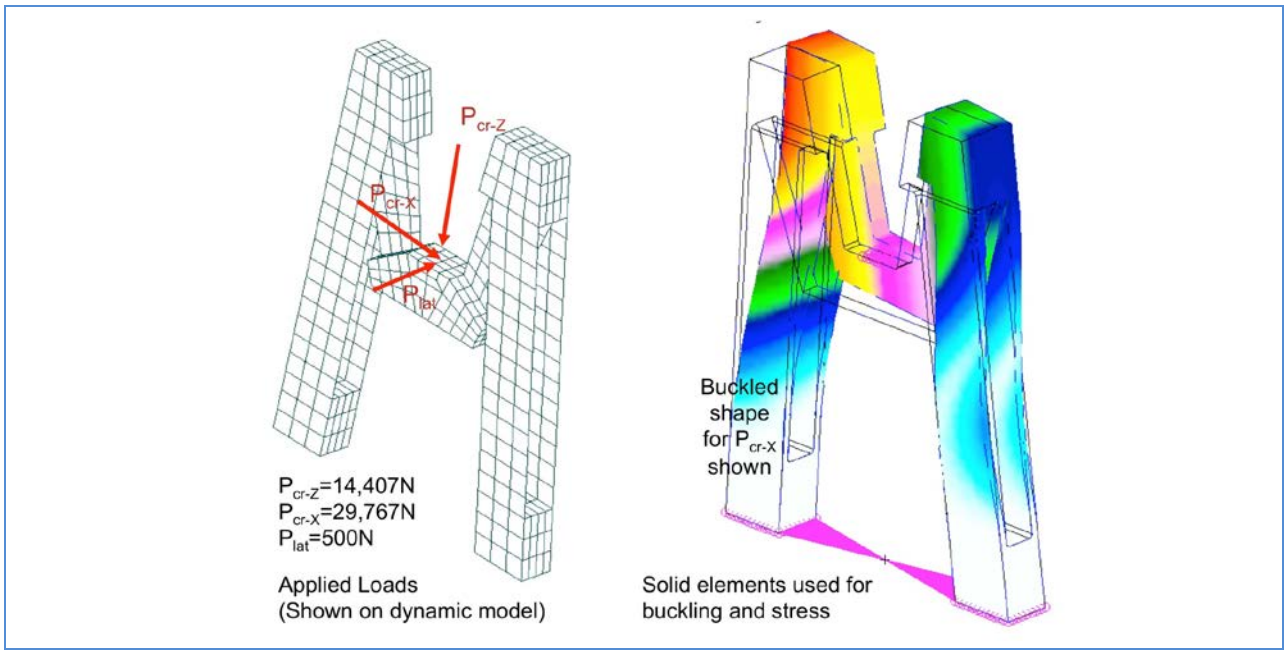

Figure 12-26: Finite element analysis of flexures

Prototype grid flexures and SiC interface bosses have been fabricated for use with the single bay grid (see Figure 12-27). The prototype flexures will first be tested to verify the finite element analysis. The SiC boss samples (including the Invar inserts) are to be stress tested to failure.

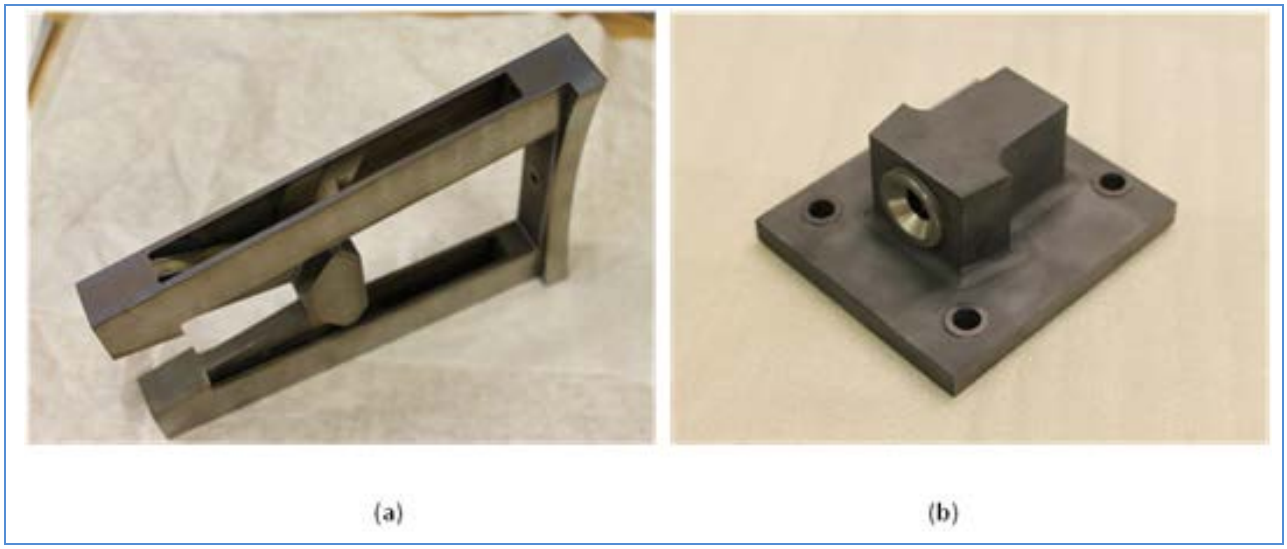

Figure 12-27: (a) Prototype flexures and (b) SiC grid bosses

12.4.1.5 Grid Thermal Straps (Interface to Cryoplate)

To reduce and control thermal distortion of the grid (and hence motion of the rafts) a system of thermal straps tying it to the cryoplate has been designed and modeled. A thermal model of the grid in the cryostat, including radiation and conduction to surrounding elements has been used to optimize the number and the arrangement of the thermal straps Analysis indicates that two straps within each grid

bay are required. Figure 12-28 shows the located on opposite faces of the bays tied close to the top of the grid and passing down to the cryoplate.

This arrangement provides the most uniform cooling of the grid, with peak to valley variations of less than a few tenths of a degree C, assuming a uniformly cooled cryoplate. A worst case model using a wider temperature profile of the cryoplate results in ~0.45°C variations in the grid temperature (see Figure 12-22 above).

The optimal thermal mechanical connection to the grid has been a focus of the grid design and manufacturing development effort. Two unthreaded holes in the SiC grid will be machined for each strap. , and the strap (with an invar nut plate, screwed down with titanium screws, from one sides (see Figure 12-29) capturing the SiC between. These inserts eliminate high stresses on the ceramic. The straps will be bolted into the inserts with a medium to improve thermal conductivity of the joint. The threaded holes in the cryoplate provide the thermal connection on the other end.

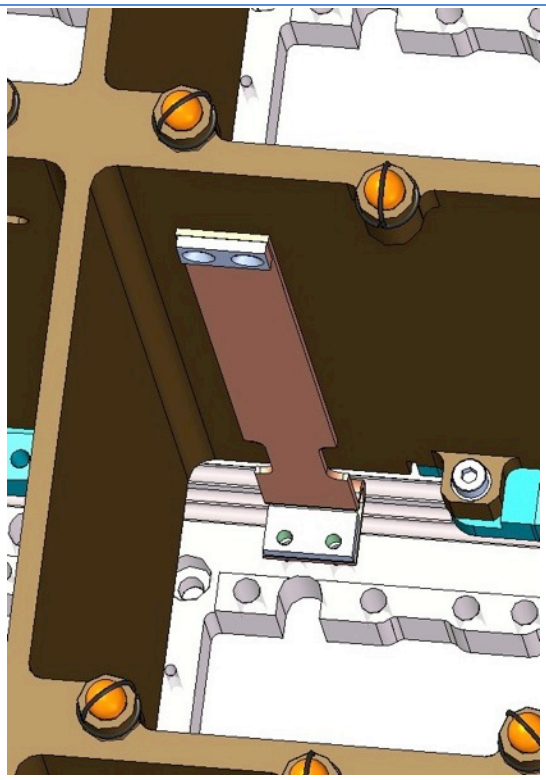

Figure 12-28: Grid showing location of thermal straps

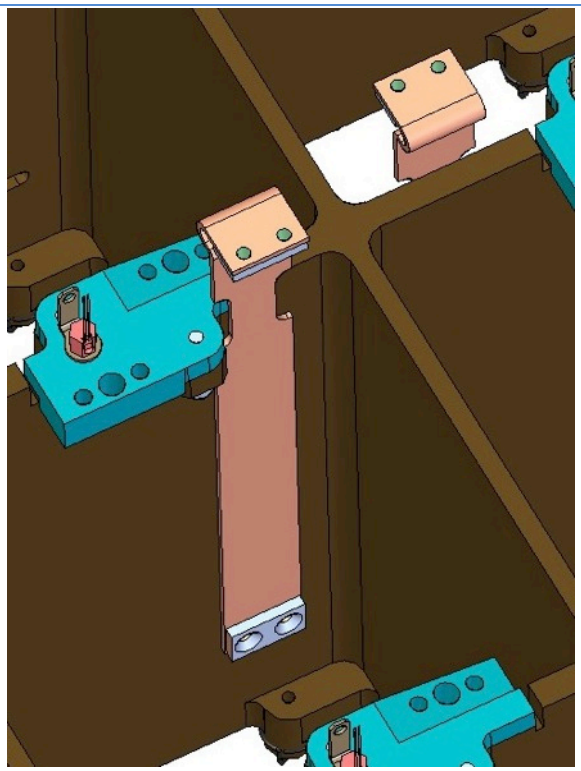

Figure 12-29: Detail of thermal strap connections and the bend in the strap for thermal compliance.

12.4.1.6 Kinematic Mounts and Raft Hold Down Features (Interface to Rafts)

The precision alignment of the RSAs on the grid during raft integration into the grid is described in detail in Section 12.5. The concept that has been adopted integrates the RAS kinematic support ball cup as a high precision feature fabricated monolithically in the grid.

The grid back surface will be fabricated flat to a few tens of microns during the initial machining phase and will remain so through the Si-Infusion phase. It will be subsequently ground flat to ~1 micron as a reference surface after final silicon infusion and sand blasting. The manufacturer will then machine the three circular protrusions in each bay where the ball cups mount stand proud of the surface by a few mm. Initially they will be ground to make a ball plane lie within about 10 microns of nominal height relative to the back of the grid. Then the manufacturer will move the grid to a special measuring and grinding machine, where they measure the balls in the ball cup heights across the grid and then grind and measure them iteratively until they lie in a common plane within the 4 micron peak to valley requirement.

The figure below shows details of the ball and cup design.

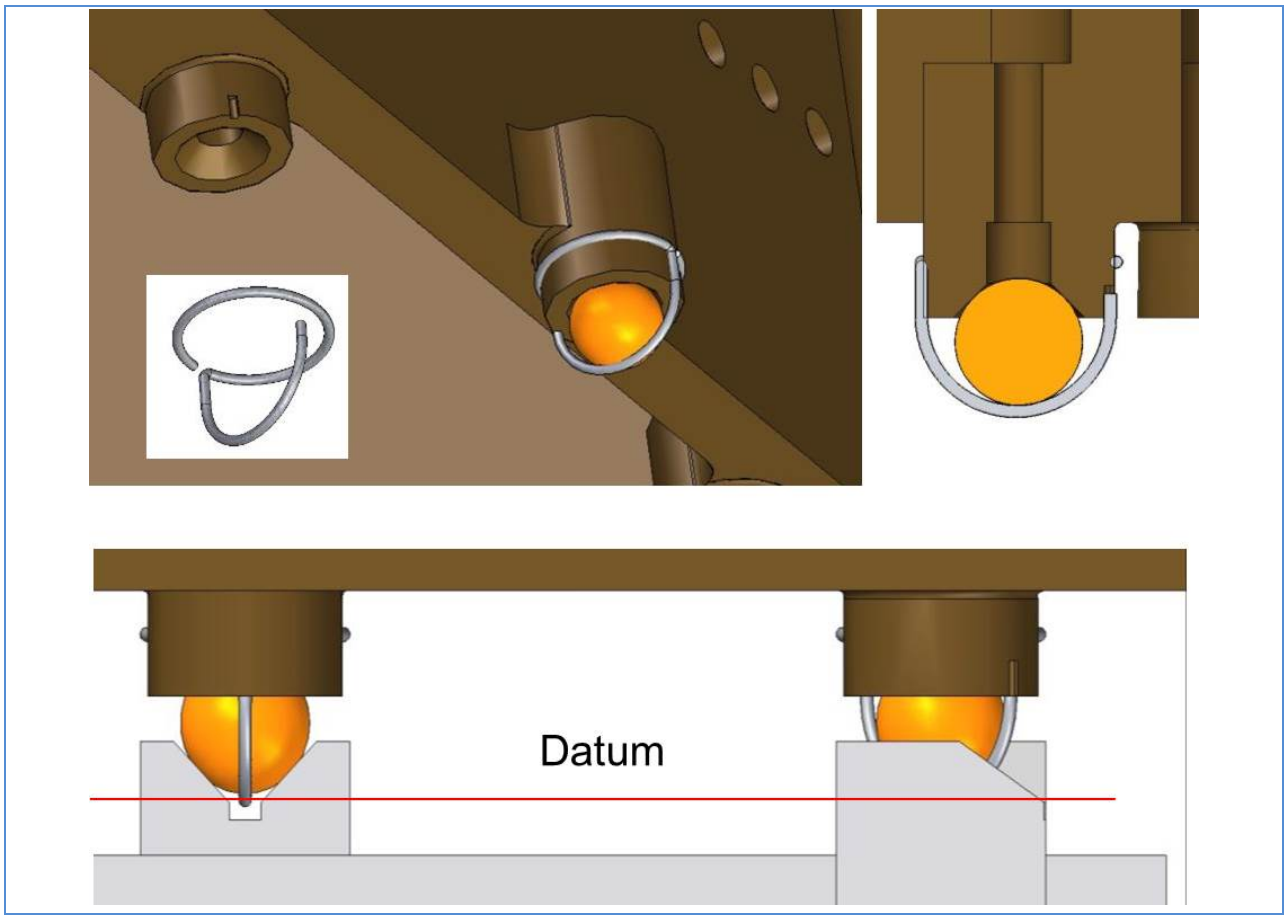

Figure 12-30: Ball and cup design, including hold down

The ball cup feature is final ground directly into the SiC grid at the last stages of grid fabrication. The total flatness (planarity) of the kinematic ball array, consisting of 75 balls (three per RSA) is to be less than 4 microns peak to valley. Any required fine adjustment of the focal plane flatness necessary during I&T of the RTMs in the cryostat can then be accomplished using a range of precision (Grade 5) kinematic ball sizes. To ensure adequate clearance between the close fitting sensors on adjacent RSAs in the completed focal plane, the position tolerance of the balls comprising the array must be less than 50 microns. A spring clip retains each ball in its cup, necessary because the Camera is assembled in the zenith pointing orientation which has the grid loaded in the downward orientation. This clip is ultimately captured in the vee of the raft, and therefore safe from coming free in the cryostat. The ball cup – ball – vee interface design of the kinematic support is sufficiently stiff to minimize the effect of variable loads

Any final height adjustments of the kinematic mount planarity is completed via the ball diameter selection. The ball diameter is nominally 8 mm. Precision balls are readily available in 100 ball lots with size variation less than 120 nanometers (1 sigma). Lots of balls will be obtained in increments of 2 to 4 microns from nominal allowing final adjustment of the completed focal plane to the required flatness.

12.4.2 Cryoplate, Cryoplate Support Flexures and Cryoshroud

The cryoplate provides:

- Mechanical support for the raft front end electronics and raft housing
- Uniform cooling for the front end electronics and the sensors
- Mechanical support and passive cooling for picture frame and perimeter shrouds, and the passive cooling of the grid via the grid straps
- Mechanical support and cooling of the two pumping chimneys

The dual role as a mechanical element and a thermal element has led to a hybrid design as a copper and stainless steel sandwich. The copper provides good thermal conductivity while the stainless steel rigidizes the structure. The poor thermal conductivity of the stainless reduces heat leaks where it is supported off four flexures to the cryostat walls. An ancillary function is that the copper plane serves as the common reference ground for the electronics.

12.4.2.1 Design of the Cryoplate

The design of the cryoplate is shown in Figure 12-31.

The cryoplate assembly weighs about 60 kg, and supports the science and corner raft electronics crates which weigh approximately 190kg. The copper cryoplate is ~1 cm thick with a stainless steel frame bolted and brazed to the backside of the plate.. Stainless support mount frames are attached to the cryoplate and ribs provide out of plane rigidity for the completed cryoplate. The copper plate is approximately square with rectangular cutouts for the science sensor RTMs and triangular cutouts for the corner sensor RTMs. These cutouts, that match the pattern in the grid, provide the mechanical and thermal attachment of the raft electronics crates to the cryoplate.

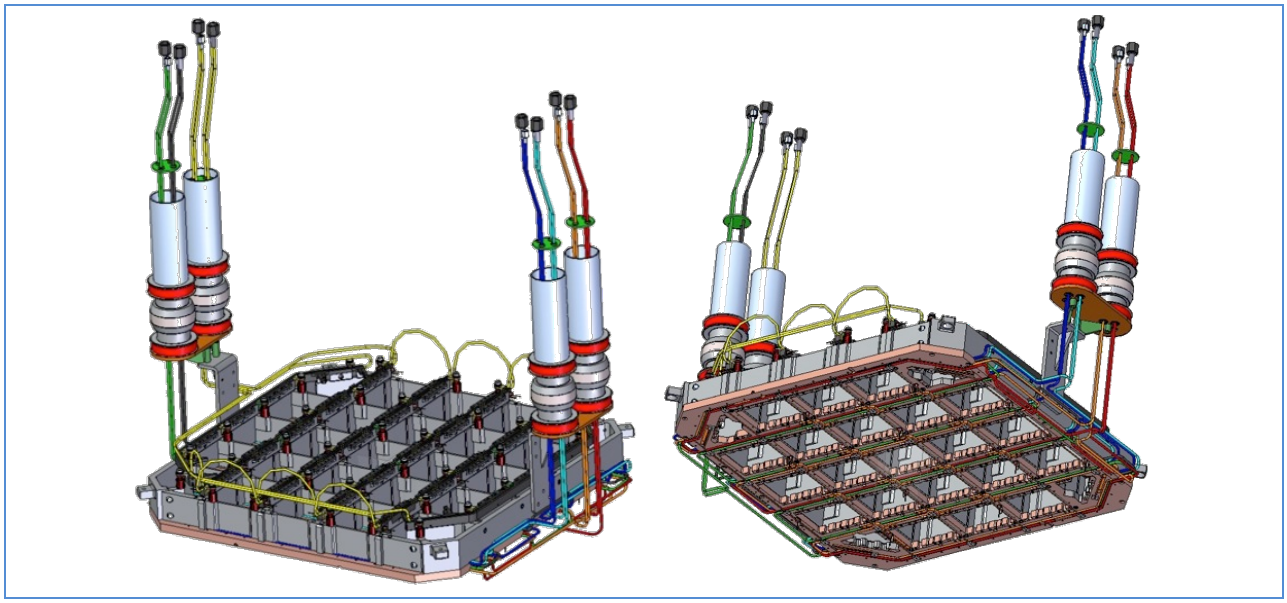

Figure 12-31: The complete cryo-cold plate (bottom and top views)

The cryoplate is mounted in the cryostat via a support ring and four flexures. The support ring is fixed within the cryostat by six columns that mount to the back side of the housing front flange at the location of the titanium grid flexures and four kinematic spherical rod end assemblies the attach to the wall of the housing. (Figure 12-32).

At opposite sides of the plate are the six inlets and six outlets for the refrigerant evaporator. Each evaporator is connected to one heat exchanger modules located in the utility trunk via the cryo-feedthrough assemblies. The refrigerant flows in the six stainless steel tube evaporators routed and brazed in channels cut in the top and bottom of the copper cryoplate.

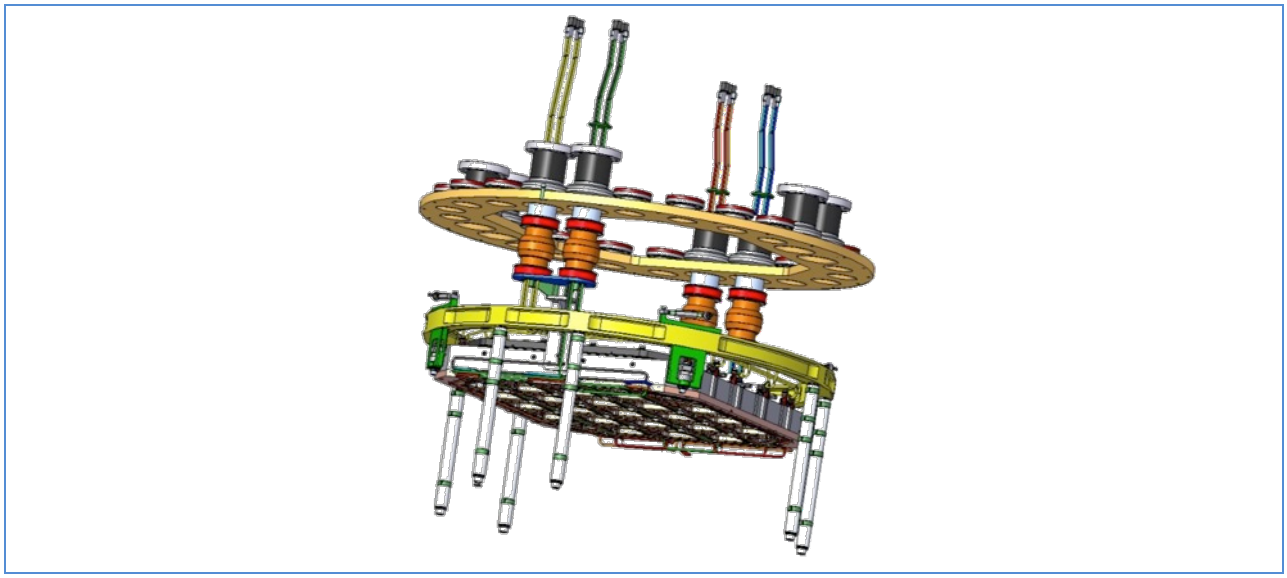

Figure 12-32: Cryoplate on its support structure with cryofeedthroughs penetrating feedthrough plate

The routing of the individual evaporators on the cryoplate is configured such as to minimize the thermal temperature effects of the possible loss of one refrigerator module. To eliminate the risk of an internal refrigerant leak, the 1/8” OD, 0.010” walled tubes are made from single length mill runs with no joints or fittings inside the cryostat vacuum envelope. All connections for the refrigeration system assembly are located on the heat exchanger side of the vacuum barrier on the cryogenic feed through.

The thermal connection of the RTM raft electronic crates to the cryoplate is made adjacent to the stainless ribs.

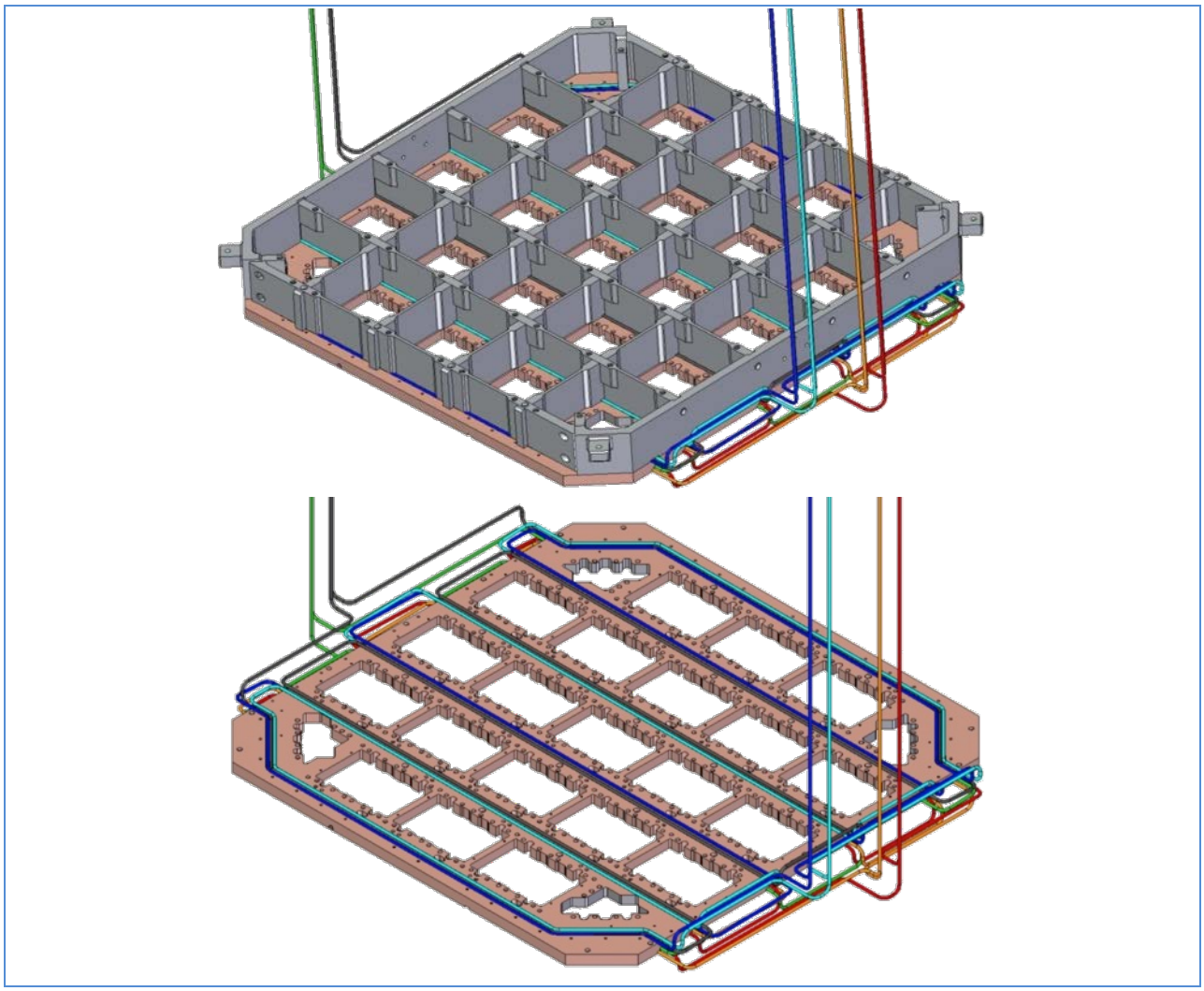

Figure 12-33: The cryoplate stiffener ribs with integral evaporators

Within each bay, there is an additional pair of connections to the two grid cooling straps. Heat removed through these straps is significantly smaller than the process heat of the sensors and the IR load on the focal plane. Holes through the cryoplate are provided adjacent to the RTM to allow access for the RSA load transfer mechanism (Figure 12-34).

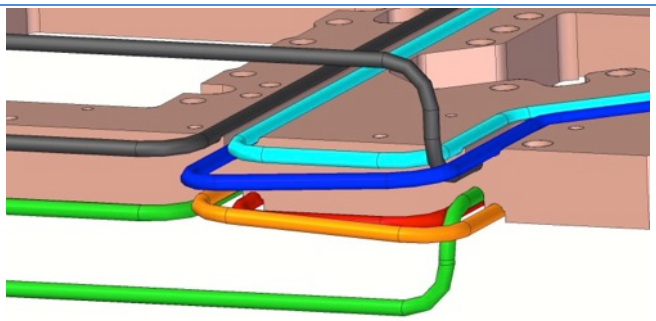

Figure 12-34: Cutaway of the channels in the cryoplate top and bottom

The make-up trim heaters are located in channels on the underside of the cryoplate. The copper plate and stainless steel support frame is sufficiently stiff to obviate any significant out-of-plane deflection of the cryoplate due to telescope repointing and seismic over loads.

Mechanical and Thermal Analysis of the Cryoplate and Flexures

A preliminary mechanical stress analysis of the cryoplate suggests that it is suitably stiff to carry the loading of the rafts (in all orientations) while introducing negligible stresses in the copper cryoplate and its brazed joints. The flexures as well are adequate for transfer of loads to the cryostat body in all orientations and accommodate the differential contraction and expansion between the cryoplate and the warm cryostat body. Preliminary thermal analysis of the cryoplate design suggests that it will provide the required +/-1.0C uniformity in temperature given the expected heat loads from the sensors, grid, support flexures and the perimeter cryoshroud.

12.4.2.2 The Cryoshroud Design

The cryoshroud is attached to the perimeter of the cryoplate. The cryoshroud is cooled by the cryoplate and extends around the grid up to the focal plane. The cryoshroud establishes a uniform thermal environment for the grid by mitigating the effects of varying spatial thermal load (and the resulting geometric distortions) from temperature gradient around the cryostat housing.

The shroud will be fabricated from copper sheet and plated to reduce emissivity and radiation load. A picture frame shroud which covers the edges of the grid extends from the top of the cryoshroud. This shroud reduces the view factor from the focal plane to the warm cryostat housing and the subsequent radiation load on the sensors. Cutouts in the picture frame shroud are required for passage of the grid flexures.

12.4.3 Coldplate Support and Shrouds

The coldplate provides uniform cooling of the science and corner readout electronic boards by the cold (-40C) refrigeration system.

There is no mechanical support function for the coldplate as the readout electronics boards are supported by an independent, thermally isolating, system inside the raft electronics crate.

The coldplate is not a “plate” as such but a series of separate bars connected by the 2 evaporator tubes brazed in the bars and supported from the cryoplate via a series of thermally isolating standoffs.

12.4.3.1 Design of the Coldplate

The coldplate is shown in Figure 12-35.

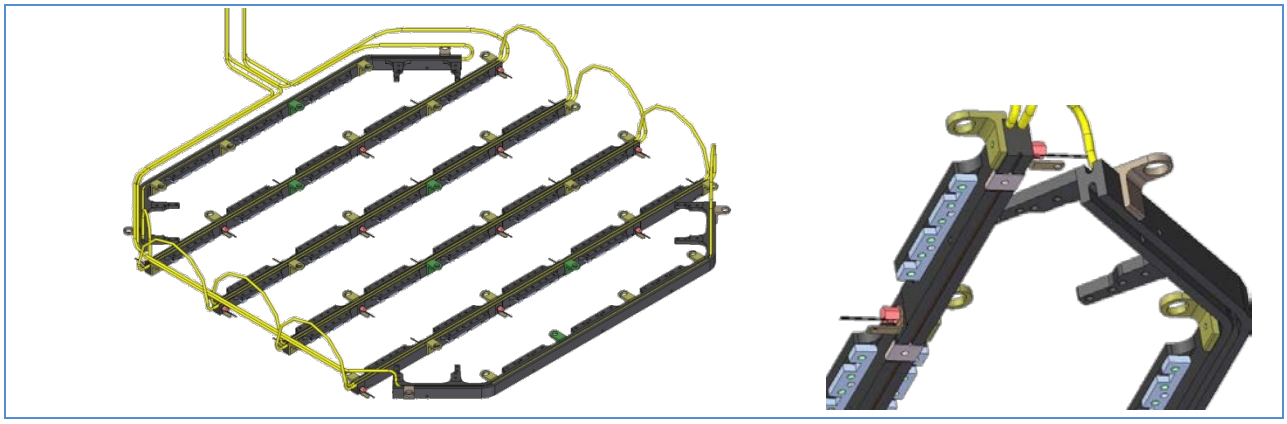

Figure 12-35: Views of the ccoldplate: (a) Top, (b) Bottom

The coldplate assembly weighs about 6kg, and cools the science and corner raft read-out electronics via cooling bars and thermal interface flexures (copper braid) mounted on those boards. The fundamental construction of the cooling system is similar to the cryoplate in the use of stainless steel evaporator loops braze in channels in copper plates. Likewise similar to the cryoplate the coldplate interconnects to its refrigeration system heat exchanger in the utility trunk via a cryo-feedthrough assembly in the back of the cryostat housing.

As in the case of the cryo evaporators, the cold system will use seamless stainless steel tubing of continuous mill run lengths inside the cryostat vacuum enclosure to eliminate the risk of refrigerant leaks. Two parallel evaporators provide redundancy.

With the coldplate 90C warmer than the cryoplate, and the raft electronic s boards (REBs) with a similar temperature difference to the raft electronics crate from which they are supported, a differential thermal motion must be accommodated. The copper bars that constitute the coldplate structure are individually mounted on the stainless stiffener ribs that run between the bays of the cryoplate. These bars are allowed to move with the relative contraction and expansion of the stiffener ribs. The copper bars of coldplate are connected to each other only by the evaporator tubes of the refrigeration system and the cooling bars on the REBs. The evaporator tubes have strain relief loops and the board cooling bars have flexible thermal straps at the interface joint. The longitudinal differential motion between the cold plate bars and the cryoplate ribs is accommodated in the support standoff interface between the two; the longitudinal position is fixed at only one standoff. These standoffs also provide the thermal isolation between the warm(er) coldplate and the cold(er) cryoplate by incorporating a serpentine geometry that creates an extended conductive path length in a compact package. Loss across an individual standoff is less than 1/2 watt. (Figure 12-36).

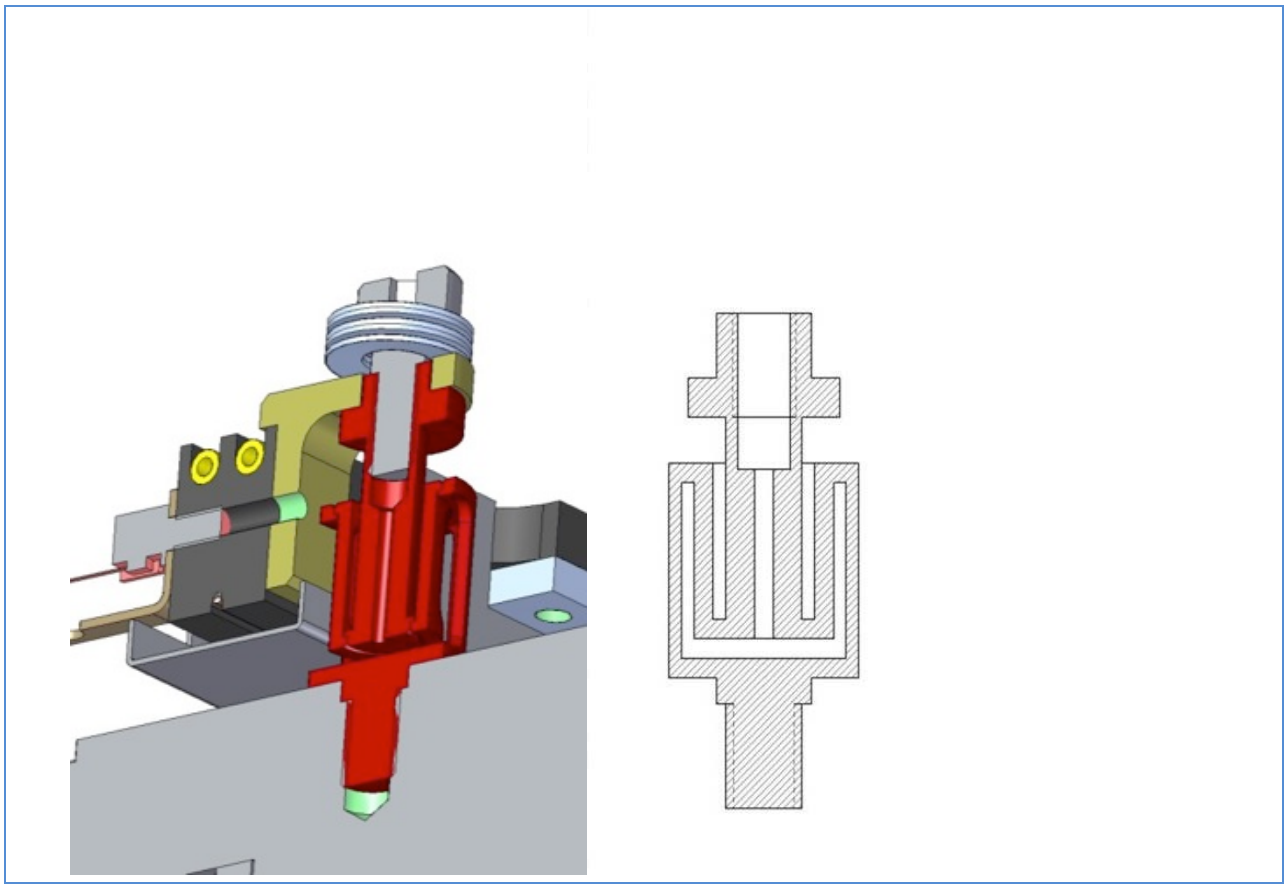

Figure 12-36: Coldplate thermally isolating standoff and cutaway showing long thermal path

The coldplate is final assembled with its dedicated thermal-vacuum feedthrough and then mated to the cryoplate (Figure 12-37). This assembly, which includes all necessary trim makeup heater, thermal instrumentation and electrical grounding and shielding hardware is checked for functional performance prior to installation in the cryostat

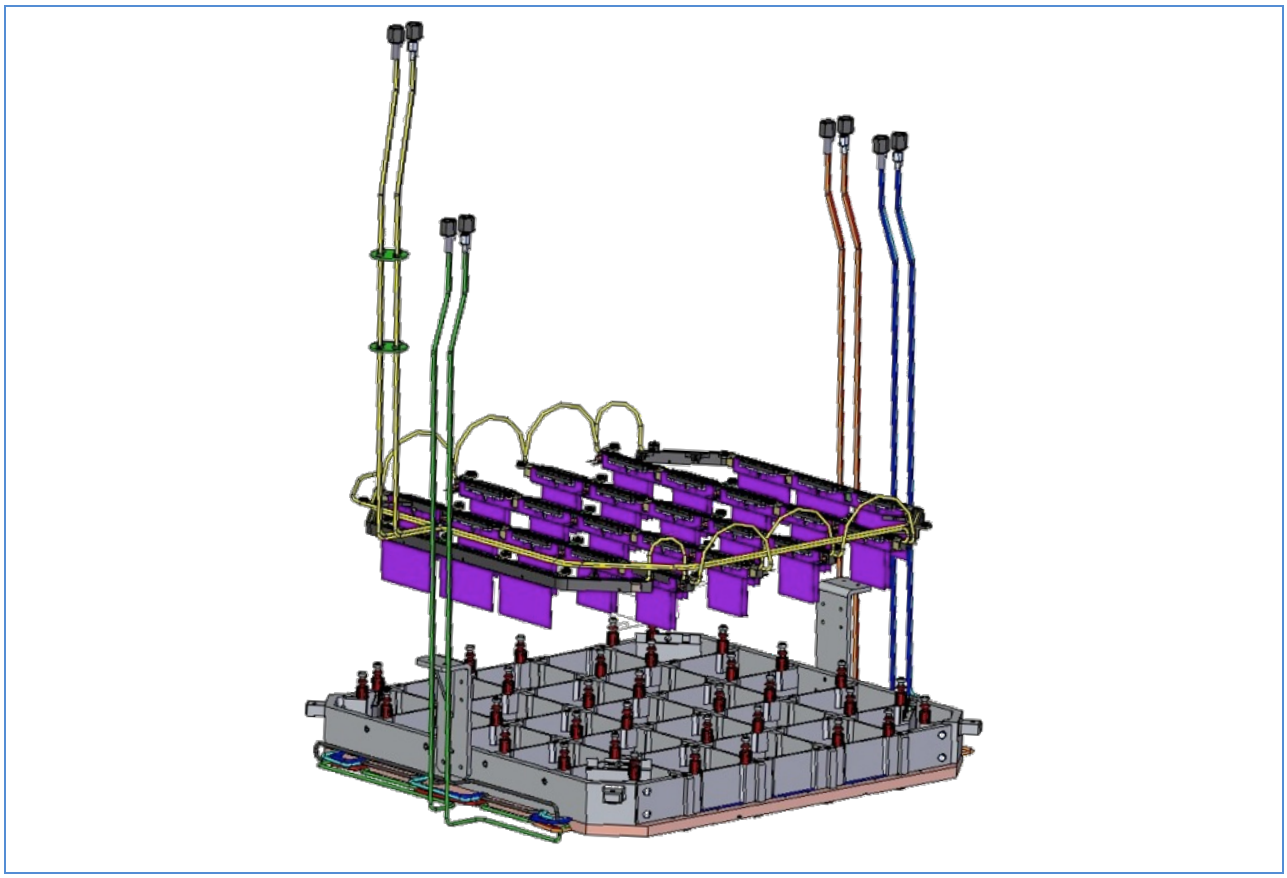

Figure 12-37: Coldplate assembly mating to cryoplate. In purple are radiation shrouds to shield the cryoplate from the warm REBs extending through the cryoplate to the coldplate.

Analysis of the Cold Plate

Preliminary thermal analysis of the coldplate design suggests that it should be able to provide the required +/-2^{o}C uniformity in temperature assuming the expected heat loads from the readout electronics and standoffs.

12.4.3.2 Shroud System

Surrounding the cryo-coldplate assembly and RTMs is a system of thermal radiation shields. (Figure 12-38). This system of shrouding reduces the radiation load from the walls of the cryostat to the cold cryoshroud surrounding the grid, the cryo-coldplate and the raft sensor assemblies These shields will be constructed of stainless sheet with nickel or other low emissivity coating.

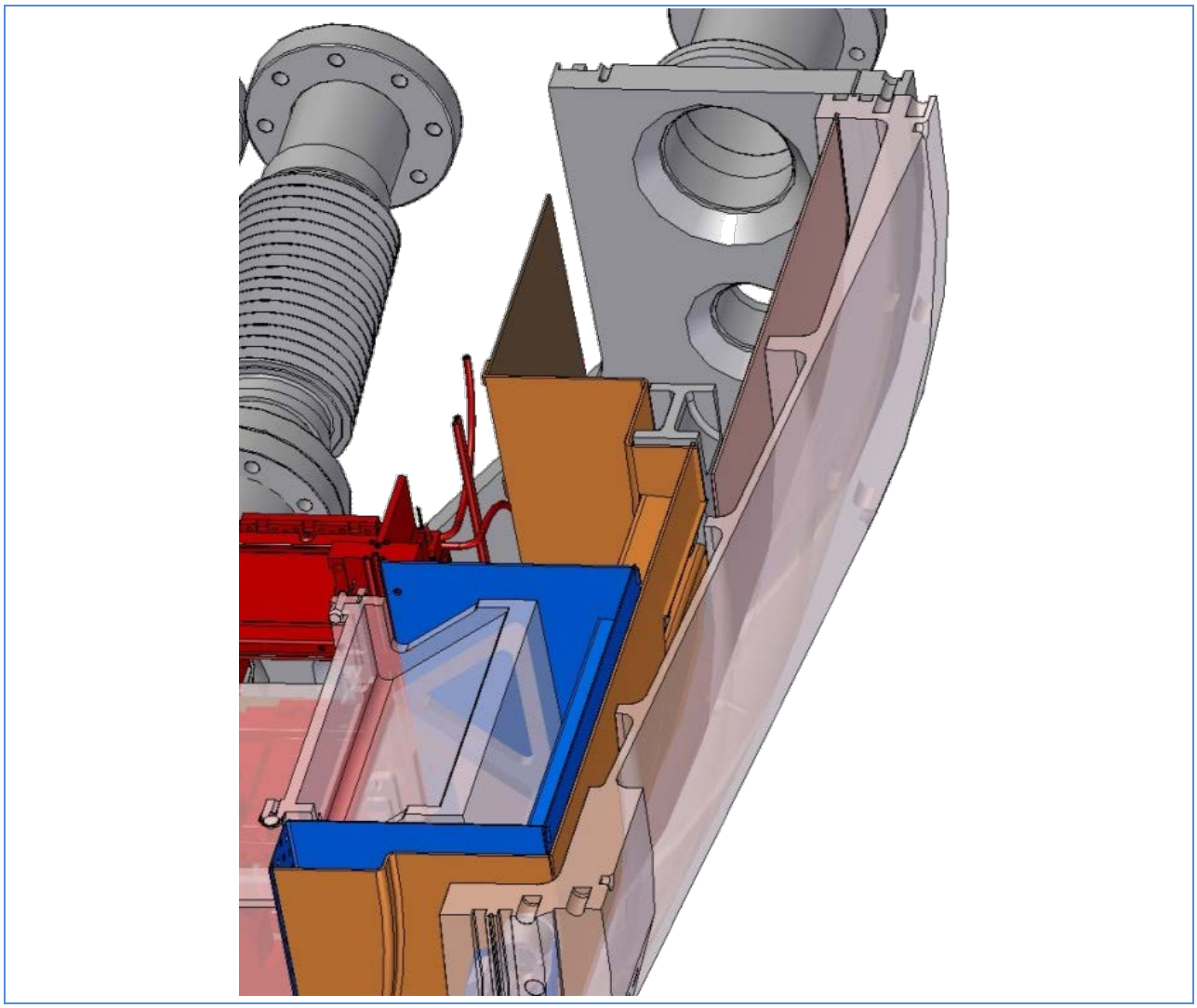

Figure 12-38: System of cold (blue), float(gold) and warm (bronze) shrouds. In red is the cryo/coldplate.

12.4.4 Vacuum and Purge Systems

As indicated earlier the cryostat vacuum is maintained locally by the three sputter ion pumps and a turbo-molecular pump mounted on the octagonal “pumping plate” at the rear of the cryostat, and the passive getter pumps located on the feedthrough flange at the rear of the cryostat.

12.4.4.1 Active Pumping and Instrumentation System

Figure 12-39 shows a detail of the layout of the rear of the cryostat. The outer feed-through plate provides 16 3-3/8 conflat flanges for installation of data, power and instrumentation cable assemblies and eight 4.5” cryo-feedthroughs(4x) for the refrigeration system, instrumentation (1X) and the getter pumps (3X). The cryostat housing vacuum components are mounted on the inner octagonal pump plate. Both the outer annular feedthrough flange and the pump plate will be constructed of aluminum. This saves mass and allows matched thermal performance to the cryostat housing.

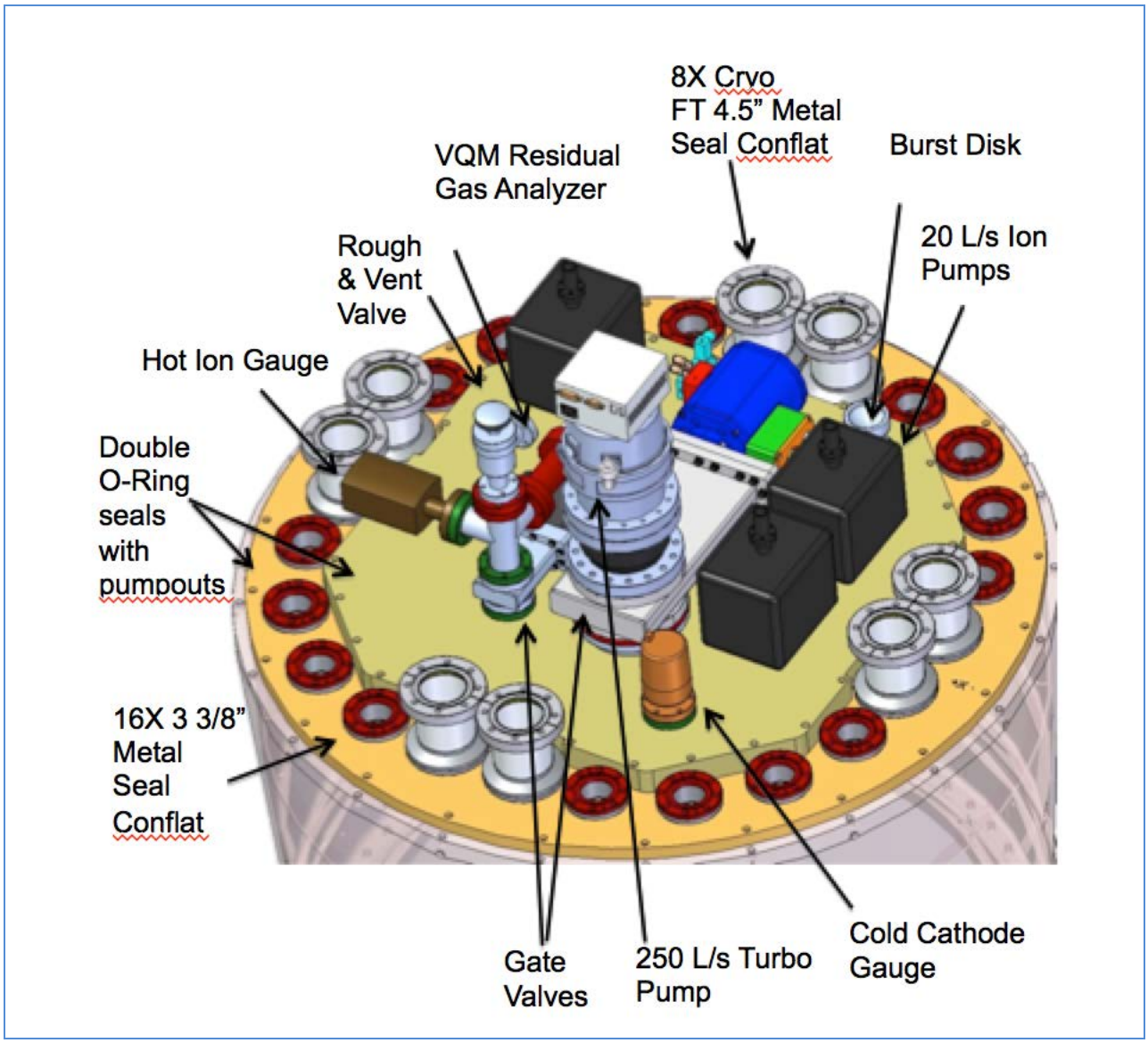

Figure 12-39: Detail of pump plate

The pump plate will include three 20 L/sec sputter ion pumps as the primary holding pump for the system. Additionally a 250 L/sec turbo-molecular pump, which will be mounted on a vibration isolator flange assembly (<0.01µm motion) via a 6 inch conflat flange with a fine mesh screen to prevent particulates from entering the pumps will provide system rough pumping and backup to the ions. The TMP will be isolatable from the cryostat vacuum envelope by a pneumatically operated gate valve. The TMP is backed by an oil free scroll pump which is located close by on a manifold and isolatable by a pneumatic valve from the TMP. There will be a cold cathode gauge mounted directly on the pump plate. A 2-3/4 inch gate valve will allow isolation of a hot cathode gauge (for filament replacement) and an RGA (vacuum quality monitor) from the cryostat housing. This gate valve also provides redundancy for the main system vent and purge valve.

Convector gauges provide control for the TMPs and also monitoring of the vacuum at the start of pumpdown. The magnetron gauge is suitable for monitoring high vacuum regime. The RGA provides continuous feedback on the partial pressures of all molecular species within the cryostat vacuum up to 200AMU once the pressure is sufficiently low. As such it will provide early warning of small leaks, outgassing of unsuitable materials, and aid in isolation of vacuum problems, as an on-board leak detector.

Throughout the rest of the system, convector gauges are used to monitor pressures. All valves will for the most part be pneumatically operated – with electrical solenoid control. Power supplies and vacuum instrumentation readout and interfaces will reside in the utility trunk.

12.4.4.2 Passive Pumping Systems

A number of getters – both evaporable and non-evaporable - have been tested in the Material Test Facility, and their pumping speed per gram of getter for various molecules and at various temperatures has been measured. Table 12-4 shows a summary of the getters tested so far.

Table 12-4: Properties of getters – measure through 0.2 µm mesh

Species	H_2	H_2O	N_2	CO_2
	x 10^{-8} Torr-Liter/Sec/gram			
Activated Charcoal GC 4x8 Mesh at 20^0 C	33	7	13	3
Activated Charcoal GC 4x8 Mesh at -100^0C	104	23	30	12
Zeolyte 3A Pelletized Hengye Corp. (warm/cold/regenerated)	87	10	70	14
Zeolyte 4A 2 to 4 micron Powder Hengye Corp. (warm/cold/regenerated)	121	68	54	25

Estim

Activated Charcoal and Molecular Sieve Pumps

The three 4.5” conflats on the feedthrough flange will be used to house charcoal and molecular sieve pumps. Molecular flow analysis (MOLFLOW and GEANT4) suggests that the best place to locate these pumps is close to the likely sources of contaminates, namely the warm circuit boards and cables.

The activated charcoal pumps will be constructed as closed cylinders attached to a conflat flange, to have as large as possible a surface area (a few hundred cm2) The 8x12 mesh coconut charcoal will be loaded into the (welded) sintered metal housing, through the conflat cover. The sintered metal housing is chosen to avoid the problems of dust. Activated coconut charcoal has been chosen because it does not need to be accessed for regeneration and it is relatively easy to cool it down by a thermal strap to the cryoplate refrigerant supply line. The broad spectrum of gettering is also appropriate. When the

system is warmed up, it will outgas whatever it has absorbed when cold, and this can be effectively pumped out by the TMP located adjacent, at the rear of the cryostat.

A non-evaporable getter such as 3A or 4A molecular sieve powder or pellets has been chosen for passive pumping. Estimates of the plateaued outgassing rate for water vapor in the cryostat focal plane region, suggest that 0.1 to 1Kg of 3A and 4A molecular sieve (powder) will reduce the residual outgassing of water vapor to $<<10^{-8}$ Torr L/sec. Unlike activated charcoal, the performance of these getters show little or no temperature dependence, but do require regeneration at high temperature greater than 200^{o}C , or replacement, when they are saturated. The molecular sieve pumps would look similar to the charcoal pumps but not require a cryostrap. Whenever the cryostat is opened, they could be removed and replaced by regenerated pumps.

12.4.5 Cryostat Refrigeration System

12.4.5.1 Motivation

Perhaps the most unique and challenging aspect of the cryostat design is the presence of a significant amount of analog and digital electronics within the vacuum space housing the cold CCD sensors. The Raft electronics represent the largest source of process heat which must be removed through the cryoplate and coldplate providing (nominal) 76.3W and 535W of cooling at -125ºC and -35ºC, respectively. While refrigeration of the coldplate can be achieved rather easily using conventional refrigerants such as R507 and a heat exchanger, a trade study was completed to evaluate options for providing the cryogenic cooling regime (-130^{o}C) required for the cryoplate.

This resulted in the adoption of a technology based on “mixed-refrigerants” developed by Micro Miniature Refrigeration, Inc. (MMR), of Mountain View, CA. LSST will utilize a specific mixed refrigerant system for which MMR holds patents. The LSST cryoplate cooling system will be composed of a set of parallel refrigeration circuits wherein each circuit represents just a modest extension of an existing MMR product which produces 30 W of cooling at 77K. To eliminate the need for cryogenic pumps moving liquid/vapor through vacuum insulated metal transfer lines, the warm and cold components of the refrigeration systems are separated. Compression of the vapor occurs on the ground in the utility room, and the Joule – Thompson expansion cooling takes place in the Camera itself, close to the cryoplate.

12.4.5.2 Detailed Description of the LSST Mixed Refrigerant System

Cryoplate Refrigeration System

The LSST cryoplate refrigeration will be accomplished by a set of six parallel refrigerators, each having a heat removal capacity of >85 W at -130^{o}C. A schematic for one of these mixed – refrigerant circuits is shown in Figure 12-40.

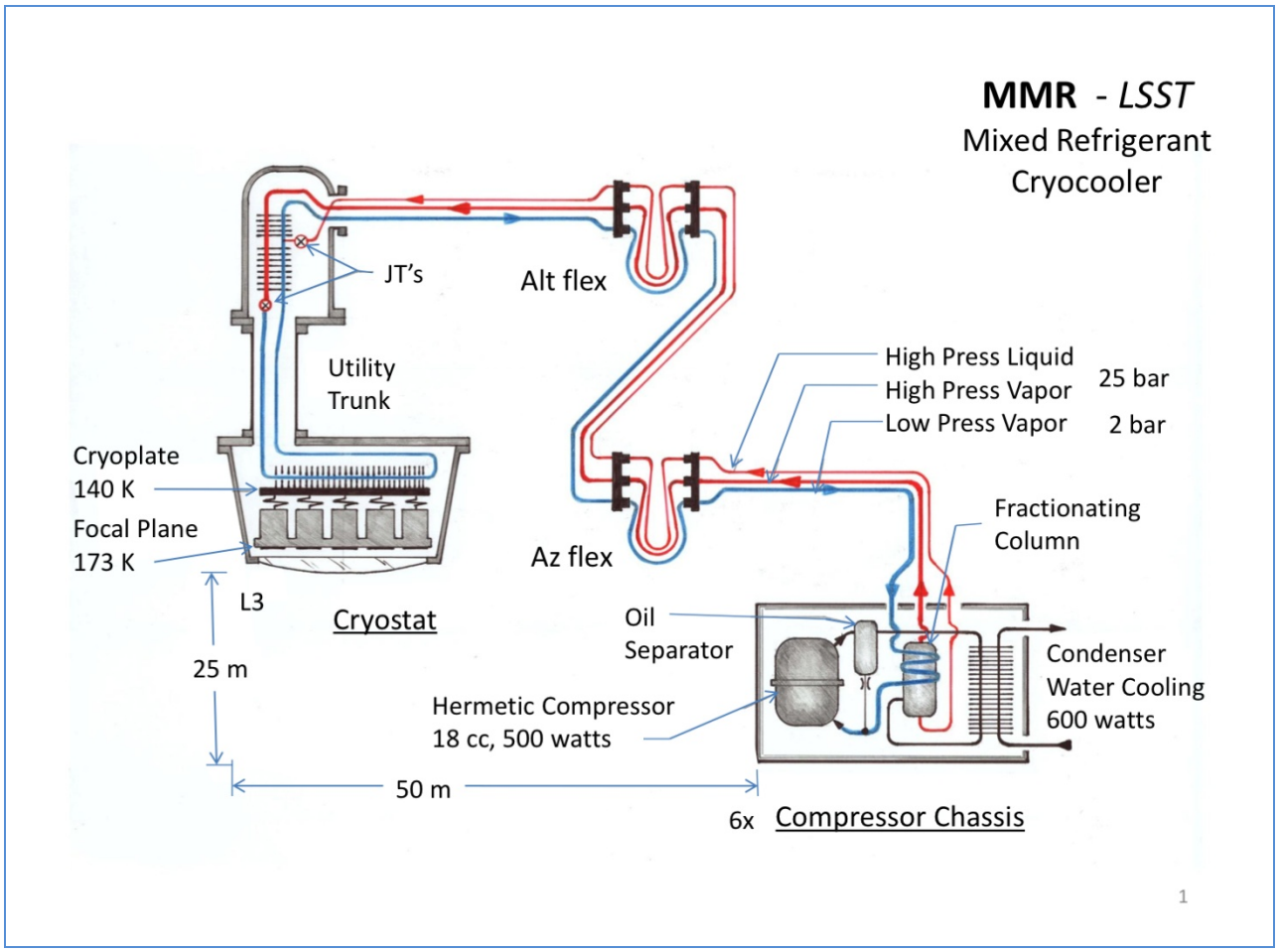

Figure 12-40: Schematic of mixed refrigerant system

Each circuit of the system works as follows. On the ground, in the utility room, a proprietary non-flammable mixture of refrigerant vapor is first compressed by an off-the-shelf commercial hermetically sealed compressor. The output of the compressor is a mixture of hot vapor which is contaminated with compressor lubricating oil. A cyclonic oil separator removes a substantial portion of the oil and returns it to the compressor via a capillary. This capillary is employed to maintain an oil seal which blocks hot refrigerant vapor from returning directly to the compressor.

The hot refrigerant mixture is next cooled to ambient temperature by a water-cooled heat exchanger. It is then separated into vapor and liquid by a fractionating column, which is water-cooled at the top. The fractionating column concentrates the residual dissolved oil in the liquid phase stream. This is a critical "self-cleaning" function, separating refrigerant into oil-rich liquid and oil-free vapor, so the vapor will not freeze and clog the downstream expansion capillaries when it ultimately reaches cryogenic operating temperatures. This oil-rich liquid stream is used to refrigerate the warmer upper stage of the low temperature heat exchanger on the Camera. Figure 12-41 shows the prototype chassis for a single circuit developed at MMR.

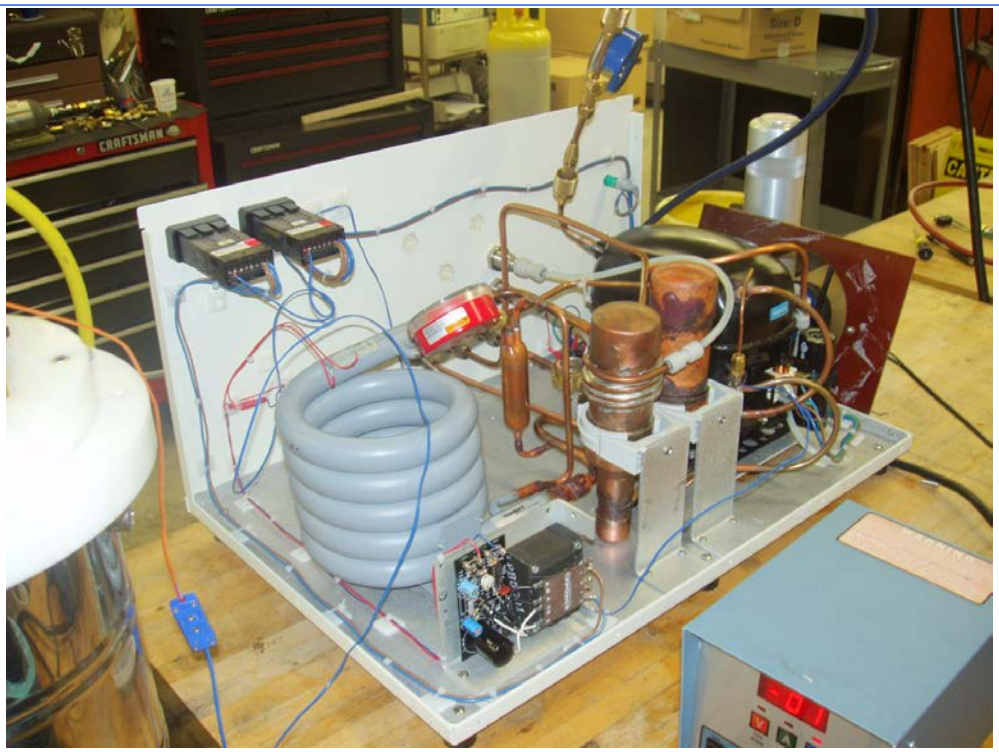

Figure 12-41: Prototype chassis holding compressor, oil separator, fractionating column at MMR lab

The~ 100 m long liquid and gas supply lines travel from the ground up to the Camera at high pressure (400 psia in 1/8" OD and 1/4" OD tubing). These small lines, being close to ambient temperature, require little thermal insulation making it simpler (in comparison to vacuum insulated transfer lines) to climb the 30m elevation. Flexible hose bridges the altitude and azimuthal rotations of the telescope, enroute to the Camera.

The liquid and gas supply lines enter the rear of the Camera in the back of the utility trunk where they subsequently enter the two vacuum insulated heat exchanger modules (4 exchangers per module). The heat exchanger module contains the set of 4 counter flow heat exchangers (CFHEX) for either the cryoplate system and/or coldplate system. There are eight in total, six for the cryoplate and two for the coldplate, sharing a common insulating vacuum housing . Four ~ 8cm diameter pipes extend the vacuum housing 1.1 m through the utility trunk, to the rear of the cryostat. These pipes carry the extended HeX, the final expansion capillary and a short section of cryogenic supply and return lines that enter and exit the cryostat. This insulating vacuum system is completely separate from the cryostat vacuum system.

A view of a typical heat exchanger is shown in Figure 12-42.

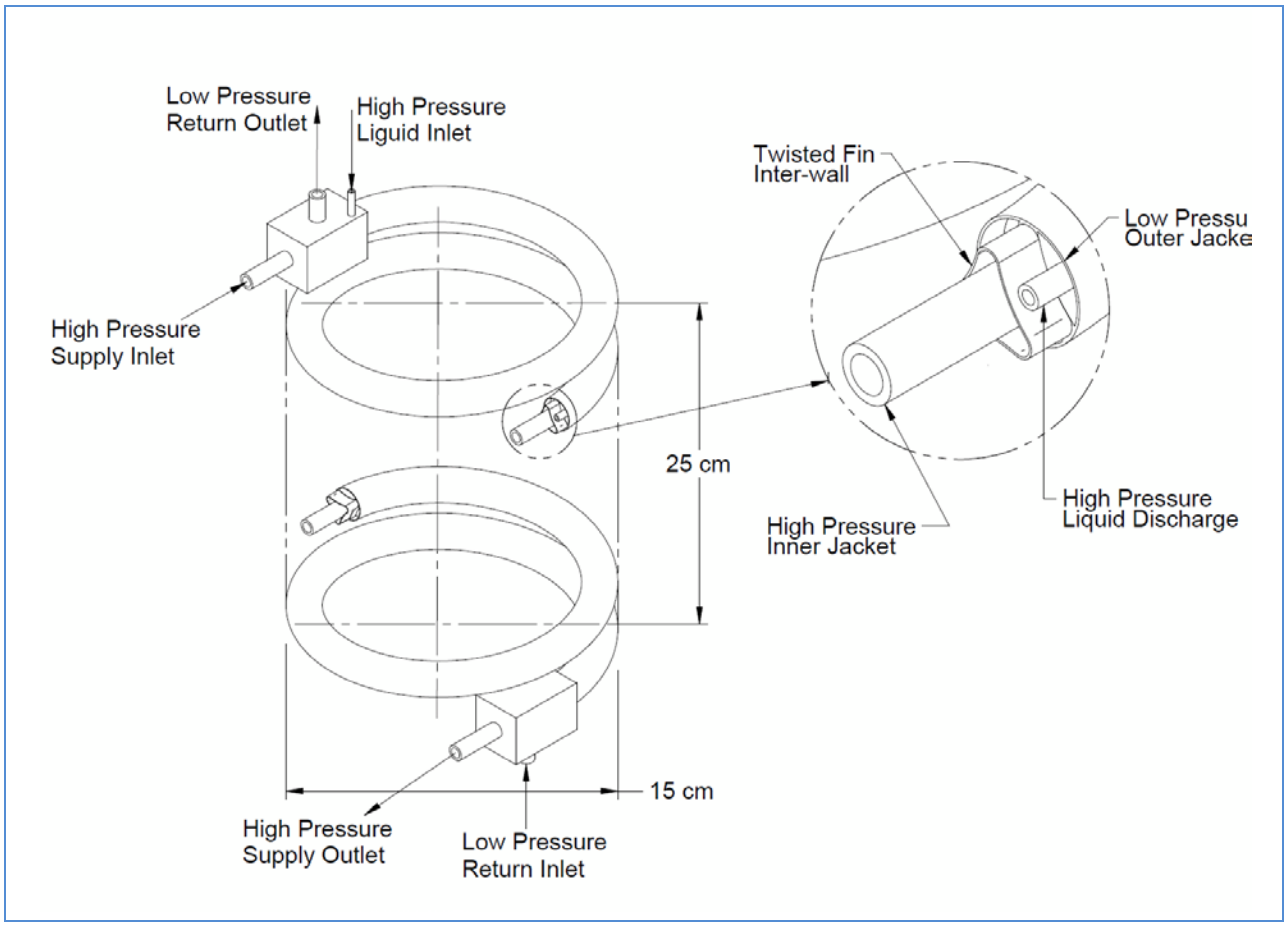

Figure 12-42: The counterflow twisted fin heat exchanger

The heat exchanger is comprised of an inner high pressure supply line with a twisted heat transfer fin along its length, within a larger copper jacket which forms the vapor return line. Near the front of the heat exchanger the incoming high-pressure liquid undergoes Joule-Thompson expansion in a short (~3 m long, 0.028 inch id) capillary and then evaporates into the low pressure (25 psia) vapor return line. This expansion and evaporation pre-cools the incoming high pressure gas, at temperatures above the freezing point of any dissolved oil.

In the balance of the heat exchanger, the pre-cooled high pressure incoming gas is further cooled by exchanging remaining heat with the outgoing low temperature and low pressure vapor returning from the cryoplate. At the cold end of the counterflow heat exchanger it undergoes Joule-Thompson expansion into a 3 m long 0.05 inch id capillary where the final mixture of gas and liquid is at the required temperature of ~-130^{o}C. A prototype of the counterflow heat exchanger is shown in Figure 12-43.

Figure 12-43: Prototype of counterflow heat exchanger, exchanger is constructed of 13mm (1/2 inch) OD copper tubing making the outer jacket, coiled to a 200mm diameter X 300 mm tall package.

The cold liquid/vapor mixture enters the cryostat vacuum through a bayonet-like feedthrough and then through shorter lines to one of six parallel evaporators in the cryoplate where the mixture removes heat by vaporization. The now cold and low pressure mixture exits the cryoplate and rear of the cryostat through the same feedthrough where it then returns back to the heat exchanger module in the utility trunk. After extracting heat from the incoming gas (as previously described), the refrigerant exits the heat exchanger vacuum, and the Camera, and returns to the ground in a ¾" OD line at near ambient temperature and low pressure (25 psia).

Description of the LSST Cold Plate Refrigerant System

A similar system is used to cool the coldplate. There, because of the higher operating temperature, a conventional single refrigerant such as R507 is sufficient to extract the ~1000 W of process heat at -40°C. The coldplate refrigeration system will require two identical parallel circuits, each feeding an evaporator on the coldplate to achieve a 1500 W total capacity. As in the cryogenic system, two compressors will be located in the utility room and two counterflow heat exchangers will be in the heat exchanger module, at the back of the utility trunk.

12.4.5.3 Control and Operations of the Refrigerant Systems

Each circuit in the system will reach its equilibrium operating temperature in ~5 hours based on early tests completed at SLAC. The actual time constant of the fully deployed system with the cryoplate mass and electronics heat loads has not been tested yet, however the system is being designed to be effectively "free running", reaching the desired operating temperature just below the optimum heat extraction efficiency point. The performance of the system is largely "engineered in" by selection of the gas/liquid mixture, the operating pressure and the detailed design of the counterflow heat exchanger. The simplest temperature control for the cryoplate that can be incorporated will be in the form of trim heaters. This would be part of a feedback loop with temperature input from sensors on each circuit in the cryo or coldplates. A trim heat of about 20 Watts will be required.

12.4.5.4 Risks and Failure Modes of Mixed Refrigerant Systems

The refrigerant system contains no flammable or toxic materials however it does flow into and out of a clean vacuum space (the cryostat) and therefore must be contained completely against leaks into the cryostat vacuum system. There are no joints in the cryostat as the evaporator lines are continuous mill run lengths. The issue of leaks into the cryostat vacuum is described in greater detail in the cryoplate design section and the cryostat feedthrough section.

As the cryostat must be installed and removed from the Camera body periodically, provision is made for venting, sealing and disconnecting long refrigerant lines, and for remaking these connections without introducing foreign contaminants into them. All demountable connections of cold refrigerant lines within the refrigeration system are made within its own insulating vacuum space, which itself is not connected to the cryostat vacuum. Any leaks within this system will be contained within it and detected by instrumentation in the refrigerant vacuum system.

A significant amount of operational experience with similar mixed refrigerant systems has been logged in the field by MMR. Their technology is used in refrigerated radiation detectors, deployed for example in thousands of sites worldwide to monitor compliance with the Nuclear Test Ban Treaty. As a result of this large sample population and enormous number of integrated running hours, the mixed refrigerant systems similar to the LSST system have been found to have only one significant operational failure mode after infant mortality issues are resolved. The failure is associated with the self-cleaning feature of the circuit, wherein a small amount of oil makes its way into the vapor circuit and freezes out, slowly plating the expansion orifice over time, and eventually plugging the line. The refrigerators are observed to be "self-healing," warming up as a result of the plugging, and subsequently flushing the frozen oil away. In LSST, periodic warming up of the system for other routine maintenance will probably serve the same function, resulting in reliable highly efficient operation.

In the design, the minimum required capacity is sufficient for 6 refrigerators to provide the total required capacity of ~540 W. We are anticipating however that the capacity of each parallel circuit will actually lie somewhere between 85 and 100 W, providing some headroom. Should the prototypes prove to have a capacity of >85W, the system would be able to run on 5 of the 6 circuits without interruption, should one circuit fail.

12.4.5.5 Status and Implementation in LSST

The mixed – refrigerant system described above has been in a prototype phase since early 2010. It is part of a contract with MMR to develop a system that meets the requirements for LSST.

As of the end of 2010, the prototype using the SG18C compressor had achieved a cooling capacity of ~100W at -130°C. This required removal of R134a from the standard LSST mixture (a 5% component of R404a) and replacement of it with other refrigerants (C2 and C3). R134a is a less well understood refrigerant and was suspected of freezing at the lowest temperatures. Figure 12-44 shows a typical curve for cooling capacity versus temperature, using one of the early refrigerant mixtures (KR15).

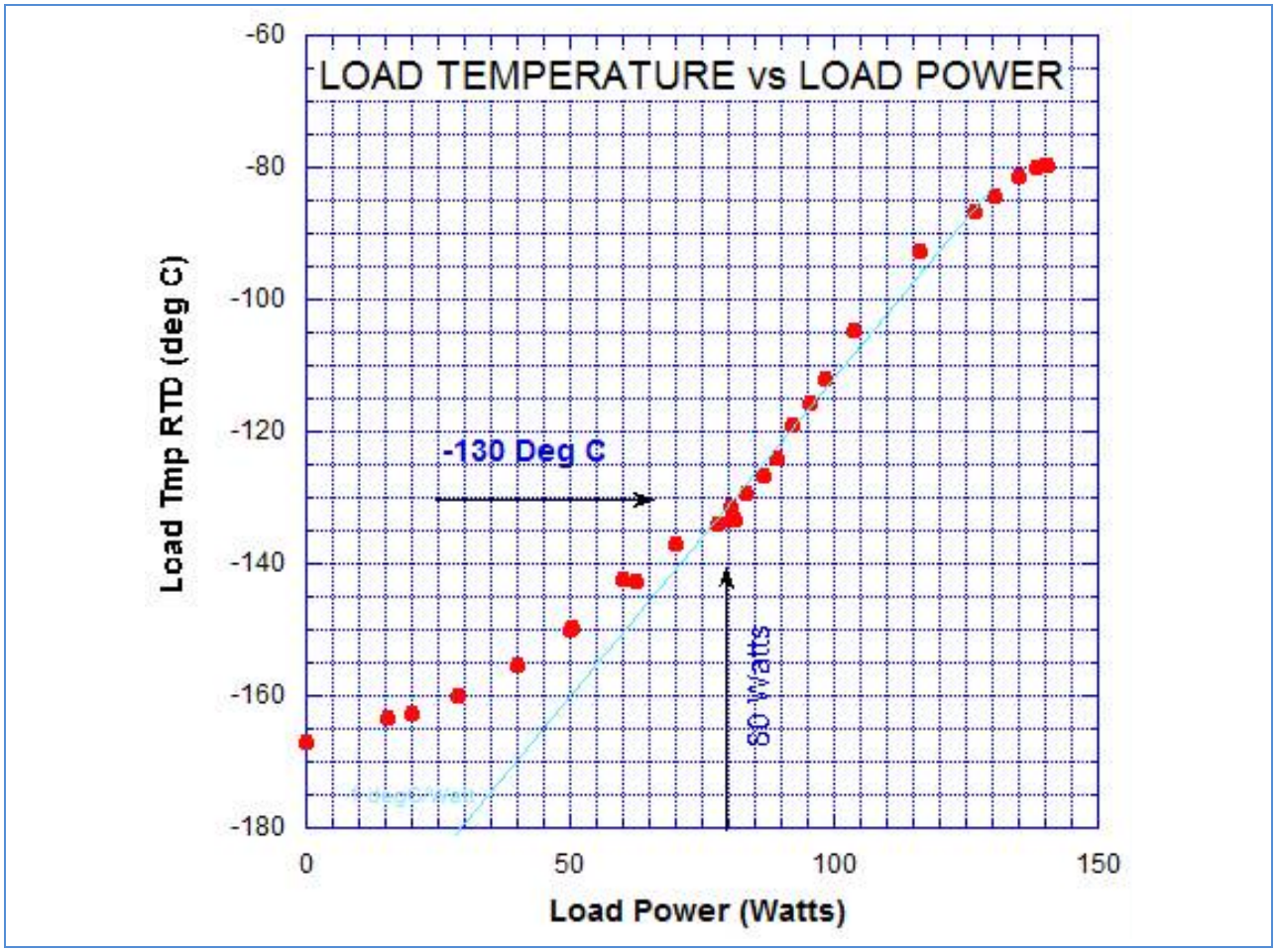

Figure 12-44: Prototype refrigerator performance

MMR has worked to optimize the refrigerant mix to achieve ease in operation and required cooling capacity. A mix based on R218 (MX29-19C) is currently in use.

Finally, refrigerant mixing and monitoring is critical to the performance of the system. While it would be ideal to have gas mixing hardware at the summit, the cost appears prohibitive. The current plan is to have sufficient pre-mixed, pre-tested, and pre-certified refrigerant available to accommodate expected losses during routine Camera servicing.

12.4.6 Feedthrough Flange Assembly, Feedthroughs, and Signal Routing

As described earlier, the rear flange of the cryostat is composed of an annular ring which contains signal, power and cryogenic feedthroughs, and a separate octagonal central plate that contains the vacuum instrumentation. The annular ring is tested and installed prior to raft integration, while the central vacuum flange is installed at the end of integration. Cable routing proceeds at several phases of the integration. Figure 12-45 shows layout of the cryo-feedthrough at the annular ring.

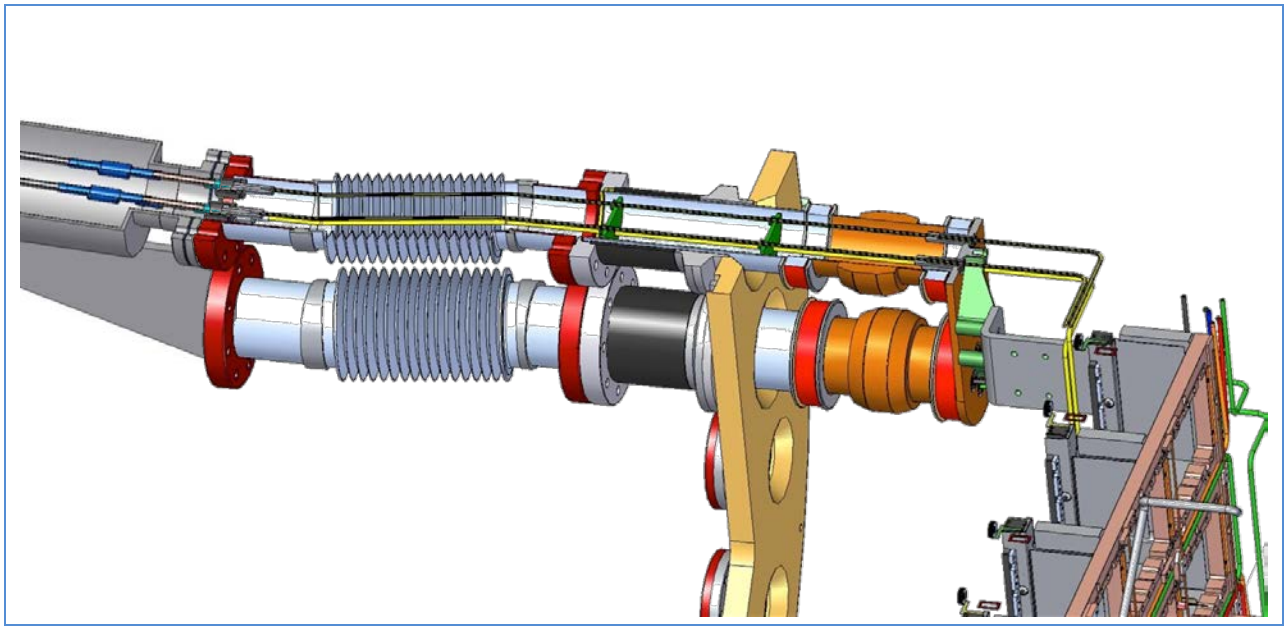

Figure 12-45: Layout of the cryo-feedthrough at the annular ring

12.4.6.1 Mechanical Description of Feedthrough Flange and Penetrations

Signal and Power Feedthroughs

The annular ring itself supports a set of 16 smaller 3 3/8” flanges each of which contains high density signal and/or instrumentation feedthroughs. The feedthrough flanges are fabricated and tested in advance and mount with knife edge seals to the annular flange.

Each feedthrough flange will provide either power or data assemblies the will support up to four science and/or corner rafts.

This arrangement works well for cable routing at the rear of the cryostat. With this organization 10 flanges provide for powering the 25 RTMs and 6 provide for data transmission for the RTMs The 8 larger flanges are used for cryogenic feedthroughs (4) and cryogenic instrumentation (1x) and getter pumps (3X).

At least one company, Douglas Electric Corporation, has been identified for custom feedthrough fabrication. To make these high vacuum quality feedthroughs by their process, each wire is individually stripped and the conductor passivated and then “potted” into an insulating epoxy core which in turn is potted into the metal vacuum flange of the feedthrough. Prototypes of these potted feedthroughs have

been tested for electrical (transmission) properties and found suitable. The epoxy as well has been tested and qualified for high vacuum use in our material test facility. As rafts are integrated, these cables from the REBs to the appropriate feedthrough are dressed, strain relieved, connected and tested.

Cryogenic Feedthroughs

The annular ring also contains four bayonet-like vacuum feedthroughs each with four 0.3cm diameter fluid lines running through it. These feedthroughs reside within the cryostat on the sides orthogonal to the pumping plenums. Three of these feedthroughs carry the 12 cryogen supply lines into the cryostat for cooling the cryoplate. One is used for the 4 cryogenic lines from the coldplate.

The feedthroughs themselves are comprised of a large diameter tube welded to the annular feedthrough flange on one end and a flange on the other. This flange is used to attach and seal the heat exchanger vacuum. A smaller inner tube is welded to this same flange and extends through the larger outer tube past the annular feedthrough plate and into the cryostat vacuum enclosure. On the end of this tube are two strain relief vacuum bellows with a ceramic electrical break in between. The end of this assembly is capped with a seal plate through which the refrigerant tubes pass. By welding the refrigerant tubes at the seal plate, the cryostat vacuum is effectively sealed for the heat exchanger vacuum. A bellows on the heat exchanger end of the assembly allows for interconnect of the refrigerant lines on the heat exchanger vacuum side. On the outside of the cryostat vacuum (but inside the refrigeration system vacuum) the individual refrigerant lines have ceramic electrical isolation breaks brazed in. These breaks in parallel with the larger break on the feedthrough assembly isolate the cryostat ground from the cryoplate ground. The overall assembly prevents a leak on the heat exchanger side from contaminating the cryostat vacuum while also providing an extended conductive path isolating the cold refrigerant lines form the warm annular feedthrough flange.

12.5 Cryostat Assembly and Test

12.5.1 Philosophy

The design of the cryostat allows for its complete assembly and testing prior to raft tower integration. In particular, all the elements of the cryostat will be assembled and tested for mechanical, vacuum, thermal, performance, and for contamination properties prior to the integration of the higher risk items (RTMs, L3 optics). Work is done in a clean room and once assembled; the cryostat need not be disassembled for the subsequent integration, save for the removal of the front L3 dummy flange and the rear octagonal pump plate. This strategy significantly reduces risks of introducing problems during raft integration, and performing work in proximity to the delicate sensors and L3 optics.

12.5.2 Cryostat Assembly and Test Sequence

An assembly fixture is mounted on the assembly stand and each element in the cryostat is mounted to this fixture in turn, starting from the front of the cryostat with the grid and flexures working back to the cryoshroud and cryoplate support ring assembly. Grid cold straps are installed and the cryoplate is mated. The outer shrouding is assembled and sensor and heater cables are routed. The feedthrough plate is fit and welded in place to the cryo-feedthroughs on the cryoplate. Cabling is interconnected and tested. After final alignment and continuity checks the cryostat housing is slid over the internal assembly

and the grid flexures are secured to the front flange of the housing. The assembly tooling is removed and the pump plate and L3 blank are made available for initial vacuum checks. Once the roughing system lines are attached, the cryostat can be pumped down, leak checked and a pump/purge and warm bakeout can be done. Cryo and cold lines can next be fitted up, leak tested and functional testing of the cryo and cold systems performed, as well as uniformity of the plates. Cold focal plane metrology can also be started to check grid flatness. When finished the cryostat is warmed up and vented. The L3 blankoff is removed as is the pump plate, in preparation for raft Integration.

12.6 Utility Trunk

12.6.1 Utility Trunk Requirements

The utility trunk houses and supports power supplies, and instrumentation and support electronics that cannot reside within the cryostat or the Camera body, but do need to be “on Camera.” The utility trunk also houses the on-Camera elements of the refrigeration system. The utility trunk provides a support, a thermal controlled environment and power for these components.

12.6.2 Utility Trunk Design

The utility trunk is cantilevered off the back of the cryostat support cylinder as shown in Figure 12-46.

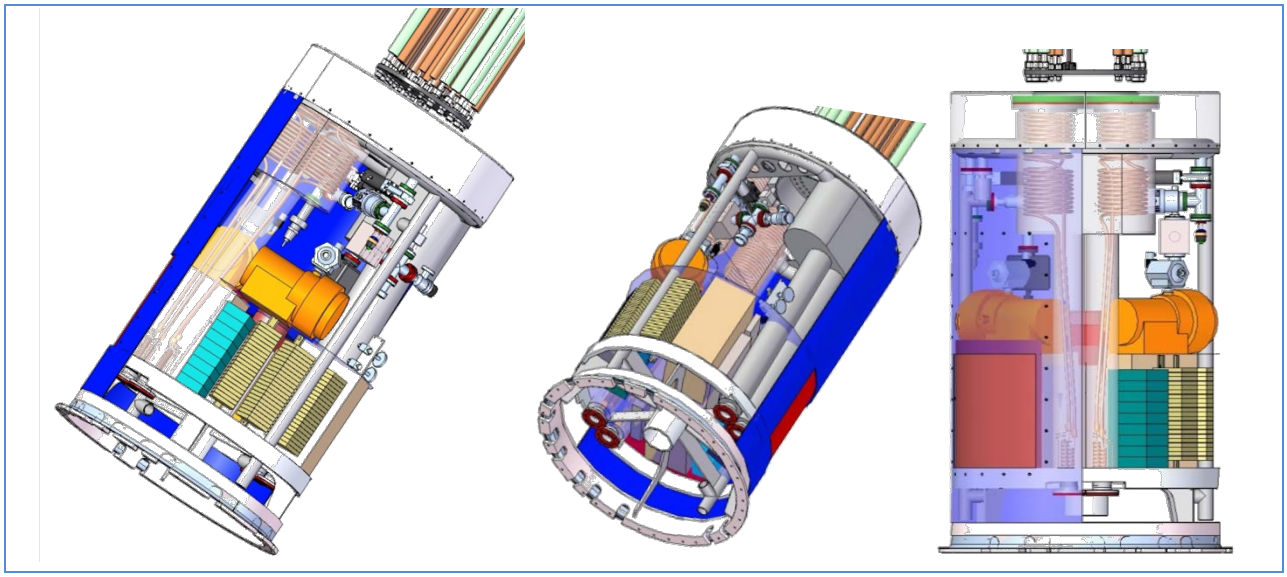

Figure 12-46: The utility trunk (three views)

The utility trunk weighs ~200 kg, divided about equally between the structure and internal contents. The utility trunk structure is comprised of a three-dimensional skeleton of welded aluminum tube, cylinders and plates. The utility trunk structure is integral with the refrigeration heat exchanger vacuum enclosure and supports the loads of the components housed in the utility trunk, while providing clear access for assembling the hardware and service during operation. To achieve this internal bracing is provided and the utility trunk cover panels are shear elements of the finished assembly. The panels are sealed to maintain a closed, clean volume inside the utility trunk. This is important since the utility trunk must

isolate the internal thermal environment from that of the telescope dome and follow the loaded cryostat into the clean room for any Camera servicing.

The side panels add structural rigidity to the utility trunk, but they can be removed to gain better access. Some elements inside the utility trunk --such as the power supply crate--are expected to need easier access, so doors have been added to the panels. The doors can be unlatched and slid open to access boards in any of the electronic crates. The doors will also provide access to key valves in the vacuum, purge and refrigeration systems.

The utility trunk is 94 cm in diameter and 179 cm long. Near the back of the cryostat it contains the vacuum pumps and gauges for managing the cryostat vacuum systems. Custom electronics crates are installed in a region that is accessible through the telescope mounting structure which allows for replacement of individual boards in the field (without dismounting the Camera) if necessary. The back third of the utility trunk contains the vacuum-insulated heat exchanger canister for the refrigeration system, along with vacuum roughing pumps and valve panels for the Camera body purge system and utility trunk cooling.

Inside the utility trunk, the structural includes interface mounting points for the components that mount in it. Table 12-5 lists the equipment housed in the utility trunk along with the subsystem that is delivering it.

Table 12-5: Utility Trunk contents

SUBSYSTEM	ITEM
Aux Elec	Power (AC and DC) conditioning and distribution
Aux Elec	Power supply crate
CCS	Networking
Aux Elec	Timing and sensor data handling
Aux Elec	Camera Protection System controller
Cryo	Heat exchanger canister for the cryostat refrigeration system
Cryo	Evacuated conduit for the refrigerant lines
Cryo	Vacuum pumps, valves, and vacuum instrumentation
CB&M	Camera purge system
Aux elec	Cable harness and trays
Cryo	UT cooling ducts and blower units

More detail may be found in Chapter 18 and earlier in this chapter. The utility trunk is designed to enable relatively quick mounting and de-mounting of the modular hardware. This simplifies both the interface development and the actual mounting process. The mechanical interfaces for most of the elements are defined simply as a set of bolt patterns and mounting rails.

The utility trunk also provides a supply of cold air for cooling electronic crates and other heat sources in the utility trunk. Glycol is brought into the utility trunk from the telescope top end cap assembly. This glycol is circulated through those elements cooled directly by glycol (e.g.: electronics crates) and also through an air-glycol exchangers. The exchanger is in a plenum which ducts and circulates the cooled air. The air is circulated through the utility trunk, down the plenum by a fan, across the exchanger, which removes heat from all sources in the utility trunk not directly cooled by glycol. Air then flows out the plenum into the back of the cryostat where elements of the vacuum system located there are cooled. The air circulates up through the utility trunk to where the heat exchanger vacuum components and additional hardware is cooled, then down the plenum and across the exchanger again. Sensors will monitor component and structure temperatures, to ensure that warm components are within their safe operating limits.

13: Filter Exchange System

13 Filter Exchange System

13.1 Introduction

The Filter Exchange subsystem provides the capability to change filters remotely during the course of nighttime Telescope operations. Given the survey nature of LSST and the multiple science programs that the observatory is supporting, filter changes will be a regular occurrence during a typical night of operation. Thus, the Filter Exchange subsystem must reliably and safely change filters quickly and with minimal impact on the night observing schedule.

The camera houses five on-board filters and includes the capability for swapping in a sixth filter during a daytime maintenance access. As shown in Figure 13-1, the filter exchange system includes three sub-assemblies to provide this functionality.

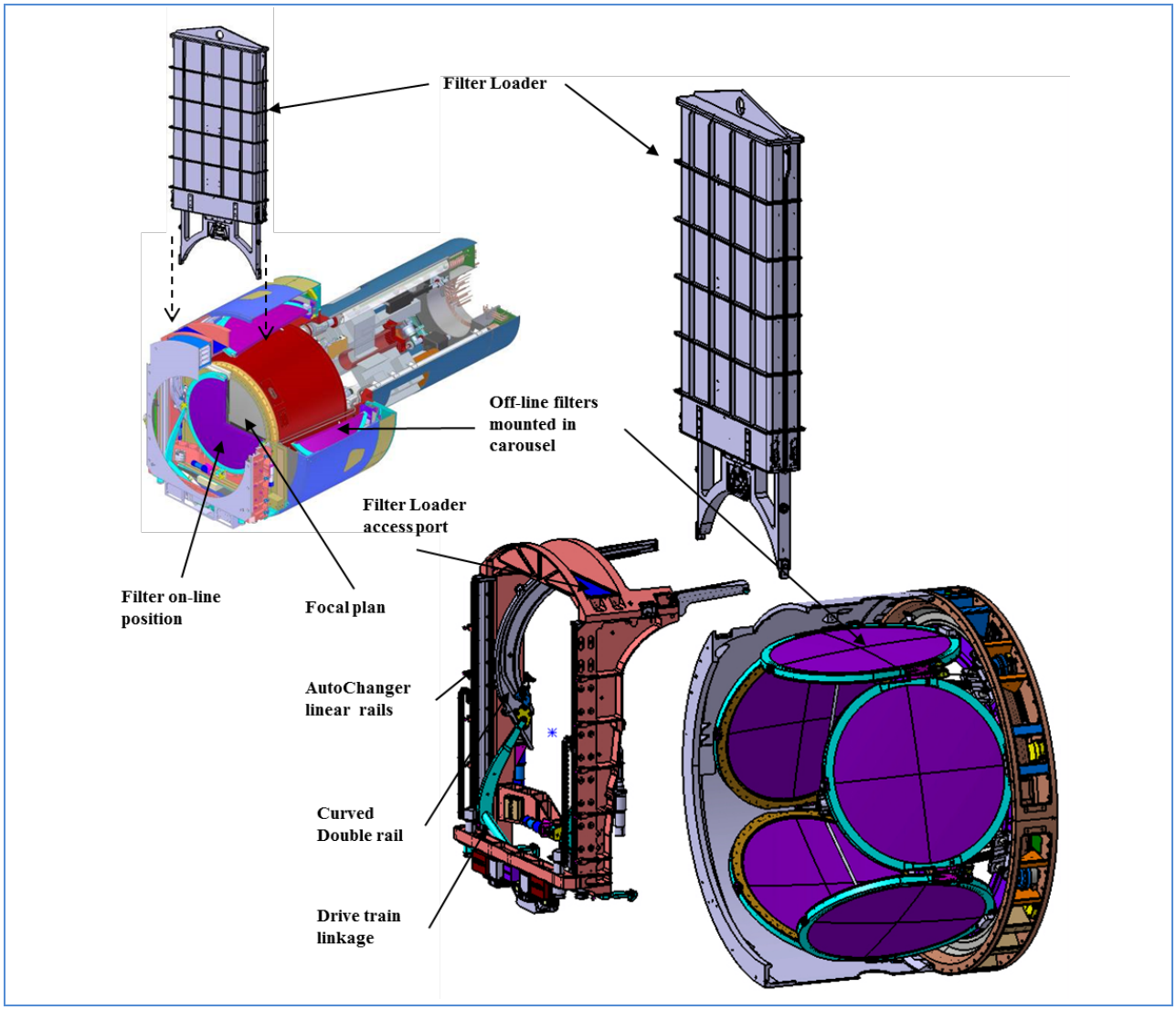

Figure 13-1: Filter exchange system components inside the camera

The Carousel holds the filters that are not in use, and moves filters into position for placing them on-line when needed. The filters sit in cradles on a ring bearing that surrounds the cryostat, with the filters oriented 90 degrees to their on-line position. The selected filter is moved into the light beam by the Auto Changer. This mechanism shuttles the filter from its slot in the Carousel, forward and around the edge of the cryostat and L3 lens, to the on-line position between the L2 and L3 lenses.

Finally, a Filter Loader is used for swapping out a filter during daytime access. The Filter Loader engages with the internal Auto Changer rails to ensure a smooth and safe hand-off of the filter. All three of these assemblies ensure that the large-diameter filters are handled safely, and can be accessed and brought on-line quickly to maximize viewing time.

13.2 Requirements

Key exchange system functionalities and performance requirements are shown in Table 13-1. These are requirements that address the filter exchange system as a whole. Specific requirements pertaining to the Auto Changer, Carousel and Filter Loader are shown in Table 13-2, Table 13-3, and Table 13-4. In the general filter exchange system requirements, the key driving requirements that drive the design deal with the physical packaging filter change time, operation reliability, and the ability to swap in external filters without removing the camera from the telescope.

The exchange system must support filters in the field-of-view. Given the large acceptance angle of the camera optics, the filter clear aperture is very large—756 mm in diameter. This is half the diameter of the camera housing itself, and leaves little room for the mechanism and structure of the exchange system. Additionally, the filters need to be stored completely within the confines of the camera housing to stay out of the light cone as well as to reduce the likelihood of particulate contamination. This eliminates design options that extend beyond the camera housing, and limits the exchange system volume to the constraints of the camera housing. This also drives lower level requirements on the cleanliness of the exchange system components, and especially of the moving parts and lubricants.

Regarding the change time, any of the filters stored inside the camera must be brought to the online position within 89 seconds. Such an operation comprises the following steps: START 1) rotate the camera so the YZ plane is parallel with gravity, 2) disengage the online filter clamps, 3) transport the filter to the empty Carousel slot in the standby position, 4) engage the Carousel filter clamp, 5) disengage filter latch, 6) move Auto Changer trucks away from Carousel, 7) rotate Carousel to the desired filter, 8) move filter trucks to filter, 9) trucks engage filter latch, 10) disengage Carousel clamps, 11) transport filter to online position, 12) engage online clamps and release the Carousel filter clamp END. Each of the steps mentioned above will be described in more detail in the following sections. These steps are enumerated here to demonstrate that the filter exchange process is complex and the time for each step must be carefully allocated with appropriate speeds and timings set to ensure reliable exchange times.

The next general system requirement that drove the design is the reliability of the exchange system. This is related to the exchange time in that running motors faster would reduce the exchange time, but would increase forces, stresses and wear rates in the components shortening their maintenance

intervals. To ensure that the filter exchange system is operational 100% of the time the camera sends an exchange command, the relationship between speed and reliability must be optimized. The scheduled maintenances are only once per year, so the exchange system is designed to operate for uninterrupted intervals of one year when subjected to all its load and cyclic environments. The annual scheduled maintenance affects the Auto Changer and Carousel components. The Auto Changer is designed to be removed and installed as a single module from the Camera Body. There will be two Auto Changer units. When a unit has been used for one year, it is removed and replaced with the other unit which has already been through a servicing and performance verification test. The Carousel is packaged tightly within the camera body volume and cannot be removed without significant de-integration of the camera. Therefore, the servicing must be done while on the camera. The electronics and motors are accessible from the perimeter of the camera. Internal parts requiring replacement, cleaning or lubrication are performed through access ports in the camera body. Should there be a failure in the Exchange System, servicing times are designed to be performed within one eight hour shift, which could be done during daytime accesses.

Finally, the requirement of being able to swap out any filter in the camera with an external filter necessitated the design of the Filter Loader. The Filter Loader is like a cartridge that removes and inserts filters from the camera via an access port built into the Auto Changer structure. A minimum of two loaders will be used for one swap-out operation. First, an empty Filter Loader would remove one of the filters from the camera and that loader would be set aside while the second loader containing the desired filter loads the filter into the camera. This operation would take place during daytime access and would take an estimated 1 hour to complete.

Table 13-1: Filter Exchange system functional capabilities and key driving requirements

Requirement Title	Requirement
	General Requirements
Lifetime	The filter exchange system shall be designed for an operating lifetime of at least 15 years
Operating environments	The exchange system shall be designed to operate in and survive the environments and loads and with the factors of safety defined in the LCA-68, the "Camera Environmental Specification"
Filter swap in place	A filter in the camera shall be replaceable without requiring removal of the camera from the telescope
	Filter Exchange System Requirements
Filter change time	The time to change filters installed in the camera shall be less than 89 seconds after receipt of command from the CCS

In addition to the overarching Filter Exchange requirements, each of the components has their own set of requirements. The Auto Changer key driving requirements are shown in Table 13-2. The most challenging Auto Changer requirements deal with maintenance and subsequent requirements. Besides holding up to the sheer number of cycles before maintenance, these subsequent requirements include ensuring precise repeatability and cleanliness without affecting other camera components. As mentioned above, the Auto Changer is designed to be removed and installed in the camera body in one piece. This is a challenging requirement because any changes in the camera body stress field caused by this operation could affect the positions of other components attached to the camera body. For example, the L1-L2 assembly, also attached to the camera body, could shift in position and introduce image error. The performance requirements of the Auto Changer deal with the positioning of the filters in the online position. This requirement is achieved through the fine adjustability of the filter online fiducials, in concert with the installation repeatability. This allows the fiducials to be adjusted and aligned in the lab, knowing that these positions are preserved after installation in the camera. The moving parts in the Auto Changer will generate particulates that could contaminate the optics, so the components are designed to seal or capture the particulates and cleaned during the annual scheduled maintenance.

Table 13-2: Auto Changer Key Driving Requirements

Requirement Title	Requirement
Design cycles	The Auto Changer shall be designed for at least 100,000 changes
Auto Changer required attitude	The Auto Changer shall be capable of moving a filter to/from the hand-off location with the Carousel with the camera X-axis horizontal and pointed at any altitude from zenith to horizon
Min maintenance cycle	The Auto Changer shall be designed for a time between planned preventative maintenance of at least 10% of its lifetime as defined by requirements C-EXCH-028 or at least 1 year, whichever is shorter.
Clear field of view	The Auto Changer mechanism and filter support hardware shall not obscure the field of view
Light scattering	All components with a direct view of the field of view shall either be shielded by light baffles, painted flat black, or treated/shaped to minimize scattering
Interface to Filter	The Auto Changer shall accommodate filters as defined in the Filter Interface Definition Drawing, document LCA-71

Carousel key driving requirements are shown in Table 13-3. Though simpler than the Auto Changer, the technical challenges of the Carousel are significant due to the extremely limited space within the camera

volume. It is tightly packaged between the Cryostat and the Camera Housing, holding 5 filters in a pentagonal configuration. The minimum static clearances are small, so the motion and dynamics must be carefully controlled. The circular ring gear drive system is attached to the Back Flange of the camera and cannot be removed without significant de-integration of the camera. Routine maintenance must thus be performed in place on the camera. Since the filter masses are all different, the combined center of gravity changes with each filter exchange. The Carousel clamps must be fail-safe because a failure could lead to a dropped filter and catastrophic results.

Table 13-3: Carousel Key Driving Requirements

Requirement Title	Requirement
Number of sockets	The Carousel shall have 5 sockets available to store filters
Design rotations	The Carousel shall be designed for at least 35,000 rotations with no refurbishment requiring removal of the camera
Design clamp cycles	The Carousel shall be designed for at least 30,000 clamp/un-clamp cycles
Min maintenance cycle	The Carousel shall be designed for a time between planned preventative maintenance of at least 10% of its lifetime as defined by requirements C-EXCH-050 and C-EXCH-106 or at least 1 year, whichever is shorter.
Interface to Filter	The Carousel shall accommodate filters as defined in the Filter Interface Definition Drawing, document LCA-71

The Filter Loader key driving requirements are shown in Table 13-4. The design is driven by the cleanliness, swap out time and the interfaces to the Auto Changer and Filter frame. The loader is itself a clean, sealed storage container for a filter. Besides this, there is a purge system, and all internal mechanisms are sealed or booted to prevent particulate contamination. The filter swap out time is estimated to be less than 1 hour, without including crane operation time. To meet such a fast swap out time, the procedure must be very simple, reliable and accurate. In order for the handoff to occur between the Auto Changer and the Loader, the Loader must extend in a precise way to engage and disengage the Auto Changer trucks.

Table 13-4: Filter Loader (Manual Filter Changer) Key Driving Requirements

Requirement Title	Requirement
Cleanliness	The filter loader shall maintain an ISO 5 (FED STD-209, class 100 equiv.) or better environment for particulates as defined in ISO 14644-1 clean room environment for a single filter during handling, storage and swap

	out operations
Manual filter change time	The time to swap out an external filter with one installed in the Camera shall be < 1 hour
Interface to Filter	The Manual Changer shall accommodate filters as defined in the Filter Interface Definition Drawing, document LCA-71

13.3 Filter Exchange System Design Description

13.3.1 Functional Design Overview

The nomenclature used for the Filter Exchange System is shown in Figure 13-2.

The total time budget to change a filter is 120 seconds where: 30 seconds to rotate the camera to vertical (+X axis horizontal) is given to the telescope, 89 seconds to perform a filter change is given to the Filter Exchange System, and one second for control system overhead goes to the CCS time budget.

To meet the 89 seconds time requirement, the Carousel and Auto Changer mechanisms must move the filters quickly around the shutter and delicate optics inside the camera body volume. To accomplish this safely, the physical envelope within which the filters can move must be tightly controlled. Since the filters are large, they cannot be stored with a simple one degree of freedom linear rail system.

The Carousel holds up to five filters and rotates around the camera bore axis to place the selected filter in the hand-off position. The filters are arrayed around the bore axis in a pentagonal configuration facing radially inward towards the center of the camera. The fail-safe clamps hold the filters in place while in the off-line position. The clamps are part of a support structure mounted to a precision circular bearing.

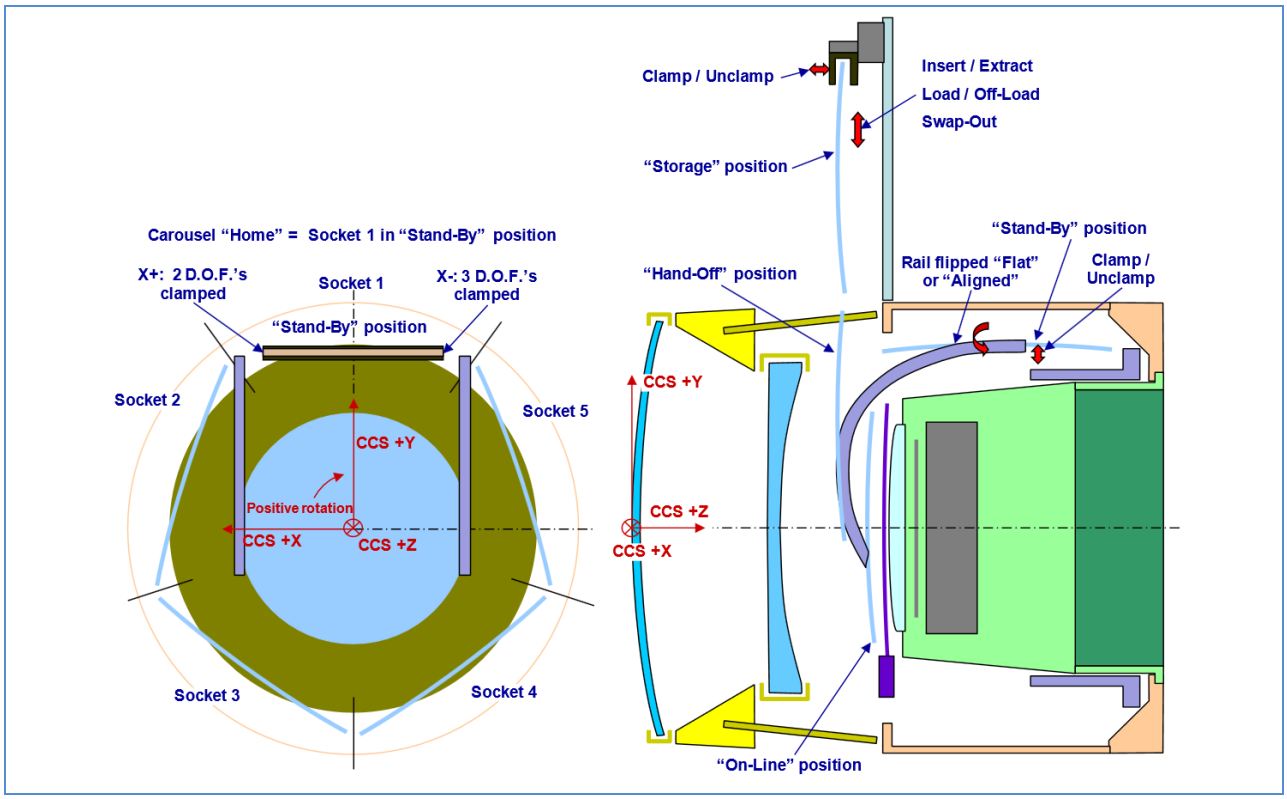

Figure 13-2: Filter exchange system nomenclature

The Auto Changer curved double rail is extended at the stand by position with a reduced section rail. That can be done because the path of the filter is straight and the shape is simpler than for the curved region. This reduced section allows the Carousel to rotate the filters into the Stand-by position without collision. The extended rail facilitates the hand-off of filters from the Carousel to the Auto Changer, guiding keys on the Auto Changer trucks into sockets in the filter frame; in the last 15 mm of the rail, the width of the rail V shape increases by 0.2 mm, which frees the truck when it starts to be centered on the filter frame, and so that the hand-off can be done without an over constraint.

When the truck is engaged in the filter frame, there are latches on the trucks. The latches are closed with electric jacks. When the frame latches onto the keys, the Carousel clamps are released and the filters are moved into the online position. The path that the filter takes from the stand-by position to the online position involves both translation and pitch rotation of the filter. The translation of the filter is defined by curved rails that guide the Auto Changer trucks.

The pitch rotation of the filter is accomplished by a pivoting following arm attached to the truck. The arm angle is defined by a roller that rides in a groove in the curved rails. The filter is moved along a pre-defined path past the cryostat into the space between the shutter and L2 into its online position. In the online position, the filter position is no longer defined by the trucks, but by stationary fiducials attached to the Auto Changer structure. See Figure 13-3: Filter change sequence

Figure 13-3 visually walks through the filter change process. Note that steps “A” and “B” and “0” are not part of the Filter Exchange System 89 second change time allocation. CCS is the Camera Control System, FCS is the Filter Control System. The FCS is a component of the Filter Exchange System. For each operation, 1 s is allocated for the control/command time. Those durations are the maximum allocated duration.

Table 13-5: Sequence maximum time allocation

N°	Operation	Sub-system	duration (second)	Time
0	CCS to FCS : Command Change filter	FCS	1	#VALUE!
1	Check the system configuration	FCS	1	2
2	Open the Online Clamps	AutoChanger	5	7
3	Check the system configuration	FCS	1	8
4	Filter goes to Stand By position	AutoChanger	9	17
5	Check the system configuration	FCS	1	18
6	Open the Latches X- and X+	AutoChanger	4	22
9	Check the system configuration	FCS	1	23
10	Empty trucks go to the Hand-off position	AutoChanger	5	28
11	Check the system configuration	FCS	1	29
12	Power on the brakes	Carousel	2	31
13	The carousel turns and put in place the new filter	Carousel	20	51
14	Release the power of the brakes	Carousel	5	56
15	Check the system configuration	FCS	1	57
16	The empty trucks go to the Stand-by position	AutoChanger	5	62
17	Check the system configuration	FCS	1	63
18	Close the Latches X- and X+	AutoChanger	4	67
19	Check the system configuration	FCS	1	68
20	Unlock the Clamp X- and X+	Carousel	2	70
21	Check the system configuration	FCS	1	71
22	Filter goes to the On-Line position	AutoChanger	9	80
23	Check the system configuration	FCS	1	81
24	Close the On-Line Clamps / Release the Clamps X+ and X-	AutoChanger Carousel	5	86
25	Check the system configuration	FCS	1	87
28	End of sequence Send information to CCS	FCS	1	88
	Total		88	

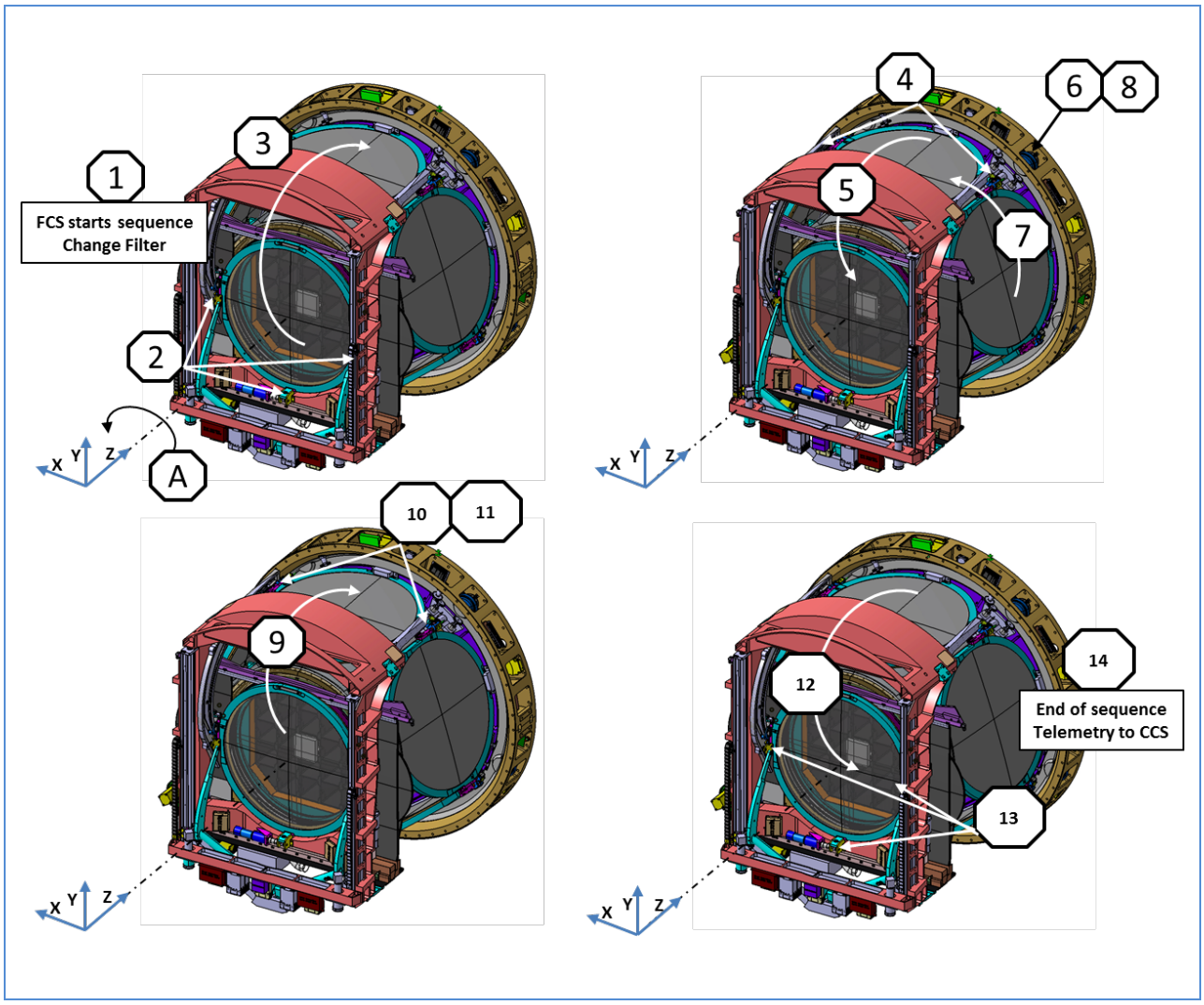

Figure 13-3: Filter change sequence

13.3.2 Electrical architecture overview

This section describes the electrical architecture of the Filter exchange. The figure below illustrates how each sub-system, the Autochanger, the Carousel and the Loader communicate with the CCS through the HCU (Hardware Control Unit), a PC104 which acts as a Ethernet - CAN Open gateway, the CAN Open is the protocol used for the communication of control-command messages of the Filter Exchange.

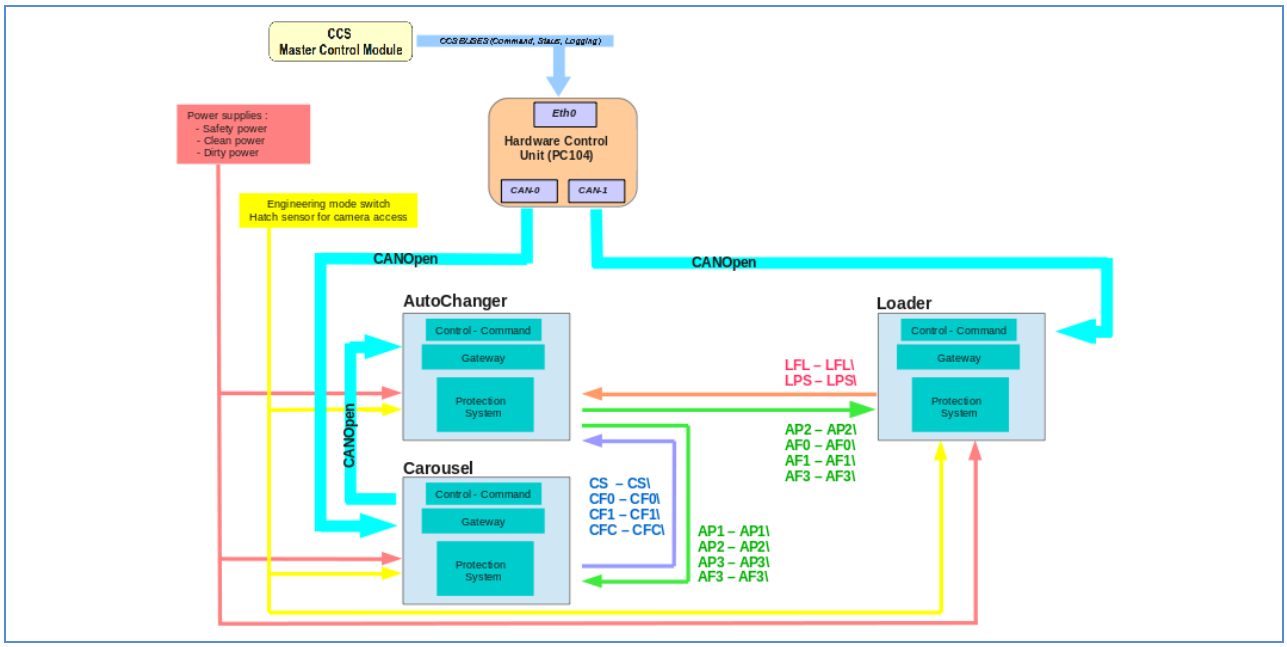

Figure 13-4: Electrical architecture of Filter Exchange

Figure 13-4 shows that the HCU (Hardware Control Unit) makes communication between the CCS and different sub-systems of the Filter Exchange through the CAN bus. Two CAN ports of the HCU are used, the CAN-0 is dedicated for the Carousel and the AutoChanger while the CAN-1 is dedicated for the Loader. Each sub-system has its own hardware devices of control-command and Protection System part embedded.

The Protection System part in a given sub-system is completely independent to other sub-systems and works without any command from the CCS. Logical equations embedded in Safety PLC need sensors status of sub-systems so complementary signals are exchanged between the Auto Changer and Carousel and between Auto Changer and Loader.

Each of the sub-systems are independently powered up by three kinds of powers:

- The Safety Power which is dedicated to power up Safety PLC.
- The Clean Power which is dedicated to power up sensors and electronic part of motor controller.
- The Dirty Power which is dedicated to power up motors, brakes, actuators.

13.3.3 Interfaces to CCS and Camera

The Filter Changer subsystem (Auto Changer, Carousel, and Filter Loader) control is through a hardware and software interface. The hardware interface between the CCS and the Filter Changer interface host is nominally a PC104 and the local device is a CanBus. The software (FCS = Filter Control System) is a written in Java and uses all the standard code provided by the CCS framework to build a software subsystem. It is built as a modular subsystem with CCS software components. Additional details can be found in Chapter 16, Camera Control System.

The interfaces to the camera are defined in a series of interface control documents (ICD) and interface definition drawings (IDD). These interface documents define the mechanical interfaces between the different assemblies, as well as define physical maximum dimensional information. Because the space to navigate a filter is so tight, these definition drawings are of extreme importance. The interface definition drawings related to the Filter Exchange System are: 1) LSST Document LCA-70, "Carousel IDD", 2) LCA-72, "Carousel Swept-Volume IDD", 3) LCA-74, "Auto Changer IDD, and 4) LCA-75, "Filter Loader IDD.

13.3.4 Controls

This section discusses the overall controls architecture for the Filter Exchange system. Sections later in this chapter describe the roles and characteristics of sensors, actuators, and other control devices on the Auto Changer, Carousel, and Filter Loader.

The Filter Exchange subsystem controllers are fully responsible for system and personnel safety. Local controllers provide hardware protection and interlocking to protect against both component or sensor failure or an erroneous CCS command. Interlock and protection sensor status is sent to the Camera Protection System (CPS). The system functions autonomously, but also accommodates manual involvement. Figure 13-5 illustrates the architecture of the control system.

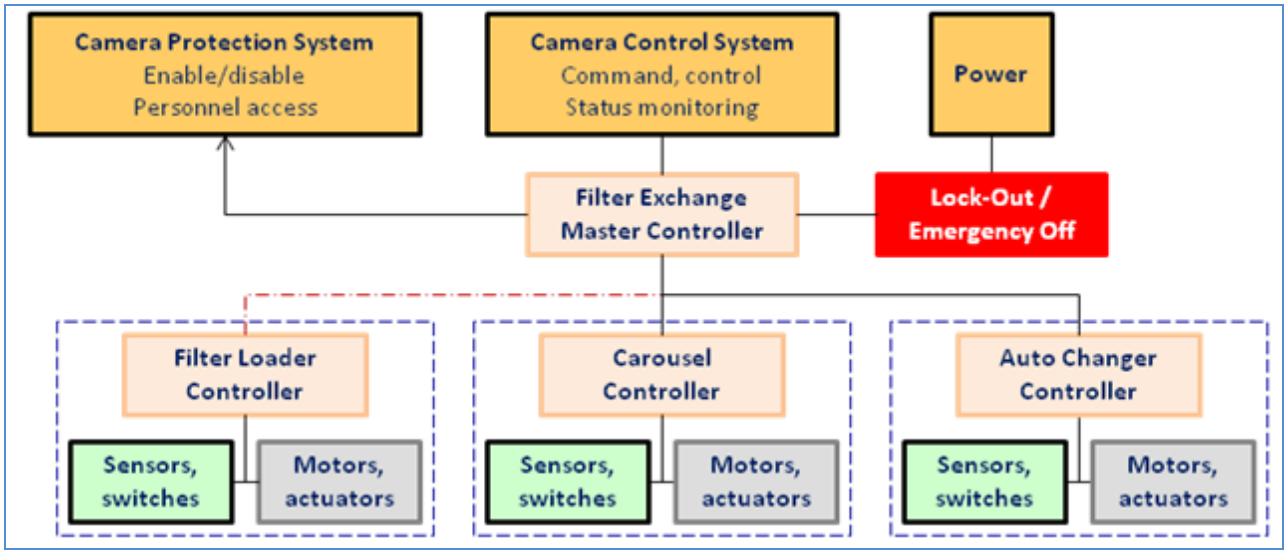

Figure 13-5: Architecture of the controls system for the Filter Exchanger

The control system for the Changer has 4 operating modes: 1) Stand alone, 2) Normal Operation, 3) Filter Swap-out, 4) Engineering Mode for Tests, Fault and Fault Recovery.

The stand-alone operation mode supports a distributed development model in which the Carousel is assembled and tested in Paris, the Auto Changer is assembled and tested in Marseille, and the Filter Loader operates autonomously in the lab.

In the normal operation mode, actions are performed with the integrated Filter Exchange system during observations from the operator's console (e.g., controlled power-up/-down to save power and reduce heat load, autonomous exchange of filters with no operator intervention needed, scrolling through carousel to re-verify the filter complement and positions).

In filter swap-out mode, actions are performed from an engineering console. The Filter Loader is engaged and added to the control logic. In Engineering Mode (Engineering_FAULT), operators can recover the system from a fault or make the system safe to protect it, prior to repair or servicing. In this operating state, some sensors or actuators may not be functioning correctly; therefore, the mode supports local "manual" operation for fault recovery (including overrides) as well as local lock-out and emergency-off switches to provide personnel hazard protection.

Finally, in Engineering Mode (Engineering_OK), technicians can put the system in a state suitable for servicing, troubleshooting, and integration. Here, some or all safety devices and enable/disable switches may be disabled and additional personnel protection protocols are added (administrative or sensors) to protect against hazards.

13.4 Auto Changer Design & Analysis

13.4.1 Auto Changer Design

Figure 13-6 shows the Auto Changer design.

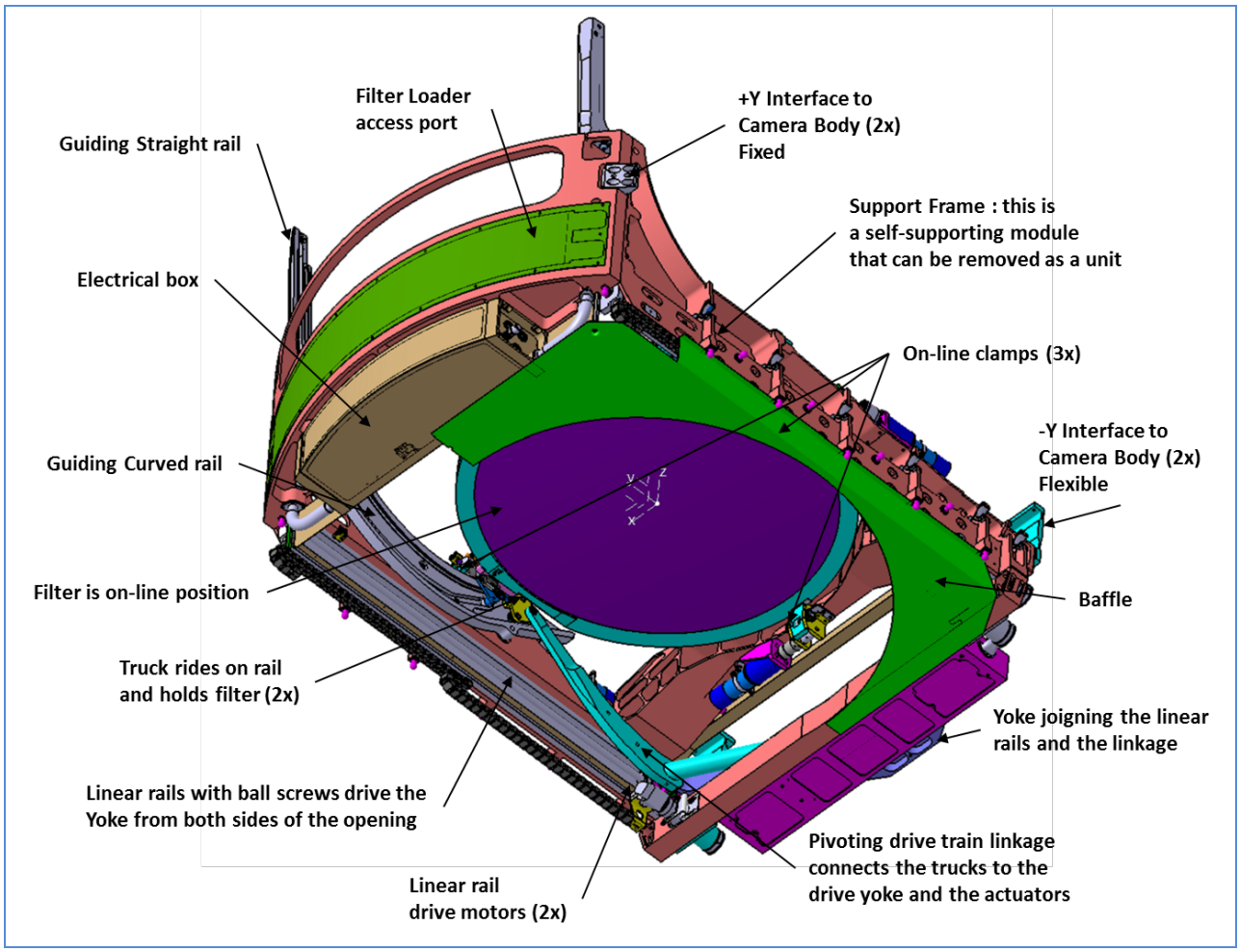

Figure 13-6: Auto Changer with a filter in the on-line position

The Auto Changer moves a selected filter from its stand-by position in the Carousel to the on-line position in the field of view of the camera optics. The filter is moved along two fixed guiding rails by trucks that roll on the rails and support the filter on either side of its equator. Each rail is comprised of two sets guide tracks, with one set supporting the weight of the filter and the second set providing control of the filter angle, as shown in Figure 13-7.

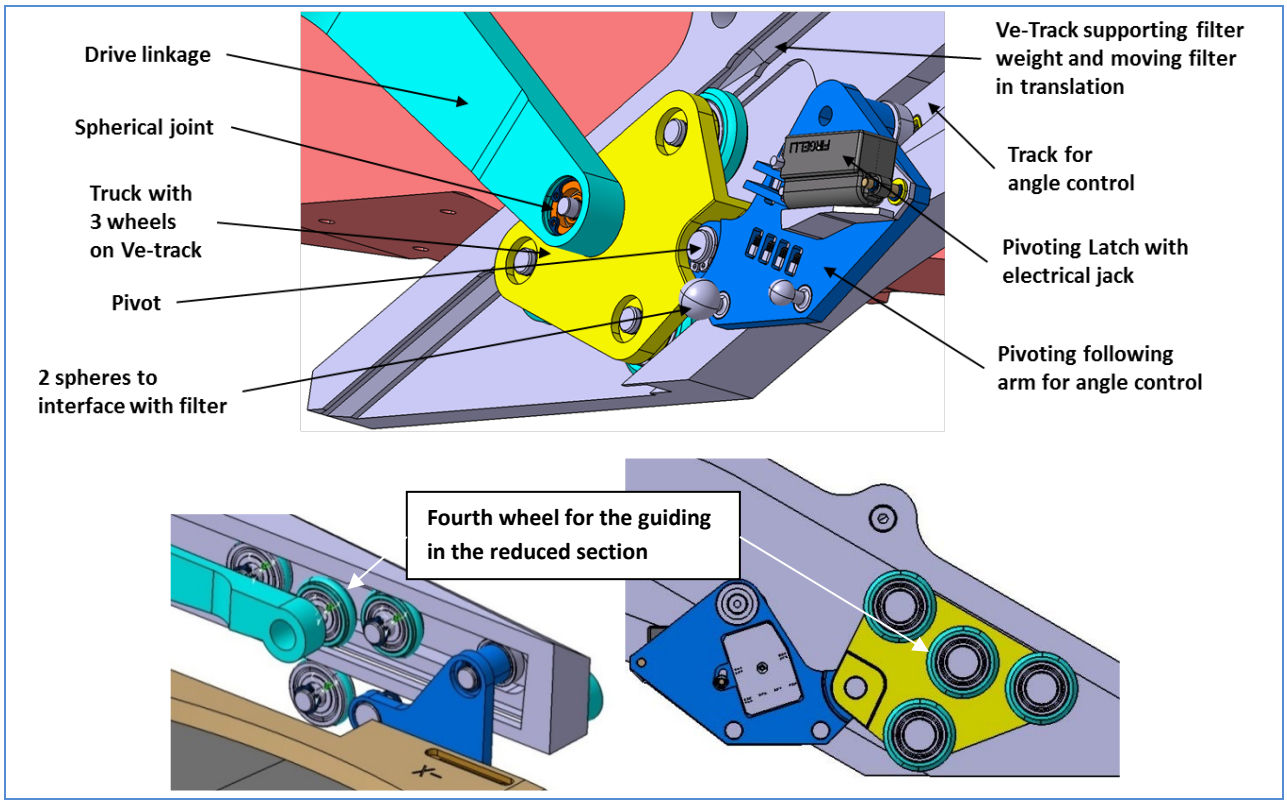

Figure 13-7: Rail detail showing two track design

As the filter is pulled away from its stand-by position on the Carousel, the spacing between the two sets of tracks on the rail changes, thereby tipping the filter and rotating it as it moves around the corner of the cryostat and into its on-line location. By varying the spacing of the tracks on the rails, the filter tip angle is tied to the rectilinear position of the filter along the rail and the sum motion is tightly controlled. Since the mechanical packaging in the camera volume is so tight, controlling the motion of the filter transit is very important. When the filter is transported between its online and standby positions, it comes into close proximity with other components in the camera volume. The closest approach of the second surface of the U-filter (the thickest filter) and the +Y edge of the L3 bezel is ~3mm. In Figure 13-8, the filter's closest approach to the camera body, cryostat, and L2 are shown. Any impact at the speeds the filter is moving would result in serious damage. The mechanical motion control of the filter change also eliminates the need for a tip-angle actuator and the attendant additional complexity. As a result, the Auto Changer includes only one actuated degree of freedom, which is provided by a linear slide and ball screw, with a linkage to tie the linear actuator to the trucks that ride along the curved rail profiles.

The Auto Changer is driven by two electronically synchronized motors with gear reducers, drive pulleys and belts running to two sets of linear slides and ball screws which straddle either side of the camera FOV. Two driven slides are used to ensure that the filter cannot jamb or get wedged in place, as can happen when driving from one side only (akin to closing a dresser drawer while pushing from one edge of the drawer). The drive train is back drivable. In case of loss of power, the mechanism stop is performed with a power-off brake on the motor shaft.

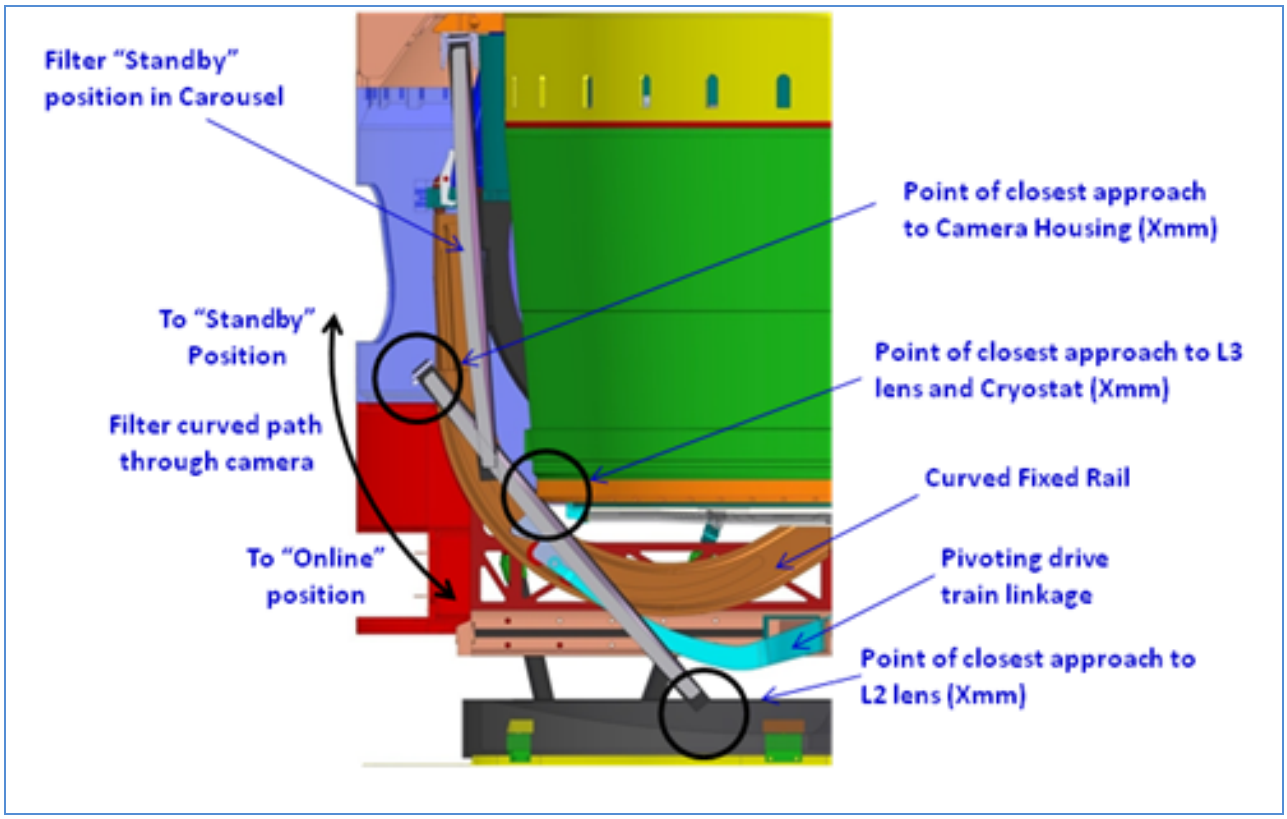

Figure 13-8: Filter curved path through camera, with points of closest approach

The carriages on the two linear drives are joined by a yoke that bridges across the FOV and provides a common central pivot point for the linkage that connects to the trucks that ride on the curved rails. While the slides are long enough to provide the full range of travel needed for a filter, their positions are constrained by the outer diameter of the camera housing. The housing effectively centers the slides on the center of the camera, which is not ideal to cover the entire range of motion of a filter. Thus, the yoke serves to offset the pivot point of the linkage to one side of the camera, which allows the slides to move the filter all the way into the FOV on the camera centerline. As the filter is moved off-line to its stand-by position on the Carousel, the linkage pivots to push the filter around the corner of the cryostat and back along the rail to the Carousel.

The C-shaped linkage mounts permanently to the two trucks with a spherical bearing to allow the trucks to pivot and to provide compliance of the joint to accommodate small misalignments and reduce the likelihood of wedging the filter.

In Figure 13-9, the guiding rail is composed of two parts: the main part with a curved shape is bolted on the Auto Changer, and a smaller part with the straight path at the Stand-by position. The smaller part is bolted and aligned on one side to the curved rail and it is bolted on the other side to the Camera body.

When the Auto Changer is removed from the camera, the smaller part of the rail is unbolted and remains inside the camera. Moreover its cross section is decreased to allow the rotation of the carousel.

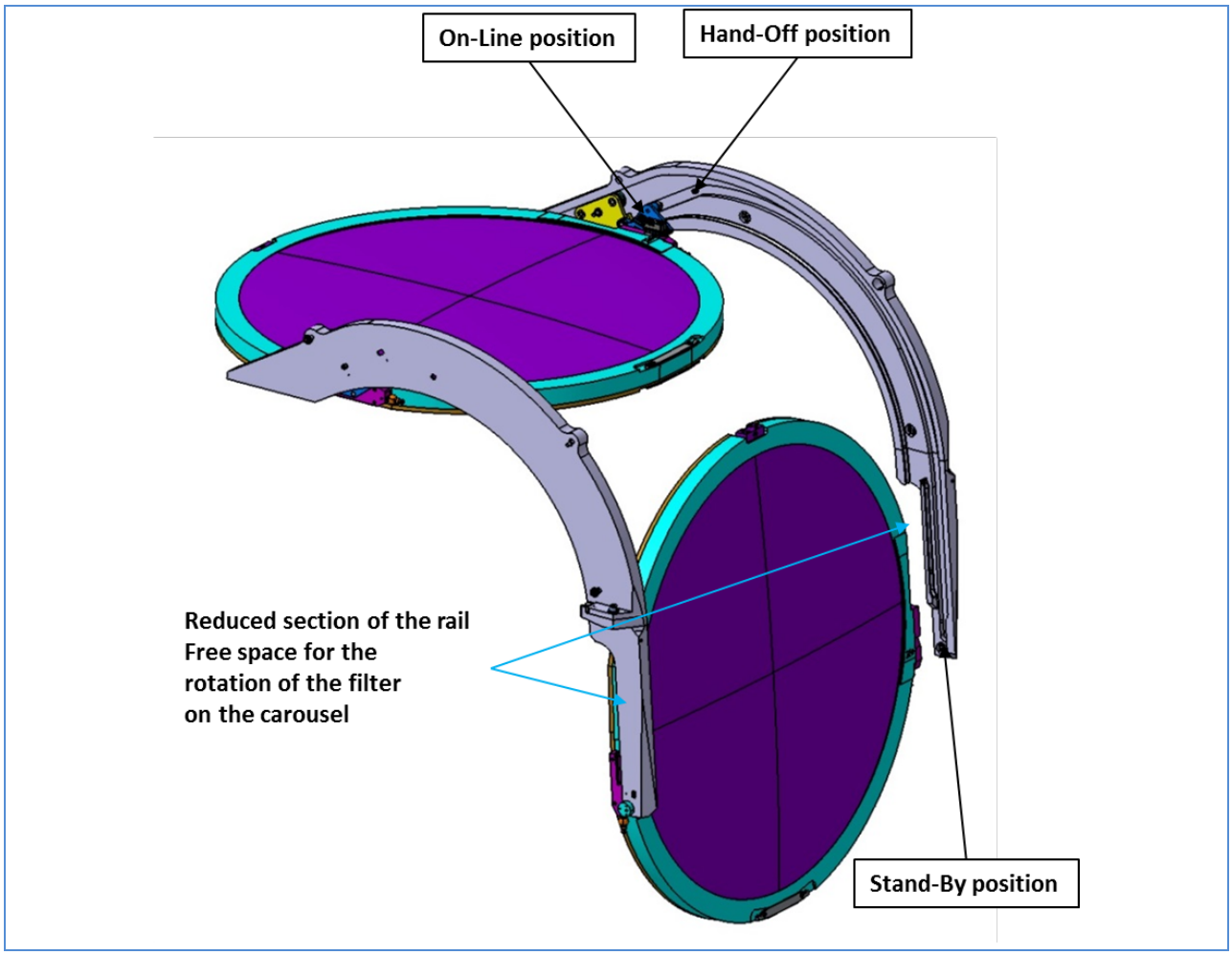

Figure 13-9: Guiding rails and filters at the on-line position and at the Stand-by position

The trucks include four wheels and a smaller fifth one (see Figure 13-7); three V-wheels support the weight of the filter and guide it along the track of the main part. The fourth central wheel replaces one of wheel for the guiding in the straight rail. The smaller fifth sits on a pivoting arm extending off the truck and rides in the second track of the rail. This provides the angular rotation for the filter. The trucks have two spheres that run into a slot on either side of the filter. The trucks also include electrical latch that runs on a tilting finger which locks the filter at each side. The latch mechanism is non-back-drive-able and cannot be released in case of loss of power. The control system ensures that the latch can only be activated when the Carousel clamp or the Loader Clamp is engaged.

As the filter approaches its online position, the weight is transferred from the trucks to support devices on the filter frame and clamps rigidly mounted to the Auto Changer structural frame. The requirements state that the filters must be held accurately and stably and must accommodate different filter masses in all camera orientations. Since all of the online position clamps have fine adjustment capabilities, tolerance stack-ups are eliminated in the alignment process during integration and assembly. The manufacturing tolerances of the filter frames, placement of the filters in the glass, and the mechanical stability of the online-clamps ensure that the positional requirements are met.

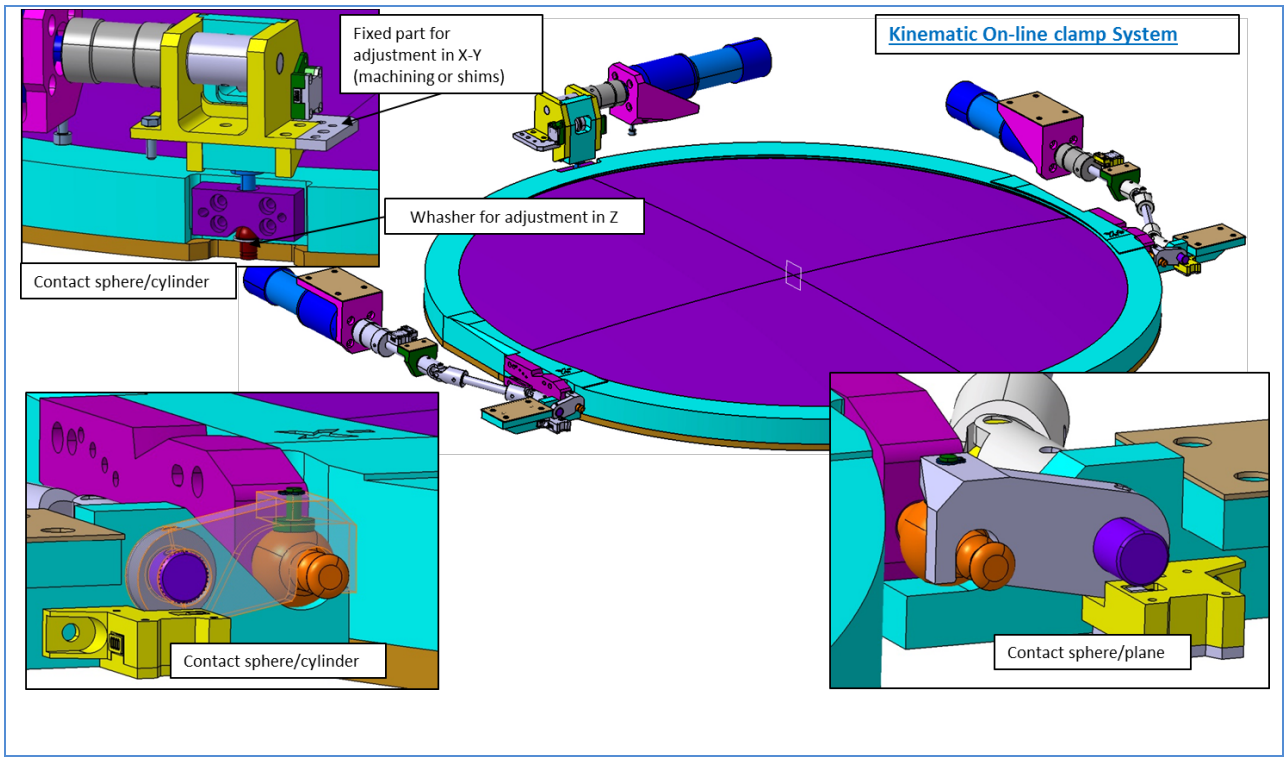

Figure 13-10: Auto Changer On-line Clamp System with kinematic support in three points

The kinematic support configuration has been chosen because of the repeatability requirement given that there are many filter frames, and in order to not constraint from clamping. The kinematic support is composed of contacts with spherical surfaces: a fixed point at the –Y side, a V shape support at the –X side and a plan support at the +X side (Figure 13-9).

The Auto Changer is supported off of the camera body by a support frame consisting of two structural beams that bridge across the enclosed volume. The frame interfaces to the camera body on the +Y side via two sets of pin and bolt joints. The pins allow freedom to rotate about the X axis while the bolt interfaces add hoop stiffness to the camera body cutout. On the –Y side of the structure, there are a set of titanium flexures to support the rail in X and Z translation while allowing compliance in the Y direction. With this interface scheme, the Auto Changer will have a highly repeatable interface while minimizing stress coupling with the camera body structure.

Each beam supports a rail and linear slide, with the entire assembly pre-aligned and integrated as a unit. Light baffles are also mounted to the support beams, to shield all components from reflecting any stray and scattered light, and to define a clean circular clear aperture for the beam as it passes through the filter.

Baffling is provided inside the camera and much of it is supported from the Auto Changer. The requirement is to reduce or eliminate glancing angle views of camera components from the incoming light cone. Optically black shrouds or coatings are used to shield as many camera components as possible. Figure 13-11 shows some of the basic baffles in the design.

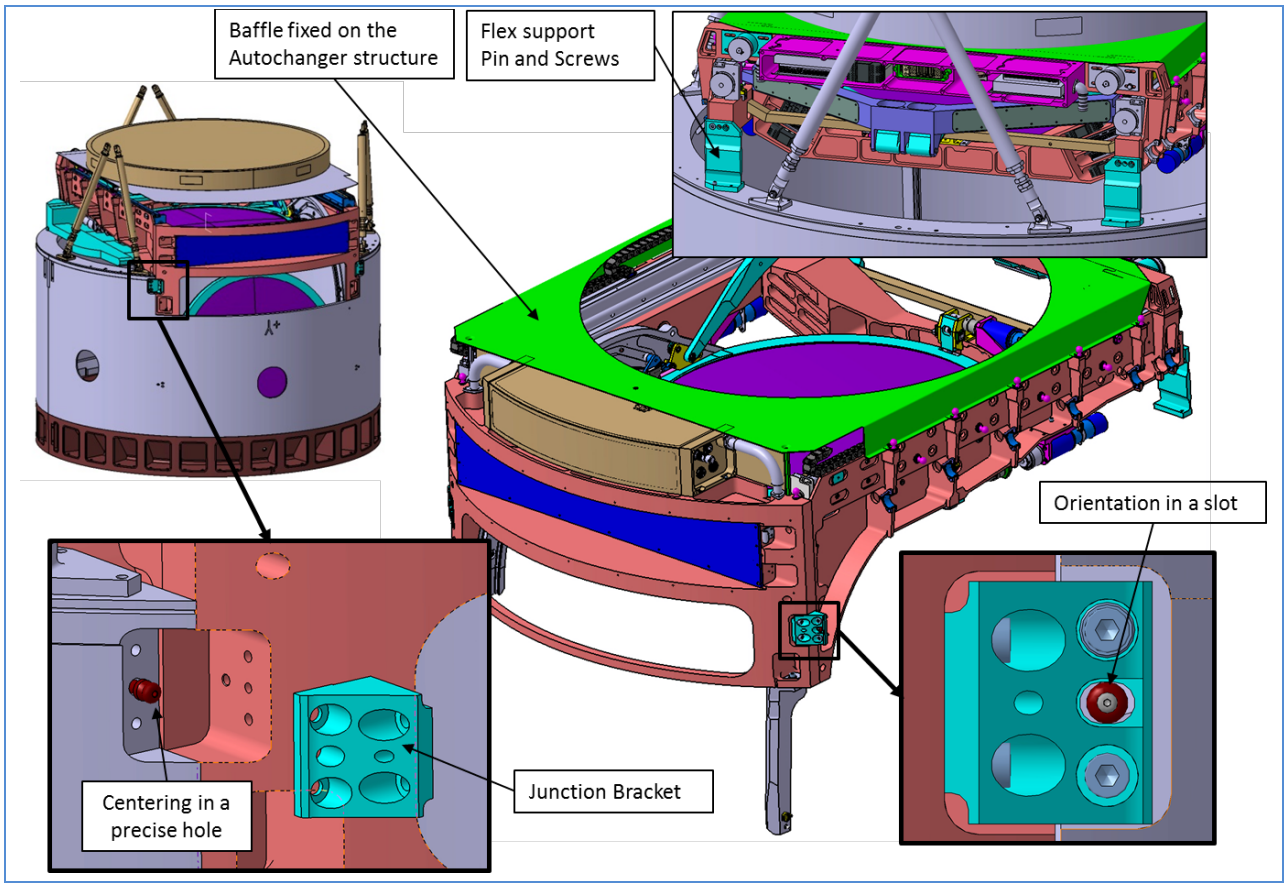

Figure 13-11: AutoChanger structure and Baffling

13.4.2 Auto Changer Protection System

Figure 13-12 shows the architecture of the Auto Changer Protection System. In this architecture, the Protection System works independently and in parallel of the control-command.

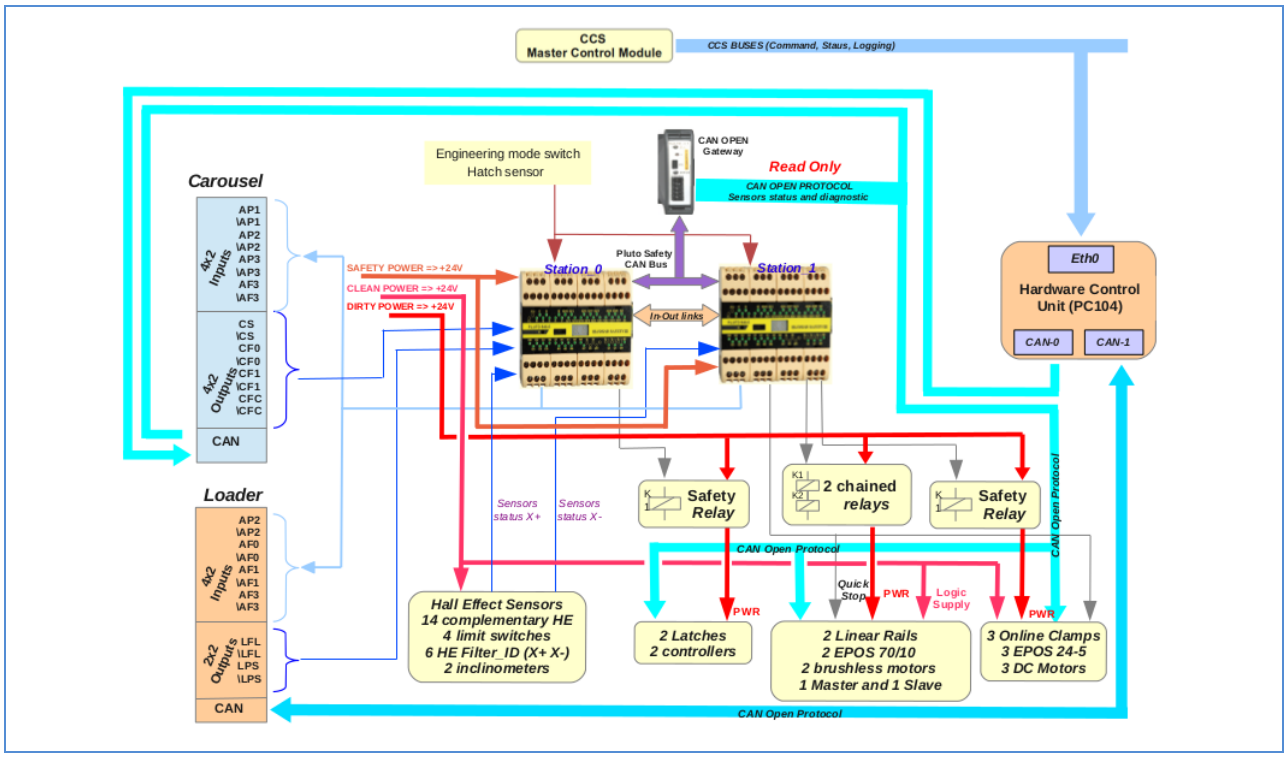

Figure 13-12: Autochanger Protection System

As it is shown in the figure, all sensors of the Autochanger are connected to the inputs of Safety PLC. The Autochanger uses two Pluto B46 as Safety PLC. Security functions implemented in Safety PLC, allow to activate the coil of relays which has for effect to power up actuators and motor controllers.

The status of the relays, activated or deactivated, depends on the result of logical equations embedded in Safety PLCs. The status of sensors and security functions involved in the Protection System are listed in a specific document “LCA-10207 Filter Exchange System Protection Logic”.

In the Autochanger there are three security functions:

- Linear Rails motor enabled.
- Clamps relays enabled.
- Latches relays enabled.

Security functions implemented in Safety PLCs of the Autochanger need also status of sensors located in the Carousel and in the Loader. For that, signals are exchanged in both directions, from and to, between Autochanger and Loader, and between Autochanger and Carousel.

In order to improve the security, signals exchanged between the Autochanger from to Carousel and from to the Loader are transmitted in the complementary mode, that allow to detect a defect, bad connection or a loss of contact.

Even if the Protection system is completely independent of the control-command, the CCS needs to know status of Autochanger sensors before starts any action. That is made thanks to a CAN open Gateway which allow to read any inputs and outputs of Safety PLC, read the status of sensors and signals connected to.

In this architecture there is also 3 separated power supplies:

- The so called “Dirty Power” which power up Clamps and Linear Rails motors.
- The so called “Clean Power” which power up all hall effect sensors, the three controllers of the Clamps, EPOS2 24-5, and the two controllers of Linear Rails motors, EPOS2 70-10.
- The so called “Safety Power” which power up the two Safety PLCs, Pluto B46.

13.4.3 Auto changer analysis

Structural analyses of the Auto Changer was performed. The load cases are defined in document LCA-68. The load cases have been applied in the analyses and the margins have been calculated following the mechanical standard given in the document LCA-280.

The method is to calculate the performance for 1g in each direction and then to combine the results to obtain the considered load case result. The seismic loads are only applied in a permanent configuration (filter clamped at the on-line position).

Table 13-6: Summary of the main load cases that were considered as well as the margin calculation equations

Load definition

Load Case	On-Telescope				Off-Telescope	
	Operable	Recoverable	Survival		Seismic-1	Seismic-2
Transverse	+2.42	+3.70	+5.70	Transverse	+0.85	+0.85
+Z-direction	+0.61	+1.17	+2.04	Vertical	+1.50	+0.60
-Z-direction	-1.44	-1.83	-2.45			
Referenced to Camera Coordinate System (CCS)				Referenced to gravity and mounting orientation		

Values are in g's, where 1 g = 9.81 m/sec²

Operational Load Cases

Load Case	Camera and Subsystems											Auto Changer, Carousel			Filter Loader
	Op-1	Op-2	Op-3	Op-4	Op-5	Op-6	Op-7	Op-8	Op-9	Op-10	Op-11	Op-12	Op-13	Op-14	Op-15
X	+1.00	+1.00	+1.00	+1.00	+0.00	+0.00	+0.00	-1.00	-1.00	-1.00	-1.00	+0.00	+0.00	+0.00	+0.00
Y	+0.00	+0.00	-1.00	-1.00	+0.00	-1.00	-1.00	+0.00	+0.00	-1.00	-1.00	+0.00	-1.00	-1.00	-1.00
Z	+0.00	-1.00	+0.00	-1.00	-1.00	+0.00	-1.00	+0.00	-1.00	+0.00	-1.00	-1.00	+0.00	-1.00	+0.00

Values are in g's, where 1 g = 9.81 m/sec² Orientations are with respect to the Camera Coordinate Systems (CCS)

Re-Pointing Load Cases

Load Case	Camera and Subsystems											Exchange System		
	Repoint-1	Repoint-2	Repoint-3	Repoint-4	Repoint-5	Repoint-6	Repoint-7	Repoint-8	Repoint-9	Repoint-10	Repoint-11	Repoint-12	Repoint-13	Repoint-14
X	+1.10	+1.00	+1.10	+1.10	+0.00	+0.00	+0.00	-1.10	-1.10	-1.10	-1.10	-0.10	+0.10	-0.10
Y	+0.00	+0.00	-1.10	-1.10	+0.00	-1.10	-1.10	+0.00	+0.00	-1.10	-1.10	-0.10	-1.10	-1.10
Z	+0.00	-1.10	+0.00	-1.10	-1.10	+0.00	-1.10	+0.00	-1.10	+0.00	-1.10	-1.10	+0.10	-0.10

Values are in g's, where 1 g = 9.81 m/sec² Orientations are with respect to the Camera Coordinate Systems (CCS)

Margin calculation

$$MS_u = \frac{\sigma_u}{SF_u \cdot \sigma_{calculated}} - 1$$

$$MS_y = \frac{\sigma_y}{SF_y \cdot \sigma_{calculated}} - 1$$

SFu and Sfy are fonction of:
- Material configuration
- Criticality level
- Use case configuration

Msu and Msy have to be positive

Results are given in the document LCA-10198.
Until now all **the margin are positive**

Trucks and Drive Train

As the parts of the drive train are moving, the first step for the calculation of the drive train is to define the loads in the different configurations. We have performed calculations with FEA model in 9 positions of the truck along the guiding rail. For each position we have collected the loads on the components for 3 orientations (Zenith, 45°, and horizon).

The drive train is used as a "transient operation". No seismic load has to be applied. But, in case of jam we added a design "stall factor" of 2 for the margin calculation. All the safety factors are defined in the Table 13-7. A margin value of 0 corresponds to a safety factor of 3.75.

Table 13-7 Definition of the safety factors for the Auto Changer Drive train

Safety factor	Value
MUF = Model Uncertainty factor	1.25
SFy = Yield safety factor	1.25
Stall factor	2
Use case = single point of failure	1.2

Total Safety factor	3.75

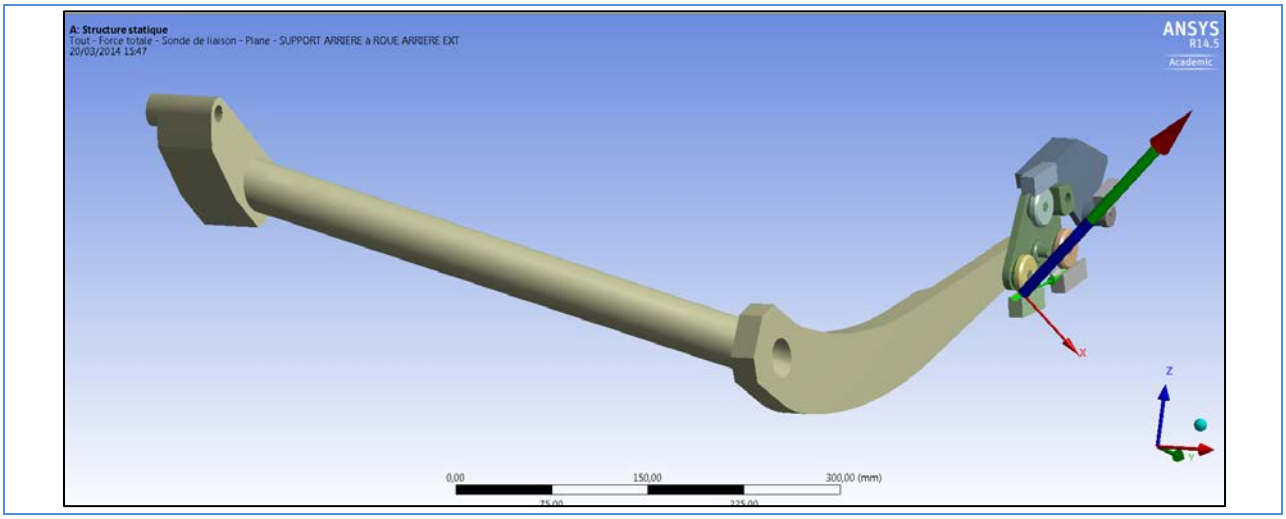

Figure 13-13: Finite Element Model in one configuration of position of the rail and the gravity direction

The loads are taken as the reaction of the joints and the contacts with the rails. They are described in details in the document LCA-10194. The maximum forces are taken for the sizing of the component and the calculation of the margin (Table 13-8)

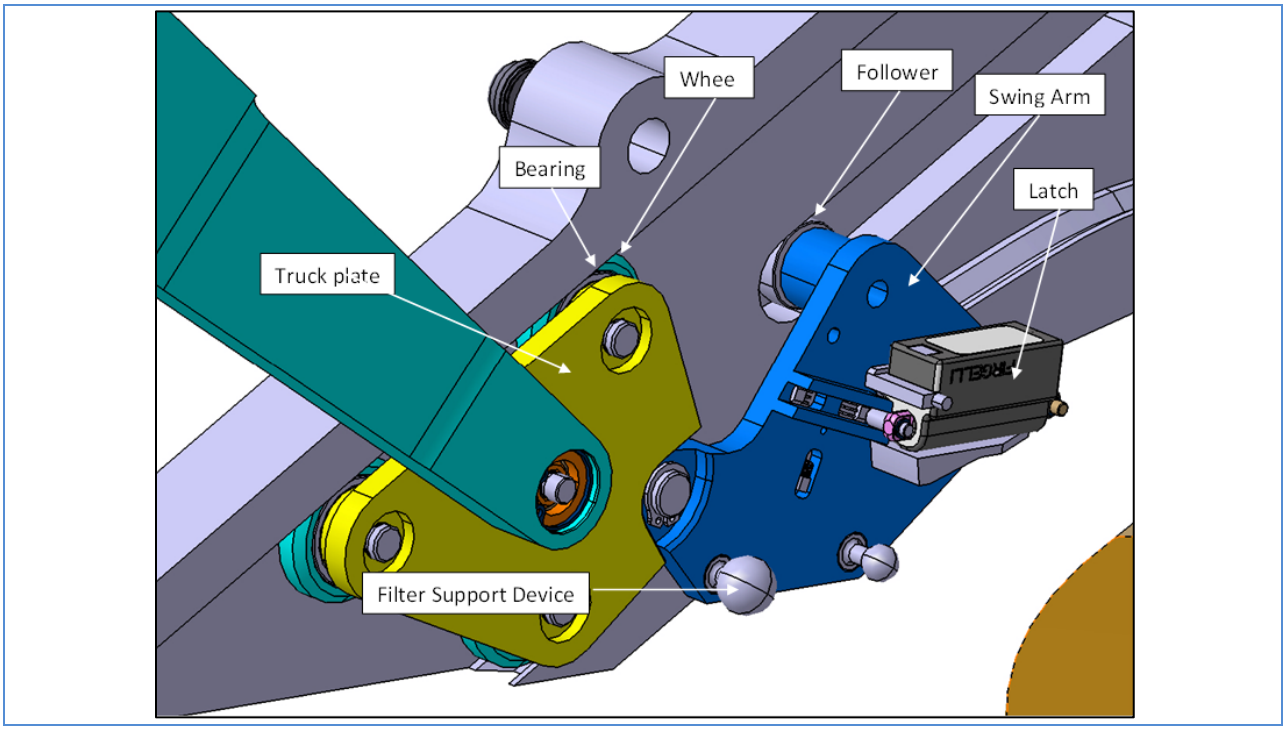

Figure 13-14: Definition of the truck components

Table 13-8: Maximum loads on each drive train components for 1 g

Force description	Value (N)
Maximum radial force on the wheel	514
Maximum axial force on the wheel	127
Maximum reaction force on one face of the rail	376
Maximum force on the follower	103
Maximum forces on the linkage • In plane • Out of plane Total	 332 81 342
Maximum force of the linkage on the Yoke : • Direction Y • Direction Z Total	 -536 -391 664
Maximum force on the linking axle	306

Depending of the component, off-the-shelves or not, the load has been compared to the technical data sheet maximum values, or it has been used in stress calculation. See examples at Figure 13-15.

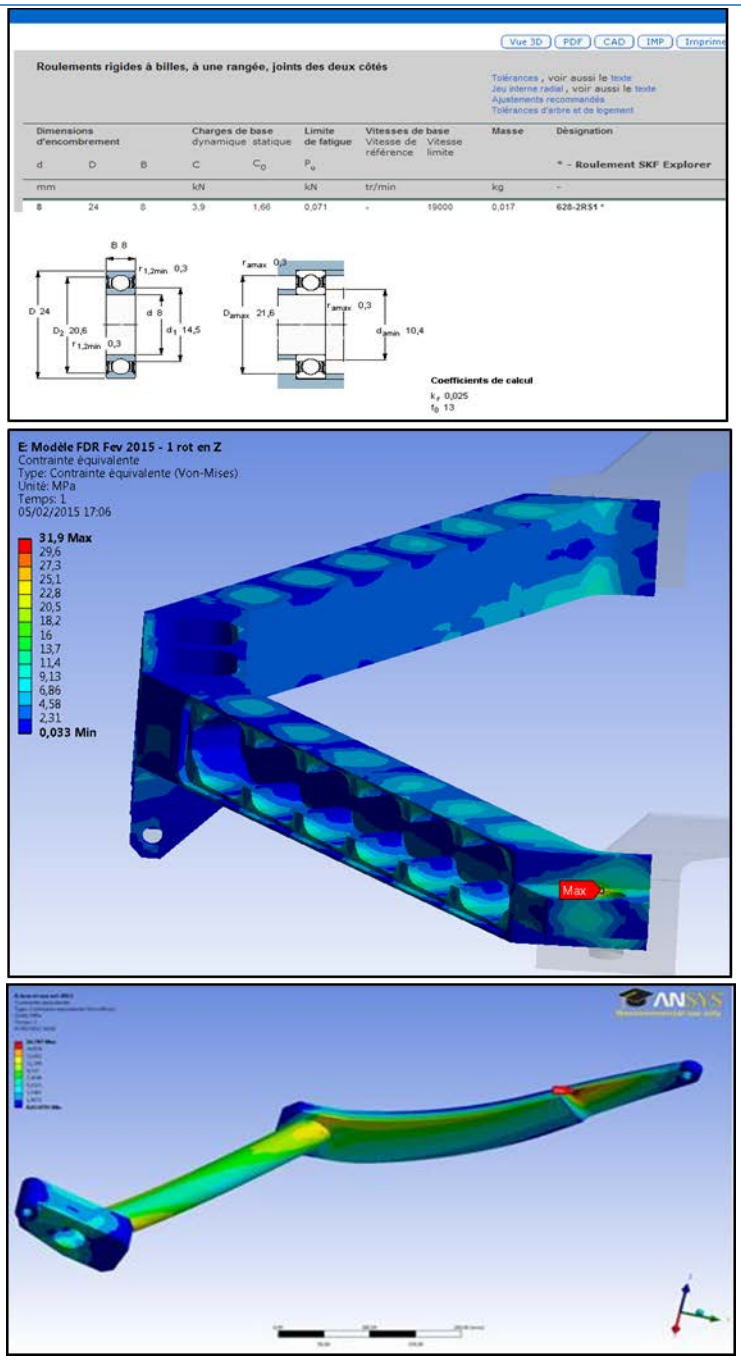

Figure 13-15: Margin calculation in reference of the data sheet or finite element Model results

For the linear rails and the motor system, we considered the maximum load on the yoke, and then we added the weight of the yoke and 100 N for the clamping in the carousel. We have taken into account of the allocated time for the travel of the filter from the on-line position to the stand-by position.

The results are:

- Travel length = 1 m in 7 seconds

- Maximum speed = 0.167 m/s
- Acceleration/deceleration = 0.167 m/s2
- Ball screw lead = 20 mm
- Maximum Rotation speed = 500 rpm = 52.4 rd/s
- Maximum total Load = 1136 N

Considering the safety factor, we have calculated the needed power and torque of the train.

- Power per rail = 190 / 2 = 95 W
- Torque per rail = 3.62 / 2 = 1.81 Nm

Then we have chosen the corresponding components and we have calculated the margin. In the worst case (seismic load), the power is off. We have calculated the margin for the brake and the reducer. The maximum torque will not damage the motor; we have checked that its max working torque is higher than the needed torque.
Table 13-9 gives the results of the margin calculation.

Table 13-9: Margin for the components of the trucks and the Drive train system

Components	Material	Msy	Msu
Wheel bearing	SKF	0.033	-
Wheel	Z160CDV12	4.2	4
Truck Plate	440 C	1.18	2.33
Supporting sphere Ø 8	Z160CDV12(treated)	0.13	0.085
Supporting sphere Ø 12.5	Z160CDV12(treated)	0.22	0.169
Follower	INA	1.05	-
Latch shaft	Z160CDV12	1.9	2.3
Linkage	6082T6	2.15	2.35
Yoke	6082T6	1.17	1.31
Linear rail Reducers	Maxon GP42C	0.32	0.77
Linear rail Brakes	Maxon AB32	-	0.06
Linear rail moment	THK SKR46-A	1.38	-
Liearn rail buckling	THK SKR46-A	3.2	-

Filter On-line Clamp system

In addition to the operational and repointing load, the seismic loads are considered for the On-line Clamp System. The filter fixation points have different degrees of freedom; each fixation point defines the boundary condition of a finite element model of the filter (Figure 13-16). An acceleration of 1g is applied in the three directions. And then we have extracted the force on each fixation point taking into account of the degree of freedom. The combination of the results allows defining the loads for each use case. For the re-pointing load case we have applied 1.1g in any direction (as specified in the document LCA-49 FiltExchSyst specification).

Filter Boundary conditions:

- A: Fixed point (sphere in a spherical hole)
- B: Fixed in Z direction and X direction (sphere in 90° V shape)
- C: Fixed in Z direction (Sphere on a plan)

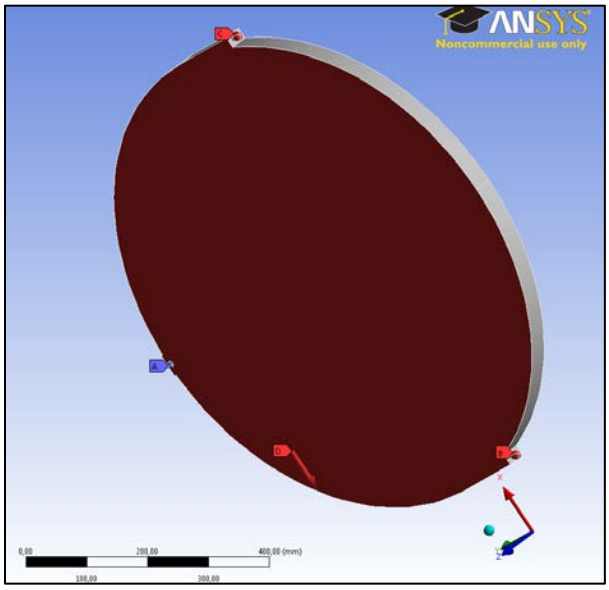

Figure 13-16: Finite element model of the filter with On-line boundary conditions

Before the calculation of the margin ,the minimum value of the clamping force required to hold the filter in place in all configurations has been extracted. The MUF of 1.25 has been applied for the clamping forces.

The results of the analysis are:

Fixation A:

- Clamping Force: 238 N
- Mechanical yield resistance under a lateral load of 1045 N

- Mechanical ultimate resistance under a lateral load of 1600 N

Fixation B

- Clamping Force: 500 N this value insures that the filter keeps in contact with the support.
- Mechanical yield resistance under a lateral load of 800 N
- Mechanical ultimate resistance under a lateral load of 1225 N

Fixation C:

- Clamping Force: 375 N
- The design of the clamps and the drive train is identical to the Fixation B which is more loaded.

In accordance with those results, we have calculated the torque on the drive train of the clamps and then the stresses and the margins in all the components. Figure 13-17 gives an example of the considered configuration.

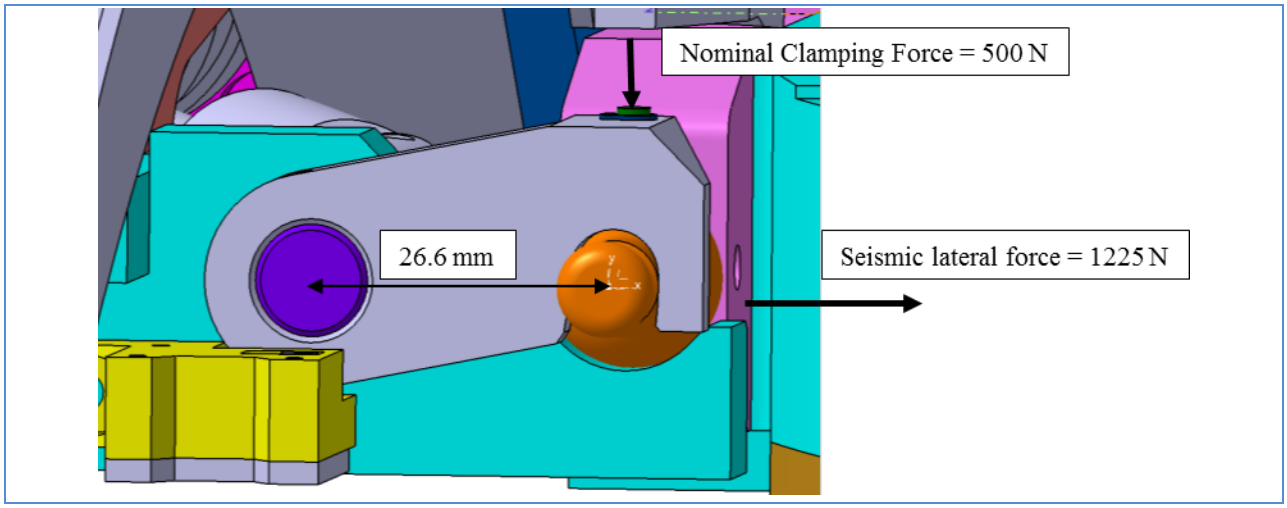

Figure 13-17: Applied Load on the V shape On-line clamp

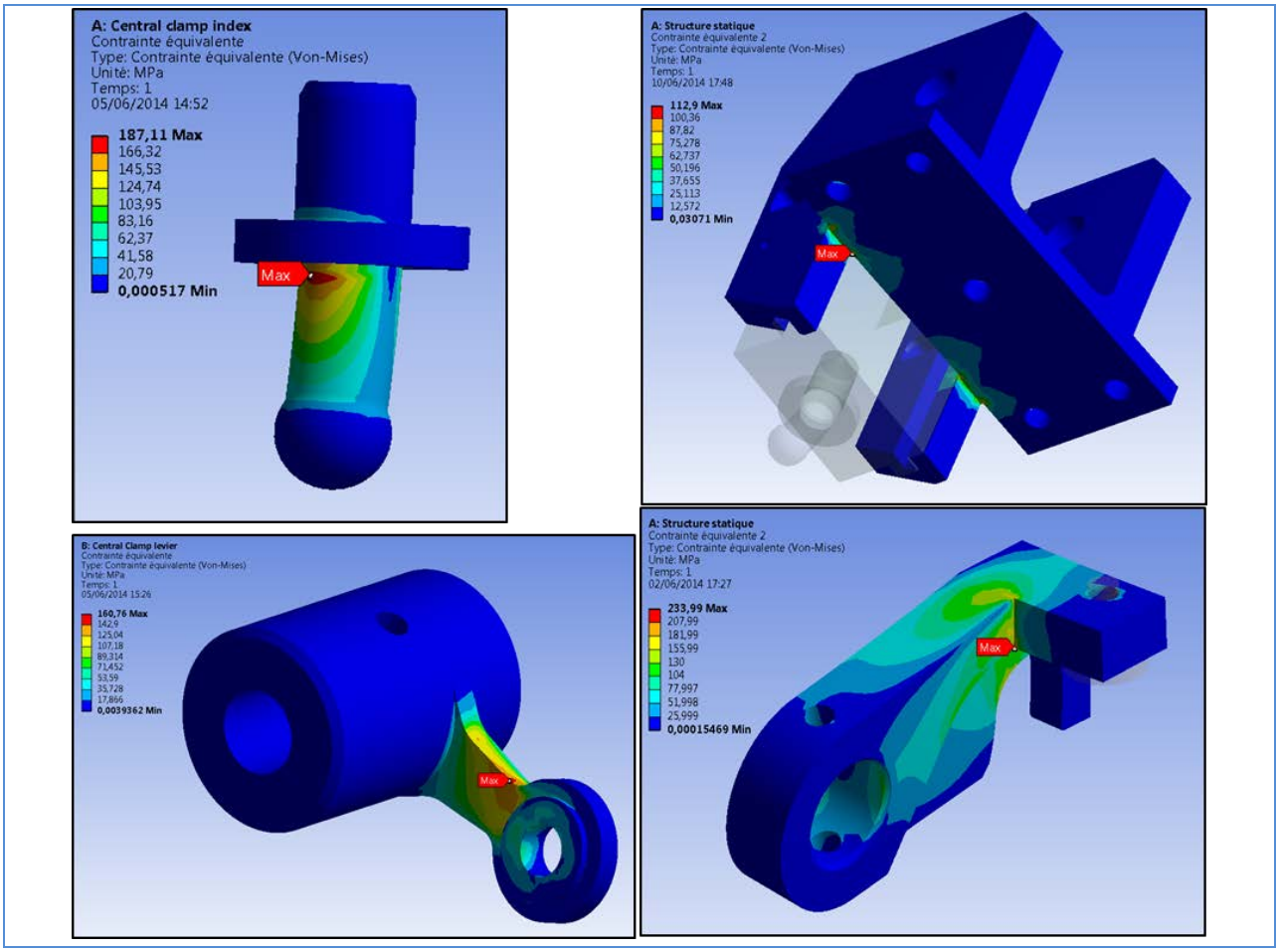

Figure 13-18: Example of the finite element models on the on-line clamp components

The Table 13-10 gives the results of the calculation. Most of the time, we only note the lower values of the margin which correspond to the seismic loads. The motor system is the same for the three clamps. The sizing is done for the most loaded one, the V shape clamp.

Table 13-10: Margin for the Filter On-line Clamp System

Components	Material	Msy	Msu
Ve shape Fixation			
Clamp arm	Z160CDV12 (treated)	1.24	1.4
Clamp pin	HRC 60	2.27	2.53
Brake	Maxon AB28	-	1.31
Reducer	Maxon GP52C	-	0.39
Reducer coupling	KTR	0.11	2.35

Components	Material	Msy	Msu
Universal joint	Steel	-	0.6
Shaft bearing	Iglidur X	21	7.6
Fixed point clamp			
Index	Z160CDV12 (treated)	1.18	1.35
Lever	TA6V	2.45	2.25
Drawer	Z160CDV12	0.32	0.68
Body	K110	0.05	0.34
Plan clamp (less loaded as the Ve shape clamp)			

Structure

The analysis of the structure has been focused on several points:

- The stress level under loads; Dead weight under specified accelerations, weight of the filter loader on the access port at the vertical position.
- The displacement of the filter under nominal loads and under the temperature variation.
- The natural frequency estimate.

All the results came from a finite element model which is describe on Figure 13-19

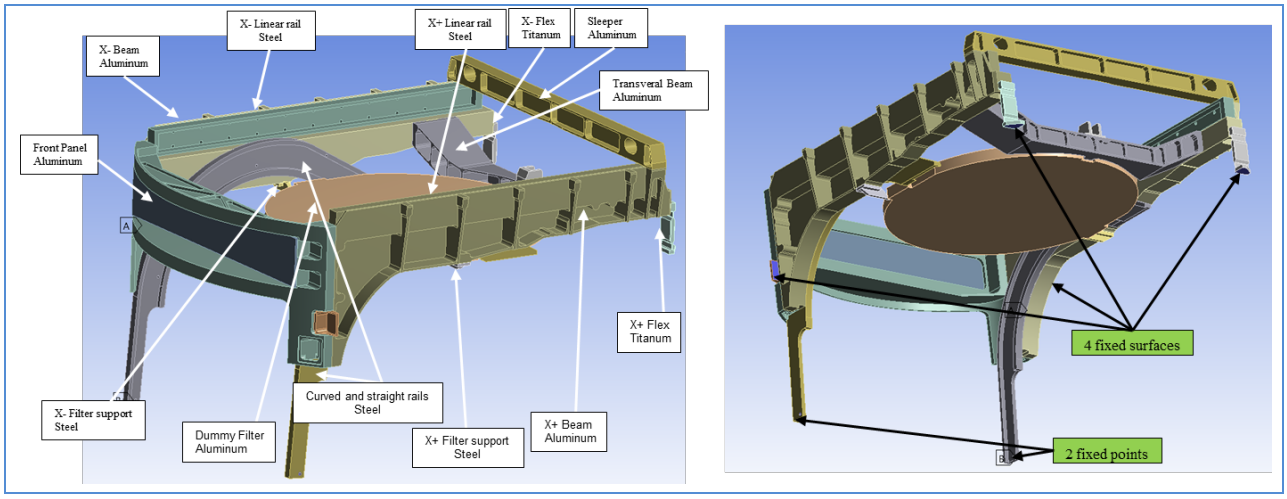

Figure 13-19: Finite Element Model for the structure analysis

The calculated margins corresponding to the highest stress value are given in the Table 13-11. The design is validated.

Table 13-11: Margin for the highest value of stress in the structure components

Components	Material	Msy	Msu
Titanium Flex	TA6V	4.17	4.51
Structure components	6082 T6	4.10	5.12
Bracket	6082 T6	1.57	1.24

Using the same model the value of the filter fixation point has been analyzed. The results have been compared to the specification of the filter position during the observation. A summary is given in Figure 13-20. The worst cases are considered. Most of the values directly meet the requirements. While the decenter when gravity is in the X direction (77 µm for 75 µm max) doesn't meet the requirement, in this direction the effect of the temperature is low and If we compare the sum of the calculated values for gravity and temperature with the sum of the specified values, then the sum is acceptable and we have room to refine the requirement in further work. It is the same configuration for the Tilt from thermal effect (76 µrad for 50 µmax). Therefore the design can be validated.

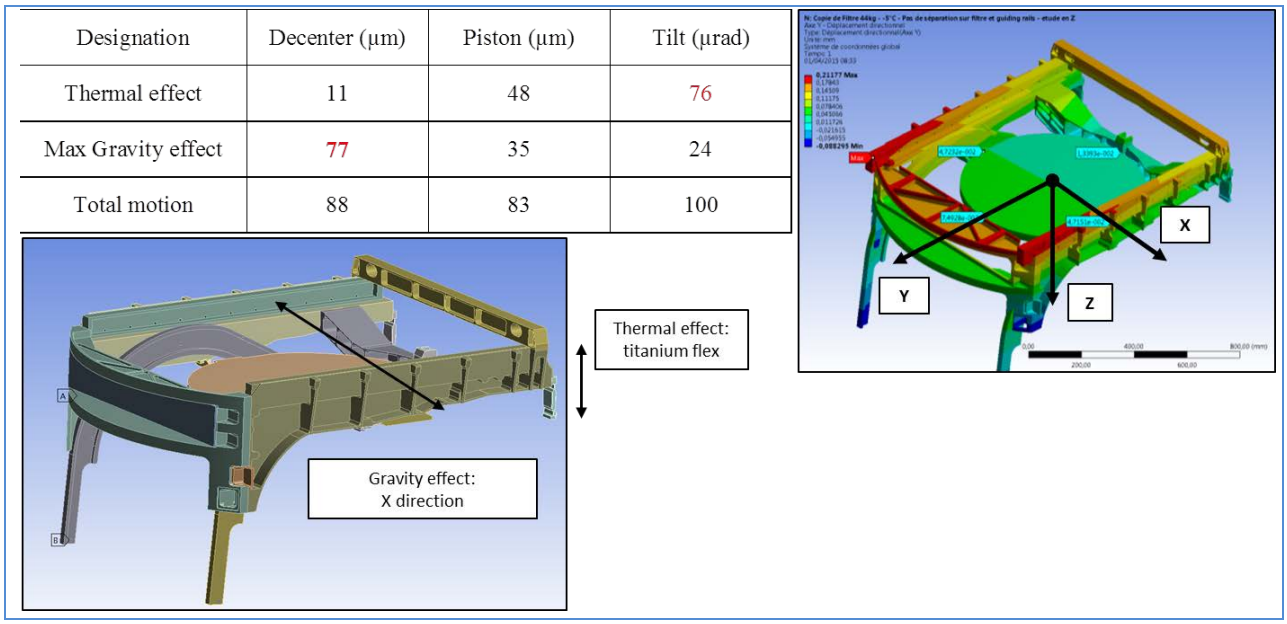

Figure 13-20: Maximum displacement of the filter under dead load and temperature effects

The calculation of the natural frequency is shown in Figure 13-21, which shows that the design meets the modal requirements.

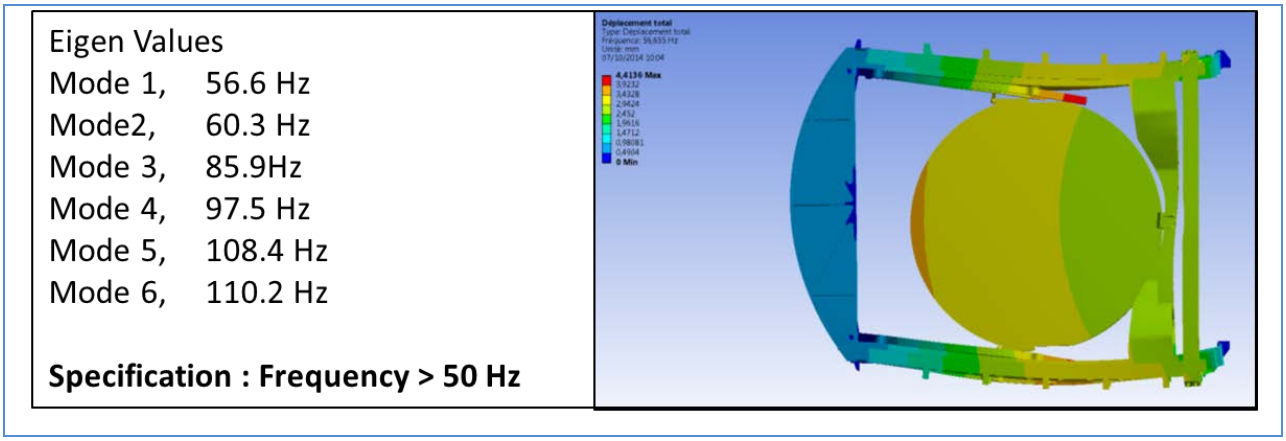

Figure 13-21 AutoChanger modal analysis

Fatigue Analysis and Maintenance Plan

Regarding the specified 100,000 filter changes for the Auto changer, we have calculated the lifetime of the components involved in the filter change.

Following the load configuration and the data sheet of the on-the-shelves components, we used various methods (Figure 13-22).

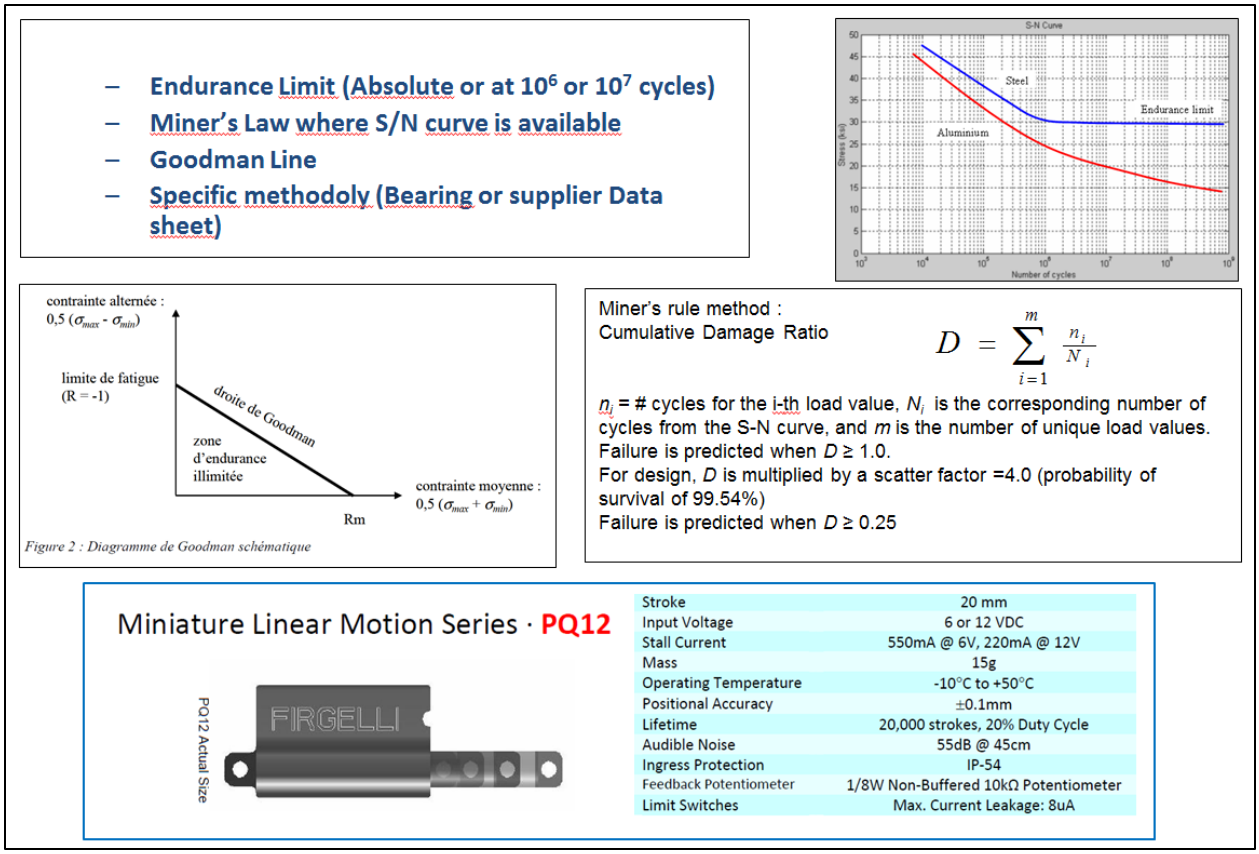

Figure 13-22 Fatigue calculation methods for the Auto Changer's components Lifetime estimate

The results allow identifying the components which need to be replaced before the end of the total lifetime. Thus we can complete the list of spare to be provided and we can define the frequency of replacement of the identified components. Table 13-12 gives an overview of the maintenance plan.

Table 13-12: Additional components supply for average and maintenance

%	Item Description	Comment	Fatigue results Complement to Overage	Replacement Plan
	Filter Exchange System			
25%	Auto Changer truck axles	Overage + Lifetime buy		
25%	Auto Changer truck wheel/bearing units	Overage + Lifetime buy		
50%	Auto Changer Latches actuators X+	Overage + Lifetime	+ 28 units	Every year

	and X-	buy (2 units)	(2 k€)	
30 %	Auto Changer truck positioning HE sensors boards	Overage + Lifetime buy (2 units)		
25%	Auto changer Driving Motor combination + controller	Lifetime buy (1 combination)	+ 6 Combinations (6 k€)	Every 4 years
25%	Auto Changer transmission device	Lifetime buy (1 set)		
15%	Auto Changer Online clamp motor combination + controller	Lifetime buy (1 combination)	+ 3 Combinations (3k€)	Every 7,5 years
25%	Autochanger Online Clamp sensors boards and contact devices	Lifetime buy		
25%	AutoChanger Safety PLC	Lifetime Buy (1 unit)		
25%	Autochanger Relay	Overage + Lifetime buy (2 units)		
50%	Auto Changer X+ and X- truck assembly	Lifetime Buy (1 unit of each)		
50%	Auto Changer linkage	Lifetime Buy (1unit)		

Analysis conclusion

Following are conclusions based on maintenance analysis:

- All the components has been calculated and validated with a positive margin. It is important in term of single point failure to check that even under the highest load the filter will not drop or there will not be any collision.
- The components which don't meet the 100 000 changes requirement are identified, they will be supplied and the maintenance plan for their replacement is defined.

13.5 Carousel Design & Analysis

The Carousel design, driven by several key requirements, depends on 1) Size, mass and stiffness of the different filters, 2) cleanliness of components for both particulate generation and low temperature

outgassing, 3) tight space constraints between the camera housing and cryostat, 4) ability to sustain the high number of cycles and maintainability, and 5) ability to operate in any camera orientation and sustain any load condition.

The Filter Carousel supports filters inside the camera body when they are not in use in the field of view (FOV). Each filter has a clear aperture diameter of 690 mm, and the heaviest has a mass of 36 kg. The Carousel can support from zero to five filters, accommodating any filter in any azimuthal location, or "socket" up to a maximum filter mass of 44kg. The filters are mounted around the perimeter of a large ring. Continuous circular ball-rails mount directly to the camera back flange and support the rotating ring which, in turn, supports the posts and clamps that hold the filter frames. The ring also supports the large ring gear that is used for rotating the Carousel to place the selected filter in the stand-by position in preparation for moving it on-line. The Carousel parts can be seen in Figure 13-23.

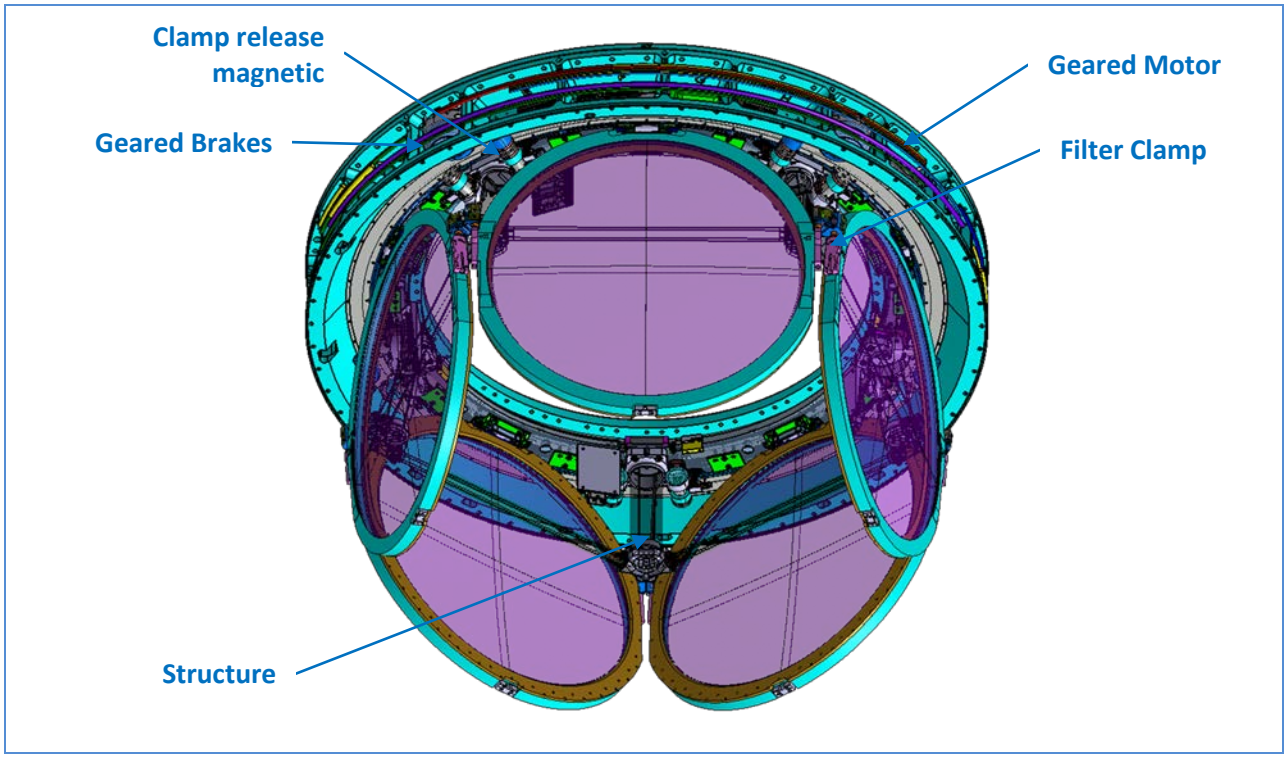

Figure 13-23: Carousel with all five filters mounted

As seen in Figure 13-24 and Figure 13-25, a circular rail is fixed on the camera back flange. Carriers, attached to the ring gear, guide the system on the rail. Motors drive the Carousel by way of pinion gears. The motors fit in cut-outs in the back flange of the camera, arrayed around the perimeter of the Carousel to provide the required torque and power in the relatively small volume available. The Carousel also uses brakes which engage the rotating ring directly and stop all Carousel motion in the event of loss of power. The Carousel can be rotated in either direction, to shorten the travel distance and reduce the time to exchange a filter. Absolute encoder monitors the position of the Carousel during rotation, to provide location information after a loss of power or control.

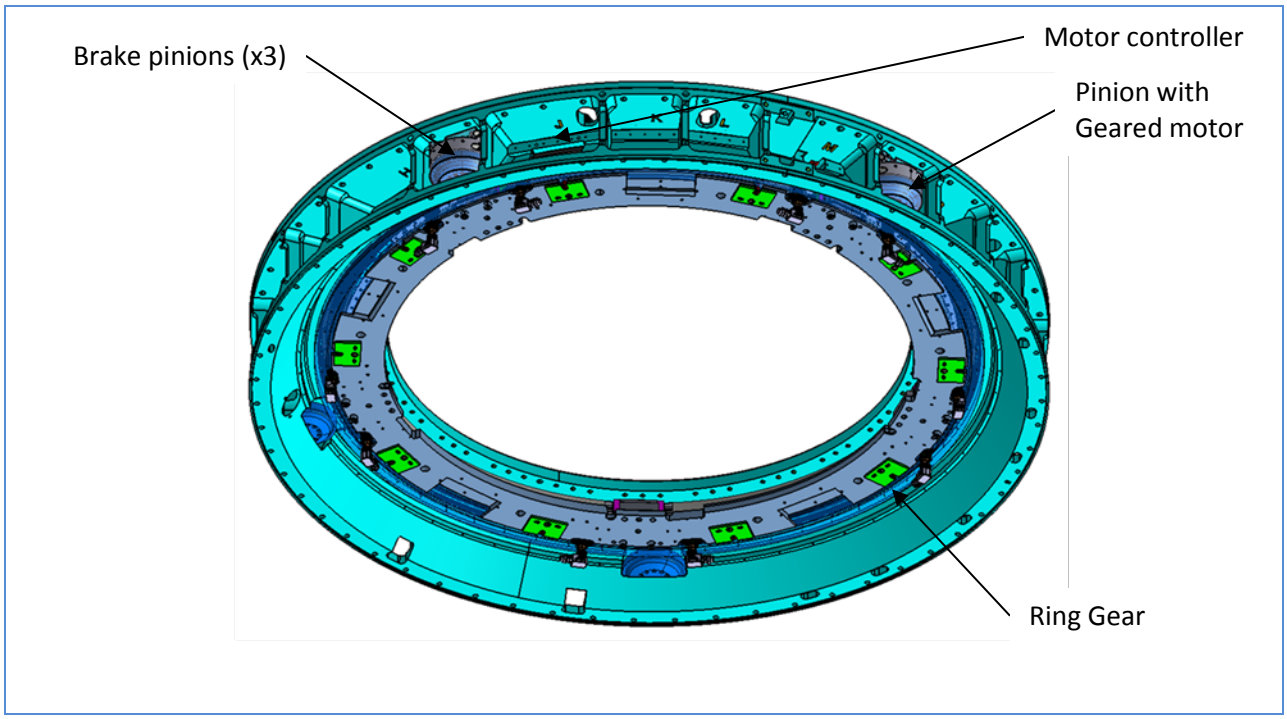

Figure 13-24: Carousel drive system

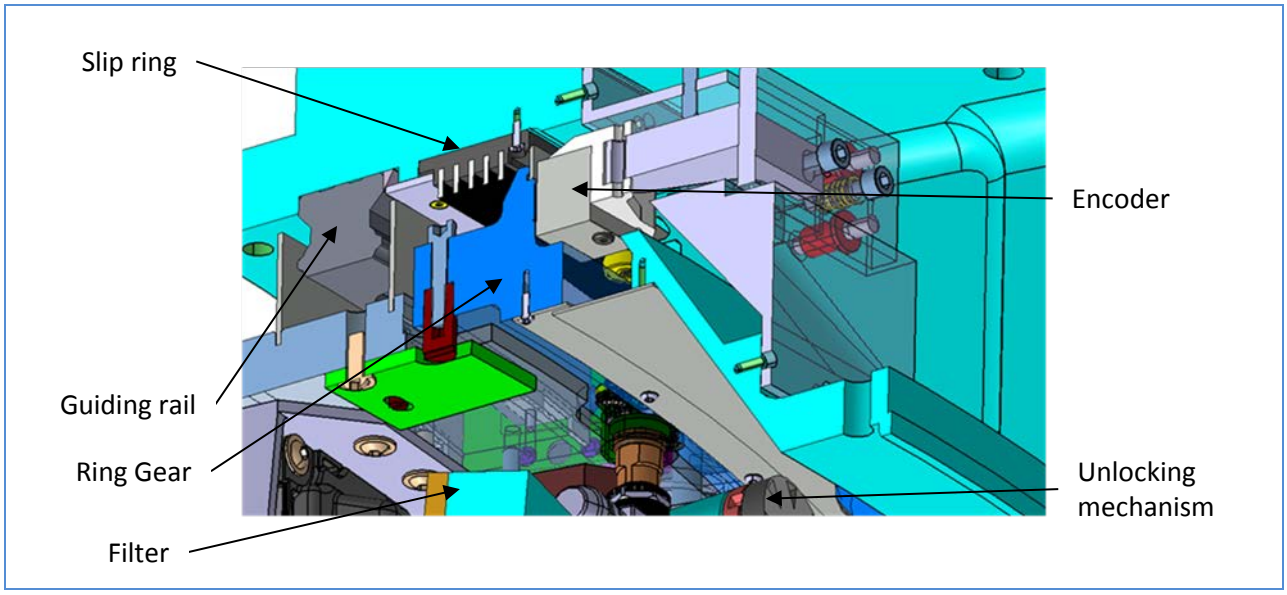

Figure 13-25: Carousel drive system cross sectional view

The five sets of filter clamps are mounted on posts that are supported off of the rotating ring of the Carousel. As shown in Figure 13-26, the clamp mechanism is spring-activated and normally clamped, ensuring that the filters are held in place even during a power failure or loss of control signal. The clamp block and mechanism must securely hold the filter during all operational and seismic accelerations and in all standard camera attitudes, while maintaining filter alignment to ensure that the filter can be successfully picked up by the Auto Changer trucks.

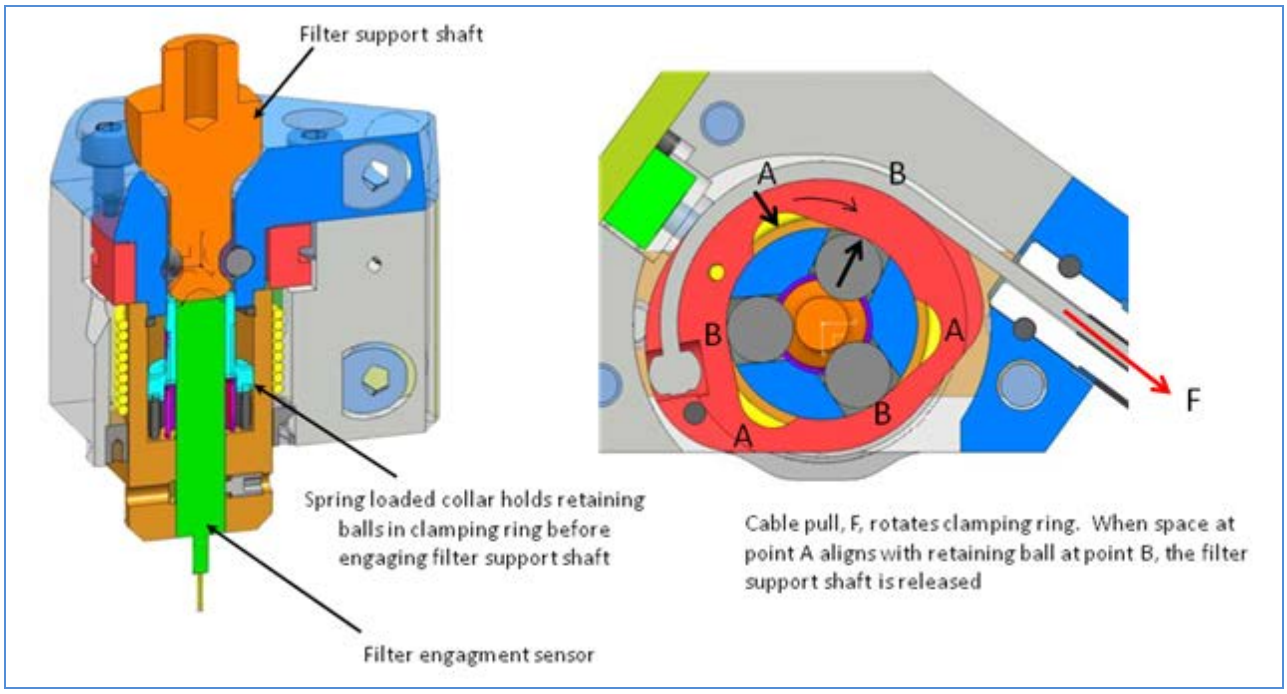

Figure 13-26: Carousel filter clamp showing retaining balls engaging on filter support shaft

The Carousel includes filter clamp release mechanisms that release the spring-activated clamps after the filter is grabbed by the Auto Changer trucks. This release mechanism is normally disengaged, so power is required to engage it and then release a filter clamp. One release mechanism will be mounted to the camera housing opposite each filter clamp at the stand-by location and used for releasing any of the filters.

Because a non-powered rotating component of the carousel is preferred, there must be a method of transferring power to the clamp mechanism release. This is done through a series of magnetic couplings, shown in Figure 13-27. The magnetic couplings transfer torque from a motor attached to the camera back flange to the filter clamp release cable. These small release motors flank the stand-by position clamps. The magnetic couplers allow for some misalignment and allow enough clearance for carousel rotation. When the selected filter is moved to the stand-by position, its half of the magnetic couplers aligns with the release motors.

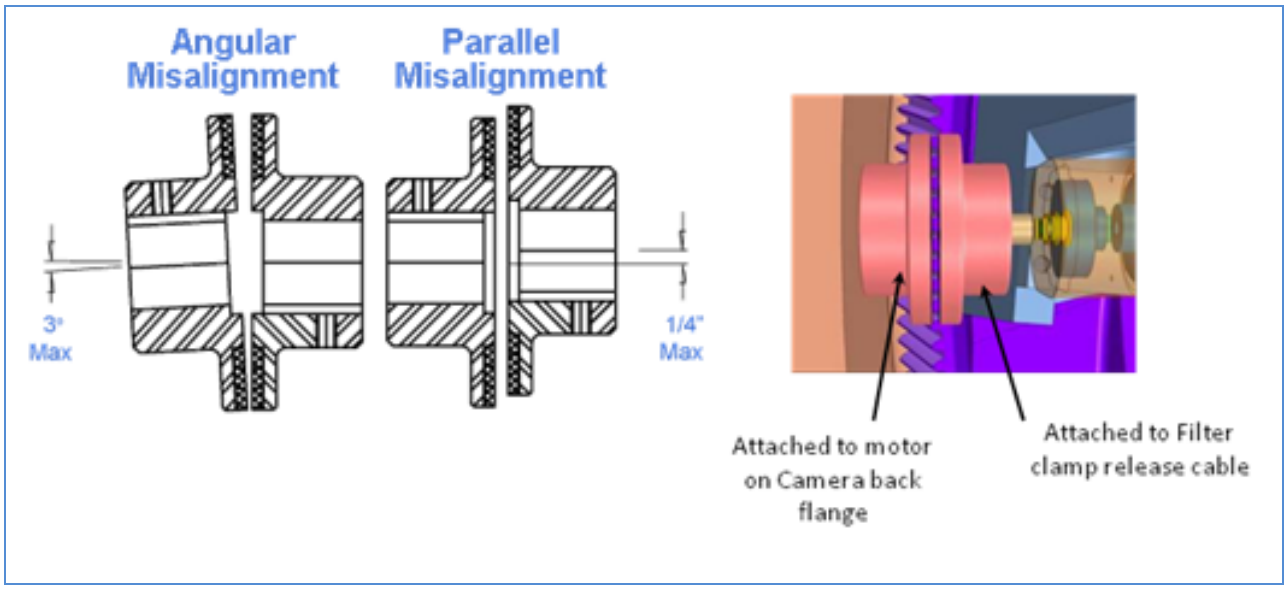

Figure 13-27: Magnetic coupling detail for clamp mechanism release

The structure holding the filters in place is a carbon fiber composite structure. The current structure, shown in Figure 13-28, is sufficient in stiffness and strength. A finite element analysis was performed to calculate the natural frequency, dynamic deflections and stresses, and the margins of safety were positives. Example results of the analysis are shown in Figure 13-29.

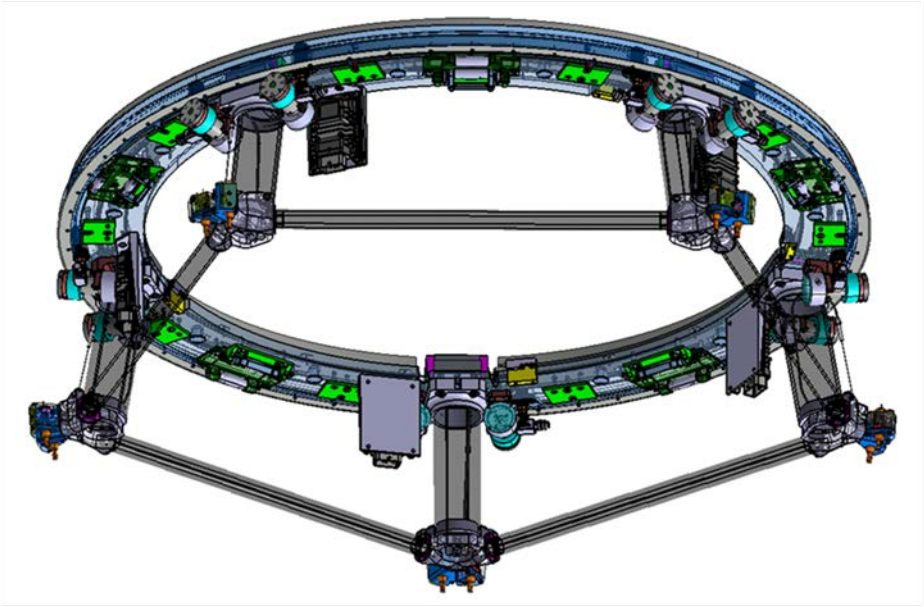

Figure 13-28: Carousel filter support structure

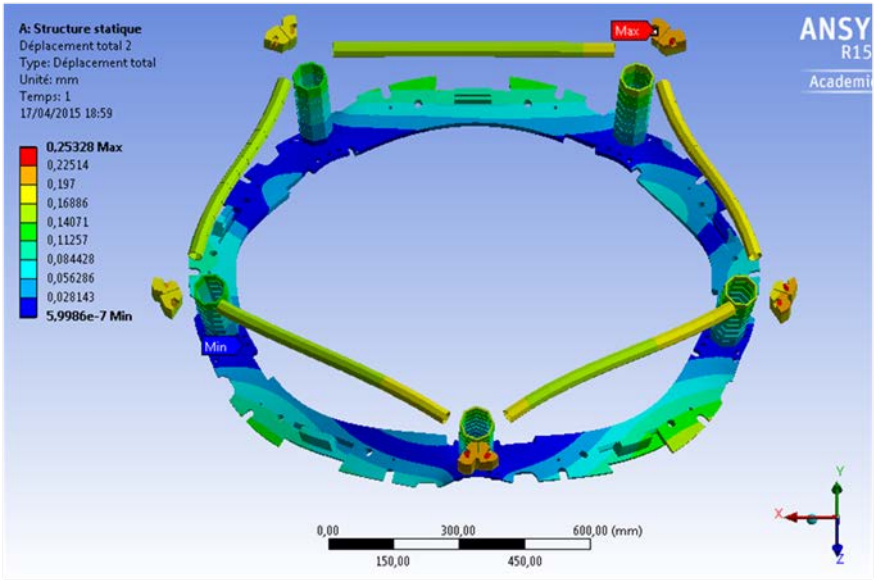

Figure 13-29: Carousel filter support structure analysis results

Simple hand calculations for highest risk items were performed for sizing the clamps. Prototyping and strength testing of the clamps has been performed to verify the operation and strength of the components. The design evolution of the filter clamp progressed from a simple proof of concept, to a fail-safe clamp, to a clamp with integrated sensors and release mechanisms, to the 4th generation prototype that refines material selections, mechanical packaging, and optimization based on previous prototypes. A visual evolution of the prototyping work is shown in Figure 13-30.

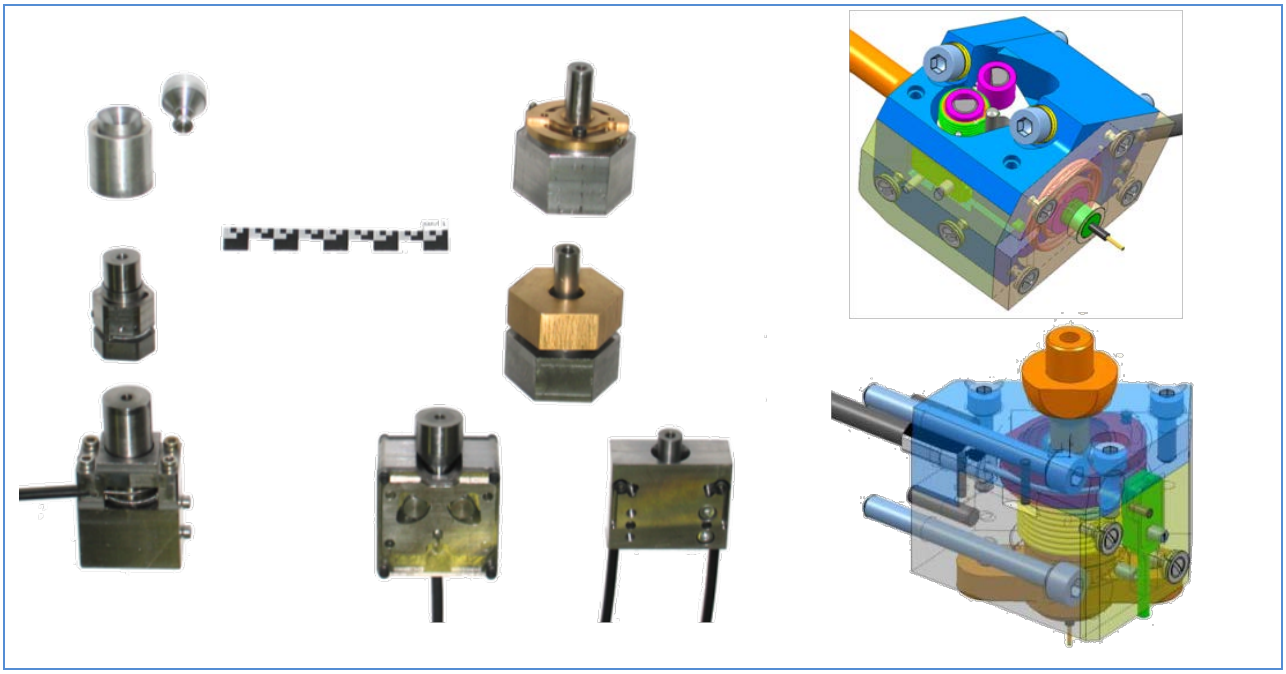

Figure 13-30: Carousel clamp prototyping work and results

Sizing of the ring gear and pinions is complete including stress analysis under worst case environmental and operational loads. The filter support structure finite element analysis has been completed for the structure and shows positive margins for all components. Clamp prototypes were successfully tested, showing load capability 5X higher than the worst case filter mass and exchange with the auto-changer on the single filter test, unlocking performance at higher than the filter mass. Calculations on contact stresses and the bearings show positive margins and a service life of greater than 15 years. The dynamic displacement of the filters is calculated to be 0.26mm which is less than the minimum static clearance. All in all, the carousel design is robust and meets all key driving requirements.

13.6 Filter Loader Design & Analysis

The Filter Loader is a piece of support equipment that is not used during normal camera operations, but solely during a servicing/access period for removing a filter from the camera and installing a new filter in its place. The Filter loader mounts to the +Y side of the camera when the telescope is in its parked position with +Y pointing up and +Z pointing to the horizon. The Filter Loader interfaces to the camera through the Filter Loader Access Port in the Auto Changer structure, as shown in Figure 13-31: Filter loader to Camera Body interface First, the dust covers on the Auto Changer and Filter Loader are removed and the Filter loader is lowered onto the Auto Changer's port. A series of fasteners are used to ensure a hermetic seal as well as prevent relative motion during the filter swap out.

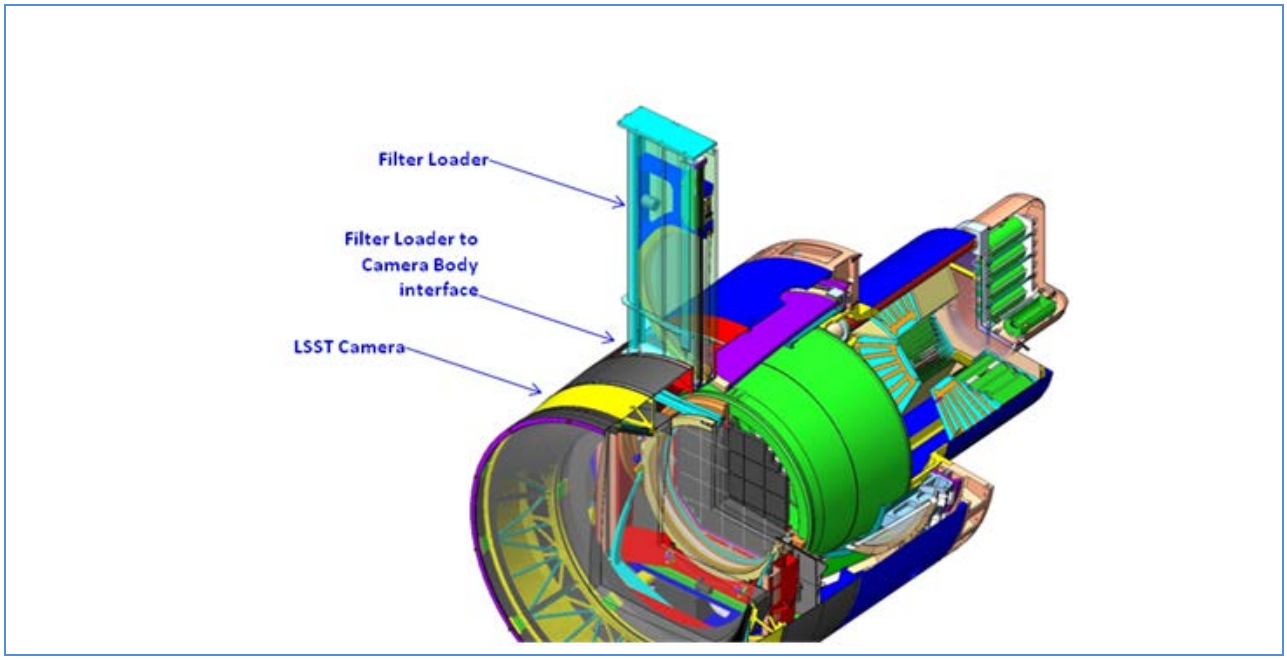

Figure 13-31: Filter loader to Camera Body interface

As shown in Figure 13-32, the Filter Loader is comprised of a clean sealed volume that houses a filter to keep it clean during the swap-out process. There are at least two identical Filter loader units: one for storing the out-going filter, and one that carries the incoming filter before it is inserted into the camera. In a filter swap out, an empty Filter Loader is first attached to the Camera. A drive motor controls the motion of the filter carrier by activating a linear motion unit. The Filter Carrier is attached to the linear

unit. To compensate misalignment between the filter and the Auto Changer the carrier is linked to the linear motion unit by four preloaded springs giving flexibility along Z and around X. Therefore during the motion a set of rollers guides (X axe) the carrier along rails located on the sides of the container. At the end of the stroke when the carrier reaches the hand-off position, the rollers escape from rails and the guiding of the filter is now done by the Auto Changer.

The filter is clamped on the filter carrier using four hooks driven by a linear jack activated by a brushless motor with gear reducer. The linear jack uses a trapezoidal screw which guaranty the system non back drivable. The carrier moves from the storage position to the hand-off position. It is driven by a brushless motor and gear reducer and guided by a linear motion unit.

At Hand-off position the filter is locked by the four hooks, in a first step. After that Filter Latch actuators of the Auto-Changer can be released. The clamping load can be applied without stresses on filter. The filter could be retracted to the storage position.

The Loader is demated from the Camera, the dust cover is replaced and the Loader is transported by the crane to the ground. The desired filter for installation, inside another Filter Loader, is lifted to the camera and the process is reversed to install the new filter.

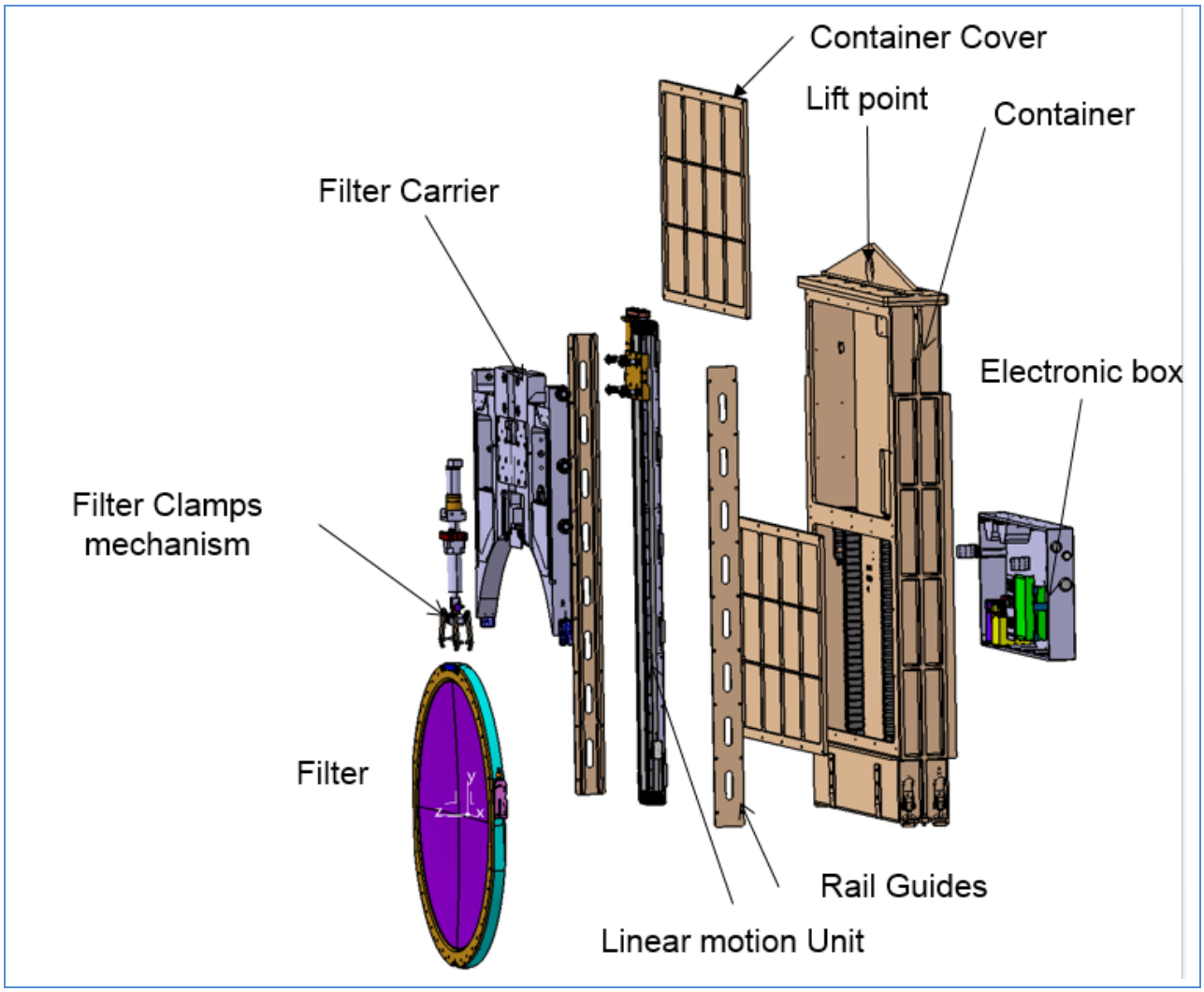

Figure 13-32: Exploded view of the Filter Loader

13.6.1 Interface with Auto-Changer

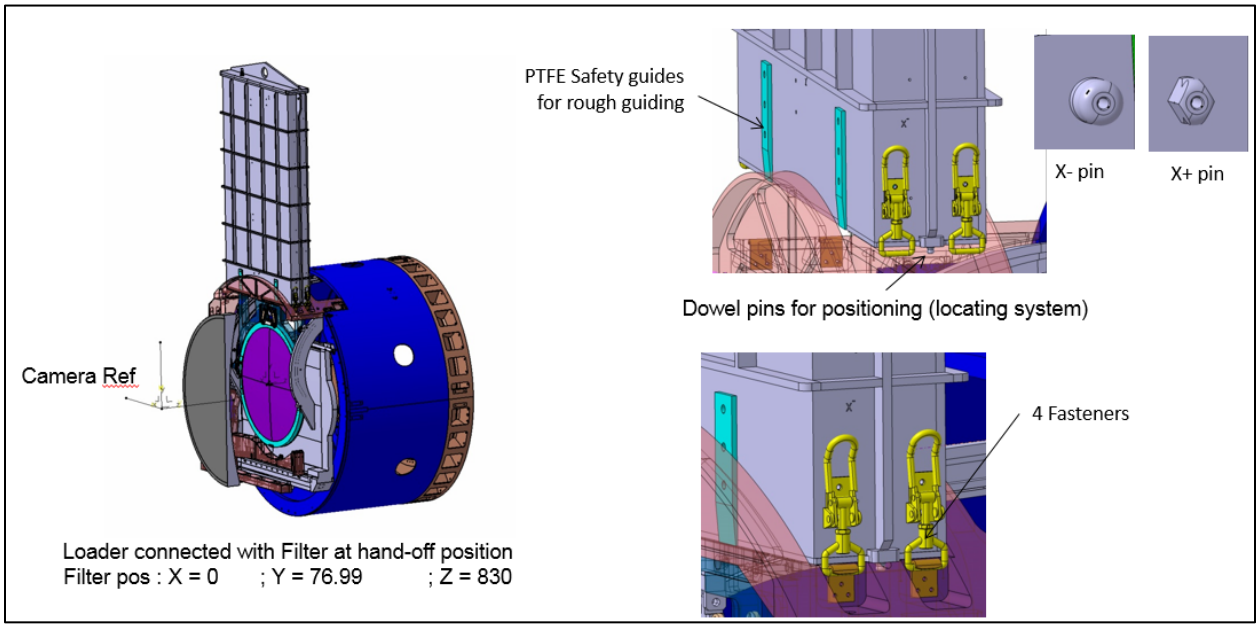

Figure 13-33: Loader interface with the Auto Changer

13.6.2 Filter Loader Container

The filter loader container should be designed to protect filters during operations and to insure a clean atmosphere equivalent to an ISO 5 clean room. It is made with six 6061 aluminum plate with machined ribs welded together. The two removable covers will be in transparent polycarbonate. It is designed to be tight. A 30µ hard anodizing will coat inner and outer surfaces. Specific places will be managed for the grounding. All openings are equipped with gaskets. A filtered N2 laminated flux system is installed on the container. All external connectors are hermetic.

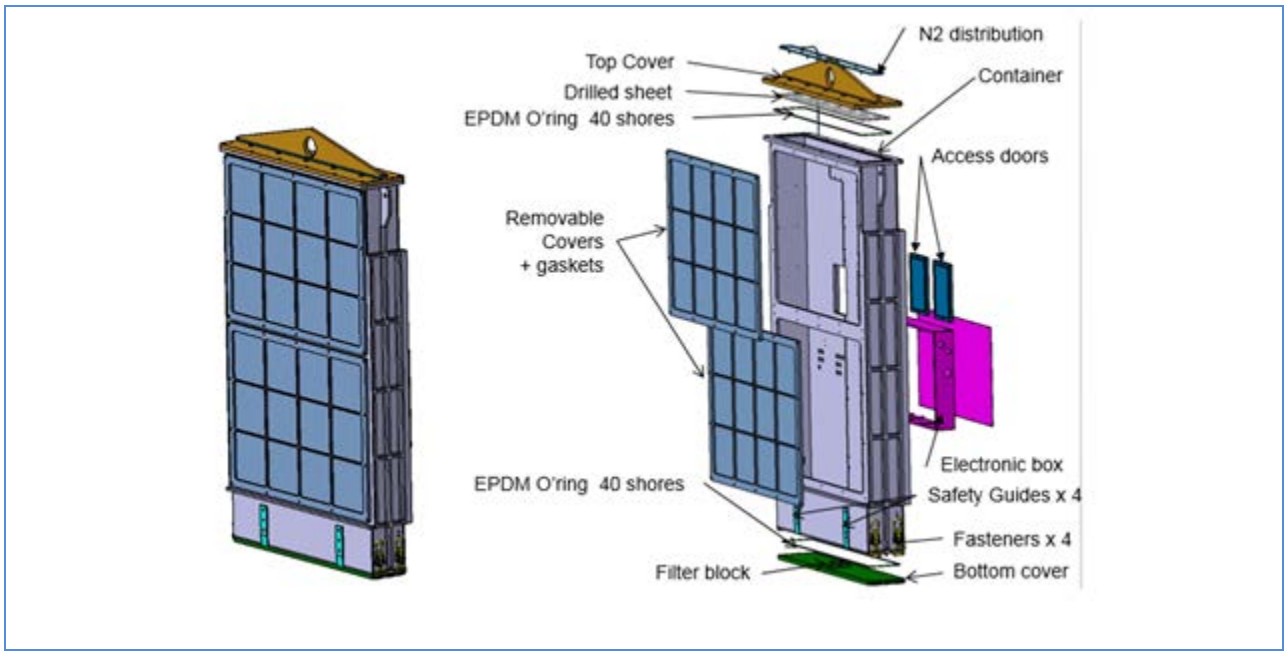

Figure 13-34: Filter Loader container

Mass: 100kg
External dimensions of the allowed envelop L = 1000 mm l = 275 mm H = 1745 mm
External dimensions of the Loader L = 983mm l = 260 mm H = 1600 mm
During transportation with the crane or the Loader cart the container is closed with a flange. The filter is maintained along Z axe by a stop part. Fasteners will be used for the closing.

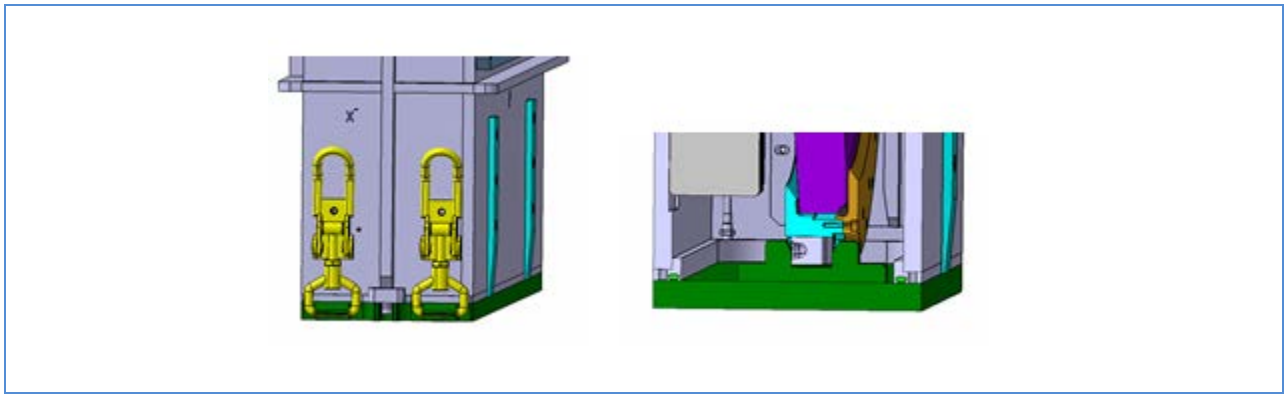

Figure 13-35: Filter Loader container fasteners

Analysis of the container body

That analysis was done to check if compression from the fasteners was sufficient to insure a contact over all of the flange surface and to learn the maximum stress on the loader container.

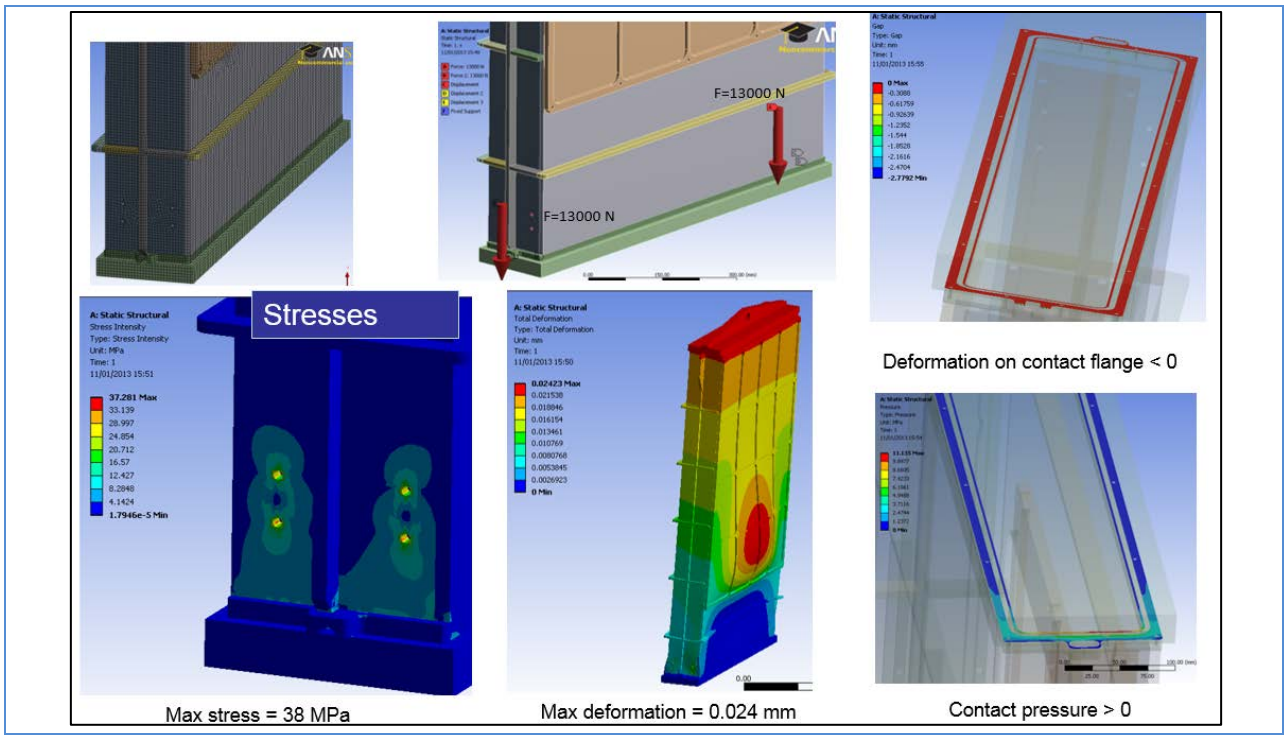

Figure 13-36: Analysis of the top Flange during handling

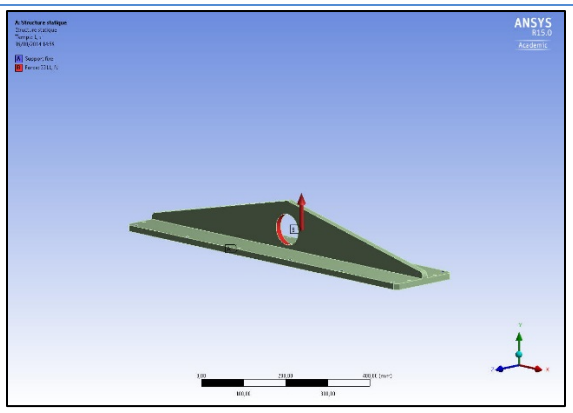

Figure 13-37: Filter loader top flange for handling

The top flange is bolted on the filter container with 12 HM 8 screws. An attachment point for handling is foreseen for the top flange.

The analysis of the top flange has been done for each handling cases. The worst case appears when motion is along Y axe.

Table 13-12: Table of margin calculations for the container and the top flange

					Safety Factors and Margins								
Components	Materiel	Use Case	Fty - Re (Mpa)or (N)	Ftu - Rr (Mpa)	Stress (MPa)/Load (N)	MUF	Use	Load Case Factor Yld	Material SFy	Msy	Load Case Factor Ult	SFu	Msu
Filter Loader Container													
Top Flange	7020	Handling Case 2 Motion on -Y	300	370	41	1,25	1,2	1,6	1,25	1,44	1	1,71	2,52
Body	6061 T6	Normal Case - connected on auto-changer	240	290	38	1,25	1,2	1	1,25	2,37	1	1,4	2,63

13.6.3 Filter Clamp Mechanism

Four hooks are used for clamping filters on the filter carrier. A 2g preload is applied to hold the filter in place. Each hook is verified to be in locked or unlocked position by 2 sensors. Two filters guides must be bolted on filter frames. The linear actuator is equipped with a trapezoidal screw to make the system non-back drivable. The force applied is checked with a force measurement sensor.

Characteristics of the clamping mechanism:

- 4 hooks are used for the clamping of the filters
- Each one is checked in locked and unlocked position by 2 sensors
- Motion controlled by an encoder
- Driven by current
- Actuator Acsys KCY 40/8 F max in traction 2000 N
- Needed Stroke : 29mm
- F required (cf. analysis) : 560 N
- Torque required : exit motor = 134 mNm / exit gear = 1.5 Nm
- Maxon ECMAX40L-24V P = 120W, T = 167 mNm
- Gear Box PM42 Torque max = 3.1 Nm

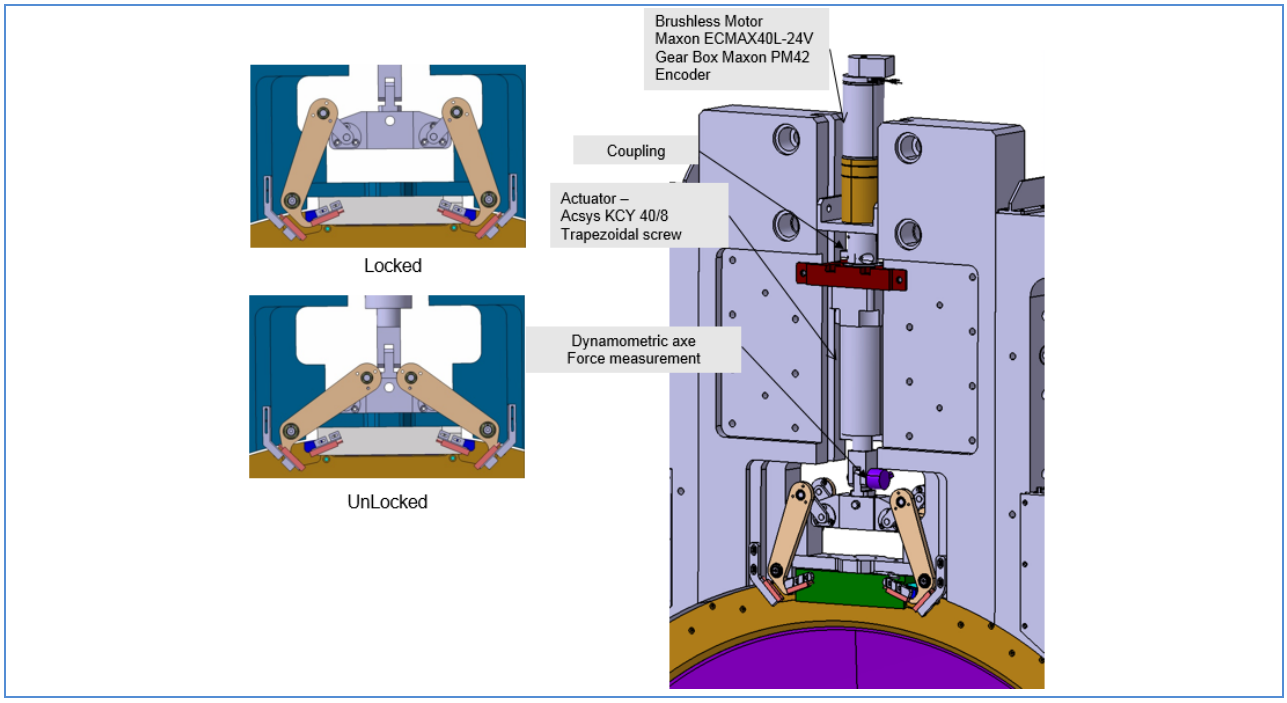

Figure 13-38: Design of the Filter Clamp Mechanism of the Loader

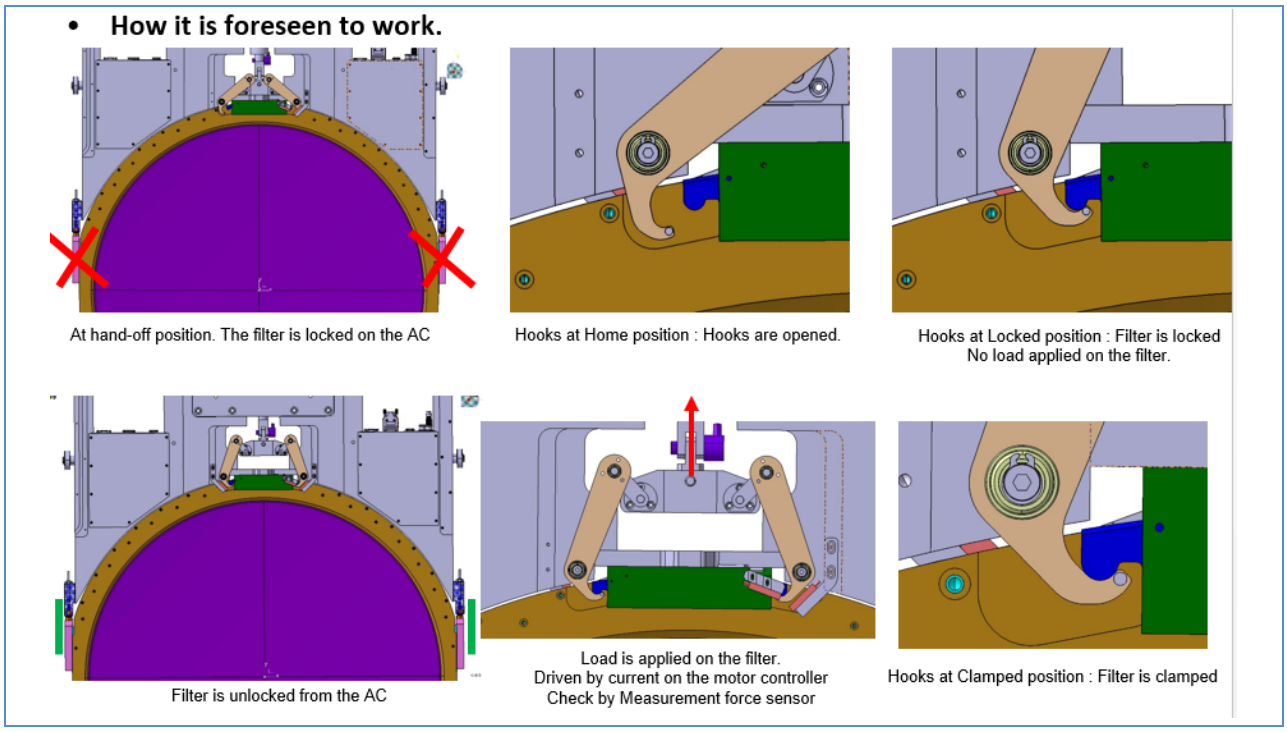

Figure 13-39: Operation of the Filter Clamp Mechanism of the Loader

Analysis of the clamp mechanism

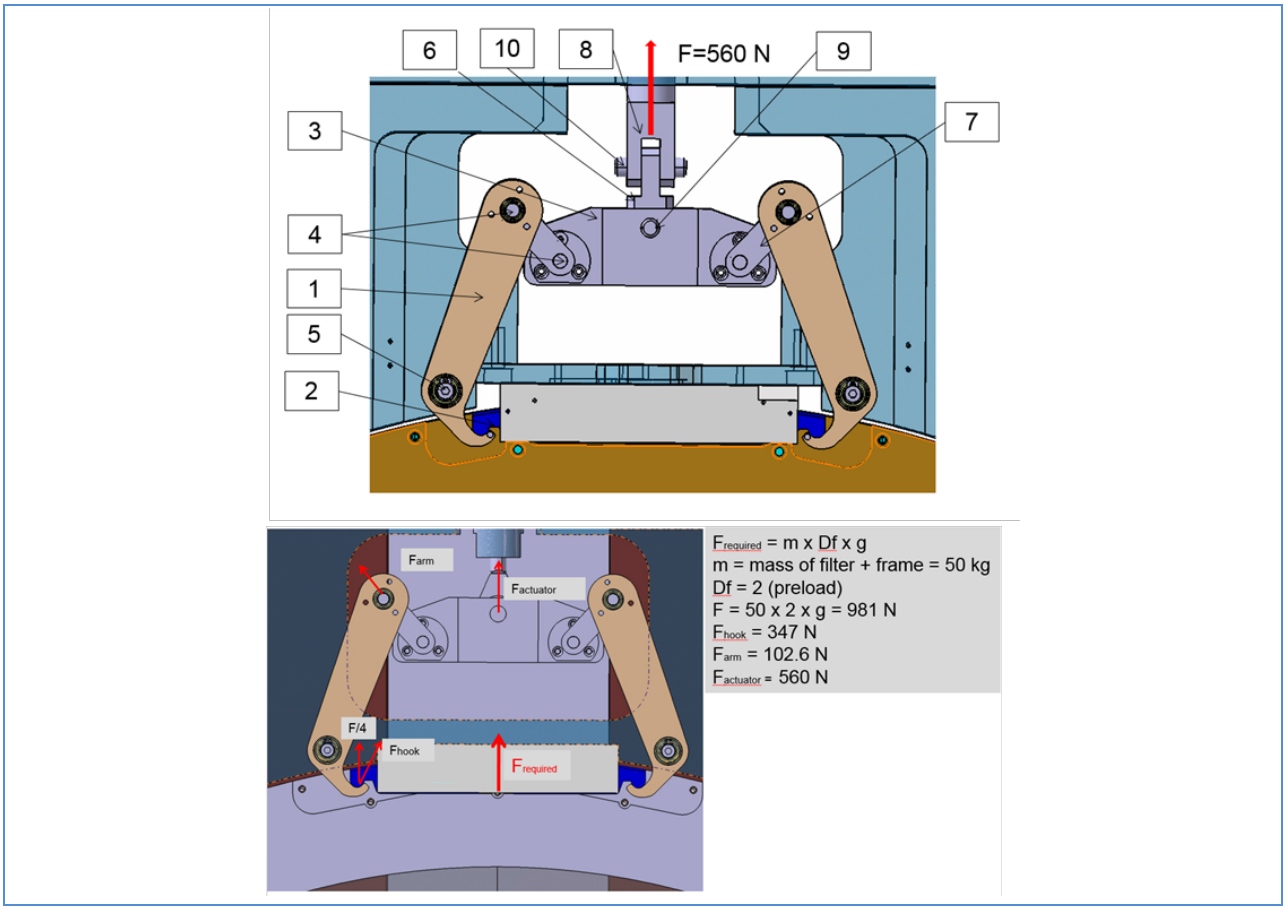

Figure 13-40: Analysis of the filter clamp mechanism

Margins calculations

Table 13-13 shows margins calculations. Only worst cases are summarized. A complete table is contained in LCA-16632 and there is a calculation note LCA-16633.

Table 13-13: Margin calculations for the filter clamp mechanism of the Loader

				Load and stress Definition															Safety Factors and Margins										
	Components	Materiel	Use Case	Fty - Fa (Mpa)or (N)	Fu - Fb (Mpa)	Nominal Load (N)	Load X (Radial (N)	Load Y (Tang (N)	Load Z (axial (N)	Stress (MPa)	Seismic Factor Lateral(g)	Seismic Factor axial (g)	Handling Factor transverse X(g)	Handling Factor gravity Y(g)	Handling Factor transverse Z(g)	handling Factor Motion X	Handling Factor Motion Y	Handling Factor Motion Z	Stall factor (x2)	MUF	Uve	Load Case Factor Yld	Material SFy	Myy	Load Case Factor Ult	SFu	Mxu	Comments
Case Nb	CLAMP MECHANISM																												
1	Hook Pivot Axe	35 Ni Cr Mo 16	Normal - Preload 2g	1050	1250	358				62	1	1							1	1,25	1,2	1	1,25	8,03	1	1,4	8,60	
2			Shearing	525	625	358				34									1	1,25	1,2	1	1,25	7,24	1	1,4	7,75	
3	Hook	35 Ni Cr Mo 16	Normal - Preload 2g	1050	1250	347				193	1	1							1	1,25	1,2	1	1,25	1,90	1	1,4	2,08	
4	Link	7020	Normal - Preload 2g	300	370	103				14	1	1							1	1,25	1,2	1	1,25	10,43	1	1,4	11,59	
5	Link Axe	35 Ni Cr Mo 16	Normal - Preload 2g	1050	1250	103				79	1	1							1	1,25	1,2	1	1,25	6,09	1	1,4	6,53	
6			Shearing	525	625	103				44	1	1							1	1,25	1,2	1	1,25	5,36	1	1,4	5,76	
7	Filter Guide	35 Ni Cr Mo 16	Normal - Preload 2g	1050	1250	347				162	1	1							1	1,25	1,2	1	1,25	2,46	1	1,4	2,67	
8	Male Strap	7020	Normal - Preload 2g	300	370	560				46	1	1							1	1,25	1,2	1	1,25	2,48	1	1,4	2,83	
9	Female Strap	7020	Normal - Preload 2g	300	370	560				13	1	1							1	1,25	1,2	1	1,25	11,31	1	1,4	12,95	Single point failure
10	Stirrup (1st model)	7020	Normal - Preload 2g	300	370	560				24	1	1							1	1,25	1,2	1	1,25	5,67	1	1,4	6,34	Single point failure
11	Stirrup (2nd model)	7020	Normal - Preload 2g	300	370	560				5	1	1							1	1,25	1,2	1	1,25	31,00	1	1,4	34,24	Single point failure
12	Male Strap Axe	35 Ni Cr Mo 16	Normal - Preload 2g	1050	1250	560				26	1	1							1	1,25	1,2	1	1,25	20,54	1	1,4	21,89	Single point failure
13			Shearing	525	625	560				14	1	1							1	1,25	1,2	1	1,25	19	1	1,4	20,26	
14	Female Strap Axe	35 Ni Cr Mo 16	Normal - Preload 2g	1050	1250	560				14	1	1							1	1,25	1,2	1	1,25	39	1	1,4	41,52	Single point failure
15			Shearing	525	625	560				7	1	1							1	1,25	1,2	1	1,25	39	1	1,4	41,52	
16	Bearing SMR 126 (6x12x4)		Normal - Preload 2g - Static	380	-	103	103				1	1							1	1	1	1	1,25	1,95	-	-	-	
17	Bearing SMR 147 (7x14x5)		Normal - Preload 2g - Static	520	-	358	358				1	1							1	1	1	1	1,25	0,16	-	-	-	
18	Axe MS proto	35 Ni Cr Mo 16	Normal - Preload 2g - Static	255	410	560				50	1	1							1	1,25	1,2	1	1,25	1,72	1	1,4	2,90	
19	Clamp for Actuator	7020	Normal - Preload 2g - Static	300	370	560				33	1	1							1	1,25	1,2	1	1,25	3,85	1	1,4	4,34	
20	Clamp for Actuator	7020	Shearing	150	185	560				19	1	1							1	1,25	1,2	1	1,25	3,21	1	1,4	3,64	
21	Sensor measurement axe	Stainless steel	Normal - Preload 2g - Static	1500	3000	560					1	1							1	1	1,2	1	1,25	0,79	1	1,4	2,83	

13.6.4 Filter Carrier

The filter carrier handles the motion of filters from storage to Hand-off position. The carrier is made of 3 machined 7020 aluminum parts.

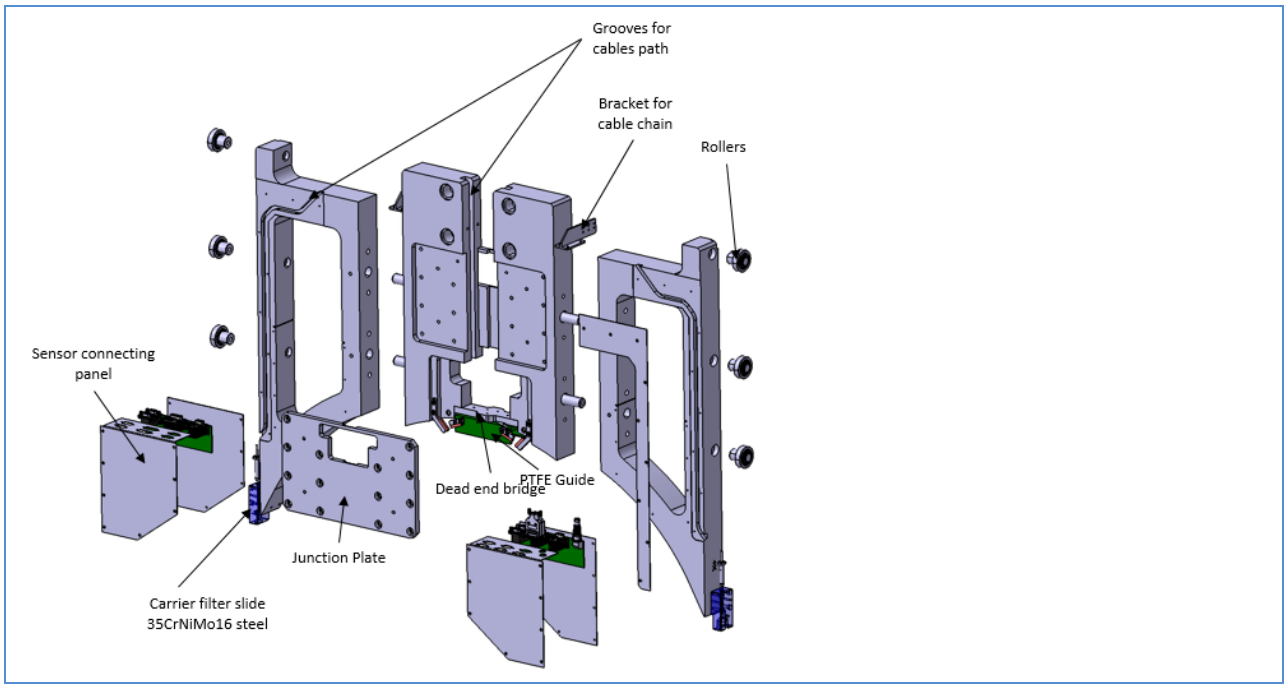

Figure 13-41: Filter Carrier for the Loader

Misalignment compensating

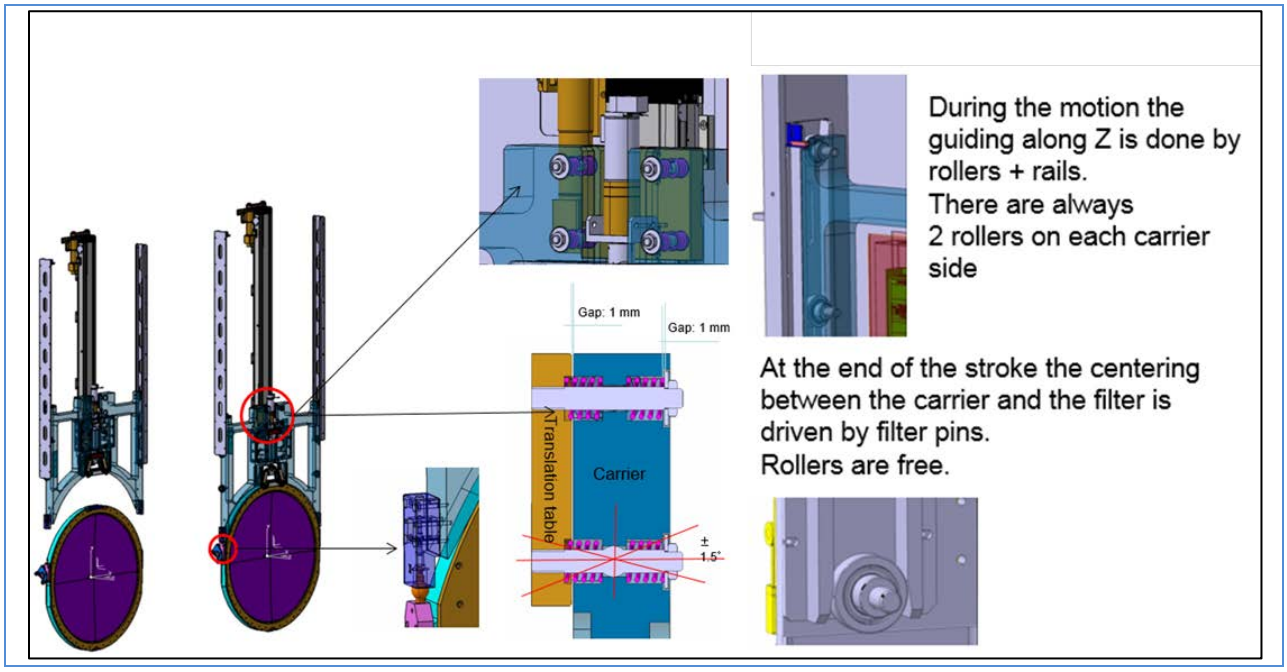

Figure 13-42: Misalignment compensating

Driving system

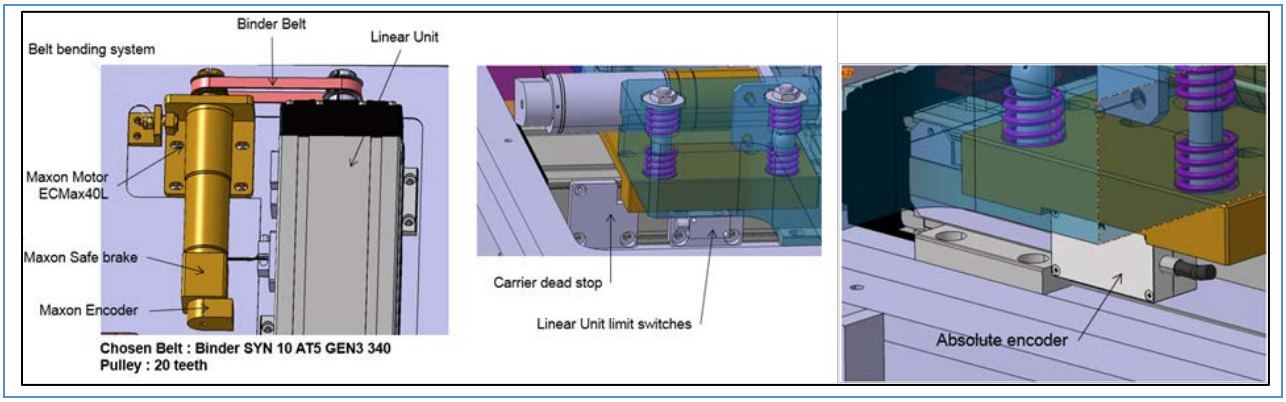

Figure 13-43: Driving system for the Loader

Characteristics of the driving system:

- Unimotion Linear unit CTV 110L - 16x5
- Linear Speed required 0.5 m/min
- Max load capability: 12300N
- Load needed: 110 kg x 1,25x g = 1375N
- Max drive torque: 12.5 Nm
- Torque required: 2 Nm
- Max Dynamic moment Mx = 1950 Nm
- Limit switches Sensors
- Linear Absolut encoder AMO GmbH - Resolution 1µ - Stroke 1220 mm - Accuracy ± 10µ
- Maxon Motor Brushless EC40 - 24 V 170W Torque = 162mNm
- Max speed: 9140 rot/min
- Maxon Planetary Gear head - Torque 15 Nm - 1:43 max speed: 228 rot/min
- Maxon Brake AB32: 24V
- Maxon EPOS Controller 70/10
- Maxon Encoder: HEDL 5540
- Maxon Shunt regulator

Analysis

Body

Calculations have been done for all different load cases: Normal, handling and seismic cases. See complete results in LCA-16332 and LCA-16333.

σ Von Mises = 41 MPa
Msy = 3.88
Msu = 4.37

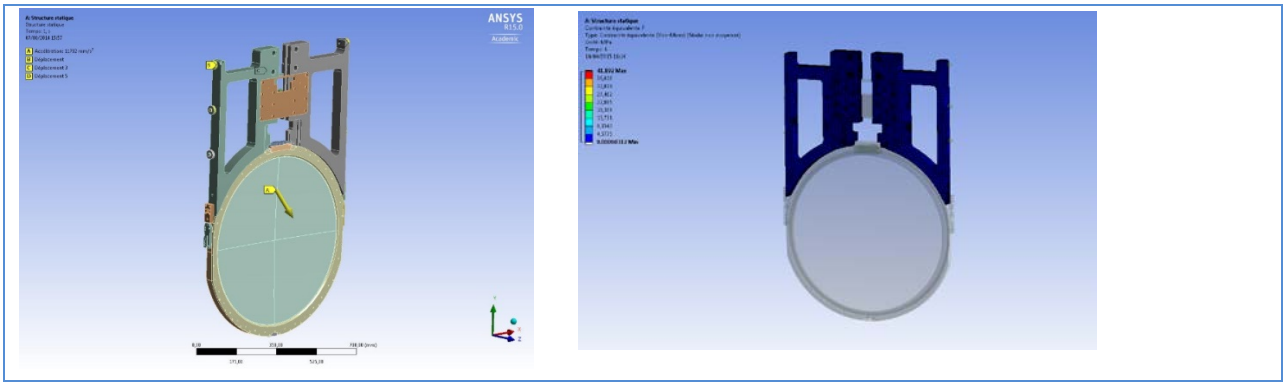

Figure 13-44: Finite element Model of the Filter Carrier for the Loader

Carrier Slide

σ Von Mises = 144 MPa
Msy = 3.86
Msu = 4.17

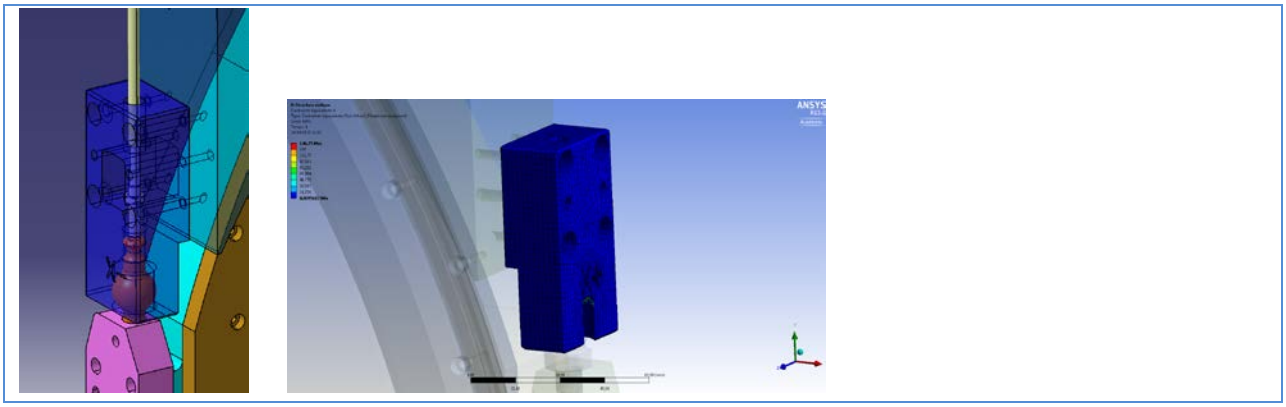

Figure 13-45: Filter carrier slide for the Loader

Pivot Axle

The Filter Carrier is supported by two pivot axles. These two axes are fixed on a plate bolted on the linear rail. Several load cases will be studied.

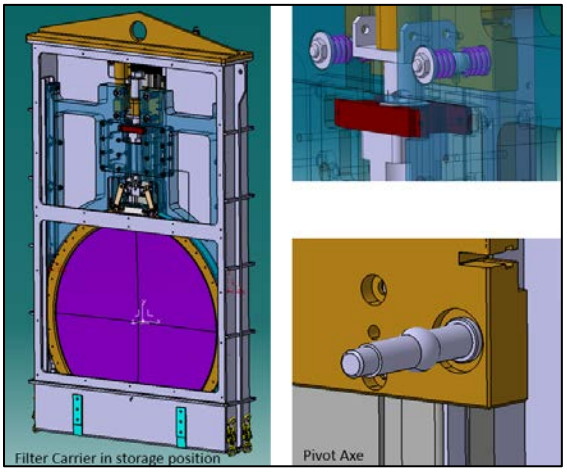

Figure 13-46: Pivot axle of the filter carrier

To simplify the analysis we calculated the forces on the Pivot Axles for each different case and then used the results in a FEA model. For the model of forces calculation see picture below.

A force equivalent at the mass of the carrier + the mass of the heaviest filter multiplied by accelerations function of the case was applied at the center of gravity.

Mass of the filter carrier + heaviest filter = 100kg

Directions are referenced to the Camera Coordinate System.

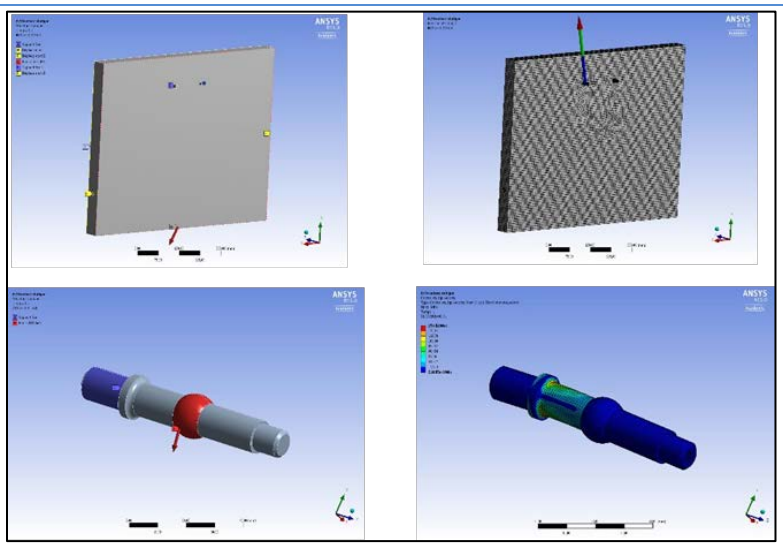

Figure 13-47: Finite Element Model for the calculation of the filter carrier pivot axle

Calculations have been done for all different load cases; normal, handling and seismic cases. Only worst cases are reported here.

	Calculated Force on pivot axe - N				
Load Cases	Fx	Fy	Fz	Von Mises Mpa	Shearing Mpa
Normal Operating mode	0	491	0	92	51
Seismic - off telescope - 1 - Transverse on X	151	795	63	154	85
Seismic-off telescope - 1 - Transverse on Z	0	738	-192	138	75
Seismic - off telescope - 2 - Transverse on X	154	-355	0	73	40
Seismic - Off telescope - 2 - Transverse on Z	0	296	-177	80	44
Handling - Case 1 & 2 Motion on ±X	44	633	-16	119	66
Handling Case 2 Motion on -Y	0	738	-24	138	76
Handling - Case 2 Motion on ±Z	0	614	-70	114	63
Handling - Case 3 & 4 Transverse on ±X	44	633	-16	119	66
Handling - Case 3 & 4 Transverse on ±Z	0	614	-70	114	63

σ Von Mises = 154 MPa
Msy = 3.54
Msu = 3.83
σ Shearing = 85 MPa
Msy = 3.1
Msu = 3.3

Roller axles

The filter carrier is guided by 6 rollers located on carrier sides rolling along two rails. These rollers take the load along the Z axis during operation. The load along Z during normal operation comes from the 4 springs used for the fixation of the carrier on the linear table. It is estimated at 200N. When the filter carrier is in storage position, the effort will be more important during handling operation or under the seismic loads. The rollers axles have been checked in all the load cases.

For the calculation it is supposed that the filter carrier is in storage position and the heaviest filter is clamped on it. Only the Z component of the effort is taken into account for that analysis. To simplify the analysis we calculated the forces on the roller axe for each different case and then used the results in a FEA model of the roller axe. The worst load case is the seismic off-telescope one. For that case we hypothesized that only 3 rollers of the six are in actual contact with the rails, 2 on one side and 1 on the other side. The system is symmetric on plane YZ so 9 different cases could appear.

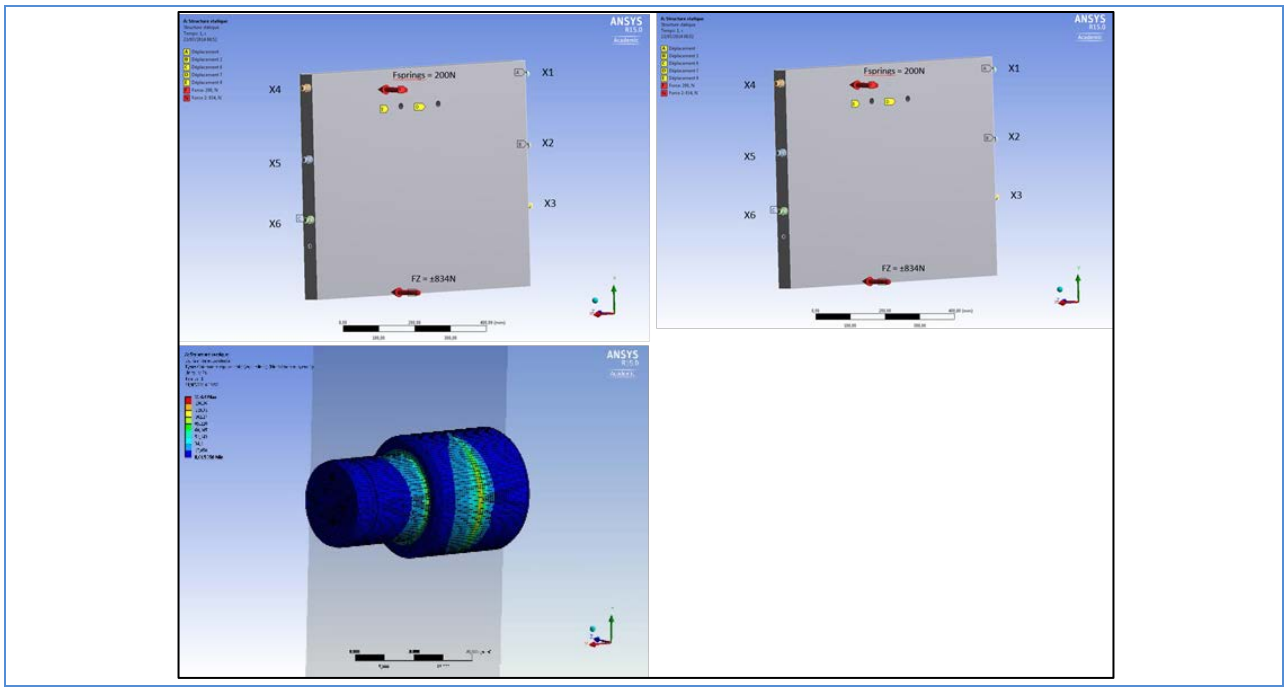

Figure 13-48: Finite Element Model for the calculation of the roller axles

Calculations have been done for all different load cases; normal, handling and seismic case. Only worst cases are reported here.

F max = 2600N
σ Von Mises = 169 Mpa
σ Shearing = 93 MPa
Msy = 3.1
Msu = 3.4

Table of margins calculation:

Only worst cases are summarized in this table. A complete table appears in LCA-16632 and there is a calculation note LCA-16633.

Table 13-14: Margin Calculation results for the Filter carrier

					Safety Factors and Margins								
Components	Materiel	Use Case	Fty - Re (Mpa)or (N)	Ftu - Rr (Mpa)	Stress (MPa)/Load (N)	MUF	Use	Load Case Factor Yld	Material SFy	Msy	Load Case Factor Ult	SFu	Msu
Filter Carrier													
Pivot Axle	35 Ni Cr Mo 16	Normal Case	1050	1250	92	1,25	1,2	1	1,25	5,09	1	1,4	5,47
		Shearing	525	625	51	1,25	1,2	1	1,25	4,49	1	1,4	4,84
		Seismic - off telescope - 1 -Transverse on X	1050	1250	154	1,25	1,2	0,8	1,25	3,55	0,8	1,4	3,83
		Seismic shearing - off telescope-1 - transverse on X	525	625	85	1,25	1,2	0,8	1,25	3,12	0,8	1,4	3,38
		Handling Case 2 Motion on -Y	1050	1250	138	1,25	1,2	1,6	1,25	1,54	1	1,71	2,53
		Handling - Case 1 & 2 Motion on -Y / Shearing	525	625	76	1,25	1,2	1,6	1,25	1,30	1	1,71	2,21
Rollers Axle	35 Ni Cr Mo 16	Normal Case	1050	1250	27	1,25	1,2	1	1,25	19,74	1	1,4	21,05
		Shearing	525	625	14	1,25	1,2	1	1,25	19,00	1	1,4	20,26
		Seismic - off telescope - 1 - Transverse on ±Z	1050	1250	169	1,25	1,2	0,8	1,25	3,14	0,8	1,4	3,40
		Seismic shearing - off telescope-1- Transverse on ±Z	525	625	93	1,25	1,2	0,8	1,25	2,76	0,8	1,4	3,00
		Handling - Case 2 Motion on ±Z	1050	1250	54	1,25	1,2	1,6	1,25	5,48	1	1,71	8,02
		Handling Case 2 Motion on ±Z / Shearing	525	625	30	1,25	1,2	1,6	1,25	4,83	1	1,71	7,12
Body	7020	Handling - Case 2 Motion or transverse on ±Z	300	370	13	1,25	1,2	1,6	1,25	6,69	1	1,71	10,10
		Seismic - off telescope - 1 - Transverse on ±Z	300	370	41	1,25	1,2	1,6	1,25	1,44	1	1,4	3,30
Carrier Slide	35 Ni Cr Mo 16	Handling - Case 2 Motion Y -	1050	1250	20,3	1,25	1,2	1,6	1,25	16,24	1	1,71	23,01
		Seismic - off telescope - 1 - Transverse on ±Z	1050	1250	144	1,25	1,2	1,6	1,25	1,43	1	1,4	3,13
Bridge	35 Ni Cr Mo 16	Normal Case	1050	1250	44	1,25	1,2	1,6	1,25	6,95	1	1,4	12,53

13.6.5 Cyclic loads

Cyclic loads analysis was also considered. It is currently assumed that there will be four manual filter changes per month. Over one year, this is 48 changes, and over the 15 year lifetime, ~720 changes. A minimum of two Filter Loaders are needed to work in tandem to execute a manual change within the 1.5 hour required timeframe. With these parameters, the cyclic loads are benign and the Filter Loader assembly is expected to perform for 15 years without maintenance.

Nevertheless for parts that are involved in cyclic motion a fatigue calculation have been done.

Results are given in LCA-17713. More over cyclic tests will be perform on test benches.

13.6.6 Control Command and Cabling

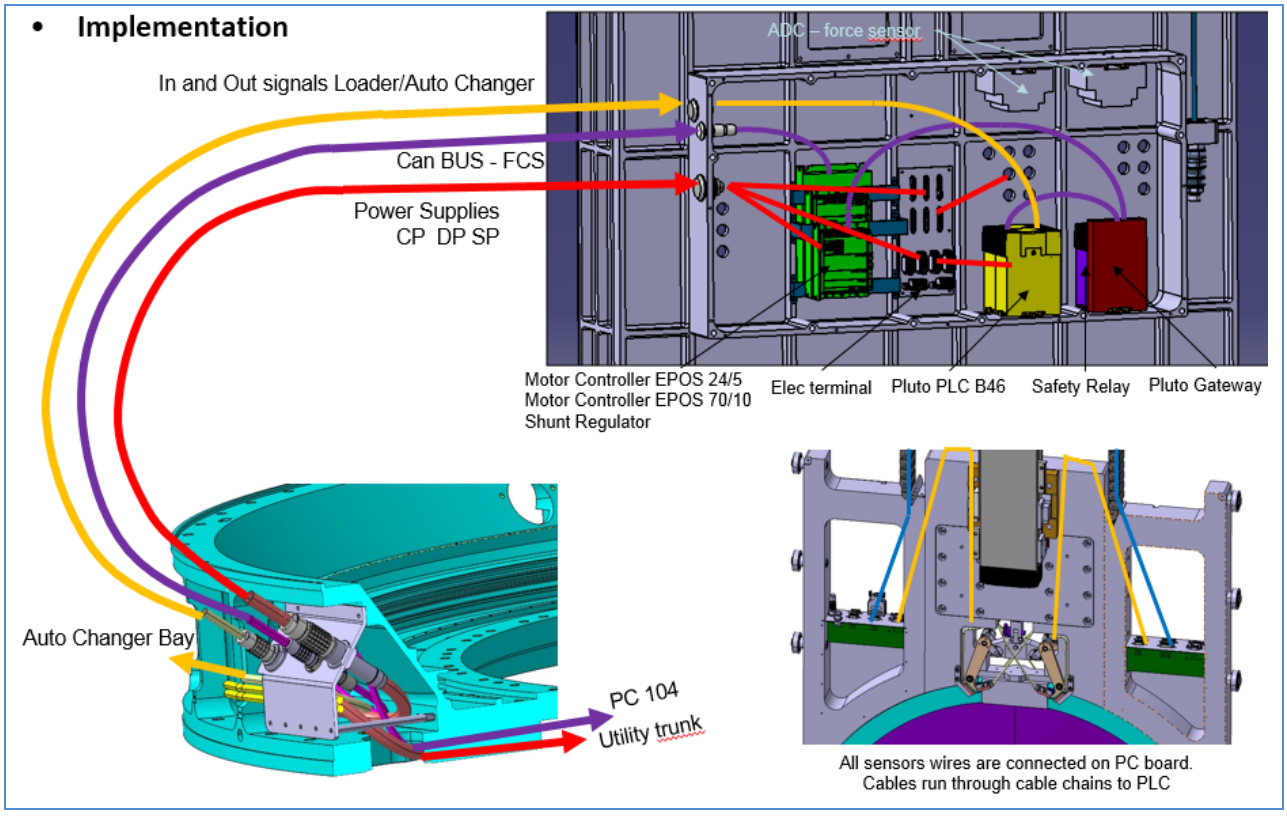

Figure 13-49 Filter Loader cabling implementation

13.7 Assembly & Test

This section describes assembly and test of the Auto Changer and Carousel. An assembly and test sequence is not presented for the Filter Loader, a relatively straightforward external system used for Camera servicing.

The overall test of the Filter Exchange system will be held on a full scale test bench and will allow testing of the compliance of the system with the specification.

Each sub-system will initially be assembled and tested on a stand-alone setup. The test will be carried out at the lab in charge of that sub-system. The sub-systems will then be shipped and assembled together on the full Scale Test Bench at LPNHE (Paris). This final facility will enable qualifying the system in a configuration very close to that of the actual Camera.

13.7.1 Auto Changer Assembly and Test

The Auto Changer assembly sequence is illustrated in Figure 13-50. Once the support frame is assembled, it is inspected for squareness and correct positioning of mount points and interfaces. Next, the curved rails are mounted on the support frame, and aligned. Trucks are fit checked before assembly continues. Once fit is verified, the drive system and motor are installed and confirmed to function as specified. Next, the yoke, linkage, and trucks are mounted; this is the first stage at which functional, load, and alignments tests on an integrated assembly can be performed. Once these verifications are complete, the on-line clamps are installed. Auto Changer assembly is complete. A full suite of functional, proof load, and alignment tests are performed before delivery for integration.

Fiducials are fixed on the structure (Figure 13-51). They define the Auto Changer reference. This reference is used for:

- Assemble the Auto Changer’s components
- Check the displacement under load
- Assemble and Align the Auto changer into the Camera

The test plan is defined and extracted from the compliance matrix. Each test will valid one or several specifications.

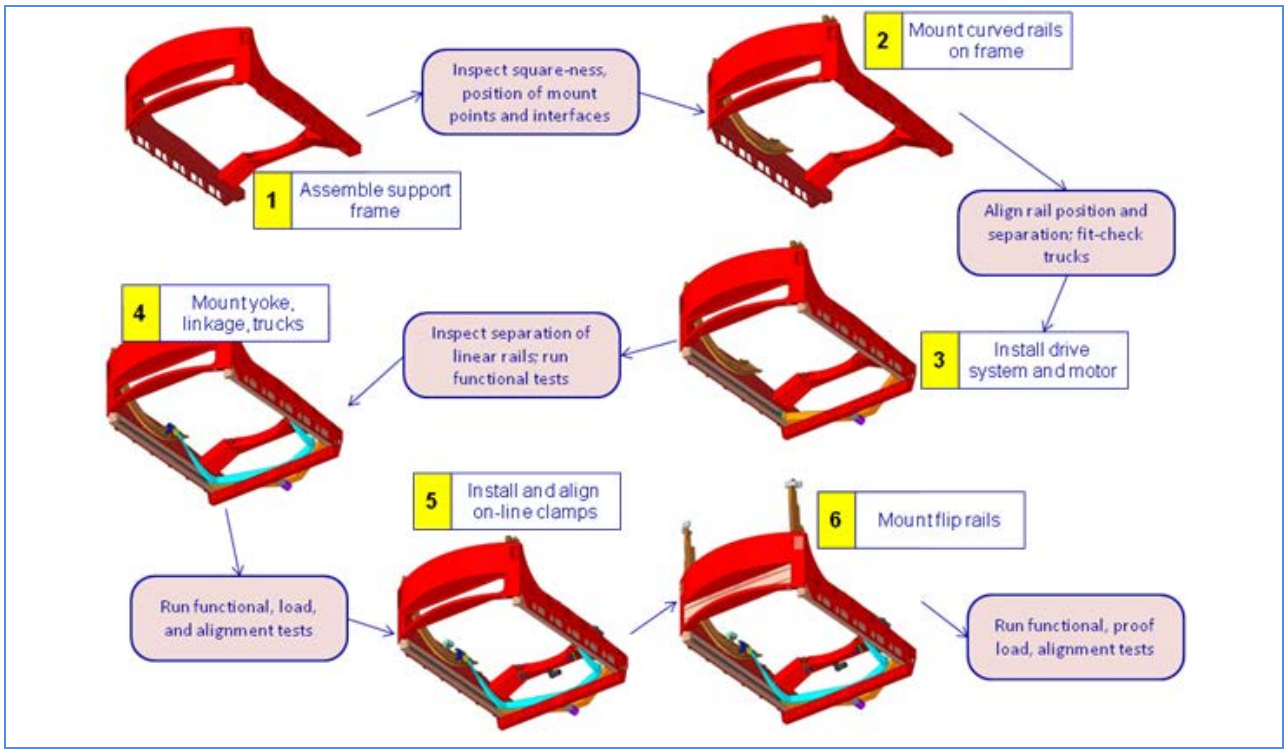

Figure 13-50: Auto Changer assembly and test sequence

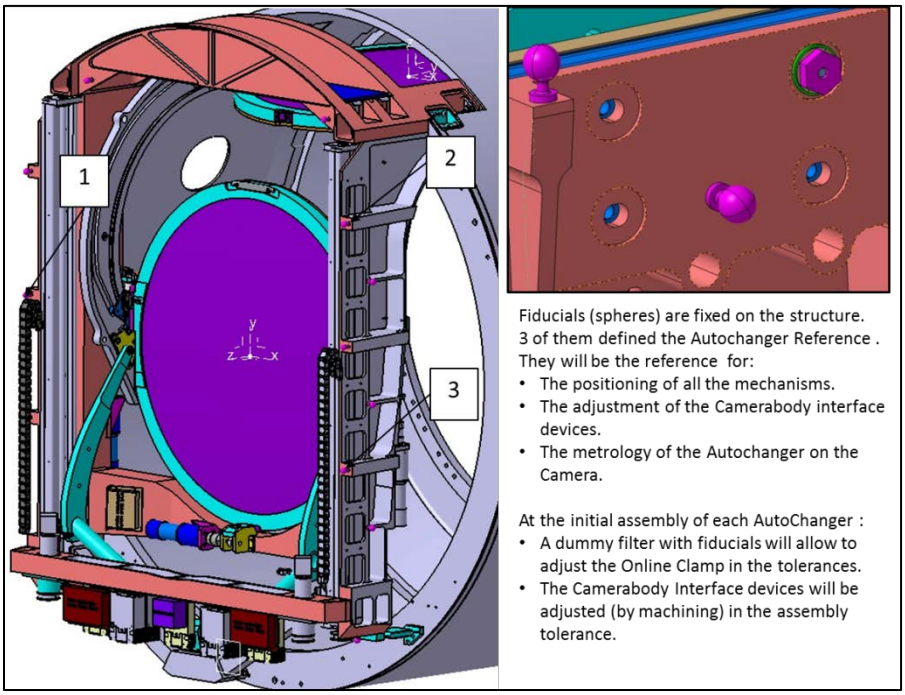

Figure 13-51: Definition of the Auto Changer reference for assembly and metrology

Figure 13-52 presents the concept for equipment required for the Assembly and Test of the Auto Changer. The design has to be finalized and integrated into a modular clean room (ISO 7). The main operation on the Auto Changer before the final assembly with the other sub-systems will be:

1. Assembly and alignment of the components. Measurement of the interfaces with the loader, the carousel, and the camera body. Measurement of the filter position in the on-line position.
2. Functional Tests on the Stand-alone test bench. Check all the requirements which don't have any interface of the other sub-systems mainly for the travel of the filter, and the repeatability of the filter in the On-line position.
   The functional tests will include:

   - Mass and Center of Gravity measurement
   - Safety test (Local Protection Module)
   - Load test at any angular position
   - Electrical consumption measurement

3. Handling Test with the crane and the dedicated cart for the transportation on the summit in a clean configuration.

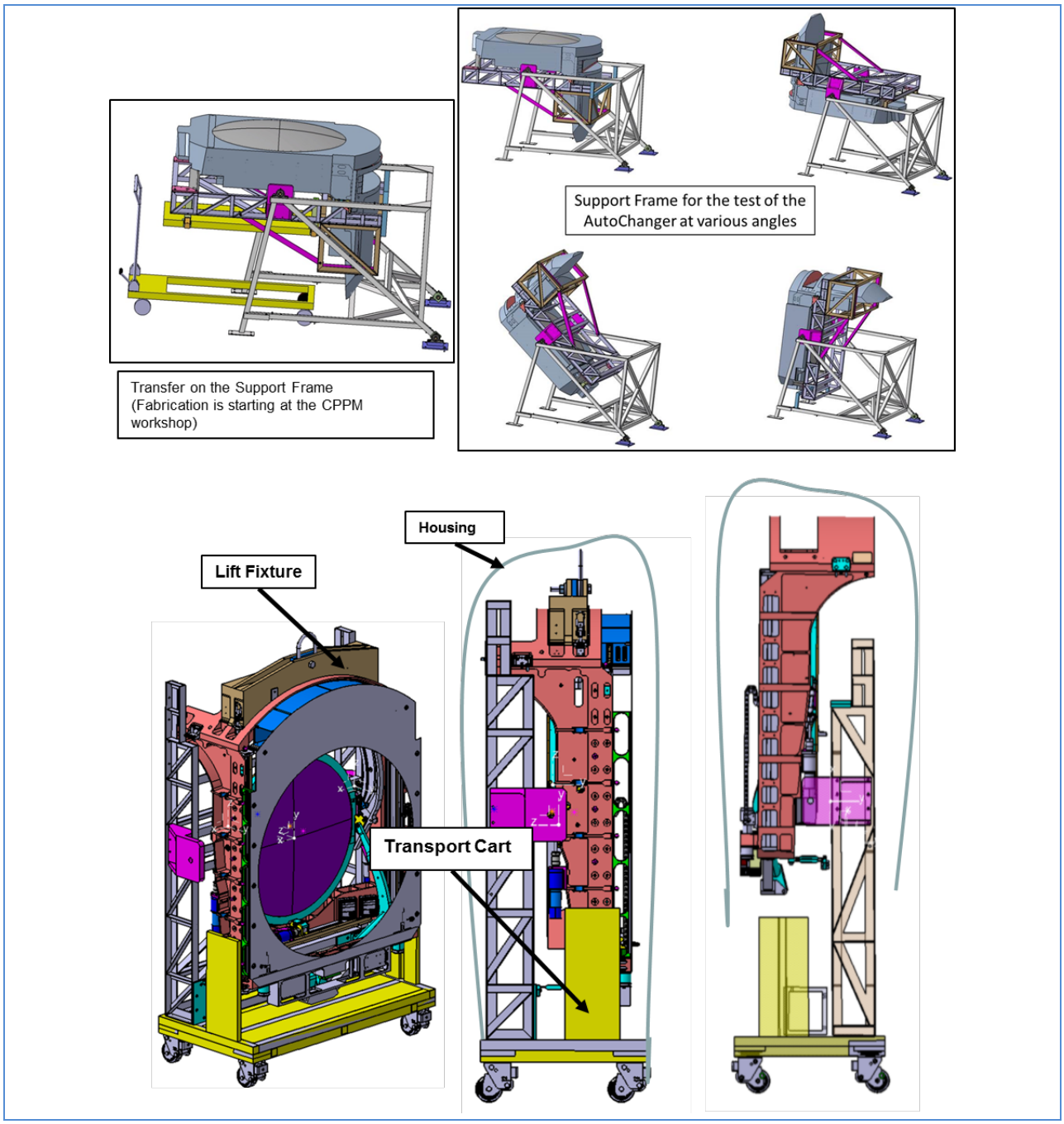

Figure 13-52: Auto Changer Assembly and Test equipment

13.7.2 Carousel Assembly and Test

The Carousel assembly sequence is illustrated in Figure 13-53. Initial steps involve mounting rails, pads, and ring gear on the unit's back flange, with verification of their flatness and concentricity. Motors, brakes, and encoders are mounted; checks are performed to confirm proper functioning of motor controllers and to verify that motors respond correctly to commands from the CCS. Next, the central support cylinder and posts are installed and the position and concentricity of the clamp mount points are confirmed. The final steps in the sequence focus on mounting the Carousel clamp and testing of the

clamp mechanism and controls, ending with a full verification test driven by the CCS using dummy filters. The Carousel is then ready for integration.

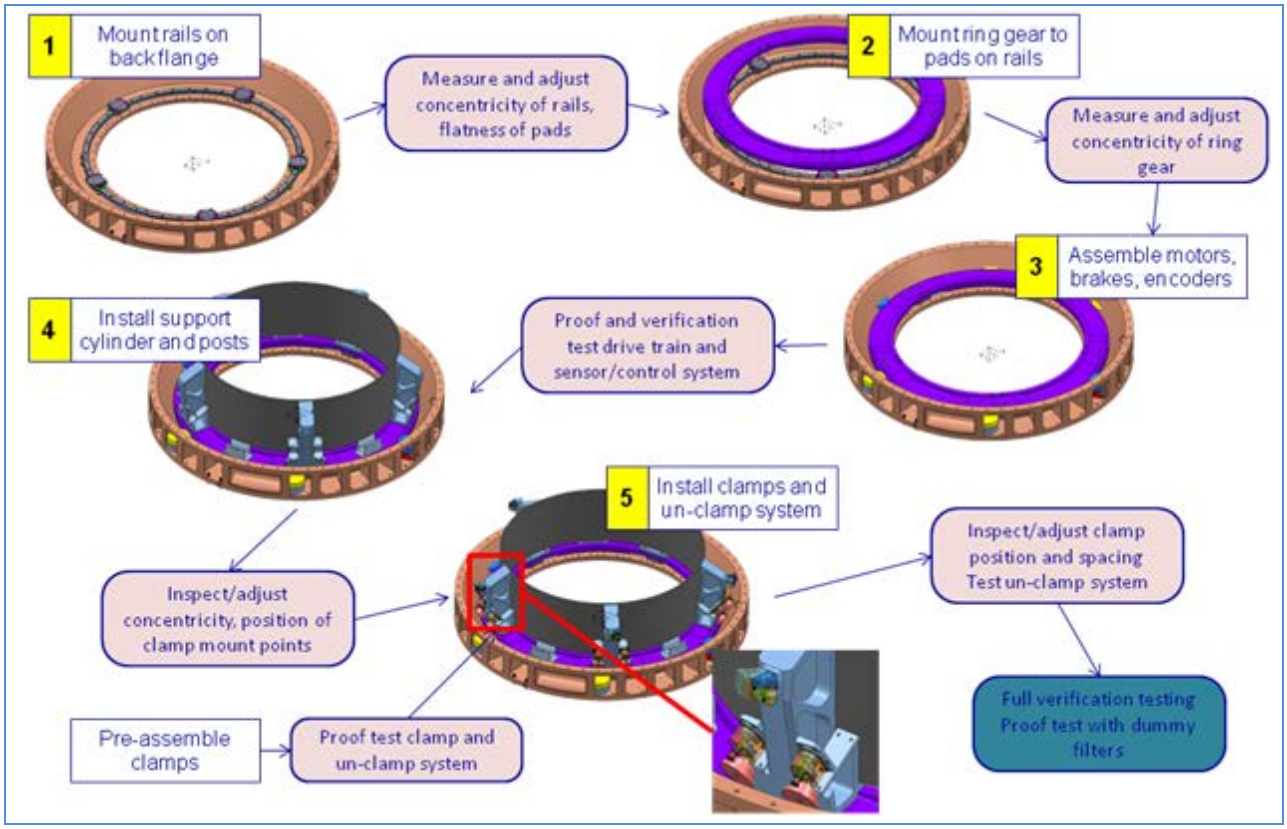

Figure 13-53: Carousel assembly and test sequence

13.7.3 Full Filter Exchange System Assembly and Test

The full Filter Exchange system will be assembled on an assembly and test bench. The test bench shall allow the assembly of the individual Filter Exchange components, and it provides interfaces emulating the camera interfaces to the Filter Exchange system. The Carousel will be assembled on a dummy Back Flange, whose design reproduces at best the design from SLAC with respect to interfaces external to the Filter exchange system, while providing exact interfaces to the Filter Exchange system. As there is no constraint on the outer envelope, and to limit manufacturing costs while providing the total stiffness, the dummy backflange is made of assembled parts. The backflange contains reference measurement points for the 3D metrological tools.

A dummy Camera body provides fixations for the Auto Changer and free volume for the loader, and provides the housing envelops. The electrical feeds run through dedicated holes in the Back Flange. The required cleanliness will be performed by the dummy camera body: sealant devices and controlled airflow inside the prototype. The Camera Body will allow accessibility tests for the maintenances procedure, training operators and dismounting mechanisms. See Figure 13-54for the assembly of dummy Camera Body on the dummy Back Flange.

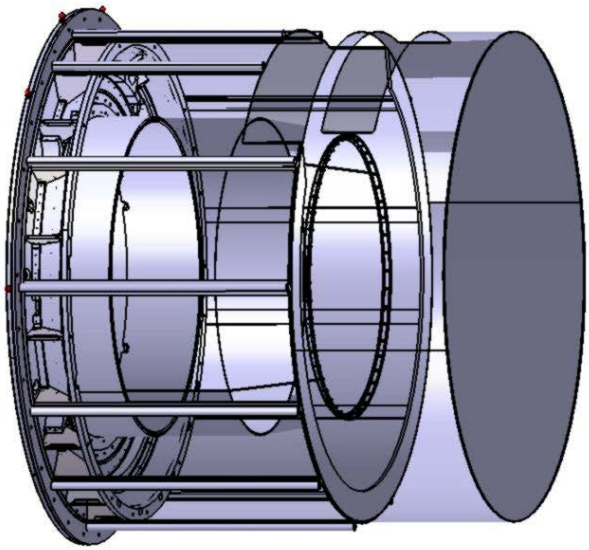

Figure 13-54: Dummy Back Flange and Camera Body envelope

The Back Flange and the Camera Body are mounted on a rotating mechanical stand which enables to put the system into any angular position observed during observations (Figure 13-54). The camera axis can rotate from zenith to nadir, with 10° overdrive, and there is a rotation of +/- 100° around the camera axis. The test bench also monitors the environmental conditions: temperature, humidity and pressure. The motors are controlled in coordination with the FCS, and the control/command of the whole system is under supervision of a CCS console. Finite element computation will ensure that the stand has the correct stiffness to hold the Back Flange and associated loads.

Dummy filters are designed to provide mechanical interfaces for the filter mount, and reproducing loads and center of mass of the filters. 7 dummy filters will be manufactured, 6 of them will reproduce the masses of the 6 LSST filters. The dummy filters are made from a base of one frame and an aluminum mass. Additional mass will be mounted on this base to vary the masses of the various filters, including qualification masses, while keeping the global envelop of the filters. In addition, one filter will be instrumented with probes to monitor accelerations and shocks during operations, and with filters dedicated to contamination tests Figure 13-55. The acceleration probe is a MSR165 data logger with a sensitivity of 0.01 g on a 15 g range, a recording rate of 1600 Hz, and can record data wirelessly. It can be configured as a shock monitor, with a tunable trigger.

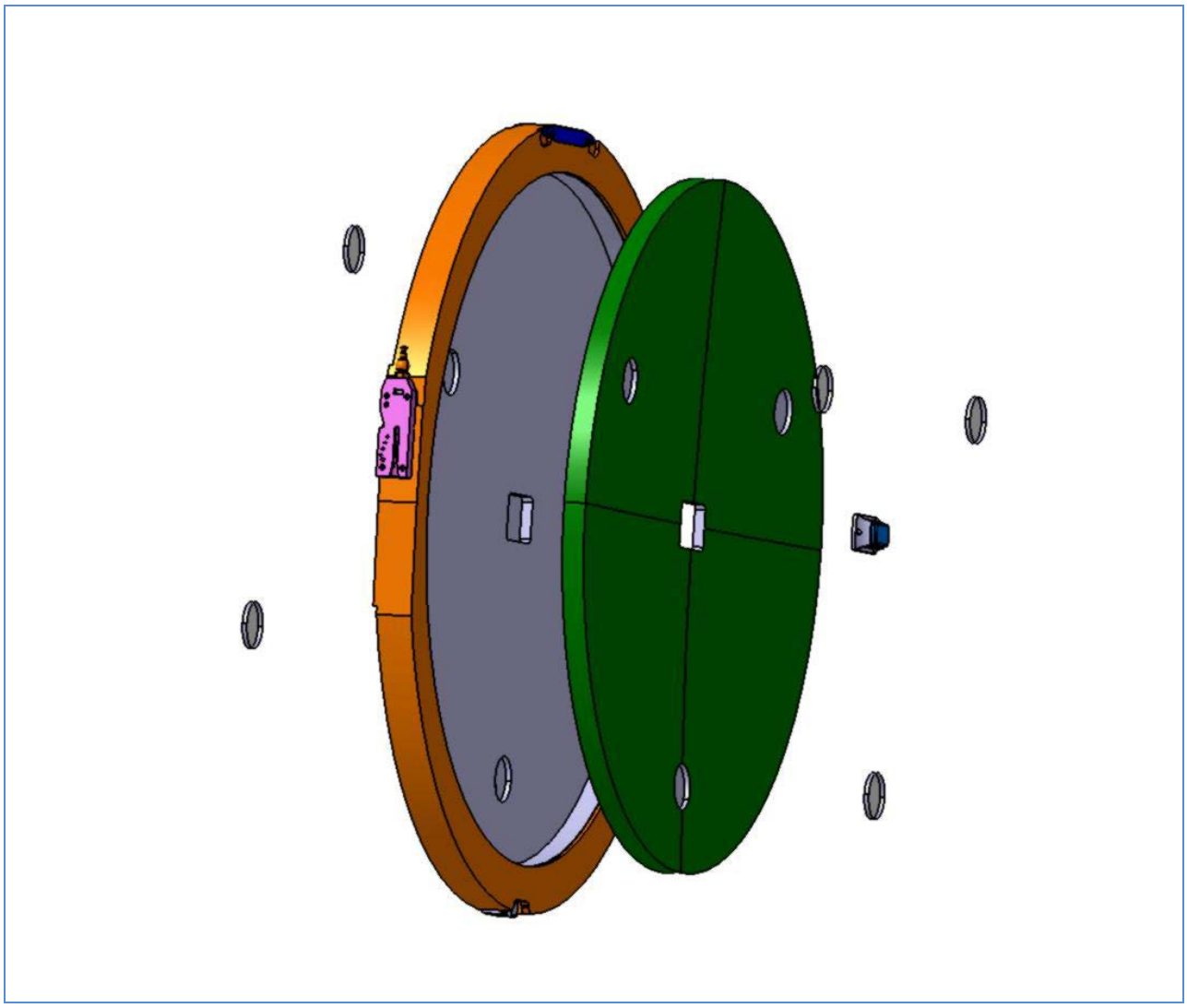

Figure 13-55: Instrumented filter design with adjustable mass, contamination filters and acceleration probe

The purpose of the test bench is to provide a facility to assemble and test the prototype. A long-run test is planned after the functionality tests will be performed. The test plan has been defined in accordance to the compliance matrix (document LCA-10757), and the test plan diagram is shown in Figure 13-56.Figure 13-56: Full Scale Prototype Test Plan diagram

After the long-run tests, the facility will be available for the integration and validation of the final system. Then the prototype will be reassembled, in order to serve as a reference model to train operators and study troubleshooting recovery procedures.

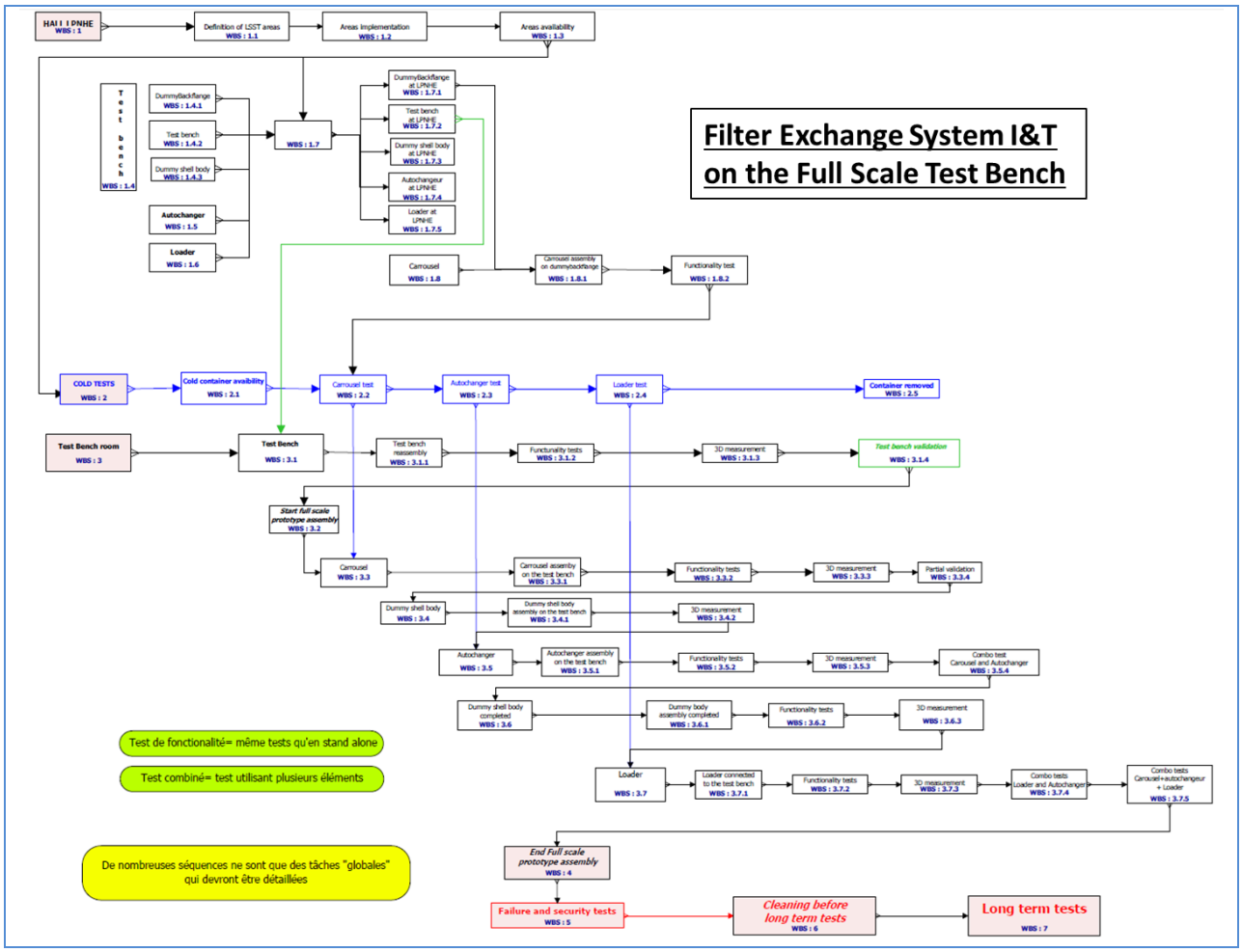

Figure 13-56: Full Scale Prototype Test Plan diagram

The tests will be held in a closed room inside the LPNHE new assembly hall in Paris. The crane in the hall will be used for the assembly on the test bench and to handle the Filter Loader when needed. The final assembly, cleaning and closing of the housing envelop will be done in a clean environment (ISO 6) build in this hall. The long test run will be done in the hall, the housing envelop and associated dry nitrogen air flow, filtered with ISO 5 filters, will emulated the expected running environment and cleanliness. The hall air is conditioned, and we will perform the long run test at 20°.

For cost reasons, the full hall, even if clean and new, will not guarantee by itself the ISO 6 level aimed at for the final assembly. The baseline is to have 2 clean room space in the hall and the associated clean area for dressing: a 25m2 x 3.5m high room to perform the final cleaning and closing of the envelops. This space will have an access from the roof to allow the usage of the crane, implying to break the room cleanness and requesting a full cleaning/requalification afterwards. And a 10m2 x 2.2 high room to perform travel unpacking, cleaning, specific packing and cleanness protection before assembly.

Before assembly on the test bench, each metallic part of the filter exchange system will be measured in order to measure the activity in term of radiation. This measurement will be made for two ranges of energy, high energy and low energy. Some specific instruments will be used for this purpose, a Ludium

Model 2241 Digital Survey ratemeter with associated probes, a Ludlum Model 44-2 which covers the energy range of 60 KeV to 1.25MeV of gamma radiation dedicated for the high energy measurement and a Ludlum Model 44-9 (Geiger Mueller) probe which allow to measure alpha, beta and gamma radiation in the range of 60 to 100keV, dedicated for the low energy measurement. The procedure of the measurement we are going to use+, is described in the document “LCA-10776 Radioactive Material Test Plan” in which is specified that the measurement will be made for an integrated time of at least one minute in the air and at the immediate proximity of the sample.

For cost reasons, thermal requirement will be tested on each individual subsystem before assembly. A cold container will be rented, and the standard dimension allow each subsystem to fit in. The operation temperature of the container allows to go as low as -20° which addresses the lower temperature range for requirements C-EXCH 143, 144 and 145. The upper temperature requirements cannot be addressed this way. Our baseline is to use the differential metrology between -10° and 20° to cross-check the thermal computations, and to extrapolate the behavior at +30°. If the conditions allows outside the hall, we may shut down the air conditioning in summer to elevate the hall temperature, but there is no guarantee on the upper bound we can reach with this procedure.

Once reassembled in the assembly room, the subsystems will be placed with a pallet truck in the container, and the internal conditions will be monitored through HTP probe. As the THK rail is the most critical piece for the thermal stress, the Carrousel will be under full scrutiny. It will be tested in all configurations: without loads, loaded with all dummy filters under qualification loads, and loaded with the most unbalanced configuration. Checks include visual inspection at low temperature, 3D measurements, analysis of instrumented filter acceleration probe. The Auto Changer will be tested with specific care to address C-EXCH197 spec on the maximum motion of the filter interface datums over the accessible temperature range. For the loader, as there is a height constraint inside of the container, a simulation load will be employed.

The integration and test of the Carrousel will be performed on the test bench after the cold tests. Functional tests will be performed with a wide range of filter loads, including the most unbalanced combinations, and the rotation time specs will be validated. 3D arms will be employed to perform the metrology, and 0.001 mm resolution 1D comparators will measure the displacement of carrousel posts with the inclination of the camera axis. Motor currents, temperature and functional parameters as well as rotation time will be monitored by the FCS. The instrumented dummy filter will record accelerations for future reference.

After carrousel integration, the dummy Camera Body will be completed and the Auto Changer assembled on the test bench. The functionality tests include a thorough inspection of Carrousel and Auto Changer interfaces, tests of filter exchange from the hand-off location at any rotation angle. 3D measurements will provide the Auto Changer installation repeatability, the filter online positioning repeatability, and follow the filter motion in the online position when rotating the camera. Motor parameters and environment conditions will be recorded by the FCS, as well as the time to change filters starting from any position on the carrousel. The instrumented filter will record accelerations. With the full prototype in place, inspection with light sensor will check that no light originating from electronic

components will reach the focal plane. We will also check that the carrousel clamps will be replaceable in situ.

Combined tests with the loader will be performed once the Auto Changer integration and tests are completed. This includes functionality tests, loading and unloading a filter, inspecting the stay-clears, and 3D measurements. The compliance with the total time to swap-out a filter will be measured, and the effect of training the crew for filter exchange will be monitored.

Once functionality tests will be completed, compliance with the FCS and failure recovery will go under scrutiny. Most of the FCS commands will be already validated at this stage, and the tests will focus on troubleshooting recovery. From the individual subsystem failure mode analysis, simulation of the corresponding signal will be implemented: fake detector signals will be sent to the protection system. In addition, bogus commands will be sent to the controllers to check the adequate LPM performances. The loss of power and safe restart from any status of the filter exchange system will also be tested.

Long duration tests will start once the prototype has been fully qualified. Carrousel will be loaded with 5 filters, and test will be performed for a range of angles. The envelop contamination goal is to reach an ISO 6. Physical measurements during the long duration tests include wear, geometry variation, alignment variation, motor consumption, filter exchange timings, and surface contamination by dust and non-volatile products. Visual inspection of sliding parts, clamping/blocking parts and lubricant behavior will be performed. The FCS will be used for the monitoring of all those parameters, and accelerometer value will be recorded on a regular basis. Pictures of all moving parts with friction will allow to judge the aging of the system. Such observation will be performed at each week day, during the filter swap-out, and at the end of each year cycle with a partial dismount which will allow access to all part subject to aging. At each end of year-equivalent cycle, abnormal flexion, alignment, geometry, screw state will be monitored. As a result, the long-duration tests will provide not only the long-term behavior, but also the method to observe the different key parts.

The long duration tests will cover many years of operating condition. The number of filter changes has been estimated to 7000 per year, with 50 swap-out with the Filter Loader. From OpSim, we expect up to 4 filter changes per hour, and up to 40 filter exchanges in 1 day, that is, 1 filter exchange every 20 minutes. The filter exchange system can accommodate for at least 6 filter exchanges per hour, keeping the running parameters at the nominal value. The equivalent of 1 year running will then take 48 days of continuous filter exchange, and 2 days of swap-outs, spread in 1-H sequences. We plan to perform at least 1-year equivalent cycle before the start of the construction of the final system. In 18 month of long-duration tests we will be able to collect data equivalent to 10 years of LSST.

During operations of the filter exchange system, some parts that age can be replaced: motors and breaks (including carrousel motor), the full Auto Changer for which 1 full spare will be build allowing for an in-place swap, loader, and clamps (for which we provision a full-set of spares). The frequency at which the elements should be changed will be determined during the long-run tests and maintenance triggers will be defined. The full scale demonstrator will be used to define how to perform each maintenance, and it will be available on the long term for the full length of the camera life, allowing to

train staff for the maintenance operations or to help performing diagnostic on an open system in case of an unexplained problem at summit.

The 1-year equivalent test will be used to monitor the contamination, following the throughput allowed change from LCA-18. For re-cleanable hardware, contamination accumulation budgets are applied separately for each interval between cleanings. The cleaning interval is assumed to be 1 year. For optical surfaces molecular contamination, the total cumulative throughput is 0.15% to 0.3% For optical surfaces particulate contaminants, the total cumulative throughput is 0.01% to 1.53%. Assessment of the contamination effects on total throughput degradation establishes the most demanding limits to particulate contamination for the focal plane, and other optical surfaces, whereas throughput change between calibrations is a less stringent requirement. Particles of size 0.1 µm diameter and larger can be considered to be opaque to optical light. For the optical elements particles below 0.1 µm have no effect on the throughput.

Due to the filter exchange system size, its large number of components and the complexity of their interactions during a filter change, the requirement to select “clean” component known to not liberate particles or NVR (non volatile residual) is not enough to guaranty that the filter exchange system will satisfy the LSST requirements in term of contamination. We consider to use 3 methods based on data collected during the “demonstrator aging run” to demonstrate that the filter exchange system qualify the LSST contamination requirement:

The evolution of the transmission over the full camera wavelength domain of fused silica test sample, located on both side of each filters, at the location of L2 and L3, will be directly measured at LMA in Lyon.

The count and size of deposited particle on key locations will be measured using a surface particle counter on site or at LMA on sample.

To further diagnose the contamination generated by the filter exchange system, a few “tape traps” will be installed in key locations, and once removed will be analyzed under microscopy.

IN2P3 LMA laboratory will bring its expertise on coating and optical metrology to the project. They will measure/characterize the small lenses & filters samples provided by vendors. The setup is based on a Perkin-Elmer Lambda 1050 able to measure very precisely transmission with an absolute precision of 0.0001% in the 175-3300nm domain on sample up to Ø110mm at an angle of incidence from 0° up to 31°. They also have surface analysis tools allowing to further characterize the origin of the transmission lost in our contamination sample.

Test samples will be put on each side of the fake filters and at the location of L3 outer surface and L2 inner surface in a way that fake as much as possible a continuous surface with the surrounding material. A few test samples will be replaced by new one at each year cycle and their transmission measured over the full camera wavelength domain. This transmission will be compared to a witness sample to estimate the total throughput lost. For the test sample we plan to use an uncoated fused silica window of 30 mm, like the Edmund #45-569 reference. It has a flat transmission of ~ 90% between 200 nm to 1500 nm,

fully covering the LSST camera wavelength domain. To distinguish the lost in throughput due to NVR or to particles, further analysis could be implemented: the shape of the transmission versus wavelength, will give a hint as particles will generate a grey extinction, and NVR will wave length dependent extinction, a surface particle count can be performed to precise the type and density of particle on the glass, detailed surface analysis could show contaminant drop if any.

We consider the option to extend the particle count on small sample as part of the throughput study to direct metrology on site of different part of the filter exchange system. Cost, time, and the need to precise contamination behavior may activate or not this option. Different type of instruments exist to perform particle counts on surface, there is in practice two types of system:

System based on “vacuum / air /liquid flow”, allowing to remove the particle from the surface and count them with a standard “clean room airborne like particle counter”. Such system are able to count really small particles (< 1 µm) but with the risk that some stay “glued” to the surface and not taken into account.

System based on optical particle count on images, which in practice for a reasonable cost (=optical system) cannot go below 0.5 µm, and in practice they are fully efficient for particle above 1-2 µm. The imaging solution seems more appropriate in our case, considering that small particles (< 0.1 µm) have no impact on the throughput, and that the test proposed in this section is seen as complementary of the transmission measurement.

The imaging solution seems more appropriate in our case, considering that small particles (< 0.1 µm) have no impact on the throughput and that the test proposed in this section is seen as complementary of the transmission measurement.

To collect particles generated by the filter exchange system, tape fixed on a removable frame can be put in key locations to trap them. In practice we propose to have a universal interface that can accommodate either a small fused silica sample or a tape and its frame. Visual inspection with microscope of the exposed tape, will allow to count the particle in function of their shape/size, which my help to identify their origin. Large particle (a few 100 µm) if any, will not be “glued” by electrostatic forces on surface, and will move in function of the camera position. This can become quite damageable for the science as then the camera transmission will become non uniform and change on quick time scale. Tape traps in key location could collect such type of large particle. Even if we don’t found such type of contaminant in the filter exchange system test, it could be interesting to consider such type of trap in the camera.

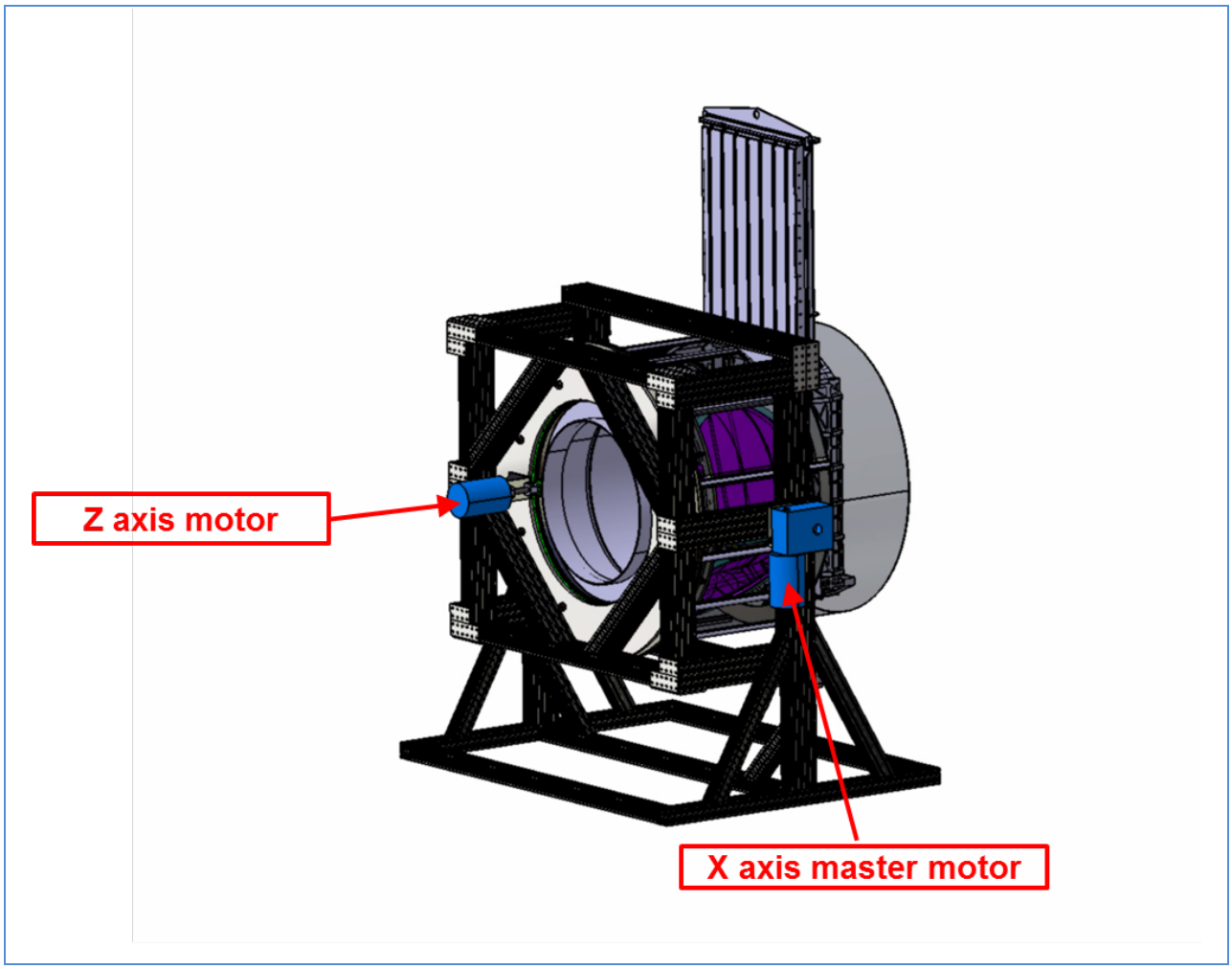

Figure 13-57: Full Scale Prototype Test Bench

14: Shutter

14 Shutter

14.1 Introduction

The LSST Camera shutter controls exposure duration and interrupts light while the image is read out and the telescope is being re-positioned for the next exposure. It is a double-bladed guillotine-style mechanical shutter that lies tightly packaged between the L3 lens-cryostat window and the filter and its exchange system. The shutter controls the length of time that the sensors on the focal plane are exposed to an image, while blocking out all stray light when closed during read-out of the CCD sensors.

As shown in Figure 14-1, the shutter is a two-blade design, where flat blades move across the focal plane to start or end an exposure. This double-acting shutter includes two shutter blade stacks. The first opens to one side to expose the field of view (FOV), beginning the exposure; then, the second blade set occludes the FOV by deploying from the opposite side, traveling in the same direction as the first. For the next exposure, the process is reversed. This provides a uniform exposure time for all pixels, since the first pixel exposed by the trailing edge of the first blade stack is also the first blocked by the leading edge of the second stack.

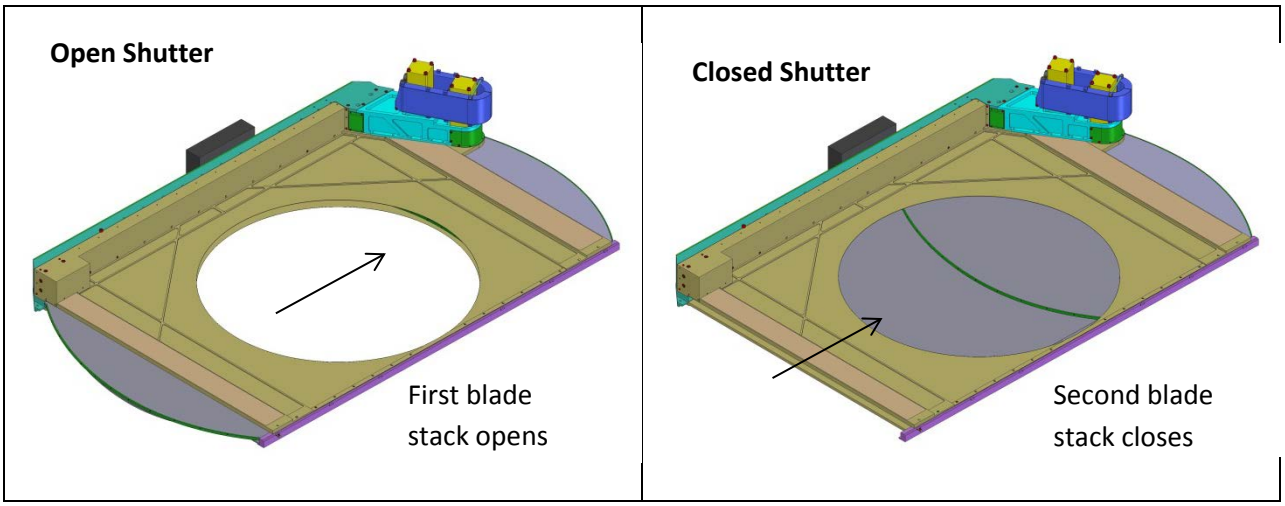

Figure 14-1: Double-acting shutter motion for an exposure

14.2 Requirements

Key requirements for the shutter are listed in the Table 14-1.

Table 14-1: Shutter driving requirements

Requirement Title	Requirement
Lifetime	The shutter shall be designed for an operating lifetime of 15 years.
Design cycles	The shutter shall be designed for at least 1E6 open/close cycles per year
Exposure duration accuracy	The accuracy of the shutter exposure duration shall be < 50 milli-seconds
Exposure duration knowledge	The exposure duration shall be known to within 300 msec with a goal of knowing the duration to 5 msec, rms.
Max opening time	The shutter open time shall be 0.98 seconds or less with a goal of 0.9 seconds.
Max closing time	The shutter close time shall be 0.98 seconds or less with a goal of 0.9 seconds.
Clear field of view	When open, the shutter and all of its constituent parts shall not obscure the field of view
Light scattering	All components with a direct view of the field of view of the internal light cone as defined in LCA-10333 shall either be shielded by light baffles, treated/shaped to minimize scattering, or coated flat black. Paint with a BRDF (Bidirectional reflectance distribution function) equal to or lower than the BRDF of LORD Aeroglaze Z306 coating is acceptable.
Light tightness	When exposed to diffuse light, the closed Camera shutter shall attenuate the light flux by 10,000 when averaged over any square centimeter as measured at a distance of 75.04 mm in the +z direction from the interface plane defined on the Shutter Interface Definition Drawing (LCA-73).

Weight	The shutter assembly mass shall not be greater than 45 kg.
Compliance with Shutter IDD	The shutter shall comply with interfaces and stay-clears defined in LCA-73
Operational loads	The shutter shall perform within specification while subject to any of the operational load cases listed in Table 1 of the LSST Camera Loads Specification (LCA-68).

Key performance requirements center on the precision of blade trajectory and knowledge of the exposure time of all pixels across the focal plane. Exposure timing and measurement precision affect the photometric accuracy of the images. Clearly, light-tightness or light attenuation when closed is another important requirement. The shutter is the only mechanism in the telescope's field of view light-cone, so it must not scatter light onto the detector plane when open, and it must also provide a "light-tight" seal when closed. Other key requirements cover the cyclic lifetime of the shutter, opening and closing at a nominal cadence of once every 15 seconds. This adds up to many open-close cycles over the life of the shutter, with minimal time available for significant maintenance.

The timing and control requirements are related to the repeatability and uniformity requirements because the timing information provided by the controller must be sufficient to enable the accurate reconstruction of the exposure timeline. Also, the shutter mechanism must maintain adequate clearances to neighboring components, independent of Camera orientation. Shutter motion control must compensate for changes in the direction of gravity. Finally, the strict contamination control requirements reflect the importance of maintaining an environment with low particulate count to minimize degradation of throughput by particles deposited on neighboring optical elements.

14.3 Shutter Design Description

14.3.1 Functional Design

Mechanical shutters for telescope cameras have been of either the roll-up window shade type as used on Hyper Suprime-Cam (Wang, S.-Y., E. J.-Y. Liaw, et al. 2008) or the rigid blade type as developed at Bonn University by Klaus Reif (Reif, K., G. Klink, et al. 2006). LSST's Camera uses rigid blades guided by linear bearings and driven through toothed belts similar to the Bonn shutters, with opening and closing blades sweeping across the focal plane from parking places at opposite ends of a common track. However, because the Camera aperture at the shutter position is 750 mm in diameter and the Camera is in the incoming optical beam of the telescope, blade parking space is limited. To reduce the area needed to park the blades, each blade set has been divided into two blades which, in the parked position, stack one above the other to conserve space. Each blade is separately driven on the drive rail by its own drive belt, but a set of two blades in a stack is driven by a single motor, coordinated by different wheel diameters on a single capstan drive shaft. At the blade tips, all blades run in a common guide rail, restrained by spring pre-loaded sliders.

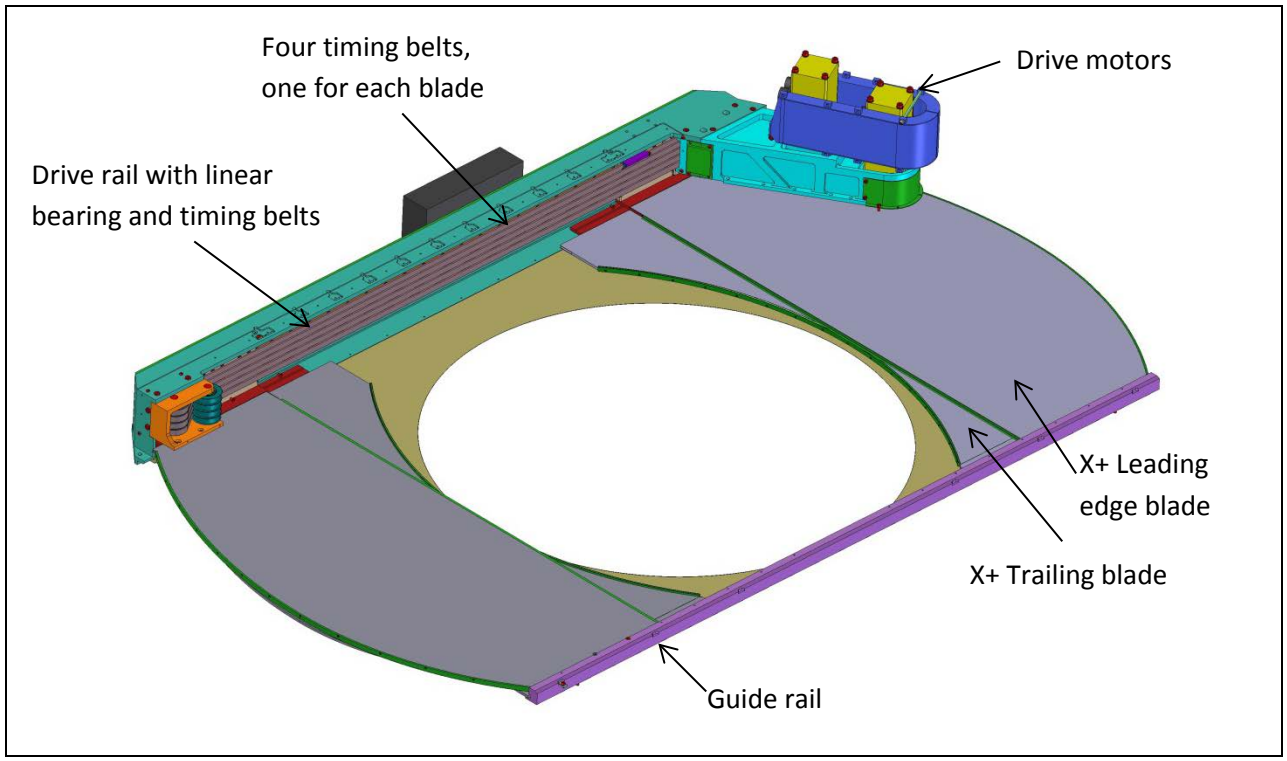

Figure 14-2: Shutter assembly with Z- garage plate and cover removed to show drive system components

Shutter operation begins with one blade set closed, covering the focal plane. Exposure starts with the closed blade stack being retracted to its stacked, parked position. Exposure ends with the extension of the opposite blade set in a coordinated telescoping motion to cover the field of view. Using two blade sets following in the same direction is necessary for uniform exposure over the field of view.

Space for shutter components is tight in the transverse and through direction, as well. Transverse to the path of blade travel, the path swept out by a filter as it is being moved into the on-line position by the autochanger barely clears the shutter track on the side of the guide rail. Consequently, both blade stacks are driven along a single drive rail, with the narrow, thin guide rail only providing out-of-plane support of the cantilevered blades.

Along the axis of the Camera, the shutter must fit in the gap between the filter and the L3 lens. This gap is very tight, constraining the shutter to thin panels and a thin double-stack of blades, made from a carbon fiber composite (CFC) lay-up to maximize rigidity for the available blade thickness.

14.3.2 Operations and Maintenance Accommodations

The shutter unit is a self-contained, modular assembly that can be removed and installed relatively quickly. Such a modular design is important for two reasons. First, it allows for the preservation of bench-top calibration and performance verification, to ensure that the as-installed unit performs in full accord with previous off-line lab testing. Also, the modular design allows the shutter to be replaced quickly during the short daytime maintenance times. Given the tight volume constraints of other Camera elements in very close proximity, it is not practical to service or repair the shutter in place.

Thus, accommodating an efficient removal and replacement of the shutter module is an important aspect of the design.

Finally, the shutter must operate in any Camera orientation. When the Camera points near zenith, gravity does not tend to act on the drive system. However, when the telescope is pointed nearer the horizon and the Camera rotated off its nominal upright orientation, the shutter drive system must drive the blades up and down against gravity. When the shutter starts its motion, the controller transfers holding torque from the brake to the motor. To prevent backsliding of the shutter blades, it is necessary for the motor to start applying torque before the brake is released.

14.4 Shutter Analysis

14.4.1 Drive System Dynamic Analysis

The full shutter system includes two stacks of two blades each, both moving on a single rail. A simulation has been made of the dynamics of a double blade stack with cantilever drive (Bowden, 2014). A schematic for the single blade model is shown in Figure 14-3. The model takes into account the rotational inertia of the drive motor and capstan, J1. The stretch and damping of the toothed drive belt are k1 and b1. The masses of the linear bearing and blade are m2 and m3, while the frictions of the two linear bearings are b2 and b3. Of major design importance is the rotational stiffness, k3, of the blade mount to the linear bearing. The ratio of k3 to the blade's rotational inertia, J3, must be stiff enough to prevent angular vibration as it is accelerated. The natural frequency of blade oscillation around its mounting to the linear bearing is about 45 hertz. A detailed finite element model of the leading edge blade has been performed to calculate the values of these parameters.

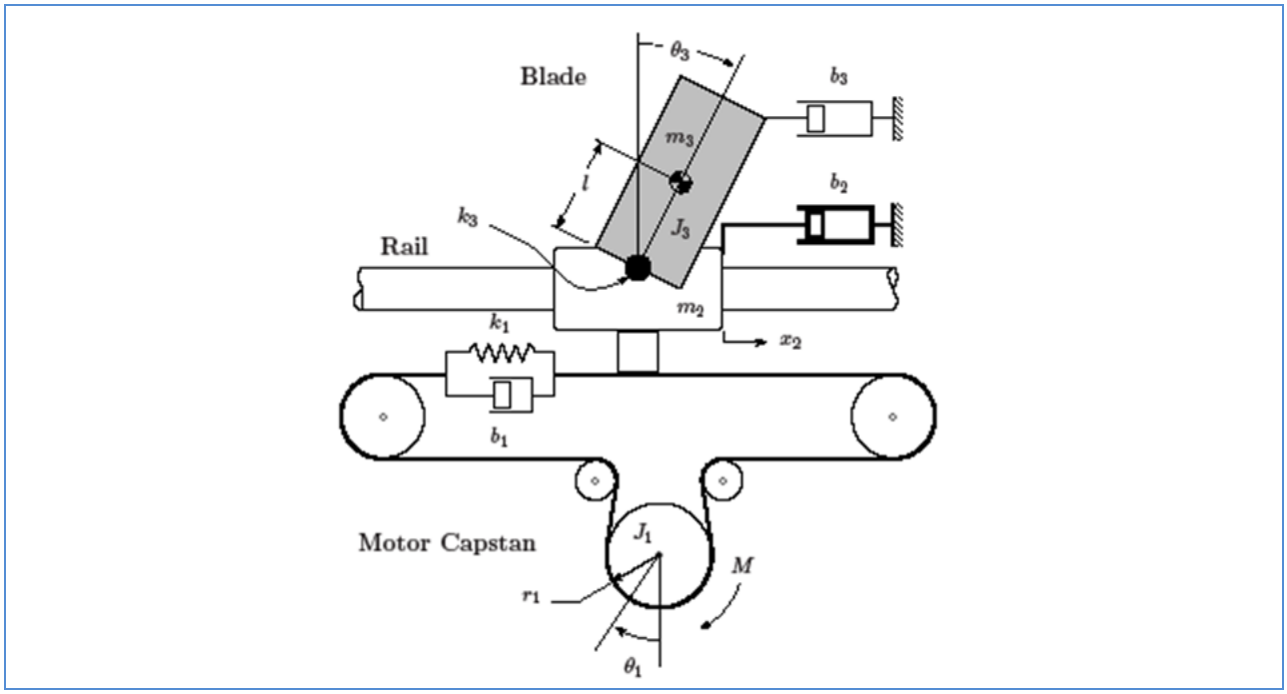

Figure 14-3: Shutter single blade model schematic

The present specifications for blade motion are a stroke of 750 mm and an actuation time of 1 second. The shutter is too large and the stroke time too short for uniform blade velocity to be used. The required accelerations and decelerations would be too great. To limit the required acceleration and sudden force reversals, blade velocity must vary continuously over the entire stroke. We have adopted a smooth point-to-point trajectory commonly used in the motion control industry called an `S'-wave, shown in Figure 14-4.

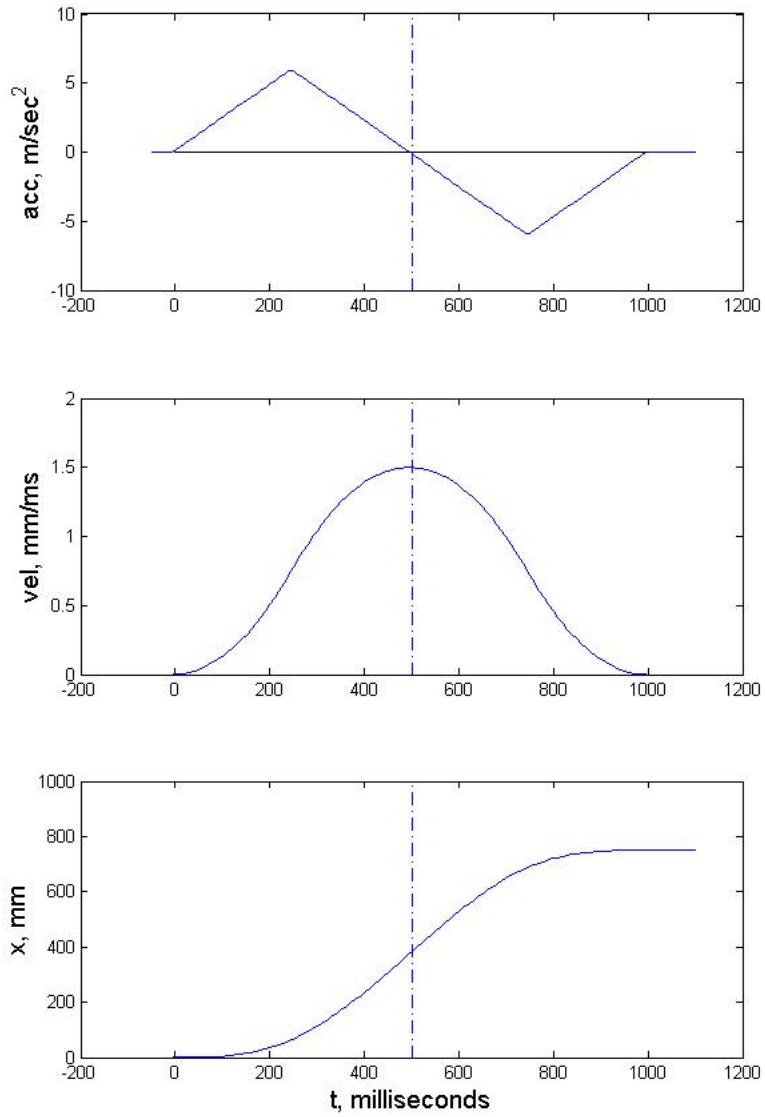

Figure 14-4: Shutter blade S-wave motion profile acceleration, velocity and position

The Bonn shutters are based on stepper motor technology used in industrial automation. Machine tools and other dynamic systems usually employ servo motor technology. The LSST shutter will use DC

stepper motors. Stepper motors have a simple holding torque for static positioning, but the selected motor includes a built-in electro-mechanical brake that will be electrically released at the start of each blade stroke. This reduces the power needed for holding blades in position when off. Standard error feedback is Proportional+Integral+Derivative or PID. Motor response has been computed for the single blade model of Figure 14-5. The feedback block diagram is shown in Figure 14-5, and the system response in Figure 14-6.

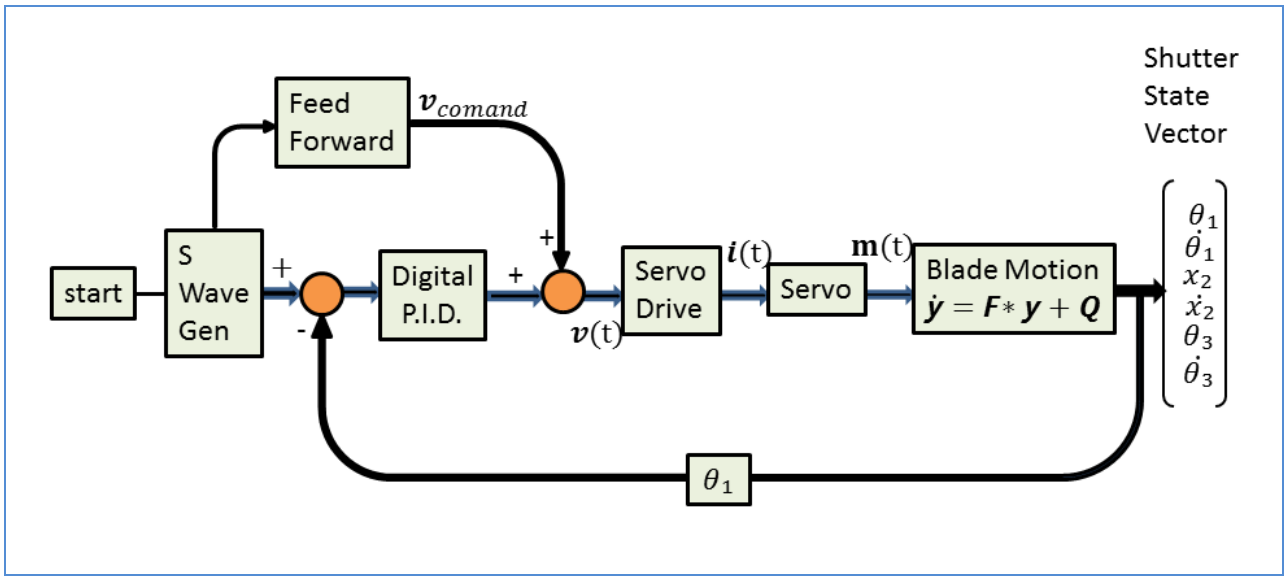

Figure 14-5: Motor and blade dynamics block diagram.

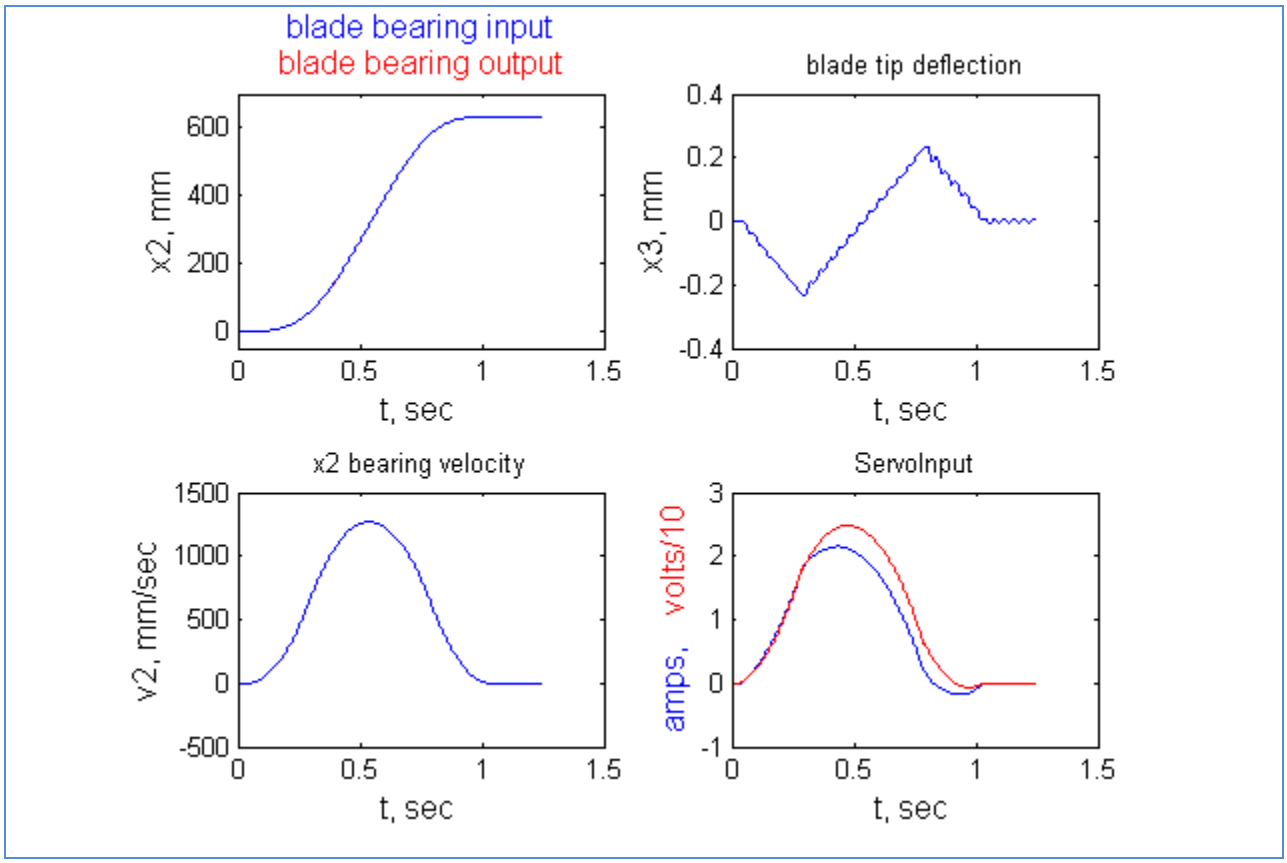

Figure 14-6: Motor and blade response to S-wave input. Peak acceleration is 0.6G.

14.4.2 Exposure Uniformity Analysis

For uniform exposure across the focal plane, opening and closing blade motions must move in the same direction with the same velocity profile, although constant blade velocity is not needed. If the shutter were mounted inside the cryostat directly in front of the focal plane, star light would be extinguished at each pixel the instant the leading edge of the shutter passes over. But the shutter is outside the cryostat, 105 mm in front of the focal plane. At the shutter plane, light converging toward the pixel is a donut shaped ring with radii of 28 mm and 20 mm. The pixel's aperture closes gradually as the shutter sweeps across this cone of light converging on the pixel. If A(t) is the exposed aperture area, the pixel exposure time is:

$$\frac{1}{A_0}\int A(t)\,dt$$

Instantaneous intensity $A(t)/A_0$ is plotted for a number of pixel locations along the shutter's path in Figure 14-7.

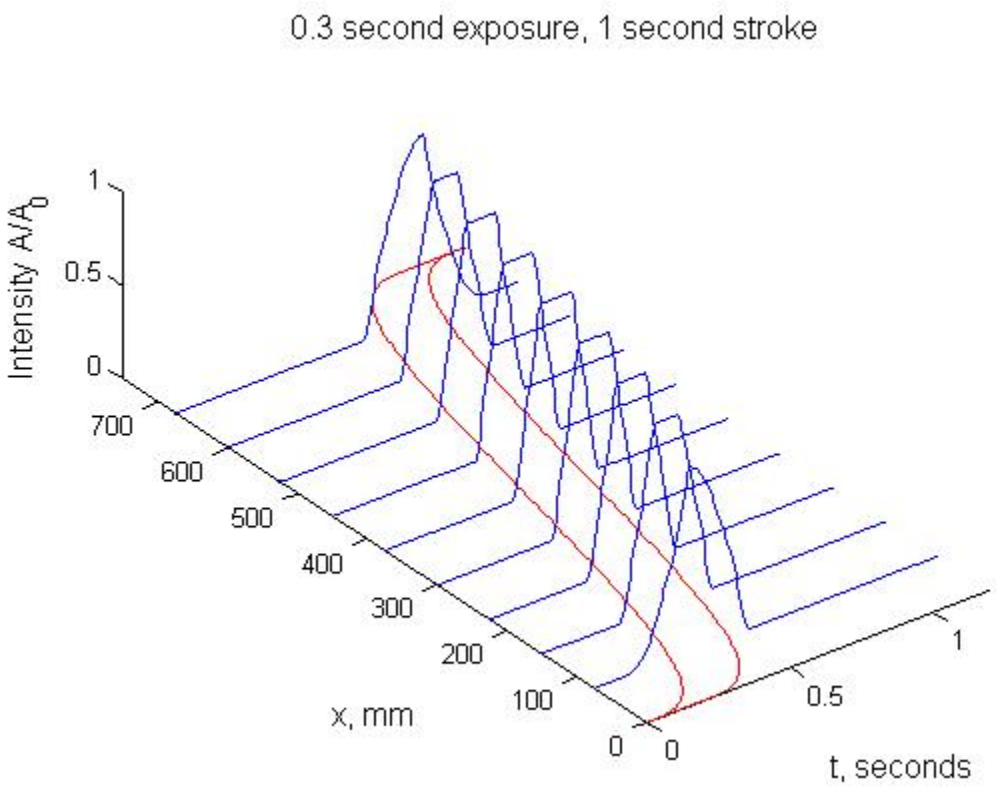

Figure 14-7: Pixel exposure for shutter at 105mm in front of focal plane. Red plots the motion of the opening and closing blade edges.

Exposure waveforms near the ends of the blade stroke are distorted by blade velocity variation across the pixel's aperture. Nevertheless, each pixel's total exposure as measured by the area under the intensity curve is everywhere the same. Figure 14-8 shows how deficits and surpluses of exposure compensate over a pixel's exposure as long as shutter opening (blue curve) and closing (red curve) trajectories match.

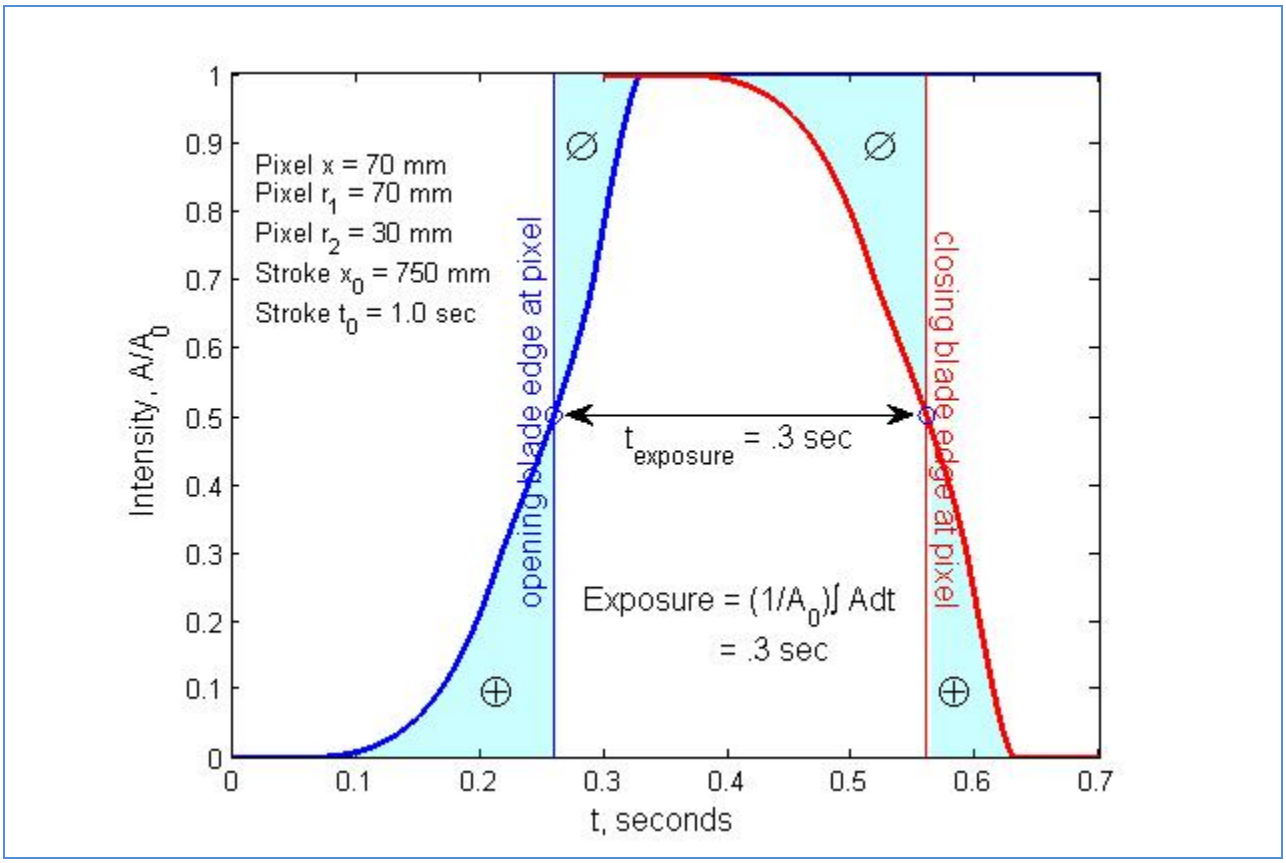

Figure 14-8: Pixel exposure geometric intensity $A(t)/A_0$ for shutter sweep across a pixel near the edge of the field of view ($x=r_1=28$mm) where the blade is accelerating.

14.4.3 Structural Analysis

There are three coupled force equations for acceleration of the motor capstan, linear bearing and shutter blade; the system is driven by a prescribed motor torque. The resultant equations of motion are of little use in calculating blade drive motion without realistic numerical values for the system parameters. Accurate values for some of these come directly from product catalogs while others depend on calculated values. A finite element analysis of the shutter blade was performed to calculate these unknown parameter values.

Numerical simulation results for the present design are heavily dependent on the numerical values of the system parameters. With the combination of published and derived parameter values, the main deviation from the desired blade motion is 0.8mm tip deflection due to cantilevered drive. The blade and its guide bearing are capable of a 45 Hz vibration but with sufficient bearing friction and a smooth application of motor torque, this vibration is not excited. A certain amount of bearing drag force is desirable to damp vibration. Mechanical noise due to individual steps or drive belt teeth is not included in this analysis.

The results of the dynamic analysis, i.e. peak accelerations, were applied to the shutter blade Finite Element Analysis (FEA) model and corresponding stresses, deflections and buckling critical loads were

calculated. The margins of safety are extremely high for the load experienced during shutter actuation. This is partly because this exposure uniformity demands extreme stiffness. Fatigue failure is not an issue.

An FEA model of the shutter was created and integrated into the full Camera model. The shutter was then subjected to all anticipated Camera loads. In addition to the mechanical properties discussed above, stresses and deformations were calculated to guide the design and optimize load paths. Because the shutter will undergo millions of cycles, it is important to understand the stress levels in the components. Similarly, displacements of the parts are also important to understand because the parts are relatively fast moving and have very small clearances. The relative displacements between the shutter internal parts and proximity to other subsystems have been calculated and shown to have adequately designed clearances. Brief discussions of the stress and displacement results are provided below.

Representative stress contour plots for the actuation direction are shown in Figure 14-9. Since the shutter components have been designed with stiffness in mind, stress levels are expected to be low. It can be seen that the induced stresses in the structure are significantly lower than the allowable stresses. The corresponding minimum margin of safety is 3.8.

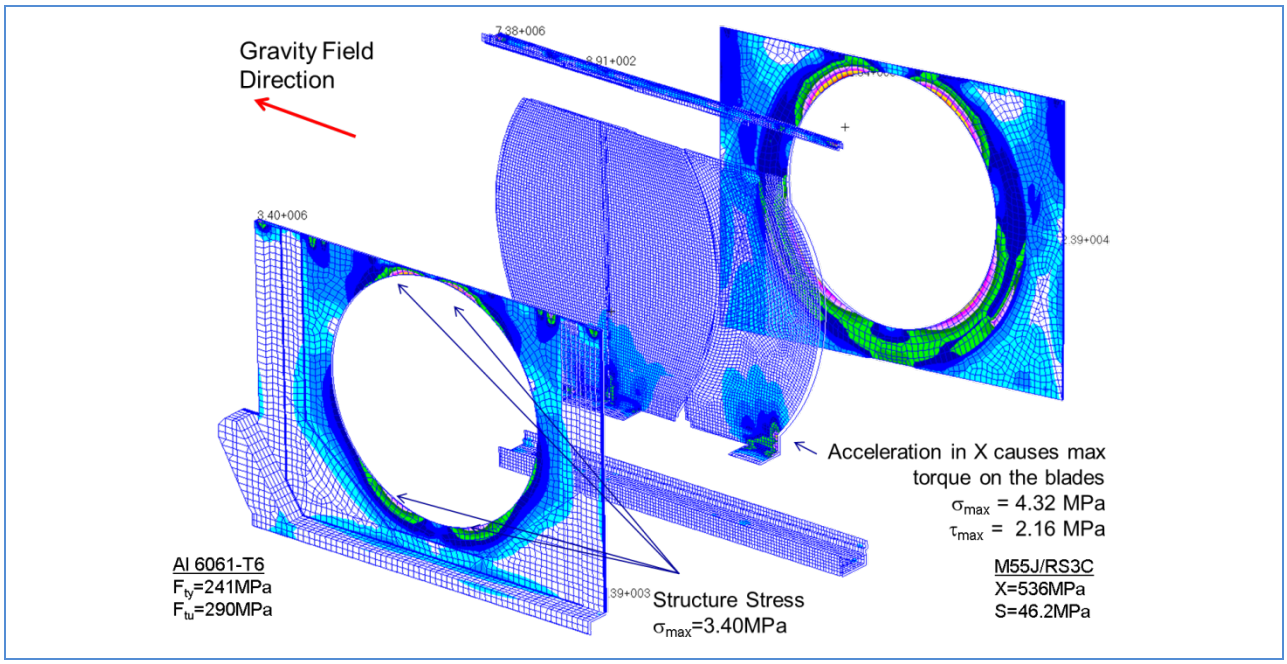

Figure 14-9: Shutter assembly stress contours when subjected to 1G acceleration in X_{CCS}

When the Camera is subjected to the full set of load cases, the shutter and other Camera components will move relative to each other. Because the clearances between the internal shutter components and surrounding subsystems are small, the shutter parts must be stiff enough to limit displacements due to gravity and operation loads. Similarly, any reduction in the gap between the shutter and other Camera components must be calculated. Deformation of the shutter when sandwiched between the filter and the L3 lens is shown in Figure 14-10. It can be seen that the shutter out-of-plane motions are greater in magnitude than the filter and L3 lens. Worst case relative displacements were assumed, i.e. that the

motions are out-of-phase and move towards each other. Looking at all of the critical clearances, the minimum gap due to dynamic motions decreases from 2.0mm to 0.50mm. This maximum dynamic motion occurs during the maximum seismic acceleration.

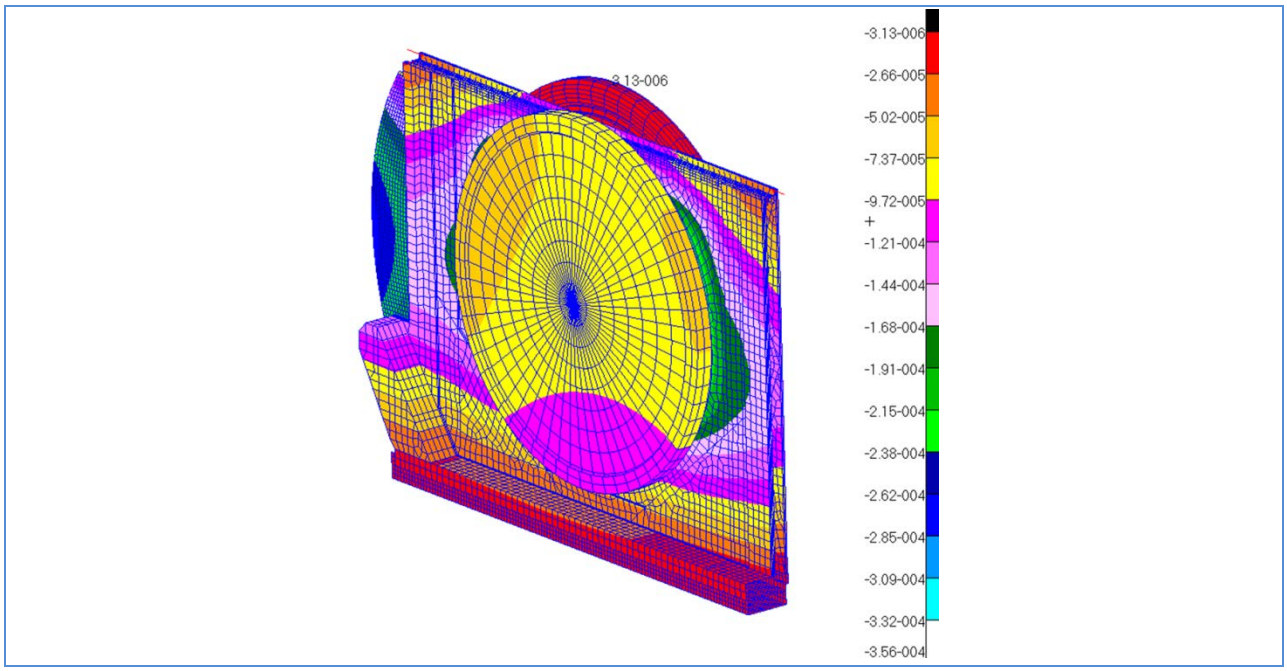

Figure 14-10: Shutter assembly displacement contours when subjected to accelerations in Z_{CCS}

14.5 Blade Position Monitoring

Position versus time knowledge defines shutter performance. Uniformity of exposure across the focal plane depends on replication of motion between opening and closing. Position detectors are needed at home and deployed positions, and a motion measuring system is needed to verify shutter performance. Trajectory resolution needs to be within fractions of a millimeter and fractions of a millisecond. Maximum blade velocity is 1.5mm/msec.

Precision of blade parking location and stroke trajectory are critical for exposure uniformity. The shutter needs 0.1 millisecond, 0.1 mm measurement sensitivity. The options for measuring position and motion are limited. Stray light from optical position sensors is not compatible with an astronomical telescope. Any sensor head mounted on the moving shutter must drag along its readout cable.

We are developing a motion detector system based on small (3 mm) neodymium/iron permanent magnets and Hall Effect magnetic switches as used in the automotive industry. Modern Hall switches are inexpensive, fast (.25 microsecond switching) with 200 gauss switching threshold. Hall switches mounted along the blade track will sense the passage of NdFe magnets mounted to the moving shutter blade.

Hall switches will be used for both setting the blade starting or ``home" location and for detecting the blade passage during the shutter stroke. Using 8 magnets on the leading blade and 3 Hall switches along

its track will produce (3 switches)*(8 magnets)*(2 switch points) = 48 switching times along the blade stroke. Spatial locations of switching points can be pre-calibrated using the servo's shaft encoder.

The blade trajectory monitor is sketched in Figure 14-11. A prototype has been built and measurements with this system indicate that the servo motor driven blade follows its prescribed S-wave trajectory with sub-millimeter accuracy.

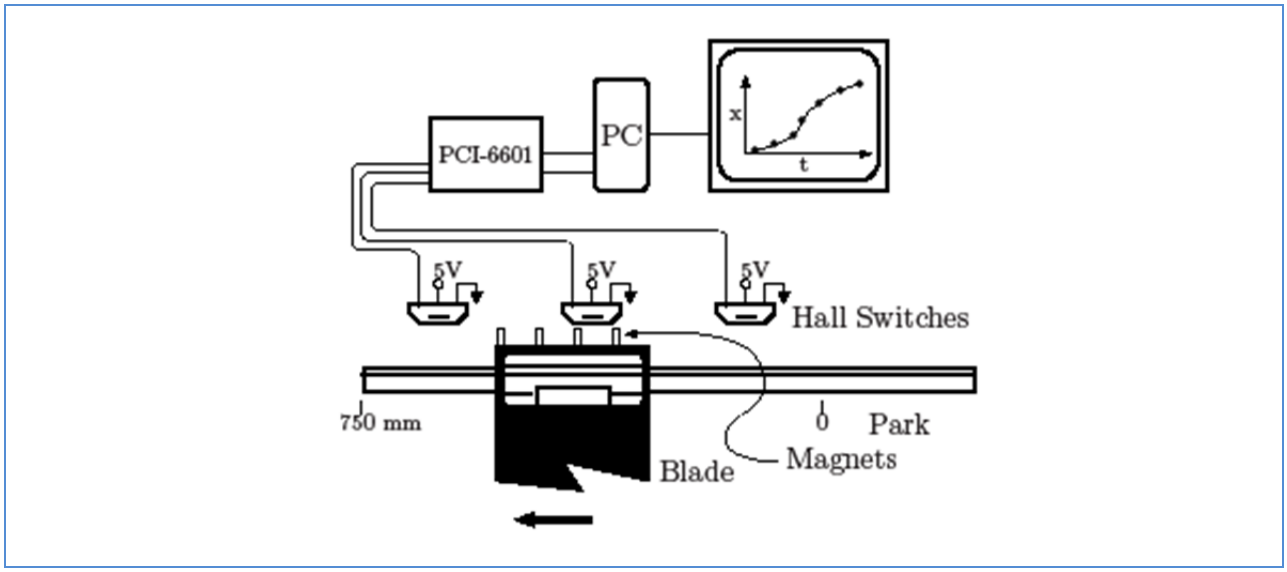

Figure 14-11: Hall switch blade trajectory monitor.

14.6 Shutter Assembly and Test

The shutter is assembled, aligned, and tested on an assembly stand, as illustrated in Figure 14-12. Assembly begins when the drive rail is mounted to the strongback support, with careful alignment of the drive rail to interface fiducials on the strongback. Motors and drive train components are then installed, and motors are verified to respond correctly to commands from the CCS. At this point, blade brackets are mounted to the timing belts and the entire drive train aligned and all instrumentation is verified to function correctly. After the drive system is verified, the shutter blade assemblies are installed, and their alignment is checked with respect to both the drive systems and guide rail.

The shutter is now run through a series of functional tests to verify all functional capabilities and command and control authority. Finally, the L3 and filter garage plates are installed to close out both sides of the assembly. Then the shutter is transferred into a light-tight box to measure exposure timing and light-tightness. When these tests are complete, the shutter is ready to be integrated into the Camera body

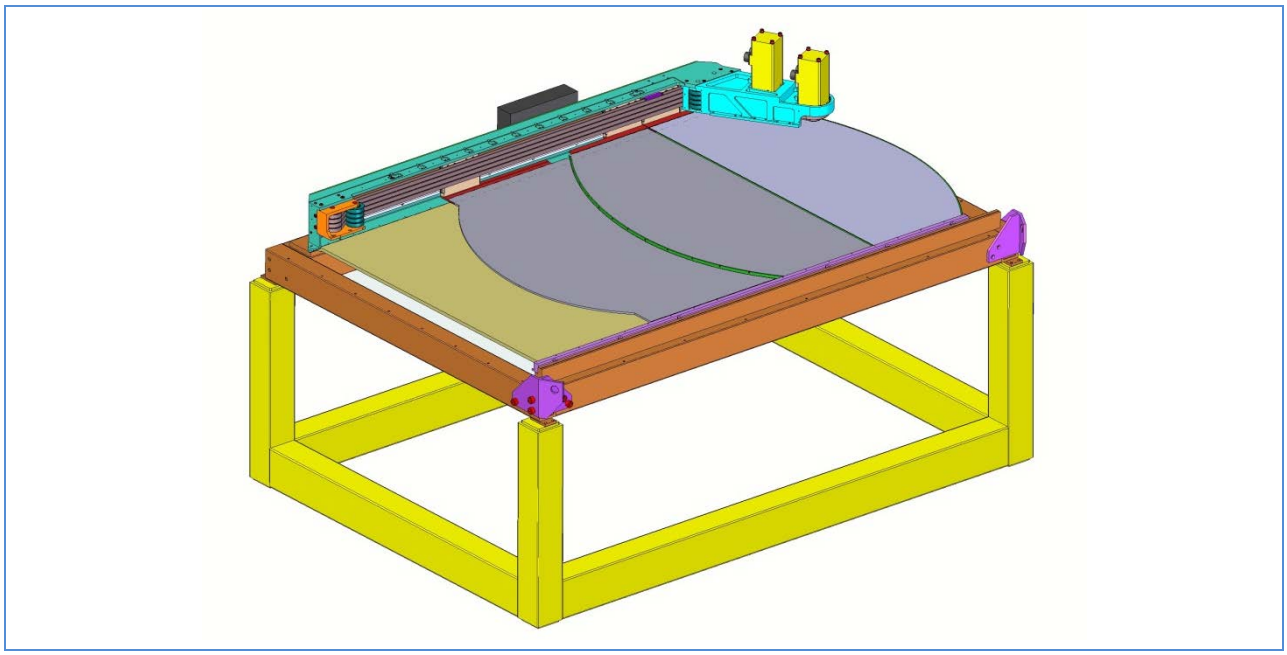

Figure 14-12: Shutter partial assembly on its assembly and test stand

14.7 References

Bowden, G (2007). LSST Camera Engineering Note Shutter Drive Dynamics, CE3-07 (Internal)

Bowden, G (2009). LSST Camera Engineering Note Shutter Blade Trajectory, CE5-09 (Internal)

Reif, K., G. Klink, et al. (2006). Bonn Shutters for the Largest Mosaic Cameras. Scientific detectors for astronomy 2005. J. Beletic, J. Beletic and P. Amico, Springer Netherlands**:** 147-152.

Wang, S.-Y., E. J.-Y. Liaw, et al. (2008). The shutter and filter exchanger system of Hyper Suprime-Cam, SPIE.

15: Camera Body

15 Camera Body

15.1 Introduction

The Camera body provides the structural backbone for all of the other Camera subsystems and also serves to regulate the temperature and environment of the Camera volume and the elements in the Camera. It consists of four primary parts: the back flange, housing, shroud, and purge system unit (located in the utility trunk), as shown in Figure 15-1.

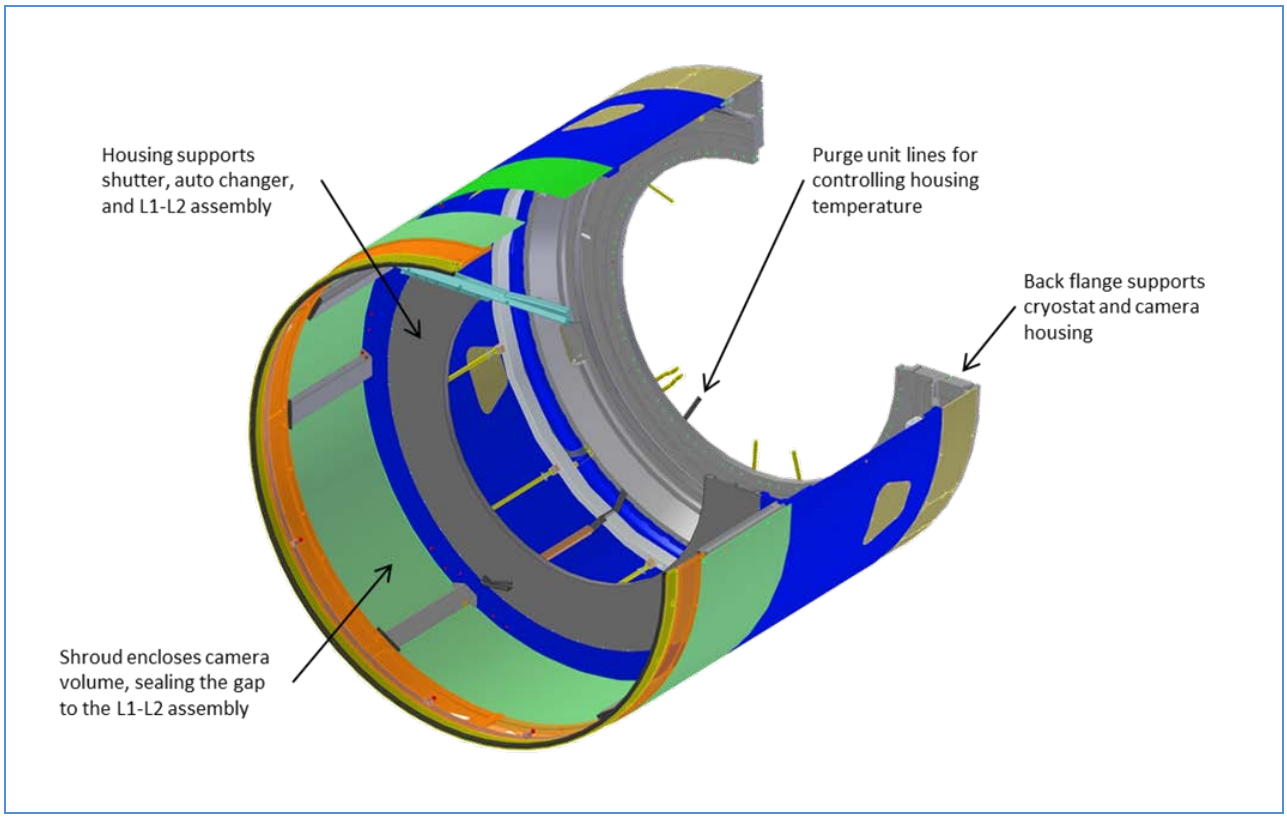

Figure 15-1: Cut-away isometric view of the Camera body, showing its constituent components

The back flange is a circular ring with a triangular cross-section machined from a monolithic aluminum forging. It includes four concentric bolt circles to provide interface attachments for the carousel, cryostat, Camera housing, integration and test stand, and telescope rotator. The back flange also houses the carousel motor, brakes and electronics assemblies and includes holes and channels for cooling ducts and cable runs from the cryostat's utility trunk into the Camera volume.

The Camera housing is a cylindrical aluminum weldment that bolts to the back flange. It provides mechanical interfaces for the autochanger, shutter, L1-L2 assembly and cableways and cooling ducts. There is a notch along the Camera housing's +Y top flange to support the autochanger module, while allowing it to be installed and removed in one piece without disturbing any other assemblies. The autochanger is further constrained on the –Y side of the top flange with flexures, and on the inner wall of the housing, where its rails are attached and aligned to the carousel. The shutter and L1-L2 assembly are also attached on the top flange. Cabling and low profile cooling ducts are routed along the inside surface of the housing. The blower and associated flow-and thermal-control components for the purge system are located in the utility trunk at the back end of the Camera.

15.2 Requirements

The Camera body key driving requirements are listed below.

Table 15-1: Camera body driving requirements

Requirement Title	Requirement
Camera mechanical interface	The camera assembly mechanical interface to the rotator shall be as defined in LCA-00126. This shall include access for installing and torqueing the outer bolt circle of the interface fasteners.
Auto Changer Interface	The Camera body shall support the autochanger as defined in the Auto Changer Interface Definition Drawing (LCA-74)
Carousel Interface	The Camera body shall support the carousel as defined in the Carousel Interface Definition Drawing (LCA-76)
Cryostat Interface	The Camera body shall support the cryostat as defined in the Cryostat Interface Definition Drawing (LCA-78)
L1-L2 Interface	The Camera body shall support the L1-L2 assembly as defined in the L1-L2 Interface Definition Drawing (LCA-77)
Shutter Interface	The Camera body shall support the shutter as defined in the Shutter Interface Definition Drawing (LCA-73)
Mass	The Camera body mass shall not be greater than 290kg.
Operational loads	The Camera body shall perform within specification while subject to any of the operational load cases listed in Table 1 of the LSST Camera Environmental Specification (LCA-68).

Requirement Title	Requirement
Seismic loads	The Camera body shall be designed to survive the seismic load cases described in Table 5 of the LSST Camera Environmental Specification (LCA-68), at all stages of assembly and integration, in any standard orientation of the assembly, and while off or in any on state.
Camera body temperature	The purge system shall be able to drive the temperature of the Camera housing at +/- 0.2 C/hr to track changes of the dome air temperature
Purge system heat removal	The purge system shall remove heat from the shutter, autochanger, and carousel according to their respective ICD's, LCA-224 and LCA-294.

These and the rest of the suite of Camera requirements are listed in LCA-55, the "Camera Body Specification." They fall within four general classes:

First, the Camera body must provide structural interfaces to all camera subsystem components and serve as the sole mechanical interface with the telescope rotator. All of the Camera body interface features must be accurately positioned to ensure adequate fit of subsystem elements.

Second, the Camera body must provide a stiff and strong structural platform for subsystem components, when subjected to changing orientations and seismic loads. When the camera structural elements distort, the optical elements move with respect to each other, resulting in image quality degradations. The Camera body structure and load paths must minimize these positional deviations and their resultant impact on image quality. Furthermore, in order to prevent dynamic coupling with the telescope top-end first mode frequency of 12 Hz, the first mode natural frequency of the Camera and its structural elements must be twice this, above 24 Hz.

Third, the Camera body must provide a clean, temperature-controlled internal environment that tracks the dome air temperature, despite changing heat loads among the subsystem components.

Finally, the Camera body must provide both outer and inner surfaces with a minimum of irregular features and reflective surfaces in order to reduce and trap stray and scattered light. This especially applies on the outside of the Camera body, where the main incoming light beam passes very near the Camera housing.

15.3 Camera Body and Purge System Design Description

As described above, the Camera body and purge system is comprised of four essential parts, the back flange, housing, shroud, and purge unit. The back flange, shown in Figure 15-2, is a toroidal ring with a right-triangular cross section and inner annular hole. In the triangular cross-section, there are bulkheads spaced at regular intervals around the flange, forming bays in the flange that open to the perimeter. These bulkheads significantly increase the strength and rigidity of the flange. Between bulkheads, the bays provide volumes for locating carousel motors and controllers as well as access regions for power disconnects for the filter loader, autochanger, and shutter. Also, both the bays and trenches cut into the face of the back flange provide channels for routing power and control lines and purge-system tubing.

Camera Control System (CCS) and power cables originating in the utility trunk pass through these channels, as shown in Figure 15-3. Similar channels are made to hold the Camera purge lines.

The back flange provides mounting bolt hole circles for fully interfacing five elements. First, the back side of the back flange includes inner and outer bolt circles for mounting the entire Camera to the telescope rotator, along with alignment pins to provide repeatable positioning. Second, the back side includes an additional pattern of tapped holes for mounting the Camera to an integration stand during Camera integration and testing. Third, the back side of the flange includes a circle of tapped holes and set of pins for positioning and mounting the fully loaded cryostat assembly. Fourth, the front face of the back flange includes another circle of tapped holes for mounting the carousel rotator rail systems, along with the fifth set of interface holes around the perimeter where the Camera housing mounts.

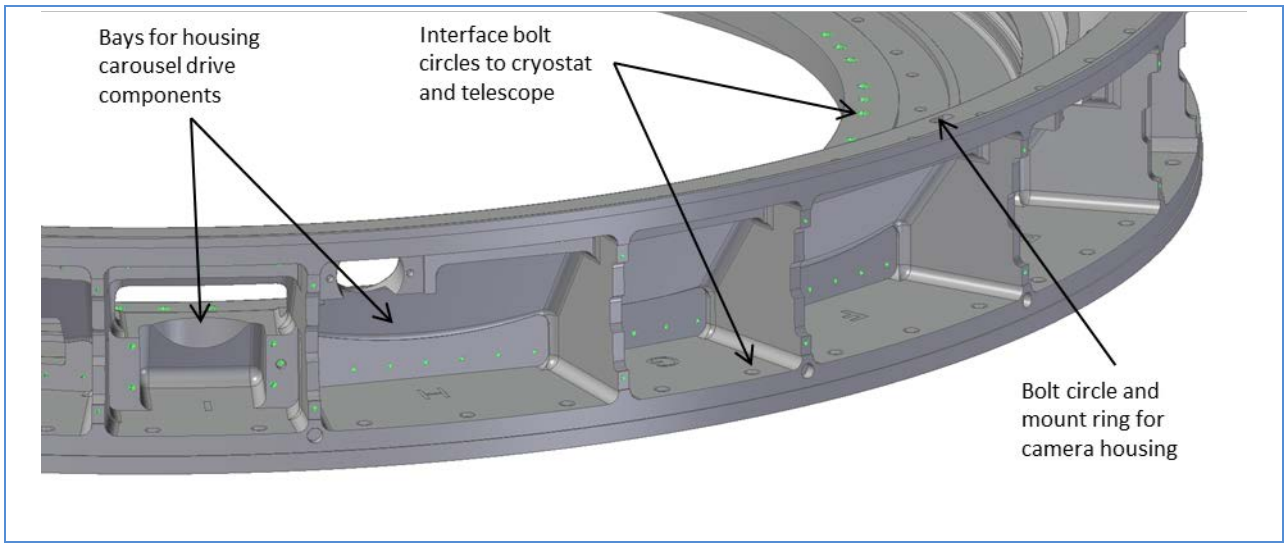

Figure 15-2: Back flange detail showing interfaces and bay mounting features for components

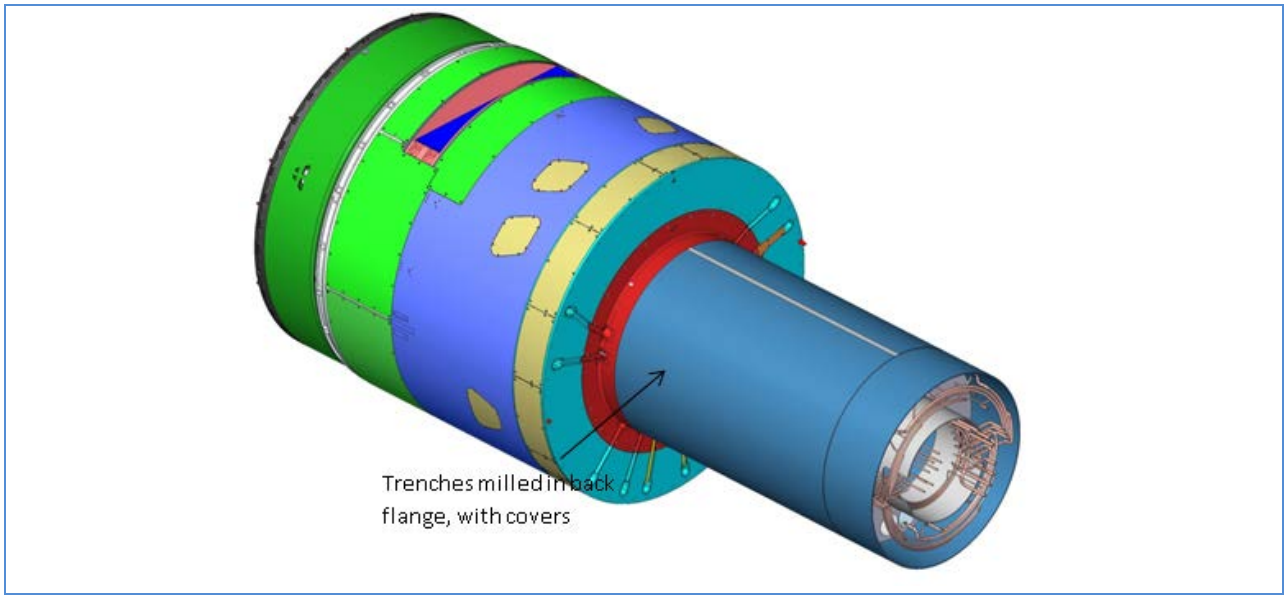

Figure 15-3: Back-end view of Camera and back flange, showing trenches cut for cabling and purge lines

The housing provides structural support and interface features for the remaining elements of the Camera that are held further forward. First, part way up the inner wall of the housing, bosses machined into the wall accurately support mounts for the end of the autochanger fixed rail. The location of these mounting bosses with respect to the back flange is very important, because it defines the location of the filter handoff position between the carousel and the autochanger.

The housing also includes access ports around its perimeter to allow for in situ servicing of the carousel clamps and autochanger rails. The holes are large enough to allow tool access but small enough to not adversely impact the stiffness of the housing or local stresses.

The housing ends in a front flange. The front end of the housing is deeply notched on the +Y side to accommodate the autochanger, so the front flange is reinforced with a bolt-in baffle ring and crossbar. These increase the stiffness of the flange to make up for the loss of continuity of the flange. The front flange and cross bar provide interface features for three components. First, the shutter mounts to two corners of the front flange on the –Y side, while on the +Y side the shutter guide rail lays against a rabbet joint in the crossbar. Second, the autochanger mounts to reinforcing features in the corners of the notch, with two flexures bolting to the –Y side of the front flange. Third, the six struts of the L1-L2 assembly attach to the front flange at six points around its perimeter.

Besides providing interface attachment points, the Camera housing also includes purge gas lines. These are bonded to the inner wall of the housing to provide uniform heating and cooling using purge gas piped in from the utility trunk purge unit.

The third element of the subsystem is the shroud. This mounts to the front flange of the housing and bridges the gap between the housing and the structural ring of the L1-L2 assembly. The shroud consists of a rigid ring at the L1-L2 assembly interface, supported by narrow columns that bridge the gap. The ring interfaces to the L1-L2 assembly with a compliant sealing gasket. The gasket is water and air-tight, but it is compliant enough to accommodate relative motion between the two as the L1-L2 assembly is aligned, and as it deflects under gravity loads. The shroud structure is covered with sheet metal panels that can be removed to access the Camera for servicing and maintenance. This provides for hermetic sealing of the Camera volume during operation, with the ability to gain access to the volume in a controlled way to minimize the introduction of contaminants during maintenance.

The final element of the subsystem is the purge system. The active elements of this system are housed in a valve box in the utility trunk, while sensors and distribution tubing are in the Camera volume. The purge unit in the utility trunk includes fan units to provide positive pressure for the purge circuits. Each of the two circuits includes particulate filtration and desiccants to dry the gas, and the temperature of each is controlled with heat exchangers using glycol cooling and electric heaters for re-heating. The system flow rates are set with manual metering valves during initial set-up, and purge gas temperature is controlled through feedback from temperature sensors in the Camera body.

15.4 Camera Body Structural Design and Analysis

A finite element analysis (FEA) model of the Camera was created and subjected to all anticipated Camera environmental loads. The environmental loads include worst case gravity orientations and

repointing impulses during normal operations, as well as non-operational cases such as during seismic events and transportation. The resulting stresses and deformations were used to guide design changes and optimize load paths for optical image quality and survivability. Worst case stress contour plots are shown in Figure 15-4, Figure 15-5, and Figure 15-6. The load conditions for the plots are for the survival seismic case where a peak 5.6g lateral acceleration is imposed on the Camera. Additionally, there is a safety factor of 3.8 applied to all of the calculated stresses. The resulting minimum margin of safety is 1.9. In practical terms, this means that the Camera body is designed to sustain more than a 20g inertial load without any sign of yielding. Such conservative analysis parameters give confidence that the design is more than adequate for strength.

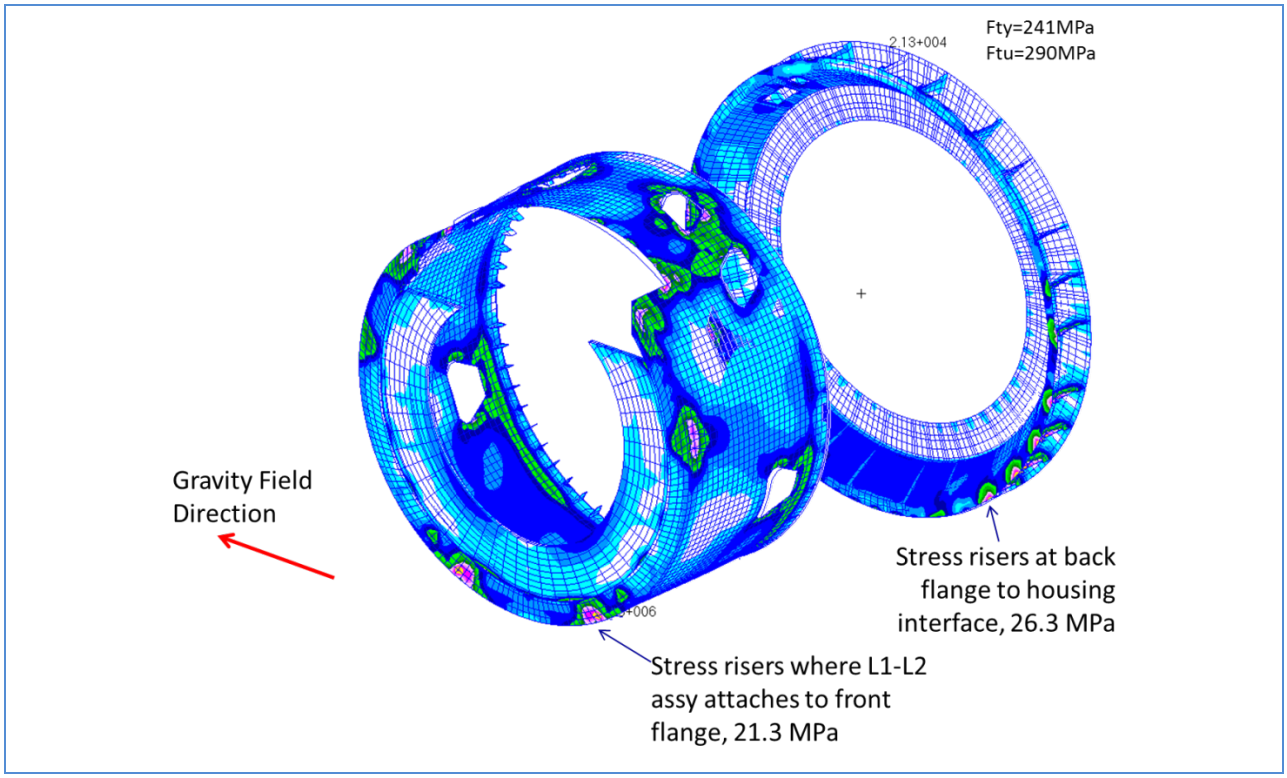

Figure 15-4: Camera body stress contours when subjected to 55.6G survival seismic acceleration in $X_{CCS}X_{CCS}$

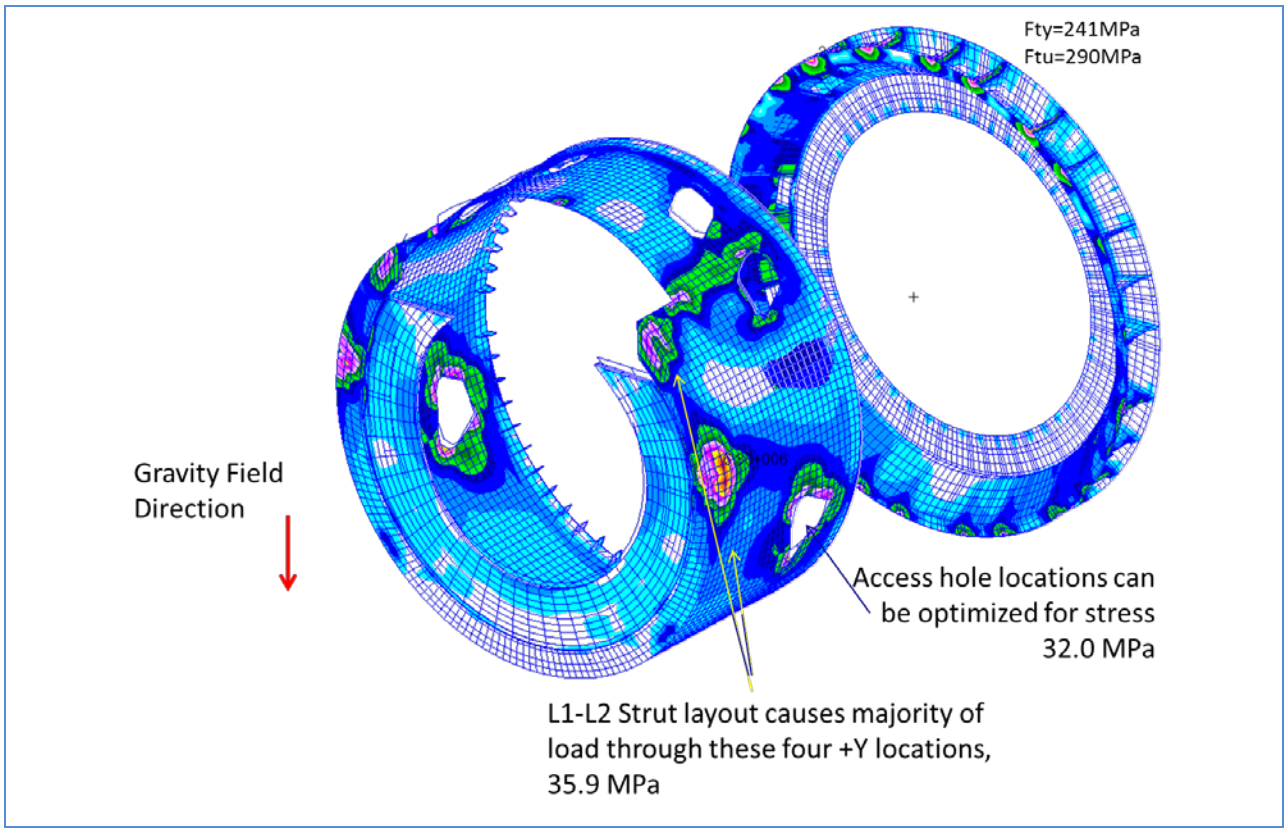

Figure 15-5: Camera body stress contours when subjected to 55.6G survival seismic acceleration in $Y_{CCS}Y_{CCS}$

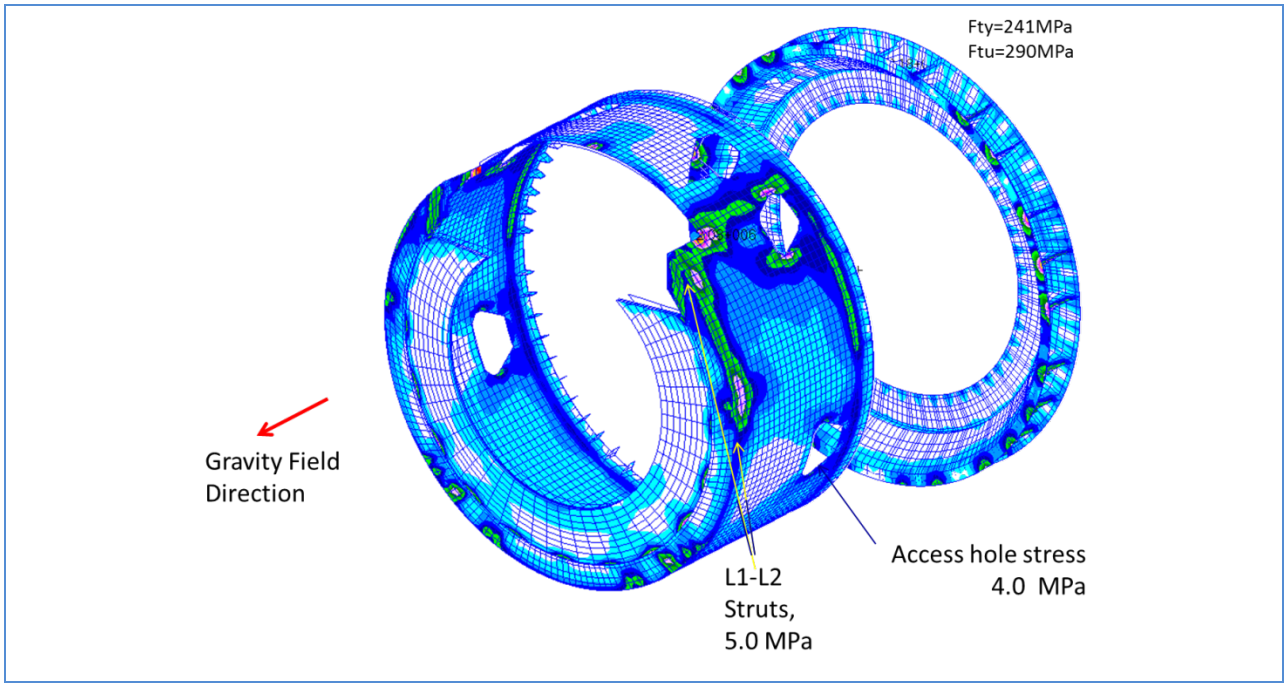

Figure 15-6: Camera body stress contours when subjected to 22.45G survival seismic acceleration in $Z_{CCS}Z_{CCS}$

The Camera requirement for minimum natural frequency is 24Hz, to ensure good modal separation from the telescope mode of 12 Hz. The integrated Camera FEA model was used to develop predictions for Camera modes including validated masses, centers of gravity (C.G.s), and structural elements for all subsystems. The normal modes analysis of the model showed the lowest natural frequency to be 25.5 Hz, which is above the requirement. Figure 15-7 shows the first mode, which is an L1-L2 assembly mode.

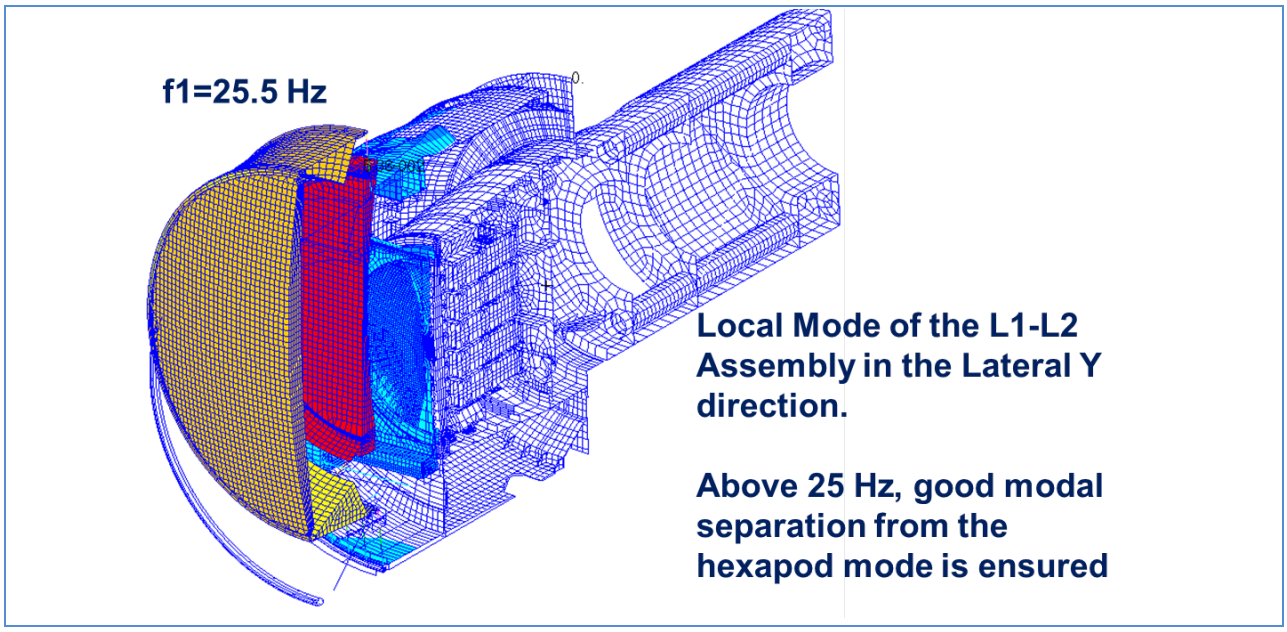

Figure 15-7: First natural frequency (25.5 Hz) ensures good modal separation from telescope.

Thermal distortions of the Camera body can induce optical image quality degradations. The Camera body was designed to minimize the impact of thermal expansions by locating the optical mounts along a plane close to the focal plane. In Figure 15-8, the distance from the Camera rotator interface is shown to the focal plane and to “Optical Element”. The optical elements in this case are L1, L2 and the online filter.

Since the Camera body and cryostat structures are both made from aluminum, they will contract and expand at the same rate. Since the interface plane at the Camera housing top flange is a small distance from the focal plane, the difference in distortion is small. The autochanger holds the filter in the online position and is mounted to the Camera housing top flange. The shutter is also mounted to the top flange. The L1-L2 assembly mounts to the top flange through six graphite epoxy composite struts. These struts have near zero coefficient of thermal expansion (CTE), so even though they experience a temperature delta, they will not change dimensionally very much. Therefore, L1-L2 optics are also thermally stable. Because of the shorter Camera body, the thermal distortion effects have been minimized.

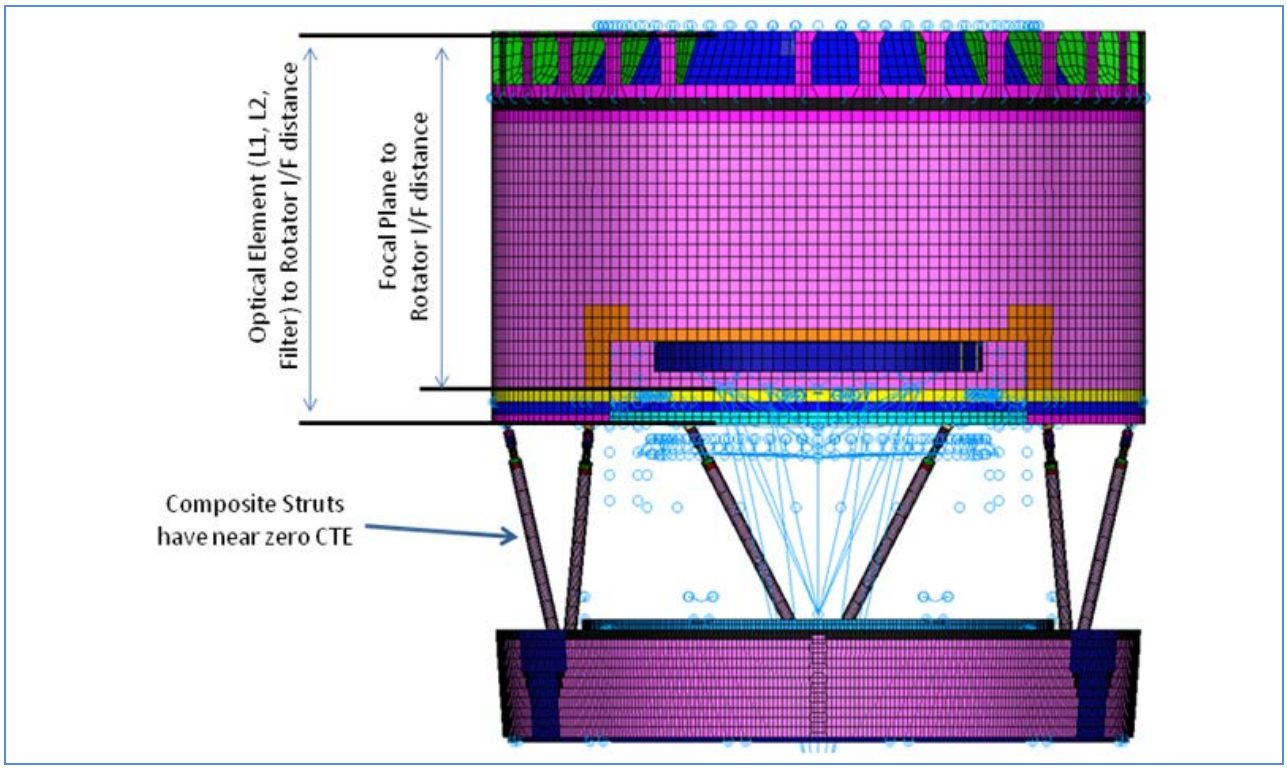

Figure 15-8: Camera Body design for thermal distortion

The preliminary structural analysis of the Camera body shows it is adequate for strength, stiffness and thermal distortion.

16: Camera Control System

16 Camera Control System

16.1 Introduction

The LSST Camera Control System (CCS) controls and coordinates the various Camera subsystems. It does the following:

- It ensures that Camera operations proceed efficiently, during science, calibration, and engineering modes.
- It monitors Camera performance, maintains a stable Camera environment and reports errors.
- It interacts with the LSST observatory, telescope, and data management control systems, sending and receiving data necessary for coordinated operations.

- It provides human interfaces both for the display of status information and to provide test, diagnostic, and debug capability.

CCS architecture is based on three main interacting components: infrastructure, worker subsystems, and consoles.

CCS infrastructure provides a set of buses used to transport messages between subsystems. These subsystems are implemented by a distributed set of Java processes. The types of messages include commands, status, logging, and alarms. CCS infrastructure includes mechanisms to control communication between subsystems. It also includes a local database, a code repository, and other utilities for support and maintenance. Figure 16-1 shows a schematic layout of the CCS architecture.

A worker subsystem is a software module, or set of modules, that provides the communication between the CCS and the corresponding Camera subsystem. For subsystems that consist of specialized hardware, the interface resides on a computer called a hardware control unit (HCU) that contains interfaces both to the CCS and to the hardware. It uses the CCS bus infrastructure to receive commands and communicate status information and telemetry. Each module also includes software (the device driver) specific to the hardware being controlled. For example, the science array subsystem (SAS) controls the science rafts through software that provides an interface to the control registers of the REBs (Raft Electronic Boards). During normal operations a master CCS module (MCM, described below) coordinates subsystem operations. Figure 16-2 shows some examples of worker subsystem architectures.

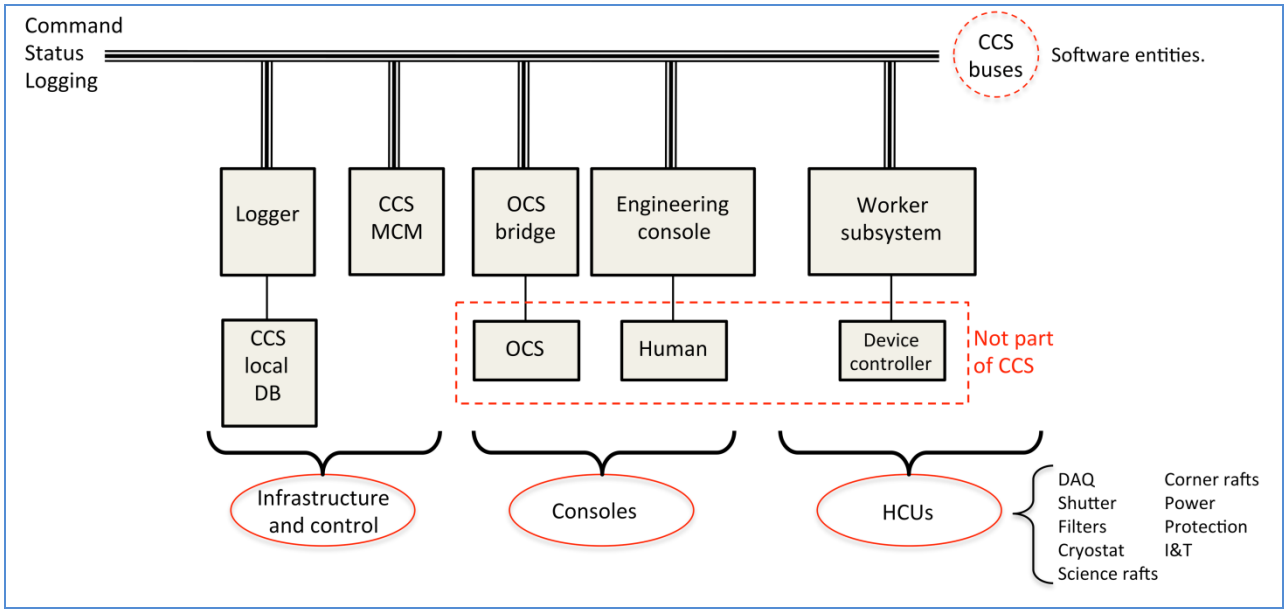

Figure 16-1: The CCS architecture. The CCS consists of three types of components, infrastructure, consoles, and worker subsystems. All internal communication is on the three CCS buses. The three buses are software entities – there is only one physical bus. CCS infrastructure provides common functionality, such as the central control logic and data logging. Consoles provide all I/O functionality: Command input and response (including user requested displays). Worker Subsystems translate signals between the Camera-wide CCS protocol to device-specific syntax. The HCU (Hardware Control Unit) hosts both the CCS interface and the device controller.

A CCS console is a process that can receive instructions (*e.g.*, from a human), issue commands to modules, and collect and display subsystem responses and Camera telemetry. In its simplest form, a command line program could allow an engineer to control the operation of a device and monitor its status. The OCS interface (called the OCS bridge) will be implemented as a CCS console. This implementation makes all command sources look the same. In short, CCS consoles "drive" the system.

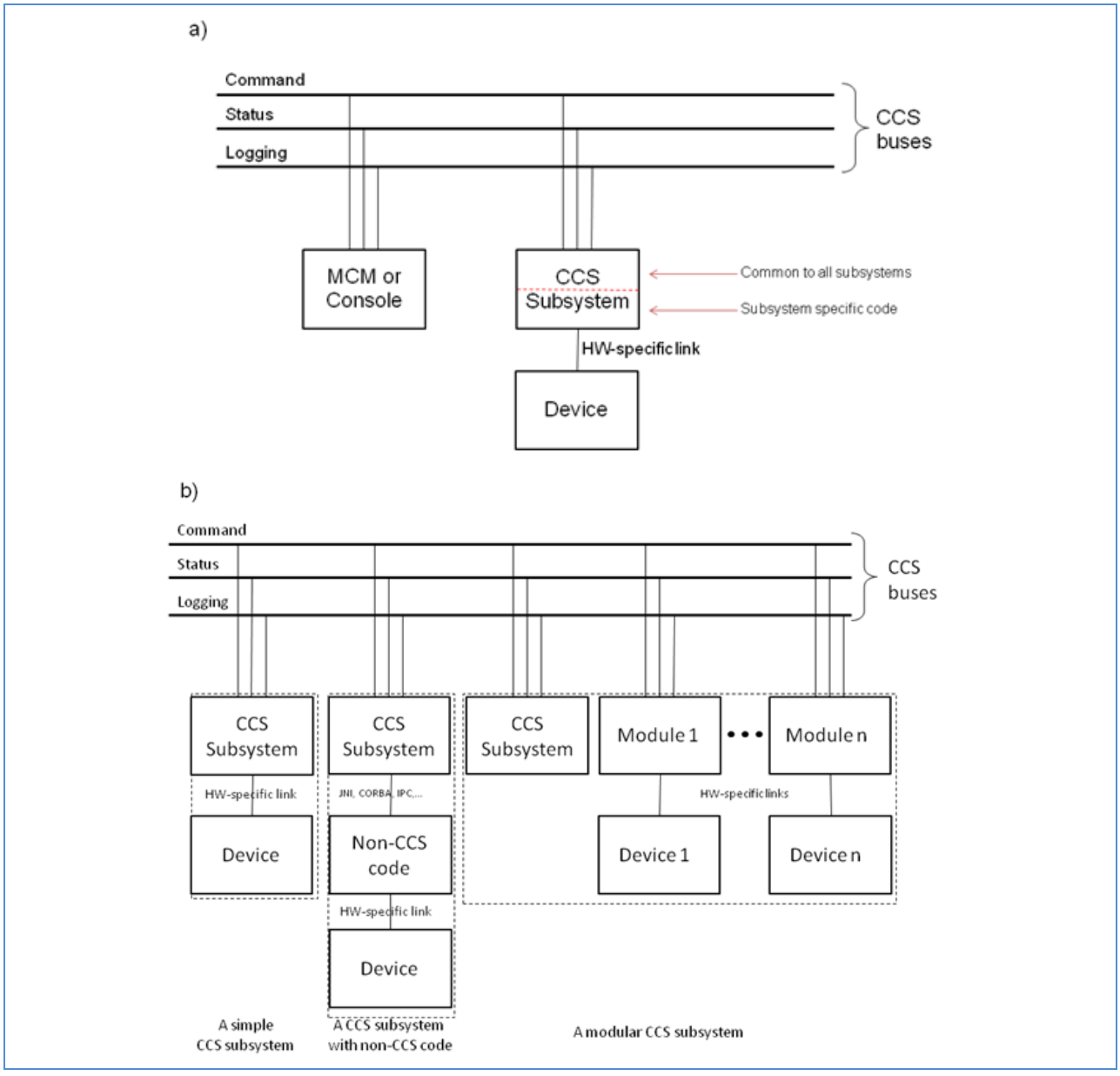

Figure 16-2: All CCS subsystems contain at least one module, a program that, on one hand, can communicate on the CCS buses and, on the other hand, can communicate with the subsystem hardware and software. (a) Commands are issued by the MCM or (in engineering mode) by a console. CCS subsystems all use the same code to communicate on the CCS buses. (b) Some subsystems may require nonstandard interfaces (*e.g.*, commercial controllers). The CCS interface must include an adaptor to accommodate it. Other subsystems may consist of several components, each controlled by a separate module. In that case, coordinated operation may be most simply done by a subsystem supervisor.

16.2 Requirements

Because the CCS is largely a coordinating system, its requirements are closely tied to the needs of the other components. The CCS will provide a common environment for commands, control, configuration, monitoring, alarms, and logging. As a consequence Camera development requires a good set of interface specifications. These specifications were an important early CCS deliverable. They have enabled the CCS to provide a uniform subsystem test stand environment, helping to simplify Camera integration and test. Our desire to provide test stands couples the CCS schedule to the various subsystem schedules, and is the principle CCS schedule driver. The following shows a summary of the key CCS requirements.

Table 16-1: Key CCS requirements

Operating modes	The CCS shall support all Camera modes, including power up sequence (under manual control), engineering mode and normal operations (under OCS control). The CCS shall report Camera mode changes to the OCS. The Camera shall provide a mechanism to allow the observatory to take and release control of the Camera.
Camera Normal operations Commanding	The camera shall support commands from the OCS to configure the camera, to change filters and to take exposures using the Command/Action/Response (CAR) model as detailed in LSE-70 "LSST Observatory Control System Communication Architecture and Protocol" when under control of the OCS (nominal mode)
Camera Commanding	When not under control of the OCS, (e.g. engineering or maintenance modes) the CCS will accept commands from engineering consoles
Telemetry delivery	The Camera will post telemetry to the observatory when it becomes possible to do so (i.e., as Camera subsystems become operational or the CCS-OCS connection becomes alive).
Camera State Notification	The CCS shall publish events whenever change of state happens, including Camera conditions that limit or prevent operations. In particular, the Camera shall publish the following events: • startIntegration • startReadout • endReadout • startShutterOpen • endShutterClose
CCS Telemetry Storage	The CCS shall have a local telemetry data base suitable for commissioning and debugging.
CCS Telemetry	The CCS shall read out and publish the Camera telemetry defined in LSE-165.
Camera Status	The CCS shall assess and report sufficient Camera health status to enable the OCS to monitor normal operations and to handle abnormal conditions.

CCS Test Stands	The CCS shall provide software and support for multiple test stand implementations of the CCS system

16.3 Architecture and Infrastructure

The CCS is structured as a distributed system, with modules communicating through three buses (control, status and logging). The buses will share network hardware; command latency will be minimized by an appropriate assignment of priorities.

Each CCS module is capable of being a master or a slave on the CCS buses. The role actually played during operation is specified during CCS configuration and is enforced by the lock manager (see below). Master modules can send commands to other modules. Slave modules receive and execute commands and post results on the status bus. In engineering mode, subsystem consoles can take control of a given subsystem. In this mode, the CCS infrastructure must ensure that subsystems do not interfere with each other. This does not include ensuring hardware safety, which is provided by a separate protection system, described in 16.6.11 below.

In order to ensure uniformity of implementation, the CCS environment provides a modular framework to ease the writing of worker subsystem modules. Common functionality is provided by the CCS infrastructure, enabling module writers to focus on subsystem-specific issues.

The Master Control Module (MCM) coordinates CCS operations. During normal operations it is the only active master. It acts as a façade, translating high level commands from the consoles into a sequence of lower level commands sent to the relevant subsystems. This coordination is a core function – the MCM must ensure that the system as a whole behaves in a sensible fashion. It is also a status aggregator: it forwards to the OCS, via the OCS bridge, a summary of the current CCS status.

The lock manager ensures that only one master subsystem is able to send commands to any subsystem, or subsystem part. If a master subsystem other than the MCM (e.g., an engineering console) needs to command a subsystem, it must request exclusive access to this subsystem. The lock manager distributes tokens to enforce exclusive access.

The local database provides two distinct functionalities: it provides a persistent storage for the subsystems configurations and maintains a history of those configurations; it also stores a selection of values published on the status bus, to be used for autonomous trending analysis

Commands to the CCS are entered via consoles and are transmitted on the CCS command bus. Commands can come from humans, automated scripts, or the Observatory Control System (OCS). In the first two cases, the console is a workstation on which a human can type or run a script. In the third case, the console is a bridge to the OCS; it can communicate on the observatory network as well as the CCS network. Consoles can also receive responses from the CCS and dispatch them appropriately (e.g., display plots on a screen or publish telemetry to the observatory).

The baseline implementation of the buses is built on top of jGroups (http://jgroups.org/), and uses three different “topics” (i.e., publish/subscribe asynchronous channels), command, status, and log. This implementation choice is well insulated in the code and could easily evolve, and an earlier implementation based on JMS (Java Message Service) is still maintained for possible future use.

Various types of data visualization and assessment are required during Camera operation, from development through integration and full operations on the mountain. The CCS design includes support for these activities. A small “diagnostic cluster” will act as a data display and analysis server. At least one large tiled display and several desktop or laptop type clients will be supported (including support for remote clients), allowing observatory or Camera operators to rapidly assess the overall quality of Camera data. This cluster will also perform enough image quality assessment to enable reliable operation when communication with data management is lost (e.g., if the connection to La Serena is down).

For source code management, CCS uses github.

(https://github.com/lsst-camera-ccs)

For code distribution, CCS uses nexus running on observatory -managed computers.

(http://dev.lsstcorp.org:8081/nexus/)

In addition, CCS uses JIRA for issue management, confluence for documentation, Jenkins for continuous integration ,and Sonarqube for code analytics.

16.4 Standards and Protocols

The CCS relies as much as possible on open source standards and protocol. Implementations are isolated from the main CCS code by interfaces, making it easy to replace them.

The core system is programmed in Java, which is portable and architecture-neutral, has good long-term perspectives, and very rich libraries. Java offers many safeguards that cut debugging time, and it is well-adapted to the envisioned hardware, which can support a standard Java virtual machine. In addition, the team in charge of CCS development has prerequisite Java skills.

CCS relies upon timestamps on telemetry, events, etc. Hence absolute and relative time-keeping across the system is required. CCS will employ standard PTP on the CCS network in keeping with observatory standard. CCS clocks will be synchronized to a master clock provided by the observatory.

Subsystems are developed using this CCS framework, without any direct usage of the lower level frameworks. In order to simplify design, production, and maintenance, subsystems must satisfy a common set of requirements defined in the table below.

Table 16-2: Common set of CCS to worker subsystem requirements

Standards

Software	Worker subsystem software must adhere to Camera standards (e.g., operating system, programming language, and coding practices).
Hardware	Worker subsystem hardware (HCUs) must host the CCS interfaces and reside in standard Camera platforms.
Uniformity	To the extent possible, the same hardware types and software packages should be used. This includes, for example, types of motor controllers, vacuum sensors, encoders, etc.
Interfaces and communications	
Architecture	Subsystems must communicate with the CCS (and other subsystems, if necessary) using the established state machine model (see figure Subsystem States) and communication protocols (e.g., on the CCS buses).
Protocols	Subsystems must communicate with the CCS (and other subsystems, if necessary) using the established communication protocols (e.g., on the CCS buses).
Cabling	Except as noted below, all communication within the Camera is via standard TCP/IP over standard cabling using commercial switches and hubs by CCS.
	Camera protection system (CPS) wiring is independent of all other cabling,
Proprietary implementations	If proprietary SW or HW is employed, Camera standard interfaces must be provided.
Commands and responses	
	Subsystems must acknowledge receipt of all commands and, if appropriate, notify the CCS of the completion status (e.g., if there is latency).
	Subsystems must self-identify (respond to “Who are you?” commands).
Timing	Timing at the millisecond level will be provided by the CCS (see LSST Camera Document LCA-50). Timing at the microsecond or nanosecond level will be provided by the precision central hardware clock.
Configuration	To the extent that the hardware (and safe and correct operation) allows, it must be possible to configure and reconfigure a subsystem at any time.
	It must be possible to compare a subsystem’s configuration parameters (including SW and HW version) with expected values.

Operating mode	Subsystems must respond to a “What operating mode are you in?” query. For each operating mode, there must be a list of commands that they will accept.
Telemetry	Subsystems must provide sufficient telemetry to monitor hardware performance and safety issues, and report all actual faults.
	Subsystems must provide, as necessary, readback and control points to the Camera Protection System.
Power and grounding	
Power feeds	Each subsystems must take its power from the following: 1 The central power distribution system as one or more regulated and controlled DC voltages - subsystem may specify voltage and current requirements . Available voltages are 5, 24, and 48 clean, and 24 and 48 dirty. 2 A “clean” 220V, 50Hz AC branch circuit 3 A “dirty” 220V, 50 Hz AC branch circuit 4
Telemetry	Auxiliary Electronics will provide telemetry and control (to CCS) of at-load voltages and currents.
Grounding	Subsystems must adhere to the overall Camera Grounding and Shielding Plan

16.5 Communications

The design philosophy for Camera cabling is to support a "loosely coupled" collection of Camera subsystems. That is, each subsystem is as independent as possible, with only power and minimal communication (command and data) connections. Camera operation relies upon reliable and performant communication between these components, controlled by the CCS. Point-to-point connections between subsystems are avoided as much as possible. Communication is provided by a typical Ethernet configuration.

The Camera utilities, control computers, and data acquisition are at fixed locations, while the Camera itself must operate both on the telescope and in the maintenance areas. Cable assemblies that connect the Camera to these fixed locations and cover significant distances are to be specified by the Camera project and provided by telescope and site services. Here, we discuss the Camera network usage and logical architecture, as seen by the CCS.

The Camera receives control (command and configuration) data from other systems and sends telemetry to other systems. Telemetry consists of any data related to the operation of the Camera system (command, control, and logging). Telemetry data will be captured and stored in the facility database. This data will be used to manage control of the Camera (from outside) and also as input to pixel data analysis. Pixel data is produced by the science, wavefront, and guide CCDs. Consumers of pixel data expect high bandwidth, low latency and high quality of service.

The networking plan for the Camera has been chosen to optimize these usage patterns. The LSST Camera networks provide:

1. A dedicated link for telemetry and control: A single CCS component (nominally, the OCS bridge) is directly connected to the wider summit network. All CCS telemetry and control communication passes through this component; that is, the Camera appears as a single node on this network. No other CCS components are directly connected to the summit network, which is maintained by the observatory. The capabilities and requirements of the summit networks are described elsewhere (see “LSST Network Design”, LSST Document-7354).

2. A local network not visible outside the Camera: Camera components in the control room, Camera body, utility trunk, clean rooms and utility room communicate over a Camera-only local area network defined by a set of switches that are part of the Camera system. The OCS bridge is connected both to the Camera network and to the wider summit network. The Camera network is a Camera responsibility.

3. Separate bulk data networks: The DAQ components of the Camera will have both Camera network connections and additional connections to networks dedicated to pixel data transport. Clients of the DAQ subsystems (which will include Camera components such as the image display) will access data on these networks. The pixel data transport networks are part of the observatory infrastructure and are maintained by the observatory. The CCS does not control or monitor communications on these networks, unless the client is a Camera component.

4. Camera protection system network. The components of the hardware protection communicate via dedicated wires, which are independent of the other CCS communication paths. This enables the protection system to function when the CCS is not operational.

Some Camera components or infrastructure may have other network interfaces. In particular, the observatory may have a dedicated management network for switch control, server administration etc. For example, rack-mount switches and servers generally have “board management interfaces” intended to allow remote power cycling, firmware upgrades etc. Development of observatory-wide standards for IT infrastructure is an observatory responsibility, and the Camera will comply with these standards as they are developed.

16.6 Worker Subsystems

16.6.1 Overview

Each worker subsystem controls and monitors one Camera subsystem, which consists of one or more hardware devices or software processes. A single CCS module controls each hardware device. Thus, a worker subsystem is a module or a set of coupled modules. A module can control one or more devices directly or indirectly via slave modules.

A module that controls a hardware device must translate commands that arrive on the CCS bus to hardware commands and signals that are sent to the device through a communication link such as a serial port, an analog or digital I/O board, or point-to-point Ethernet. A CCS command will typically become a sequence of hardware commands. A module must also gather status information coming from the devices and format and publish it on the status bus.

16.6.2 Operating Modes

Communication with a device control module depends on the CCS operating mode. In normal mode, the commands sent to a control module must come from the Master Control Module (or, in the case of a complex interface, from the module that controls the subsystem). In engineering mode, some commands can be sent directly from an engineering console to the control module.

For example, in the current prototype, we can send the following commands from the console:

- Normal mode: “Put the r filter online” (goes to the Filter Control System (FCS), the top-level control module for the Filter Exchange subsystem)

This command is converted by the FCS module to a sequence of commands to the carousel and autochanger control modules. The control modules translate these commands into the appropriate commands to the hardware device drivers.

- Engineering mode: “Stop the carousel” (goes to the carousel module)

This command is sent directly to the carousel module, where it is translated for the hardware device drivers.

Note: Command names are illustrative, and are not the actual syntax.

The CCS framework provides a way to build an interface as a tree of modules. The high-level control modules are the part of the interface visible to CCS. The lowest level modules are drivers in charge of controlling hardware elements and are reusable.

The framework handles the routing of commands sent on the command bus. Depending on the mode (normal or engineering), the commands can only be sent to the top-level module, or to any module.

Modules can provide status data that may be filtered or processed by the top-level module before publication on the status bus. Log messages are published on the logging bus if they pass the current filters.

CCS modules that communicate with Camera subsystems live in two environments (CCS and subsystem). The CCS environment is provided by a standardized set of Java classes that implement all of the CCS protocols. The device-specific code inherits these classes, so that implementation of a worker subsystem does not entail rewriting any CCS code. This simplifies code development and enhances code maintainability.

16.6.3 Filter Changer

The Filter Exchange subsystem consists of three mechanical components: the loader, the carousel, and the autochanger. The interface software to each component is a CCS module. A fourth module, the FCS, coordinates operation during the normal operating mode.

The loader holds a filter that is not yet on the Camera. When it is attached to the Camera, this filter can be loaded into an empty socket in the carousel. The reverse operation (unloading a filter) is also possible.

The carousel holds five filters, one in each socket. By rotating the carousel to a particular socket's "standby" position, a filter can be moved by the auto-changer into the optical path (the "online" position).

The autochanger moves filters between the standby position on the carousel and the online position in the optical path. It consists of two trucks that move along two rails, plus a flip rail that extends the other two rails. The flip rail must move so that:

- It is aligned with the other two rails when a filter is being moved by the autochanger, and
- It is moved out of the way when the carousel rotates.

The physical link between the CCS worker subsystem host, nominally a PC104, and the local device is a CanBus. The communication protocol is CANopen. (http://www.canopen.us/)

16.6.4 Shutter

The purpose of the shutter system is to provide precisely-timed exposures and to ensure that the exposure duration is uniform across the whole Camera aperture. This implies that the system is capable of accurately measuring the positions of the shutter components as a function of time (their motion profile) and is capable of precise control of shutter movement. A single CCS module controls the shutter.

The shutter consists of two blade stacks, each driven by its own motor, located on opposite sides of the Camera aperture. Each blade stack consists of two blades, each blade sized to cover slightly more than one-half of the Camera aperture. The blades move together in an overlapping telescoping manner from the parked position, where the blades are stacked on top of one another, to the extended position, where the blades barely overlap.

When the shutter is closed, one of the blade stacks extends completely over the Camera lens, while the other is parked (out of the aperture). In the shutter open state, both stacks are in their parked

positions. Thus to perform a timed exposure, the extended blade stack is moved to its parked position while the other stack is subsequently moved to its extended position. For a 15-second exposure, only one blade stack will move at a time, but exposures shorter than about one second will require that both blade stacks are moving simultaneously.

Sensors are used to define the parked position of each blade stack, as well as its travel limits. Additional sensors are used to record the motion profile of these blades. The effective exposure time at any point on the focal plane is recovered (10ms accuracy) from recorded motion profile of the blade trajectories. The sensor timestamps are recorded with 1ms (differential) accuracies. .

16.6.5 Focal Plane Subsystems

Three CCS focal plane subsystems control the activities of the 25 rafts in the focal plane housing. The rafts support 189 science-imaging sensors, four wavefront imaging sensors, and eight guide array sensors.

The Science Array Subsystem (SAS) controls the 21 science rafts, each with nine CCDs through interfaces to the raft electronics boards (REBs). Each REB hosts local intelligence to read out the CCDs, transmit data, monitor/set temperatures and voltages. Control, monitoring and programming of the REB is accomplished via registers and a timing synchronization interface, discussed below.

The Wave Front Array Subsystem (WAS) controls the four wavefront sensors in the corner rafts. These nominally operate synchronously with the science sensors and are covered by that discussion. However, during engineering or testing modes, the WAS may be operated independently.

The Guider Array Subsystem (GAS) controls the eight guide array sensors (two in each corner raft) in a similar fashion but nominally with an orthogonal duty cycle – when SAS/WAS sensors are integrating/reading the GAS sensors are active/quiescent. The control interface is essentially the same, but latency and data delivery requirements dictate a somewhat different scheme.

These subsystems run on one or more computers located in the control room. In each case, the register interface to the REBs is provided by the DAQ/Raft Interface (DRI) software package in the DAQ Camera subsystem. The DRI is a set of C++ classes that extends the remote register protocol portion of the DAQ RCI over the network to the CCS. The DRI then allows for monitoring and control of all rafts.

Control and monitoring of the focal plane is accomplished by reading and writing registers in each REB. The SAS will sample and publish thermal data on the CCS status bus and set heater currents (or voltages) as directed by the CCS thermal subsystem.

16.6.6 Data Subsystems

The principle function of the Camera's Data Acquisition (DAQ) Systems is to acquire, process, and buffer incoming data from the Camera's Focal Plane Subsystems. Data from these subsystems is then made available to the DAQ System's clients. The science, wave front, and guide data acquisition comprise separate CCS subsystems (SDS, WDS, and GDS, respectively). However, the interfaces are nearly identical, so all three are described here.

Each DAQ subsystem provides a control interface, the DAQ-Control Interface (DCI) that performs a function similar to the DRI described above (16.6.5). The CCS uses the DCI to configure and monitor a DAQ subsystem. Given the many client services that the DAQ subsystems support, the DCI will be used primarily for monitoring and configuring those aspects that are Camera specific. Other aspects, for example those specific to data management, will also be configured from data management via the CCS using the DCI.

16.6.7 Reference Clock

The DAQ also provides the fast (nominally 100 MHz) clock that orchestrates the data acquisition. The fast clock is generated in the DAQ. External synchronization is not necessary. This clock is distributed to all the REBs in order to maintain synchronous operation.

16.6.8 Power Distribution

The Camera Power Distribution System (CPDS) supplies required power to the on-Camera subsystems. See Chapter 18 and Figure 16-3.

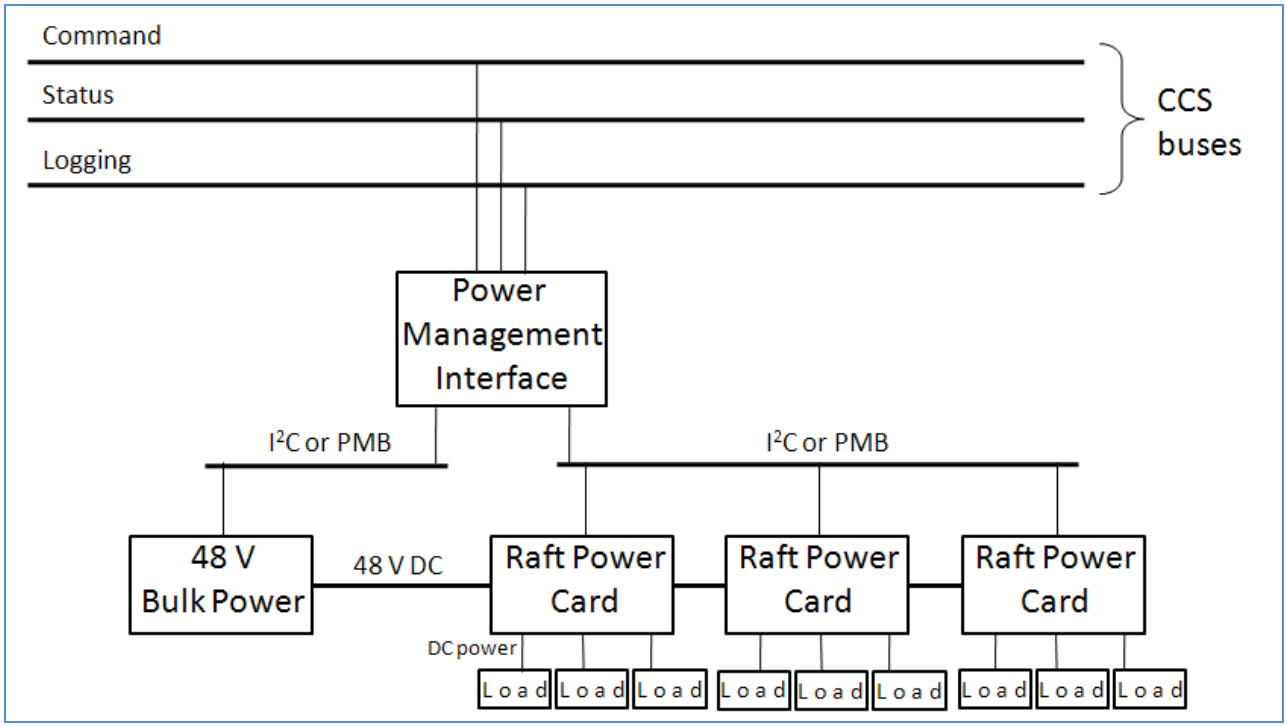

Figure 16-3: The power distribution architecture. The power management interface communicates with the 48 V bulk power supply and the raft power cards by PM buses (similar to I2C). We show separate buses because, until hardware is chosen, we don't know if the devices are compatible.

The CPDS resides in one or more crates inside the utility trunk. A CPDS crate can contain a number of power supplies as well as an HCU. Each science and corner raft tower is supplied by a separate isolated power supply called a Raft Power Card (RPC). The RPCs and the HCU are connected via the crate backplane, which carries PMBus (similar to I2C), 48V, 5V (standby), and control signals. Power is sent through the backplane via connectors to the cryostat (and then on to the raft towers and other auxiliary modules).

The HCU provides the CCS interface to the RPC's and other power supplies (e.g., for the shutter motors). The CCS will be able to monitor voltages, currents, and temperatures. It will also be able to control voltages and set voltage, current, and temperature limits and alarms.

16.6.9 Vacuum

The cryostat that holds the focal plane is a vacuum vessel. To maintain Camera performance and ensure sensor integrity, the vacuum must be monitored and controlled. If vacuum integrity is compromised, the Camera Protection System (CPS, see Chapter 6) and CCS must respond appropriately. The role of the CCS will be to monitor the vacuum parameters and warn of incipient problems before CPS is activated.

16.6.10 Thermal Control

Thermal control of the Camera is needed to optimize performance of Camera components and to minimize effects on seeing. The Camera is divided into several, largely independent, thermal zones: Camera body, utility trunk, in-cryostat electronics and the focal plane array itself in a "cryo zone."

The first three zones are well-enough contained that CCS interaction is solely by means of set points. However, the cryo zone has the most critical uniformity, stability, and monitoring requirements. It also depends on distributed monitoring and control functions: Temperatures are monitored on each CCD and each raft baseplate, heat is removed via the cryoplate, and trim heaters on the raft baseplate will adjust the temperatures as needed. This architecture requires that control be implemented in CCS "Raft Thermal Control" processes that have access to the full set of Camera telemetry.

Off the telescope, the cryo and cold refrigeration systems and the purge gas systems reside in the Camera utility room. These systems are controlled and monitored as well. Auxiliary devices such as the cryo/cold heat exchangers and the transport lines will be monitored. Coordination with the vacuum subsystems is also expected.

16.6.11 Protection System

Each subsystem implements its own protection system, which receives status signals from subsystem sensors and, based on those signals, sends permit signals back to the subsystem. Subsystem protection must be able to protect the subsystem hardware from damage when there is no connection to the CCS or to other external entities. When the CCS is connected, subsystem protection will send telemetry to the CCS interface for monitoring.

When the Camera is integrated (i.e., when more than one subsystem is connected), there will also be a protection master. Its purpose is to manage any inter-subsystem dependencies. The protection master receives status information from its own sensors in various subsystems and, acting on that information, controls devices that are in other subsystems. In other words, the protection master handles protection that crosses subsystems.

In general, the protection master does not handle signal paths whose logic could be wholly-contained within a single subsystem, but it does handle all those paths in which a permit used by one subsystem is derived from status signals from one or more other subsystems.

In many cases, status signals are themselves the result of complex logic. For example the cryoplate temperature-high status may be derived from a network of 17 temperature sensors in a manner that provides redundancy and minimizes false failure signals.

A schematic of the high-level logic of the protection system is shown in Figure 16-4.

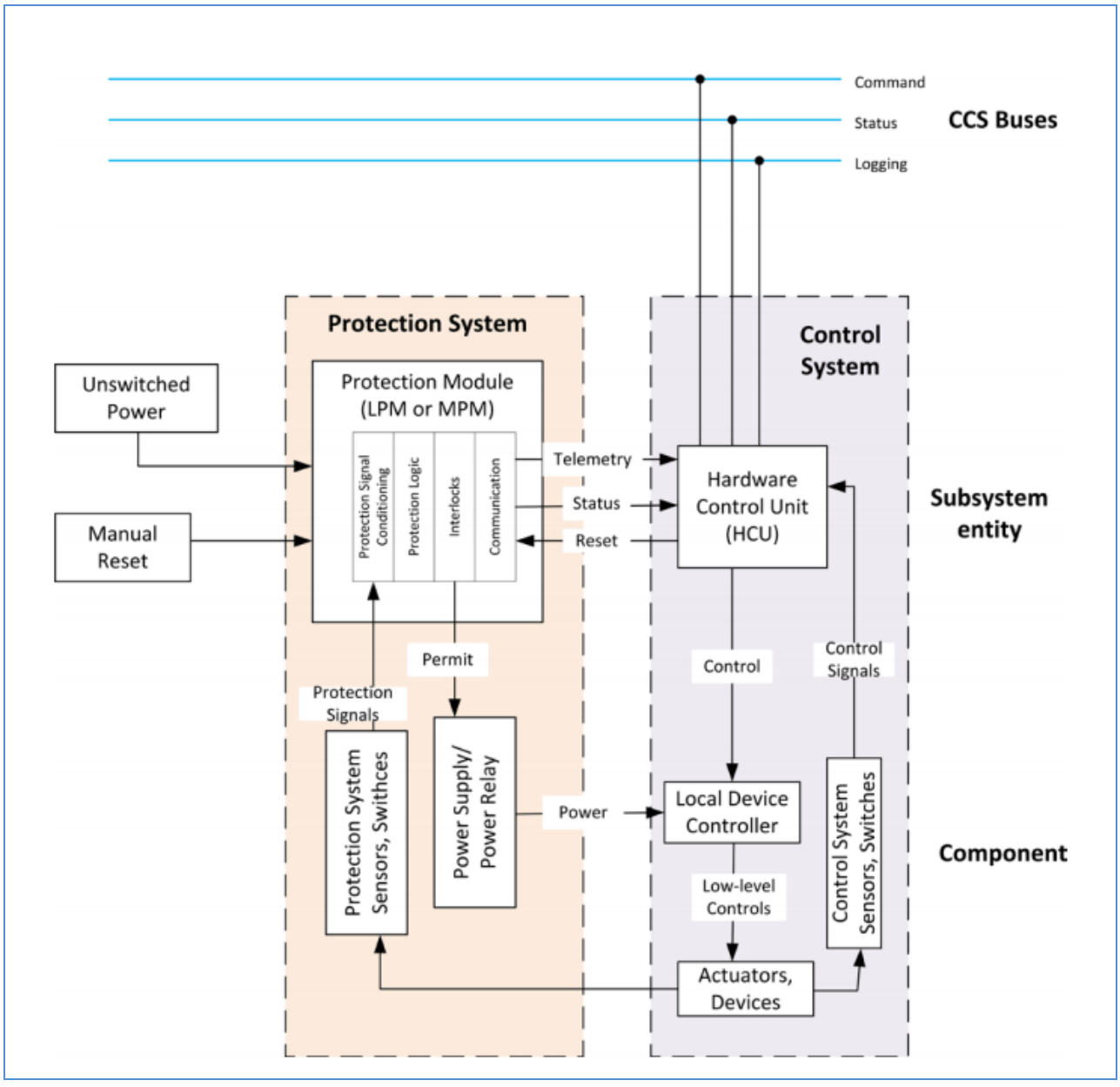

Figure 16-4: The Camera protection system architecture (see LSST Camera Document LCA-139). All connections between Camera protection components are provided by a network that is independent of the CCS. The CCS MCM can communicate with the protection master, but only to request status and telemetry. Each CCS subsystem module has similar communications with its subsystem protection, although the details will vary.

The protection systems will appear to the CCS as a standard subsystem. The CCS will monitor the status of all inputs, outputs, and some internal states. The only commands that the CCS may send to the protection system are status resets. (All failure states will be latched.).

The protection systems will be implemented with high reliability logic and input/output hardware. In most cases this is commercial safety rated PLCs and a small number of IO modules.

17: Data Acquisition System

17 Introduction

17.1 Overview

The Camera Data Acquisition (DAQ) subsystem connects directly with the sensors and electronics contained on the Camera Focal-Plane-Array (FPA). The FPA is partitioned as 5 x 5 grid of 25 individual rafts. Each raft is a self-contained set of sensors and corresponding electronics. Located in the FPA center are 21 science rafts. Each science raft contains nine sensors and three Raft-Electronics-Boards (REBs). Each REB is responsible for managing three sensors on the raft. The four corner rafts each

contain one wavefront sensor, two guiding sensors and two REBs. One REB manages both guiding sensors while the other the single wavefront sensor. Each REB, independent of location, contains a single link that forms the REB electrical and logical connection to the DAQ system. Consequently, each science raft contains three links and each corner raft contains two links for a total of 71 independent links serving as an interface to the DAQ system.

The entire FPA contains 189 science sensors, four wavefront sensors and eight guiding sensors. From a DAQ perspective, each sensor is electronically identical and contains roughly 16 megapixels. Pixels are digitized with 18 bits of precision. In nominal operation, both science and wavefront sensors are exposed for 15 seconds and digitized and completely read out in no less than two seconds. However, in contrast, a subset of the pixels from each guiding sensor is acquired with a faster cadence, averaging 9 Hz.

When read out, pixel data from the video channel of a sensor is moved to the REB of the sensor, where the data is potentially aggregated with data from other sensors and is emitted onto the REB link to the DAQ system. Data emitted on a link will be called sensor pixel data, or where the context is clear, simply data.

With respect to an FPA, its corresponding DAQ system must satisfy four necessary functions:

- Acquire, buffer and catalog its acquired pixel data.
- Provide both buffered and streaming access to these data.
- Generate and distribute a common system reference clock.
- Provide access to its electronics for the purpose of configuration, monitoring and control.

These four functions are expressed through a set of five different DAQ system capabilities. These capabilities provide for:

- Notification, through subscription of incoming data.
- Retrieval of buffered data for both science and wave-front sensors.
- Access to streaming interface for guiding.
- Access to FPA electronics for purposes of configuration, monitoring & control.
- Management of reference clock and timing.

Users access these capabilities through application-specific-software on commodity hardware. Any such software is considered a DAQ system client. The execution platform for a client is a host. A host is a commodity processor operating under LINUX connected to the DAQ system through a 10-gigabit Ethernet. Clients gain access to the various DAQ services through a set of software interfaces provided by the DAQ system. These interfaces hide from the client the underlying communication mechanisms implemented between host and DAQ system. Figure 17-5 summarizes the relationships between the DAQ, its FPA and clients..

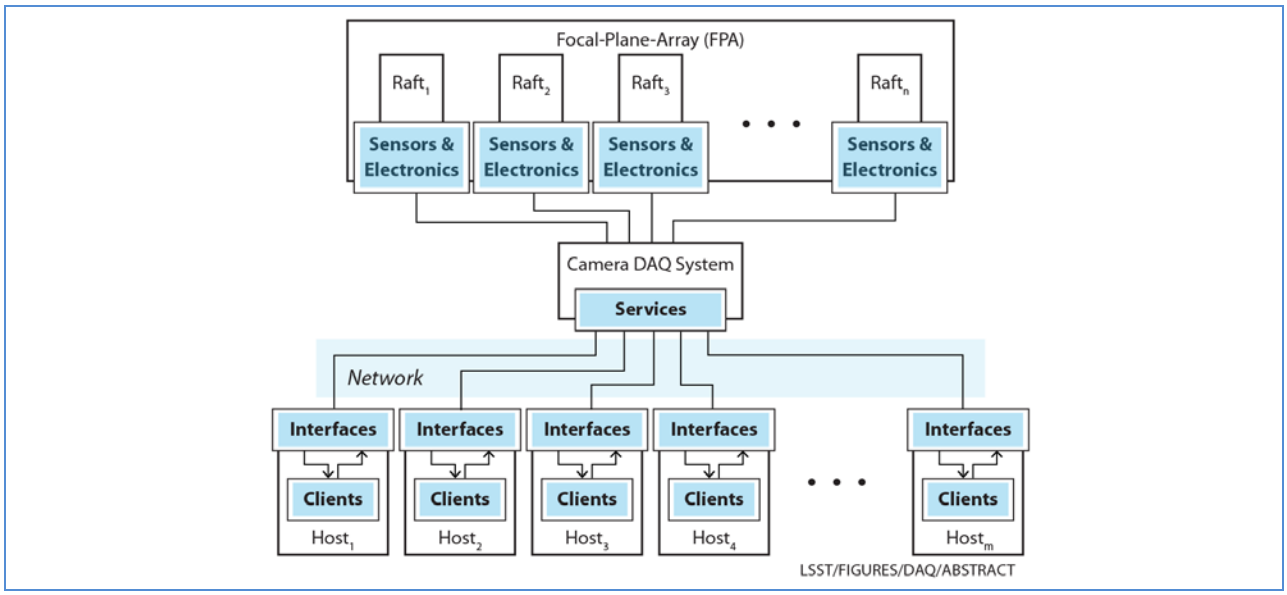

Figure 17-5: Abstract model of the DAQ system and its interfaces

17.2 Focal Plane Arrays and DAQ Systems

The overview of this document implies that only a single FPA is produced by the Camera project, and that is the FPA for the Camera delivered to the observatory. In fact, a variety of FPAs will be produced to support a number of different activities. These activities include:

- Development of raft electronics as well as both CCS and DAQ subsystems
- Sensor/Raft production
- I & T and Sensor/Raft acceptance
- DM data challenges
- Early path-finding and the commissioning camera
- Raft maintenance on the summit

Each one of these activities will require DAQ subsystem support; however it is likely that some or many of the DAQ systems will coexist within a common networking infrastructure. The activities associated with each of these systems will generate and persist data products, and inevitably, the data products generated by one system will require comparison to data products produced by other systems. To differentiate between DAQ systems, a unique name is allocated and assigned to each system. A name is used to qualify any addressable components within its corresponding system. In addition, all data products generated by a system, including especially images, will be tagged with the name of the corresponding system.

17.3 Clients

Images, with data acquired from the science rafts and suitably formatted and processed, constitute the principal science product of the Camera. The primary client for those data is the Data-Management (DM) system. Images with data acquired from the corner rafts are used by the telescope for control of

its adaptive optics system as well as by DM to supplement science analysis, and therefore, the clients for those data are both DM and the Telescope-Control-System (TCS).

Note that while DM and the TCS are certainly the primary clients of the DAQ system, they are not the only clients. Observatory operation, and the need to monitor the Camera's health as well as to perform diagnostics in the event of failure, all require access to image data. Given typical observatory operation, it is likely many of these accesses will occur concurrently.

In order to support these usage patterns, the DAQ architecture is designed for an arbitrary number of clients distributed over an arbitrary number of hosts. The DAQ architecture is also designed to assure quality of service for each client. The architecture provides a total aggregate communication bandwidth in excess of 1.1 Terabits/second between a DAQ system and its hosts.

17.4 Time

All components of the observatory are required to synchronize their respective clocks. This synchronization allows for temporal correlations between events generated across the various observatory subsystems. To this purpose, the DAQ system maintains a Time-Of-Day (TOD) counter that the system may deterministically sample to mark and identify in time any "interesting" occurrence. The TOD is a 64-bit counter incrementing at the Camera system clock rate and initialized by the DAQ system with the "time of day" as determined by the observatory.

17.5 Images and Metadata

To characterize the pixel data associated with an exposure, the exposure is tagged with additional metadata. The combination of metadata and pixel data is an image. One primary component of metadata is the identifier of the image. When triggering an exposure, the client is responsible for creating and assigning a unique image identifier. Identifiers serve two functions:

- They differentiate images while resident in the catalog.
- Through association, they reference the image's associated storage bucket.

Metadata has its origin in four sources:

- Each (raft) bay of the FPA.
- Each board of each raft of the FPA.
- Internally, with the DAQ system itself.
- Externally, with the client triggering an exposure.

The DAQ system is responsible for the rendezvous of the various metadata along with their corresponding pixel data to form an image.

Each raft of the FPA will contribute at least, but not limited to the following metadata:

- Raft and board address.
- Sensor type.

Each board of the FPA will contribute at least, but not limited to the following metadata:

- Type. One of REB, GREB, or WREB and whether or not the board is emulated.
- Serial Number.
- FPGA version (both for SCI and raft specific logic).
- Register schema information.
- The contents of a specified set of registers.

The DAQ system will contribute at least, but not limited to the following metadata:

- Data Acquisition Name.
- Operating System Version information.
- RDS and IMS versioning information.

The client will contribute at least, but not limited to the following metadata:

- A unique image Identifier.
- A set of client specific opaque data.

17.5.1 The Storage Array

The DAQ system for the observatory is required to buffer its acquired images for at least two days of typical operation. This requirement derives from an observatory requirement to maintain operation for as many as two days in the event of an interruption of service between summit and base facility. Interruptions could occur, for example, if the communication links between summit and base are down, or services at the base facility are unavailable due to scheduled maintenance. The functional component of the DAQ system maintaining and managing that two-day buffer is called the storage-array.

For reasons of performance and reliability at altitude, flash rather than rotational media is chosen as storage media. Based on an observatory model that takes into account typical night observation patterns as well as daytime calibration, 48 hours of buffering corresponds to roughly 35 terabytes of image data. The need to provide for an equal number of hours of simulation data doubles that amount and Camera maintenance and diagnostic requirements adds an additional 15 terabytes for a total storage requirement of around 85 terabytes.

To provide contingency as requirements mature, the storage array is sized somewhat larger at 132 terabytes. This is not a hard limit, with higher density drives total capacity could trivially grow to double that amount. Further, if required, the storage architecture provides a graceful growth path to reach what is an essentially unlimited amount.

The usage model for the storage array is based on the premise that images are written once, but read many times. Therefore, the necessary write bandwidth is straightforward to quantify and must be able to keep up with the total read-in rate of approximately 3.5 gigabytes/second. The necessary read bandwidth is somewhat more difficult to quantify, as it depends on a concurrency model, which in turn

depends on the observatory's "operational concepts" model, which remains a work in progress. However, a model, maintaining "Quality-Of-Service" guarantees for at least four concurrent clients is considered a reasonable approximation. This corresponds to a necessary read bandwidth of approximately 15 gigabytes/second.

Given the relative immaturity of the observatory's operations model, the total available bandwidth of the storage array is designed purposely large, on the order of 100 gigabytes/second. That bandwidth scales as additional storage is added at roughly the rate of one gigabyte/second for each additional terabyte of storage.

17.5.2 The Image Bucket

The storage array is partitioned into units of buckets. A bucket is the container for one image. Buckets are sized to contain the largest image that may be generated by the FPA and stored by a DAQ system. The number of buckets is configuration driven. When it is created, each bucket, is assigned an identifier (the bucket ID). A bucket ID is used to reference the stored data and metadata of an image. Once assigned, a bucket ID is unique for all time. Deleting a bucket does not allow the identifier to be reused. Buckets are created and populated with their corresponding image by the system when the image is triggered. Buckets are allocated and deleted by the DAQ system as necessary.

17.5.3 The Image Catalog

The storage array has an associated catalog. A catalog is composed of a hierarchy of folders and images. Catalogs contain folders and folders contain images. The principal function of the catalog is to return to a client the bucket corresponding to a specific image contained within a specific folder. Each folder in a catalog is addressed by its name. A name is simply an ASCII string of arbitrary length assigned when the folder is created. The set of folder names must be unique within a catalog. The client has access to the following operations on a catalog:

- Create, rename and delete its folders
- Retrieve the Bucket ID for a given image in a given folder
- Retrieve all Bucket IDs for a given folder
- Move one or more images from one folder to another

To formalize the management of the storage array during operation, a DAQ system contains a number of predefined, "well-known" folders. As needs mature this set may be extended, however, to this point the catalog contains the following well-known folders.

- The Freelist: The buckets associated with the images in this folder are candidates for reallocation by the DAQ system. Allocation from the Freelist will be in insertion (FIFO) order. That is, the oldest, inserted image will be the first candidate for allocation. The Freelist will be initially populated by a DAQ system when configured.
- Pending archival: This is the initial, default location for created images. Data Management will assume any images in this folder are to be archived.

- Pending catch-up: This folder contains the set of images acquired while service to the base facility was interrupted. Data Management will assume any images in this folder are to be archived.
- Simulation: This folder contains the set of images to “play back” when the DAQ system is being driven in simulation. The composition and names of the images in this folder are reserved to the DAQ system.

17.6 Amplifier Addressing

FPA electronics digitize their data in parallel in units of amplifiers. Consequently, for purposes of both subscription and identification, the smallest unit of addressability is also the amplifier. An FPA contains a variable number of amplifiers ranging from one all the way to the 3216 amplifiers contained within the FPA of the production Camera. However, independent of specific FPA, the schema for locating an amplifier is identical. In this scheme, an amplifier address is encapsulated and encoded in 32-bits as illustrated with Figure 17-6 below:

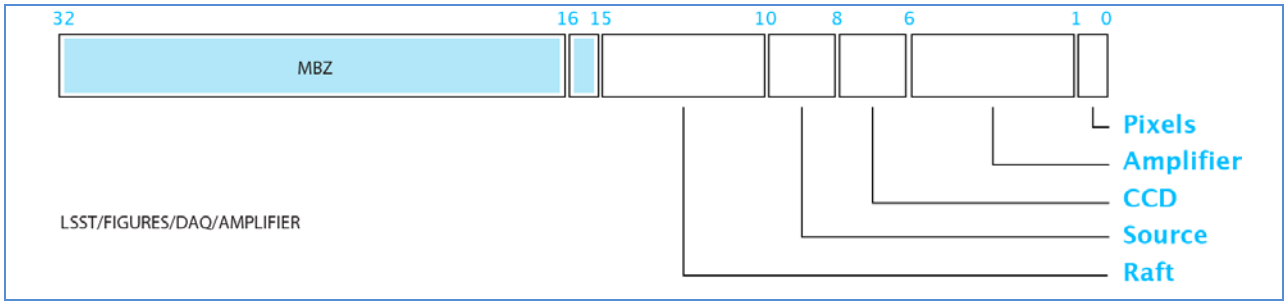

Figure 17-6: Amplifier addressing

Where:

- Pixels: A flag that specifies whether the address fields described below reference pixel data or metadata. If this field contains zero (0), the reference is to metadata. If this field has a value of one (1), the reference is to pixel data.
- Amplifier: Specifies the amplifier relative to the CCD specified below. This field contains a small enumeration corresponding to the physical location of the amplifier within a CCD. Amplifier locations are defined in [yyy]. The value of this field may vary from zero to fifteen. Numbers sixteen to thirty are considered invalid and must not be used. The value thirty-one is reserved as a wildcard specification and depending on context could mean either “any” or “all.”
- CCD: Specifies the CCD containing the amplifier, relative to the Source specified below. This field contains a small enumeration corresponding to the physical location of the CCD managed by a single source. CCD locations are defined in [yyy]. The value of this field may vary from zero to two. The value three is reserved as a wildcard specification and depending on context could mean either “any” or “all.”
- Source: Specifies the Source containing the amplifier, relative to the Raft specified below. This field contains a small enumeration corresponding to the physical location of the link within a raft. Link locations are defined in [yyy]. The value of this field may vary from zero to two. The

value three is reserved as a wildcard specification and depending on context could mean either “any” or “all.”

- Raft: Specifies the Raft containing the amplifier, relative to its FPA. This field contains a small enumeration corresponding to the physical location of the raft within a FPA. Raft locations are defined in [yyy]. The value of this field may vary from zero to twenty-four. Numbers twenty-five to thirty are considered invalid and must not be used. The value thirty-one is reserved as a wildcard specification and depending on context could mean either “any” or “all.”

17.7 Image Data Organization

Pixel data for an image is organized in two dimensions. In the x dimension data are specified by their spatial source relative to their FPA, while in the y dimension data are specified as they evolve in time. Dimensions in x are measured in units of Amplifiers, while dimensions in y are measured in units of Slices.

Independent of total size, an image is always divided into 128 equal sized time-slices. Slices increase monotonically in time. For example, data contained in time-slice one was always read-out earlier then data in time-slice two. Note that at the nominal readout rate a slice corresponds to roughly 16 milliseconds of data.

It is convenient, therefore, to consider pixel data as an array of n x m dimension, where n is equal to the number of amplifiers whose data were acquired and m is always 128 slices. For example, one column corresponds to the pixel data from one specific amplifier, from beginning to end of read-out. Or as another example, the first row corresponds to data from all amplifiers from beginning to 16 milliseconds into read-out.

Both row zero and the array element (0, 0) have special meaning. Any row zero element contains metadata. Note that this implies metadata is acquired and stored before its corresponding pixel data. Element (0,0) corresponds to the metadata, which is common to all elements of an image.

Image data organization is represented pictorially as shown in Figure 17-7.

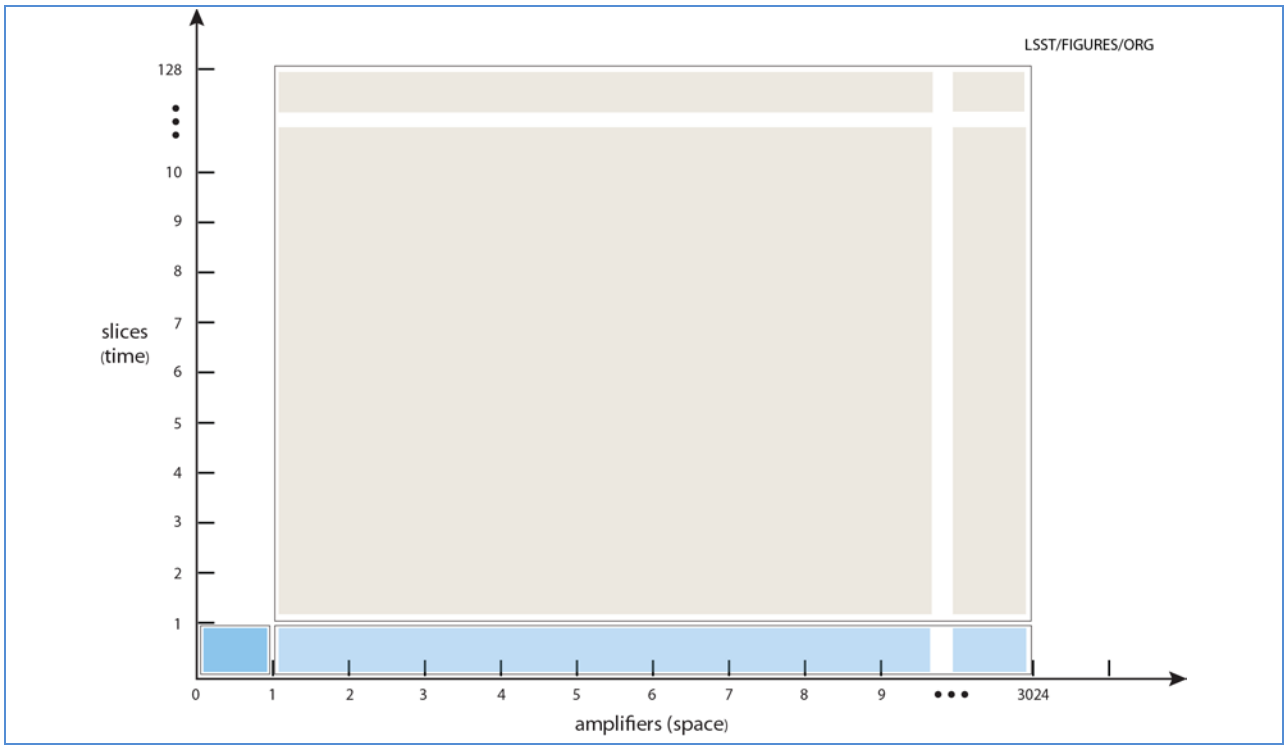

Figure 17-7: Image data organization

In Figure 17-7, regions shaded brown indicate pixel data of an image and regions shaded blue indicate the corresponding metadata of the image. Typically, when referencing image data, clients are interested in more than one and less than all the elements of its array. Therefore, it's convenient to specify a reference to a region, rather than to a single coordinate. Such a specification will be called a Region-Of-Interest (ROI) . An ROI is characterized by two parameters:

- The coordinate of its first element
- Its size (in units of rows and columns)

17.8 Image Access

Clients access image data only from stored images. That is, clients only gain access to image data after the data is committed to the storage array. However, once written, that data remains accessible until its reuse (nominally 48 hours after the image was created).

As described above, as data arrive to a DAQ system, they are quantized in units of slices and stored. As slices are stored, events are produced. An event is a small, concise message describing a slice and the container in which its data can be found. Its message contains the following information:

- A Bucket ID: This identifier specifies a container holding an image's pixel and metadata.
- A ROI: This ROI specifies the slice acquired and committed to the storage array.

Events are made known to clients through a publish-subscribe paradigm. Using that paradigm, clients subscribe to events the system publishes. The client subscribes using an appropriate method of the IMC

software interface. This method takes an ROI as an argument. This ROI specifies the events that interest the client. Once a subscription has been registered, the client waits on the arrival of its corresponding events. This implies that access to data is a two-step process: The client waits on an event and as events arrive, uses the event information to fetch the corresponding data.

Quantizing data in slices adds pipeline latency to the nominal two-second readout time. That latency is roughly equal to the time for the system to buffer and store one slice.

17.9 Camera Operation

To minimize cost and maintenance, the summit has a single DAQ system to service the Camera in all Camera modes of operation. In order to do so, the system design takes into account three questions:

- How does the system allow for Camera maintenance?
- Where can the hosts that must interact with the system be located?
- How does the system support Data Management at the base-facility?

The nexus for the DAQ System is the Camera Data System (CDS) located in the computer room at the summit. The computer room is fixed in place and does not move. However, the same cannot be said for the Camera, which on arrival at the summit as well as during planned or unplanned maintenance is off the telescope and located in the observatory cleanroom.

To deal with this eventuality, the Camera-side of the CDS has permanent fiber plant and connections to the two possible locations of the Camera, the telescope or clean-room suite. In this fashion, as the Camera moves, no physical re-cabling is necessary. Instead, using a software interface, the DAQ system is simply reconfigured to “point” at the appropriate set of fibers.

A third option exists. It is also possible the DAQ system is operable, but the Camera is unavailable. Such a condition exists in the early path-finding for the observatory as well as when an instance of the DAQ system must participate in a data challenge. To deal with this eventuality, the system contains a two-day emulation of the Camera, with a permanent set of connections between it and the remainder of the DAQ system.

17.10 Reuse and the DOE Detector R & D Program

In order to minimize both development costs and schedule risk, the implementation of the DAQ system draws heavily on the concepts as well as the hardware, firmware and software developed out of the SLAC /DOE Detector R & D program on large-scale Data Acquisition Systems . This program’s fundamental premise is that application specific, arbitrarily sized DAQ systems may be constructed by derivation from a small number of generic, reusable building blocks. These blocks are the Reconfigurable Cluster Element (RCE), the Cluster, the Cluster Interconnect and as a physical substrate ATCA .

17.11 Architecture

A major design goal is to maximize reusability wherever appropriate. Therefore, while the usage of science, wavefront and guider data varies, their acquisition inherits from a common hardware, firmware

and software foundation. This leads to a single hardware abstraction of the DAQ system as shown in Figure 17-8.

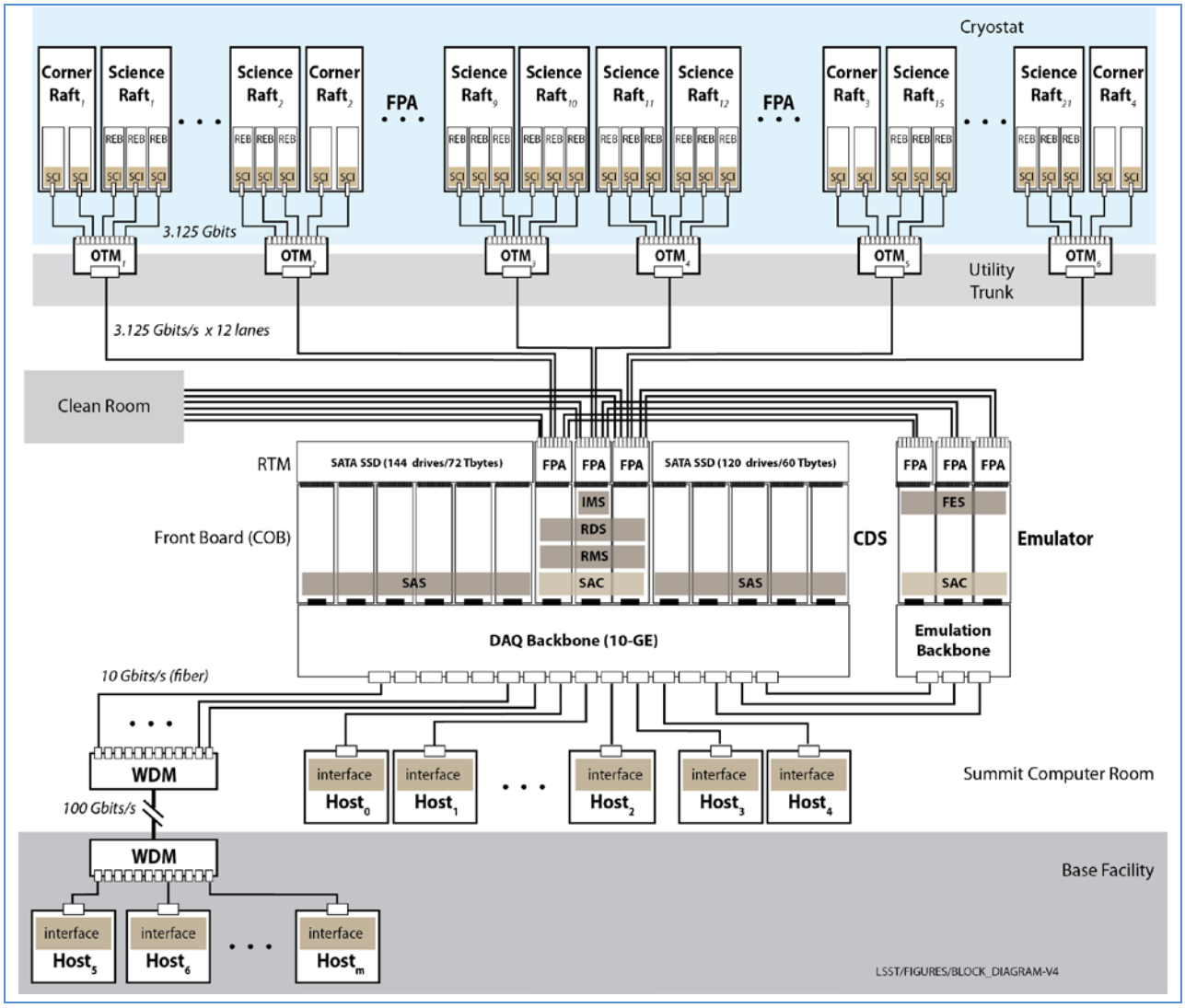

Figure 17-8: Block diagram of the LSST Camera Data Acquisition System

The blocks in the diagram represent the various functional components either provided by, or interfaced with the DAQ system. Shaded blocks within blocks represent system software or firmware. One somewhat unique feature of the system architecture is how its components are distributed over geographically disparate locations, starting from within the Camera cryostat on the summit and continuing to the observatory base facility located in the city of La Serena almost 100 km away. The diagram expresses this feature by arranging its functional blocks by their observatory location, with blocks closest to the Camera at the top and blocks furthest away at the bottom. The following sections briefly describe each block starting from within the cryostat.

17.11.1 The Source Communication Interface

The Source-communication-Interface (SCI) is a pure firmware block located within the cryostat. In actuality, an SCI resides within an FPGA contained within a Raft-Electronics-Board (REB). In turn, a REB is itself contained within a raft. Both REB and FPGA are provided by their respective science and corner raft subsystems.

Each science raft contains three REBs with each REB servicing three CCDs. Each corner raft contains two REBs. One REB services the two guiding sensors of the corner raft and the other REB services the single wavefront sensor. For its corresponding REB, an SCI provides the following: synchronous timing and control, monitoring and configuration of its electronics, and serialization and transmission of its sensor video data.

In total, the FPA contains 71 SCIs, with each SCI having a single, high-speed serial link with the CDS. That serial link is full-duplex having physically disparate transmit and receive signals carried on a copper lane. Lanes are converted to optical fiber at the cryostat boundary by the Optical Transition Module (OTM). The decision to convert to fiber optics outside rather than inside the cryostat was predicated on the Camera's strong desire to minimize the amount of electronics inside the cryostat. Note that independent of science or corner raft the design and implementation of their respective SCIs are identical.

17.11.2 The Optical Transition Module

The OTM is a hardware block located on the boundary between Camera cryostat and utility trunk and has the straightforward electrical responsibility of converting the high-speed, serial links emanating from SCIs from copper to light and light to copper. Physically the OTM is simply a small printed-circuit-board (PCB) containing fiber-optic transceivers. The PCB is co-located on a flange of the cryostat endplate and serves as the mechanical and vacuum penetration for link signals. One edge of the board is exposed to the cryostat (the "vacuum" side) and manages signals as copper, and the other edge of the board is exposed to the utility trunk (the "air" side") and manages signals as light.

Each OTM services up to 12 SCI-Links, where a link is carried to the OTM's "vacuum" side as two copper, differential pairs. Each pair contains transmit and receive signals with the pair duplicated for purposes of redundancy. The OTM contains on its "air" side, two, 12-channel, full-duplex transceivers, again duplicated for purposes of redundancy. One copper pair connects to one channel of the primary transceiver and the other pair to one channel of the secondary transceiver.

As the two transceivers are intended to provide redundancy, only one transceiver is powered at a time. Each transceiver employs MT ferrules as its fiber-optic physical standard, consequently the "air" side interface consists of two, twenty-four strand fiber-optic cables; one for each transceiver.

The FPA contains 71 SCIs, whose links are distributed uniformly over six OTMs. In turn, those six OTMs are distributed uniformly over the annulus of the cryostat end plate.

17.11.3 The Camera Data System

The CDS is the central core of the DAQ system and is located in the computer room of the summit facility. The CDS is a combination of hardware, firmware and software. Physically, the CDS is a 14-slot ATCA shelf with a full-mesh backplane. Its front slots are occupied with identical PC boards called COBs, while its rear slots are occupied with one of two types of Rear-Transition-Modules, or RTMs. Those two types are:

- The FPA/RTM. This RTM provides a fiber-optic interface for up to 96 SCI-Links. The RTM also includes an accurate "Time-Of-Day" clock, which is used to establish the absolute time at which images are created.
- The SSD/RTM. This RTM contains up to 24, 1.8" flash, SATA-II drives. Each drive is base-lined with a capacity of ½ terabyte of flash media (solid-state-disk). All 24 drives operate in parallel and provide an aggregate read/write bandwidth of almost five gigabytes/second and a total storage capacity of 12 terabytes.

A COB contains eight DPM-RCEs and a single DTM-RCE. Although physically identical, SDS COBs are differentiated by their corresponding RTMs and by the firmware and software their RCEs execute. The 14 COBs may be grouped by logical function into two sets:

- The FPA. This set contains three COBs each paired with a FPA/RTM. Its three RTMs are connected to the FPA's 71 SCIs. Each of its DPM-RCEs is capable of controlling and managing the data from up to three SCIs . The "wiring" between RCE and SCI is rich enough to allow each SCI to physical exist in one of the three zones without need for physical re-cabling. These three zones are:
    - The Camera's SCIs residing on the telescope.
    - The Camera's SCIs residing in the clean-room.
    - The Camera's SCIs being emulated by the DAQ system.
- The storage array. This set contains 11 COBs each paired with a SSD/RTM. It hosts the software and firmware dedicated to providing uniform, external access to its RTM's 264 SATA-II drives.

The full mesh backplane of the shelf combined with the switching contained within each of its 14 COBs constitutes a fully provisioned, non-blocking, Layer-2 Ethernet switch with 238 10-Gigabit ports. This switch is referred to as the DAQ backbone. A group of 126 ports of the switch are permanently connected to the s 126 RCEs of the shelf. The remaining 112 ports are reserved for connection to the DAQ network.

From a functional rather than physical perspective, the principal responsibility of the CDS is to host the software necessary to express the services provided by the DAQ system. .

17.11.4 The DAQ Network

All CDS RCEs connect to a single Ethernet (the DAQ network). The backbone for this network is contained within the CDS. This network extends over the entire observatory, including the computer

room of the summit, the downlink (WDM) equipment connecting summit and base facility, and the inside the base facility itself, where it penetrates into the equipment housing the DM infrastructure and secondary control-room.

A host wishing to gain direct access to the services provided by the DAQ system must be connected to the DAQ network. All network traffic not related to the DAQ system is both physically and logically segregated off this network. This implies that a host must be dual-homed, with one interface connected on the DAQ network and the other to the outside world.

As this network is physically isolated at Layer-2, it is also logically isolated at Layer-3. TCP/IP configuration and management will be dictated by the needs of its corresponding DAQ system. This includes, for example assignment of IP addresses.

17.11.5 Timing Distribution and the System Clock

Timing for the sensors and electronics of the FPA is synchronous. That is, the FPA:

- Is driven by a common system clock.
- Receives and acts on, simultaneously a common set of commands.

The source for both clock and commands is the CDS. This implies a significant fan-out to components geographically distributed. This fan-out is implemented in coordination with the link-protocol between CDS and SCI.

17.12 Support for DAQ and Camera Development

The DAQ development schedule is prioritized to provide development support of increasing fidelity and capability to other Camera and observatory subsystems. In order to facilitate that support, the DAQ system is designed for backward compatibility. As it evolves, adding new features existing systems in the field can, as needed be upgraded. The components that make up DAQ support for test stand are shown in Figure 17-9.

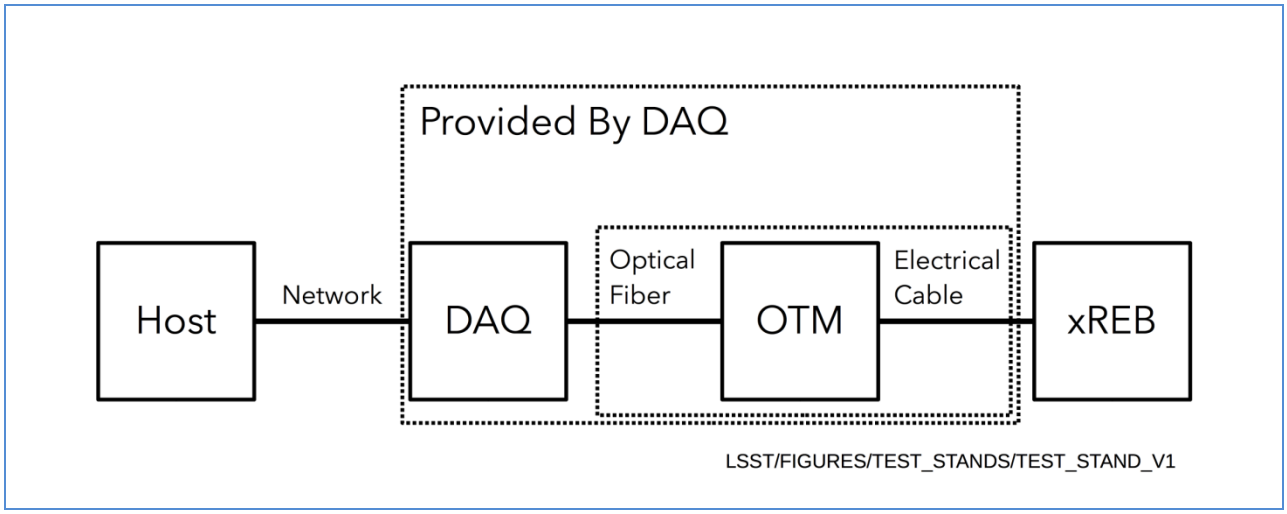

Figure 17-9: Test stand components

Note the DAQ subsystem provides not only a DAQ system, but also additionally an OTM along with its associated cabling. The DAQ system and OTM evolve independently, each in a series of well-defined versions. For the DAQ system versions are labeled V0 through V5. Each version represents a combination of additional hardware, firmware, or software; with V5, the last version representing the production system carried to the observatory. As not every test stand requires the full-blown functionality of V5, not all DAQ systems in the field will advance to V5. The versions, their components and uses are described in Table 17-3.

Table 17-3: DAQ Versions

DAQ Version	Description	Uses
V0	1. Prototype DAQ hardware 2. Prototype software interfaces	Five systems in various locations in the field.
V1	1. Preproduction COB hardware. 2. The hybrid RTM 3. Production software interfaces 4. *Ephemeral*, limited size storage array	1. CCS development 2. Science raft development 3. Corner raft development 4. I&T raft acceptance 5. DAQ development
V2	Synchronous clock distribution (using PGP-2)	
V3	*Persistent*, flash based storage array	
V4	1. Raft emulation 2. FPA/RTM 3. Storage RTM	1. DM data challenge 2. Commissioning camera 3. Camera production system
V5	Crosstalk correction	

Over the project lifetime, there are three versions of the OTM. Any OTM version is interchangeable with any version of the DAQ system . For a given test stand, the appropriate selection of OTM is typically based on three criteria:

- How many REBs must the OTM support?
- Where is the OTM located with respect to its DAQ system?
- Which interface they use.

Note that each OTM version requires a different cable solution for both the electrical and optical side. The different versions are enumerated in in Table 17-2:

Table 17-2: OTM Versions

OTM Version	Name	Description
V0	Raft Transition Board 1 (RTB1)	Connects a single SCI over a prototype PAL
V1	Raft Transition Board 2 (RTB2)	Connects a single SCI over a production PAL
V2	Optical Transition Board (OTM)	Connects up to 12 SCIs over a production PAL

17: Data Acquisition System

17 Introduction

17.1 Overview

The Camera Data Acquisition (DAQ) subsystem connects directly with the sensors and electronics contained on the Camera Focal-Plane-Array (FPA). The FPA is partitioned as 5 x 5 grid of 25 individual rafts. Each raft is a self-contained set of sensors and corresponding electronics. Located in the FPA center are 21 science rafts. Each science raft contains nine sensors and three Raft-Electronics-Boards (REBs). Each REB is responsible for managing three sensors on the raft. The four corner rafts each

contain one wavefront sensor, two guiding sensors and two REBs. One REB manages both guiding sensors while the other the single wavefront sensor. Each REB, independent of location, contains a single link that forms the REB electrical and logical connection to the DAQ system. Consequently, each science raft contains three links and each corner raft contains two links for a total of 71 independent links serving as an interface to the DAQ system.

The entire FPA contains 189 science sensors, four wavefront sensors and eight guiding sensors. From a DAQ perspective, each sensor is electronically identical and contains roughly 16 megapixels. Pixels are digitized with 18 bits of precision. In nominal operation, both science and wavefront sensors are exposed for 15 seconds and digitized and completely read out in no less than two seconds. However, in contrast, a subset of the pixels from each guiding sensor is acquired with a faster cadence, averaging 9 Hz.

When read out, pixel data from the video channel of a sensor is moved to the REB of the sensor, where the data is potentially aggregated with data from other sensors and is emitted onto the REB link to the DAQ system. Data emitted on a link will be called sensor pixel data, or where the context is clear, simply data.

With respect to an FPA, its corresponding DAQ system must satisfy four necessary functions:

- Acquire, buffer and catalog its acquired pixel data.
- Provide both buffered and streaming access to these data.
- Generate and distribute a common system reference clock.
- Provide access to its electronics for the purpose of configuration, monitoring and control.

These four functions are expressed through a set of five different DAQ system capabilities. These capabilities provide for:

- Notification, through subscription of incoming data.
- Retrieval of buffered data for both science and wave-front sensors.
- Access to streaming interface for guiding.
- Access to FPA electronics for purposes of configuration, monitoring & control.
- Management of reference clock and timing.

Users access these capabilities through application-specific-software on commodity hardware. Any such software is considered a DAQ system client. The execution platform for a client is a host. A host is a commodity processor operating under LINUX connected to the DAQ system through a 10-gigabit Ethernet. Clients gain access to the various DAQ services through a set of software interfaces provided by the DAQ system. These interfaces hide from the client the underlying communication mechanisms implemented between host and DAQ system. Figure 17-1 summarizes the relationships between the DAQ, its FPA and clients..

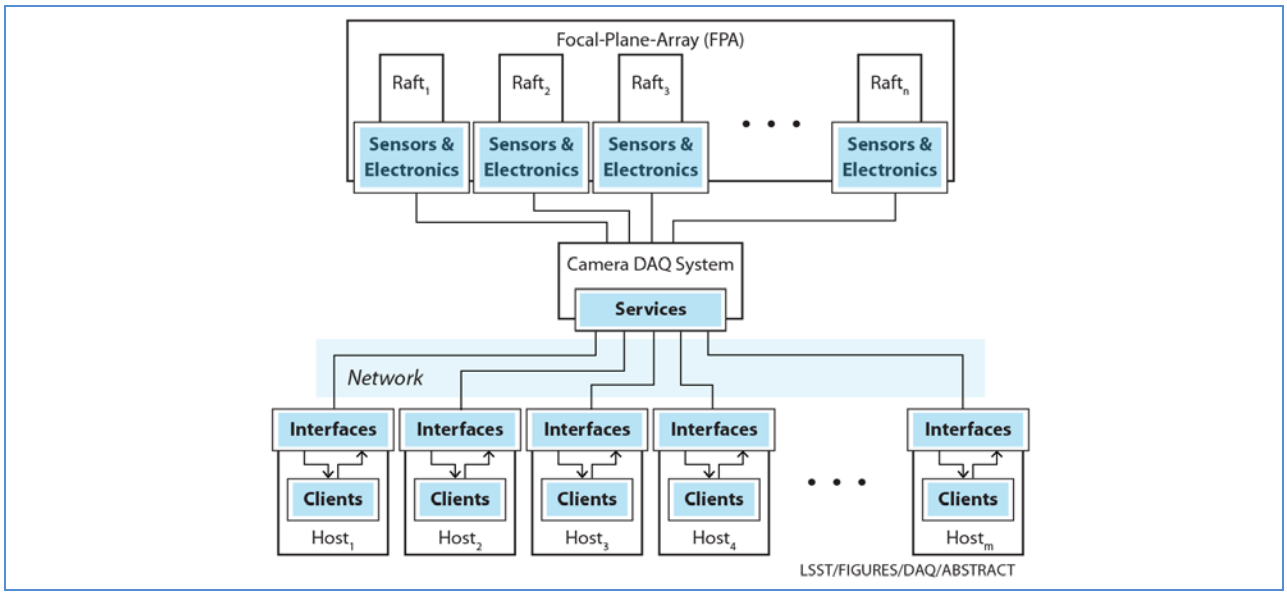

Figure 17-1: Abstract model of the DAQ system and its interfaces

17.2 Focal Plane Arrays and DAQ Systems

The overview of this document implies that only a single FPA is produced by the Camera project, and that is the FPA for the Camera delivered to the observatory. In fact, a variety of FPAs will be produced to support a number of different activities. These activities include:

- Development of raft electronics as well as both CCS and DAQ subsystems
- Sensor/Raft production
- I & T and Sensor/Raft acceptance
- DM data challenges
- Early path-finding and the commissioning camera
- Raft maintenance on the summit

Each one of these activities will require DAQ subsystem support; however it is likely that some or many of the DAQ systems will coexist within a common networking infrastructure. The activities associated with each of these systems will generate and persist data products, and inevitably, the data products generated by one system will require comparison to data products produced by other systems. To differentiate between DAQ systems, a unique name is allocated and assigned to each system. A name is used to qualify any addressable components within its corresponding system. In addition, all data products generated by a system, including especially images, will be tagged with the name of the corresponding system.

17.3 Clients

Images, with data acquired from the science rafts and suitably formatted and processed, constitute the principal science product of the Camera. The primary client for those data is the Data-Management (DM) system. Images with data acquired from the corner rafts are used by the telescope for control of

its adaptive optics system as well as by DM to supplement science analysis, and therefore, the clients for those data are both DM and the Telescope-Control-System (TCS).

Note that while DM and the TCS are certainly the primary clients of the DAQ system, they are not the only clients. Observatory operation, and the need to monitor the Camera's health as well as to perform diagnostics in the event of failure, all require access to image data. Given typical observatory operation, it is likely many of these accesses will occur concurrently.

In order to support these usage patterns, the DAQ architecture is designed for an arbitrary number of clients distributed over an arbitrary number of hosts. The DAQ architecture is also designed to assure quality of service for each client. The architecture provides a total aggregate communication bandwidth in excess of 1.1 Terabits/second between a DAQ system and its hosts.

17.4 Time

All components of the observatory are required to synchronize their respective clocks. This synchronization allows for temporal correlations between events generated across the various observatory subsystems. To this purpose, the DAQ system maintains a Time-Of-Day (TOD) counter that the system may deterministically sample to mark and identify in time any "interesting" occurrence. The TOD is a 64-bit counter incrementing at the Camera system clock rate and initialized by the DAQ system with the "time of day" as determined by the observatory.

17.5 Images and Metadata

To characterize the pixel data associated with an exposure, the exposure is tagged with additional metadata. The combination of metadata and pixel data is an image. One primary component of metadata is the identifier of the image. When triggering an exposure, the client is responsible for creating and assigning a unique image identifier. Identifiers serve two functions:

- They differentiate images while resident in the catalog.
- Through association, they reference the image's associated storage bucket.

Metadata has its origin in four sources:

- Each (raft) bay of the FPA.
- Each board of each raft of the FPA.
- Internally, with the DAQ system itself.
- Externally, with the client triggering an exposure.

The DAQ system is responsible for the rendezvous of the various metadata along with their corresponding pixel data to form an image.

Each raft of the FPA will contribute at least, but not limited to the following metadata:

- Raft and board address.
- Sensor type.

Each board of the FPA will contribute at least, but not limited to the following metadata:

- Type. One of REB, GREB, or WREB and whether or not the board is emulated.
- Serial Number.
- FPGA version (both for SCI and raft specific logic).
- Register schema information.
- The contents of a specified set of registers.

The DAQ system will contribute at least, but not limited to the following metadata:

- Data Acquisition Name.
- Operating System Version information.
- RDS and IMS versioning information.

The client will contribute at least, but not limited to the following metadata:

- A unique image Identifier.
- A set of client specific opaque data.

17.5.1 The Storage Array

The DAQ system for the observatory is required to buffer its acquired images for at least two days of typical operation. This requirement derives from an observatory requirement to maintain operation for as many as two days in the event of an interruption of service between summit and base facility. Interruptions could occur, for example, if the communication links between summit and base are down, or services at the base facility are unavailable due to scheduled maintenance. The functional component of the DAQ system maintaining and managing that two-day buffer is called the storage-array.

For reasons of performance and reliability at altitude, flash rather than rotational media is chosen as storage media. Based on an observatory model that takes into account typical night observation patterns as well as daytime calibration, 48 hours of buffering corresponds to roughly 35 terabytes of image data. The need to provide for an equal number of hours of simulation data doubles that amount and Camera maintenance and diagnostic requirements adds an additional 15 terabytes for a total storage requirement of around 85 terabytes.

To provide contingency as requirements mature, the storage array is sized somewhat larger at 132 terabytes. This is not a hard limit, with higher density drives total capacity could trivially grow to double that amount. Further, if required, the storage architecture provides a graceful growth path to reach what is an essentially unlimited amount.

The usage model for the storage array is based on the premise that images are written once, but read many times. Therefore, the necessary write bandwidth is straightforward to quantify and must be able to keep up with the total read-in rate of approximately 3.5 gigabytes/second. The necessary read bandwidth is somewhat more difficult to quantify, as it depends on a concurrency model, which in turn

depends on the observatory's "operational concepts" model, which remains a work in progress. However, a model, maintaining "Quality-Of-Service" guarantees for at least four concurrent clients is considered a reasonable approximation. This corresponds to a necessary read bandwidth of approximately 15 gigabytes/second.

Given the relative immaturity of the observatory's operations model, the total available bandwidth of the storage array is designed purposely large, on the order of 100 gigabytes/second. That bandwidth scales as additional storage is added at roughly the rate of one gigabyte/second for each additional terabyte of storage.

17.5.2 The Image Bucket

The storage array is partitioned into units of buckets. A bucket is the container for one image. Buckets are sized to contain the largest image that may be generated by the FPA and stored by a DAQ system. The number of buckets is configuration driven. When it is created, each bucket, is assigned an identifier (the bucket ID). A bucket ID is used to reference the stored data and metadata of an image. Once assigned, a bucket ID is unique for all time. Deleting a bucket does not allow the identifier to be reused. Buckets are created and populated with their corresponding image by the system when the image is triggered. Buckets are allocated and deleted by the DAQ system as necessary.

17.5.3 The Image Catalog

The storage array has an associated catalog. A catalog is composed of a hierarchy of folders and images. Catalogs contain folders and folders contain images. The principal function of the catalog is to return to a client the bucket corresponding to a specific image contained within a specific folder. Each folder in a catalog is addressed by its name. A name is simply an ASCII string of arbitrary length assigned when the folder is created. The set of folder names must be unique within a catalog. The client has access to the following operations on a catalog:

- Create, rename and delete its folders
- Retrieve the Bucket ID for a given image in a given folder
- Retrieve all Bucket IDs for a given folder
- Move one or more images from one folder to another

To formalize the management of the storage array during operation, a DAQ system contains a number of predefined, "well-known" folders. As needs mature this set may be extended, however, to this point the catalog contains the following well-known folders.

- The Freelist: The buckets associated with the images in this folder are candidates for reallocation by the DAQ system. Allocation from the Freelist will be in insertion (FIFO) order. That is, the oldest, inserted image will be the first candidate for allocation. The Freelist will be initially populated by a DAQ system when configured.
- Pending archival: This is the initial, default location for created images. Data Management will assume any images in this folder are to be archived.

- Pending catch-up: This folder contains the set of images acquired while service to the base facility was interrupted. Data Management will assume any images in this folder are to be archived.
- Simulation: This folder contains the set of images to “play back” when the DAQ system is being driven in simulation. The composition and names of the images in this folder are reserved to the DAQ system.

17.6 Amplifier Addressing

FPA electronics digitize their data in parallel in units of amplifiers. Consequently, for purposes of both subscription and identification, the smallest unit of addressability is also the amplifier. An FPA contains a variable number of amplifiers ranging from one all the way to the 3216 amplifiers contained within the FPA of the production Camera. However, independent of specific FPA, the schema for locating an amplifier is identical. In this scheme, an amplifier address is encapsulated and encoded in 32-bits as illustrated with Figure 17-2 below:

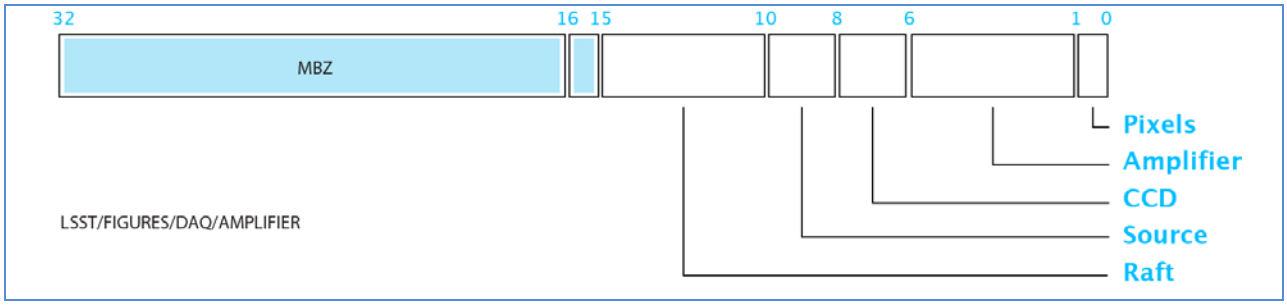

Figure 17-2: Amplifier addressing

Where:

- Pixels: A flag that specifies whether the address fields described below reference pixel data or metadata. If this field contains zero (0), the reference is to metadata. If this field has a value of one (1), the reference is to pixel data.
- Amplifier: Specifies the amplifier relative to the CCD specified below. This field contains a small enumeration corresponding to the physical location of the amplifier within a CCD. Amplifier locations are defined in [yyy]. The value of this field may vary from zero to fifteen. Numbers sixteen to thirty are considered invalid and must not be used. The value thirty-one is reserved as a wildcard specification and depending on context could mean either “any” or “all.”
- CCD: Specifies the CCD containing the amplifier, relative to the Source specified below. This field contains a small enumeration corresponding to the physical location of the CCD managed by a single source. CCD locations are defined in [yyy]. The value of this field may vary from zero to two. The value three is reserved as a wildcard specification and depending on context could mean either “any” or “all.”
- Source: Specifies the Source containing the amplifier, relative to the Raft specified below. This field contains a small enumeration corresponding to the physical location of the link within a raft. Link locations are defined in [yyy]. The value of this field may vary from zero to two. The

value three is reserved as a wildcard specification and depending on context could mean either “any” or “all.”

- Raft: Specifies the Raft containing the amplifier, relative to its FPA. This field contains a small enumeration corresponding to the physical location of the raft within a FPA. Raft locations are defined in [yyy]. The value of this field may vary from zero to twenty-four. Numbers twenty-five to thirty are considered invalid and must not be used. The value thirty-one is reserved as a wildcard specification and depending on context could mean either “any” or “all.”

17.7 Image Data Organization

Pixel data for an image is organized in two dimensions. In the x dimension data are specified by their spatial source relative to their FPA, while in the y dimension data are specified as they evolve in time. Dimensions in x are measured in units of Amplifiers, while dimensions in y are measured in units of Slices.

Independent of total size, an image is always divided into 128 equal sized time-slices. Slices increase monotonically in time. For example, data contained in time-slice one was always read-out earlier then data in time-slice two. Note that at the nominal readout rate a slice corresponds to roughly 16 milliseconds of data.

It is convenient, therefore, to consider pixel data as an array of n x m dimension, where n is equal to the number of amplifiers whose data were acquired and m is always 128 slices. For example, one column corresponds to the pixel data from one specific amplifier, from beginning to end of read-out. Or as another example, the first row corresponds to data from all amplifiers from beginning to 16 milliseconds into read-out.

Both row zero and the array element (0, 0) have special meaning. Any row zero element contains metadata. Note that this implies metadata is acquired and stored before its corresponding pixel data. Element (0,0) corresponds to the metadata, which is common to all elements of an image.

Image data organization is represented pictorially as shown in Figure 17-3.

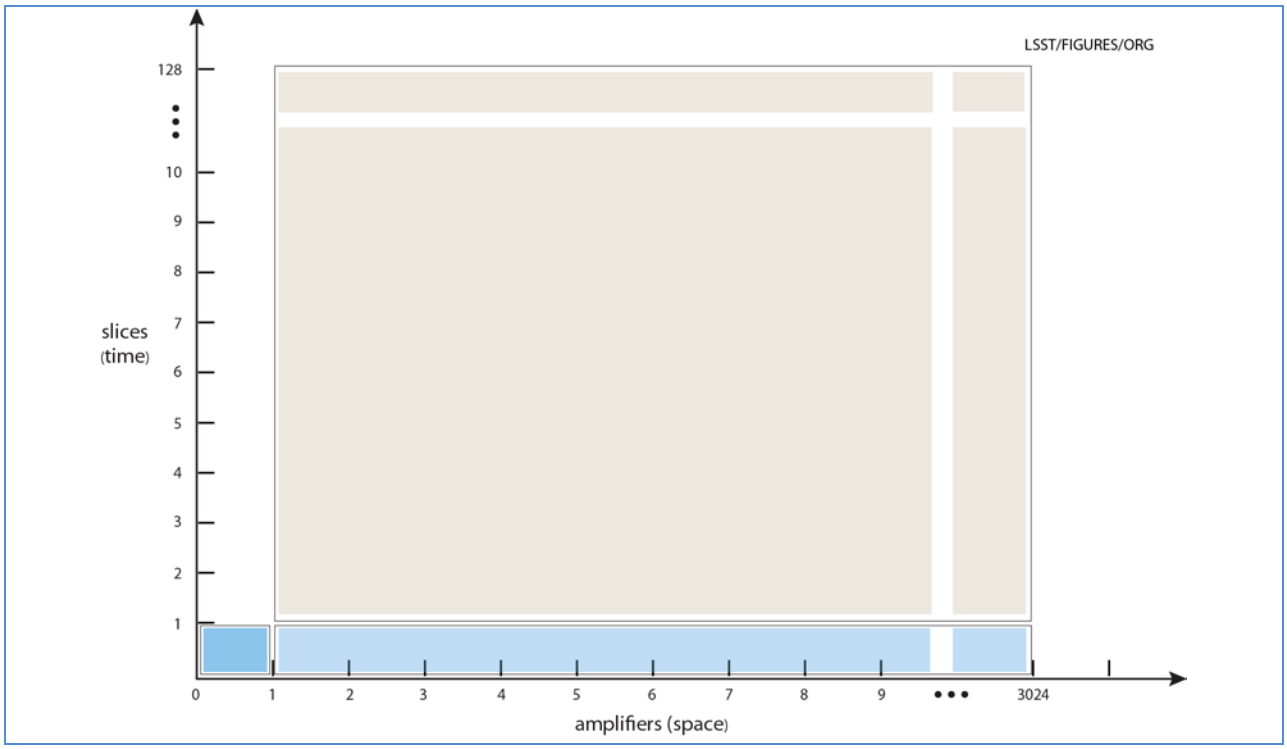

Figure 17-3: Image data organization

In Figure 17-3, regions shaded brown indicate pixel data of an image and regions shaded blue indicate the corresponding metadata of the image. Typically, when referencing image data, clients are interested in more than one and less than all the elements of its array. Therefore, it's convenient to specify a reference to a region, rather than to a single coordinate. Such a specification will be called a Region-Of-Interest (ROI) . An ROI is characterized by two parameters:

- The coordinate of its first element
- Its size (in units of rows and columns)

17.8 Image Access

Clients access image data only from stored images. That is, clients only gain access to image data after the data is committed to the storage array. However, once written, that data remains accessible until its reuse (nominally 48 hours after the image was created).

As described above, as data arrive to a DAQ system, they are quantized in units of slices and stored. As slices are stored, events are produced. An event is a small, concise message describing a slice and the container in which its data can be found. Its message contains the following information:

- A Bucket ID: This identifier specifies a container holding an image's pixel and metadata.
- A ROI: This ROI specifies the slice acquired and committed to the storage array.

Events are made known to clients through a publish-subscribe paradigm. Using that paradigm, clients subscribe to events the system publishes. The client subscribes using an appropriate method of the IMC

software interface. This method takes an ROI as an argument. This ROI specifies the events that interest the client. Once a subscription has been registered, the client waits on the arrival of its corresponding events. This implies that access to data is a two-step process: The client waits on an event and as events arrive, uses the event information to fetch the corresponding data.

Quantizing data in slices adds pipeline latency to the nominal two-second readout time. That latency is roughly equal to the time for the system to buffer and store one slice.

17.9 Camera Operation

To minimize cost and maintenance, the summit has a single DAQ system to service the Camera in all Camera modes of operation. In order to do so, the system design takes into account three questions:

- How does the system allow for Camera maintenance?
- Where can the hosts that must interact with the system be located?
- How does the system support Data Management at the base-facility?

The nexus for the DAQ System is the Camera Data System (CDS) located in the computer room at the summit. The computer room is fixed in place and does not move. However, the same cannot be said for the Camera, which on arrival at the summit as well as during planned or unplanned maintenance is off the telescope and located in the observatory cleanroom.

To deal with this eventuality, the Camera-side of the CDS has permanent fiber plant and connections to the two possible locations of the Camera, the telescope or clean-room suite. In this fashion, as the Camera moves, no physical re-cabling is necessary. Instead, using a software interface, the DAQ system is simply reconfigured to “point” at the appropriate set of fibers.

A third option exists. It is also possible the DAQ system is operable, but the Camera is unavailable. Such a condition exists in the early path-finding for the observatory as well as when an instance of the DAQ system must participate in a data challenge. To deal with this eventuality, the system contains a two-day emulation of the Camera, with a permanent set of connections between it and the remainder of the DAQ system.

17.10 Reuse and the DOE Detector R & D Program

In order to minimize both development costs and schedule risk, the implementation of the DAQ system draws heavily on the concepts as well as the hardware, firmware and software developed out of the SLAC /DOE Detector R & D program on large-scale Data Acquisition Systems . This program’s fundamental premise is that application specific, arbitrarily sized DAQ systems may be constructed by derivation from a small number of generic, reusable building blocks. These blocks are the Reconfigurable Cluster Element (RCE), the Cluster, the Cluster Interconnect and as a physical substrate ATCA .

17.11 Architecture

A major design goal is to maximize reusability wherever appropriate. Therefore, while the usage of science, wavefront and guider data varies, their acquisition inherits from a common hardware, firmware

and software foundation. This leads to a single hardware abstraction of the DAQ system as shown in Figure 17-4.

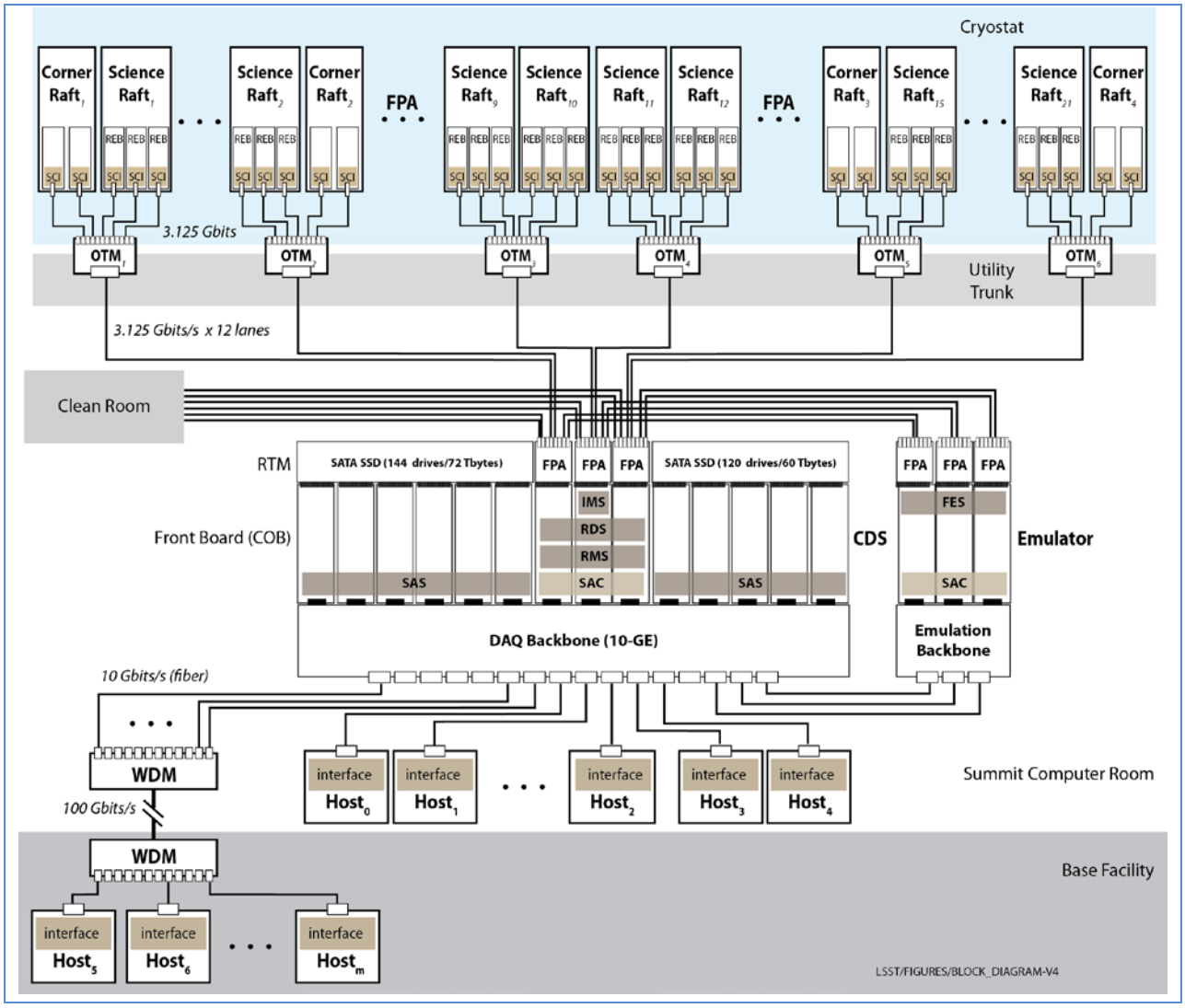

Figure 17-4: Block diagram of the LSST Camera Data Acquisition System

The blocks in the diagram represent the various functional components either provided by, or interfaced with the DAQ system. Shaded blocks within blocks represent system software or firmware. One somewhat unique feature of the system architecture is how its components are distributed over geographically disparate locations, starting from within the Camera cryostat on the summit and continuing to the observatory base facility located in the city of La Serena almost 100 km away. The diagram expresses this feature by arranging its functional blocks by their observatory location, with blocks closest to the Camera at the top and blocks furthest away at the bottom. The following sections briefly describe each block starting from within the cryostat.

17.11.1 The Source Communication Interface

The Source-communication-Interface (SCI) is a pure firmware block located within the cryostat. In actuality, an SCI resides within an FPGA contained within a Raft-Electronics-Board (REB). In turn, a REB is itself contained within a raft. Both REB and FPGA are provided by their respective science and corner raft subsystems.

Each science raft contains three REBs with each REB servicing three CCDs. Each corner raft contains two REBs. One REB services the two guiding sensors of the corner raft and the other REB services the single wavefront sensor. For its corresponding REB, an SCI provides the following: synchronous timing and control, monitoring and configuration of its electronics, and serialization and transmission of its sensor video data.

In total, the FPA contains 71 SCIs, with each SCI having a single, high-speed serial link with the CDS. That serial link is full-duplex having physically disparate transmit and receive signals carried on a copper lane. Lanes are converted to optical fiber at the cryostat boundary by the Optical Transition Module (OTM). The decision to convert to fiber optics outside rather than inside the cryostat was predicated on the Camera's strong desire to minimize the amount of electronics inside the cryostat. Note that independent of science or corner raft the design and implementation of their respective SCIs are identical.

17.11.2 The Optical Transition Module

The OTM is a hardware block located on the boundary between Camera cryostat and utility trunk and has the straightforward electrical responsibility of converting the high-speed, serial links emanating from SCIs from copper to light and light to copper. Physically the OTM is simply a small printed-circuit-board (PCB) containing fiber-optic transceivers. The PCB is co-located on a flange of the cryostat endplate and serves as the mechanical and vacuum penetration for link signals. One edge of the board is exposed to the cryostat (the "vacuum" side) and manages signals as copper, and the other edge of the board is exposed to the utility trunk (the "air" side") and manages signals as light.

Each OTM services up to 12 SCI-Links, where a link is carried to the OTM's "vacuum" side as two copper, differential pairs. Each pair contains transmit and receive signals with the pair duplicated for purposes of redundancy. The OTM contains on its "air" side, two, 12-channel, full-duplex transceivers, again duplicated for purposes of redundancy. One copper pair connects to one channel of the primary transceiver and the other pair to one channel of the secondary transceiver.

As the two transceivers are intended to provide redundancy, only one transceiver is powered at a time. Each transceiver employs MT ferrules as its fiber-optic physical standard, consequently the "air" side interface consists of two, twenty-four strand fiber-optic cables; one for each transceiver.

The FPA contains 71 SCIs, whose links are distributed uniformly over six OTMs. In turn, those six OTMs are distributed uniformly over the annulus of the cryostat end plate.

17.11.3 The Camera Data System

The CDS is the central core of the DAQ system and is located in the computer room of the summit facility. The CDS is a combination of hardware, firmware and software. Physically, the CDS is a 14-slot ATCA shelf with a full-mesh backplane. Its front slots are occupied with identical PC boards called COBs, while its rear slots are occupied with one of two types of Rear-Transition-Modules, or RTMs. Those two types are:

- The FPA/RTM. This RTM provides a fiber-optic interface for up to 96 SCI-Links. The RTM also includes an accurate "Time-Of-Day" clock, which is used to establish the absolute time at which images are created.
- The SSD/RTM. This RTM contains up to 24, 1.8" flash, SATA-II drives. Each drive is base-lined with a capacity of ½ terabyte of flash media (solid-state-disk). All 24 drives operate in parallel and provide an aggregate read/write bandwidth of almost five gigabytes/second and a total storage capacity of 12 terabytes.

A COB contains eight DPM-RCEs and a single DTM-RCE. Although physically identical, SDS COBs are differentiated by their corresponding RTMs and by the firmware and software their RCEs execute. The 14 COBs may be grouped by logical function into two sets:

- The FPA. This set contains three COBs each paired with a FPA/RTM. Its three RTMs are connected to the FPA's 71 SCIs. Each of its DPM-RCEs is capable of controlling and managing the data from up to three SCIs . The "wiring" between RCE and SCI is rich enough to allow each SCI to physical exist in one of the three zones without need for physical re-cabling. These three zones are:
    - The Camera's SCIs residing on the telescope.
    - The Camera's SCIs residing in the clean-room.
    - The Camera's SCIs being emulated by the DAQ system.
- The storage array. This set contains 11 COBs each paired with a SSD/RTM. It hosts the software and firmware dedicated to providing uniform, external access to its RTM's 264 SATA-II drives.

The full mesh backplane of the shelf combined with the switching contained within each of its 14 COBs constitutes a fully provisioned, non-blocking, Layer-2 Ethernet switch with 238 10-Gigabit ports. This switch is referred to as the DAQ backbone. A group of 126 ports of the switch are permanently connected to the s 126 RCEs of the shelf. The remaining 112 ports are reserved for connection to the DAQ network.

From a functional rather than physical perspective, the principal responsibility of the CDS is to host the software necessary to express the services provided by the DAQ system. .

17.11.4 The DAQ Network

All CDS RCEs connect to a single Ethernet (the DAQ network). The backbone for this network is contained within the CDS. This network extends over the entire observatory, including the computer

room of the summit, the downlink (WDM) equipment connecting summit and base facility, and the inside the base facility itself, where it penetrates into the equipment housing the DM infrastructure and secondary control-room.

A host wishing to gain direct access to the services provided by the DAQ system must be connected to the DAQ network. All network traffic not related to the DAQ system is both physically and logically segregated off this network. This implies that a host must be dual-homed, with one interface connected on the DAQ network and the other to the outside world.

As this network is physically isolated at Layer-2, it is also logically isolated at Layer-3. TCP/IP configuration and management will be dictated by the needs of its corresponding DAQ system. This includes, for example assignment of IP addresses.

17.11.5 Timing Distribution and the System Clock

Timing for the sensors and electronics of the FPA is synchronous. That is, the FPA:

- Is driven by a common system clock.
- Receives and acts on, simultaneously a common set of commands.

The source for both clock and commands is the CDS. This implies a significant fan-out to components geographically distributed. This fan-out is implemented in coordination with the link-protocol between CDS and SCI.

17.12 Support for DAQ and Camera Development

The DAQ development schedule is prioritized to provide development support of increasing fidelity and capability to other Camera and observatory subsystems. In order to facilitate that support, the DAQ system is designed for backward compatibility. As it evolves, adding new features existing systems in the field can, as needed be upgraded. The components that make up DAQ support for test stand are shown in Figure 17-5.

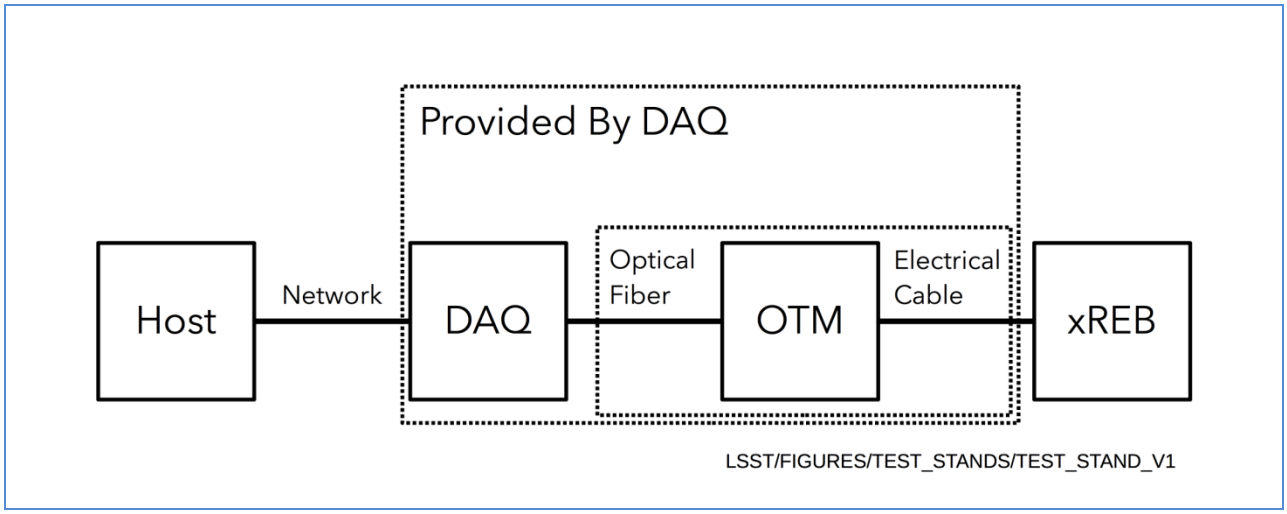

Figure 17-5: Test stand components

Note the DAQ subsystem provides not only a DAQ system, but also additionally an OTM along with its associated cabling. The DAQ system and OTM evolve independently, each in a series of well-defined versions. For the DAQ system versions are labeled V0 through V5. Each version represents a combination of additional hardware, firmware, or software; with V5, the last version representing the production system carried to the observatory. As not every test stand requires the full-blown functionality of V5, not all DAQ systems in the field will advance to V5. The versions, their components and uses are described in Table 17-1.

Table 17-1: DAQ Versions

DAQ Version	Description	Uses
V0	1. Prototype DAQ hardware 2. Prototype software interfaces	Five systems in various locations in the field.
V1	1. Preproduction COB hardware. 2. The hybrid RTM 3. Production software interfaces 4. *Ephemeral*, limited size storage array	1. CCS development 2. Science raft development 3. Corner raft development 4. I&T raft acceptance 5. DAQ development
V2	Synchronous clock distribution (using PGP-2)	
V3	*Persistent*, flash based storage array	
V4	1. Raft emulation 2. FPA/RTM 3. Storage RTM	1. DM data challenge 2. Commissioning camera 3. Camera production system
V5	Crosstalk correction	

Over the project lifetime, there are three versions of the OTM. Any OTM version is interchangeable with any version of the DAQ system . For a given test stand, the appropriate selection of OTM is typically based on three criteria:

- How many REBs must the OTM support?
- Where is the OTM located with respect to its DAQ system?
- Which interface they use.

Note that each OTM version requires a different cable solution for both the electrical and optical side. The different versions are enumerated in in Table 17-2:

Table 17-2: OTM Versions

OTM Version	Name	Description
V0	Raft Transition Board 1 (RTB1)	Connects a single SCI over a prototype PAL
V1	Raft Transition Board 2 (RTB2)	Connects a single SCI over a production PAL
V2	Optical Transition Board (OTM)	Connects up to 12 SCIs over a production PAL

18: Auxiliary Electronics

18 Auxiliary Electronics

18.1 Introduction and Requirements

The LSST Camera is a large and complex device, but all of that complexity is directed at a single goal: to provide very high resolution images at, for an astronomical instrument, a very high repetition rate. The Focal Plane Array (FPA), which is the heart of the Camera, is described in detail in Chapters 8, 9, 10 and 11. This chapter describes the Auxiliary Electronics subsystem, which provides electrical and electronic support functions needed to allow the FPA and the rest of the Camera to operate properly.

Auxiliary electronics support functions are organized into three groups: power distribution, monitoring, and hardware protection. This chapter focuses mainly on power distribution and monitoring. Hardware protection is covered in Chapter 6.

The requirements for auxiliary electronics support functions come directly from science requirements imposed on the subsystems being supported, or they come or from general requirements for Camera design. For example, the low noise level required of the electronics for the FPA implies a low noise, high-stability power supply; it is a direct requirement that can be translated into a power supply specification.

However, high-availability is a general requirement for all Camera parts; this general requirement is not so easily translated directly into a power supply specification.

Here are the general Camera requirements that influence auxiliary electronics support functions:

- High availability – The requirement for highly reliable hardware and relatively easy replacement of individual boards or modules wherever possible.
- Low power – The requirement for low-power consumption in the Camera and especially inside the cryostat where cooling is difficult. Power and the associated cooling are always expensive in terms of space and reliability, and for an astronomical instrument, design must avoid generating heat plumes in the optical path.
- Built in test and monitoring – The requirement to ensure timely maintenance, and therefore, high reliability.
- Compact size and low mass – The requirement to fit within space available without overloading the telescope mount and drive.

18.1.1 Support for the Focal Plane Array

The focal plane array (FPA) consists of 21 Science Raft towers mounting 189 CCDs (nine per raft) and four Corner Rafts mounting two guide sensors and one wave front sensor. Each of these twenty five rafts is an independent mechanical and electrical object capable of operating as a stand-alone Camera. Even after integration into the cryostat grid, each raft is treated as an independent electrical object in terms of power, control path, and data path.

18.1.2 Mechanical Interfaces

Physical dimensions of each electrical and electronic device are a critical part of the auxiliary electronics design. Given location of the Camera in the optical beam of the telescope, there are tight constraints on available space for devices, and space is largely cylindrical rather than the rectangular.

Location of electrical and electronic parts also is critical. The Camera is not easily accessible when it is mounted on the telescope; much of the outside of the Camera is hidden behind features such as the secondary mirror or the hexapod.

While the Camera can be demounted from the telescope for full servicing, that is a non-trivial effort that takes many days. As a result, it is important to put as many critical components in areas accessible while the Camera is mounted on the telescope.

Fortunately, a significant portion of the Camera body where shutter and filter mechanisms are located can be accessed with the Camera on the telescope, and in addition, there is a region inside the hexapod, forward of M2 that can be accessed via walkways built into the telescope. The baseline design places as much as possible of the critical electronics (not, of course, the focal plane electronics) in regions that are readily accessible. Figure 18-1 shows a cutaway of the entire Camera with the filter and shutter region on the left (in red) and the utility trunk on the right.

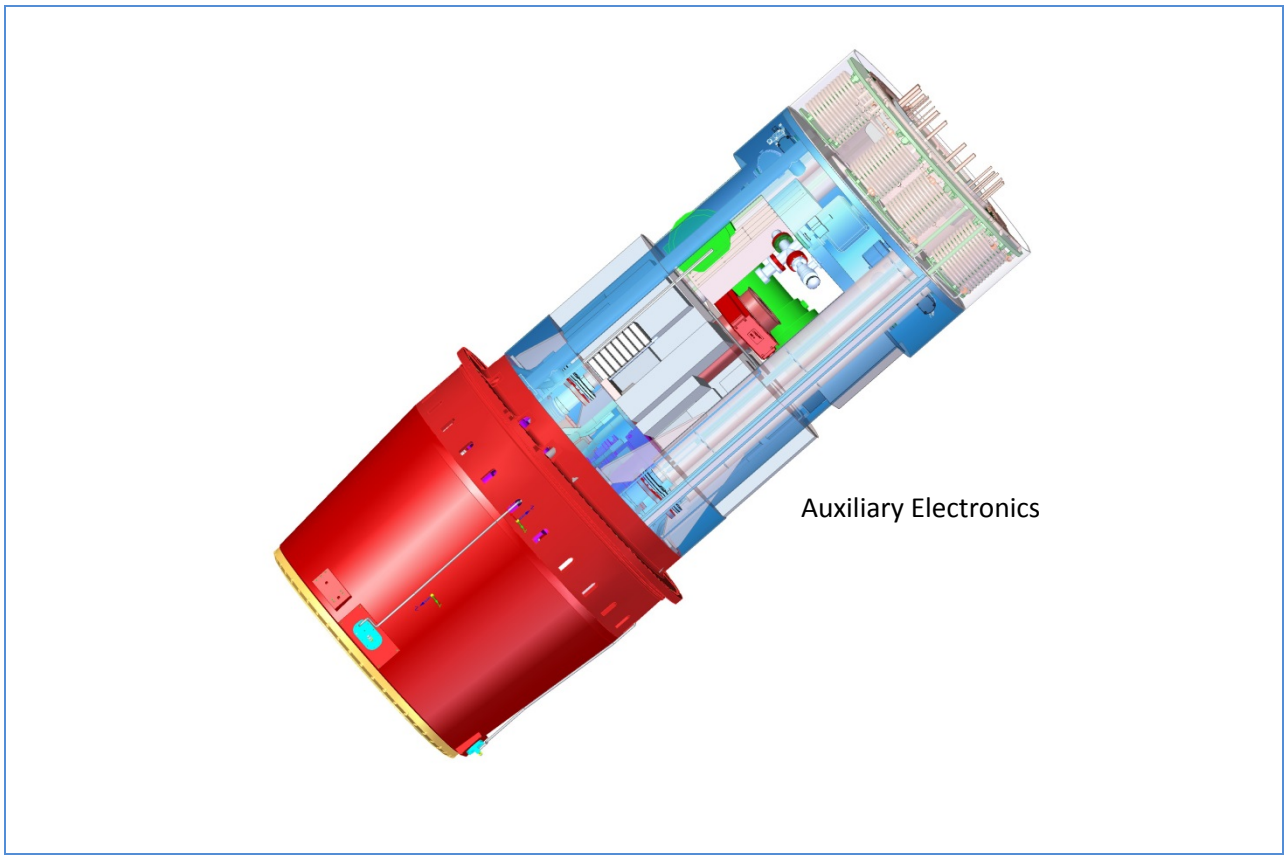

Figure 18-1: Picture of overall utility trunk, electronics chassis area

The region marked “Auxiliary Electronics” illustrates how power supply crates as well as the AC and DC power distribution chassis are placed along the length of and arranged inside the cylindrical utility trunk volume; a detailed view of this region is shown in Figure 18-2 below.

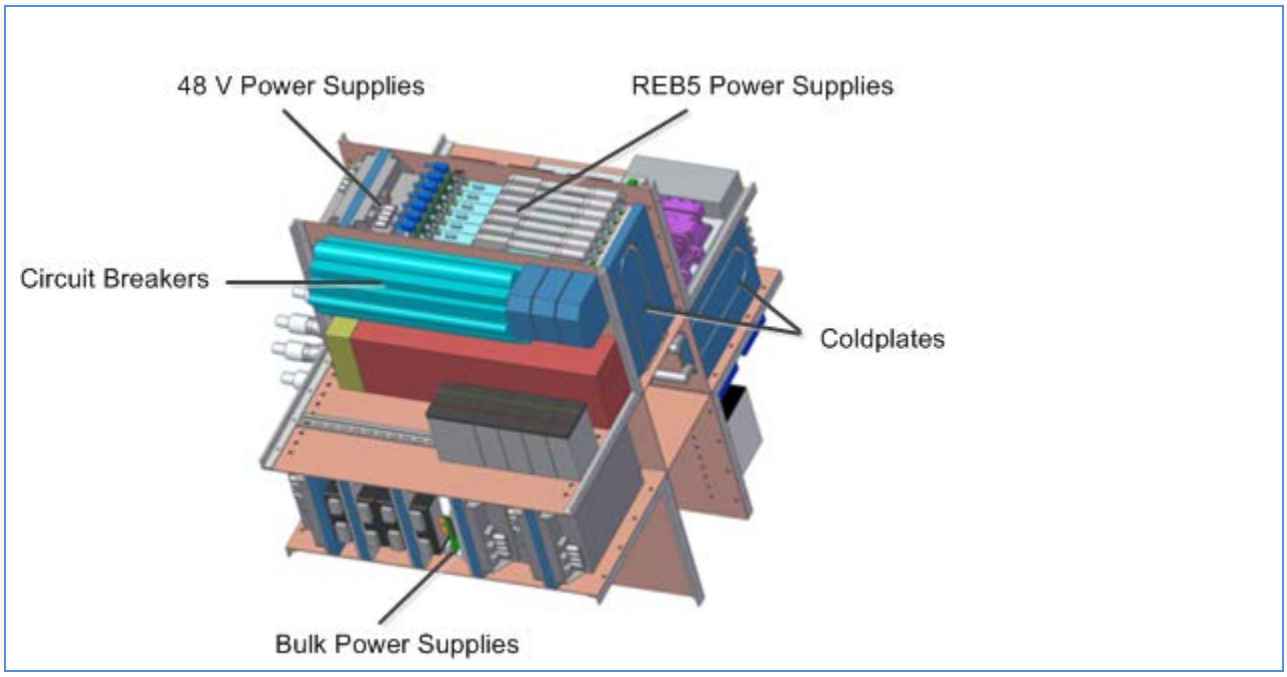

Figure 18-2: Current design for integration of power supplies and auxiliary electronics chassis in utility trunk

18.2 Power Distribution

Power is provided to the Camera from the Observatory via a dedicated AC feed from an electrostatically shielded Δ -Y transformer used solely for feeding the Camera. For the baseline design, a 380Y/220V 50 Hz five-wire feed (three phases, neutral, and safety ground) has been specified, as shown in Figure 18-3.

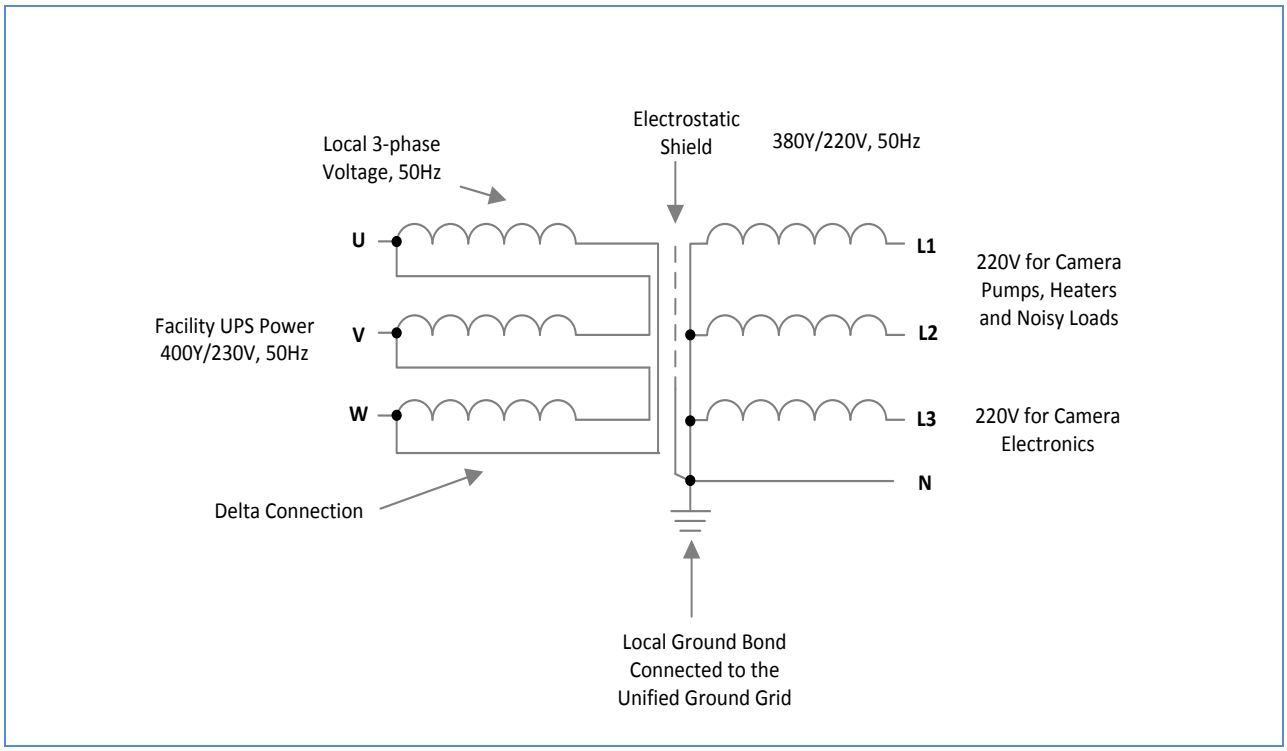

Figure 18-3: 380/208 50 Hz five wire feed

Once inside the Camera the AC power will be filtered once again (immediately at the AC disconnect after the breaker panel) to isolate the Camera from possible external disturbances and the phases will then be divided into “clean” and “dirty” loads as shown in Figure 18-4.

Loads described as “dirty” are those which could inject noise into the power system either because of sharply changing currents with normal operation as with motors starting or stopping or because the load could be prone to instabilities or breakdowns as, for example, high voltage vacuum gauges.

Isolation between clean and dirty is obtained simply putting those loads on separate AC phases. In addition there will be LC filters not only at the Camera input but also at each separate AC load bus.

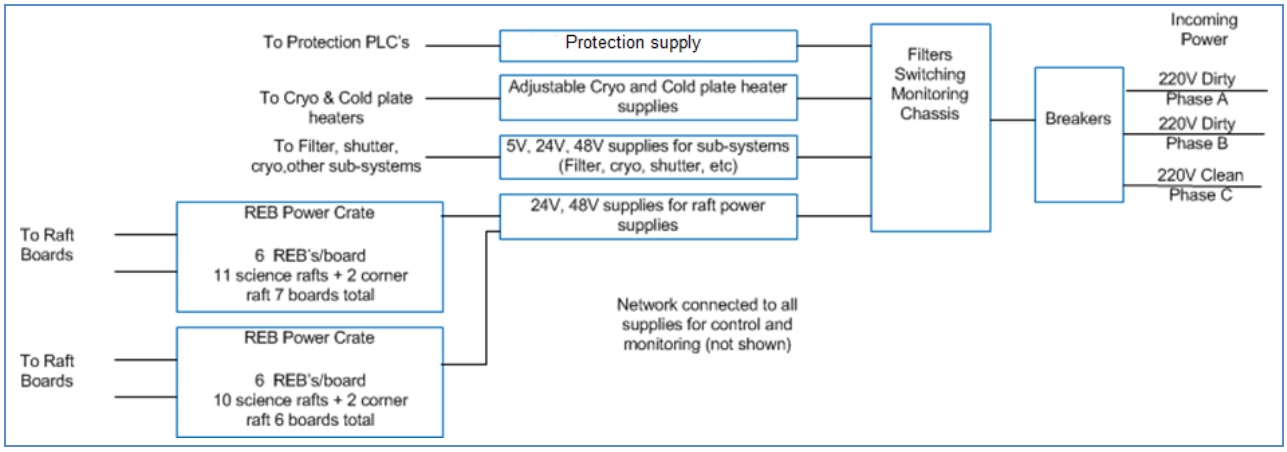

Figure 18-4: Division of Camera “clean” and “dirty” power loads

The major loads are listed in Table 18-1. The input supply must be able to supply the maximum peak power. The cooling load for the Camera is, of course, only the maximum average power as long as the thermal time constants of the various parts of the Camera are less than duty cycle of any of the loads – so, for instance, the shutter only operates for one second out of eighteen.

Table 18-1: Major Camera electrical loads, with estimated peak power

Load	Type of Power	Load Location	Regulator Location	Note
Raft Electronics Board (REB)	DC	Cryostat	Utility Trunk (UT)	Most sensitive
Fiber Conv	DC	UT	UT	
CCS Hdw	DC	UT/C Body	UT	
CCS Network	DC	UT	UT	Cu Ethernet
Vacuum Pumps	DC / AC	Rear of Cryostat	None	Unregulated
Vacuum Gauges	DC	Rear of Cryostat	UT	Moderate regulation
Filter Exchange	DC	Camera Body	UT	CAN Bus
Shutter	DC	Camera Body	UT	

18.2.1 Raft Power

The Science and Corner Rafts are probably the best understood loads and the most sensitive. In baseline design, several different well-regulated DC voltages are specified; from a low of 5V to a high of 70V.

The baseline plan for this power, the Power Distribution System (PDS), is to have a number of custom raft power boards in the electronics crate volume. The boards will be fed from the 48V power bus. A PC104 single-board computer allows for CCS compatible control of the PDS, which distributes 48V and control commands to the individual power boards.

Each power board provides the multiple independent supplies to Science or Corner Rafts. Each board is individually monitored for voltage and current as well as faults, and each board has individually adjusted voltage, current, and thermal limits.

Any single Raft Electronics Board (REB) and any single supply for that board can be individually turned on or off and, by the same token, sequenced in a suitable way. Each supply is an independent DC-DC converter with isolated outputs so that the power system does not cross-couple the rafts.

Prototypes of individual supply modules using commercial DC-DC controller chips have been constructed and were measured to have performance close to what is required for the final system. Packaging all the required supplies in a space-efficient fashion will not, however, be a simple task.

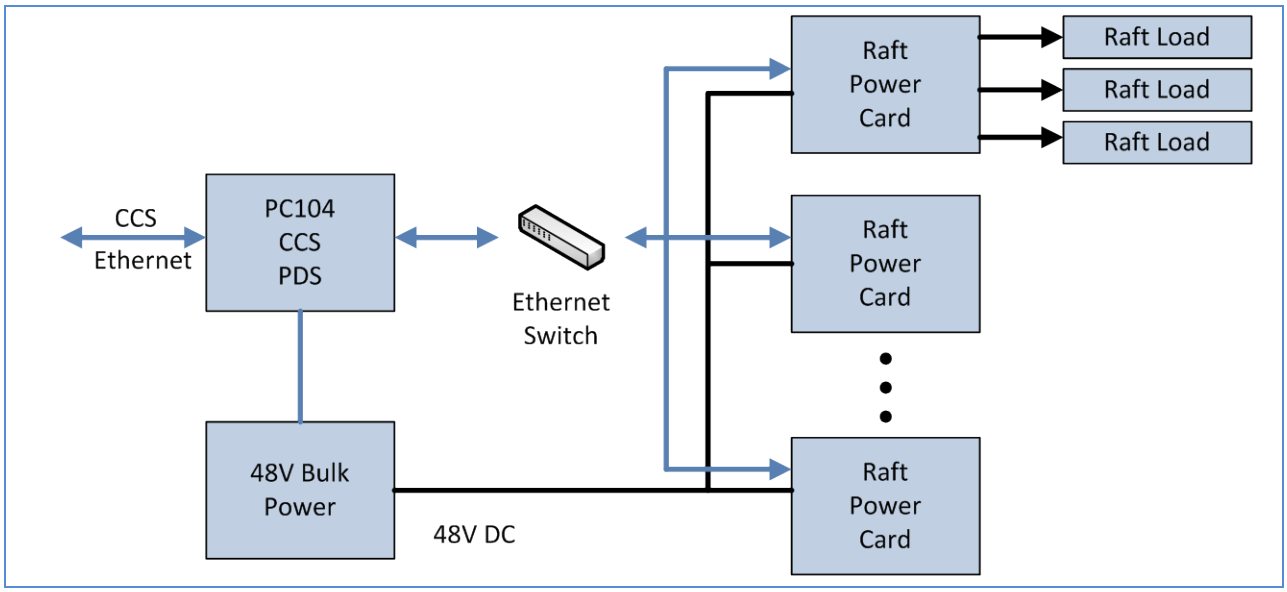

Figure 18-5: Ethernet interface of raft power cards to the controlling PC104

As indicated in Figure 18-5, the individual raft power boards are expected to have an Ethernet interface to the controlling pc104 by way of a shared Ethernet switch. Using the switch simplifies packaging and provides ample bandwidth for the anticipated number of control commands and parameter reads that will occur per second.

18.2.2 Control and Monitoring of Power

As noted previously, the project baselines a system with complete control (on/off and voltage set point) and complete monitoring of output voltage and current for each of the supply voltages for each load.

Assuming seven independent voltages for each raft, there will be 175 on/off controls, 175 voltage set points, 175 current monitors, and 175 voltage monitors that are all readout via the controlling pc104 that interfaces with CCS.

In addition to board-level monitoring, the standard DC-DC controller chips in the power supplies each include independent over-voltage and over-current set points that can drive digital alarms sent to CCS. Those digital alarms are independent of the continuous precision-monitoring measurements by the CCS that allow trending and serve to diagnosis possible problems early.

18.3 Optical and Network Communications

Dataflow within the Camera and from the Camera to the observatory is over two separate sets of high speed serial links. The main science data flow is carried via a custom high speed protocol - first over copper from each raft to the utility trunk and then by optical signals for long haul transmission to the DAQ components in the observatory control room.

All control and monitoring inside the Camera is over a set of standard Ethernet links that tie together the various CCS nodes that are implemented in commercial processors (of baseline pc104 form factor).

An external TCP/IP fiber link and a redundant fiber link from the off-Camera CCS servers to the Camera connect to a commercial switch in the utility trunk. The switch converts optical to copper TCP/IP and instantiates point-to-point connections to each CCS hardware component in the Camera. The switch is located in the accessible power control and auxiliary electronics area of the utility trunk in order to allow easy replacement and servicing.

18.3.1 Fiber Routing

After the science data is converted to fiber, those fibers (and the standard TCP/IP fibers connecting to the CCS) are routed to a disconnect or interface patch panel near the rear of the utility trunk.

In order to keep the number of fiber junctions as low as possible (and so avoid signal loss), the copper signals from the rafts are input to Optical Translation Module (OTMs) at the back of the cryostat. The OTMs are custom boards that serve as vacuum feedthroughs (providing electrical connectors to the REBs on the vacuum side, and fiber optic connectors on the air side).

18.3.2 Internal Ethernet Distribution

The CCS Ethernet connection from the outside world to the Camera arrives at the rear of the Camera along with the high speed fibers in a fiber patch panel. This pair of high speed fibers (including an appropriate number of redundant fibers) operates as an ordinary TCP/IP link and is an extension of the CCS network in the observatory.

This fiber Ethernet connection is routed inside the utility trunk to a commercial switch. This switch provides copper connections to each of the CCS nodes in the Camera body and utility trunk. All of these connections are run as standard commercial CAT6 with RJ45 connectors, but routed along with the rest of the Camera power and control wiring in order to make the most efficient use of volume and to avoid any possible interference effects.

18.3.3 Control and Monitoring of Communications

The commercial network switch will have the normal suite of monitoring and management tools characteristic of modern high-end switches. The custom protocol data fibers incorporate a somewhat simpler set of monitoring protocols which are explained in detail in Chapter 17.

18.4 Support Electronics

In addition to the custom or semi-custom electronics described above, there are a number of electronic functions that are performed by commercial electronics. The system-level challenge is to select devices that function as needed and also do not interfere in some subtle way with other operations of the Camera – for instance by adding excessive electrical noise, thermal load, or mechanical vibration.

To avoid unwanted interference from commercial devices, the specifications and performance of those devices will be evaluated as stringently as the custom and semi-custom electronics.

The commercial electronics devices are organized into three groups: motor controllers and sensors, vacuum controllers and sensors, and temperature controllers and sensors. The following subsections identify possible problem areas with these devices and the planned mitigation strategies.

18.4.1 Motor Controllers and Sensors

There are moderately powerful motors used to open and close the Camera shutter and to change the filters. Each motor is part of a more complex mechanism with a variety of sensors providing information and other operations (for example, clamps for the filters) that need to be monitored and turned on and off in a controlled way.

The baseline plan is to use commercial motor controller boxes matched to the motors selected for the mechanical design. It will be necessary to find accessible space in the Camera body for these commercial boxes and to provide a hardware interface between the CCS system and commercial motor controllers – the interface may be as simple as a standard RS-232 connection.

The somewhat more difficult challenge is to provide the proper hardware interface to the sensors and actuators required by the shutter or filter system. There are a wide variety of sensors and actuators that are involved in the baseline shutter and filter system designs.

There are many different commercial pc104 (the CCS baseline single-board computer physical standard) boards that can provide the interface to sensors and actuators. The problem comes down to finding the best suited boards in terms of functionality, power dissipation, and reliability, while keeping the types of boards selected as small as possible to simplify sparing and maintenance.

18.4.2 Vacuum Controllers and Sensors

In the baseline cryostat design, the insulating vacuum is maintained by using turbo pumps during non-observing periods and by continually monitoring the state of the vacuum using multiple commercial vacuum gauges. The auxiliary electronics must provide the capability for CCS to monitor the vacuum gauges and to turn turbo pumps on and off as necessary.

Monitoring and control of the pumps and gauges requires hardware interfaces between the CCS and those devices. In order to be near the vacuum devices and not require very long cable runs while still being located in accessible areas, these hardware interfaces will be placed in the utility trunk directly behind the cryostat.

The commercial vacuum gauges typically interface to their own commercial controllers, which provide human and machine readable interfaces. However, those controllers tend to be quite large and would be difficult to fit into the volume available. The Camera does not require the direct human interface for the gauges. In most cases, the machine interface can be provided by a very simple bridge circuit which requires a DC exciting voltage and an ADC to digitize the bridge difference voltage.

Since this interface requirement is easily accomplished by some channels of the PDS plus the standard pc104 analog interface boards, the problem resolves itself into selecting the optimal interface boards and creating a suitable wiring harness.

The turbo pump power on/off can be accomplished by an SCR switch on the turbo pump AC power line with that switch controlled by a CMOS level from the pc104 interface board. The same pc104 board can

be used to monitor the temperature of the turbo pump and any other quantities related to the vacuum system.

18.4.3 Temperature Controllers and Sensors

Auxiliary electronics must also provide the capability for the CCS to monitor and control temperature in areas of the cryostat, utility trunk, and Camera body.

The most critical temperature in the Camera is that of the CCD sensors of the focal plane in the cryostat. The sensors must be kept at a stable temperature to a fraction of a degree. The cryo system described in Chapter 12 removes excess heat from the focal plane, and temperature of the sensors is maintained in a highly stable condition by small make up heaters mounted to each raft (nine CCDs).

Each CCD also mounts a precision RTD temperature sensor, which is read by the CCS through the REB system. The control loop is closed by the CCS, which calculates the value of makeup heat needed for each raft. No extra hardware outside the raft-tower assembly is needed to accomplish this. However, the cryo system and a similar system that pulls heat from the cold plate in the rear of the cryostat need to be controlled to a few degrees.

Power-dissipating objects inside the Camera body and the utility trunk also must be kept sufficiently cool, and the exterior of the Camera must be maintained near ambient in order to not cause a heat plume in the telescope beam – all of these conditions require some level of thermal control.

The details of thermal control in the Camera body and utility trunk are not as critical as for thermal control in the cryostat (order one rather than one-tenth degree) and are still under study. Thermal control in the Camera body and utility trunk requires low precision control loops to be closed through CCS using, as much as possible, the same hardware interfaces used for the other CCS functions.

All on-Camera interface hardware will be located in the utility trunk. There will clearly be some CCS hardware also in the observatory utility room to interface with compressors for the cryo system and cold plate system.

19: Integration and Test

19 Integration and Test

19.1 I&T Scope and Description

The Integration and Test (I&T) organization serves as the implementation side of the system engineering effort. Where system engineering focuses on flowing down requirements, defining interfaces, and assessing technical risk, the I&T effort works to ultimately close out technical risks, fulfill all system interfaces, and verify that all requirements are met. As with system engineering, Camera integration and test planning started early in the conceptual design phase of the Camera and continues as Camera subsystem requirements and designs mature, and interfaces firm up.

Camera integration and test efforts at the conceptual design stage involve the development of plans for the safe and timely integration of hardware delivered by subsystems into the complete Camera.

Testing is also carried out to verify that Camera requirements have been met. This has been accomplished by focusing on three areas. First and foremost, considerable effort has gone into providing input into the requirements and conceptual designs of subsystem hardware to ensure that the hardware can be safely integrated, that it includes the necessary design features to do so, and that subsystem interfaces and requirements reflect these optimizations.

The second area of focus has been in developing the plans and sequence of events for integrating and testing the Camera. This methodical process has helped to identify and resolve design and interface problems, as well as to extract requirements for integration fixtures and processes. It has also helped us in developing verification test concepts and the overall test methodology.

Third, integration planning efforts have helped us to develop requirements and designs for both the I&T facilities and workflow, as well as the infrastructure and fixtures needed to accomplish the work. This three-pronged I&T development work has resulted in a more robust Camera conceptual design as well as strong I&T plans and concepts.

19.2 Camera Integration

19.2.1 I&T Principles During Conceptual Design

Three overarching design principles originating with the I&T development effort have guided the Camera design as it has evolved and been refined. First, Camera components should be modular, self-contained and tested at the unit level. This allows for independent assembly of components and sub-assemblies at remote locations within the collaboration, as well as early in-process testing of the modules before they are integrated in the Camera. This both reduces the risk of problems during Camera integration, and it speeds the final integration process. Component modularity also improves serviceability by reducing the interdependencies between components, and allowing them to be serviced and removed with minimal disturbance of neighboring components. In short, the design of every subsystem in the Camera has been influenced by this principle.

Second, only pre-tested and verified sub-assemblies and components are integrated into the Camera assembly. All key Camera sub-assemblies will be both functionally and performance tested prior to installing in the Camera, thereby minimizing the risk of downstream failures at higher levels of integration. Furthermore, performance is again verified after integration in the Camera, but before subsequent work is performed. Such incremental testing ensures that the outcome of each integration step is verified to be successful, and that any process or procedural problems are caught early.

Third, early planning for integration and testing—and the related servicing activities during operations—is essential during the development phase, and it provides a strong base for implementing the design and starting construction. The Camera mechanical package is heavily constrained by its optical and structural requirements, and the control systems require tight inter-relationships among subsystems. Thus, planning for and understanding how these subsystems are brought together and tested is required to ensure that they operate as expected when they have been fully assembled.

19.2.2 Subsystem Deliverables and Verification Condition

I&T planning efforts during the conceptual and preliminary design phases have resulted in a clear understanding of subsystem deliverable hardware, and the condition in which it will be handed off for integration. This has proved invaluable for defining subsystem scope, budgets, and work, as well as for identifying how subsystem components fit into the flow of work during integration and test.

As subsystems have approached final designs, the I&T team has assisted subsystems to ensure that a clear set of deliverables is understood and that manufacturability issues have been addressed. Subsystem deliverables are listed in Table 19-1, and a general description of the classes of deliverables is given below.

Table 19-1: List of Camera deliverables, organized by type and subsystem, showing the quantity required for the completed Camera assembly

Deliverable	Subsystem
Integrating Structures	
Cryostat	Cryostat
Camera body	CB&M
Utility trunk structure	Cryostat
Control Elements	
Control system	CCS
SDS	DAQ
Units	
Science raft tower	Sci Raft
Corner raft tower	Crnr Raft
Power supply crate	Aux. Electronics
Shutter	CB&M
L3 lens assembly and L3 flat assembly for I&T	Optics
L1-L2 assembly	Optics
Filters	Optics
Distributed Systems	
Refrigeration system	Cryostat

Deliverable	Subsystem
Protection system	CCS (& Aux Electronics)
Filter Exchange System	CB&M

19.2.2.1 Integrating Structures

The cryostat, Camera body, and utility trunk are key deliverables in that they provide support structure off of which everything else mounts. Thus, these structures include interfaces to components from many subsystems, and I&T efforts cannot start without them.

Subsystem verification testing of these units will be done at the subsystem level, but verification testing will require more test and simulator hardware from I&T to ensure that all interfaces have been verified.

19.2.2.2 Control Elements

The analog integrating elements for Camera control systems are the CCS and SDS hardware and accompanying software. Similarly, these interface with multiple Camera subsystems and provide the sole control and data acquisition interface for them. Because of this, early versions of the CCS and SDS will serve as test crates for other subsystem hardware. Test crates of the CCS and SDS will actually be used even during subsystem prototype testing, so design qualification of CCS and SDS functionality and features will be incremental and proceed along with verification of command, control, and data flow interfaces to subsystem hardware. As Camera integration proceeds, then, CCS and SDS units will already be verified at the individual interface level and will continue to be used and developed throughout the I&T process.

19.2.2.3 Subsystem Unit Deliverables

Science raft towers, Corner raft towers, the power supply crate, shutter, and optics all are delivered as pre-tested units ready to mount and plug in. These “unit-level” deliverables will be fully verified prior to delivery. Their interfaces are much more straightforward and will be initially verified at the unit level using simulators and test crates. Thus, receiving tests in I&T only repeat previously passed tests at the Camera level.

19.2.2.4 Distributed Systems

The refrigeration system, system electronics crates, and Filter Exchange subsystem are geographically distributed systems. These will be assembled and tested at the subsystem level, but must be disassembled and re-assembled during Camera integration. Thus, verification testing will need to be re-done to ensure that workmanship of the final assembly was adequate and all systems meet their requirements.

19.2.3 Integration and Test Sequence Overview

The Camera integration and test process begins with successful Pre-Ship Reviews for subsystem deliverable components. This is when subsystem component test data is reviewed and verification of requirements checked. The goal of this review is to check that a component is indeed ready to be integrated into the Camera, with any non-compliances, open issues or outstanding tests identified and the risks associated with them understood and accepted. If the risks are deemed unacceptably high, then the component needs to stay with the subsystem organization, since they have the infrastructure

and knowledge base to work through any issues. Ultimately, we want to make sure we know exactly what we are going to be integrating into the Camera.

The Camera is comprised of three completely separate mechanical assemblies: the cryostat, utility trunk, and Camera body. The cryostat contains the detector plane sensors, and analog and digitizing electronics. The utility trunk supports the system electronics, power supplies, and purge/thermal systems. The Camera body houses the shutter and Filter Exchange System along with supporting the L1-L2 assembly. These three assemblies are integrated along parallel paths until very late in the I&T process, then brought together just prior to full verification and calibration testing. Keeping these three sub-assemblies along parallel integration paths improves our ability to respond to problems that arise during the I&T process, and it reduces the risks inherent with assembly processes with a long, single-thread critical path.

A further risk reduction effort involves using incremental and repeat testing of components. This chain of tests starts at the subsystem verification level, then proceeds through acceptance testing within the I&T organization, then post-integration testing and further combined testing at higher levels of integration. Such successive testing reduces the risk of component failure at high levels of integration, and it helps in trending, troubleshooting, and diagnosing problems that do occur during system-level testing.

19.2.4 Cryostat Integration and Test Sequence

Cryostat integration begins with the already-verified cryostat sub-assembly, which provides essential risk reduction for the downstream integration activities. First and foremost, pre-verification of cryostat services reduces system safety hazards associated them. The cryostat pressure vessel is proof-tested, and all load-carrying structures are strength-tested, including the grid, cryoplate, and coldplate.

Furthermore, the integrity of all vacuum joints is tested at the component level, including the vacuum-tightness of the high-pressure refrigerant lines and channels. Sub-assembly testing also serves to verify the functionality of the vacuum and purge systems, along with the refrigeration and heater circuits in the cryostat. Finally, early testing of the cryostat allows us to ensure that all components are aligned correctly and meet all interface constraints.

All of this subsystem-level testing of the cryostat allows for full sell-off of cryostat subsystem requirements prior to the start of integration, significantly reducing the risk of failure or loss of functionality later on. Colocation of the cryostat subsystem and I&T will also allow coordinated testing and preparation of the cryostat.

When the cryostat is received from subsystem testing, all fluid lines and vacuum systems are fully tested and complete, the feedthrough plate is assembled and all feedthroughs pre-tested, so the primary work involved in the integration process is the installation of raft towers and their accompanying raft control modules. The science raft and corner raft tower assemblies are fully modular, and the two share many common design features lending themselves to automated I&T processes.

The raft modules have been designed to accept standardized insertion tooling and allow for uniform insertion, mounting, connecting, and testing processes. This will also easily accommodate the use of pathfinder and simulator hardware such as mechanical test rafts to reduce risk to the high-value components. The insertion process is performed vertically to reduce tooling deflection and the risk associated with that.

A detailed integration sequence has been developed and is summarized in Figure 19-1. This allows for loading the 25 bays of the cryostat in any order or sequence, depending on the demands of the delivery schedule. Conceptual designs of the insertion tooling components have also been developed. This sequencing and tooling development has led to a process with discrete steps and stop points to maximize safety and to allow for discipline specialists as appropriate at each step.

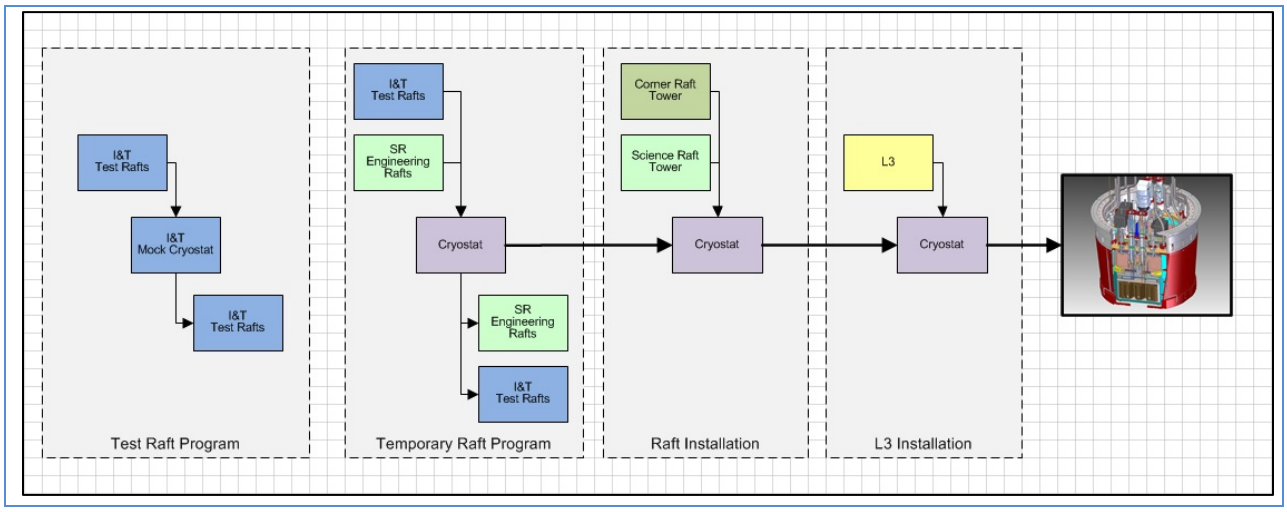

Figure 19-1: Cryostat integration and test sequence

Cryostat integration begins with mounting the cryostat onto the Bench for Optical Testing (BOT), which also serves as the raft integration stand. This stand provides a repeatable and stable mounting for the loaded cryostat. The raft integration fixture consists of two main components. First, a tip/tilt adjustable waffle plate attaches to the pump plate flange. Then a custom x/y/z/theta stage attaches to the waffle plate above the raft bay to be integrated. All processes are performed vertically, with the L3 entrance window removed and the cryostat pointed down to the ground.

For a given bay of the grid, raft towers are inserted from below. The integration fixture, attached near the top of the cryostat, reaches completely through the target bay in the cryostat until the insertion arm extends out past the front face. Prior to positioning a raft tower for integration, an alignment jig is attached to the gantry and drawn into place. Alignment measurements are taken using several different metrology tools. After removing the alignment jig, a raft tower is positioned upside-down under the cryostat using the large BOT x/y stage. The insertion arm is then bolted to the back end of the raft tower. The raft tower is then pulled up into the cryostat through the grid. As the raft tower is inserted, the integration fixture is able to make small adjustments to correct for misalignments.

As the raft tower comes near its mounting point, several imaging devices (telecentric cameras) will be used to ensure clearance on all sides of the raft tower, specifically monitoring the raft sensor assembly (RSA). While monitoring clearances and slowly drawing the raft tower into place, the V-blocks on the RSA engage the balls on the grid. With the RSA now fixed to the grid, the raft electronics crate (REC) module is pulled 6.5mm further until its back end comes to rest on the front face of the cryoplate.

The pre-loaded spring hold-down system for the raft accommodates this relative motion between the RSA and REC module. At this point, the integration fixture is holding the REC module to the cryoplate against the pre-load force of the hold-down springs. The installation process is completed by installing and torqueing down screws that hold the REC module to the cryoplate. Once the screws are in place and torqued, the integration insertion arm is disconnected from the back of the REC module and withdrawn from the cryostat.

Mechanical integration is completed by transferring the attachment point of the pre-load hold-down springs from their temporary location on the sides of the REC module to their permanent support points on the back of the grid. This load transfer is done by rotating the cam feature of the hold-down so it locks into place on the grid.

The final step of the integration process involves plugging in the connectors from the vacuum feedthrough pigtails to the back of the raft electronics board (REB). This completes electrical integration of all components inside the cryostat vacuum enclosure. Subsequent functional testing uses test hardware connected to the pigtails on the outside of the cryostat, verifying workmanship for all internal connector mates as well as ensuring that all raft tower systems are alive.

This identical integration process is repeated for all 21 bays of the grid and similarly for the four corner rafts. The process does not require any access from neighboring bays, so it is independent of the order in which the bays are integrated. Furthermore, since each bay is mechanically and electrically independent of its neighbors, the integration process can—and will—be halted at times to cool down the assembly and run cold performance tests. These tests are also performed on the Bench for Optical Testing (BOT) stand. After the integration fixturing is removed, the cryostat is closed up with an optical flat on the front and the pump flange on the back. Cold testing will be performed to verify performance of the raft towers, and the metrology system in the BOT will measure the flatness of the detector plane at its operating temperature. Using the BOT stand for both raft integration and optical testing the cryostat allows the cryostat to remain in one place throughout cryostat integration.

19.2.5 Utility Trunk Integration and Test Sequence

The utility trunk houses and supports much of the electrical and thermal infrastructure to operate the Camera. This includes the system electronics, power supplies, and purge and thermal systems for the cryostat, Camera body, and utility trunk itself. During operation, the utility trunk is mounted to the back of the cryostat and cantilevers away from the focal plane, through the telescope rotator and hexapod.

The Utility Trunk is a stand-alone structure that is cantilevered off of its base and it is designed to be fully removable. During integration either the actual Utility Trunk (UT) or a temporary version of the UT will be used in place with required components installed as they become available and are needed.

Where possible, the final versions of utility trunk hardware will be used but in some cases use of prototypes may be required. Use of a neighboring utility rack is the preferred method of integration but the complexity of connectors made this difficult, so the I&T and cryostat teams have been working together to find the best solution.

Utility trunk hardware will initially be received from the Cryostat group, having already been load tested and with the cooling system already commissioned. The UT stand accommodates connections to all of the components that mount to it. For the electronics crates, this includes skids for installing and mounting the crates and connections to the air cooling ducts. Camera purge and thermal control systems will be built up on a modular support frame that can be easily connected to the structure, and cable and tube runs will allow for their integration.

System electronics and purge system units will also be received from other subsystems, already pre-tested and ready for integration. Cryostat support systems will be integrated first. This includes the power supply and network crates, and the vacuum and refrigeration system support elements, along with their cabling and tube runs. Additional cabling and tubes will be added to bridge the gap between the utility trunk stand and the cryostat while the utilities are more distant than in the final utility trunk configuration. The utilities will remain in this configuration for much of the cryostat I&T process. When the cryostat is fully loaded with rafts utilities will be moved into the final utility trunk assembly and then will be mounted to the cryostat at the final close-out, just prior to integrating it in the Camera.

After the cryostat is inserted into the Camera, the remaining components will be installed in the utility trunk. This includes the Camera purge and thermal control system and the remaining power supplies and controllers that support operation of Camera components—notably the shutter and Filter Exchange System. These are also modular, so they can be integrated relatively easily and connected to pre-installed cables.

The last step of utility trunk integration is installation of the covers around the structure to seal the inside. Once this is complete, the utility trunk volume will remain clean even after the Camera is moved out of the cleanroom.

19.2.6 Camera Integration and Test Sequence

Camera integration begins with assembly of the outer housing, continues with re-assembly of the Filter Exchange System and mounting of the shutter, and ends with insertion of the fully-loaded cryostat and mounting of the L1-L2 assembly. While the cryostat integration includes repetitive steps that lend themselves to automated processes and fixturing, components being integrated into the Camera are all one-off units that have unique interfaces and assembly methods.

As shown logically in Figure 19-2, the first step of the Camera integration process is the assembly and test of the outer body structure. The outer housing and back flange are delivered by the Camera Body and Mechanisms subsystem, but are assembled and tested by the I&T group, since they form the structure off of which the rest of the Camera is mounted.

First, the back flange (with the filter carousel preinstalled by IN2P3 collaborators) is aligned and mounted to the Camera support stand. Then, the outer housing is bolted to the back flange, its alignment is checked, and it is proof-tested using weights to simulate the loads of all constituents of the Camera. The integrating stand allows for rotation of the Camera around its Z-axis, so the proof-testing will qualify the Camera structure to carry its proof-weight in all orientations.

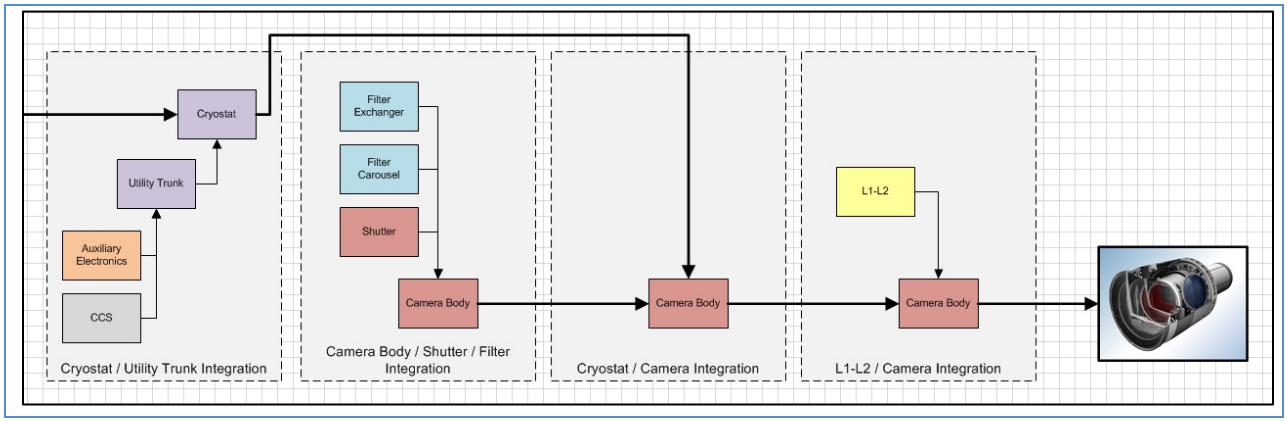

Figure 19-2: Camera integration and test sequence

With the camera structure tested, component integration begins. First, cabling pigtails and purge system plumbing lines are installed inside the housing and terminated at the back flange. Then, the carousel is installed onto the back flange. This currently requires partial disassembly of the carousel, alignment, and mounting to the flange. The carousel ring and structure are then reassembled, electrically integrated to the control and power systems through the pigtails, and re-tested to verify full functionality. Small design changes are currently being evaluated that should minimize the amount of carousel disassembly and reassembly required.

After the carousel is tested, the autochanger is installed and aligned. It, too, is electrically integrated by way of the cable harness pigtails, and then tested on its own and as an assembly with the carousel. This functional verification testing is all a repeat of the subsystem-level testing, and is done to verify that the re-assembly and alignment was done correctly.

The final Camera integration step is integration of the shutter. For the shutter to be integrated the autochanger is removed, which provides access to the front of the L3 lens where the shutter is positioned. The shutter is moved into place using integration/servicing rails that accurately and stably position the assembly during the integration process. This is essential, since the final position of the shutter is mere millimeters away from the L3 lens, and any incidental contact with the lens could scratch the lens.

After the shutter is installed, checked for accurate alignment, and functionally tested, the autochanger is re-installed. This removal/re-installation process will be used to access the shutter for maintenance, so initial integration serves as an important check of the procedures and timing. A second/spare autochanger and filter loader will be installed and tested at this time.

With all contents integrated into the Camera, the cryostat and L1-L2 assemblies can be integrated. The cryostat is integrated first. It is installed horizontally, using a C-Hook to support it while rails guide it into the Camera through the back flange. The cryostat support cylinder bolts to the back flange then the position of the final assembly is surveyed to ensure that the L3 lens and detector plane components are correctly aligned to the Camera.

The cryostat is integrated with utility trunk already in place, so there is no electrical integration needed. However, Camera components that have heretofore been operated off of test crates are now integrated to installed electronics in the utility trunk.

The final step of the integration process is mounting and alignment of the L1-L2 assembly. This involves the mechanical connection of the assembly to the front of the Camera, as well as inter-connection of the purge lines and temperature sensors to the Camera body purge/thermal system. After the Viton skirt is mounted to seal up the Camera, the purge/thermal system is functionally tested to demonstrate that it can maintain the internal temperature of the Camera.

While the integration process described above is sequential, we actually have considerable flexibility in the order of integration. In particular, the cryostat and L1-L2 assembly can be installed and removed at any time during the Camera integration process. This, for example, allows us to test-fit the cryostat inside the carousel, if needed, or mount the L1-L2 assembly to test the purge system. The sequence described above simply maximizes the access and reduces risk during the process, but it can be modified as the design matures, if needed.

19.3 I&T Infrastructure

19.3.1 SLAC I&T Facilities

Camera integration and testing will be carried out in new clean room facility located in the SLAC IR-2 hall. The facility includes approximately 1875 square feet of class 1,000 clean room with anteroom, 1500 square feet of office space in the IR-2 control room, and 160 square feet of cooled computer server space. A floor plan of the facility is shown in Figure 19-3. This facility was completed in May 2015.

The clean room facility is subdivided into two rooms. The larger of the two includes multiple workstations and storage racks for storage of clean components. Penetrations exist that could allow for thermal-vacuum test chambers, a laminar flow hood and environmental chamber as needed. The larger room also has a higher ceiling with a 5-ton gantry crane, as well as windows, a pass-through, intercom, and cable interconnects with an electronics room outside the clean room. This allows for “remote” testing by engineers not in the clean room, while still providing good communication and visual feedback.

The smaller auxiliary clean room will be used for raft receiving tests and for corner raft development work. The clean room includes key card locks to control access, and a gowning and cleaning ante-room to minimize the introduction of contaminants.

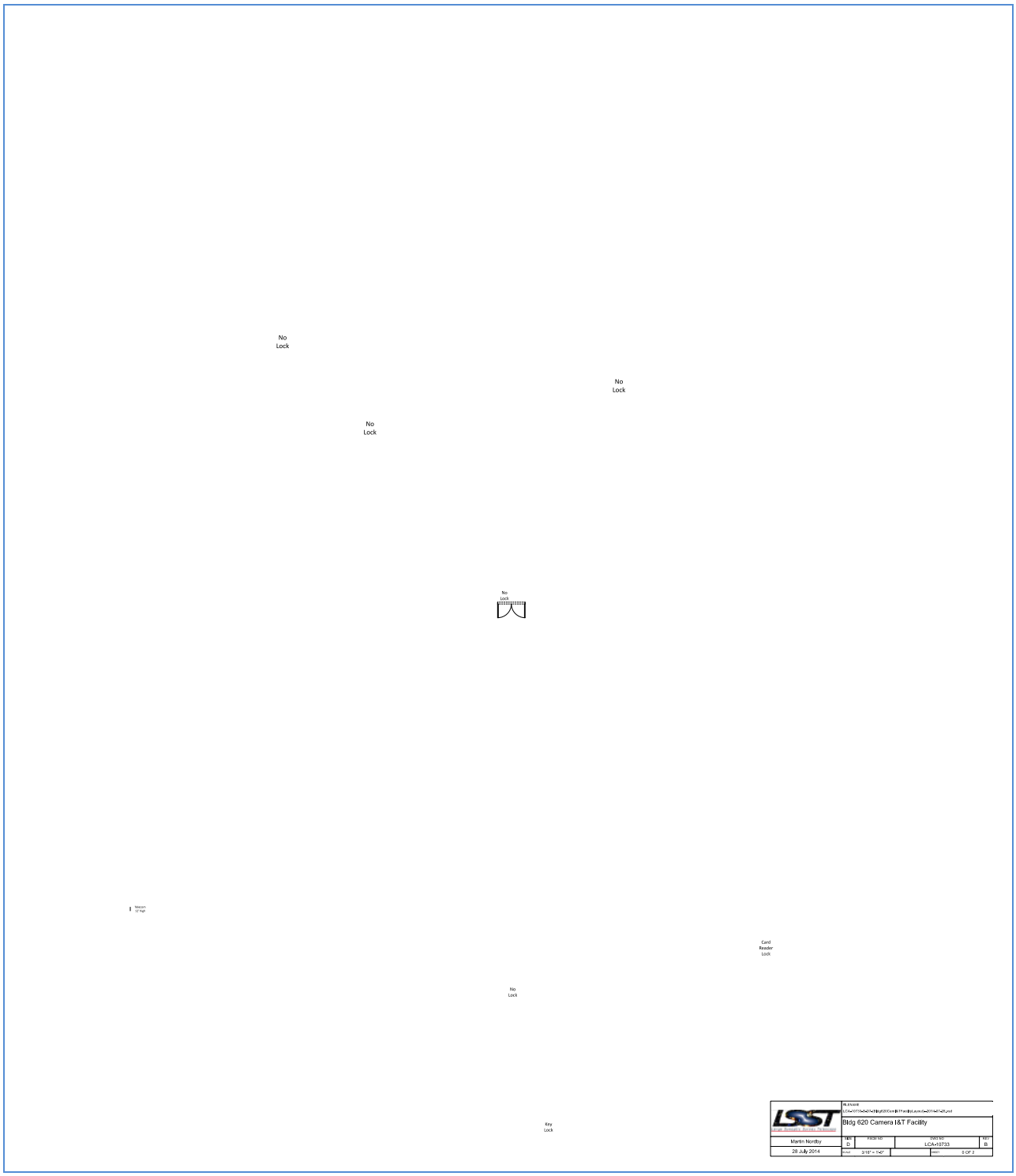

Figure 19-3: Floor plan of the SLAC Building 620 (IR-2) integration facility, showing the clean rooms and ante-room, as well as the general flow of integration work through the facility

Inside the clean room a dedicated air-handling system maintains a temperature- and humidity-controlled environment. HEPA filtration and top-down air flow is used, with high-capacity return ducting in the walls. Since much of the camera hardware and support equipment is heavy, the floor is

directly on the concrete building pad, so a false-floor return plenum is not use. The room also includes boil-off dry nitrogen and filtered dry-air purge systems, and a dry-pipe sprinkler system. Room environmental conditions are continuously monitored and their states are remotely-accessible over the internet. This includes temperature and humidity as well as oxygen deficiency. All parameters are tracked against preset limits and an automated alarm system provides remote calling and paging of technicians and managers if any preset limit is approached or reached.

The clean room also includes a number of anti-static controls. First, it includes a full-coverage anti-static floor as well as grounding points throughout for personnel ESD control and equipment safety grounds. Furthermore, wrist grounding tethers are used and gowns include metal strands to reduce static build-up.

Outside the clean room, IR-2 also includes large loading and staging areas and some space used by the LZ experiment. A separate utility area (B624) is allocated for utilities and cooling water. The clean room facility forms a stand-alone structure inside the larger building, and the entire building—including the roof of the clean room—is covered by a large crane.

Facility use plans and support equipment designs have been developed along with the design of the Camera. This was partially necessitated by the large physical size of the Camera. Beyond the integration sequences described above, step-by-step integration processes were developed for the large sub-assemblies. Each step was evaluated for height, floor-space and access constraints within the facility clean rooms, to ensure that the rooms could support all required activities.

Integration sequence evaluation was also performed to assess the requirements and configuration for the support fixturing that is needed. This has resulted in a comprehensive list of the support hardware, along with requirements imposed on the hardware to fulfill its function during the I&T process. This is discussed in Section 19.3.2, below.

We have identified two important requirements that will be needed to support Camera integration activities. First, to reduce the risk of introducing contaminants into the cryostat, a class 1,000 clean room was constructed. While calculations indicated that a class 10,000 clean room with a class 1,000 partitioned area for raft integration was sufficient, obtaining class 1,000 throughout the entire clean room was available at the same total cost.

Finally, the auxiliary clean room will also be outfitted with an Alum-a-Lift to provide safe and precise rigging and hoisting of the single raft and corner raft cryostat between its various test stations. We expect to perform these moving operations many times during the integration process.

19.3.2 Mechanical Support Equipment and Fixturing

Mechanical support fixturing and equipment have been developed concurrently with the integration sequences for Camera hardware. As noted above, tight space constraints within the Camera have driven an early look at integration plans and sequencing. This holds for the development of fixture preliminary designs, as well. For the key integration fixtures listed in Table 19-2, Camera design constraints as well as the physical dimensions of the facility have driven their design.

Table 19-2: Fixtures that are instrumental to Camera mechanical integration, and key functionalities of each

Key Fixture	Function
Camera Integration Stand	Support stand for Camera in +Y up, -Z up, +Z up orientations, plus intermediate angles; includes pivots to allow controlled rotation of the Camera using the crane; can be rigged and lifted with the Camera; includes provision to move it using air bearings; includes earthquake braces and tie-downs as needed; provides free access to both ends of the Camera.
Bench for Optical Testing (BOT)	Optical bench and support structure for focal plane metrology system, flat field, Fe55 and spot projector testing; includes XY-table for positioning optical flat under the cryostat L3 opening. A raft integration fixture can also be attached to the cryostat while in this stand. The fixture consists of a precision z-stage mounted to an x/y/theta stage. This second stage is attached to a tip/tilt waffle plate matching the grid pattern that is mounted to the cryostat feedthrough flange. All axes have a brake to lock them in place; accepts interface frames for mounting science, corner , and test raft towers.
Single Bay Electro Optical Test Stands	Copy of the Test Stand 7 (TS7) dewar used in the Science Raft subsystem for raft level testing. Copy of the Test Stand 8 (TS8) electro-optical test system used in the Science Raft subsystem for raft level verification.
Single Bay Metrology Stand	A variant of the Test Stand 5 (TS5) metrology system that holds the TS7 dewar horizontally; A reference flat located opposite the dewar window. XYZ stage that moves Keyence heads to scan raft flatness.
Cryostat cart	Supports cryostat in horizontal or vertical orientation; wheeled to transport cryostat between clean rooms; re-cleanable; includes a pivot to allow the cryostat to be rotated by the crane; accommodates installation of the utility trunk; accommodates picking up the cryostat with the C-Hook.
Cryostat C-hook lifting fixture	Mounts to the cryostat support cylinder and supports it while it is installed in the Camera; does not use or block access to the mounting holes for mounting the cryostat to the back flange; suitably hooked to allow for insertion of the cryostat while the Camera is in the saddle stand; balanced so it hangs horizontal with no extra load on it; includes provisions for adding balancing weights to level the cryostat before insertion; re-cleanable.
Saddle Stand	Supports Camera during integration with fully loaded cryostat assembly; provides a platform for shipping Camera; allows for L1-L2 integration at the summit facility.

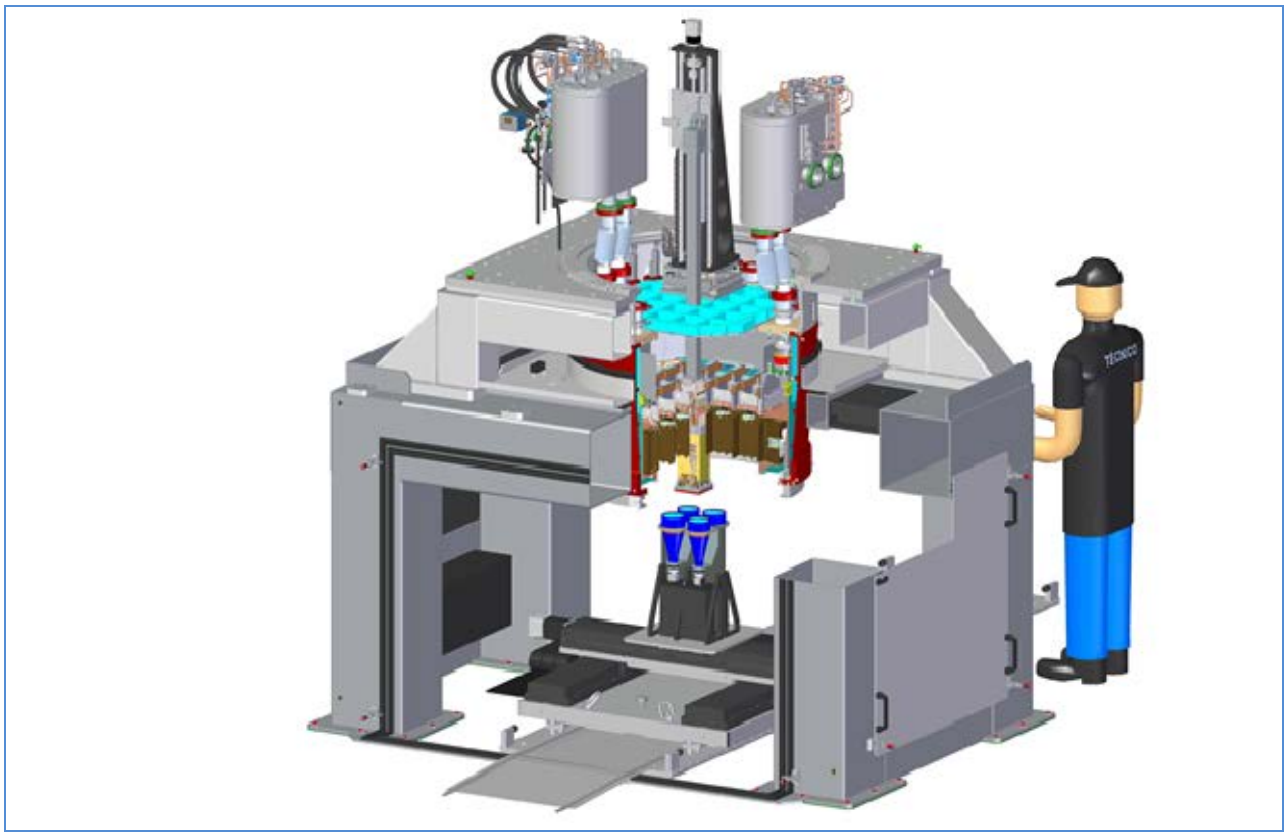

Figure 19-4: Raft tower integration on the BOT stand. All raft integration and electro-optical cryostat testing takes place on the BOT stand without the need to move the cryostat.

One particularly complex fixture is the raft tower integration fixture. The design of this fixtures is shown in Figure 19-4. The BOT stand provides repeatable positioning of the cryostat but also allows the cryostat to remain in one location throughout cryostat integration. The integration fixture is attached to the top of the cryostat, and provides four degrees of controlled motion for inserting a raft tower. The remaining two degrees are adjusted via the waffle plate that holds the fixture.

Transverse and drilling rotation motions are used for accurately centering a raft tower over any of the 25 bays, while the plunge direction moves the raft tower into position within the cryostat. These motions will be driven by Aerotech controllers with fine adjustments.

The full complement of fixtures needed for Camera integration and test is listed in Table 19-3. While many of these are provided by the I&T group, others will be delivered by subsystems along with their camera components. Often, these fixtures will have already been used in subsystem assembly and test operations, so their functionality is relatively well understood. Other of the fixtures will go on to be used for Camera integration on the telescope and subsequent maintenance. In either case, they and their operating procedures will be checked and operated first using pathfinders or load-test hardware to verify that they meet their requirements, prior to use with Camera hardware.

Table 19-3: Fixtures and mechanical support hardware needed for Camera integration. This shows the subsystem providing the hardware, as well as the phase of integration in which it is used

Fixture or Equipment	Providing Subsystem	1. RTM Acceptance	2. Cryostat Initial Testing	2a. Mechanical Test RTM Integration	2b. Thermal Test RTM Integration	2c. Eng-grade RTM Integration	2d. Sci RTM Integration	2e. Crnr RTM Integration	3. Cryostat Close-Out, Utilities Integration	4. Camera Preparation	5. Exchange System Integration	6. Shutter Installation	7. Cryostat Integration to Camera	8. Utilities Interconnection	9. Optics Integration	10. Final Test and Delivery	Maintenance	ICD / Specification
General Supports																		
Camera Integration Stand	I&T									X	X	X			X	X	X	
Camera Integration Frame	I&T									X	X	X			X	X	X	
Camera Saddle Support Stand	I&T												X	X				
Back Flange mounting hardware	I&T																X	LCA-284
Duplicate Rotator	Tel										X	X			X	X		LSE-80
Camera lift fixture	CB&S									X						X	X	LCA-284
Utility Trunk lift fixture	Cryo								X				X				X	LCA-10848
RTM Acceptance Equipment																		
Crnr Raft Tower support frame	CRft	X						X									X	LCA-292
Crnr Raft Tower lift fixture	CRft	X						X									X	LCA-292
Crnr Raft Tower transport container	CRft	X						X									X	LCA-292
Crnr Raft Tower single-bay test cryostat	CRft	X															X	LCA-292
DAQ Stand (V1)	DAQ	X																LCA-11683
Test rafts (5 SciRft)	I&T	X		X	X													LCA-11561
Optical Table to support TS7/TS8	I&T	X																LCA-291
Single-bay Metrology System	I&T	X															X	
Single-bay Installation Process Stand	I&T	X															X	
Single-bay TS7 Lift Fixture	I&T	X															X	
Sci Raft Tower support frame	SRft	X					X										X	LCA-291
Sci Raft Tower lift fixture	SRft	X					X										X	LCA-291
Sci Raft Tower transport container	SRft	X					X										X	LCA-291
Sci Raft Tower Single-bay Cryostat (TS7)	SRft	X																LCA-291
Sci Raft Tower single-bay Electro-Optical Stand (TS8)	SRft	X															X	LCA-291
Cryostat Integration and Test																		
Support cylinder (early delivery) for proof test	Cryo		X															LCA-10848
Proof test load for support cylinder	I&T		X															LCA-10848
Fe55 test flange	I&T		X	X	X	X	X										X	
L3 Aluminum Blank	Cryo		X	X	X													
L3 lens purge system	I&T		X	X	X	X	X	X	X								X	LCA-10848
L3 Lift	I&T		X	X	X	X	X	X	X									
Veritcal Cryostat Lift Fixture	Cryo		X	X	X	X	X	X	X									LCA-10848
Raft Tower Integration Gantry	I&T			X	X	X	X	X									X	
Science raft gantry integration bracket	I&T			X	X	X	X										X	LCA-291 (LCA-10731)
Corner raft gantry integration bracket	I&T							X									X	LCA-292 (LCA-XXXX)
CCS test stand	CCS			X	X	X	X	X	X							X	X	
DAQ test stand (V8)	DAQ					X	X									X	X	LCA-11683
Cryostat interface h'ware to integration stand	I&T		X	X	X	X	X	X	X								X	
BOT / Metrology Stand	I&T			X	X	X	X	X	X								X	
Alt vac-insulated refrig transport line	Cryo				X	X	X	X									X	LCA-10848
Stand-alone support for Heat-X Can	Cryo				X	X	X	X									X	LCA-10848
Refrig line umbilicals to wall panel (2 sets)	Cryo					X	X	X	X							X	X	LCA-10848
Ball/nest assemblies with 5x overage	Cryo			X		X	X	X										LCA-10848
Test crate w/HCU, LPM, cabling, software	Cryo				X	X	X	X	X								X	LCA-10848
Refrig ground unit duplicate system	Cryo					X	X	X	X							X	X	LCA-10848
Camera Body Test Equipment																		
Dummy changer flange	CB&S									X								
Camera housing proof test fixture	CB&S									X								LCA-284
Camera housing proof test equip	CB&S									X								LCA-284
Camera housing proof test weights	CB&S									X								LCA-284
Back end cover plate	CB&S								X	X	X							LCA-284
Pressure test front end cover plate	CB&S									X								LCA-284
Pressure test equipment	CB&S									X								LCA-284
Purge unit aux stand-alone housing	CB&S									X								LCA-284

Fixture or Equipment	Providing Subsystem	1. RTM Acceptance	2. Cryostat Initial Testing	2a. Mechanical Test RTM Integration	2b. Thermal Test RTM Integration	2c. Eng-grade RTM Integration	2d. Sci RTM Integration	2e. Crnr RTM Integration	3. Cryostat Close-Out, Utilities Integration	4. Camera Preparation	5. Exchange System Integration	6. Shutter Installation	7. Cryostat Integration to Camera	8. Utilities Interconnection	9. Optics Integration	10. Final Test and Delivery	Maintenance	ICD / Specification
Filter Exchange System Equipment																		
Filter mass/interface simulators (5)	Exch Sys										X				X			LCA-286
Proof test add-on weights (5 sets)	Exch Sys										X							LCA-286
Filter Loader (2)	Exch Sys										X				X	X	X	LCA-286
Filter storage cartridges/box	Exch Sys										X						X	LCA-286
Filter Loader docking station	Exch Sys										X				X	X	X	LCA-286
Filter Loader cart	Exch Sys														X	X	X	LCA-286
Auto Changer lift fixture	Exch Sys										X						X	LCA-286
Auto Changer servicing frame/box	Exch Sys										X						X	LCA-286
Auto Changer Mass Simulator	I&T																X	LCA-286
Mechanical filter assembly (2)	Optics										X							LCA-338
Shutter Fixturing																		
Shutter insertion/removal rail	CB&S											X				X	X	LCA-289
Shutter servicing frame/box	CB&S											X				X	X	LCA-289
Shutter lifting fixture	CB&S											X				X	X	LCA-289
Dummy L2 lens region	CB&S											X						LCA-289
L2 lens protector	CB&S											X			X		X	LCA-287
Cryostat Insertion Fixtures																		
Cryostat cart	I&T								X								X	
Cryostat C-hook lift fixture	I&T								X								X	
Cryostat insertion guide rails	I&T								X								X	
Optics Fixturing																		
L1-L2 upright support stand	Optics														X			LCA-287
L1-L2 flat support stand	Optics														X			LCA-287
L1-L2 lift fixture	Optics														X		X	LCA-287
L1-L2 transport container	Optics														X		X	LCA-287
L1 lens cap	Optics														X	X	X	LCA-287
L3 optical flat	Optics					X	X	X	X				X		X		X	LCA-287
L3 lens cap	Optics					X	X	X	X				X		X		X	LCA-287
L3 transport container	Optics														X		X	LCA-287
L3 Installation fixture	Optics					X	X	X	X								X	LCA-287
Camera Test Equipment																		
Camera calibration optical bench (CCOB)	I&T														X	X	X	
Mass properties measurement table	I&T															X		
Thermal test equipment	I&T															X		
Modal test equipment	I&T															X		
Diagnostic cluster and data store	I&T						X	X	X							X	X	
Other Test Equipment																		
Getter pump re-generation system	Cryo																	
Utility Trunk front end close-out	Cryo								X									LCA-10848
Vacuum pump cart	Cryo						X	X	X							X	X	
Vacuum leak detector	Cryo						X	X	X							X	X	
Transportation																		
Camera Shipping Container	I&T															X		
Transportation monitoring equipment	I&T															X		
Environmental control equipment	I&T															X		
Shipping crates for suppport equipment	I&T															X		
Aerogo air casters	I&T															X		
Filter transport/storage crate	Optics															X		LCA-287
Inspection Equipment																		
Faro arm	I&T									X	X	X	X	X	X			
Through-bore inspection stand	I&T									X								
Forward-access inspection stand	I&T										X	X						

19.3.3 Verification Test Stands and Software

There are three separate test stands used in verification testing:

1) Single raft test dewar copied from Science Raft subsystem test stands.

2) Bench for optical testing (BOT) for cryostat-level tests with ^{55}Fe tests, metrology scan, point sources, flat fields and multi object projectors.

3) Camera Calibration and Optical Bench (CCOB) test-stand

Each of the several verification test-stands requires custom software to acquire data, analyze the data, and produce summary reports. In some cases the data acquisition includes the regular readout of the rafts, while in other cases (for instance, the metrology testing), data acquisition involves an entirely separate data stream.

For those tests reading out the rafts, the Camera Control System (CCS) will interface to the optical source, movable stage, and other controllable elements needed in these tests by way of dedicated hardware control units (HCUs) for the test equipment. Verification software scripts must be able to control both the readout of the rafts and these special test elements in an integrated fashion. In addition, the data stream must include both raft data and information from the external test elements.

Each stand will require a software suite, consisting of user-level scripts, backed with data acquisition software, data management, data analysis software, and software to generate summary reports. Version control of the verification test suites will be maintained. While the single raft test stand will utilize software developed for raft acceptance testing, the other test suites will be written specifically for I&T. However, some of the cryostat-level tests overlap in functionality with the single raft tests, allowing for shared software development. A software team has been developing reusable tools for electro optical testing at the sensor, raft and I&T levels.

Both cryostat-level and Camera-level tests will involve the readout of the full focal plane, with the total data volume from tests expected to be as large as a month of LSST data. A rough estimate of the total data volume for all cryostat- and camera-level tests is over 100 TeraBytes. The full images may be visualized with the system to be developed for LSST. Compute facilities to analyze the test suite data must allow rapid turn-around time for verification tests and the production of test reports.

A rough estimate of the computing needed to support test data analysis is 1 core per CCD or about 200 cores total, available throughout the cryostat and camera I&T phase. A diagnostic cluster will be used for immediate processing. SLAC computing resources will also be utilized as data is transferred from IR2 to SLAC computing clusters.

19.4 Verification Testing

19.4.1 Overview

Verification testing is performed at four different stages of the Camera assembly. Individual rafts are tested in a dedicated single raft dewar to ensure they have been delivered to SLAC intact, to ensure that

there is no material that would cause contamination and to determine their metrology calibration. Second, testing at the cryostat level is performed, initially with a combination of test and engineering rafts, to ensure that temperature, flexure, metrology, noise and linearity specifications are met, and to establish all procedures for raft assembly. These verification tests are also performed with the science rafts, with the cryostat either partially or fully loaded. Third, optical verification tests are performed on the assembled Camera, to ensure that L1 and L2 meet their alignment specifications. Finally, verification tests are performed on the fully assembled Camera to ensure that the system-wide specifications such as Camera throughput are met.

19.4.2 Single Raft Tower Verification Testing

Individual rafts towers are tested in a dedicated dewar, capable of CCD, metrology and contamination testing. The CCD-level verification testing ensures that delivered raft towers still meet their specifications and enables retesting should that be necessary for any individual raft tower over the long time period for integration. The CCD-level verification tests follow the description below. Dark images are used to verify the noise specification. Flat-field images at different intensities verify the linearity, full-well, dead or hot pixel and dead column specifications. The test stand contains a ^{55}Fe source to verify the diffusion, or PSF, specification. This testing is accomplished with a copy of the BNL "TS8 cryostat and test stand but modified to also support metrology testing.

The single-raft dewar will also be used to perform a metrology calibration for each raft at operating temperature. As the discussion of metrology indicates, there is no adjustable fixture to set the height of individual rafts; instead the size of the ball/ball-nest assembly can be reduced in size by lapping. To determine the size needed, the absolute height of the raft is calibrated. This measurement is made during the same cool-down cycle as the raft verification test.

Lastly, the received rafts are tested for material contamination, using a residual gas analyzer (RGA), prior to installation in the cryostat.

19.4.3 Cryostat Verification Testing

The assembly of rafts and electronics into the cryostat was described above; here we describe the verification testing performed along with this assembly. Both the cryostat and the utility trunk will have been received at this point. Note that the metrology ball nests in the grid will be planarized, and their deflection measured at temperature and in different orientations.

Test rafts, consisting of accurate mechanical models of the raft including the CCD surface, raft mechanical structure with correct weight distribution will be constructed. Additionally, test rafts with test electronics to produce the expected heat load are being studied to determine both required fidelity and the utility of a full thermal load test.

The test rafts are used to validate the raft assembly procedure, and test rafts will be used to initially populate the cryostat grid. Both integration procedures and the metrology system be verified using the cryostat filled with test rafts.

The cryostat will be rotated around two axes to test the detector plane flatness, and grid flexure, for the full range of orientations. We also verify the contamination specification with the associated getters using an RGA.

Once these tests are passed, and the assembly procedure validated, a subset of these test rafts will be replaced with engineering grade rafts. Engineering rafts consist of complete raft hardware and electronics, but loaded with engineering grade CCDs.

Two engineering rafts will be constructed and delivered by the Science RAFT subsystem. The cryostat will be filled with a combination of engineering and test rafts. With this configuration, we again verify metrology, flexure, temperature, and contamination specifications.

An optics bench capable of producing both an image as well as a flat field illumination is used for verification testing at the cryostat level. The cryostat will be equipped with a flat glass window and ^{55}Fe sources capable of illuminating the full focal plane from will be incorporated in a small standoff between the cryostat and L3 flange assembly. Dark images are used to verify the noise specification, now with multiple rafts installed in the cryostat. Likewise artificial images are used to verify the cross-talk specification, both across amplifiers of a single CCD, across CCDs in a raft, and finally from raft to raft. Flat field images are used to verify the linearity and full-well specifications. Of course, since the engineering grade CCDs will not, by definition, meet all CCD requirements, allowance for CCD quality is made in this round of verification testing.

Next, the installation of science rafts begins. Test and engineering rafts are removed, and the installation of science rafts begins with an empty cryostat. After a subset of the grid is populated with rafts, the cryostat is cooled down and again equipped with the flat glass window and ^{55}Fe source. The metrology tests are performed to verify flatness and flexure specifications. The suite of optical tests described above is performed to verify noise, linearity, full-well, crosstalk and image quality specifications. Finally, all rafts are installed, and the test suite is repeated for a full verification test at the cryostat level. This installation plan currently calls for installation of 2 rafts, then 9 + 4 corner rafts and finally 21 + 4 corner rafts. This plan will be adjusted according to the raft delivery schedule.

19.4.4 Optical Alignment

The L1-L2 assembly will undergo a computer generated hologram (CGH) test and the L3 lens will undergo null testing to verify that they are made to specification, as described in Chapter 7. The overall alignment of the three optical elements, in tip/tilt, piston and decenter will be made based on an integrated optical test. An alignment plan was presented and reviewed in 2013 and consists of laser surveying of known fiducials. Additional in-situ tests may also be possible to exploit the CCOB to infer the optical alignment using the location of ghost images.

19.4.5 Camera System Verification Testing

The complete assembly of the Camera, including the L1-L2 assembly, the filter assembly, the shutter, the L3 window together with the cryostat and utility trunk is described above. At this point, Camera system level verification testing is performed. Many requirements will have been verified by the subsystem tests described previously and cannot be individually retested. However, other requirements may only

be verified at the system level. An example of the latter are the Camera optical throughput requirements, which combine the effects of the optical elements, L1, L2, each filter and L3 combined with the CCDs. Such requirements are therefore also verified at the Camera system level.

Verification testing at the system level divides into several areas: temperature control and exposure, mechanical flexure, optical throughput and image quality.

The temperature of the Camera must be carefully controlled with respect to the ambient air temperature, and the Camera must be capable of operating over a wide temperature range. The entire Camera will be assembled and operated in either a subsection of the IR-2 clean room or in a softwalled annex in IR-2 that will be capable of being heated or cooled to explore the full temperature survival range.

The temperature will be slowly raised or lowered, using temporary room heating or cooling, to cover this survival range. Likewise, the relative temperature of the Camera body with respect to the ambient air temperature, and the temperature of the back-end electronics will be verified.

The cryostat temperature control loop, the temperature variation across the focal plane and the temperature stability in the focal plane will all have been verified at the cryostat level. These temperature requirements will also be verified under the range of operating temperatures present in the Camera level tests.

The entire Camera structure will be tested for mechanical flexure and vibration with dedicated sensors, micrometers and accelerometers, or with survey metrology. Static tests, where the Camera is moved from one orientation to another via a crane, will enable tests of the static flexure of the Camera elements. Small impulses delivered to the Camera will test the vibrational amplitude and frequency spectrum of the Camera. It should also be possible to introduce external vibration, at the expected amplitude and frequency spectrum from the telescope, during optical image quality tests.

The optical throughput requirements, specifying the minimum throughput as a function of filter, and the throughput stability and repeatability requirements will be verified using a Camera system level test stand, the Camera calibration optical bench (CCOB). The data produced by the CCOB may also be used as calibration data for the Camera.

The CCOB consists of an independent mount with movable XY stages capable of covering the entire Camera aperture. The CCOB provides a controlled broad-band illumination pattern onto the Camera, in either a wide-beam or narrow-beam configuration. Filters, corresponding to the LSST filter set, may be used to limit the wavelength of the beam. The beam may enter L1 at normal incidence or at a range of angles corresponding to the LSST beam envelope.

A National Institute of Standards and Technology (NIST) calibrated photo-diode is used to make an absolute measurement of the CCOB intensity to compare against the intensity measured by the Camera. The CCOB will thus be capable of measuring the throughput as a function of angle of incidence, position in the aperture and wavelength, enabling verification test of all system optical throughput requirements.

Lastly, work on developing a verification test, again at the Camera system level, for the overall Camera image quality is planned. While it is not possible to reproduce the full aperture F1.2 beam produced by the full LSST, we expect that another input beam may be used to test the image quality.

19.4.6 Metrology

19.4.6.1 Detector Plane Flatness

As described above, the Camera detector plane is comprised of nine CCD sensors mounted to each of 21 identical science rafts, along with two guide sensors and one wavefront sensor mounted to each of four identical corner rafts. Each of these rafts are kinematically mounted and held to the cryostat grid structure, while the grid itself is mounted to the cryostat housing by way of three flexures.

The image quality error decomposition analyses has characterized the behavior of each part of this complex mechanical assembly and its impact on overall image quality. These analyses have shown that due to LSST's fast beam, detector plane flatness is an important contributor to image blur and ellipticity.

Allowed flatness terms for detector plane components are dominated by an 18 µm (PV) flatness at the assembled raft level, together with an additional irreducible 4 µm (RMS) flatness error contribution for the integration of the rafts onto the grid. The detector plane metrology program is intended to directly measure the as-built flatnesses, both at the subsystem component and assembly level as well as for the entire detector plane assembly.

19.4.6.2 Metrology Plans

Delivery of a Camera that meets these overall flatness tolerances will require coordinated efforts between production and assembly at the sensor, raft, cryostat, and integrated Camera levels. At the sensor and raft level, this effort involves measuring flatness of the packaged sensors and completed raft. Raft-level measurement, in particular, will involve both surface flatness measurement as well as sensor selection to bring the nine independent sensors into tolerance with respect to a best-fit plane.

For the cryostat, much of the metrology will focus on measuring and adjusting the co-planarity of the grid interface balls and measuring changes in flatness due to gravity-induced deflections and cool-down distortions. Finally, after rafts are integrated onto the grid, metrology measurements will track integrated flatness and distortions of all sensors on the detector plane at both room- and operating-temperature as well as over a range of operational orientations.

Throughout the process of assembly and integration, starting from the packaged sensors through the raft production and Camera integration, the following non-contact surface height metrology facilities will be used:

1) Sensor surface screening facility: used for sensor acceptance measurements (Science Raft subsystem)

2) Raft assembly metrological facility: to provide feedback for absolute sensor height adjustment and verify overall raft assembly flatness (Science Raft subsystem)

3) Raft acceptance test facility: used for raft acceptance at I&T prior to integration, to measure overall raft flatness and height off its interface vee-blocks (Science Raft subsystem and I&T)

4) Ball calibration facility: measures height ball for pairing to individual grid locations (I&T)

5) Long-throw differential surface metrology facility: measures flatness of integrated sensors through L3 lens or an optical flat, at room- and operating-temperature and over multiple orientations (I&T)

Repeated measurements will be made on parts and sub-assemblies at the various facilities to synthesize a coherent model for the physical detector plane, which is compliant to image quality flatness requirements under operating conditions. To partially illustrate this approach, we describe in the following section the measurement plans that will establish the required detector plane figure, and provide some of the relevant measurement and repeatability tolerances demonstrated in our prototype metrology facility.

19.4.6.3 Metrology Facility

Our non-contact surface metrology strategy is based on stitching multiple, redundant and overlapping individual sub-mappings of the "finite element" plane of detectors relative to a floating reference whose stability is critical only over the short duration of the scans, typically 600 seconds. The approach removes otherwise tight and expensive thermal control requirements of the BOT stand, which would also place scheduling constraints on the measurements, stemming from long thermal timescales of large masses.

The stitching algorithm was outlined and demonstrated by a Monte-Carlo simulation (Rasmussen et al. 2006), where the raw measurement accuracy was improved upon by the availability of multiple measurements providing intermediate references, or "hops" – essentially an exercise of the central limit theorem with extensive book-keeping. This approach improves fidelity for the various in situ measurements, including verifying detector plane figure under representative conditions, positioned behind the vacuum barrier optic L3. These measurements will be made with relatively large standoff distances between the detector surface and the measurement head (typically 150mm) due to the intervening L3 lens.

Ultimately the in situ measurements will include ambient, *in vacuo* warm and cold measurements as seen through L3. The cryostat will also be tilted to a representative operational extreme, 45 degrees from zenith to measure and confirm the predicted degree of gravity-induced deflection of the grid and raft mounts, prior to its integration into the Camera.

19.4.6.4 Prototype Results

The general non-contact, differential displacement measurement approach applied to surface height metrology has already been shown to yield key quantities relevant to the focal plane buildup flatness error budget. These are summarized in Figure 19-5, and represent the sum total of measured resolutions and repeatabilities performed under different conditions and for different purposes.

We expect to obtain significantly better results for the kinematic mount disassembly repeatabilities and for parts wear-in amplitude prior to contact point passivation: representative materials, combined with a smaller number of parts making up the load stack (ball nests will now be manufactured within the SiC grid structure, with the only stack height degree of freedom adjustable by ball diameter selection). Details are described more fully in the metrology and precision assembly development plan.

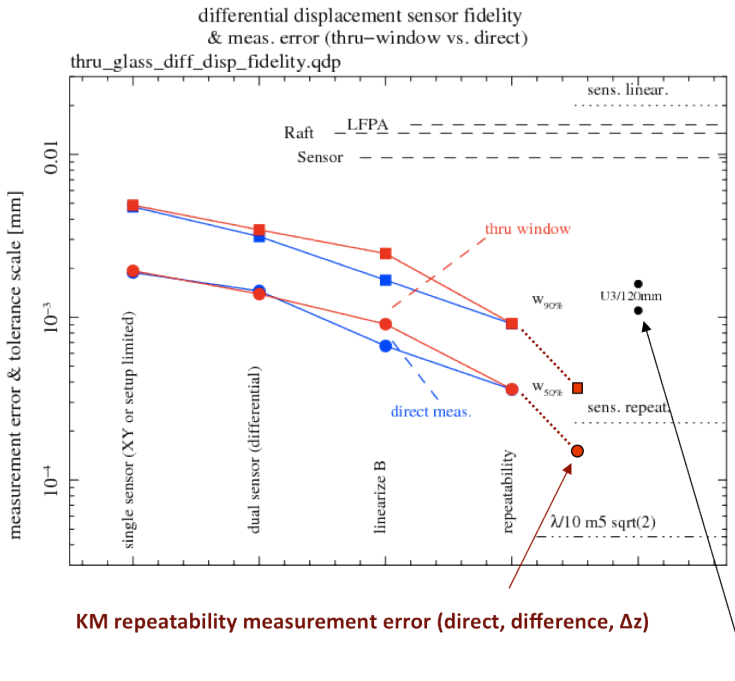

Demonstrated Quantity	Surface height variation (rel.)
Measurement error 3min single/ 6min single/50rep	270nm/220nm/ 100nm
KM Disengage/ engage error	170nm
KM Disassemble/ reassemble error	200nm-4µm
Controlled abrasion under load (Ti/SS440)	< 1.6µm wear-in per ΔT=45°C slew; passivation onset @ 4µm wear-in.

(expect controlled abrasion for representative parts to suffer only ~5% of these numbers.)

Shown: Leitz PMM 12106 (CMM) advertised standard & high (volumetric) uncertainties U3 for 120mm translation

Figure 19-5: The plot on the left is a status summary for thru-window, non-contact, differential metrology prototype results. The demonstrated repeatabilities are a few percent of the build tolerances for the focal plane: the measurement precision is sufficient

19.5 References

LCA-17. LSST Document Archive. LSST Camera Image Quality Error Tree (FWHM).

LSST Document Archive, Document-9491. LSST Camera Focal Plane: Metrology & precision assembly development plan review.

Rasmussen, A. P., L. Hale, et al. (2006). Focal plane metrology for the LSST camera, SPIE.

20 Safety Assurance

20 Safety Assurance

20.1 Introduction

20.1.1 LSST Safety Program

The LSST project is committed to optimizing safety for the project within the constraints of operational effectiveness, schedule, and cost through all phases of the project lifecycle. The project will utilize engineering and management principles, criteria, and techniques to assure a systematic approach to hazard identification, risk assessment, risk reduction, and risk acceptance.

Defining the safety effort is necessary and is accomplished by developing appropriate safety plans. The “LSST Safety Program” establishes the approach to integrating safety into the overall LSST project. The “LSST Camera System Safety Program Plan (SSPP)” identifies the approach to integrating safety into all phases of the Camera project. The site specific Safety Health and Environmental (SHE) plans for the collaborating institutions will be developed as required. A brief outline of the plans is provided below:

- LSST Safety Program (LSST Document LPM-18)

This is the overall project safety plan that establishes for the LSST project: the responsibilities of LSST project management, the LSST Safety Manager, and the LSST Project Safety Council; the requirements for SHE plans for participating institutions; the requirements for hazard analysis and safety reviews; and the identification of pertinent top-level regulations, codes, and compliance standards.

- Performance and Safety Assurance Plan(LSST Document LCA-00138-B)

  The scope of this plan includes the Camera system safety program, environment, safety, and health (ES&H) plans and the means by which personnel and environmental safety processes are managed across the Camera collaboration.

- LSST Camera System Safety Program Plan (LSST Document LCA-31-A)

  This plan is based on ANSI/GEIA-STD-0010 “Standard Best Practices for System Safety Program Development and Execution”. The Camera SSPP establishes for the Camera project the following: the system safety program organization, management, and responsibilities; the methodology of system safety; the program deliverables; and, the hazard analysis process.

- Institutional Safety Implementation Plan

  Collaborating institutions and contractors are expected to have established safety programs in place. The Institutional Safety Implementation Plans will provide the detailed guidelines and/or define procedures for activities at these institutions that involve Camera equipment. The local institution will be responsible for generating these plans.

20.2 Personnel and Environmental Safety and Health

SLAC ES&H policy states the following: “SLAC is committed to protecting the health and safety of on-site personnel, the public, and the environment as it carries out its scientific mission.” The implementation of this policy is the responsibility of all SLAC personnel. The integration of safety into all phases of the LSST Camera project including: design, construction, test, and operation, is the responsibility of the SLAC LSST program team. This team is supported by the SLAC ES&H Division.

SLAC institutional safety processes and programs will complement and support the LSST System Safety Program. The Experimental Project Review Process and the Work Planning and Control (WPC) program are two of these. The Experimental Project Review Process is a formal peer review process. Identified safety Subject Matter Experts (SME), Safety Officers, or other designated personnel are called upon to review an experimental project, identify safety issues, and work with the experimental project to satisfactorily resolve identified issues. This process assures adequate safety review has been accomplished. This process is ongoing for the Camera project. The WPC program is focused on the activity of workers. This program is a formalized, standardized, and documented process for considering and mitigating risks when planning, authorizing, releasing, and performing work.

Camera subsystems will be responsible for the safety, including integration and test activities at their home institutions. The site specific SHE plans and integration and test procedures will formally establish safety requirements for these locations. The safety of Integration and test activities at SLAC will be

managed by both institutional safety procedures and programs as well as Camera-specific safety requirements and procedures. The safety of on-summit integration and test and operations will be governed by Chilean Regulations, Codes, and Standards, AURA requirements, as well as LSST specific procedures and programs.

20.3 System Safety Program

The LSST Camera System Safety Program (SSP) is based on ANSI/GEIA-STD-0010 "Standard Best Practices for System Safety Program Development and Execution". The Camera SSPP describes the tasks and activities associated with the Camera SSP, which has the purpose of identifying the hazards of the Camera project and imposing design requirements and management controls to prevent mishaps and mitigate their impact. Elements of the SSP are identified and briefly described below:

- System Safety Program Plan (SSPP)
  The SSPP describes the Camera project organization and the safety roles and responsibilities for the Camera Project Manager, the Camera System Safety Engineer, the Camera Subsystem Managers, and the Camera System Safety Working Group. The SSPP also describes the methodology for hazard identification, risk assessment, risk reduction, and risk acceptance. A description of the six risk mitigation strategies is explained as well as the methods utilized to verify mitigation actions have been implemented. System safety deliverables are identified with a schedule for completion tied to Camera project milestones.
- Preliminary Hazard Analysis (PHA)
  The PHA identifies safety-critical areas and provides an initial assessment of hazards and requisite mitigation, controls and follow-on actions. A functional and physical description of the hardware is included, as well as a description of hazards and mitigation plans. Hazards associated with the proposed design or function are evaluated for hazard severity, hazard probability, and operational constraints, based on the best available data including mishap data from similar systems and other lessons learned. The Camera Hazard List, LSST Document LCA-15, is a spreadsheet tabulation that captures the identified hazards and characterizes the risk, causes, effects, and controls.
- Hazard Analysis Report (HAR)
  The HAR is developed as a follow-on of the PHA and refines the assessment of hazards consistent with the Camera final design. This includes updating hazards to match the design and capturing hazards associated with interfaces in their final designs. The HAR also documents the validation that requisite controls are incorporated into the final design and operations plans.

- Operating and Support Hazard Analysis (O&SHA)
  The O&SHA evaluates hazards introduced into the system by activities associated with operations and support procedures, and evaluates the adequacy of the procedures to eliminate, control, or abate the hazards.

20.3.1 Hazard Analysis Report

This section contains a summary discussion of the hazards and proposed hazards controls identified in the HAR and is organized by Camera subsystems. The hazards are organized by type and include the following: thermal and cryogenic, pressure and vacuum, mechanical, structural, electrical, environmental, fire, control, and contamination and materials. The physical and functional descriptions of the subsystems are contained in the HAR.

20.3.1.1 Optics

Thermal and Cryogenic

The L3 lens forms the vacuum barrier for the cryostat. Exposure to the -100°C environment may either embrittle the glass or cause thermal contraction and generate stresses beyond the allowable limit resulting in failure. This risk has been assessed by analyzing the black body radiative cooling load, which is the maximum radiative heat transfer possible. These worst case conditions do not pose a hazard to the lens.

The L1 lens is exposed to the dome environment inside the telescope and therefore the extreme temperatures of the mountain top environment. These extremes would produce relatively large differential radial expansion and contraction between the lens and its support ring, which stresses the flexures that bridge between them. Overstressing these highly-loaded flexures could ultimately result in failure. This risk has been controlled by designing the flexures to survive a temperature range much larger than they should ever be exposed to.

Pressure and Vacuum

During operation, both the L1 and L3 lenses are exposed to pressure and vacuum differentials which stress the glass. Overload due to either condition could result in lens failure. This hazard is mitigated by designing for the maximum pressure differential and providing pressure relief valves to ensure the volumes do not exceed their rated pressure.

Failure of the L3 vacuum gasket could result in an uncontrolled venting of the cryostat and the introduction of contaminants or water vapor which could damage the detectors. The vacuum gasket and back-up O-ring will be designed and tested to tolerate the vacuum load combined with the shearing produced by contraction of the flange relative to the lens.

Mechanical

The L1 lens is open to the dome and is at risk by personnel or equipment during access to the Camera. A lens cap will be used to cover the lens during extended access and the Camera will be accessed from the side.

The L2 lens is fully within the Camera housing. However, to remove the shutter or autochanger from the Camera, the region between L2 and L3 is accessed by personnel and handling hardware. During this operation, there is a potential for personnel, tools, or handling fixtures contacting the L2 surface, damaging either the coating or even scratching the lens. To protect the lens, rails are used for removing the shutter and autochanger, and a cover can be installed to completely cover L2.

Structural

The L1-L2 assembly could be exposed to distortions imparted on the assembly by distortions in the rest of the Camera. However, the kinematic hexapod support ensures that no loads can be transmitted into the L1-L2 assembly.

A flaw or micro-crack in the glass could cause a failure in L1 or L3, the two lenses that are under stress due to pressure loads. This risk is mitigated in two ways. Fracture analysis is performed to establish the maximum allowable crack size. The lens is then inspected to verify that there are no cracks of that size; this inspection can be repeated if a problem is suspected.

20.3.1.2 Filter Exchange System

Thermal

The motors and actuators that drive the filter exchange mechanism are used only intermittently, so the average heat load is low and heat is removed by air flow. If the carousel or autochanger drive system were to stall due to some mechanical failure, the motor would heat up. This would be temporary since the position and the force or torque feedback instrumentation would stop the motor.

Mechanical

The Filter Exchange subsystem uses a variety of mechanisms to perform its function, and loss of function of either a mechanism or monitoring instrumentation can result in hazards to the equipment or personnel. These hazards are grouped into the following classes: collision, dropping, mechanical failure, and personnel injury.

If an action is inadvertently executed while the system is in a state that is not safe for that action, physical collision of parts could occur. Examples of this include: moving the filter to its parked position while the carousel is not rotated into its correct orientation or rotating the carousel while a filter is in transit. These actions would likely result in damage to the mechanism and possibly to a filter as well. This hazard is being controlled by having instrumentation to monitor the state and position of every moving mechanism. Commands can only be executed if all instrumentation provides positive indications that mechanisms are in their correct location.

The second mechanical hazard is inadvertent dropping of a filter at the hand-off between the carousel and autochanger. While this is perceived to be the biggest concern for the system, qualitatively it falls into the same class of hazard as a collision: loss of knowledge of the state of the hardware. As with the collision hazards, the dropping hazard is being mitigated by using instrumentation to monitor the condition of each clamp that is used for holding the filter.

Mechanical failure, the third class of hazard, is the broadest class and most difficult to mitigate. Many parts are single-point failure parts where loss of function or outright failure could damage the system. For all of these parts, we will use hardware purchased to national standards and proof test all hardware prior to use.

Degradation of other components could result in a “softer” failure or prolonged decrease in performance that could ultimately result in a system failure. Gradual degradation of performance could indicate wear that may result in failure if ignored. We have three methods to mitigate such a hazard. First, prototype testing will provide empirical data for establishing maintenance intervals for the moving components. Second, we will monitor trends in the performance of the systems by collecting data on motor currents to look for slow changes that signal an impending problem. Finally, if a failure of some

kind does somehow occur, over-current trips on the motors will stop the actuators before any secondary over-loading can occur.

The final class of mechanical hazards in the Filter Exchange subsystem is injury to personnel working around the system. The autochanger, in particular, has a number of pinch points and apertures that open and close. A lock-out/tag-out system is used to disable all mechanisms in the Filter Exchange subsystem when personnel are working around it, and a “panic button” will be available to cut power to all mechanisms.

Structural

Structural loads in the Filter Exchange sub system are generally small, relative to the dimensions of the members. The sole exception is the pivoting C-shaped linkage that transfers the linear motion of the actuator to the curved motion of the trucks that follow the path of the rails. The linkage is pinned at both ends, so there is no bending moments imparted on it. However, the relatively thin members will experience high axial loads along the line of action between the pinned mounts that result in bending and twisting of the members. Structural failure or buckling of the linkage would likely stop the trucks in their tracks, but it may also damage either the filter or even the neighboring shutter. Structural failure of the linkage is mitigated by using closed sections to improve its stiffness against twisting and buckling. Also, the linkage will be proof tested to qualify the safe working load of the design.

20.3.1.3 Shutter

Mechanical

The shutter is comprised of moving parts, so mechanism failure constitutes the primary hazard associated with the components. Given the proximity of the L3 lens to the moving shutter blades, one hazard is that a blade could contact the lens and scrape it, thereby ruining its optical quality. To reduce the likelihood of this happening, the shutter blades are guided from both of their ends by carefully aligned rails and the blade design will be tested to ensure that it does not flutter or vibrate.

Another hazard is of blades colliding with each other. Since we have two sets of blades running on the same track, there is a risk that both blade sets are actuated simultaneously and collide at in the center of the aperture. If this were to occur, the shutter blades would be damaged, and the L3 lens would likely be scratched, as well. This is prevented by monitoring and control of shutter blade position. Thus, one blade set cannot be actuated unless there is a positive signal that the other set is out of the way. Since only one blade set moves at a time, we can ensure that the path is clear prior to actuating either set of blades.

The final mechanical hazard is a pinch hazard for personnel. Since the blades occlude an aperture, there is a possibility that a finger could get pinched by the closing blade. We expect to have shields to deflect objects out of the path of oncoming shutter blades, and will also use administrative controls including lock-out/tag-out procedures and protective covers to reduce the possibility of pinching from occurring.

Structural

The shutter is supported at its four corners off of the Camera housing, and is intentionally designed to be somewhat flexible to reduce force due to over-constraints. Also, it is very light, so forces and stresses on components will be very low. Thus, we do not anticipate any credible structural failure scenarios for the shutter.

20.3.1.4 Cryostat

Thermal and Cryogenic

The cryoplate and grid and components mounted to them operate at cold and cryogenic temperatures. A significant hazard to these components is loss of temperature control, leading to temperatures exceeding normal operating ranges. At both extremes, this hazard is handled by temperature instrumentation on the cryoplate and coldplate to ensure they do not exceed their operating ranges, as well as sensors on the electronics to track temperature while the units are operating.

Pressure and Vacuum

The cryostat is evacuated during normal operation. However, failure of an O-ring seal, a leak through a feedthrough pin, or a leak across a welded seam in the housing could result in an uncontrolled venting of the volume. Such a venting could introduce contaminants and water vapor into the clean cryostat, which would freeze onto the cold CCDs. Also, a rapid venting may produce large pressure differentials across components in the cryostat, leading to unexpected loads on components.

The risk of uncontrolled venting is reduced by using double O-ring seals with an intermediate vacuum groove at all bolted joints. Thus, the failure of one of the seals can be detected immediately and repair plans put in place, while the second seal is still functioning.

Structural

Components in the cryostat are subject to four possible sources of structural failure. First, the large temperature differences in the cryostat can lead to high stresses from differential contraction. We are reducing this risk by using flexures to support the cryoplate, coldplate, and the grid. Structural failure hazards can originate with brittle materials failing prematurely. Some materials may embrittle at cold temperatures. The grid is manufactured from a ceramic which tends to be less fracture-tough than most metals. In both cases, brittle failure hazards are mitigated with a conservative analysis and test program to ensure that even under worst-case stress conditions the material is not stressed to failure.

Non-linear failures can also occur with buckling of the cryostat vacuum housing under combined loads of vacuum and seismic accelerations or of the thin-bladed flexures. Such non-linear failure scenarios are being mitigated with conservative analysis and component qualification test programs to ensure all such structural components have large margins of safety.

Finally, accidental overpressure of the cryostat during venting could result in damage to an O-ring seal, feedthrough, or failure of the vacuum vessel itself. This is being addressed by designing the cryostat to

carry overpressure loads, over-pressure proof-testing it, then also providing a burst disk to ensure that an over-pressure cannot exceed this limit.

Control

The cryostat contains elements of thermal, vacuum, and power systems which rely on the functioning of each other and of elements outside the cryostat. Many of these functions are commandable from the control system, as well. Loss of control, operator error, or failure of one component could produce a more significant problem or failure elsewhere in the system. These hazards are mitigated by implementing enable and disable control for functions handled by a single controller. For those that bridge between controllers or outside of the cryostat, functional interdependencies are monitored and actions allowed or disallowed by the Camera protection system. This will ensure that prevented actions that could damage another subsystem are disabled.

Environmental

When the cryostat is not cold, it will be vented and at atmospheric pressure. Since any contaminant in the cryostat can migrate to and possibly damage the detectors, the cryostat will always be vented with clean and dry nitrogen gas. However, when personnel are working on the cryostat, we will use flow restrictors and oxygen-deficiency monitors as required to detect any unacceptable build-up of this simple asphyxiant.

Fire

The refrigerant used in the cryoplate and coldplate cooling channels is not flammable, but in a fire they will burn, and the combustion products can be toxic to personnel. Inside the cryostat, these materials are fully contained in their channels, and in the event of a leak, there are no ignition sources within the cryostat and the nitrogen purge reduces the possibility of combustion. Outside the cryostat, the refrigerants may pose other hazards.

Materials and Substances

The release of the refrigerant used in the cryoplate and coldplate cooling channels into the cryostat may be harmful to the CCD detectors and severely impact the cleanliness of the cryostat. Furthermore, the gases may also be greenhouse gases. Risk of release of refrigerant in the cryostat vacuum is being reduced by utilizing continuous mill run lengths of tubing, thereby eliminating all joints and connections in the cryostat.

20.3.1.5 Refrigeration system

Thermal and Cryogenic

Given that the primary function of the refrigeration systems is to cool components, one of the primary classes of hazards associated with the systems is overcooling or uncontrolled cooling. First, overcooling could occur if the heat source at the electronics in the cryostat is removed. This could happen due to either a planned turn-off or unplanned shut-down of the systems. In either case, the refrigeration system could provide far more cooling capacity than needed, which could cool down components inside the cryostat too much, or cool down the return lines, creating condensation and ice build-up. Both

symptoms of overcooling are addressed by two mitigators. First, the refrigeration cycle has an inherent temperature floor, below which it cannot function, which is established by the peak pressure and the refrigerants being used. All hardware in the system is survival-tested to this limit to ensure that it can tolerate exposure to these temperatures. Furthermore, temperature sensors are used both for fine control of the system and for monitoring health and safety of the system. If the lines were to cool down beyond their preset limits, the system would shut down.

Another possible source of overcooling is the loss of vacuum in the valve box. This could produce icing of the heat exchanger coils. While this is not preferred and would require recovery effort to repair the leak, this would likely not damage the heat exchangers. Furthermore, the possibility of a leak is mitigated by pressure and leak testing of the vacuum vessel, as well as monitoring of the vacuum pressure during operation. Sudden, catastrophic leaks in well-sealed all-metal vacuum vessels are not common, and any incipient leak is detected by upward trends of the vacuum pressure.

Pressure and Vacuum

The refrigeration systems are under high pressure and rely on large changes in pressure of the working gas to remove heat from the Camera. Thus, over-pressurization is a real hazard within the system. There are two possible causes for such a hazard, located along different points of the circuit. First, in the utility room at the compressor, if a valve were inadvertently closed, the compressor could overpressure the ground circuit of the inlet lines. Up in the valve box, a similar situation could be produced if the free-expansion orifice were to get plugged with frozen oil. In either case, the inlet line pressure would increase. Three controls mitigate this risk. First, the compressor includes overpressure shut-off capability to ensure it is not damaged. Second, the lines include burst disks as a last resort. Also, all lines and fittings in the circuit are rated and proof tested to beyond the maximum operating pressure, set by the relief pressure of the burst disk.

A similar overpressure scenario could occur on the low-pressure return line, due to a pinch in a line or valve closure. Here, also, relief valves and pressure-tested lines ensure that any overpressure is accommodated. Even though the return lines nominally operate at a lower pressure, they are rated and tested to the same level as the supply lines. This ensures that the entire circuit is pressure-rated to the same maximum operating pressure.

A different type of overpressure could occur in the valve box, if a high-pressure heat exchanger developed a leak. Here, the normally-evacuated valve box would fill with refrigerant until it equalized in pressure with the high-pressure inlet line. This pressure is much more than the vacuum vessel typically handles. Such a scenario is addressed first by the vacuum pump on the valve box, which would pump out any refrigerant from a small leak. Larger leaks would be handled by an over-pressure burst disk in the valve box, which could accommodate the mass flow of the largest design leak in a heat exchanger.

Fire

The hazard of a flammable refrigerant has been eliminated by designing the systems to use non-flammable refrigerants only. None of the constituents of the refrigerant mixture are flammable or explosive.

Materials and Substances

The second hazard associated with a fire is that if a fire were to occur, the fumes and combustion products from the burning refrigerant are harmful to human health and the environment. This is a known hazard for the refrigerants in the systems. This is addressed in multiple ways. First, fire due to overheating in the refrigeration system itself is mitigated by monitoring the temperature of the compressors in the utility room. In addition, emergency procedures for the dome and support building will include provisions for the possible presence of hazardous fumes.

Apart from a fire, an accidental release of refrigerant in the utility room may pose a risk of asphyxiation. While the refrigerant mixture is at room temperature while in the room, it is under pressure and some of the constituents are heavier than air. A release in the closed volume of the room may displace air. This potential hazard is being addressed as the system is being developed and sized. If the volume of refrigerant is large enough to pose a hazard, the room may need to be outfitted with an oxygen-deficiency monitor or auxiliary ventilation system.

Contamination

There are three possible sites for contamination in the observatory: CCDs and the L3 lens in the cryostat, and the mirrors in the telescope. Within the cryostat, the risk of contamination due to inadvertent leak of refrigerant is reduced by utilizing continuous mill run lengths of tubing, thus eliminating all joints and connections.

In the utility trunk, a leak in a hose or tube fitting could release gaseous refrigerant into the air, where it could contaminate the surface of the M2 mirror which surrounds the Camera. This is mitigated first designing with adequate safety factor and second by pressure-testing the entire system prior to use.

20.3.1.6 Science Raft Tower

Thermal and Cryogenic

The science raft tower modules are designed to operate at very low working temperatures. However, as with any such system, the hardware can be damaged if the safe operating temperature range is exceeded either on the cold end or hot side. For the science rafts, over-cooling or rapid cooling could damage either the circuit boards due to larger-than-expected thermal stresses, or the detectors themselves. These risks are mitigated by the design of the refrigeration systems, which have an operational floor based on the thermodynamics of the working fluids. Also, the raft tower test program includes qualification and acceptance tests that cover the full survival temperature range of the system. Furthermore, qualification tests demonstrate that the raft tower is capable of surviving a much larger number of temperature cycles than will be experienced in the planned operating life of the Camera.

On the hot side, sensors or boards could overheat during bench testing of components during integration. Here, mechanical failure is not possible, since components are all designed to endure much larger temperature gradients on the hot side. The most sensitive part of the assembly on the high temperature side is the Parlene C passivation coating which is damaged by extended exposure to

temperatures over 80 °C. All cryostat bake-out steps will be carefully controlled and monitored to ensure that maximum temperatures are not exceeded.

Structural

The raft tower is a relatively benign structural assembly, with low loads and high margins of safety. Most components are sized to maximize thermal conductivity, including the bolted joints in the assembly, thus mounting points are multiply-redundant and significantly overdesigned for carrying the structural loads. Two parts pose the most significant structural hazards of the assembly. The loaded rafts are held on their kinematic balls by three pre-loaded springs, to ensure that the loads and deflections are unchanging. However, failure of a spring or support feature would release the raft, causing it to drop out of its ball sockets and either hit the L3 lens or more likely to swing down and damage sensors in neighboring rafts, both of which would cause significant damage to the Camera. This significant risk element for a single-point failure item is being mitigated on three fronts. First, the design of the spring mechanisms is fail-safe to the loss of a spring. The spring itself is a compression spring, which is fully contained and guided to eliminate any possibility of buckling or loss of compression. The support feature that holds the spring units to the grid has also been designed to ensure that it is always fully engaged. Second, the system is designed with relatively high margins of safety on all components. Finally, the design is being prototyped and strength qualification tested to determined safe working loads, then production units will be proof-tested prior to use.

The second hazard risk associated with the structural design is the machined ceramic components that support the CCD sensors. Silicon-carbide ceramic is used for these to maximize heat conductivity and reduce thermal contraction of the assembly. However, the ceramic is more brittle than most metals and typically fails by fracturing, not yielding. The ceramic components are designed to minimize stress concentrations and sharp corners where chipping may occur, and installation tooling prevents collision of adjacent ceramic parts. A design option under consideration is the use of threaded ceramic differential screws for height adjustment. While three screws are used to position and support each sensor, only two are needed to support it, so the screws are redundant structures. Failure of one screw would not result in loss of a sensor, but would likely result in its misalignment only, and possible particulate generation. The likelihood of such a hazard is being reduced by prototype testing to ensure that the screw can carry not just the expected support and thermal contraction loads, but also those associated with misalignment and adjustment forces. Also, a more fracture-tough ceramic is being used to reduce the likelihood of a failure of the material.

The science raft tower assemblies include hundreds of threaded fasteners and thousands of surface-mount electronic components. Due to the sensor-down orientation of the tower in operation, components which become free due to thermal cycling could fall onto the underside of a CCD, possibly causing mechanical breakage or electrical shorting. The design incorporates a conductance barrier between the front end cage (FEC) and raft sensor assembly (RSA), and captive hardware where possible to mitigate this risk. Thermal cycling tests with dummy assemblies also address the likelihood of such an occurrence.

Electrical

The sensor read-out and digitizing electronics includes low-voltage power conditioning, clocking, and signal processing. As with any electronics system the two most common hazards are over-current or short-circuits and over-voltage due to power supply failure or electro-static discharge (ESD). Over-current and overvoltage protection is built into the circuitry of the power supply design and the design is intentionally divided into independent units of low total power sourced to each raft electronics board (REB), so this hazard is addressed at the source in the circuit designs. ESD hazards are the more serious of the hazards. This is mitigated by locating over-voltage protection diodes at all sensitive nodes where this is possible, and by administrative controls for handling of all devices including low-voltage circuits. This includes standards for packaging for storage and delivery of components, design criteria for test benches and clean room materials, and protocols for handling and testing of ESD-sensitive parts. While only a few components in the raft tower are ESD-sensitive, the entire cryostat assembly will be treated with ESD precautions.

Contamination

The primary contamination risk for raft towers is contamination of the sensors by materials outgassing inside the cryostat vacuum. Such an event could significantly affect the response of the CCD sensors and possibly irrevocably damage them, making this a significant hazard. Raft towers include three possible sources of contamination for the CCDs: outgassing of component materials, release of contaminants due to catastrophic failure of an electrical component, and inadvertent introduction of contamination during processing of assemblies.

Contamination due to materials outgassing is being addressed at the source with a materials and part characterization test facility. This is intended to test every material that is used in the cryostat to determine the quantity of outgassing and constituent materials being deposited, then also to assess the effect of deposited material on the system throughput. During production, this will be expanded to include component-level testing of all assemblies, both to qualify the assembly and test processes, and for a final acceptance test prior to delivery. Furthermore, getter canisters are installed in the cryostat vacuum to trap some fraction of condensable contaminants.

The most likely source of contamination is cross-contamination of parts during processing, assembly, or testing. This source is address by process controls invoked by the Camera Contamination Control Plan (CCP), which defines clean room facility requirements, handling protocols, and cleaning procedures for all components being used in the Camera.

20.3.1.7 Corner Raft Tower

Hazard risks in the corner raft towers are identical to those in the science raft towers, given their very similar design.

20.3.1.8 System Electronics

Thermal and Cryogenic

Any of the active devices, but especially the power systems, can be damaged or cause damage to nearby components if the cooling is not active while the systems are powered and they overheat. The time constants for damage from overheating are relatively long—on the order of tens of minutes—so that protective measures based on monitoring a rise in temperature would be fully effective. The primary method of mitigation will be monitoring and control by the CCS. Device temperatures are also monitored by the Camera protection system. This provides a hardware over-temperature interlock to shut down any device that exceeds its allowed temperature limit.

Electrical

Component failures or shorts in active devices could result in over-current. To protect against that possibility, the power supply system not only monitors currents into the various loads but implements over-current and over-voltage protection for all loads. This provides first order but not complete protection against catastrophic failures in the loads.

Another possible source of shorts to ground or other potentials is the abrasion of cabling. To protect against such a possibility, the cable plant is protected in all areas where abrasion or rubbing could occur to prevent cut-through of or failure of the insulating materials.

Fire

If the utility trunk volume is purged with air, some of the electronics objects may pose a fire hazard. However, the energy densities are relatively low, so this is not expected to be a significant hazard. To mitigate against this, board designs use fire retardant materials such as FR-4. The Camera protection system shall include some level of smoke detection within the utility trunk and Camera body. The need for active fire suppression is not anticipated but is under investigation.

20.3.1.9 Camera Body

Structural

The Camera housing, sealing skirt, and L1-L2 assembly form an enclosure that is pressurized at a very slight positive pressure. The Viton sealing skirt will vent any excess pressure and a pressure-relief valve will ensure that in all circumstances the pressure in the Camera volume never exceeds its limits.

Since the Camera housing and back flange provide the primary structural support for the Camera, there is a risk that over-stressing or failure of one structural element could result in large-scale damage or collapse. To mitigate this, we are designing the flange and housing with conservative margins even under extreme seismic loading conditions.

Environmental

The hermetic seals that make up the Camera volume ensure that Camera components and optics operate in a clean, low-humidity environment. However, failure of any one of these seals could result in the introduction of contaminants into the volume. Such a failure is mitigated by slightly over-pressuring

the volume to ensure that any leaks that form result in a net outward flow. Instrumentation will monitor both the internal pressure and flow rate of purge gas, so a leak can be identified.

If dry nitrogen is used as the purge gas, the Camera volume will be oxygen-deficient and a hazard for personnel accessing the Camera for servicing. Here, oxygen-deficiency monitors and administrative controls will be used to reduce this risk.